NEW DEVELOPMENTS IN EXPERIMENTAL ANALYSIS OF TORSIONAL VIBRATION FOR ROTATING SHAFT SYSTEMS

by

Toby J. Miles

BEng, DIS, AMIMechE

A Doctoral Thesis submitted in partial fulfilment
of the requirements for the award of
Doctor of Philosophy of Loughborough University

July 1997

ABSTRACT

The torsional vibration of rotating shafts contributes significantly to machinery vibration and noise but is notoriously difficult to study experimentally. New developments are reported which address the need for appropriate measurement tools, through improved understanding of the laser torsional vibrometer (LTV) and the application of modal analysis techniques.

The LTV was developed previously for non-contact measurement of torsional oscillation. This thesis describes comprehensive theory to account for the sensitivity of its measurements to shaft motion in all degrees of freedom. The significance of this sensitivity is compared with the instrument noise floor and typical torsional and lateral vibration levels. Optimum instrument alignments are thereby specified to ensure immunity to all lateral motion. A new technique is proposed permitting unambiguous measurement in situations where conventional use of an LTV shows unavoidable lateral vibration sensitivity. Simultaneously, a previously unattained measurement of shaft bending vibration is derived. Practical application is demonstrated with measurements from an engine crankshaft, with identification of the first bending mode and estimation of its bending vibration amplitude.

Experimental torsional modal analysis on rotating systems has had limited progression due to the absence of a versatile means to apply an instrumented torque. A novel device has been developed to provide a controllable and measurable torsional excitation, based on the principle of eddy current braking. Together with an LTV to measure response, estimation of the torque input permits frequency response functions to be obtained without modification to the system under test. This system achieves full modal analysis from a rotating shaft using conventional techniques for data processing, with derivation of natural frequencies, mode shapes and damping factors. Results from simple shaft systems consider the variation of modal parameters under rotating conditions.

Application of this technology is clearly demonstrated in studying the behaviour of a centrifugal pendulum vibration absorber (CPVA) used to control the resonant modes of a shaft system. Accurate measurement of each individual pendulum tuning is achieved, with examination of other effects related to successful absorber design. These results are complemented by novel use of the LTV to study the actual pendulum motion. The depth of information obtained underlines the analysis potential made possible by these advances in torsional vibration measurement.

ACKNOWLEDGEMENTS

I would like to express my sincerest thanks to Dr. Steve Rothberg and Dr. Margaret Lucas, my supervisors for this research, for their invaluable guidance, encouragement and advice throughout its duration. This project was funded by a bursary from the Department of Mechanical Engineering at Loughborough University.

I am also grateful for the assistance and advice of the technical staff in the department, most notably Bob Ludlam and the workshop technicians, the I.C. engines laboratory and Alan Wilkinson. Additionally, I would like to acknowledge the Department of Aeronautical and Automotive Engineering and Transport Studies for the use of their engine facilities in part of this work.

Finally, I must thank my parents, family, friends and colleagues to whom I am indebted for their support, patience and understanding during the last four years.

This thesis is dedicated to you all.

'I will lift up mine eyes unto the hills from whence cometh my strength'

CONTENTS

Nomenclature

A	Cross-sectional area of magnetic circuit
A_g , A_i	Cross-sectional area of air-gap and iron respectively
A_m	Area of electromagnet flux acting on disk
$\underline{\boldsymbol{A}}$	Torsional system characteristic matrix
B, $\vec{\boldsymbol{B}}$	Magnetic flux density
$\underline{\boldsymbol{B}}$	Shaft-ground torsional damping coefficient matrix
B_g , B_i	Magnetic flux density in air-gap and iron of magnetic circuit respectively
B_n	Shaft-ground torsional damping coefficient
B_0	Peak value of sinusoidal magnetic field
C	Generalised LTV factor
$\underline{\boldsymbol{C}}$	Shaft torsional damping coefficient matrix
C_n	Shaft torsional damping coefficient
d	Perpendicular beam separation
$\hat{\boldsymbol{d}}$	Unit vector parallel to perpendicular beam separation
d_h	Suspension hole diameter
d_m	Electromagnet diameter
d_p	Suspension pin diameter
$d\vec{l}$	Arbitrary circuit element vector
$d\vec{S}$	Arbitrary surface element vector
D	Diameter of excitation disk
$\vec{\boldsymbol{E}}$	Electric field intensity
f	Frequency
f_A , f_B	Doppler frequency shift at points A and B
f_{beat}	Beat frequency
f_D	Doppler frequency shift of laser light
f_L	Frequency of laser light
F_m , $\vec{\boldsymbol{F}}_m$	Force from eddy current braking effect

$f_{\hat{x}}$	Beat frequency with $\vec{\theta}_x$ motion only
$f_{\hat{y}}$	Beat frequency with $\vec{\theta}_y$ motion only
f_1 to f_4	Beat frequency from LTV positions 1 to 4
g	Actual air-gap length between electromagnets
h	Disk thickness
H	Magnetic field strength
$\hat{i}$	Direction of direct laser backscatter
I	Current
I_c	Inductor core loss current
I_e	Inductor supply exciting current
I_m	Inductor magnetising current
$\underline{I}$	Identity matrix
$\underline{J}$	Inertia matrix
J_n	Inertia
$\vec{J}$	Current density
J_C	CPVA carrier moment of inertia
J_E	Effective inertia of a single CPVA pendulum
J_P	Pendulum bob moment of inertia about its centre of gravity
J_{TOTAL}	Total effective inertia of the CPVA
k_{1e}	LTV demodulator constant
$\underline{K}$	Torsional stiffness matrix
K_n	Torsional shaft stiffness
K_N	Torque-current proportionality constant
K_1', K_2'	LTV constants excluding incidence angle
K_1, K_2	LTV proportionality constant
l	Distance of applied braking force from shaft axis
l_g	Length of air-gap in magnetic circuit
L	Inductance
L_P	Pendulum length

m	Pendulum bob mass
M	Moment applied by braking system
M_h	Time-varying or harmonic moment applied by braking system
n	Rotation order, counter (Appendix B)
$\hat{n}$	Arbitrary unit vector
n_r	Resonance tuned order of CPVA
N	Number of turns in coil winding
N_p	Number of pendulums on absorber carrier
N_R	Shaft rotation frequency
$\underline{P}$	Modal matrix
$\underline{\tilde{P}}$	Mass normalised modal matrix
r, r_1, r_2	CPVA suspension arrangement dimensions
$\vec{r}$	Position vector of generalised point P
$\vec{r}'$, $\vec{r}''$	Position vectors of generalised point P after finite rotations
$\vec{r}_a'$, $\vec{r}_a''$	Position vectors after finite rotations
$\vec{r}_b'$, $\vec{r}_b''$	Position vectors after finite rotations
$\vec{r}_A$, $\vec{r}_{Ao}$	General and initial position vector of point A
$\vec{r}_B$, $\vec{r}_{Bo}$	General and initial position vector of point B
$\vec{r}_P$, $\vec{r}_{Po}$	General and initial position vector of generalised point P on shaft surface
R	Radial position of pendulum axis
R_{AB}	Lumped electromagnet resistance
R_c	Electromagnet core loss resistance
R_g	CPVA suspension dimension
R_m	Magnetic Reynolds number
R_w	Coil winding resistance
$\hat{s}$	Unit vector defining LTV incidence arrangement
t	Time
T	Retarding torque
$T_{applied}$	Torque applied to rotating shaft system

T_C	Torque acting on carrier
T_n	External applied torque
T_N	External applied torque column vector
T_{shaft}	Shaft torque
U	Component of velocity along line of direct laser backscatter
$\vec{v}$	Velocity vector for moving conductor
$\vec{v}_P$	Velocity components of point P due to angular lateral motion
V	Voltage
$\vec{V}$	Total translational velocity
$\vec{V}_A$, $\vec{V}_B$	Velocity vectors at points A and B
V_c	Volume of conductor in magnetic flux
V_{ind}	Induced e.m.f.
$\vec{V}_P$	Total velocity of particle P
$\vec{V}_Q$	Velocity of arbitrary particle Q
$\vec{V}_x$, $\vec{V}_y$, $\vec{V}_z$	Translational velocity components in orthogonal directions
V_1 , V_2	LTV output voltages
$\hat{x}$	Unit vector parallel to X-axis
X_{AB}	Lumped electromagnet reactance
X_L	Inductor reactance
X_m	Electromagnet coil reactance
$\hat{y}$	Unit vector parallel to Y-axis
$\hat{z}$	Unit vector parallel to Z-axis
$\hat{z}_R$	Shaft rotation vector
Z	Electrical impedance
$\underline{Z(\omega)}$	Torsional shaft system impedance matrix
α	LTV incidence angle
β	LTV incidence angle
γ	Pendulum displacement relative to carrier rotation axis

δ	Angle defining relative alignment of LTV beams and shaft
δ_s	Skin depth
ΔC	Fluctuation in LTV factor
$\overrightarrow{\Delta r}$	Change in $\bar{r}$ due to finite rotation
$\overrightarrow{\Delta z}$	Change in shaft rotation vector due to angular lateral vibration
$\overrightarrow{\Delta z_1}$, $\overrightarrow{\Delta z_2}$	Changes in shaft rotation vector
$\Delta\omega_R$	Fluctuation in shaft rotation frequency, torsional vibration
$\Delta\Omega$	Generalised torsional vibration
ζ	Damping factor
$\bar{\theta}$	Arbitrary finite rotation vector of magnitude θ about unit vector $\hat{n}$
θ_C, Θ_C	Carrier displacement about shaft axis
θ_n	Torsional vibration displacement
θ_R	Angle between normal to LTV laser beam plane and shaft rotation axis
θ_s	Angle defining direction of laser scattering observation
θ_v	Angle defining particle velocity vector
$\bar{\theta}_x$	Rotation vector of magnitude θ_x about $\hat{x}$ (pitch motion)
$\bar{\theta}_y$	Rotation vector of magnitude θ_y about $\hat{y}$ (yaw motion)
$\bar{\theta}_z$	Rotation vector of magnitude θ_z about $\hat{z}$ (roll motion)
$\bar{\theta}_1, \bar{\theta}_2$	Finite rotation vectors
Θ	Torsional vibration displacement column vector
$\underline{\lambda}$	Eigenvalue matrix
λ_i	Eigenvalue
λ_L	Laser light wavelength
Λ	Magnetic flux linkage
μ	Refractive index
μ_0	Relative permeability of free space
σ	Electrical conductivity
ϕ	Magnetic flux

ϕ_g, ϕ_i	Magnetic flux in air-gap and iron of magnetic circuit respectively
ϕ_H	Hooke's joint inclination angle
ϕ_P, Φ_P	Pendulum displacement relative to its suspension axis
ψ	Phase difference between supply and magnetising currents
Ψ	Forced torsional vibration solution column vector
ω	Angular frequency
ω_d	Damped natural frequency
ω_n	Undamped natural frequency
ω_P	Pendulum natural frequency
ω_R	Shaft angular rotation frequency
ω_x	Angular frequency of θ_x motion
Ω	Angular rotation frequency

1. INTRODUCTION

While the study of translational vibration is well developed, experimental analysis of the torsional vibration of rotating components is notoriously awkward. This thesis introduces new developments to address the deficit in the available measurement tools for rotating shaft systems. This is achieved through progression in the understanding of the operation of the laser torsional vibrometer and in the application of modal analysis techniques to study the torsional vibration characteristics of rotating shafts.

1.1 Vibration of Rotating Shafts

The wide use of rotating machinery throughout the industrialised world demonstrates the importance of experimental and analytical techniques to understand its behaviour. Applications such as marine, aircraft and automotive propulsion systems, electrical power generation, machine tools and medical equipment are prime examples in which dependable operation is critical and where component failure can incur significant penalties. For reliable operation over long periods of service, vibration measurements are a primary concern, from early design and development work to condition monitoring during operation. However, it is apparent that measurement of vibration directly from rotating components is an exacting problem for engineering metrology. Historically, only representative measurements from non-rotating components and machine housings can be easily achieved.

Machine vibrations can provide an indication of the health of the machine, as high levels of vibration imply high levels of stress, noise and reduced component fatigue life. In the early developmental life of a machine, rotordynamic measurements can determine if design requirements have been met and then, subsequently, in the commissioning stage to satisfy the user that the machine meets specification. During service life machinery diagnostics can identify the causes of failures and malfunctions, with condition monitoring schemes and maintenance programs used to provide early prediction of fault conditions.

Every point on a structure can have its motion completely defined by six co-ordinates or degrees of freedom, three translational and three rotational. Translational vibrations of a shaft, a simple example of which is the cylindrical whirl orbit of a rigid-rotor in Figure 1.1a, have been the main emphasis of many vibration studies, primarily due to the ease of obtaining measurements. Rotational vibrations about the two axes orthogonal to the undisturbed shaft rotation axis and thus constituting a change in direction of the shaft rotation axis, are labelled angular lateral, or bending vibrations. An example of this latter motion is the conical whirl orbit shown in Figure 1.1b. Rotational vibrations about the shaft rotation axis are referred to as torsional vibrations.

Lateral vibration of a rotating shaft is easily coupled to the external motion of the machine. Therefore it can often be adequately implied from measurements on the machine casing. However this is not the case with torsional vibration, which may not be apparent as a vibration problem at the casing until a failure occurs. Ideally this parameter should be measured directly from the rotating component with a non-contact technique. Torsional excitations act on all rotating machinery, most notably in reciprocating engines due to the inertia forces of the piston mechanism and gas pressure forces from the combustion process. Further examples include impulsive loads occurring during a machine process such as a punch press, shock loads applied to electrical machinery from generator line faults and gear mesh frequencies. These excitations constitute a potential concern when the system torsional natural frequencies are close to a driving frequency in the operational range of the machine.

This thesis describes developments in experimental techniques for the study of rotational degrees of freedom for rotating shaft systems, most specifically the analysis of torsional vibration. In addition, the effects of rotating shaft angular lateral vibrations are an important consideration in this work.

1.1.1 Torsional Vibration

Torsional vibration of a rotating shaft is conventionally defined as the speed fluctuation of an axial shaft element and, therefore, superimposed on the mean rotation there is a fluctuating component which can be related to the oscillatory twist along the shaft.

Visualisation of this condition is complicated by the fact that vibration problems associated with rotating shafts are difficult to instrument and thus observe firsthand.

The numerous vibration problems due to torsional oscillations usually result from an inappropriate mix of flexibility and inertia of system components, creating a system torsional natural frequency which coincides with a strong excitation at some point in the machine operating speed range. As with any resonance of a structure this results in fatigue stresses and symptoms indicative of torsional vibration problems include low or high cycle fatigue failures, fretting wear at gear teeth and induced lateral motion and noise radiated from gearboxes, coupling deterioration and shaft and keyway cracking [1-1 to 1-3]. Typical problems in automotive, marine propulsion and industrial applications include torsional oscillation of reciprocating engine crankshafts and excitation of transmission system driveshafts. Coupled torsional-lateral motion has been linked to bearing damage resulting from journal impacts [1-4].

Classification of problems due to torsional vibration can be based on the number of stress cycles before failure [1-5]. At one extreme, if the vibration magnitude is too high for the drive components failure can occur after only a few cycles, with examples including supply faults on electrical machines, surges in centrifugal compressors, material feed problems in rolling mills and synchronous electrical motors designed for limited starts and stops. Alternatively, 'infinite' life applications subject to periodic or continuous torsional vibration are diesel engines, reciprocating compressors, geared drives, grinding mills, crushers and metal rolling mills, where the issue is not component durability but vibration of connected components and associated noise.

Despite this obvious importance, torsional vibration measurement has not been widely used in machinery diagnostics and maintenance, as traditional measurement systems require modifications to be made to the machine or have performance limitations. Section 2.1 reviews the range of techniques which have been used for the measurement of this dynamic parameter. Application of torsional vibration measurement for preventative maintenance on rotating machinery has been limited, although it has been used to monitor the health of viscous dampers [1-6], torsional vibration absorbers [1-7], flexible couplings and gear trains in service [1-8]. The invention of an instrument based on the principles of laser Doppler velocimetry has made the measurement of torsional vibration a straightforward practical possibility [1-9].

Almost one hundred years have elapsed since the first studies of torsional vibration were undertaken and developments up to 1969 are comprehensively reviewed by Ker Wilson [1-10]. Initial concerns were directed at the multi-cylinder reciprocating steam engines which powered transatlantic liners, with failures in the propeller shafting due to torsional oscillations. Numerous mechanical systems were developed for deriving measurements of this motion which highlighted the large fluctuations in the twist of the driven shafts. More advanced studies became necessary as the use of larger, high-speed diesel engines for submarine propulsion saw failures in propeller shafting and engine crankshafts. These developments included the first attempts at controlling the vibration by means of special devices. Rapid development of the internal combustion engine for marine propulsion contributed greatly to the study of torsional vibration as the occurrence of crankshaft failures increased. The engineering research department of Lloyd's Register of Shipping made valuable contributions to the specification of recommended limits for torsional vibration stress and full-scale fatigue testing of shafts. Advances in modelling of torsional effects permitted natural frequencies of shaft systems and critical speed zones to be accurately predicted [1-11].

From 1935 onwards the urgency of problems in marine engineering applications was superseded by advances in knowledge from the aeronautical industry. Considerable progress was made in analytical developments for complicated shaft systems including branched systems and geared assemblies. Additionally, this included the development of instrumentation for the measurement of torsional vibration, such as the torsiograph, which was suitable for both bench and flight testing. The resistance strain gauge was also developed as a useful tool for determining the vibratory response of structural components, including the measurement of shaft torsional strain. The main drive for these studies was that higher powers with reduced structural weight would be achieved through advanced understanding of the inherent vibration problems.

During this period various devices were developed to control undesired torsional vibration including the rubber element absorber and viscous friction damper using silicon fluid as the damping medium. In addition, the centrifugal pendulum vibration absorber was employed successfully on many radial aero-engines which, in addition to reducing vibratory stresses in the power plant system, gave a marked reduction in wear of engine and airscrew components and smoothing of the torque pulsations. These latter devices have been used subsequently to good effect in aero-engine, automotive, industrial and marine applications.

In the modern marketplace for passenger cars the objective noise level and its subjective character are important design parameters, driven by legislation and market forces. The requirements of lower fuel consumption and higher power output conflict with the necessity for comfortable noise and vibration levels in the vehicle and low external radiated noise. Reductions in the weight of the powertrain and vehicle body increase the sensitivity to these problems and recent developments in the automotive industry have identified torsional vibration as an important measurement in NVH studies. This has become more significant in recent years due to lower overall engine noise and improvements in performance. Torsional vibration absorbers and dampers have been applied to automotive engines with the aim of achieving NVH improvements, through the use of these devices on the crankshaft, drivetrain and more recently with the dual function of controlling shaft bending vibration [1-12] as discussed in the following section. Most small and medium-sized petrol engines have stiff enough crankshafts and appropriately low excitation to avoid excessive torsional stresses. These auxiliary dampers and absorbers are used primarily for NVH benefits through changes in the rotation cycle motion and the reduction of gear impacts [1-13].

As a further example, concerns related to torsional vibration increased with the application of high torque, low speed diesel engines to achieve improved fuel economy and emissions in the heavy duty power trains of trucks [1-14]. Reductions in the torsional vibration output from the gearbox can improve the noise and vibration of the drivetrain, by reducing the rattle noise produced by the manual transmission during idling [1-15]. Driveline rattle originates from teeth impacts of unloaded gears undergoing high angular acceleration and for a small automotive petrol engine transmission noise can be higher than engine noise at low speeds, with the rattle appearing as a disturbing component of vehicle interior noise [1-16]. Recent approaches which have had good effect include two-mass flywheels, dampers and various clutch and coupling configurations [1-17 to 1-19]. These have given improvements in idle and acceleration rattle noise in addition to substantially reduced transmission of torsional vibration to the driveline and axles.

A number of links have been identified between torsional vibration and the noise and vibration of reciprocating engines. Torsional vibration of a crankshaft can be coupled with axial vibration as the cranks flex along the shaft axis and in geared systems where relative oscillation of the gears results in reaction forces at the bearings, exciting lateral vibration. Fundamental work has explored relationships between crankshaft torsional vibration and noise for diesel engines, where torsional resonance of the crankshaft excites the stationary crankcase [1-20]. In addition, torsional vibration has been seen to couple with shaft vibrations in other senses. For example, in vehicle drivelines the torsional vibration of the engine crankshaft can give rise to gear rattle in the transmission and booming noise through coupling to bending vibration in the driveshaft [1-21]. For reciprocating engines the effective inertia of the mechanism varies with angular position twice per revolution cycle, hence termed 'secondary inertia', which may create torsional secondary resonance [1-22, 1-23]. Unexpected torsional failures in large, low-speed marine diesel engine crankshafts initially identified this non-linear behaviour as a practical problem. Coupling mechanisms between torsional and transverse vibration of a shaft can dissipate energy and therefore increase the damping of torsional vibration [1-24]. These coupling effects can result from the reaction forces at gearbox bearings [1-25] and, with reciprocating engine crankshafts, through the bearings and piston to the block. These effects have been explored for a simple single-cylinder engine [1-26].

Torsional vibration has the potential for problems in a wide range of industrial machinery. Examples in heavy industry applications include torsional resonances in a large grinding mill and a cement kiln with dual motor drives and transient torsional vibration in a metal rolling mill [1-5]. Additional torsional vibration problems include the self-excited oscillations observed on large induction motor drives used for road tunnel ventilation, evident by noise and chatter due to gear impacts caused by torque reversal [1-27]. The dynamic torsional response of machine tool drive systems can be seen to influence the stability of the drive system and ultimately the quality of the machining process. The design of machine tool gearboxes has been investigated for better dynamic performance and this knowledge applied to a typical small horizontal milling machine [1-28].

Electrical machinery applications also demonstrate problems of torsional vibration. In electrical power generation transmission systems, faults and planned switching operations have the potential for reducing the fatigue life of turbine-generator shafts due to the induced transient oscillations [1-29]. Subsynchronous resonance has resulted in a number of shaft failures and estimation of torsional response and fatigue damage has been used in the analysis of system operating requirements. Direct on-line starting of electrical induction motors generates a considerable pulsating torque, causing large transients of both torque and speed which can create problems when connected to mechanical loads such as fans or pumps. Acceleration of the high inertia load subjects the interconnecting shaft to high stress levels and there are reported cases of the interconnecting shafts having been sheared on start-up [1-30]. These effects have been considered for down-hole pumps used in oil production where it was shown that the induction motor has negative damping on the shaft torsional vibration during start-up [1-31]. The combination of torsional vibrations in induction motor drive systems and eccentricity of the machine rotor can lead to large lateral oscillations of the shaft, with torsional vibration sources including excitation by the electrical supply system, asymmetry of rotor or stator due to damaged components and torque pulsations of the load [1-32].

A multitude of problems are therefore related to the torsional vibration of rotating shafts and experimental measurement is clearly important. The trend of engineering development towards higher operating speeds and reduced material mass emphasises the significance of vibration analysis in determining the safety and reliability of engineering components. Although modelling of torsional system characteristics is reasonably well developed, comprehensive validation of these models is prevented by the absence of suitable experimental techniques. A real need can therefore be perceived for the development of measurement procedures for detailed study of torsional behaviour, to verify theoretical predictions and allow interpretation of the observed response for identification of model refinements.

1.1.2 Angular Lateral Vibration

Considering the other rotational degrees of freedom of a rotating shaft, it is apparent that there a number of applications in which angular lateral motion is important. This motion can be considered as occurring when the target shaft rotation axis undergoes a change in direction and includes bending or whirling of a flexible shaft. For practical arrangements, as in reciprocating engines for example, the excitation inherent in the machine operation and the configuration of the shaft will give rise to a complex bending motion of this component. Therefore there are noise and vibration implications through transmission of this energy to the stationary components of the machine. Generally there are a number of situations which can give rise to shaft whirling or bending vibrations [1-33]. Rotor imbalance is a common problem and is always synchronous with shaft speed. Other rotordynamic concerns include vibration due to shaft misalignment, loose bearing housings or shaft rubs, bearing faults, gear conditions, shaft cracks and the effects of blades and vanes.

As with torsional vibration, measurement of actual shaft motion should ideally be obtained directly from the component, often with complicated instrumentation requirements. Angular lateral vibration of a rotating shaft is inherently difficult to measure and usually inferred from translational vibration response, with reported measurements using accelerometers attached to a stationary housing which is carried by a retro-fitted bearing on the shaft of interest [1-34, 1-35]. Studies of engine crankshaft vibration have also included measurements of the lateral motion with strain gauges attached to the shaft [1-36] or eddy current displacement sensors [1-37]. Modal analysis of lateral vibration of a shaft under non-rotating conditions has been used to identify natural frequencies of the system [1-35, 1-38, 1-39].

Systems to measure shaft vibration can be used to consider angular lateral shaft vibration by measurement of translational displacement, velocity or acceleration [1-33, 1-40, 1-41]. Non-contacting displacement transducers, eddy current or proximity probes, provide a measurement of the relative motion between the shaft and its housing, with typically two orthogonal probes in use. Installation requires access through the machine or bearing housing and the probes are usually put in place on initial assembly of the machine. Shaft lateral vibration can also be assessed, to a limited degree, from measurements taken on the stationary housing with the use of velocity transducers or accelerometers. Laser Doppler vibrometry has been applied to the measurement of the lateral vibration of rotating shafts, with potential advantages due to non-contact operation and inherent immunity to shaft run-out [1-42, 1-43]. However, with radial vibration measurements spurious components can corrupt the resultant signal, masking the intended measurement. Additionally, non-contact measurement of rotational degrees of freedom has been achieved from non-rotating structures by optical means through the use of a conventional scanning laser vibrometer [1-44] and a newly developed dual beam laser vibrometer [1-45]. A six degree of freedom laser vibrometer has also been developed for measurement of the complete dynamic response of a point on a structure [1-46, 1-47]. At present, application of laser technology to the measurement of lateral vibration of rotating shafts has been limited.

In addition to the torsional vibration problems introduced in the previous section, angular lateral vibration of reciprocating engine crankshafts has particular importance in automotive NVH studies. Low-order bending vibrations have concerns in engine reliability while high-order vibrations due to firing pressure are influential on powerplant noise and vibration [1-48]. One solution is to increase crankshaft stiffness but the increased diameter increases friction in the engine, degrading fuel consumption and power output. Optimum design of a shaft would require assessment of the actual bending vibrations.

Crankshaft bending vibration is believed to be the main source of engine 'rumble', a troublesome low and mid-frequency noise that reduces passenger comfort, particularly during acceleration [1-49]. The rumbling noise is induced by the combustion impact resulting in the application of impulsive forces to the main bearings of the engine [1-36]. These vibrations are then transmitted to the vehicle body and this structure-borne noise is radiated as airborne noise inside and outside the vehicle. These NVH problems have been addressed with sound quality control measures such as a flexible flywheel to control the bending resonance of the crankshaft-flywheel system [1-38] and dual-mode dampers to reduce bending vibrations of crankshafts and driveshafts in addition to the torsional vibration [1-12, 1-13, 1-35, 1-36, 1-49], particularly when the frequencies of crankshaft and powertrain bending resonances are close [1-34]. Changing the dynamic properties of the crankshaft-flywheel system can give additional improvements in sound quality at idle speed [1-50]. Other effects related to this shaft motion include the occurrence of booming noise in vehicles reducing comfort levels due to bending vibrations in the drivetrain shafts [1-21].

Shaft angular lateral vibration is of interest in the research reported here for two main reasons. Primarily, the significance of the complete shaft motion on the measurement obtained with a laser torsional vibrometer (LTV) is considered. Subsequently, the use of the LTV is discussed for minimisation of these effects and to give maximum sensitivity to pure torsional vibration. Further to this, it is possible to derive an estimate of the bending vibration of a rotating shaft with an extension of this non-contact method, representing a further step forward in the use of laser technology for vibration measurement.

1.2 Outline of the Thesis

This thesis takes the following format, describing a number of original research contributions which advance knowledge in the experimental measurement and analysis of torsional vibration of rotating shaft systems.

This introductory chapter has defined the significant concerns related to torsional vibration of rotating shafts. In addition, the effects of shaft angular lateral vibration and problems associated with its analysis were introduced. Chapter 2 introduces the wide range of experimental methods developed for the measurement and excitation of torsional vibration. The aims of the programme of work reported here are thereby identified in relation to this published literature.

Accurate, non-contact measurement of the torsional oscillation of rotating components is achieved by the LTV, with advantages over conventional techniques. The optical geometry of the instrument offers inherent immunity to lateral shaft vibration in most cases, but is demonstrated in Chapter 3 to be sensitive to specific types of target vibration under certain circumstances. Following development of the fundamental theory of the instrument, this effect is considered in depth with exploration of the significance of this cross-sensitivity in comparison to the instrument noise floor and torsional and lateral vibration levels found in practice. Guidelines are thereby proposed for accurate assessment of genuine torsional oscillation with minimisation of any measurement discrepancies by optimisation of the optical geometry used. In this way complete immunity to all lateral shaft vibrations can be achieved.

Subsequently, a technique is proposed which permits unambiguous measurement of shaft torsional vibration in situations where conventional use of a single LTV is demonstrated to show unacceptable sensitivity to lateral vibration. Experimental results validate the theory developed, with measurements from an engine crankshaft demonstrating the practical application of this new technique. Simultaneously, this technique is shown to give measurement of the bending vibration of a rotating shaft. These experimental results give a deeper insight into the complex lateral motion of a reciprocating engine crankshaft in operation.

The LTV is therefore demonstrated as a versatile and robust means of measuring torsional vibration response for most applications. However, in the absence of suitable excitation methods, experimental analysis of the torsional vibration characteristics of rotating shaft systems has not been well developed. A novel method of exciting torsional vibrations is presented in Chapter 4, which addresses the limitations of previous approaches and permits modal analysis techniques to be used to study the torsional vibration response of rotating systems. Real-time determination of the torque input to the rotating shaft system by non-contact means and the LTV measurement of system response allow torsional vibration frequency response functions to be obtained for the first time. This experimental approach is used successfully on a rotating system, with conventional modal analysis techniques for data processing, to extract the torsional modal parameters. Experimental results consider the effects governing modal parameters under rotating conditions.

In Chapter 5 an application of this new experimental technique is demonstrated in the study of a centrifugal pendulum vibration absorber (CPVA), a device for controlling the torsional vibration of a shaft system. This device needs to rotate in order to function and therefore could previously only be considered experimentally in limited depth. With the new information obtained through torsional modal analysis, the practical operation of the CPVA can be explored in detail. Accurate measurement of the tuning of the device is achieved and limitations in its practical behaviour can be identified. Additionally, novel application of the LTV allows the motion of the individual pendulums to be studied.

Conclusions drawn from this research are presented in Chapter 6 together with important areas identified for further work. Advances in the understanding of the operation of the LTV, the measurement of rotating shaft bending vibration and the use of torsional modal analysis for rotating shaft systems are all areas which will permit a greater depth of study to be realised in the design and development of a wide variety of rotating machinery.

2. BACKGROUND TO RESEARCH

This chapter identifies and reviews previous published work directly relevant to this study. Firstly, experimental methods for measurement of torsional vibration are discussed. The second section then presents methods which have been used to excite torsional vibration to facilitate testing of shaft systems and components.

2.1 Measurement of Torsional Vibration

The measurement of torsional vibration from rotating shafts provides an exacting problem for transducer design, with most conventional methods costly to set up in terms of machinery downtime, calibration and alignment. There is a need for a user-friendly instrument which can take measurements almost immediately in on-site situations. The primary requirements are for a device which can give accurate measurement of the torsional vibration of a rotating shaft and can be easily moved from one location to another along the shaft axis. Additionally, it must not change the dynamics of the shaft and should be easily installed on an existing machine. It was only through the advent of laser technology that a solution was found which overcame these difficulties and surpassed the basic limitations of other systems.

It is important to make a comparison between the two generic measurement types used to study torsional vibration. Torsion measurements and angular motion measurements can produce radically different results when applied at the same point on a shaft. The former, which includes strain gauges and all forms of torque transducer, produces a measure of the vibratory shear strain across the instrumented shaft section. The latter gives the oscillatory angular motion at a point, whether this is in terms of an angular displacement, velocity or acceleration signal. A torsion measurement system will have a maximum signal in regions where the variation of angular velocity is minimum, that is across the node of a torsional mode shape. It is therefore important to consider the transducer type, position and the number of measurement locations required to determine fully the shaft system torsional vibration behaviour. Conventionally, torsional vibration is measured as the speed fluctuation of the shaft at a point, as considered for this research.

Cyclic speed fluctuation [2-1] is complete rolling motion of an essentially free-free shaft system as though it were a rigid body, as the external vibratory torque is balanced by the inertia torque of the system. This 'roll' component is the same at all points along the shaft and produces no twist and therefore no stress in the shaft and would not be measured by a torsion-type measurement system. Although this rolling motion of the whole shaft occurs without producing torsional stresses in the shafting, it is not desirable in certain applications. These include geared systems to avoid load reversals and tooth impacts, electrical generator sets where it results in voltage variations and systems with rubber couplings.

Torsional vibration is usually not coupled to the lateral motion of the shaft and as a result limited estimation of the torsional behaviour can be determined without direct measurement. Alternative methods to derive a suitable signal from consideration of other parameters have been discussed [2-2] and compared with strain gauge telemetry and gear tooth carrier signal demodulation. These approaches can provide useful information related to torsional response with the use of conventional vibration instrumentation. Measurement of casing or bearing acceleration has limited sensitivity to torsional vibration and is affected by lateral vibration. The use of proximity probes to measure machine gear displacement allows consideration of lateral motion and can provide supporting information. A further non-intrusive approach is to mount matched vibration transducers in the vertical direction, equidistant from the driven or driving component shaft centreline. Subtraction of the signals gives an indication of the reactive torque absorbed by the component and synchronous tracking of the resultant signal and other component reactions during transient periods can give evidence to discriminate between torsional and lateral responses. However, none of these approaches provides a consistent measure of shaft torsional response and for accurate consideration of torsional vibration it is therefore necessary to obtain measurement of the rotating shaft motion directly.

2.1.1 Shaft Strain Gauges

The most common method of measuring torsional vibration uses strain gauges bonded to the surface of the rotating shaft [2-3, 2-4]. A cylindrical bar subjected to torsion has the directions of principal strain at 45° to the longitudinal axis of the bar. Shaft torque can be measured by one or two gauges in appropriate alignment on the bar and through the use of four suitably aligned gauges the possibility of bending or axial strains affecting the measurements is eliminated.

Strain gauges consist of either thin resistance wire arranged in a zig-zag pattern and glued between paper covers, or a 'foil gauge' produced by etching a grid in a copper-nickel or gold-silver layer deposited on a thin flexible plastic base. When cemented onto a shaft, the surface strain is transmitted through the base to the wires of the gauge, causing its cross-sectional area and hence resistance to change in proportion. For determination of torsional strain on the surface of a shaft, the usual arrangement is in the form of a Wheatstone bridge with four strain gauges oriented along the directions of principal strain and on opposite sides of the shaft to derive only shear strain. The signal is transferred from the rotating parts via a slip-ring arrangement, radio telemetry or a rotary transformer.

Two main types of signal can be electrically derived for torsional vibration measurement with these systems [2-4]. The strain gauges can be used as a simple d.c. bridge with amplification, but with the limitation that its frequency response is suitable only down to a few Hz, preventing static calibration of the system. Alternatively, an amplitude-modulation system can be used in which a carrier signal from a constant frequency oscillator is applied to the strain gauge bridge. Bridge unbalance variations due to torsional strains modulate the amplitude of this signal and the output is demodulated as required.

Strain gauges have been used successfully in numerous applications, including the crankshaft of an operating automotive engine [2-5]. They can provide accurate measurement of true strain at their position on the shaft when properly installed, although the time and effort required for installation and calibration of a system may be prohibitive. The torsional vibration motion at a point can be deduced from the measurement of torsional strain using this method. However, this requires knowledge of the dynamic characteristics of the system in order to determine mode shapes and lacks sensitivity to detect small twists.

As an alternative to fixing discrete strain gauges, prefabricated shaft sections are commercially available with calibrated strain gauge systems installed. However, retrofitting of such devices, if feasible, may affect machine performance. Various manufacturers use design variations of the basic principle to give improvement over the inherent limitations of these systems [2-6]. Alternative arrangements of the instrumented test section can reduce the overall transducer length and increase its torsional stiffness but are best suited to large scale applications.

Recent developments have seen the use of piezoelectric material for sensing shaft torsional strain, as an electric current is induced in this material when it undergoes mechanical deformation. However, this approach has been restricted to small-scale, non-rotating applications to date. Shear mode piezoelectric transducers of a ring or shell type bonded onto the surface of a shaft have been used in the active vibration control of a simple structure [2-7]. Alternatively, piezoelectric strip wrapped around a circular shaft has been utilised as a transducer, but this arrangement was demonstrated to be sensitive to both torsional and bending vibration [2-8].

2.1.2 Torque Transducers

Other methods for the measurement of dynamic shaft torque measure the relative twist over a known length of test shaft, which is assumed to be perfectly elastic. The main difference between these methods is the technique used to detect the relative angular displacement over the length of the test shaft and a number of systems are in current use and available commercially.

These devices have been termed 'transmission dynamometers' or in-line torque transducers and commonly take the form of a test length of shaft which is inserted at a suitable point in the shaft system. A number of such systems are described in review papers by Gindy [2-9] and Fleming [2-10], the latter discussing measurement systems for specific application to torque measurement in automotive power trains. These include measurement of the phase shift between pulse train signals obtained from locations at either end of the test shaft section to give a signal proportional to torque across this region. These signals can be derived from magnetic sensors monitoring the passage of gear-wheels, a technique that is discussed fully in Section 2.1.4 for the measurement of speed fluctuation. Alternatively, an arrangement of photo-cells can be used to sense the light returned from illuminated reflective strips fixed to the shaft ends. As a further variation, two slotted disks can be fixed to either end of the test section and arranged adjacent to one another. Differential twist of the shaft changes the alignment of the slots which is detected by a change in the light transmitted thought the slots with a photocell arrangement. However, the main restrictions with these techniques are the poor transient response and accuracy.

A novel non-contact system is the magneto-elastic, or magnetostrictive, torque transducer as the torque applied to a shaft of ferro-magnetic material alters the permeability of the material, thus changing the coupling between the windings of the sensor coils [2-9, 2-10]. However, the dynamic response is limited to frequencies below the crankshaft rotation frequency due to signal-to-noise problems related to shaft run-out. Recent advances in laser technology have explored the non-contact measurement of torque in a shaft, utilising speckle phenomena to provide the signals from the ends of the test section [2-11].

The commercial in-line torque transducer used in experimental stages of this research is based on the principle of variable torque-proportional transformer coupling [2-12]. Two concentric cylinders are shrunk onto the shaft on either side of the torsional test region and two concentric coils are attached to the stationary housing. The cylinders have coinciding rows of slots and rotate with the shaft between the stationary coils. A constant frequency alternating current is applied to the primary coil, internal to the cylinders. When a torque is applied across the ends of the transducer, the deformation zone undergoes an angular deformation and the slots start to overlap. A torque-proportional e.m.f. is therefore induced in the external secondary coil which is converted into a calibrated torque signal by the signal conditioning electronics. A variation of this system is the reluctive torque transducer, or torsional variable differential transformer [2-9].

Although strain gauges and torque transducers provide adequate measurement of twist across a length of shaft, if actual torsional motion of a point on the shaft is to be monitored then these systems are not suitable. Additionally, the restriction that measurements can only be obtained from an appropriately instrumented shaft section prevents full consideration of a system's vibratory response.

2.1.3 Seismic Torsiographs

Torsiographs comprise a rotary seismic inertia mounted on bearings and restrained by a form of torsional spring, resulting in a low torsional natural frequency. When the vibration frequency of the input shaft is higher than the resonant frequency of the transducer spring-mass system the mass is isolated from the torsional vibration. It therefore rotates at a constant speed and can be used as a reference point for measuring machine shaft torsional vibration. The main differences between various systems exist in the methods used for measuring the relative motion between the input shaft and the mass, deriving a mechanical motion or voltage output proportional to the angular oscillation of the shaft. Various forms exist and significant developments have been comprehensively reviewed in the identified references.

Mechanical torsiographs were first reported in 1916 [2-13, 2-14], primarily based on the Geiger instrument shown in Figure 2.1. The shaft section is coupled to the shafting of the machine under test by a belt and pulley system, or in high speed devices by direct drive. The mass is enclosed in a casing rigidly attached to the vibrating shaft, and any torsional vibration results in relative motion between the seismic mass and casing. A system of levers arranged between the two components transmits the vibratory motion to a recording arrangement situated on the stationary body of the instrument. Seismic types of torsiograph with belt drives can be used to obtain measurements at intermediate points on the shafting, although due to access requirements measurements are commonly taken from the free end of a crankshaft. Difficulties are met with belt-drive mechanical torsiographs due to limits of frequency response when signal components associated with multi-cylinder medium to high speed engines are to be examined. In addition, the recorded waveform needs careful analysis to determine the vibration characteristics and torsiographs do not respond accurately at low frequencies which is critical for most heavy machinery. A further development of these devices was the optical torsiograph [2-16], which used a tilting mirror actuated by the relative movement between the seismic mass and its mounting shaft, extending the working range of mechanical equipment for high frequency applications before alternative electrical equipment had been developed.

Electrical torsiographs, such as the Sperry MIT equipment [2-17] and Sunbury electromagnetic pick-up [2-18] produced a voltage output proportional to the oscillatory angular velocity of the shaft. This allowed a smaller, lightweight pick-up to be utilised, compared to mechanical devices where sensing, amplifying and recording functions were combined in one unit. Armature-type coils were fitted to the torsiograph shaft with their outputs connected to slip-rings. Surrounding this arrangement was a permanent magnet fixed inside the brass casing which acted as the seismic mass, freely supported on plain bearings and with no elastic connection to the pick-up shaft. Oscillations of this shaft reproduce those of the engine shaft and the device therefore gives an output voltage via the slip-rings, proportional to the rate of cutting lines of magnetic flux by the armature windings. Direct-drive of the torsiograph is preferred for indication of the high-frequency components, although the unit can be belt-driven. The devices have a flat response over their working range, with a lower frequency limit of the order of 15-30Hz which can be improved by increasing the seismic mass.

Further variations of the instrument were based on the same fundamental principles and include the capacitance type torsiograph in which the seismic mass and its outer casing form the two electrodes of a capacitor [2-19]. The capacitance change of the pick-up due to the relative vibratory motion between these components modulates the carrier frequency voltage supplied from an oscillator and this signal is frequency demodulated to obtain the required output. Other novel forms make use of strain gauges and optical systems to measure the relative motion of the seismic mass and are reviewed by Verhoef [2-20]. This includes a hand-held torsional vibration pick-up that is merely pressed against a rotating driveshaft and, although limited to low frequency operation, can provide an instant measure of torsional vibration.

Practical limitations of these devices arise from the need to withstand high vibration levels, requiring robust support bearings, and the implications of restricted frequency ranges. Recent developments in torsiographs are rare with the emergence of simpler, more user-friendly instrumentation.

2.1.4 Carrier Signal Devices

These devices act as a source of 'carrier signal', with any torsional vibration, or speed fluctuation of the shaft, producing a variation of this signal. Figure 2.2 shows the type of signal that is produced, for example, by a magnetic transducer sensing the passing of gear teeth. Frequency or amplitude demodulation of the signal yields the torsional vibration response, providing the frequencies of interest are sufficiently lower than the carrier wave. An upper limit on the usable frequency range is imposed by the Nyquist sampling theorem. Granere [2-22, 2-23] and Hershkowitz [2-24] provide comprehensive reviews of these methods as commonly used for measuring torsional vibration and the circumstances under which measurement errors are induced due to improper use. The phase-displacement type of torque transducer described previously in Section 2.1.2 uses essentially two of these arrangements to measure relative twist in a shaft section.

The use of gear teeth and a magnetic displacement transducer or proximity probe provides a good method of obtaining measurements. Often the machine to be analysed has a suitable gear installed and there may be no exposed shaft ends for attachment of an encoder. However, there may be no choice of the number of teeth available and it is essential that the gear has been machined to close tolerances as nicks, chips and machining irregularities will introduce spurious harmonic components into the signal. The use of evenly spaced marks machined into the face of a flywheel is a further option, although 'run-out', or variation in the gap between the wheel and transducer, causes the pulse width for each hole to vary resulting in extraneous signal components. An alternative to this is a radially slotted disk with a proximity transducer or optical light-switch used to monitor the slot passing frequency, which is demodulated as before to give a voltage analogue of the crankshaft speed and torsional oscillations. Lateral run-out or shaft whirling components can be eliminated from the torsional vibration signal derived from these methods by summing the signals obtained with two transducers appropriately mounted on opposite sides of the shaft of the gear or wheel [2-25].

The optical encoder is a precision device which couples to the free end of a rotating shaft, consisting of a disk with accurate radial markings which give a pulse every time they pass a photocell. This device requires accurate mounting if the output is to represent actual shaft motion so that relative torsional or radial motion between the disk and casing of the encoder, due to eccentricity or misalignment, does not contaminate the measurement. The encoder is an attractive alternative due to its clean digital pulse train output, reliability and low cost [2-2]. The optical encoder has the further advantages of low moment of inertia and transverse effective mass compared to seismic devices. However, the free end required for attachment prevents measurements from being obtained from points along the shaft and with a flexible coupling used to connect the shaft and encoder an upper frequency limit is dictated by resonance of the system. An alternative method of deriving measurements from an optical encoder has been considered where, instead of demodulating the pulse frequency, the encoder output is electronically compared to the output of an oscillator running at the same frequency as the mean shaft rotation [2-26]. The difference between the two signals is the torsional vibration of the shaft.

Photo-etched tape with accurate black and white bars running across it can also be used, with the main advantage that it can be fixed around a shaft without requiring an exposed end [2-27]. The passage of the white stripes was detected with a fibre-optic probe for ease of access. However, the discontinuity point where the two ends of the tape overlap looks like a transient, or instantaneous speed change which gives spurious spectral peaks in the frequency domain at synchronous frequency and its multiples. This is an obvious drawback as in most studies of the vibration of rotating machinery, measurements at the rotation frequency and its harmonics are of paramount importance. Alternative solutions to this problem include prediction of the unwanted synchronous signal amplitude, or use of a computer to produce an optimally spaced line width for each application.

With regard to signal processing of the transducer output, optical and magnetic sensors and proximity probes all derive a carrier signal with the predominant 'gear-tooth' passing frequency. The proximity probe gives an output voltage proportional to the instantaneous probe/tooth gap and therefore torsional vibration modulates only the frequency of this signal. A frequency modulated carrier signal is also produced by the optical sensors. Frequency modulation (FM) systems are used to perform the demodulation and signal conditioning. The resulting analogue output signal has a d.c. amplitude proportional to the mean shaft speed and an a.c. component corresponding to torsional vibration velocity.

However, the magnetic transducer output is amplitude and frequency modulated as the voltage produced is proportional to the instantaneous velocity of the gear tooth. 'Envelope detection' is used in amplitude modulation (AM) systems to produce a d.c. voltage proportional to the amplitude of the signal, directly related to instantaneous shaft speed as before. An alternative approach is the side-band system which only utilises the transducer, to give a frequency-modulated carrier signal, and a spectrum analyser. By expanding the analyser window about the carrier frequency, a symmetrical array of smaller side-band peaks can be observed either side of the main carrier signal and the torsional oscillation frequency and amplitude can be determined from these. Comparison of FM, AM and side-band systems with strain gauge measurements from the same test-rig, under a range of steady-state and transient conditions showed that all systems can be used to derive torsional vibration frequencies accurately [2-27]. The side-band system was deemed to be most accurate under steady-state conditions due to its simplicity, although this method was found to be unsuitable for transient measurements. Some problems were experienced with the amplitude modulation system due to lateral whirling or 'run-out' of the gear teeth, which has less effect on the carrier wave derived by frequency modulation based methods.

These techniques all provide convenient methods for the derivation of a signal representing the torsional vibration behaviour of a point on a shaft. However, the limitations of each are apparent in terms of inaccuracies which can be introduced through inappropriate matching of the technique to the application and problems of using an appropriate mounting location. This reinforces the need for an accurate, easy to use method for the measurement of this quantity from a series of locations along a rotating shaft with the minimum of alteration of the system under test.

2.1.5 Time Interval Measurement

A digital version of the analogue demodulation techniques of Section 2.1.4 can make use of the pulse train generated by an encoder, a toothed wheel and pick-up [2-28, 2-29] or a tape fixed around the shaft with a series of black and white stripes [2-27]. Instead of using these arrangements to produce a carrier signal, the duration of the passage of the individual teeth or stripes can be timed to derive a measure of the surface velocity of the shaft. The signal from the transducer is used to turn on and off a counter connected to a high frequency oscillator and computer processing converts the values recorded for the passing time of each tooth or stripe into angular velocity.

The sources of errors in this measurement method have been identified as aliasing, problems with measurement of the tooth passing time and the demodulation process, tooth spacing variation and movement of the magnetic pick-up [2-29]. Further reductions in measurement errors have been achieved by the use of multi-bit data acquisition processes to measure accurately the tooth passing time with a low sample rate. Additionally, improvements in the frequency response of the digital demodulation technique improved the measurement accuracy. For the striped tape system, problems were again experienced due to the uneven spacing of the stripes, although by recording the signal at a constant shaft speed with no shaft excitation the digital noise could be subtracted from each digital record to obtain corrected data [2-27]. One claimed advantage of this prototype system is in the monitoring of transient signals for accelerating or decelerating shafts.

A more advanced development of this approach derives measurements of the torsional and translational vibration at a point on a rotating shaft, intended for application to automotive powertrains [2-30]. The shaft surface velocity is measured by timing the duration of the passage of the light and dark stripes and this velocity can be related to lateral motion of the shaft axis and angular fluctuations about the rotation axis. Timing information from three photocell probes arranged around the shaft can be used to determine measurements of the translational motion of the shaft centre in two orthogonal axes and its rotational motion. The data acquired is processed by computer to solve the equations of motion and decouple the torsional and translational motions. Inconsistencies in the tape stripe width are accounted for by recording characteristic data for the tape on the shaft at a constant speed with no lateral vibration. Problems encountered with the 'joining strip' are overcome by placing a highly reflective section over it for synchronisation and reference. The system was demonstrated on a small test-rig to give good comparison with a laser torsional vibrometer [2-31]. Further validation was carried out on a test-rig comprising a simple two inertia system driven through a Hooke's joint, with measurement of both torsional and lateral components [2-32].

This relatively inexpensive system is simple to install and requires only the attachment of the tape and access for the non-contacting optical head and flexible optical fibres which transmit the light from the high intensity halogen source. Simultaneous measurement of translational shaft velocity is a significant development and the system can be expanded for multiple channel use providing simultaneous monitoring of a series of points along the shaft. However, the measurement of torsional vibration is not easily obtained requiring considerable computing power to derive the measurements. Additionally, careful alignment of the system relative to the axis of the shaft is required to avoid errors in measurement and its use is restricted to shafts of circular cross-section.

2.1.6 Torsional Accelerometers

Accelerometers can also be used for torsional vibration measurement by using a diametrically opposed pair of matched transducers. This can be during stationary testing of torsional systems [2-33] or on a rotating system using slip-ring connectors and standard linear accelerometers mounted tangentially on a split collar, with the outputs summed to derive a measure of torsional motion and to cancel lateral motion sensitivity [2-34]. Comparison of torsional vibration measurements with an optical encoder on a shaft system incorporating a gearbox showed good agreement at frequencies up to the torsional resonance of the encoder at around 1500Hz. Errors were seen to occur once per revolution with the accelerometers due to gravity effects interacting with the misalignment of the effective axis of the assembly. Additionally, problems were experienced when lateral vibration of the shaft caused the slip ring brushes to lose contact. The higher natural frequency of the accelerometer assembly gave operation up to 3kHz, although at low frequencies, typically less than 25Hz, the small accelerations result in an unacceptable signal to noise ratio. Fundamentally, this approach is most suited for torsionally stiff shaft systems as the signal to noise ratio is optimal at higher frequencies

A novel torsional accelerometer has been developed with the unique feature that the seismic mass is a fluid and a pressure transducer is used as the sensing element [2-35]. Its structure is illustrated in Figure 2.3 and consists of a fluid filled helical loop connected to a central axial channel in which the pressure transducer is mounted. A differential pressure is generated when the fluid in the helix is accelerated in response to torsional motion. This device has the benefits of minimal sensitivity to all linear and cross-axis torsional accelerations due to the channel configuration and small levels of accelerometer rotation axis eccentricity also had minimal effect on its output. Good comparison was demonstrated with a conventional torsiograph for excitation frequencies up to 300Hz and this device was equally suited to rotating and non-rotating applications. Its capabilities were also compared to those of a toothed wheel system for the measurement of torsional motion of generator sets for torsional fatigue life predictions [2-36]. The angular accelerometer was superior due to its immunity to lateral vibration of the engine which induced small motions of the casing of the toothed wheel system. Problems identified with the accelerometer operation include the effect of severe crankshaft translations which would occasionally cause the slip rings transferring the pressure sensors signal to bounce, increasing noise. Additionally, the transducer signal could be corrupted by the intense electromagnetic radiation from the generator set.

2.1.7 Optical Techniques

A number of systems which use optical phenomena to measure torsional oscillation of rotating shafts have been explored and are discussed here, in addition to the use of laser Doppler velocimetry (LDV) which is introduced in the following section.

Following the development of a high resolution system to measure the static angle rotated by a cylinder through the detection of speckle displacement [2-37], a laser-based system for the measurement of rotational speed and torsional vibrations for semi-reflective target shafts has been proposed [2-38, 2-39]. For this system the time delay between the passage of a speckle pattern between two detectors is tracked. The speckle pattern is formed by the backscattering of a collimated beam of coherent laser light illuminating the shaft and carries information on angular position as minor indentations in the shaft surface influence the speckle pattern in the far field. The light returned from the object is collected by a lens and focused onto two detectors placed exactly in its Fourier plane, thereby providing two signals which are essentially identical. As the detectors are optically placed in the ultimate far field, the time delay between the two signals is independent of the shaft curvature and the distance from detector to shaft and corresponds to the passage of surface scattering structures located angularly on the target. Tracking of the time delay for maximum covariance facilitates measurement of the instantaneous shaft rotation speed.

As with Doppler-shift based instruments the system calibration is independent of the shaft radius and insensitive to translational motion of the target. Additionally, reflective objects can be targeted directly without any mounting of retro-reflective material as the signal strength is estimated to be higher than with other laser-based systems. Potential limitations to the practical implementation of these complex systems include the inability to obtain measurements from arbitrary cross-sections of rotating shafts and sensitivity to large-scale shaft translational motion. In further discussion of this technique, comparison was made of detector arrangements for the two generic types of laser vibrometers, namely those which determine the Doppler shift from two laterally displaced positions on the target shaft surface and those which cross-correlate the passage of a speckle pattern from two angular positions as discussed above [2-40].

Other techniques using optical systems have been applied to the measurement of dynamic transmission error in geared systems, defined as the relative torsional displacement of the input and output shafts of a gearbox. A high degree of accuracy is required over a large speed range and the earliest satisfactory technique for measuring transmission error, although limited to 1:1 gear ratios, could be used over a range of load conditions [2-41]. The image of an optical grating attached to the driving shaft of the gearbox under test is overlaid on an identical grating attached to the driven shaft. In the absence of any transmission error the overlap between the image of the first and the second grating remains constant. Transmission errors between the two shafts change the amount of overlap, allowing more or less light to pass through the gaps of the second grating. The intensity of this light is measured with a photodetector whose output is therefore directly proportional to the transmission error. Refinement of this system has enhanced its performance with the accuracy limited only by the pitch accuracy of the gratings and typically of the order of 5 arc seconds [2-42].

Further improvements to this system have addressed the optical arrangement creating the Moiré fringe pattern from which the analogue measurement of relative torsional displacement is derived in real-time [2-43]. The system included methods to achieve cancellation of translational shaft vibrations, thereby ensuring pure sensitivity to rotational displacement, and allowed application to a 3:1 gearbox with an accuracy better than 1 arc second. This system was subsequently installed on a 4MW test-rig to investigate the noise and vibration of high speed, high power geared systems, clearly demonstrating its ability to measure both static and dynamic transmission errors to high accuracy [2-44].

For comparison, measurement of transmission error with a laser torsional vibrometer was considered [2-43]. Sufficient resolution could not be achieved with the laser instrument as the transmission error component was estimated to be two orders of magnitude lower than the shaft torsional vibration component. Additionally, two instruments would be required for measurement of the relative torsional displacement of the gearbox input and output shafts. However, the demanding requirements of accuracy for this specialised application far surpass those for torsional vibration measurement, necessitating the use of the sophisticated, custom techniques described.

2.1.8 Laser Doppler Velocimetry (LDV)

The application of laser Doppler velocimetry (LDV) [2-45] to translational vibration velocity measurement is now established as a technique complementing the use of more traditional transducers. The measurement of solid surface velocity has been developed from laser Doppler anemometry (LDA) which was used primarily for non-intrusive measurement in fluid flows [2-46, 2-47].

The basic principle of LDV requires the detection of the Doppler frequency shift in coherent light when it is scattered from a moving object. The magnitude of this Doppler shift is proportional to the instantaneous target-object velocity in the direction of incidence of the laser beam. By tracking and measuring this frequency shift, which is generally of the order of MHz, a time resolved measure of the solid surface velocity can be made. The fundamental principles of LDV are further explained in Chapter 3, relating to the operation of the laser torsional vibrometer which is introduced below.

The cross (or dual) beam laser Doppler velocimeter [2-46] created a method for measuring tangential surface velocities without contact. However its use was limited by the inclusion of frequency shifting devices which add to the expense, size and optical geometry. These components are not necessary in the application of this technology to rotating components, as the mean rotation speed of the target shaft gives a unidirectional surface velocity. A laser torsional vibrometer was constructed by Halliwell et al [2-48], based on the cross-beam geometry, and is shown in Figure 2.4. Demodulation of the Doppler signal gave a time-resolved analogue of the surface velocity, the fluctuating part of which is proportional to torsional vibration velocity. The device was used to measure torsional oscillations of the crankshaft of a six cylinder in-line diesel engine and the results compared well with those obtained using a slotted disk system.

The cross-beam velocimeter suffers a number of practical disadvantages. Due to the converging lens system the intersection region of the laser beams, where the target surface must remain, is typically less than 1mm in length. As a result the target shaft must have an essentially circular cross-section and the instrument should be tripod-mounted at a fixed distance as large amplitude solid-body movement of the target or instrument will prevent measurements from being achieved. Additionally, components of solid-body oscillation in the direction of tangential surface velocity are indistinguishable from torsional oscillations. Limitations are also imposed on the working speed range by the electronic demodulator due to the fixed optical geometry and the need for easy optical access and careful alignment. These points prevented the cross-beam instrument from becoming a practical instrument and laser technology for torsional vibration measurement did not progress further until the development of an alternative optical geometry.

An early development of LDV considered the instantaneous measurement of rotation speed of solid bodies or the vorticity of fluids with scattering seed particles [2-49]. The optical arrangement uses a birefringent prism or diffraction grating to derive two beams from the same laser source with a set angular separation and orthogonal polarisation which are focused at separate points in the measuring volume. The backscattered light is collected from the two spots and recombined, having undergone a Doppler shift due to the velocity of the target in this volume. After passing through a polarising filter the light interferes on a photodetector giving rise to a beat frequency. This frequency is related to target rotation only and is independent of the radius of the target rotation and the absolute spot position on the surface, dependent only on the distance between the spots. This measurement is inherently insensitive to collective translations providing the target remains in the measuring volume. The technique was verified experimentally for measurement on a rotating scattering object and, although the potential for measurement of fluid flow vorticity was discussed, the use of this technique for torsional vibration measurement was overlooked.

An arrangement of parallel laser beams was proposed by Watanabe et al [2-50] and it was demonstrated that this geometry can be used to measure shaft rotational velocity regardless of the profile of the object or translational motion of the rotating target. In the practical form, light from a laser is split into two beams which are given slightly different frequencies using a Bragg cell frequency shifting device, enabling detection of rotation direction. The beams are then made parallel and focused onto the surface of the rotating body by a lens. As before, the combined backscattered light from the two points is detected by a photomultiplier with a beat frequency proportional to the rotational velocity of the body. Retro-reflective tape was used to increase the intensity of back-scattered light and experimental results verified the technique through measurement of the very low speed of a rotating drum (less than 3.5rpm). However, the possibility of using this system for the measurement of real-time fluctuations in the shaft rotation speed, or torsional vibration, was not recognised.

The potential of the parallel beam arrangement for the measurement of torsional vibration was first realised in the laser torsional vibrometer (LTV) developed by Halliwell et al [2-51 to 2-54] as shown in Figure 2.5. This ingeniously simple optical arrangement provides a compact and robust solution which overcomes the limitations of previous techniques for the practical measurement of torsional vibration. The laser light is divided into two beams which impinge on the shaft and the light collected in direct backscatter from each point undergoes different Doppler shifts. When this backscattered light is recombined and mixed on the surface of a photodetector, heterodyning takes place and a beat frequency is produced in the photodetector output equal to the difference frequency between each Doppler shifted beam. This beat frequency is therefore proportional to target rotation speed N_R as follows [2-54];

$$f_{beat} = \left(\frac{4\mu\pi d}{\lambda_L}\right) N_R \cos\theta_R \qquad \{2.1\}$$

where μ is the refractive index of the surrounding medium, assumed to be unity for air, d is the laser beam separation, λ_L is the laser wavelength, and θ_R the angle between the normal to the laser beam plane and rotational axis of the target shaft. The photodetector output is analysed by a suitable Doppler signal processor, essentially a frequency to voltage converter which produces a time-resolved analogue of the beat frequency. Torsional vibration is seen as a fluctuation in rotation speed, with a corresponding fluctuation in output voltage.

Retro-reflective tape is applied to the target shaft to allow use of a low powered laser and for ease of alignment. Measurements with this instrument are unaffected by the cross-sectional shape of the target, therefore allowing use on components of arbitrary cross-section. In addition to use on the side of a shaft, it can be targeted on the end-face, offering significant advantages in situations of restricted access. Additionally, the system uses a minimum of optical components and has straightforward signal processing requirements. The LTV can be effectively hand-held and gives good agreement with existing methods of measuring torsional vibration. The accuracy of the instrument was tested through comparison with a cross-beam velocimeter and agreement between the two instruments was to within 0.5dB. Additionally, a dynamic range of 80dB was claimed for torsional displacement measurement which encompasses the range typically found in practice [2-51]. Measurement of the torsional displacement of a six-cylinder turbocharged diesel engine was also considered [2-53]. The results agreed closely, over the speed range considered, with those from a slotted disc system fixed to the end of the crankshaft, similar to systems described in Section 2.1.4. The optical arrangement of the LTV has been commercially realised in the Brüel & Kjær Torsional Vibration meter Type 2523 [2-55].

An alternative torsional vibrometer is commercially available, based on a very similar principle with identical advantages to those discussed above [2-56]. However, a birefringent prism is used to split the laser light into two parallel beams and recombine them after backscattering from the target. A modular system allows a more powerful laser source to be used, thus allowing measurements from untreated matt surfaces if required. Additionally, a Bragg cell module can be incorporated to permit measurement of bi-directional angular motion without a mean rotation speed.

An important concern with these instruments which are based on the principles of laser Doppler velocimetry is the characteristic noise floor. A typical example of this is shown in Figure 2.6, the spectrum of an LTV output for a target shaft rotating at a constant speed, that is in the absence of torsional vibration. The spurious peaks result from the noise in the LTV signal due to the formation of 'speckles' in the backscattered laser light. Component wavelets of the coherent incident laser beam are dephased on scattering from a target that is rough on the scale of the optical wavelength. Constructive and destructive interference of these wavelets results in a chaotic distribution of high and low light intensities on the surface of the LTV's photodetector, referred to as a speckle pattern. With the LTV a speckle pattern is obtained from each of the two laser beams and the photodetector output is derived from summation of all the speckles on its surface. Changes in the speckle pattern due to the rotation of the target shaft modulate the photodetector output and the resulting noise repeats with a period equal to that of the target shaft rotation.

This gives the LTV a noise floor which has a spectrum typical of a pseudo-random signal, consisting of a fundamental peak at the rotation frequency and higher order harmonics of similar magnitude. This spurious information is described as pseudo-vibration [2-57, 2-58] and the actual spectrum is particular to the target surface speckle dynamics in each measurement situation. Therefore data interpretation requires a degree of judgement to distinguish genuine low level torsional vibration from this pseudo-vibration as, in practice, the torsional vibration frequencies of interest are usually at integer multiples of rotation, coinciding with the speckle noise peaks. This effect is apparent in the experimental data presented in later chapters at low magnitudes of torsional vibration response.

A torsional vibrometer based on optical fibre technology has been developed, offering some apparent advantages over other systems [2-59]. The sensor is based on the laser

Doppler principle, but uses single-mode optical fibres for laser beam delivery. The main advantage of this approach is that it allows a flexible light guide between the optical source and processing circuitry and has a potentially miniature and rugged lightweight probe which can be used in otherwise inaccessible locations. The laser beam is split into two parts in a single mode coupler to give the two target probe beams and the beams backscattered from the target subsequently interfere in this coupler. Depending on the optical arrangement of the fibres, the vibrometer can be operated in two ways. A differential mode gives direct, independent, instantaneous measurement as with other laser torsional vibrometers, requiring reflective tape to be used on the target to ensure sufficient backscatter of light. Alternatively a reference mode utilises back reflections from the ends of the fibres at the probes to form a reference beam, with the instrument output comprising the individual frequency shifted components from the two measurement points and no combined differential beat signal. This latter arrangement can use significantly lower illuminating power and a poorly reflecting target surface but the required beat frequency must be derived electronically by combining the two individual frequency shifts. Further limitations of the system are the target focus and operating distances, which are determined by the focal length of the probe lenses.

The techniques described previously have utilised a form of differential mode interferometer which optically acquires the difference of two parallel velocity vectors at separate points on the rotating object. The resulting beat frequency at the photodetector output is then directly proportional to the absolute value of the target angular velocity. However, the backscattered beams must have sufficient intensity to heterodyne and generate a signal on the photodetector, requiring a retro-reflective coating on the target shaft. Additionally, measurements can only be made if the rotation speed exceeds a certain value, otherwise no useful carrier frequency will be generated, and the technique does not provide directional information without the use of frequency shifting devices.

These inherent disadvantages are addressed in an alternative system, which has been realised as a commercial instrument, in which the two tangential velocity components are acquired separately with independent interferometers [2-60, 2-61]. A single laser is used for both halves of the instrument to give a compact optical head. The resulting signals are combined electronically to provide the required measurements of mean rotation velocity and rotational vibration. A further refinement is the heterodyning of each signal beam with a reference beam which provides optical amplification of the signal. This improves the sensitivity, permitting measurements to be obtained from untreated shaft surfaces and removing the necessity to attach retro-reflective tape to the shaft. Direction sensitivity and measurements of rotational velocity without a mean rotation speed are achieved by the optical frequency offset in each interferometer configuration. This is similar to the techniques used in translational laser Doppler vibrometry techniques [2-62, 2-63] and created with a Bragg cell in this case. However, the optical complexity of this arrangement is clearly apparent with implications for alignment and capital cost. Signal processing hardware requirements are substantial in order to process two very high frequency carrier signals and to separately track the two input signals.

The significance of these techniques for obtaining measurements of torsional vibration with ease from rotating shafts is considerable and highlights their hitherto under-utilised potential in machinery monitoring. Limited examples include the use of an LTV to achieve in-situ measurement from the crankshafts of large marine propulsion diesel and generator sets [2-64]. This allowed diagnosis of failures in important viscous shear torsional dampers, thereby avoiding the need for 'downtime' associated with traditional damper health monitoring procedures such as viscous fluid sampling. Other developments include novel techniques for assessing the condition of tuned elastomeric dampers, which were successfully employed on the rubber damper of a six-cylinder turbocharged automotive diesel engine [2-65].

Due to the inherent advantages of the LTV developed by Halliwell et al [2-54] in offering a simple and compact solution for the measurement of torsional vibration, this arrangement was used for the basis of the subsequently reported research. Its optical geometry offers immunity to shaft or instrument axial motion and radial motion such as a cylindrical whirl orbit thereby providing significant advantages over traditional torsional vibration transducers. However, in this thesis torsional vibrometers are demonstrated to have measurable sensitivity to angular lateral vibration, where the shaft rotation vector undergoes a change of direction relative to the LTV such as the conical whirl orbit of

Figure 1.1b. This effect is considered in depth for the first time in Chapter 3 where the theory of the instrument's operation is expanded to explore its sensitivity to all senses of lateral vibration of a rotating shaft.

Torsiograph systems, strain gauges and slotted disk arrangements have therefore been superseded by the use of laser technology. The inherent problems of torsional vibration measurement have been solved, providing a robust and non-contact, easy to set up, align and calibrate measurement with improved immunity to solid body motion of the shaft or instrument. Expensive machinery downtime is therefore avoided and the instrument represents a significant step forward in rotating machinery diagnostics.

2.2 Experimental Excitation of Torsional Vibration

The use of modal analysis for vibration testing of non-rotating engineering structures is well established [2-66]. To investigate the vibration behaviour of a system experimentally with this method it is important to be able to study its response to a known input. However, while a range of measurement techniques for torsional vibration were discussed in the previous section, the lack of suitable torsional excitation methods has prevented development of equivalent analysis tools. System characteristics may change during rotation so it would be advantageous to obtain measurements under these conditions. For example, the performance characteristics of a vibration damper or absorber should be verified through testing under conditions approximating those in service. Only in this way is it possible to ensure the many influences controlling the behaviour of the system are accurately reproduced. The application of modal analysis to torsional vibrations would permit the study of a shaft system's characteristics during design and development procedures, rather than examining its response in the final application. The resulting data can then be used in validation of theoretical models and development of design changes.

The primary requirements of any apparatus for creating torsional vibration experimentally are that it should be controllable, consistent and able to provide a torque input of appropriate magnitude and frequency. It should cover a bandwidth suitable for exciting the torsional vibration modes of interest to determine the performance characteristics of the test system. The torque magnitude required will depend on the shaft arrangement under test and the aims of the experimentation. Measurement of this torque input is usually achieved by strain gauge or torque transducer system and modifications to the shaft system to accommodate the excitation system and instrumentation may be an important consideration. The development of a system for applying a known torque to a rotating system is therefore a demanding problem.

The following sections introduce a range of approaches which have been utilised for the torsional vibration excitation of shaft systems. These have been developed for specific test applications and are seen to have a number of inherent limitations, particularly for application to torsional modal analysis which is discussed in detail in Chapter 4.

2.2.1 Non-Rotating Apparatus

Non-rotating test-rigs have been used due to their simplified construction and ease of vibratory amplitude measurement. However, this class of test cannot be used for examining damper or absorber assemblies whose operation depends on rotational speeds or if the frictional torque depends on centrifugal action. In addition they do not reproduce the influence of rotation on distribution of damping and lubrication fluids.

The fundamentals of these test-rigs are reviewed by Ker Wilson [2-67]. For quality-checking the damping characteristics of viscous fluid dampers, the assembly is fastened to one end of a thin torsion rod, forming a simple torsional pendulum. Twisting the damper casing through a predetermined angle and then releasing it causes the pendulum to perform damped torsional oscillations. These oscillations can be compared with suitable standards to determine the effectiveness of the device. An alternative system uses an unbalanced mass driven by a variable speed drive, thus producing a sinusoidal inertia torque on the absorber assembly. A range of frequencies can be covered due to the once per cycle torque variation of the exciter disk and the amplitude is controlled by changing the eccentricity of the mass. Other arrangements include an eccentric rocking lever mechanism and a lever following a sinusoidal-profile cam to provide the desired oscillatory motion [2-68]. These methods have been used for crankshaft fatigue testing and to determine the slipping torque of solid-friction dampers under dynamic conditions.

A more powerful out-of-balance mass exciter has been developed suitable for tests on the larger sizes of damper used on large, slow-speed marine engines [2-67]. As shown in Figure 2.7, a number of planet-pinions each driving an out-of balance mass are equally spaced around a sun-wheel. One of the pinions is driven through a flexible shaft by a variable speed motor and gearbox and the drive is transmitted to the other pinions by the sun-wheel. A sinusoidal torque is imposed on the test assembly, with a frequency determined by the planet pinion rotation speed. Exciters of this type have been used in a number of other applications including determination of the effective inertia of variable pitch airscrews and torsional fatigue tests on marine engine shafting.

Two methods of excitation were used for experimentally investigating the torsional modes of the shaft of a 900MW steam turbine generator [2-33]. A 'shaker' was used which consisted of two out-of-balance disks rotating in opposite directions mounted on a support which was clamped to the shaft on one side of its centreline. The force input was measured with piezo-electric transducers and by sweeping through the required frequency range the response of the shaft to the sinusoidal torque could be determined as it floated at zero speed on its oil films. Transient or shock torque excitation was also used, achieved by applying a force from the turning gear ratchet. A hydraulic piston pushed the ratchet on a short stroke to engage the gear wheel mounted on the rotor. The force applied to the gear by the ratchet was measured with a transducer fitted inside a special attached 'shoe'. Again, the rotational speed of the shaft before the test was zero although the shaft turned slowly for a short while after the application of the shock.

The use of hydraulic systems for torsional excitation is discussed in Section 2.2.3 and non-rotating systems of this type can be relatively straightforward to instrument. However, as with all these approaches, the limitations of not adequately simulating service conditions prevent study of the required behaviour of the shaft system under test. It is therefore important to derive measurements under rotating operating conditions where possible and the techniques discussed here are unsuitable for this task.

2.2.2 Rotational Mechanical Exciters

A test-rig where the required torsional vibration function can be superimposed on steady rotation of the shaft is necessary when the effects of rotation are likely to exert a significant influence on the performance of the shaft assembly under test. A number of approaches have been explored which utilise a mechanical method to apply a controllable torsional vibration to the rotating shaft. These are more sophisticated alternatives than running the machine through its operating speed range and measuring the effect of the fundamental and other dominant harmonics of running speed in exciting torsional resonances.

A common technique utilises a Hooke's joint as a device for calibrating torsional vibration measuring equipment [2-67]. Two shafts are connected by such a joint which consists of two forked members, one mounted on the driving or input shaft and the other on the driven or output shaft, connected by a cross-piece. This permits the shafts to be aligned with rotation axes that have an angular offset. When the input shaft is driven at a constant angular velocity, although both shafts complete a revolution in the same time period, the angular velocity ratio for the two shafts varies as a function of the inclination angle between the shaft axes and the angular position of the input shaft and a torsional vibration, or more correctly a speed fluctuation, is superimposed on the rotation of the output shaft. This has a principal sinusoidal component at a frequency equal to twice the input shaft rotation frequency and a smaller 4th order component. There are also motions at 6th and 8th orders but these amplitudes are insignificant in practical applications. The magnitude of these components can be derived from consideration of the kinematics of the joint components and are discussed with respect to the experimental results in Chapter 3.

This method is suitable for accurate simulation of vibration amplitudes up to $\pm 2°$, corresponding to setting the Hooke's joint at an inclination angle of approximately 20° [2-69]. For use as an accurate calibration device the apparatus needs to be carefully designed and manufactured to ensure uniform rotation of the driving shaft and to minimise undesired torsional vibration induced by geometric discrepancies [2-67]. Although the apparatus can be used to simulate various torsional excitation frequencies through adjustment of the operating speed, it can only simulate a 2nd order torsional vibration and a much smaller 4th order fluctuation. It therefore has limited use in testing order-tuned torsional vibration absorbers. Rigs with Hooke's joint excitation are used for endurance tests on absorber and damper assemblies as service conditions can be easily simulated. The effects of centrifugal forces on the stability of component parts can be studied as can the behaviour and influence of damping and lubricating fluids. Service temperatures can be reproduced by encasing the test assembly in an environmental chamber.

A parallel-displacement type calibrator has been developed, with the aim of obtaining vibratory and rotary motion by a simpler device than a Hooke's joint [2-68]. A driven shaft has an arm attached to the free end carrying a projecting pin and a sliding block. The block slides in a forked arm attached to the end of a second shaft. This is mounted on a plate which may be moved in a horizontal direction normal to the shaft axes. By laterally displacing the axes of the shafts, cyclic variation of the second shaft angular velocity occurs. The frequency of this vibration is equal to the running speed, with the amplitude controlled by the relative displacement of the shaft axes. Shaft alignment and component wear has an appreciable effect on the motion accuracy.

A simple torsional vibration exciter was used as a demonstration model for the measurement of Torsional Operational Deflection Shapes (TODS) [2-70]. A thin steel shaft had two aluminium flywheels mounted at the ends and could be rotated at variable speed. Two permanent magnets were mounted axially on the supporting frame either side of one of the flywheels, with two matching magnets positioned on the flywheel. When the rotor system is rotating the attraction between the moving and fixed magnets gives a momentary deceleration of the flywheel. This impulse is applied once per revolution creating a first order excitation. The rotational speed and hence frequency of excitation was adjusted to coincide with the first torsional natural frequency of the shaft system, resulting in a resonant condition.

A number of other mechanical systems have been used successfully in practice [2-67]. One of the simplest types, suitable for dealing with small absorber and damper assemblies, utilises a multi-lobed cam with a profile designed to produce simple harmonic motion of the roller follower. The frequency of the excitation is seen to be equal to the number of lobes multiplied by the shaft rotation speed. Various systems for loading the cam have been utilised to provide the necessary torque.

The out-of-balance mass type of exciter utilising planetary gears, described as a non-rotating device in Section 2.2.1, was developed into a device which revolves with the test shaft [2-67]. The planet-pinions and their attached masses, which are fixed to the exciter carrier, are driven from a sun or annular wheel. The variable speed drive, a heavy flywheel to minimise speed fluctuations, the exciter assembly and component under test are all mounted on the same shaft with appropriate instrumentation to measure the shaft strain and vibratory motion. In contrast to the majority of other mechanical techniques described, this method can provide an excitation with a frequency independent of rotation. By using a completely independent drive system for the sun-wheel, excitation of any order and hence frequency throughout the speed range can be achieved. It is possible to control the magnitude of the excitation during testing by changing the relative phase of two equal sets of out-of-balance masses. Exciters of this type have been used for neutralising a harmonic torque acting by rotating the fixed sun-wheel locking plate to adjust the torque phase until the measured vibratory amplitude is a minimum. This device has been used in studies of machine tool and radial drill 'chatter' during machining operations.

These systems either provide a steady-state sinusoidal torque excitation, or some form of rotation order-related function. In contrast, a novel device has been developed which applies a torque impulse to a rotating machine and is referred to as a 'torsional impact hammer' [2-71, 2-72]. A diametrical arm acts as a guide for two equal mass sliders which are initially constrained at the centre of the device near the rotation axis by a trigger mechanism. Releasing the sliders allows them to move outwards under centrifugal force, increasing the moment of inertia of the 'hammer' and applying a braking torque impulse to the parent system. This torque ceases when the masses reach the end of their travel. The amplitude and profile of the torque impulse imparted to the shaft system can be calculated from the physical characteristics of the device and the shaft speed and it was demonstrated that the impulse contains useful excitation up to ten times the rotation frequency. Experimental results were presented with the hammer attached to a simple two-inertia system, exciting the first torsional resonance of the system. Results were restricted to rotation speeds above 800rpm due to inherent operational limitations. To obtain useful torque amplitudes either the shaft speed must be relatively high or the mass and final radius of the sliders must be large. Additionally, the machine under test must be stopped after each impact for the masses to be re-constrained.

It is apparent that these mechanical excitation techniques are limited in both control of the magnitude and frequency of excitation, independent of rotation speed, and the frequency range which can be attained. Substantial modification of the shaft system to accommodate the torque input device and associated instrumentation is unavoidable and changes the system's dynamic behaviour.

2.2.3 Hydraulic Systems

The use of hydraulic actuators has also been explored for torsional excitation, requiring novel development for application to rotating systems in order to apply a suitable torque over a reasonable frequency range. Early use of this technology is discussed by Knight [2-73] who considered two previously developed electro-hydraulic exciters for studying the torsional vibration response of machine tools. One of these could only be used on non-rotating machines, with the oil flow in the input valve controlled by a sine-wave generator and providing excitation up to 350Hz [2-74]. The second used a pump driven via gears from the shaft under test which delivered fluid through an electrically controlled servo-valve. This generated a static delivery pressure with a superimposed pressure oscillation. In addition to the disadvantages of its installation requirements it could only be operated above a speed of 450rpm to give suitable delivery pressure.

A number of commercial systems are available which make use of hydraulic mechanisms to excite a shaft system torsionally. Developments in servo-valve technology have provided powerful electro-hydraulic torsional exciters with a large range of static and dynamic torques and improved frequency limits. More recent developments have included commercially available systems with precise computer control for specifying excitation frequencies and amplitudes. Rotary Vibrators manufactured by Servotest have the capability for angular torque excitation and continuous rotation [2-75]. Peak torque input is specified as 4kNm at 500Hz with measurable excitation up to 1kHz. An electric or hydraulic motor is used to drive the rotation and is isolated from the exciter shaft system via a torsionally soft coupling. Team Corporation manufactures similar devices, utilising a hydraulic actuator and high performance servo-valve set optimised for high frequency operation [2-76]. For non-rotating applications a 'torsional table' is available which converts linear vibration of a hydraulic shaker into angular motion. More importantly their Rotating Vibration Test System is an electro-hydraulic rotary actuator designed to operate while rotating, with similar operational specifications to the previous commercial system described. A drive motor is used to provide the rotation and the actuator output shaft requires attachment of a position sensor, torque sensor and an angular accelerometer.

These devices can operate at substantially greater torque input magnitudes and over a considerably wider frequency range than other systems. As a result this technology is used by damper and absorber manufacturers for a variety of testing purposes, including in-service simulation, fatigue tests and development testing to examine elastomeric material properties and viscous fluid behaviour. Other applications of these systems include vibration and fatigue testing for fan and turbine blades, couplings and transmission components, simulation of crankshaft, camshaft, gear train or drive coupling induced vibration and in combination with a dynamometer to simulate loads experienced by automotive engines and other prime-movers. This form of excitation system has also been used in the investigation of idling rattle noise in truck clutch systems [2-77]. The primary limitation to the frequency range is supply of sufficient pressure to ensure suitable acceleration of the actuator mechanism together with oil column resonance which restricts the upper frequency of excitation. Measurement of the torque input to the rotating components under test can only be achieved with a torque transducer or strain-gauged section of shaft. Additionally, they require rigid attachment to a shaft system under test, affecting the dynamic response of the system. Furthermore, the capital cost of this equipment is substantial.

2.2.4 Electrical Excitation

The use of this type of torque excitation has the potential for creating a readily controllable excitation in terms of frequency and amplitude. The simplest method of electrical excitation is to drive the test system with a directly-coupled single phase a.c. motor which runs at a rotation frequency determined by the variable frequency a.c. supply [2-67]. In addition to the constant driving torque component the input contains a fluctuating component at twice the frequency of the electrical supply, therefore with an order number equal to twice the number of motor pole pairs. This technique cannot be used for investigating the response of the test system to excitations of different order numbers as this is a fixed relationship with rotation speed. Use is further restricted to the range where these harmonics are strong enough to excite resonance.

Further examples of electrical torsional exciters include various electromechanical devices developed primarily for testing centrifugal pendulum vibration absorbers [2-67]. One arrangement consisted of a modified two-pole shunt d.c. motor, with one bearing removed at the end at which the armature is connected to the main shaft. A steady d.c. current was supplied to the field coils and the armature was fed via the commutator from a 3-phase alternator, driven by a variable-speed motor. This arrangement imposed an oscillatory torque on the main shaft at the frequency of alternator output. Rotation and oscillation torque frequencies could be varied independently so the order of excitation can be any required value within reasonable frequency range limits. An alternative system used a winding-less two-pole armature mounted within a cylindrical field frame. This frame carried two sets of windings, one of which was connected through slip-rings to an external d.c. supply and provided electromagnetic coupling with the armature. The second set was connected to an a.c. supply with adjustable frequency and amplitude. The armature is rotated by an independent variable speed d.c. motor and the complete assembly rotates at this speed. An alternating torque of any selected frequency was superimposed on the steady rotation by the a.c. winding on the field frame. With this and the previous arrangement, excitation power was insufficient to force non-resonant vibration of the shaft system of sufficient amplitude for accurate measurements to be achieved.

In studies of machine tool drive system response, Knight [2-73, 2-78] developed two electromagnetic exciters based on previous research. The first used the principle of the reluctance motor in which a slotted cylindrical cage was rigidly attached to the main shaft of the exciter [2-79]. This cage was situated between the two similarly toothed rings of the rotor, which ran freely on the exciter shaft, with a circular coil fixed between each set of rotor teeth and supplied with direct current via slip-rings. This imparted an oscillatory torque to the machine drive due to the magnetic force on the cage bars. An approximately sawtooth waveform was applied and the frequency was varied by changing the rotor rotation speed relative to the cage and machine shaft. The torque output was almost constant for a fixed current input over the range 50Hz to 400Hz, with a maximum torque of approximately 5Nm, although below 15Hz the output was erratic. The electrical input for this exciter was simply a d.c. supply but excitation of a specific frequency was awkward, requiring fine adjustment of the drive spindle and exciter rotor rotational speeds.

The second exciter created a readily controllable sinusoidal torque input and its construction is detailed in Figure 2.8 [2-74]. The main body of the exciter, which was free to rotate on the shaft, consisted of an outer steel ring and a central boss with a number of rigidly attached permanent magnets. A glass-fibre moulding containing a corresponding number of coils was situated in the air-gap between the magnets and the ring and was rigidly clamped to the exciter shaft. Alternating current was fed to the coils via slip-rings generating forces between the magnet system and coil moulding. The magnet and ring assembly were isolated from the main shaft by means of a cross arm and four soft springs, to have a low (10Hz) resonance and above this frequency the assembly moved with the shaft. The torque output was demonstrated up to a magnitude of 2.3Nm and frequency of 500Hz once the low frequency system resonance had been exceeded. A signal generator and large power amplifier provided the input signal with easy control of frequency and amplitude. The torque output of this and the previous device were measured by strain gauges installed on the shaft connecting the exciter to the machine under test. These exciters were complicated to design and build and it was necessary to modify the measured response of the system to correct for the added inertia.

Vance and French [2-27] described a test-rig consisting of two large spur gears connected by a thin shaft, driven through a flexible coupling by a d.c. motor. Torsional excitation was provided by superimposing an a.c. voltage onto the d.c. supplied to the field connections of the motor to produce a pulsating torque of variable amplitude and frequency. In a similar method, a.c. current was superimposed onto the d.c. signal driving the test system motor through the use of a rotating converter [2-80]. The disadvantage of this system was that low frequency excitation cannot be obtained with this type of converter.

Various modern electrical motor drives have the potential for use as torsional excitation systems. The control electronics are connected to a power circuit which supplies the input to the motor, with a low level signal controlling the speed. Application of an input with both d.c. and a.c. voltages will cause the motor torque to have mean and oscillatory components. This technique is restricted by the response of the power electronics, the inertia of the motor and its electromagnetic characteristics, preventing the attainment of high frequency torque oscillations of a reasonable amplitude.

A commercially available a.c. servo-drive has been demonstrated as a combined drive motor and torsional exciter for small rotating test-rigs [2-81, 2-82]. This consisted of a servo-motor powered by a three-phase transformer and servo-amplifier which was fitted with an external control circuit into which the torsional oscillation signal was provided from a waveform generator. For the drive running unloaded with a sinusoidal input the torque input was 10Nm up to 200Hz, decreasing to 1Nm at 2kHz. Broadband (random) excitation was also possible at frequencies up to 250Hz. A torque transducer with associated telemetry system provided measurement of the torque in the shaft between the system under test and the drive system. This system has been used in the study of a simple gearbox, shafts couplings [2-83], and in the investigation of secondary resonance effects of reciprocating engines [2-84].

Although electrical excitation systems offer significant advantages over other techniques for torsional excitation of rotating shafts, they are still limited by the same fundamental problems. Modification of the system under test is necessary to incorporate the excitation device. Additionally, measurement of the torque applied requires the use of a strain gauge or torque transducer to be inserted in the shaft system. Both these factors can unacceptably change the system response from the actual situation under investigation.

The work reported in Chapter 4 introduces a new method of torsional excitation offering a simple, effective and low expense solution to this problem overcoming the disadvantages of previous techniques. It is apparent that this technology has the potential to provide a depth of information previously unobtainable, through the application of modal analysis techniques to examine the torsional vibration behaviour of a rotating shaft system.

3. OPERATION OF THE LASER TORSIONAL VIBROMETER IN THE PRESENCE OF LATERAL VIBRATIONS

The laser torsional vibrometer (LTV) provides a solution to the exacting problem of torsional vibration measurement from rotating shafts [3-1]. It has seen use in a range of applications including examining speed fluctuations of tape recorder drives, vibration studies on automotive petrol and diesel engines, failure diagnosis in viscous shear torsional dampers on large marine propulsion diesel engines and generator sets and large electric motor drives in the petrochemical industry. However, it is rare to be able to describe vibration behaviour in only one co-ordinate or degree of freedom on a rotating component. Previous work [3-2] has discussed the insensitivity of the instrument to radial and axial shaft vibration or instrument movement - distinct advantages over traditional torsional vibration transducers. This chapter looks in depth at the effects of all shaft motions on the measurements derived by an LTV.

Initially, the fundamental principles of the instrument are presented and comprehensive theoretical treatment examines how the LTV is sensitive to specific lateral shaft motions. Subsequent discussion quantifies this cross-sensitivity of the instrument in instances which have the potential to cause ambiguity in the measurements recorded. These predictions are based on experimental results and highlight the significance of this behaviour. This permits operational guidelines to be suggested for the use of the instrument during shaft lateral motion. Ultimately, a solution is proposed which permits unambiguous measurement of shaft torsional vibration in a situation for which conventional use of an LTV would otherwise show unacceptable sensitivity to lateral motion. Simultaneously, this technique can provide an assessment of the angular lateral, or bending, vibration of a rotating shaft and this new measurement is introduced at the end of the chapter.

3.1 Laser Vibrometry

Developed from the principles of laser Doppler anemometry (LDA), the measurement of solid surface vibration velocity with laser Doppler velocimetry (LDV) is now a well established experimental technique. The basic principle of LDV requires the detection of the Doppler frequency shift in coherent light when it is scattered from a moving object.

3.1.1 Doppler Shift of Scattered Light

The change in frequency of the light scattered from a moving object is detailed in Figure 3.1. Laser light of frequency f_L and wavelength λ_L is incident on a particle Q moving with velocity $V_Q(t)$ and observed in the direction shown. The Doppler frequency shift of the incident laser beam is derived as [3-3];

$$f_D = \frac{2V_Q(t)}{\lambda_L}\cos\theta_v \sin\frac{\theta_s}{2} \qquad \{3.1\}$$

The direction in which the scattering is observed is defined by angle θ_s and θ_v is the angle between the velocity vector and the bisector of the angle between the source and scattering directions. The refractive index of the surrounding medium is assumed to be unity.

Generally, with laser vibrometry, measurements are taken in direct backscatter, aided by the use of retro-reflective tape, so $\theta_s = \pi$. The magnitude of the Doppler shift is then proportional to the instantaneous target velocity in the direction of the backscattered light and this defines the sense of target velocity resulting in a positive Doppler shift. By measuring and tracking this Doppler frequency shift a signal can be derived proportional to the velocity vector, $U(t)$, parallel to the line of incidence in which case {3.1} reduces to;

$$f_D = \frac{2U(t)}{\lambda_L} \qquad \{3.2\}$$

With the use of lasers in or near the visible spectrum the scattered light has a frequency of the order of 10^{15}Hz and so the Doppler shift cannot be monitored directly with a photodetector. Therefore, to obtain a signal which can be detected the scattered light is mixed on the photodetector surface with another light beam from the same coherent source. This process produces a heterodyne or 'beat' in the photodetector output with a frequency, typically of the order of MHz, equal to the difference in frequency between the two beams and therefore dependent on the instantaneous target velocity. Hence, demodulation of the output from the photodetector with an appropriate Doppler signal processor produces a time-resolved analogue of the target vibration velocity.

For translational vibration measurement this second beam is referred to as a reference beam and is derived from the single laser source with the use of a beam-splitter as shown in Figure 3.2. This beam has its frequency pre-shifted by a known amount to remove ambiguity in the direction of target motion measured. All laser Doppler vibrometers use this basic principle, primarily differing only in the type of frequency-shifting device used and the technique used to demodulate the photodetector output. Various commercial devices have been developed to measure the translational vibration of a solid surface [3-4 to 3-6].

3.1.2 The Laser Torsional Vibrometer

In the laser torsional vibrometer (LTV), introduced previously in Section 2.1.8, the second laser beam is arranged to be parallel to the first, using a configuration of beam-splitter and mirror, and is also incident on the target shaft as was shown in Figure 2.5. The resulting beat frequency in the photodetector output is then proportional to the instantaneous shaft rotation speed. Amongst other inherent advantages, this eliminates the need to introduce a frequency pre-shift because the velocity component resulting from the mean rotation speed provides a 'carrier frequency'. Torsional vibration is seen as a fluctuation in rotation speed of the illuminated shaft element, with a corresponding fluctuation in beat frequency and hence instrument output voltage.

The Doppler shift of a single laser beam incident on a solid surface can be related to the motion of this target in all six of its degrees of freedom. The LTV has previously been shown to be insensitive to translational shaft vibration or instrument movement. Rotational vibration about the two axes orthogonal to the undisturbed shaft rotation axis, however, causes a change in direction of the shaft rotation axis and does influence the performance of the instrument. This motion will be referred to as 'angular lateral vibration' as defined earlier in Section 1.1.2. For the consideration of engine crankshaft motion this is more specifically described as bending vibration. This effect modulates the beat frequency detected and gives rise to signal components indistinguishable from the intended measurement of shaft torsional vibration. The importance of these components is analysed for accurate assessment of torsional vibration with conventional use of an LTV and for new developments of this technology.

3.2 Advances in the Theory of Operation of the Laser Torsional Vibrometer

This section details the development of comprehensive theory which fully describes the effects of all shaft motions on the operation of the LTV. Initially, the six velocity components of a point on a shaft are considered, with particular consideration given to angular lateral motion. Subsequently, the measurement obtained from the LTV is derived, showing its dependence on specific types of lateral motion.

3.2.1 General Definition of Motion of a Point on a Rotating Shaft

Consider the general case of a point P on the surface of an arbitrarily shaped shaft, located by position vector $\vec{r}_P$ with respect to the shaft axes, as illustrated in Figure 3.3. The main co-ordinate system $OXYZ$ is fixed in space, with the undeflected shaft rotation axis (i.e. in the absence of any vibration) defining the Z-direction and the X-direction determined in the subsequent analysis of Section 3.2.2 and thus defining the right-hand set of co-ordinates.

The instantaneous velocity vector at P can be related to motion in its six degrees of freedom, as derived in subsequent sections. This comprises the three translational motions $\left(\vec{V}_x + \vec{V}_y + \vec{V}_z\right)$ and components related to the angular rotations of the shaft. These are defined as the motion of the point at angular velocity Ω about the shaft rotation axis $\hat{z}_R$ and angular lateral motion which results in the angular displacement of this primary shaft rotation vector $\hat{z}_R$ relative to the fixed co-ordinate axis $\hat{z}$. This latter motion is described as rotations about the two co-ordinate axes, X and Y, of the stationary reference frame $OXYZ$, making use of the unit vectors $\hat{x}$ and $\hat{y}$. These rotations of the shaft axis are conventionally described as pitch and yaw respectively [3-7]. The magnitude of this angular motion is assumed to allow small angle approximations to be applied, for consistency in vector addition as discussed in the following sections.

3.2.1.1 Finite Rotations of the Shaft Axis

It is important to note that finite rotations of a rigid body about specified axes, although expressed as vectors, do not obey the commutative law of addition [3-8]. For example, two consecutive rotations about different axes applied to a position vector will give different final positions if their sequence is reversed, in contravention of the commutative law of addition or parallelogram law. This important property should be noted when considering the change in direction of the shaft rotation vector due to shaft angular lateral vibration as consisting of finite rotation vectors about the X and Y axes.

Consider the general case of the motion of a position vector $\vec{r}$ of fixed magnitude describing an arbitrary point P in space. The vector undergoes a finite rotation $\vec{\theta} = \theta\hat{n}$, where θ is the magnitude of the rotation about an axis having the unit vector $\hat{n}$. As shown in Figure 3.4, after the rotation P has moved to P' and the position vector $\vec{r}$ becomes $\vec{r}\,'$. The final position vector can be expressed as;

$$\vec{r}\,' = \vec{r} + \overrightarrow{\Delta r} \qquad \{3.3\}$$

An expression for $\vec{r}\,'$ can then be derived in terms of the original position vector and finite rotation vector;

$$\vec{r}\,' = \vec{r} + (1 - \cos\theta)[\hat{n} \times (\hat{n} \times \vec{r})] + \sin\theta(\hat{n} \times \vec{r}) \qquad \{3.4\}$$

Extending the general case, two consecutive rotations are applied to the position vector $\vec{r}$, designated $\vec{\theta}_1 = \theta_1\hat{n}_1$ and $\vec{\theta}_2 = \theta_2\hat{n}_2$ and defined as before. Denoting the position vectors locating point P after the first and second rotations as $\vec{r}\,'$ and $\vec{r}\,''$ respectively, these expressions can be derived with the use of {3.4}. Appendix A details the development of these expressions and it is demonstrated that if the sequence of rotations is reversed a different form of the final position result is obtained. This confirms that finite rotations do not obey the commutative law of addition, unless the two rotations are about a common axis or are infinitesimal. Assuming infinitesimal rotations the final positions for the two sequences of rotations, designated $\bar{r}_a''$ and $\bar{r}_b''$, are equivalent and can be derived as;

$$\bar{r}_a'' = \bar{r}_b'' = \bar{r} + (\theta_1 \hat{n}_1 + \theta_2 \hat{n}_2) \times \bar{r} \tag{3.5}$$

This general case can be applied to the rotation axis system introduced in Section 3.2.1, with the aim of resolving the angular lateral displacement of the rotating shaft into the fixed orthogonal reference frame *OXYZ*. The time-varying shaft rotation vector $\hat{z}_R$ can be described by the fixed unit vector $\hat{z}$ and a fluctuating component $\overrightarrow{\Delta z}$ related to the angular lateral vibration;

$$\hat{z}_R = \hat{z} + \overrightarrow{\Delta z} \tag{3.6}$$

Defining the rotation angles consistent with a conventional right-hand set of axes, initially the unit rotation axis vector undergoes a pitch rotation $\bar{\theta}_x = \theta_x \hat{x}$, followed by a yaw rotation $\bar{\theta}_y = \theta_y \hat{y}$. Figure 3.5a shows how the rotation axis is displaced by these rotations. The general result for this order of angular lateral rotations therefore defines the vector describing the movement of the shaft rotation axis as;

$$\overrightarrow{\Delta z}_1 = (\cos\theta_x \sin\theta_y)\hat{x} - (\sin\theta_x)\hat{y} + (\cos\theta_x \cos\theta_y - 1)\hat{z} \tag{3.7}$$

Alternatively, the order of the rotations can be reversed and the rotation axis is rotated by finite rotation vector $\bar{\theta}_y$ and then $\bar{\theta}_x$. This is shown in Figure 3.5b which indicates how the order of execution of the two vectors changes the final position of the rotation axis vector. The vector describing the displacement of the shaft rotation axis in this case is therefore;

$$\overrightarrow{\Delta z}_2 = (\sin\theta_y)\hat{x} - (\sin\theta_x \cos\theta_y)\hat{y} + (\cos\theta_x \cos\theta_y - 1)\hat{z} \tag{3.8}$$

For the addition of true vectors the final position should be independent of the order in which they are applied, thus satisfying the commutative law of addition. This implies that {3.7} and {3.8} are equal, while it is clear that this is not the case.

The assumption of infinitesimal rotations is valid for typical estimates of shaft angular lateral vibration magnitudes. Additionally, when considering the experimental case it is not appropriate to define an order in which to consider the rotations of the shaft about the *X*- and *Y*-axes. In light of this, small angle approximations can be made. Equations {3.7} and {3.8} then give equivalent results and the resulting displacement vector can be derived from either of these expressions or the general case of {3.5};

$$\overrightarrow{\Delta z_1} = \overrightarrow{\Delta z_2} = (\theta_y)\hat{x} - (\theta_x)\hat{y} \qquad \{3.9\}$$

This angular displacement of the shaft rotation vector $\hat{z}_R$ relative to the fixed co-ordinate axis $\hat{z}$ will affect the velocity component of point *P* related to shaft angular velocity Ω.

3.2.1.2 Velocity Components of a Point on the Shaft

In addition to velocity components of *P* due to translational motion and rotation about the shaft axis, there are seen to be components of its velocity due to angular lateral motion of the shaft which are independent of shaft angular velocity. The position of point *P* on the shaft is defined as $\bar{r}_P$. Through extension of the general case of {3.5}, the change in position vector during time increment Δt due to angular lateral shaft vibration is defined, including the third component, θ_z, described as roll or spin about the $\hat{z}$ axis;

$$\overrightarrow{\Delta r_P} = (\theta_x\hat{x} + \theta_y\hat{y} + \theta_z\hat{z}) \times \bar{r}_P \qquad \{3.10\}$$

Subsequently, the velocity components of point *P* due to this motion can be determined from the time derivative of its position vector;

$$\begin{aligned} \bar{v}_P &= \frac{d\bar{r}_P}{dt} = \lim_{\Delta t \to 0} \frac{\overrightarrow{\Delta r_P}}{\Delta t} \\ &= \dot{\theta}_x(\hat{x} \times \bar{r}_P) + \dot{\theta}_y(\hat{y} \times \bar{r}_P) + \dot{\theta}_z(\hat{z} \times \bar{r}_P) \end{aligned} \qquad \{3.11\}$$

However, in practice it is not possible to distinguish between the torsional vibration of the rotating shaft element and the θ_z component of angular lateral vibration. It is therefore appropriate to make the approximation of including both in a generalised angular velocity, Ω. This includes the approximation, in accordance with previous assumptions of small angles of rotation, that the θ_z motion can be described about $\hat{z}_R$, rather than $\hat{z}$. The complete velocity vector of point *P* on the shaft surface of Figure 3.4, resulting from all motions of the rotating shaft, can then be stated, assuming the shaft element under consideration to be rigid;

$$\vec{V}_P = \left(\vec{V}_x + \vec{V}_y + \vec{V}_z\right) + \Omega\left(\hat{z}_R \times \vec{r}_P\right) + \dot{\theta}_x\left(\hat{x} \times \vec{r}_P\right) + \dot{\theta}_y\left(\hat{y} \times \vec{r}_P\right) \qquad \{3.12\}$$

The velocity of an arbitrary point on the shaft surface is seen to be comprised of three sets of components, with the first term of {3.12} due to solid-body translation of the shaft element. The second velocity component, dependent on the main shaft rotation, includes the torsional vibration of primary interest and components due to angular lateral vibration of the shaft rotation axis. The last two terms relate to the angular lateral motion about *X* and *Y* axes and are independent of the shaft rotation.

3.2.2 Comprehensive Theory of LTV Operation with Lateral Shaft Motion

The schematic optical configuration of the LTV to be used in this theoretical development is shown in Figure 3.6, where the laser beam from the instrument is split into two parallel beams by a beam-splitter and mirror. This shows the general case of target configuration with the two LTV beams incident on the side of a shaft of arbitrary cross-section. The shaft is rotating at frequency $\omega_R(t)$, about the axis defined by $\hat{z}_R(t)$ whose time dependency allows for changes in direction. However, the time factor is not written in subsequent development, using ω_R and $\hat{z}_R$ for brevity of expression. The two equal intensity beams are of perpendicular separation *d* and impinge on the shaft surface at points *A* and *B*. These beams are collected in direct backscatter in the direction defined by the unit vector $\hat{i}$, usually assisted by the use of retro-reflective tape, and recombine on the photodetector where they heterodyne. This produces a beat frequency equal to the difference frequency between the two Doppler shifted beams.

Consistent with the analysis of the previous sections, the main stationary co-ordinate system *OXYZ* is fixed in space, with the undeflected shaft rotation axis, in the absence of any vibration, defining the Z-direction. The shaft rotation axis $\hat{z}_R$, free to undergo changes of direction, is assumed to be identical at each of the incidence points A and B over the length of shaft element of interest.

The angles associated with the alignment of the LTV will be defined before considering the angular lateral motion. These incidence angles which define the relative position of the instrument and target shaft are resolved into two orthogonal planes, as shown in Figure 3.7. Considering them separately, angle α is between the direction of backscatter of the laser beams and the direction of the undeflected shaft rotation axis. Angle β is between the plane formed by the two incident laser beams and the plane of the cross-section of the target shaft, perpendicular to the undeflected rotation axis. The 'ideal' instrument set-up is that for which the plane defined by the two LTV beams is parallel to the shaft cross-section, therefore with angle α at 90° and angle β at 0°. The X-axis of the fixed co-ordinate system is thus defined as parallel to and in the direction of laser beam backscatter vector $\hat{i}$ for this special case. However, for reasons of access it is often necessary to align an LTV with α at an angle other than 90° and β at an angle other than 0°. For the general instrument set-up detailed in Figures 3.6 and 3.8, the plane of the laser beams (or more accurately unit vector $\hat{d}$, parallel to the perpendicular beam separation) has undergone a rotation about the X-axis, changing angle β, followed by a rotation about the Y-axis, changing angle α. These angles are defined using right-handed convention.

The arbitrary incidence points A and B are located on the shaft surface by position vectors $\vec{r}_A$ and $\vec{r}_B$ respectively, as shown in Figure 3.6. Translational motion of the shaft is defined by solid body motion vector $\vec{V}$ and the shaft is assumed to have angular lateral motion which results in the displacement of the rotation vector $\hat{z}_R$ relative to the fixed unit vector $\hat{z}$. This has been previously described as rotations in the two orthogonal planes about the two co-ordinate axes X and Y.

3.2.2.1 Definition of Measurement Derived by LTV

Each of the laser beams undergoes a Doppler shift f_D when scattered by the moving shaft surface and light collected in direct backscatter has its frequency shifted by an amount given previously by {3.2}. In the system under consideration, light backscattered from the points A and B undergoes Doppler shifts f_A and f_B where;

$$f_{A,B} = (2/\lambda_L)\,\hat{i}.\vec{V}_{A,B} \qquad \{3.13\}$$

When the backscattered light is mixed on the surface of the photodetector, heterodyning occurs and the output from the detector is modulated at the difference or 'beat' frequency f_{beat} which is shown to be;

$$f_{beat} = |f_A - f_B| = (2/\lambda_L)\left|\,\hat{i}.\left(\vec{V}_A - \vec{V}_B\right)\right| \qquad \{3.14\}$$

Following the format of equation {3.12} the total components of velocity at points A and B on the shaft surface, resolved in the direction of the backscattered laser beams, are;

$$\hat{i}.\vec{V}_A = \hat{i}.\vec{V} + \hat{i}.\left[\omega_R(\hat{z}_R \times \vec{r}_A)\right] + \hat{i}.\left[\dot{\theta}_x(\hat{x}\times\vec{r}_A) + \dot{\theta}_y(\hat{y}\times\vec{r}_A)\right] \qquad \{3.15a\}$$

$$\hat{i}.\vec{V}_B = \hat{i}.\vec{V} + \hat{i}.\left[\omega_R(\hat{z}_R \times \vec{r}_B)\right] + \hat{i}.\left[\dot{\theta}_x(\hat{x}\times\vec{r}_B) + \dot{\theta}_y(\hat{y}\times\vec{r}_B)\right] \qquad \{3.15b\}$$

Deriving the difference-velocity vector term the following expression is obtained, demonstrating immunity of the instrument to any translational motion of the shaft as this component is detected by both beams and thus cancels on heterodyning;

$$\begin{aligned}\hat{i}.\left(\vec{V}_A - \vec{V}_B\right) = {} & \omega_R\left[\hat{i}.(\hat{z}_R \times \vec{r}_A) - \hat{i}.(\hat{z}_R \times \vec{r}_B)\right] \\ & + \left[\dot{\theta}_x \hat{i}.(\hat{x}\times\vec{r}_A) - \dot{\theta}_x \hat{i}.(\hat{x}\times\vec{r}_B)\right] \\ & + \left[\dot{\theta}_y \hat{i}.(\hat{y}\times\vec{r}_A) - \dot{\theta}_y \hat{i}.(\hat{y}\times\vec{r}_B)\right]\end{aligned} \qquad \{3.16\}$$

Rearranging each of the terms it can be seen that;

$$\begin{aligned}\hat{i}.\left(\vec{V}_A - \vec{V}_B\right) = {} & \omega_R\left[\hat{i}.\left(\hat{z}_R \times (\vec{r}_A - \vec{r}_B)\right)\right] \\ & + \left[\dot{\theta}_x \hat{i}.\left(\hat{x}\times(\vec{r}_A - \vec{r}_B)\right) + \dot{\theta}_y \hat{i}.\left(\hat{y}\times(\vec{r}_A - \vec{r}_B)\right)\right]\end{aligned} \qquad \{3.17\}$$

From this and with regard to Figures 3.6 and 3.8 it is apparent that subtraction of the position vectors for the points A and B results in the vector $\vec{BA}$ joining these points;

$$\hat{i}.\left(\vec{V}_A - \vec{V}_B\right) = \omega_R\left[\hat{i}.\left(\hat{z}_R \times \vec{BA}\right)\right] + \left[\dot{\theta}_x \hat{i}.\left(\hat{x} \times \vec{BA}\right) + \dot{\theta}_y \hat{i}.\left(\hat{y} \times \vec{BA}\right)\right] \qquad \{3.18\}$$

This expression shows the sensitivity of the instrument to separate components related to the shaft rotation speed and angular lateral vibration. The first term gives the measurement of shaft rotation speed and hence torsional vibration which is of principal interest. This is, however, a function of the rotation vector $\hat{z}_R$ and development of this expression in subsequent sections will quantify this sensitivity of the instrument to angular lateral vibration of the shaft. The second term also implies sensitivity of the instrument to angular lateral motion of the target shaft about the orthogonal axes but it is independent of shaft rotation. This component of angular motion could be detected even if the shaft were not rotating. Both of these measurement components are considered separately in the following analysis in order that their effects on the LTV measurements can be investigated.

3.2.2.2 Angular Lateral Motion of Rotation Axis

Initially, the first term of {3.18} will be considered and is superscripted '(1)'. The shaft rotation vector $\hat{z}_R$ is assumed to comprise a fixed part $\hat{z}$ and a time-dependent part $\vec{\Delta z}$ as defined in {3.6}. By rearranging the scalar triple product the effect on the instrument measurements can be explored;

$$\hat{i}.\left(\vec{V}_A - \vec{V}_B\right)^{(1)} = \omega_R\left[\hat{i}.\left(\hat{z}_R \times \vec{BA}\right)\right] = \omega_R\left[\hat{z}_R.\left(\vec{BA} \times \hat{i}\right)\right] \qquad \{3.19\}$$

The vector product is then expanded;

$$\left(\vec{BA} \times \hat{i}\right) = \left|\vec{BA}\right| \left|\hat{i}\right| \sin(\delta + \pi/2)\, \hat{s} \qquad \{3.20\}$$

where $\hat{s}$ is a unit vector perpendicular to both $\overrightarrow{BA}$ and $\hat{i}$ with $(\delta + \pi/2)$ as their included angle, as shown in the arbitrary arrangement of Figure 3.8. It is convenient to define a unit vector $\hat{\boldsymbol{d}}$ in the direction of a perpendicular line joining the parallel beams as shown, where;

$$\hat{\boldsymbol{d}} = \hat{\boldsymbol{i}} \times \hat{s} \qquad \{3.21\}$$

The perpendicular beam separation is d and it can be seen from Figure 3.8 that;

$$\left|\overrightarrow{BA}\right| = d/\cos\delta \qquad \{3.22\}$$

Furthermore, examination of the figure allows the following relationship to be derived;

$$\left(\overrightarrow{BA} \times \hat{\boldsymbol{i}}\right) = d\hat{\boldsymbol{d}} \times \hat{\boldsymbol{i}} \qquad \{3.23\}$$

Using $\{3.20\}$ and $\{3.22\}$, equation $\{3.19\}$is rearranged to give;

$$\hat{\boldsymbol{i}}.\left(\vec{V}_A - \vec{V}_B\right)^{(t)} = \omega_R d(\hat{z}_R.\hat{s}) \qquad \{3.24\}$$

These last two expressions demonstrate that the dependence on $\overrightarrow{BA}$ and δ, which are shape sensitive, has been lost and therefore the parallel beam arrangement can be used on a shaft of arbitrary cross-section without penalty.

Rearranging $\{3.21\}$, the unit vector $\hat{s}$ can be substituted to give the following expression for the scalar product in $\{3.24\}$ which aids subsequent simplification;

$$(\hat{z}_R.\hat{s}) = \hat{d}.\left(\hat{i} \times \hat{z}_R\right) \qquad \{3.25\}$$

The expression for the rotation axis vector $\hat{z}_R$, defined in equation {3.6}, is used to expand the scalar product on the left-hand side of {3.25};

$$\hat{z}_R.\hat{s} = (\hat{z}.\hat{s}) + \left(\overrightarrow{\Delta z}.\hat{s}\right) \qquad \{3.26\}$$

Hence, it is possible to consider initially only the fixed part $\hat{z}$ of the shaft rotation vector, whereby;

$$\hat{z}.\hat{s} = \hat{\boldsymbol{d}}.\left(\hat{i} \times \hat{z}\right) = -\hat{\boldsymbol{d}}.\hat{y}\sin\alpha \qquad \{3.27\}$$

where α is the included angle between the two unit vectors $\hat{i}$ and $\hat{z}$ and the unit vector perpendicular to them both is $\hat{y}$, as shown in Figure 3.8. The scalar product $\left(\hat{\boldsymbol{d}}.\hat{y}\right)$ can then be deduced to give the result;

$$\hat{z}.\hat{s} = -\cos\beta\sin\alpha \qquad \{3.28\}$$

In considering the angular lateral motion of the shaft from the variable part of equation {3.26}, it is possible to split the scalar product $\left(\overrightarrow{\Delta z}.\hat{s}\right)$ into components relating to the axes in use, through consideration of the three orthogonal components of $\overrightarrow{\Delta z}$.

$$\overrightarrow{\Delta z}.s = \hat{\boldsymbol{d}}.\left[\left(\hat{i} \times \left(\overrightarrow{\Delta z}\right)_x\right) + \left(\hat{i} \times \left(\overrightarrow{\Delta z}\right)_y\right) + \left(\hat{i} \times \left(\overrightarrow{\Delta z}\right)_z\right)\right] \qquad \{3.29\}$$

As discussed in Section 3.2.1.1, it is necessary to make the assumption of infinitesimal rotations for the angular lateral motions, which significantly simplifies this analysis. The resulting vector $\overrightarrow{\Delta z}$ describing the displacement of the shaft rotation axis was defined in {3.9} and is used to expand the variable part of the scalar product of {3.26} to consider the appropriate components;

$$
\begin{aligned}
\overrightarrow{\Delta z}.\hat{s} &= \hat{d}.\left[\left(\hat{i}\times\theta_y\hat{x}\right)+\left(\hat{i}\times(-\theta_x)\hat{y}\right)\right] \\
&= \hat{d}.\hat{y}\left(\theta_y\right)\sin(\pi/2-\alpha)+\left(-\theta_x\hat{i}.\left(\hat{y}\times\hat{d}\right)\right) \\
&= \left(\theta_y\cos\alpha\cos\beta\right)+\left(-\theta_x\sin\beta\right)
\end{aligned}
\tag{3.30}
$$

Thus, equation {3.30} highlights part of the sensitivity of the LTV to angular lateral motion of the shaft element under examination. Combining {3.28} and {3.30}, the following expression defines the motion of the shaft in two orthogonal fixed frame axes, assuming infinitesimal rotations as discussed.

$$
\hat{z}_R.\hat{s} = \left(-\cos\beta\sin\alpha\right)+\left(\theta_y\cos\alpha\cos\beta\right)+\left(-\theta_x\sin\beta\right) \tag{3.31}
$$

It can be concluded that this sensitivity of the LTV to angular lateral shaft motion is readily quantifiable. The beat frequency components related to this motion and the shaft rotation speed are given from {3.14} as;

$$
\begin{aligned}
f_{beat}^{(1)} &= \frac{2}{\lambda_L}\left|\hat{i}.\left(\vec{V}_A-\vec{V}_B\right)^{(1)}\right| \\
&= \frac{2}{\lambda_L}\left|\omega_R d\left[\left(-\cos\beta\sin\alpha\right)+\left(\theta_y\cos\alpha\cos\beta\right)+\left(-\theta_x\sin\beta\right)\right]\right|
\end{aligned}
\tag{3.32}
$$

3.2.2.3 Sensitivity to Angular Lateral Motion Independent of Rotation Speed

In this section the velocity terms from equation {3.18} due to angular lateral motion about the co-ordinate axes which are independent of the main shaft rotation speed will be addressed. The velocity terms as a result of this motion which give a beat frequency on the photodetector will be denoted by the superscript '(2)' and are derived from;

$$
\hat{i}.\left(\vec{V}_A-\vec{V}_B\right)^{(2)} = \dot{\theta}_x\hat{i}.\left(\hat{x}\times\vec{BA}\right)+\dot{\theta}_y\hat{i}.\left(\hat{y}\times\vec{BA}\right) \tag{3.33}
$$

This expression can therefore be expanded making use of the vector relationships defined in Section 3.2.2.2. Considering the first term which is dependent on the pitch motion θ_x

of the shaft it can be seen that;

$$\dot{\theta}_x \hat{i}.\left(\hat{x}\times\overrightarrow{BA}\right)=\dot{\theta}_x\hat{x}.\left(\overrightarrow{BA}\times\hat{i}\right)=\dot{\theta}_x\hat{x}.\left(d\hat{d}\times\hat{i}\right) \qquad \{3.34a\}$$

This makes use of the relationship of equation {3.23} which demonstrated that the operation of the instrument is independent of the shaft cross-section and hence the position of the incidence points. Further development of this expression gives;

$$\begin{aligned}\dot{\theta}_x \hat{i}.\left(\hat{x}\times\overrightarrow{BA}\right)&=\dot{\theta}_x d\hat{d}.\left(\hat{i}\times\hat{x}\right)\\ &=\dot{\theta}_x\left(d\hat{d}.\hat{y}\right)\sin\left(\pi/2-\alpha\right)\\ &=\dot{\theta}_x d\cos\beta\cos\alpha\end{aligned} \qquad \{3.34b\}$$

Similarly, the second term of equation {3.33} related to the yaw motion, θ_y, of the shaft can be deduced;

$$\begin{aligned}\dot{\theta}_y \hat{i}.\left(\hat{y}\times\overrightarrow{BA}\right)&=\dot{\theta}_y\hat{y}.\left(\overrightarrow{BA}\times\hat{i}\right)=\dot{\theta}_y\hat{y}.\left(d\hat{d}\times\hat{i}\right)\\ &=\dot{\theta}_y\hat{i}.\left(\hat{y}\times d\hat{d}\right)\\ &=\dot{\theta}_y d\sin\beta\end{aligned} \qquad \{3.35\}$$

These terms describe further sensitivity of the LTV to pitch and yaw motion when the instrument is set up with arbitrary incidence angles. Hence, the components of the beat frequency related to this motion and independent of the shaft rotation speed can be stated, by substitution of the above expressions into {3.18} and {3.14};

$$\begin{aligned}f_{beat}^{(2)}&=\frac{2}{\lambda_L}\left|\hat{i}.\left(\vec{V}_A-\vec{V}_B\right)^{(2)}\right|\\ &=\frac{2}{\lambda_L}\left|d\left[\left(\dot{\theta}_x\cos\beta\cos\alpha\right)+\left(\dot{\theta}_y\sin\beta\right)\right]\right|\end{aligned} \qquad \{3.36\}$$

3.2.2.4 Comprehensive Theory for All Shaft Motions

Combining equations {3.32} and {3.36}, the expression describing the resultant beat frequency detected by the photodetector in the LTV can be ascertained. This is related to all motions of the shaft, which are now specified as being time dependent again;

$$f_{beat} = \frac{2}{\lambda_L}\Big| \omega_R(t) d\Big[\big(-\cos\beta\sin\alpha\big) + \big(\theta_y(t)\cos\alpha\cos\beta\big) + \big(-\theta_x(t)\sin\beta\big)\Big] + d\Big[\big(\dot{\theta}_x(t)\cos\beta\cos\alpha\big) + \big(\dot{\theta}_y(t)\sin\beta\big)\Big]\Big| \qquad \{3.37\}$$

This demonstrates that, as a result of the combination of incidence angles α and β, there is sensitivity of the LTV to all angular motions of the shaft. There are two sets of terms, one dependent on the shaft rotation speed $\omega_R(t)$ and the other independent of it.

Considering the rotation speed term to consist of a mean and a fluctuating component, or torsional vibration, so $\omega_R(t) = \overline{\omega}_R + \Delta\omega_R(t)$, then {3.37} is expressed as follows;

$$f_{beat} = \frac{2d}{\lambda_L}\Big| \overline{\omega}_R\Big[\big(-\cos\beta\sin\alpha\big) + \big(\theta_y(t)\cos\alpha\cos\beta\big) + \big(-\theta_x(t)\sin\beta\big)\Big] + \Delta\omega_R(t)\Big[\big(-\cos\beta\sin\alpha\big) + \big(\theta_y(t)\cos\alpha\cos\beta\big) + \big(-\theta_x(t)\sin\beta\big)\Big] + \Big[\dot{\theta}_x(t)\cos\beta\cos\alpha + \dot{\theta}_y(t)\sin\beta\Big]\Big| \qquad \{3.38\}$$

This expression can be used to predict the spectral components of the resultant signal from an LTV in use on a laterally vibrating shaft. The first term gives the mean d.c. level of the instrument output, proportional to the target rotation speed. Multiplying out the other terms and extracting the time-dependent parts from the fixed coefficients relating to the alignment of the instrument (*d*, α and β) allows discussion of the components resulting from shaft lateral vibration;

$\overline{\omega}_R\theta_y(t)$ and $\overline{\omega}_R\theta_x(t)$ are terms related to the angular lateral vibration of the shaft, and proportional to the mean rotation speed.

$\Delta\omega_R(t)\theta_y(t)$ and $\Delta\omega_R(t)\theta_x(t)$ are cross-terms which will each introduce components at the sum and difference frequencies of angular lateral and torsional vibration.

$\dot{\theta}_x(t)$ and $\dot{\theta}_y(t)$ are the angular lateral velocities of the shaft and are contained in the terms independent of the shaft rotation speed.

In the theoretical development of Section 3.2.2, lateral shaft vibration of the form of a cylindrical whirl orbit was shown to affect each laser beam equally and the vibrometer is therefore immune to this sense of motion, as discussed in previous work [3-2]. However, it has now been shown that the instrument is sensitive to lateral vibration in a whirl orbit where the shaft rotation vector undergoes a change of direction, described here as the combination of pitch motion about the *X*-axis and yaw motion about the *Y*-axis. This problem is significant in certain experimental alignments of the LTV as the effects of angular lateral vibration will be indistinguishable from genuine torsional vibration. From equation {3.38} the magnitude of any error components will depend significantly on the LTV incidence angles, α and β, and the angular lateral motions, $\theta_x(t)$ and $\theta_y(t)$.

Practical limits to the ranges of α and β values are determined by the scattering of sufficient light from the target shaft and the minimum value of f_{beat} which can be demodulated. For example, the following angular ranges are quoted for the Brüel & Kjær Type 2523 LTV when using retro-reflective tape [3-9]. For side of shaft measurements, where the ideal arrangement is with the laser beams normal to the axis of rotation, a minimum α of 35° is recommended, limited by scattered light intensity. For end of shaft measurements α should be between 30° (limited by f_{beat} value) and 55° (limited by scattered light intensity). Values of β up to 75° are considered acceptable in reducing the effective beam separation which may be necessary, for example, on very small diameter shafts, but operation with $\beta \neq 0°$ is generally unusual. However, the sensitivity to angular lateral vibration demonstrated in this work indicates the undesirability of using the instrument in these arrangements.

Optimum operation of the instrument is achieved when the plane of the incident laser beams is perpendicular to the rotation axis, then $\alpha = 90°$ and $\beta = 0°$ to give:

$$f_{beat} = \frac{2}{\lambda_L} d\omega_R(t) \qquad \{3.39\}$$

When aligned in this way sensitivity to variations in $\omega_R(t)$ is maximised and small amplitudes of angular lateral vibration will have little effect on instrument output. Use of the instrument at other incidence angles increases the sensitivity to angular lateral motion, in addition to a reduction in the sensitivity to torsional vibration, but is often necessary because of restricted access to the measurement location.

Conventionally, the LTV is used with incidence angle $\beta = 0°$ to maximise the sensitivity of the instrument to torsional vibration for the given incidence angle α necessitated by the available optical access. The measurement derived from a rotating shaft undergoing the motions described is determined from equation {3.37} as;

$$f_{beat} = \frac{2}{\lambda_L} d\left| \omega_R(t)(-\sin\alpha) + \left[\omega_R(t)\theta_y(t) + \dot{\theta}_x(t)\right]\cos\alpha \right| \qquad \{3.40\}$$

The second term of this expression indicates the sensitivity of the instrument to angular lateral vibration about both the *X*- and *Y*-axes, becoming more sensitive to both as the incidence angle α is decreased towards zero. Obviously this is of concern if the LTV is to be used for accurate assessment of the torsional vibration behaviour of a rotating shaft. Experimental results in subsequent sections validate this theory through measurement of simulated torsional and angular lateral vibration. This aims to quantify the severity of this sensitivity on the performance of the instrument.

3.3 Experimental Validation

To consider the operation of the LTV in full it is important to validate the beat frequency expression of {3.37} and investigation of the LTV sensitivity to the various shaft motions is described in the following sections. For validation of the torsional vibration sensitivity the LTV measurements are compared with the calibration standard of the Hooke's joint. Further to this, the sensitivity of the instrument to angular lateral motion is demonstrated experimentally.

3.3.1 Hooke's Joint Calibrator

Despite the commercial availability of the LTV, validation of its performance has been limited. Comparisons have been made with conventional torsional vibration transducers during development of the instrument but only limited independent calibration methods exist. The Hooke's joint, or universal coupling, has been widely used as a device suitable for checking the accuracy of torsional vibration measuring equipment over a large range of motion amplitudes [3-10, 3-11] and was introduced in Section 2.2.2. Although the Hooke's joint cannot been calibrated by absolute means, it can be used as a suitably accurate calibration device, reproducing predictable magnitudes of rotating shaft speed fluctuation. In this instance it is considered with the aim of validating the sensitivity of the LTV to torsional vibration, in the absence of any lateral vibration effects. As a result, the resulting beat frequency in the photodetector signal is entirely dependent on the rotation speed and its fluctuating components.

Figure 3.9 shows the typical arrangement where a driven shaft is connected through a Hooke's joint to a driving shaft rotating with a constant speed. Although both shafts complete a revolution in the same time period, their angular velocity ratio is not constant during the revolution. The speed fluctuation on the output shaft has a predominant 2nd order component, which increases in magnitude with the inclination angle ϕ_H between the shafts, and a smaller 4th order component.

The apparatus was substantially rigid to minimise distortion under load and utilised a heavy flywheel and flexible rubber coupling to maintain uniform rotation of the driving shaft. Care was taken to minimise any backlash in the Hooke's joint and related components. This is confirmed by the nominally zero output given when the shafts were run in line, with any measured torsional vibration, neglecting measurement technique noise floor effects, due to small errors in the geometry of the apparatus [3-10]. Vertical misalignment of the Hooke's joint would also give a non-zero output at 0° shaft inclination but is not apparent with this apparatus. The driven shaft support plate is pivoted at the Hooke's joint to allow the horizontal inclination ϕ_H of the driven shaft to be set in the range -30° to +30° for the required speed fluctuation amplitude. A calibrated scale marked on the main base allowed alignment of the inclination angle of the two shafts to within ±0.5°. The LTV was set up to measure the speed fluctuations directly on the output half of the Hooke's joint.

Figures 3.10 and 3.11 show the variation in second and fourth order torsional vibration respectively for the output shaft of the rig taken at three rotation speeds. During the experimentation, the predominantly sinusoidal nature of the output shaft speed fluctuation could be confirmed by viewing the LTV output on an oscilloscope. The amplitudes of the second and fourth order speed fluctuations can be easily calculated theoretically [3-10, 3-11] and are included on the two figures. The experimental results from the LTV for second order compare extremely well with theory up to the maximum amplitude considered of $\pm 4°$. The torsional vibration displacement of the driven shaft is independent of rotation speed, permitting direct comparison of results from each speed value. A slight inclination angle 'zero-error' can be identified from the two graphs, although this systematic offset between the theoretical and experimental values is only apparent through consideration of the full inclination angle range of -30° to +30°. It should be noted that the range of second order torsional vibration amplitudes seen here is excessive as in real situations, such as diesel engine crankshafts, maximum levels are typically of the order of 1° peak.

The experimental results for fourth order speed fluctuation in Figure 3.11 give good agreement with theory, on consideration of the systematic offset error in the inclination angle. There is clear indication of the 'noise floor' for the instrument in this situation, with the lower limit of measurement apparent at a value of approximately 10m°. This lower limit results from the characteristic speckle noise peaks in the spectrum of the instrument's output at the rotation frequency and its harmonics, as discussed in Section 2.1.8. This is of fundamental concern when attempting to measure very low levels of torsional vibration at integer orders of rotation speed, as in this situation. In addition, at these low levels small geometrical discrepancies and the effects of wear in the Hooke's joint are emphasised.

Concerns related to the accuracy of the Hooke's joint have minimal effect on the results obtained, primarily due to the simplicity of the experimental arrangement in which there is no load and negligible inertia on the output shaft. The experimental results correlate well with the theory used, showing the LTV to give accurate and consistent measurements over a range of speeds and vibration amplitudes when compared against this standard independent calibration method.

3.3.2 Effects of Shaft Angular Lateral Vibration

Experimental validation was carried out to investigate the lateral vibration terms in the beat frequency expression of {3.37}. A rig was designed to simulate angular lateral vibration, offering accurate angular tilt motion of a rotating shaft section as shown in Figure 3.12. A precision dynamic shaker was used to drive a section of gear rack in a linear direction. The gear rack meshes with a large diameter gear, which rotates back and forth to provide the required angular lateral motion about either the *X*- or *Y*-axis, depending on the relative alignment of the rig and LTV. A small d.c. motor carrying the target shaft section was mounted on top of the gear. The amplitude and frequency of the motion and the shaft rotational speed were all readily controllable, providing a large dynamic range for experimentation.

It was seen in initial qualitative tests that the LTV, when conventionally aligned with the incident laser beam in the *X-Z* plane as defined in development of the theory, was sensitive to both θ_y and θ_x motions. As apparent from theoretical predictions, the magnitude of the former component was proportional to mean rotation speed, whilst that of the latter was not. The following experimental results address the terms in the beat frequency expression dependent on the rotation speed, considered previously as $f_{beat}^{(1)}$ in Section 3.2.2.2. Quantitative examination of terms independent of rotation speed, previously labelled $f_{beat}^{(2)}$, and the cross-terms identified in equation {3.38} is to be the subject of further work.

The rotation dependent components due to angular lateral motion will be considered separately by obtaining appropriate forms of the beat frequency equation of {3.37}. If the shaft only undergoes angular lateral motion about the *Y*-axis, $\vec{\theta}_y = \theta_y \hat{y}$, the beat frequency is given by;

$$f_{\hat{y}} = \frac{2}{\lambda_L}\left| \omega_R(t) d\left[\left(-\cos\beta\sin\alpha\right) + \left(\theta_y(t)\cos\alpha\cos\beta\right)\right] + d\left[+\dot{\theta}_y(t)\sin\beta\right]\right| \quad \{3.41\}$$

With incidence angle $\beta = 0°$ the lateral vibration term independent of rotation speed is removed;

$$f_{\hat{y}} = \frac{2}{\lambda_L}\left| \omega_R(t)d\left[-\sin\alpha + \theta_y(t)\cos\alpha\right]\right| \qquad \{3.42\}$$

Alternatively, if the shaft is considered to undergo only angular lateral motion about the X-axis, $\vec{\theta}_x = \theta_x \hat{x}$, with incidence angle $\alpha = 90°$ the term independent of rotation speed is removed and the beat frequency is given by;

$$f_{\hat{x}} = \frac{2}{\lambda_L}\left| \omega_R(t)d\left[-\cos\beta - \theta_x(t)\sin\beta\right]\right| \qquad \{3.43\}$$

In these simplified cases the components of the beat frequency resulting from the angular lateral motion are readily estimated and the magnitude of each of these terms is proportional to the rotational speed of the shaft. The beat frequency expressions of {3.42} and {3.43} can be rewritten to be equivalent to;

$$f_{beat} = \frac{2}{\lambda_L} d\left| \omega_R(t)C \right| \qquad \{3.44\}$$

where C is a generalised factor representing the terms related to the instrument alignment and shaft angular lateral vibration. In the absence of angular lateral vibration the mean value of C is defined as $\overline{C}$. The resulting beat frequency when a steadily rotating shaft undergoes angular lateral vibration would be equivalent to that resulting from a shaft element rotating at a mean speed Ω with a torsional vibration $\Delta\Omega$. Beat frequency expressions for each of these cases can be derived from {3.44}. Therefore, the variations in beat frequency due to fluctuations in C or Ω can be equated to give:

$$\frac{2}{\lambda_L} d\left| \overline{C}(\Omega + \Delta\Omega) \right| = \frac{2}{\lambda_L} d\left| \left(\overline{C} + \Delta C\right)\Omega \right| \qquad \{3.45\}$$

where ΔC corresponds to the magnitude of fluctuations in C. For the simplified cases of equations {3.42} and {3.43}, considering each angular lateral vibration component dependent on rotation speed in isolation, the relationship of {3.45} is conveniently rearranged in the form of an apparent speed fluctuation ratio, due only to the separate angular lateral motions;

$$\left[\frac{\Delta\Omega}{\Omega}\right]_{\hat{y}} = \frac{\theta_y}{\tan\alpha} \qquad \{3.46a\}$$

$$\left[\frac{\Delta\Omega}{\Omega}\right]_{\hat{x}} = \theta_x \tan\beta \qquad \{3.46b\}$$

For the experimental validation, the apparatus in Figure 3.12 was run at a series of rotation speeds, with the lateral vibration frequency fixed at 20Hz. Two arrangements were considered for these tests; θ_y motion with the LTV at a series of α incidence angles with $\beta = 0°$ and θ_x motion with the LTV at a series of β incidence angles and $\alpha = 90°$. In each of these two arrangements the LTV was tested throughout the range of incidence angles, within the limits of scattered light intensity and the Doppler signal processor. The laser beam separation was adjusted for each measurement to ensure the signal was within the operating range of the instrument Doppler processor.

Figures 3.13 and 3.14 show the close agreement between experimental results for the θ_y angular lateral motion and theoretical predictions as a function of the incidence angle α. The continuous lines are theoretical data predicted using equation {3.46a} while the discrete data points correspond to tests at rotation speeds of 30Hz, 45Hz and 60Hz for each of the chosen vibration amplitudes. The apparent torsional vibration values are presented in terms of $\Delta\Omega/\Omega$, which allows direct comparison of results for each rotation speed. Figure 3.13 shows the results from viewing the end face of the shaft, a technique often used with the LTV in engine measurements where a pulley or gearwheel often provides the most convenient access. Figure 3.14 displays the values obtained when the laser beams are incident on the side of the shaft.

Lateral motion in the θ_x sense and its relationship with inclination angle β is shown in Figure 3.15. As in the previous case, the experimental results and theoretical values from equation {3.46b} agree closely.

Minor estimated errors of $\pm 1°$ exist in measurement of α and $\pm 0.5°$ in β due to alignment tolerances and results are found to lie within these limits. The magnitudes of the harmonic speckle noise peaks present in the instrument output were also recorded during the experimentation and seen to give an average $\Delta\Omega/\Omega$ value of 3×10^{-4}. This experimental investigation confirms that angular lateral vibration can induce error components of significant magnitude into the measured signal.

3.3.3 Engine Vibration Measurements

A series of measurements from automotive engines were made to examine the magnitude of the angular lateral vibration cross-sensitivity in practical situations, relative to the instrument noise floor and typical levels of torsional vibration.

The torsional vibration was measured on the crankshaft pulley of a four-cylinder four-stroke 2.0 litre direct injection diesel engine. The instrument was tripod-mounted and arranged with $\alpha = 50°$ for reasons of access. Engine crankcase lateral vibration effects were minimal as the engine was rigidly clamped to fixed supports on the main test bed. Figure 3.16 shows the variation of the main orders of vibration measured for the diesel engine under load over its working speed range at full throttle. These values are expressed as a speed fluctuation ratio $\Delta\Omega/\Omega$ for comparison with the values obtained in the preceding section. The second order exhibits the most severe torsional vibration, with a maximum $\Delta\Omega/\Omega$ of 0.021 (602m° displacement) at 1300rpm. Smaller torsional resonance effects are clearly apparent for the eighth and sixth orders.

Measurements were also made on a four-cylinder four-stroke 2.0 litre fuel injection petrol engine and for the speed range covered under load a second order maximum $\Delta\Omega/\Omega$ of 0.049 (1420m°) at 1040rpm was recorded. A minimum level of significant torsional vibration at any order for each engine was estimated to be $\Delta\Omega/\Omega = 0.001$.

Actual engine yaw and pitch vibrations were assessed to determine limits within which the operation of the LTV will give accurate measurement. This was achieved with two accelerometers mounted on the engine block a known distance apart. Accounting for the phase between the two signals and with suitable calibration, an estimate of the angular lateral motion of the block could be obtained. Tests on the previous four-cylinder petrol engine, which was mounted on resilient, elastomeric engine mounts as in a vehicle, gave a peak yaw amplitude of 36m° for second order vibration when running under load and full throttle at 545 rpm. The maximum pitch amplitude was approximately 10m° for second order at 775rpm.

To highlight further the discrepancies in LTV measurements due to angular lateral vibration of the target shaft, two LTVs were set up to measure simultaneously the torsional vibration of the crankshaft pulley of the resiliently mounted petrol engine used previously. One was set at $\alpha = 20°$ (very sensitive to angular lateral vibration) and the other at $\alpha = 60°$ (marginally sensitive to angular lateral vibration), arranged to be incident in the yaw (*X-Z*) plane. The second order torsional vibration measured with each of the two instruments is shown in Figure 3.17.

Above 1400rpm the values for both instruments are approximately equal. However, as the speed decreases the difference between the measurements increases up to a value of approximately 180m° at 1000rpm as a result, it is suggested, of angular lateral vibration of the rotating target. Since it is not possible to find the phase between the torsional and lateral motions in this configuration, an accurate figure for genuine angular lateral vibration cannot be derived. Assuming the yaw and pitch amplitudes to be equal, an estimate of the motion of the crankshaft pulley can be made from the beat frequency expression of equation {3.40} for this arrangement. Considering the phase between the two orthogonal motions, θ_y and θ_x, a lower limit of shaft angular lateral vibration which would result in a difference of this magnitude between the two LTV measurements, is estimated to be of the order of 50m°. This is approximately twice the value measured for motion of the engine block but is of appropriate magnitude when compared to published data considering the effects of engine crankshaft bending vibrations [3-12].

3.3.4 Guidelines for Use in the Presence of Angular Lateral Vibrations

To ensure accurate assessment of torsional vibration it is necessary to identify incidence angle ranges where the sensitivity of the LTV to yaw and pitch vibration is of importance. The experimental data discussed in Section 3.3.3 is presented in Figure 3.18 to give a clear indication of the magnitude of errors expected. The typical noise floor level defines a minimum above which the sensitivity to angular lateral vibration becomes significant. The maximum and minimum levels of $\Delta\Omega/\Omega$ measured during the engine tests are included. Additionally, the error induced by angular lateral vibration is predicted from the value of crankshaft pulley angular motion at second order, $\theta_x = \theta_y = 50\mathrm{m}^\circ$, estimated from the simultaneous LTV measurements and assuming the same phase relationship between the two motions as before.

This estimate of yaw and pitch motion defines the operating limits for use of the LTV on any machine in which the target shaft experiences these levels of angular lateral vibration at this order. Comparison can therefore be made between the relative magnitudes of angular lateral vibration induced components, genuine torsional vibration and the LTV noise floor, highlighting particular operating regimes where the sensitivity to angular lateral vibration becomes of concern in this typical application. These guidelines are important when use in these configurations is necessitated by shaft access limitations.

It is apparent from Figure 3.18 that for $\alpha < 70^\circ$ the magnitude of signal components induced by angular lateral vibration is potentially very significant and it is recommended that use of the LTV in this incidence angle range is avoided if possible. In the range $70^\circ < \alpha < 80^\circ$ the error components are of measurable magnitude and caution should be exercised in the interpretation of data if it is unfeasible to avoid use in this arrangement. Finally, for $80^\circ < \alpha \leq 90^\circ$ the error components are of similar or smaller magnitude than the instrument noise floor level and operation of the LTV is effectively immune to all lateral vibration, allowing reliable and accurate measurement of torsional vibration. Additionally, hand-held operation of the LTV can be advantageous in some measurement situations, but the same incidence angle recommendations apply. Human body movement may induce changes in the instrument output in the same way as angular lateral vibration due to relative motion of the LTV and target shaft. Tripod mounting in these cases, while not essential, is preferable [3-13].

The next section considers new instrumentation configurations to remove this sensitivity to angular lateral vibration, ensuring accurate assessment of shaft torsional vibration when access limitations prevent the optimum instrument alignment from being used. Additionally, novel techniques are considered to assess the angular lateral vibration itself directly from the rotating shaft.

3.4 Measurement of Pure Torsional Vibration from a Laterally Vibrating Shaft

Experience has shown that while it is common to align an LTV with incidence angle $\beta = 0°$, restricted access often demands use with α at an angle other than 90°. As demonstrated previously, there will in general then be some measurable sensitivity to angular lateral vibrations and it will not be possible to make an unambiguous measure of torsional vibration though the conventional use of a single LTV. It is proposed that with the use of two suitably aligned torsional vibrometers, a measure of pure torsional vibration can be derived in these situations.

Simultaneously, this technique can give an assessment of the shaft bending vibration - a measurement not previously realised by non-contact means. Up to this point the general term angular lateral vibration has been used to describe the angular displacement of a rotating shaft, as this can result from motion of the whole machine or rotating shaft. However, the term bending vibration will be now be used to describe the yaw and pitch motions, particularly with respect to engine crankshafts,

In this new configuration two LTVs are arranged symmetrically at equal and opposite incidence angles as shown in Figure 3.19, on either the side (Arrangement A) or end face (Arrangement B) of the shaft. With $\beta = 0°$ in both cases, the sensitivity of each vibrometer to bending vibrations is limited to those terms detailed in equation {3.40} which will modulate the mean beat frequencies measured by the two instruments.

Figure 3.20 shows that with a nominally specified incidence angle α there are four possible arrangements of the LTV relative to the shaft. It should be noted that positions 1 and 4 on the side of the shaft are assumed equivalent to the respective measurement positions 1' and 4' on the end face of the shaft. Following previous convention for determining the sign of these incidence angles with rotation about the *Y*-axis, the four positions are aligned respectively at angles; +α, (π-α), (π+α), and -α. Substituting these angles into equation {3.40} the following expressions for the beat frequencies are derived;

$$\begin{aligned} f_1 &= \frac{2}{\lambda}\left| d\left[-(\omega_R(t)\sin\alpha)+\left(\omega_R(t)\theta_y(t)+\dot{\theta}_x(t)\right)\cos\alpha\right]\right| \\ &= \frac{2}{\lambda}d\left[\omega_R(t)\sin\alpha-\left(\omega_R(t)\theta_y(t)+\dot{\theta}_x(t)\right)\cos\alpha\right] \end{aligned} \tag{3.47a}$$

$$\begin{aligned} f_2 &= \frac{2}{\lambda}\left| d\left[-(\omega_R(t)\sin(\pi-\alpha))+\left(\omega_R(t)\theta_y(t)+\dot{\theta}_x(t)\right)\cos(\pi-\alpha)\right]\right| \\ &= \frac{2}{\lambda}d\left[\omega_R(t)\sin\alpha+\left(\omega_R(t)\theta_y(t)+\dot{\theta}_x(t)\right)\cos\alpha\right] \end{aligned} \tag{3.47b}$$

$$\begin{aligned} f_3 &= \frac{2}{\lambda}\left| d\left[-(\omega_R(t)\sin(\pi+\alpha))+\left(\omega_R(t)\theta_y(t)+\dot{\theta}_x(t)\right)\cos(\pi+\alpha)\right]\right| \\ &= \frac{2}{\lambda}d\left[\omega_R(t)\sin\alpha-\left(\omega_R(t)\theta_y(t)+\dot{\theta}_x(t)\right)\cos\alpha\right] \end{aligned} \tag{3.47c}$$

$$\begin{aligned} f_4 &= \frac{2}{\lambda}\left| d\left[-(\omega_R(t)\sin(-\alpha))+\left(\omega_R(t)\theta_y(t)+\dot{\theta}_x(t)\right)\cos(-\alpha)\right]\right| \\ &= \frac{2}{\lambda}d\left[\omega_R(t)\sin\alpha+\left(\omega_R(t)\theta_y(t)+\dot{\theta}_x(t)\right)\cos\alpha\right] \end{aligned} \tag{3.47d}$$

It is clear from these expressions that $f_1 = f_3$ and $f_2 = f_4$, making LTV outputs derived in these cases equal. Initial experimental investigations confirmed that torsional vibration signals were in-phase with each other for all four positions of the LTVs. Referring to Figure 3.20, the LTV signal components due to $\theta_y(t)$ motion, with a magnitude proportional to rotation speed, relative to position 1 were in-phase at position 3 and out-of-phase at positions 2 and 4, confirming the predictions of equations {3.47a to d}. Further preliminary tests confirmed the sensitivity of the LTV to $\theta_x(t)$ motion when aligned in this arrangement. It was seen that the magnitude of this component was independent of rotation speed and the LTV signals had the same relative phase relationships as for the $\theta_y(t)$ sensitivity. Therefore all bending vibration components were in phase with each other for LTV alignments with parallel incidence vectors, as predicted by the theory.

The proportionality constant of the LTV at position 1 is K_1, which incorporates the geometrical and optical constants, together with the demodulator constant k_{1e}. Therefore the voltage output from the LTV can be written as follows, with similar expressions for the other positions;

$$V_1 = K_1\left[\omega_R(t) - \left(\frac{\omega_R(t)\theta_y(t) + \dot{\theta}_x(t)}{\tan\alpha}\right)\right] \qquad \{3.48a\}$$

where;

$$K_1 = k_{1e}\frac{2}{\lambda}d\sin\alpha \qquad \{3.48b\}$$

If simultaneous measurements are taken with two LTVs from positions 1 (or 3) and 2 (or 4), utilising the calibration factors shown, the sum of the outputs provides a real-time measurement of rotation speed;

$$\frac{V_1}{K_1} + \frac{V_2}{K_2} = 2\omega_R(t) \qquad \{3.49\}$$

The mean value is proportional to the mean rotation speed and the fluctuating component provides the totally unambiguous measure of torsional vibration velocity, immune to all angular lateral shaft vibration regardless of the incidence angle α. This arrangement therefore provides a means to achieve accurate measurement of pure torsional vibration from a laterally vibrating shaft where restricted optical access precludes the use of a single LTV with the incidence angle in the previously specified range of $80° < \alpha \leq 90°$.

Obtaining the difference in the instrument outputs gives the following signal;

$$\frac{V_1}{K_1} - \frac{V_2}{K_2} = \frac{2}{\tan\alpha}\left[\omega_R(t)\theta_y(t) + \dot{\theta}_x(t)\right] \qquad \{3.50\}$$

This indicates the possibility of non-contact evaluation of the bending vibration of a rotating shaft and this notoriously difficult measurement has not been achieved previously. However, the two bending vibration terms always have the same sign as each other at any of the incidence positions, as seen in equations {3.47a to d}. It is therefore not possible to derive a measurement purely dependent on one of these orthogonal motions through addition or subtraction of these signals. A measurement obtained in the manner of {3.50} will have sensitivity to both yaw and pitch, with the magnitude of the resultant signal dependent on the relative phase between the components and their individual amplitudes. The following section demonstrates the potential of this technique with partial validation. Further work should consider the development of a means to resolve the $\theta_y(t)$ and $\theta_x(t)$ components and is discussed in Chapter 6.

3.4.1 Experimental Validation

Simulation of angular lateral motion in one plane is used here to demonstrate the derivation of pure torsional vibration from a shaft exhibiting bending vibration. If the shaft vibrates angularly around only the *Y*-axis, measurement of the bending motion can also be achieved if the two LTVs are aligned with their beams incident in either the *X-Z* or *Y-Z* plane. This single axis vibration condition rarely occurs in practice and, as a result, completely unambiguous measurement of shaft angular lateral vibration cannot yet be achieved with this technique. However, it was shown in Section 3.4 that unambiguous measurement of torsional vibration can be attained in all cases, with complete immunity to all lateral shaft motion.

The experimental set-up was as shown previously in Arrangement A of Figure 3.19, with two LTV's arranged initially at $\alpha = 45°$ and incident on the side of the shaft. This angle was chosen as a satisfactory compromise of three factors: sensitivity to torsional vibration, sensitivity to bending vibration and to ensure sufficient intensity of light collected. Equations {3.48 to 3.50} confirm the influence of the incidence angle α on the sensitivity of these measurements. At $\alpha = 90°$ there is maximum sensitivity to torsional vibrations as with a single LTV. As α approaches $0°$ the sensitivity to bending vibrations increases and at intermediate values there is sensitivity to both vibrations. The experimental rig introduced in Section 3.3.2 was used to simulate the bending vibration of a rotating target.

An accelerometer was fixed to the rack which rotated the gear wheel, providing an independent measure of the shaft angular lateral vibration. An a.c. ripple was added to the d.c. motor drive causing its speed to fluctuate, thereby simulating torsional vibration. An independent measure of this speed fluctuation was provided by a third LTV set with $\alpha = 90°$ such that the measurement was effectively insensitive to the angular lateral vibration of the shaft. For this experimental study only $\theta_y(t)$ bending vibration was simulated and this is adequate for proof of the principle described. As described in Section 3.4, in the processing of the results the sum and difference of the calibrated signals from the instruments were used to give the required measurements.

Figure 3.21a shows simultaneous time domain signals from the two LTVs incident on the side of the shaft. The combined effect of the torsional and bending vibration is clearly apparent but it is not possible to distinguish between them with this measurement. The spectrum of one of the LTV signals is presented in Figure 3.21b showing the components at, nominally, 25Hz for bending vibration and 45Hz for torsional vibration.

Figure 3.22a shows the resolved torsional vibration obtained by processing the two LTV signals in accordance with equation {3.49}. This measurement of torsional vibration can be compared with the independent LTV in the spectra of Figures 3.22b & c, with close agreement between the resolved and the independent levels. This technique therefore provides a measure of pure torsional vibration in situations where measurement with a single LTV would be ambiguous due to sensitivity of the instrument to bending vibration of the target shaft.

Equation {3.50} demonstrates the sensitivity of the difference signal to both $\theta_y(t)$ and $\theta_x(t)$ senses of motion. However, with the angular lateral motion constrained to $\theta_y(t)$ only in the experimental situation, dividing {3.50} by {3.49} normalises the bending vibration measurement by the rotation speed, deriving an exact measure of the angular displacement of the rotating shaft;

$$\left(\frac{V_1}{K_1}-\frac{V_2}{K_2}\right)\Bigg/\left(\frac{V_1}{K_1}+\frac{V_2}{K_2}\right)=\frac{[\theta_y(t)]}{\tan\alpha} \qquad \{3.51\}$$

Figure 3.23a shows the bending vibration measurement in the time domain resolved in accordance with equation {3.51}. The independent measurement of bending vibration of the shaft is compared with the resolved signal in the spectra of the two signals shown in Figures 3.23b & c. As before, close agreement is seen between the resolved and genuine levels.

The sensitivity of the technique to bending vibrations can be improved if required. This is achieved by decreasing the incidence angle α and in this instance necessitates that the LTVs are incident on the end face of the shaft as in Arrangement B of Figure 3.19. Figure 3.24 shows a different measurement, obtained from the end face of the shaft with $\alpha = 15°$. The angular motion of the shaft derived with the laser technique agrees closely with the accelerometer measurement, within the limit of the rack motion following that of the gear rotation in the test apparatus. From this result the minimum measurable bending vibration is estimated to be of the order of 1m°. Additionally, the signal to noise ratio for bending vibration measurements has been improved by reducing the incidence angle α and it was estimated that the noise base has been reduced by almost an order of magnitude compared to the previous measurement. As for torsional vibration measurements using this technology, the lower limit of measurement for bending vibration components at multiples of rotation speed, is defined by the level of speckle noise harmonics.

Angular lateral, or bending, vibration has been notoriously difficult to measure and, therefore, this use of laser vibrometry for non-contact measurements of shaft vibration represents a further step forward in the use of this technology for machinery diagnostics. However, simultaneous sensitivity to yaw and pitch motion prevents direct independent measurement of each quantity and further work is intended to resolve the individual components. This technique has now been proven in a laboratory situation and the following section describes its application to a practical measurement.

3.4.2 Diesel Engine Crankshaft Vibration

A 2.0 litre DI compression ignition (diesel) engine was used as a first practical example to demonstrate the measurement of pure torsional vibration and crankshaft bending vibration. The engine was connected to a dynamometer, allowing a range of loads and speeds to be considered. Two LTVs were arranged at equal incidence angles to the shaft centreline in the manner discussed in Section 3.4, as shown in Arrangement B of Figure 3.19.

In this alignment measurement by a single instrument would be contaminated by angular lateral vibration. Initially the instruments were aligned by hand with the laser beams incident on the centre bolt of the engine crankshaft pulley and approximately similar α incidence angles. In a practical arrangement of this nature it is difficult to measure the incidence angles precisely. However, accurate alignment was achieved through use of the instrument calibration to equalise their incidence angles. It can be generally stated for LTV1 that the mean d.c. output voltage is given by;

$$\overline{V}_1 = K_1'\overline{\omega}_R \sin\alpha \qquad \{3.52\}$$

where K_1' is a general constant including all the terms in equation {3.48b} except the incidence angle. In the experimental arrangement the position of LTV1 is fixed and the incidence angle of LTV2 adjusted until;

$$\frac{\overline{V}_1}{K_1'\overline{\omega}_R} = \frac{\overline{V}_2}{K_2'\overline{\omega}_R} = \sin\alpha \qquad \{3.53\}$$

Both LTVs are then aligned at the same incidence angle, α, as required. In the experimentation the two instruments were aligned to be sensitive to both bending and torsional vibration at approximately $\alpha = 35°$. A third torsional vibrometer was set up at $\alpha = 75°$, an arrangement much less sensitive to shaft bending vibration, to provide an independent measure of torsional vibration for comparison. Time history data from the first two LTVs were recorded simultaneously on a digital oscilloscope and processed to give the resolved torsional and bending vibration measurements for a series of engine speeds under full load.

Figure 3.25 shows a typical torsional vibration signal measured on the engine at 750rpm, from one of the LTVs at $\alpha = 35°$. At this rotation speed the 2nd order crankshaft torsional vibration dominates the response and the influence of shaft bending vibration on this measurement is not clearly apparent. Figures 3.26a to c show the frequency spectra of the three torsional vibration measurements obtained, from one of the LTVs at $\alpha = 35°$, the independent instrument and the resolved signal from the two equally-aligned LTVs. The main orders of torsional vibration, namely 2nd, 4th and 6th, are clearly evident in each case and comparison of these spectra highlights important differences due to bending vibration sensitivity. It is apparent that the magnitude of the resolved measurement components are closer to the independent measurement than those of the single LTV. This is a result of the single instrument measurement of Figure 3.26a being affected by crankshaft bending vibration. The independent LTV measurement in Figure 3.26b, closer to the ideal incidence angle, has much reduced bending vibration sensitivity but still contains a small component due to this motion. However, the resolved measurement in Figure 3.26c, derived with the new technique, is immune to crankshaft bending vibration, and highlights the discrepancies apparent in the other two results. Additional minor differences between the measurements may be attributed to the fact that it was not possible to obtain the results from the independent LTV simultaneously.

In addition to the discrepancies identified at the main harmonic vibration orders for the single LTV measurement, the concentration of response in the frequency range 300Hz to 500Hz is quite different to that of the resolved signal. This section of the frequency spectra has been expanded in Figures 3.27a & b for both these measurements. The spectra are significantly different and the substantial contribution due to bending vibration sensitivity is clearly apparent in the single LTV measurement. The resolved measurement has a clear peak at 375Hz which is due to excitation of the crankshaft at one of its torsional resonant modes. This is in agreement with previous torsional vibration surveys on this diesel engine, such as that presented in Figure 3.16, where the minor resonances observed for 6th and 8th orders give an estimation of the frequency of the first torsional mode at approximately 350Hz. This component cannot be identified in the single LTV spectrum due to the other signals present, highlighting the importance of this technique for accurate assessment of torsional vibration.

Subtraction of the two LTV signals derives a measure of the bending vibration of the engine crankshaft and an example of this is shown in Figure 3.28, which is significantly different from the torsional vibration response of Figure 3.25. The repeating pattern of impacts from the firing of the four cylinders can be clearly seen, occurring over a two revolution time period as expected for a four-stroke engine. The largest impact is that of cylinder 1, closest to the pulley position, consistent with previous experimental studies of crankshaft behaviour [3-14 to 3-16]. Minor variations between impact sequences occur as a result of combustion cyclic variability. Previously, with simulated bending vibration about a single axis, calibrated units could be used to give a direct measure of the angular motion. However, as has been discussed previously, this signal is sensitive to both yaw and pitch motions and direct assessment of either bending vibration magnitude cannot be determined. Therefore, in this situation bending vibration measurements are presented in units of 'rad/s' appropriate to the actual signal derived.

The frequency spectrum of this motion is shown in Figure 3.29 with significant differences from the torsional vibration spectra. In addition to the distinct bending vibration peaks occurring at the main vibration orders, the first four orders of rotation, the spectrum shows a large concentration of vibration response in the 350-500Hz range, which was seen previously to corrupt the measurement from the single LTV at $\alpha = 35°$. It is proposed that the peak at 455Hz is due to resonance of the crankshaft in a bending mode, excited by the combustion impulses.

It is important to note that when observing, in a stationary co-ordinate system, the bending vibration of a rotating shaft, the vibration undergoes a frequency transformation related to the rotation speed. This occurs as a result of the whirling motion of the rotating shaft being projected onto the co-ordinate axes in which the measurement is made. The genuine motion of the shaft is obtained, although it is described in terms of the stationary co-ordinate parameters θ_y and θ_x. For example, in the experimental bending vibration spectrum the biggest components at low frequencies are at odd rotation orders rather than the expected multiples of the dominant second order motion. Detailed theoretical discussion of these effects has been covered by a number of sources [3-17, 3-18].

Figure 3.30 shows the time trace of the crankshaft bending vibration measurement, band-pass filtered around this resonant frequency, with the main component of this motion clearly apparent. From equation {3.50} the resultant measurement is seen to depend on the magnitudes of the $\theta_y(t)$ and $\theta_x(t)$ motions and their relative phase. For equal magnitudes of each motion, at higher frequencies the 'velocity' component, $|\dot{\theta}_x(t)| = \omega_x|\theta_x(t)|$, will dominate the response. From this filtered time trace of the bending vibration measurement, assuming all the signal to result from $\dot{\theta}_x(t)$ motion, the magnitude of angular lateral motion at the crankshaft pulley position is estimated to be 12m°. Additionally, the estimated damping for this mode is in the region of 5% of critical damping.

Results recorded for five speeds of the engine under load showed a similar concentration of response in the 350-500Hz range with similar levels of signal magnitude. Other modes of interest were present, such as vibration modes of the engine block, and further investigation would clarify the exact mechanisms governing the response. The total resultant angular displacement measured will not result exclusively from bending displacement of the shaft, but will include the angular displacement of the engine on its mountings. However, this effect will occur at frequencies much lower than the crankshaft bending.

The natural frequency of the crankshaft was confirmed by basic experimental modal analysis results taken from the stationary engine crankshaft with an impact hammer used to strike the central bolt on which an accelerometer was mounted. During these tests it was seen that the lateral natural frequency of the crankshaft was dependent on its angular position. This gave natural frequencies in the range 456-476Hz, dependent on the position of the con-rods. The example FRF of Figure 3.31 shows clearly the first bending mode of the crankshaft. Further modal analysis on the crankshaft pulley alone (mounted on the engine and also separately on an experimental bench) identified the first natural frequency of the outer ring moving laterally on the rubber insert (the first diametrical mode) to be at approximately 700Hz. This confirms that the motion recorded from the engine is due to the actual crankshaft bending vibration.

Although analytical modelling of crankshaft response has been comprehensive, experimental work measuring crankshaft bending on a rotating engine has been limited, primarily due to a lack of suitable measurement techniques. Previous approaches have used accelerometers mounted on a stationary housing and coupled to the crankshaft through a bearing [3-12, 3-14] or an arrangement of strain gauges attached to the shaft [3-19]. As such no direct comparison with published results could be made, although comparable values of crankshaft bending mode frequencies have been obtained under non-rotating conditions for similarly sized spark ignition engines [3-14, 3-16, 3-20].

The use of two LTVs for measurement of pure torsional vibration from the crankshaft of an automotive diesel engine undergoing angular lateral vibration has been practically demonstrated. Measurement with a single LTV was seen to exhibit unacceptable sensitivity to lateral motion in this situation. In addition, this technique has been used to investigate the bending motion of the engine crankshaft, clearly showing its motion due to cylinder firing impacts. Whilst not giving unambiguous resolution of this motion, due to inherent sensitivity of the signal derived to yaw and pitch components, this permitted estimation of the first natural bending frequency of the crankshaft excited by the combustion impulses, together with the vibration amplitude and the modal damping. Development of this technique into a robust experimental tool for application to a range of shaft systems is discussed in Chapter 6.

4. TORSIONAL MODAL ANALYSIS OF ROTATING SHAFT SYSTEMS

In the absence of suitable excitation and measurement techniques, experimental analysis of the torsional vibrations of rotating shaft systems has not been well developed. System characteristics may change due to rotation and so it is important to obtain measurements under rotating conditions. This chapter describes the development of a novel method of exciting torsional vibrations for a rotating system. In combination with a laser torsional vibrometer (LTV) to measure response, real-time determination of the torque input allows torsional vibration frequency response functions to be obtained by non-contact means. This versatile technique achieves full modal analysis from a rotating shaft system, including derivation of natural frequencies, mode shapes and damping factors.

Initially, the concept of modal analysis is introduced, identifying the requirements and objectives of this area of vibration testing. Previous investigation of modal techniques for torsional vibration is discussed, identifying inherent limitations and factors which directly influence experimental studies of this nature. Development of the novel excitation method is then described, detailing the theory of its operation and experimental investigation including calibration of the torque input to the system under test. Experimental results are presented for three and four inertia systems, with discussion of modal frequencies, mode shapes, damping factors and constraints of the excitation system. This validates the use of this excitation method for experimental torsional modal analysis, with potential application to a variety of rotating shaft systems.

4.1 Modal Analysis of Rotating Shaft Systems

Vibration problems can present design limitations to many engineering components and the experimental study of translational vibration characteristics has been well documented. As opposed to measuring the response of a machine or structure under 'operating conditions', simultaneous measurement of both an applied excitation and the resulting response of a structure allows derivation of its dynamic properties. Measurements of this type are usually referred to as 'mobility measurements' and are commonly determined as 'frequency response functions' or FRFs. These represent the complex relationship, in terms of magnitude and phase, between the input and response. This type of experimental study is known as 'Modal Testing' and is extensively described in the near-definitive text of Ewins [4-1]. It is defined as 'the processes involved in testing components or structures with the objective of obtaining a mathematical description of their dynamic or vibration behaviour'. This model can then be used for validation and refinement of finite element analyses or other theoretical models and for exploring the effect of modifications to the structure.

Modal testing requires the integration of three components, namely the theoretical basis, experimental measurements and data analysis. The aim of this work is not to redefine modal analysis but to apply the theory and techniques developed for translational vibration to the study of torsional vibration of a rotating structure. Direct analogies can be made between the two areas and consideration will be given to how the requirements for torsional vibration differ from those for translational vibration.

The data analysis stage for torsional vibration behaviour, in which curve-fitting procedures are applied to the measured results to derive a mathematical description of the system characteristics, is identical to that of translational measurements. It is in the area of experimental measurement that the developments reported here make a significant contribution to modal testing, allowing excitation and response derivation. This permits frequency response functions to be generated for input directly to conventional modal analysis software.

4.1.1 Analysis of Translational Shaft Vibration

Modal testing of translational vibrations for rotating structures has been explored in previous research as introduced below. Significant problems are apparent in the measurement and excitation of a rotating structure's dynamic behaviour and these concerns are directly applicable to torsional vibration studies.

Furthermore, it is well known that rotating machinery components cause non-symmetric terms to appear in the system matrices of the equations of motion [4-2 to 4-6]. This can be due to rotor anisotropy, cross-coupled damping and bearing properties, gyroscopic effects and other rotation speed dependent modal parameters. Difficulties in modal analysis of rotating structures arise from the skew-symmetric matrices and the resulting eigenvalue problems. For full understanding of the physical modal characteristics it is necessary to consider the forward and backward modes which result from this behaviour. Conventional modal analysis has been applied for identification of modal parameters from rotating systems [4-5, 4-7]. However, this required the development of generalised theory, rather than using the conventional assumptions of symmetric system matrices, with implications for the measurements required to derive a full description of system characteristics. Alternatively, a complex modal testing theory was developed for rotor systems which considered the directivity of the forward and backward modes [4-8, 4-9]. However, the modal testing theory problems of rotating system torsional vibrations are less significant due to symmetric mass, damping and stiffness matrices.

A range of excitation methods has been used to excite rotating shaft lateral vibration for modal analysis, including impact hammer and electrodynamic shaker excitation [4-8]. Of particular interest to the work reported in this thesis is the use of active magnetic bearings (AMBs) [4-10, 4-11]. Whilst originally used to provide contact-free levitation of a rotor, these bearings can simultaneously apply lateral excitation of rotating shaft systems and have the capacity for active vibration damping. The bearing force input is measured in two orthogonal directions and, with simultaneous measurement of the rotor lateral response, FRF measurements can be assessed. Control of the amplitude and phase relationship between the orthogonal bearing forces applied allows selective excitation of forward and backward eigenmodes for simulation of imbalance and other effects.

Accurate measurement of the excitation forces is a primary concern to ensure valid FRF data. Three main strategies have been used to measure the force applied by magnetic bearings. Linearisation of the AMB force-current relationship allows the current signal to be used as a direct measurement of the force applied. However, accurate measurement requires the displacement amplitude to be small compared to the air-gap between the bearing yokes and the rotor. Furthermore, simplifications are made regarding the electromagnetic effects of core saturation, hysteresis and eddy currents which cannot be accounted for directly. The applied forces can also be calculated from the flux density in the air-gap between the stator and rotor, measured with Hall effect sensors inserted into the magnetic circuit [4-10]. The force exerted by the AMB calculated from this signal accounts for eddy current and magnetic hysteresis effects giving an order of magnitude improvement in measurement accuracy over computation of the force from the current signal. This system was used in parameter identification of the radial rotordynamic coefficients of bearings, seals and other components in centrifugal pumps due to fluid-structure interaction forces and rotation speed [4-12].

In the third approach, the insertion of piezoelectric force transducers between the machine foundation and AMB stator allows measurement of the orthogonal forces applied to the rotor [4-9]. This was used in modal parameter identification for vibration control of a flexible rotor-bearing system and the forces were measured by a three-axes tool dynamometer. Accurate calibration of the transducer requires the minimisation of cross-coupling between the two orthogonal directions and the finite stiffness of the transducers can distort high frequency measurements. Random noise was used as the excitation function for the AMB system and FRFs demonstrated that with the rotor at rest the modal frequencies in perpendicular directions are identical. However, with the shaft rotating at increasing speed the modes separated into forward and backward types, due to gyroscopic effects, and could be accurately distinguished. The control system developed was used effectively for improving the stability of the transient and steady-state response of the lightly damped rotor system.

In addition to the practical problems regarding application of a measured force input and determination of its response, components of response due to operational excitation can invalidate regions of the measured FRFs in these translational vibration tests. This influence might be apparent in a number of ways and possible indications to its occurrence would be apparent in the coherence of the recorded FRF. The effect of disturbances other than the applied excitation would appear as noise in the measured response, thus degrading the spectra recorded. This could be random noise or, if directly related to rotation, another excitation applied to the structure and the measured response cannot then be directly attributed to the single measured force input. Non-linear behaviour of the rotating system is a further possible source of low coherence and these effects are discussed in later sections in relation to measured torsional FRFs and modal analysis.

4.1.2 Previous Developments in Torsional Modal Analysis

The problems associated with measurement of rotational mobilities from static structural components have been considered in previous work, highlighting the neglect of these parameters in conventional modal testing [4-1]. These concerns are echoed in the study of torsional vibrations and therefore progress has been limited in the experimental analysis of rotating shaft systems. This is due to difficulties encountered in achieving a controllable excitation and in measuring this input and its response.

Previously developed torsional excitation systems have included a variety of mechanical devices and electrical systems as introduced in Section 2.2. However, these methods lack either adequate control over or measurement of the input torque function to permit modal analysis. Additionally, they often require extensive modification of the assembly under test to accommodate the excitation system and instrumentation. Measurement of the torque input is usually only facilitated by the use of strain gauges or a torque transducer inserted into the shaft system, which has a number of inherent problems.

Limited torsional modal analysis has been performed successfully on non-rotating systems using conventional vibration testing equipment, with accelerometer pairs providing the measure of torsional response. A simple laboratory rotor-shaft system was studied in this way, excited by an impulse hammer input eccentric to the shaft centreline [4-13]. At another extreme, torsional modal analysis was achieved on a large stationary turbogenerator shaft [4-14]. This assembly was excited by a harmonic input from an eccentrically mounted out-of-balance disk device or by shock excitation from the turning gear ratchet.

The dynamic torsional behaviour of a non-rotating fixed end shaft with three flywheels was studied experimentally using a piezoelectric strip wrapped around the shaft surface [4-15]. This sensor was used to measure the system response by monitoring the potential differences occurring across the piezoelectric component and torsional excitation was applied with an impact hammer. Cross-sensitivity to bending vibration could not be excluded, with the relative sensitivity to bending and torsional components determined by the alignment of the piezoelectric strip axis relative to the shaft axis. Alternative arrangements of piezoelectric material, such as shear-type transducers incorporated in tubular structures, have been used for both sensing and active control of torsional vibrations [4-16]. The structural response of a simple shaft was considered in terms of a transfer function through processing of the measured torsional response from one piezoelectric transducer and the swept-sine input signal to a driving transducer.

However, in many cases, system characteristics may change due to rotation under working conditions. For instance, system torsional vibration damping depends on the fluid film in bearings and has proved difficult to determine accurately in previous experimental studies [4-17]. Additionally, there are applications where centrifugal forces exert a significant influence on performance, for example in the testing of centrifugal pendulum vibration absorbers, as discussed in Chapter 5, which need to be rotating in order to function.

In further examples of torsional modal analysis, the torsional mode shape, or more correctly operational deflection shape, of a simple rotating shaft system has been measured although the excitation method was simply a multiple of rotation speed and not instrumented [4-18, 4-19]. Limited frequency response measurements have been obtained from rotating systems using electromagnetic excitation devices to investigate the behaviour of machine tool drives [4-20, 4-21]. However, attachment of these exciters and measurement of the input and response, using strain gauges and accelerometers respectively, necessitated considerable modification to the shaft system, thus changing its vibration characteristics. Other excitation methods suitable for torsional modal testing include the use of an a.c. servo-drive [4-22], which can apply both single-frequency sinusoid and broad-band signals, and a novel 'torsional-hammer' [4-23, 4-24] which imparts a torsional impulse to a rotating system. For both these methods it is only possible to measure the torque input to the test shaft with an in-line torque transducer.

4.1.3 Factors Specific to Torsional Systems

The main aspects of the modal testing procedure can be identified, in order that a direct parallel between translational and torsional modal analysis can be made. To perform torsional modal analysis on a system during rotation, the main requirements are therefore a practical measurement transducer, permitting a series of measurements from the rotating system to be easily obtained, and a controllable and measurable method of torsional excitation. Conventional vibration analysis techniques can then be utilised for signal processing, data analysis and dynamic modelling.

The mechanical arrangement for supporting the rotating system will determine the assumptions that can be made regarding its boundary conditions. Obviously, for a rotating system, a bearing arrangement is required, together with a drive input to provide the rotation. These will dictate whether the system boundaries are considered to be free, grounded or at some intermediate condition.

A number of torsional vibration measurement techniques have been presented in previous chapters and it was seen that a versatile and robust means of measuring torsional vibration response is provided by the laser torsional vibrometer (LTV). This chapter introduces the development of a practical means by which to provide the second key instrumentation component of a torsional modal analysis system - a controllable and measurable torsional excitation. The novel excitation device enables torsional excitation to be applied by non-contact means and a measure of the torque input to be derived without substantial modification of the rotating test system. Important requirements for instrumentation of the torque input and vibration response are that they should have minimal interference with the system under test and have suitable dynamic ranges.

A range of signals could potentially be applied with the excitation system, whether in the form of a single sinusoid for swept-sine testing or more complex excitations including random and impulse inputs. Signal processing should be appropriate to each test and the aim of this work is to utilise the same techniques and hardware as for translational modal testing. The main considerations regarding the practical application of a measured force input and determination of the response for modal analysis of the lateral vibrations of rotating structures are relevant to experimental torsional vibration studies. Additionally, components of response due to operational excitation can invalidate regions of the measured FRFs.

This chapter describes how the excitation system developed is used successfully, with conventional modal analysis techniques for data processing, to extract the torsional modal parameters from a rotating system.

4.2 Instrumented Excitation of Torsional Vibration

A number of criteria must be satisfied for a versatile torsional vibration excitation system to be of practical use on a wide variety of rotating systems. The torque input should be of suitable frequency range and magnitude for the system under test, offering control of the amplitude and waveform for optimisation of modal test procedures. Measurement of the input torque is required to derive calibrated data and physically significant modal parameters. Application and measurement of the excitation are required to be minimally intrusive so as not to affect the dynamic behaviour and to complement the significant inherent advantages of the LTV and a single-point torque input will ensure compatibility with existing modal analysis software. The following sections describe the development of a non-contact system that addresses these requirements.

The basic principle of this excitation method is that of eddy current braking of a rotating disk with the use of electromagnets. Although the use of electromagnetic forces is certainly not new to the field of modal testing, the theoretical operation of this excitation system is complicated by the complex coupling between the physical parameters of the system. The aim of the subsequent discussion is to introduce the concept of eddy current braking, explore the limitations in modelling and demonstrate its operation in practice. It is not intended to develop a full analytical model of the system but to consider its operating principles and how these relate to the torque input and measurement of this quantity.

A schematic of the system for applying a torque to the rotating shaft assembly is shown in Figure 4.1, identifying the main components and the transfer of energy which determines its operation. It is the understanding of this complex interaction between the electrical, electromagnetic and mechanical aspects of the system that will be discussed here.

Introducing the basic operation of the torque input system, the voltage applied to the electromagnets produces a current in their coils resulting in the creation of a magnetic field. This in turn interacts with the rotating conducting disk, as described below, to apply a torque retarding its motion through the induction of eddy currents. All these factors are inter-connected through the behaviour of the magnetic field set up by the electromagnets.

4.2.1 Eddy Current Theory

Eddy currents are the result of electromagnetic induction and their occurrence can be deduced from Faraday's law or, more generally, from Maxwell's equations [4-25]. They occur in any electrically conducting component that is subject to changes in flux, as a result of time-varying excitation or motion [4-26]. The main effects of eddy currents in a conductor are heating, creation of a magnetic reaction field and the forces resulting from interaction of the inducing and reaction fields [4-27]. The first two effects result in a number of problems in the design of electrical power equipment requiring such measures as lamination of transformer cores and rotating machine armatures, to prevent the generation of large eddy currents and corresponding losses in performance.

The third effect described is utilised in a variety of electromechanical devices. Brakes based on eddy current principles are used when rapid deceleration of a flywheel is essential and where the substantial kinetic energy of the rotating masses could cause excessive component heating with alternative methods, as in reversible rolling mills [4-28] or where a constant load is required for cable unwinding or machining processes [4-29]. Eddy current clutches or couplings can provide stepless speed control over a wide range [4-29, 4-30]. Further applications of this principle include electricity supply watt-hour meters [4-31] and devices such as the homopolar generator, also known as Faraday's disk generator, which is used to generate d.c. power at low voltage and high current [4-32 to 4-34]. Some analogue electrical instrumentation meters use an eddy current damper, consisting of a light aluminium disk mounted on the indicator shaft and moving between the poles of a permanent magnet which steadies the motion of the needle for rapidly fluctuating measurements [4-35, 4-36].

Eddy currents have been used for non-contact application of forces for translational vibration testing. An exciter for light structures was developed to complement the non-contact optical measurement techniques used for vibration analysis [4-37]. The eddy currents induced in a thin conducting plate interact with the magnetic field from a permanent magnet attached to the excitation coil and apply a force to the object. This force is dependent on the material and thickness of the object and its distance from the exciter. A non-contacting electromagnetic exciter has also been developed for ferromagnetic targets [4-38]. The target material sets up its own magnetic field when placed in an external field from the exciter coil and the fields interact to produce a mechanical force. A transducer between the exciter coil and ground measured the force applied to the test structure. The exciter operation is dependent on the magnetic properties of the exciter and target and therefore small non-linearities exist in the excitation force due to hysteresis in the magnetic circuit magnetisation curve. This distorts the applied sinusoidal input current to give significant harmonics in the resulting field. The force applied is proportional to the square of the incident field, which is assumed in turn to be proportional to the coil input current. Hence, with a sinusoidal input current the measured force input consists of a constant component and one at twice the input signal frequency. Modal analysis using this device was successfully demonstrated on a small cantilever beam.

The operation of the eddy current braking system to be used here is based on the electromagnetic reaction principle, or Lenz's law, considering the force on a moving conductor in a magnetic field. The fundamental theory of its operation is well documented [4-39]. Considering the general case of Figure 4.2 a thin, conducting but non-magnetic finite plate moves through a region of uniform magnetic field $\vec{B}$ at a constant velocity $\vec{v}$. Non-magnetic in this instance implies that the relative permeability of the material is equal to that of free space, μ_0. A current density $\vec{J}$ is induced in the region of the plate in the flux and is related to the induced electric field $\vec{E}$ by Ohm's law thus;

$$\vec{J} = \sigma\vec{E} = \sigma\vec{v} \times \vec{B} \qquad \{4.1\}$$

where σ is the conductivity of the plate material. This current is directed downwards, in the direction of $\left(\vec{v} \times \vec{B}\right)$ and the circuit is completed in the less restricted, but less well defined, remainder of the plate external to the flux region. These induced eddy currents, being in a magnetic field, will transfer to the plate a magnetic force per unit volume which is;

$$\frac{\vec{F}_m}{V_c} = \vec{J} \times \vec{B} = \sigma\left(\vec{v} \times \vec{B}\right) \times \vec{B} \tag{4.2}$$

where V_c is the volume of conductor in the region of the magnetic field. If all the vectors are at right angles as shown, the magnitude of the magnetic force on the volume of plate material entering into the flux region, opposing its motion, is given by;

$$\left|\vec{F}_m\right| = \sigma|\vec{v}|\left|\vec{B}\right|^2 V_c \tag{4.3}$$

A different way to consider this effect, directly based on Lenz's Law [4-25], sees that as the section of plate enters the magnetic field and is penetrated by it, a current is generated which tries to prevent the establishment of this field. The direction of this current is such that the magnetic field produced is opposite to that of the magnet and a force results opposing the motion of the plate. As the plate conductivity is finite the induced eddy currents cannot establish a field large enough to completely cancel the imposed magnetic field as part of the energy goes into heating the plate.

Expanding this theory to the specific case used in this work, the plate of Figure 4.2 is considered to be part of a rotating disk of thickness h mounted on a central shaft and rotating at a constant angular speed Ω, as detailed in Figure 4.3. The tangential force of magnitude F_m, applied at a mean distance l from the centre of rotation, will apply a moment retarding the rotation due to the flux of magnitude B acting in an area A_m. The moment M can be derived from {4.3} as [4-31];

$$M = lF_m = l\sigma(\Omega l)B^2\left(A_m h\right) \tag{4.4}$$

A suitable arrangement of magnets to provide the magnetic field will therefore apply to a rotating disk of a shaft system what will be subsequently referred to as a retarding torque.

4.2.1.1 Previous Studies of Eddy Current Braking

The treatment of eddy current braking theory in the preceding section is sufficient to introduce the concept, although some simplifications have been made. A number of previous experimental and theoretical studies have considered the constant torque braking of a rotating disk with this eddy current mechanism. These have addressed the complex interaction between the important controlling factors, including the resistance of the current path external to the pole region, the eddy current magnetic field (or armature reaction) and skin depth effects. These effects change the torque-speed characteristics from the linear relationship of {4.4}, with increasing effect at higher rotation speeds, by altering the assumed magnetic flux through the disk in this simple case. The important points are now summarised for subsequent development of a practical excitation system. Very limited previous work could be identified concerning application of a harmonic torque with an eddy current braking system using electromagnets.

The resistance of the external current path due to a finite edge dimension of the conductor has been addressed [4-40], extending theory which was developed for a translating conducting strip [4-41] to consider thin disks at 'low' speeds. From equation {4.4} it is apparent that the torque increases with the radial pole position but, simultaneously, the outer path of the eddy currents becomes constricted by the periphery of the disk. The optimum position was experimentally determined to be at approximately 80% of the disk radius, comparing well with theoretical predictions and previous studies [4-35]. The applied torque and eddy current distribution were also predicted for a finite dimension rotating disk where two identical magnet systems are mounted diametrically opposite on either side of the shaft axis [4-42]. This avoids the unbalanced force on the disk which results from the single magnet arrangement.

Any adverse effects of the magnetic field due to the induced currents in the disk are considered negligible for braking systems with hard magnetic poles and low operating speeds [4-42]. However, this situation is complicated by the use of electromagnets to produce the exciting flux as the permeable pole pieces are subjected to a demagnetising effect, due to the magnetic field of the induced eddy currents. With increasingly high rotational speeds the effective flux rapidly decreases and the braking torque, after reaching a maximum, is seen to decrease due to this 'armature reaction'. The effect of the magnetic field due to the induced currents has been included in prediction of the force-speed and flux-speed characteristics of eddy current brakes, comparing well with experimental results [4-43]. Resistivity factors were evaluated to account for the pole dimensions and their proximity to the edge of the disk for a number of different pole configurations. Additionally, the modelling of an eddy current brake has been considered for the purposes of studying feedback control of its operation [4-44]. Non-linearities were introduced into the global system model through assumptions regarding the magnetisation curve of the electromagnetic system.

The characteristic regions of the torque-speed relationship have been defined in theoretical analysis and related to experimental studies of the air-gap magnetic field, where three different behaviour regions were observed [4-45]. At low rotation speeds the magnetic field resulting from the induced eddy currents is negligible in comparison with the exciting field. The air-gap magnetic field is then only slightly different from that at zero speed and the above expression of {4.4} for braking torque holds true. A critical speed zone is defined where the braking torque exerted is a maximum, due to the trade-off between the conflicting factors of increasing speed and reduced total magnetic field in the air-gap. Above this point, at high speed, the applied torque becomes inversely proportional to the speed as the original magnetic field between the poles is reduced by the field of the currents induced in the disk.

In addition to the magnetic field due to induced eddy currents affecting the effective magnetic field of the electromagnet, penetration of the magnetic field through the rotating disk is limited by the skin depth [4-46]. In the generalised case, a varying magnetic field incident on a non-magnetic conductor of conductivity σ will induce eddy currents on the surface which will decrease exponentially to $1/e$ of their amplitude in a distance called the skin depth δ_s. This is defined as [4-47];

$$\delta_s = \sqrt{\frac{2}{\mu_0 \sigma \omega}} \qquad \{4.5\}$$

where μ_0 is the permeability of free space and ω is the angular frequency of the incident magnetic field. Hence, if the skin depth is sufficiently small, the magnetic field cannot penetrate the conductor and this phenomenon is often used for electromagnetic shielding at high frequencies. In the case discussed in this section, with a constant (time invariant) magnetic field through the disk, the angular frequency of the field is effectively the rotation speed Ω. For the eddy current braking system the skin depth should ideally be larger than the disk thickness. This will ensure an essentially constant eddy current density with depth through the disk to maximise the braking torque applied.

This effect has been seen experimentally through braking torque measurements on a thick copper disk over a range of rotation speeds [4-48]. It is characterised by definition of a magnetic Reynolds number, based on the skin depth expression and used in previous studies as a modulus to give a non-dimensional measure of the effect of motion on magnetic fields [4-49]. For the case of a rotating disk the magnetic Reynolds number is defined, using previous notation, as;

$$R_m = \mu_0 \sigma h(\Omega l) \qquad \{4.6\}$$

At low speeds the skin depth is bigger than the disk thickness, while at high speeds it becomes comparable with the disk thickness. Experimental results were presented for the range $1 < R_m < 30$, from the negligible skin effect region to that in which it is dominant. It is deduced from skin effect theory that, as the speed of the disk is increased, the eddy currents and their induced magnetic fields tend to concentrate in a progressively thinner layer near the surface of the conductor. As for armature reaction effects, skin effect results in a loss of braking force at high speeds. The skin effect was analysed for thick disks, as found in eddy current brake dynamometers [4-50]. In prediction of the braking torque for thin disks the effective resistance and inductance of the plate remain constant at high speeds. However, if the thickness of the plate is greater than the skin depth, the resistance and inductance vary considerably at high speeds. From equation {4.6} it is apparent that this condition occurs if either the thickness or velocity of the plate are sufficiently large.

Both armature reaction and skin effects are closely related and change the torque-speed characteristics from the relationship of {4.4} with increasing effect at higher rotation speeds. The identified studies of constant torque application to a rotating disk with an eddy current brake demonstrate the complexity involved in development of an accurate theoretical model to predict the torque applied. However, experimental development of such a device should account for these factors and provide a basis for integration of these aspects into the comprehension of the complete excitation system.

4.2.1.2 Application of Electromagnets for Eddy Current Braking

For the creation of the magnetic field for the braking system it is important to consider the limiting factors that relate specifically to the use of electromagnets. Figure 4.3 shows the basic arrangement which has been used by previous researchers for eddy current disk brakes [4-44, 4-45] and the theoretical flux line pattern which results from this. In the current study two electromagnets with 'pot-type' cores as shown in Figure 4.4, originally intended for holding applications, are used to create a magnetic field to act on the rotating disk. The resulting flux pattern is more complicated than that of Figure 4.3, preventing any accurate prediction of the eddy current pattern. However, it is evident from consideration of the velocity, magnetic field and induced eddy current field vectors that, whatever the direction of the applied magnetic field, the torque acting on the disk will always retard its motion.

The magnets used were readily available and the simple mounting design is useful for alignment purposes. This allowed a basic system to be implemented for investigation of the feasibility of this technique. They are 80mm in diameter and, with 24V d.c. applied to a single electromagnet in its intended application, a maximum holding force of 2100N is stated by the manufacturers [4-51]. Additionally, the inherent magnetic force or magnetic remnance is a maximum of 5% after the supply has been removed. A system using two C-core magnets with specially wound coils was also investigated with the aim of increasing the magnetic flux and reducing the circuit inductance. However, this was found to be inferior to the arrangement shown as it was unable to create a magnetic flux of sufficient magnitude. Other electromagnet forms which are conventionally used to give high magnitude flux densities in the air-gaps of such arrangements, which might be used in the design of a dedicated system, include the use of coned pole tips to reduce the area over which the flux is acting [4-52].

The most significant problem in estimation of the torque supplied by the brake using previous expressions is determining the magnetic flux density in the air-gap of the electromagnet arrangement. For the pole system used this is not easily achieved as the magnets are outside their normal operating mode. Only a very rough estimate of the flux density can be derived based on the holding capacity of the electromagnets. The factors determining the flux density in the magnetic circuit and more importantly the air-gap region are highlighted below.

Considering the generation of a constant magnetic flux by the system, the basic operation of the electromagnets is as follows [4-53]. The application of a d.c. voltage across the electromagnet input causes a current to flow, related to the resistance of the coils. This current produces a magnetomotive force which can be defined as a magnetic field of strength *H*. The magnetic flux density *B* in the magnetic circuit can then be determined, based on the properties of the core material.

The electromagnets used have a predominantly iron core construction. This ferromagnetic material is magnetically soft allowing rapid change of magnetisation with the applied coil field and this attribute is utilised in transformers and electrical machinery. The iron core intensifies the magnetic flux inside the coil by a factor termed the relative permeability. For ferromagnetic materials the relative permeability varies considerably for different values of the applied field strength [4-53], giving a non-linear magnetisation curve which is usually obtained experimentally. The upper magnetisation limit is reached when the material domains are all orientated with their axes in the direction of the applied field and the core is then said to be saturated, restricting further increases in flux density. Additionally, the magnetic hysteresis loop of these materials results in some flux density remaining in the material after the excitation has been removed from the coil and this magnetic remnance contributes to the varying relative permeability.

However, for air there is a linear relationship between the magnetic flux density and field strength, related by the permeability of free space μ_0. Air-gaps are used in magnetic circuits to make the magnetisation characteristic more linear [4-53]. This significantly reduces the influence of all the effects related to the iron core and would allow a linear relationship between coil current and magnetic flux density between the electromagnet faces to be assumed. Therefore, although the iron in the electromagnets will contribute to the reluctance of the magnetic circuit, most of the magnetomotive force will be used to overcome the reluctance of the air-gap. The flux ϕ in a magnetic circuit is related to the flux density B and the cross-sectional area A of the circuit by;

$$\phi = BA \tag{4.7}$$

The magnetic circuit for the electromagnet system can be considered to have the iron in series with the air-gap and so the flux in the iron $\phi_i(= B_i A_i)$ is equal to the flux in the air-gap $\phi_g(= B_g A_g)$. The flux distribution under the poles is assumed to be uniform and if flux fringing in the air-gap is negligible then the flux in the gap is confined to the same cross-sectional area as in the iron, so $A_i = A_g$. Hence, the magnetic flux density is the same throughout the magnetic circuit, so $B_i = B_g$. An expression can then be derived for the circuit magnetic flux density as this is dominated by the presence of the air-gap and seen to be linearly related to the current in the electromagnet coils I [4-54];

$$B_g = \frac{\mu_0 NI}{l_g} \tag{4.8}$$

where N is the number of coil turns for the electromagnet and l_g is the length of the air-gap in the magnetic circuit. The 'ampere-turns' could therefore be determined for an ideal electromagnet to give the required value of the flux density in the air-gap B_g by ignoring the reluctance of the magnetic circuit path through the iron. This expression is the same as that for an air-cored solenoid of identical length to the air-gap, so the iron concentrates the flux at the intended point but is discounted in consideration of the circuit reluctance. Accurate measurement of the small gap length is essential for estimation of the flux density.

Limitations to this theory include the effects of leakage and fringing of the flux around the circuit. Air is not a perfect magnetic insulator, so the flux is not completely confined to the magnetic circuit, resulting in some leakage which could be approximated for. Additionally, when the magnetic circuit is interrupted by a gap, fringing occurs as the flux tends to bulge out in the gap, reducing the flux density, although for large pole-face areas and small gap lengths fringing is minimal. Its effect increases when the gap length is of the same order of magnitude as the core cross-sectional dimensions and this can be compensated for in calculations by increasing the effective cross-sectional area of the gap.

The non-magnetic, conducting disk used in the braking system has minimal effect on the magnetic circuit. It can be assumed to be replaced by air for the purposes of the magnetic theory, as aluminium has an almost identical relative permeability to that of free space, μ_0 [4-54]. Copper would work equally as well and has a conductivity over 1.6 times that of aluminium giving potential increases in applied torque. An iron-based material such as steel would work in theory to give a braking effect due to its conductivity. However, the effect of its ferromagnetism would increase the flux density in this region of the electromagnetic circuit and alter the flux-current relationship of the system. Therefore, although a torque would be applied to the disk, the linearity assumption resulting from the influence of the air-gap is no longer valid. Additional effects such as magnetic saturation of the iron would serve to prevent these simplifications from being used.

Combination of equations {4.4} and {4.8} defines the basic relationship between the electromagnet current and the moment applied to the rotating disk;

$$M = l^2 \sigma \Omega A_m h \left(\frac{\mu_0 N I}{l_g} \right)^2 \qquad \{4.9\}$$

The applied moment is therefore proportional to the square of the magnetic flux density in the air-gap and, due to the near-linearity of the magnetic circuit resulting from the influence of the air-gap, this magnetic flux is proportional to the current I in the electromagnet coils. However, due to the effects discussed in 4.2.1.1, namely resistance of the eddy current path, armature reaction and skin effect, it is necessary to determine the actual torque-speed relationship experimentally. An approximate expression for the retarding torque can therefore be stated as;

$$T = K_N I^2 \qquad \{4.10\}$$

where K_N is a speed dependent constant which is a function of the parameters in equation {4.9}. In practice, the torque input of the electromagnets would be calibrated for each rotation speed range with the constant K_N determined experimentally. The following sections demonstrate the experimental validation of this expression and the problem is compounded by the application of a harmonic torque input as discussed in Section 4.2.2.

4.2.2 Application of a Time-Varying Input to the Electromagnets

The subsequent discussion considers the application of a harmonic torque input with the eddy current brake. This highlights the differences with the constant torque case and introduces those concerns specific to this situation through consideration of fundamental theory governing the system behaviour. Following the structure of Figure 4.1, which showed the inter-related aspects of the torque input system, this section will discuss the use of the electromagnets to apply a harmonic flux to the rotating disk. By applying a time-varying voltage to the coils the magnetic field through the disk varies with time, applying a fluctuating torque to the shaft system. Development of a comprehensive analytical model of the excitation system for a harmonic voltage input is beyond the scope of this work and very limited prior research has considered problems with both time-varying magnetic flux and motion of a conductor.

In addition to the system behaviour with a time-varying magnetic field applied to the excitation disk, the sinusoidal current in the electromagnets has important effects. It is therefore necessary to discuss the operational characteristics of this aspect of the excitation system to consider the relationship between the voltage input to the electromagnets, the current in the coils and the generated magnetic flux. The operation of the electromagnet system under the influence of a sinusoidal input can be considered in two main areas; inductor behaviour and modelling of the electromagnet impedance.

4.2.2.1 Inductor behaviour

The electromagnet system is effectively an inductive component with a large ferromagnetic core. Although the presence of the iron in magnetic circuits generally causes the relationship between flux and current to be non-linear, the inclusion of the air-gap between the two halves of the system serves to linearise this, as discussed in this section. The arrangement of the two connected electromagnets will be considered as a single component and the lumped parameters discussed include all effects of the magnetic circuit and the mutual inductance of the two coils.

For pure inductance L in a single-phase a.c. circuit, the current I resulting from application of a sinusoidal voltage V of frequency f is as follows [4-55];

$$I = \frac{V}{2\pi f L} = \frac{V}{X_L} \qquad \{4.11\}$$

where X_L is the inductive reactance and is seen to be proportional to frequency. However, the electromagnet inductor system is not a pure inductance because of the resistance of the coils and the relative permeability of the ferromagnetic core.

If a simple coil is wound on a ferromagnetic core, the non-linear relationship between magnetic flux density and field intensity causes the current in this inductor excited by a sinusoidal input voltage not to be purely sinusoidal [4-56]. These losses in the energy supplied to the inductance are usually lumped together but can be split into two main components for which empirical expressions have been derived [4-26]. Hysteresis loss is due to power dissipated as heat in the core material due to the work done in reorienting the magnetic moments of the material. Eddy current losses occur as a result of the currents induced in the core material by the alternating flux from the coil. However, it can be assumed that when a sinusoidal voltage V is applied to this simple coil, a sinusoidal flux ϕ is established in the magnetic circuit and the flux linkage of the coil of N turns is [4-56];

$$\Lambda = N\phi \qquad \{4.12\}$$

This induces an e.m.f. that is essentially equal to the applied potential difference. The time-varying exciting current in the inductor I_e is determined from the ferromagnetic properties of the core configuration and material. Thus, the waveform of the current in the coil can be derived from the flux linkage versus exciting current $(\Lambda - I_e)$ relationship loop for the core and winding. At low frequencies this loop is predominantly the same as the magnetisation characteristic (*B-H*) loop for the core but at higher frequencies it is broadened by the effect of eddy currents induced in the core material. The main result is that the steady-state current waveform consists of the fundamental and smaller magnitude harmonics.

With the electromagnet system proposed in the work reported here the dominating influence of the air-gap which determines the reluctance of the magnetic circuit, with the non-magnetic disk used in the excitation system as discussed in Section 4.1.2.2, gives an approximately linear relationship between applied current and flux linkage. This magnetisation curve implies that both the flux in the air-gap and the coil current can be assumed to vary sinusoidally with the applied voltage. This linear behaviour of the magnetic circuit should be apparent in experimental results with little distortion of the current waveform. Although it was assumed that a sinusoidal flux was created by a sinusoidal input voltage no attempt was made to measure it in this study. Validation is implied by the single frequency harmonic torque excitation applied to the excitation disk.

The phasor diagram of Figure 4.5 shows the relationship between the applied voltage V and the fundamental component of exciting current I_e for the electromagnet system, neglecting any resistance of the coil windings [4-56]. This is related to the flux linkage of the coil Λ and hence flux ϕ in the air-gap of the magnetic circuit as shown. The current I_e lags the applied voltage by less than 90° and leads the resulting flux ϕ and can be resolved into two components, I_c and I_m. I_c represents a sinusoidally varying current in phase with the applied voltage, accounting for all the power dissipated in core losses. I_m represents a sinusoidally varying current in phase with the flux which lags the applied voltage by 90° and the supply current by phase angle ψ.

The impedance of the electromagnetic system was measured experimentally in order to demonstrate the factors discussed. This was achieved by monitoring the voltage applied to the coils and the resulting current in the circuit. A 'pseudo-random' broad-band input for the frequency range under consideration was applied and a spectrum analyser used to derive the system impedance as a transfer function of the two parameters. Measurements were taken for a series of rotation speeds throughout the operating range. The results are shown in Figure 4.6 and as expected the impedance magnitude and phase increase with frequency, due to the changing resistance and reactance of the system. In addition, the impedance is seen to change in profile with rotation speed, due to the interaction of the electromagnets and rotating disk. This data is used in subsequent estimation of the current components in the electromagnet circuit.

The electromagnet system used in this study is not ideally suited to this application due to the large impedance and the losses associated with the large iron core. Possible improvements include laminated electromagnet cores to reduce eddy current losses, constructed of material specifically designed for a.c. applications with a narrow hysteresis loop. Similar issues have been addressed in the development of a non-contact electromagnetic exciter for translational modal analysis and strategies were proposed to compensate for the non-linearity of the magnetisation curve [4-38]. The system could be linearised by reducing the current and therefore operating on a small part of the characteristic curve. Alternatively, the magnetisation curve could be measured and this data used in a computer-controlled system to develop the required coil excitation input to give a sinusoidal magnetic field.

4.2.2.2 Modelling of the Electromagnet Impedance

In order to analyse the behaviour of the electromagnets a simplified model of the coil impedance parameters can be used. A suitable approach in common use [4-56] proposes a number of assumptions which give a sufficiently accurate representation of a 'real' inductor and the equivalent circuit of the model is shown in Figure 4.7a. The resistance of the coil windings, which was neglected in the preceding section, is included in the lumped resistive element R_w to account for the energy dissipated in power losses as heat. The ferromagnetic cores of the electromagnets introduce hysteresis and eddy-current losses into the system. As discussed previously, if the flux linkage of the coil and its exciting current are sinusoidal, the exciting current I_e can be resolved into a magnetising component I_m and a core loss component I_c, which are shown in Figure 4.7a. For the equivalent circuit, this loss can be attributed to a purely resistive element R_c in parallel with a purely inductive element X_m which carries the fundamental magnetising current. The magnetic flux in the air-gap which acts on the disk is assumed to be proportional to this magnetising current component.

In Figure 4.7b the inductor model is shown in series form with the lumped resistive and reactive elements R_{AB} and X_{AB} which are equivalent to the parallel form of Figure 4.7a. The real and imaginary parts of the experimentally measured electromagnet impedance from Figure 4.6 could be equated to these elements of the impedance model, as the total impedance of the electromagnet circuit in complex notation is given by;

$$Z = (R_w + R_{AB}) + jX_{AB} \qquad \{4.13\}$$

Rearrangement of these circuit parameters into the parallel form of Figure 4.7a allows expressions for the resistive core element and the inductive element to be stated;

$$R_c = R_{AB} + \frac{X_{AB}{}^2}{R_{AB}} \qquad \{4.14a\}$$

$$X_m = X_{AB} + \frac{R_{AB}{}^2}{X_{AB}} \qquad \{4.14b\}$$

This permits theoretical estimation of the supply current and the current in each branch of the model inductor circuit, the inductive component and the loss resistance, from the phasor relationships between applied voltage, impedance and current.

Figure 4.8 shows the estimated supply current I_e which passes through R_w, using the experimental electromagnet impedance measurements in this inductor model, for the shaft rotating at 1000rpm for a 60V (pk-pk) sinusoidal input across the frequency range. This branches into the two circuit elements, R_c and X_m, and can be compared with an estimate of the magnetising current I_m in the reactive element X_m. There is close agreement between the magnitudes of I_e and I_m although it is obvious that the phase lag of the magnetising current relative to the input voltage increases with frequency more rapidly than the supply current. At the maximum frequency of 100Hz the phase lag of the magnetising current relative to the supply current, which will subsequently be labelled ψ, is approximately 20°. For the full range of rotation speeds considered, the phase of the magnetising current was predicted to lag the supply current by 32.5° at 200rpm, decreasing with increasing speed to 19.8° at 1200rpm.

The variation of supply and magnetising currents with frequency can be attributed to the behaviour of the lumped parameters. It is apparent that the phase lag of the magnetising current relative to the electromagnet supply voltage is not equal to 90°, as was discussed for the basic model of Section 4.2.2.1. This is due to the voltage drop across the winding resistance R_w, so in this case it lags the voltage across AB by 90° which changes phase with the supply voltage with frequency due to the changing relative values of the lumped parameters. The resistive core losses at low frequencies are much smaller than the winding resistance so the current in the electromagnet I_m establishing the field is approximately the same as the overall current value I_e. However, with increased frequency the impedance of the coil system increases, decreasing the overall current drawn from the supply and, in turn, the magnetic flux incident through the disk with implications for the torque applied. The resistive core losses are also seen to increase until they are increasing at a similar rate to the reactance. Therefore the phase of the impedance changes very little at high frequencies as seen in the experimental results of Figure 4.6. Neither the core loss resistance nor the impedance of the electromagnet system were seen to be linear functions of frequency.

4.2.3 Eddy Current Braking with a Time-Varying Flux

Differences in the eddy current braking mechanism will now be discussed which occur due to the application of a time-varying flux by the electromagnets. This results in a fluctuating torque being applied to the excitation disk and builds on the valid assumptions of the constant torque case.

The mechanism by which eddy currents are induced in the disk remains the same but the potential complication to the excitation system operation is in the magnitude of torque generated. The expression developed for the steady-state case in {4.4} considers the application of a time-invariant magnetic field. However, Faraday's law of electromagnetic induction for moving circuits fundamentally considers the electromotive force (e.m.f.) induced when a general closed conducting loop C moves with velocity $\bar{v}$ in a time-varying magnetic field $\bar{B}$ [4-25]. The induced e.m.f. V_{ind} around the loop which encloses a surface S is derived by considering contributions by the surface element $\mathrm{d}\bar{S}$ due to the movement of circuit element $\mathrm{d}\bar{l}$. In a conductor this e.m.f. causes a current to flow which, for the experimental system under consideration, is described as an eddy current. For the general case, integrating over the entire circuit C derives the following expression;

$$V_{ind} = -\int_S \frac{\partial \bar{B}}{\partial t} \cdot \mathrm{d}\bar{S} + \oint_C \bar{v} \times \bar{B} \cdot \mathrm{d}\bar{l} \qquad \{4.15\}$$

This is obtained from the total rate of change of flux linkage for the loop in which there are separate contributions due to the time-varying field and the relative motion between the conductor and lines of flux. These are known respectively as transformer and motional e.m.f.s and in the general case both must be included to derive the total induced e.m.f. [4-57 to 4-59].

The first term of {4.15}, the transformer e.m.f., occurs where a rigid stationary circuit has a time-varying magnetic flux passing through it. This is independent of the conductor motion, depending only on the rate of change of flux, so the conductor can be assumed to be stationary. The second term considers the motional e.m.f.s which are induced where a circuit, in whole or part, moves in a magnetic field and cuts the flux, independent of the space variation of the flux. This depends only on the instantaneous flux density and it is assumed at that instant that the flux density and velocity are constant. From the general statement of {4.15} the time-invariant flux case of Section 4.2.1 can be derived, where only the motional e.m.f. is present. Motional effects give rise to the electric field which is observed in the moving frame of reference of the conductor and known as the Lorentz field [4-60]. This results in the previously discussed force on the conducting disk as it moves through a constant magnetic flux. Lenz's law can be used to define the directions of each of these effects and states that induced currents, which flow when an induced voltage is present, produce magnetic fields which oppose the changing flux through the circuit [4-25].

The physical system for the induction of an e.m.f. consists of a mutually inter-linked electrical and magnetic circuit. When the circuit moves through a time-varying flux both types of e.m.f. are induced and superposition can be used as there is a linear relationship between the induced e.m.f. and magnetic flux for each. The two effects are usually considered in isolation due to the complications arising from the co-ordinate systems in use. The induction of eddy currents by these two mechanisms has been introduced in previous theoretical treatment of the subject, although with only limited consideration of motional currents [4-61]. For the torque input system used here, the e.m.f. induced by the magnetic field drives currents through the conducting disk material proportional to the conductance of the circuit, which in turn interact with the applied magnetic field to give the braking torque. The full relationship between the torque and a harmonically varying flux applied to the disk depends on the direction and relative magnitude of each effect, which can contribute differently to the resultant eddy current distribution in the disk, depending on the rotation speed and frequency of excitation. In the case considered here there is superposition of the two induced e.m.f.s both temporally and spatially, which would necessitate substantial development of {4.15} to model the system. Application of this general expression is not straightforward in practical situations without a definite closed contour. To consider the e.m.f. induced and resulting force on the conductor it is necessary to define carefully the region in which the induction occurs.

Theoretical consideration of problems of this nature, with both induced transformer and motional e.m.f.s, has been extremely limited due to the inherent complexities in developing a comprehensive understanding of the simultaneous occurrence of these two effects. It is therefore difficult to identify examples which clearly demonstrate the phenomena involved. Theoretical treatment of a similar situation considered a Faraday disk generator with a time-varying magnetic field applied across its whole area [4-62]. It was demonstrated that both components of e.m.f. are generated in the disk, but the transformer e.m.f. was seen to be entirely circumferential and so would have negligible influence on the braking effect in our application. Another example is that of a 'cup-motor' with a.c. excitation of the main winding, for which the flux distribution and generated torque were calculated [4-63]. However, the field-rotor arrangement used for that case with a uniform current pattern assumed in the rotating cylinder results in a significantly different system to that considered in this work.

It was demonstrated in Section 4.2.1 that the motional e.m.f. induced will have a radial direction in the region of the magnet poles with the circuit completed in the remainder of the disk. The currents resulting from the transformer effect will be predominantly confined to the pole region and in a circulatory sense, attempting to oppose the changes in magnetic flux which are occurring [4-34]. A rough estimate of the current flow pattern in the disk may be possible but it is extremely difficult to ascertain how the two induced currents will interact. Additionally the electromagnet pole configuration used in this experimental system will further complicate the resultant eddy current pattern in the three-dimensional situation under consideration.

The eddy currents induced within a non-magnetic conductor when an alternating time-varying magnetic field is applied tend to cancel the magnetic field within the conductor and therefore increase its effective resistance to current flow and magnetic field penetration. This is known as the skin effect and the skin depth related to transformer-induced e.m.f.s can be calculated in a similar manner to that described for motional e.m.f.s in Section 4.2.1.1 [4-46]. For a magnetic field with a frequency of 100Hz incident on an aluminium surface the skin depth is 8.3mm. For the frequency range of interest and the disk thickness used later in the experimentation (5mm), these currents will not cause the disk material to exhibit magnetic shielding effects, which would impair the performance of the torque excitation system. In addition, eddy currents are only induced in the region local to the magnets with the experimental arrangement in use, so different 'circuits' of the plate material are subjected to this influence as the disk rotates. Further investigation would require accurate modelling of the eddy currents induced in the rotating disk and this is not known to have been achieved previously.

Therefore, for the time-varying eddy current braking considered here, the transformer e.m.f. will be discounted as it is assumed that the direction and magnitude of these components will not significantly affect the braking force generated. The motional e.m.f., which has a radial direction in the disk section between the electromagnet magnet poles, therefore dominates the braking mechanism. Experimental results in subsequent sections reinforce the assumption of negligible effect of transformer e.m.f.s. on the braking torque.

The simple expression of {4.4} can therefore be used in derivation of the torque generated by the system, based on only the motional e.m.f.. If the magnetic flux incident on the section of disk in the air-gap is considered to be sinusoidal;

$$B = B_0 \sin \omega t \qquad \{4.16\}$$

then the moment applied to the disk can be derived from {4.4} as;

$$\begin{aligned} M_h &= \left(l^2 \sigma \Omega A_m h\right)\left(B_0 \sin \omega t\right)^2 \\ &= \left(l^2 \sigma \Omega A_m h B_0^{\ 2}\right)\left(\frac{1-\cos 2\omega t}{2}\right) \end{aligned} \qquad \{4.17\}$$

With the practical system described, application of a sinusoidal voltage across the electromagnet coils applies a retarding moment, or torque, to the disk with a steady-state component and a component at twice the frequency of the applied voltage. This is evident from consideration of the flux, eddy-current and velocity vectors so, whatever the polarity of the magnetic field, the torque acting on the disk is always retarding the disk rotation. As a result the torque applied by the excitation system does not exactly parallel use of a conventional electrodynamic shaker in translational modal analysis due to the d.c. component in the force. It is assumed that this constant torque does not detrimentally affect the torsional vibration response of the shaft system and the excitation device provides excitation for the purposes of modal analysis as required. The occurrence of a d.c. offset in the input signal, in addition to the fundamental frequency, will cause the torque input to have a component at the fundamental frequency together with the d.c. and twice fundamental frequencies determined from equation {4.17} [4-38].

Although the discussion up to this point has been primarily concerned with the application of a single frequency sinusoid to the rotating assembly under test, the device has the potential for creation of a variety of input torque functions. These can follow the form of conventional modal analysis utilising swept-sine or broad-band inputs, speeding up the test procedure and improving the versatility of the technique as an experimental tool.

4.2.4 Measurement of Torque Input to the Shaft System

The potential of the electromagnetic system has been introduced theoretically as a means of creating a controllable and measurable torque input to a shaft system. For practical torsional modal analysis, accurate measurement of the applied torque is required. Methods to achieve this will be discussed in this section, for both validation of the excitation system and its subsequent use in torsional vibration testing of rotating shafts.

The theoretical relationship between the torque applied to the shaft system, the magnetic flux in the air-gap and the current in the electromagnet coils has been defined;

$$T \propto B^2 \propto I^2 \qquad \{4.18\}$$

Experimentally it is possible to measure any of these three quantities and hence obtain a signal proportional to the torque applied to the shaft system. Similar methods have been used for active magnetic bearings (AMBs) used to apply excitation to rotating shafts for translational modal analysis, discussed in Section 4.1.1 [4-9 to 4-12]. All of these approaches have inherent disadvantages to be addressed in development of this concept.

4.2.4.1 Torque Measurement

Ideally, measurement of the actual torque applied to the shaft system would be the best approach. However, using conventional transducers it is difficult to measure the torque input applied by this non-contact system to a rotating shaft system, although two possible methods to achieve this can be identified. An in-line torque transducer inserted into the shaft system, such as the systems discussed in Section 2.1, can be used to measure the torque in a section of the shaft and the applied torque derived from this. Alternatively, by mounting the electromagnet system bracket with a transducer between it and ground, measurement of the reaction on the magnets can be used to infer the dynamic moment applied to the system.

Complications exist in the practical application of either of these systems. In the first instance, mounting of an in-line shaft torque transducer necessitates modification of the rotating system under test. Additional requirements of transferring the measurement from the rotating system to the signal processing hardware impose operational restrictions.

More significantly, for a shaft system with 'free-free' boundary conditions, the torque measured by an in-line shaft transducer is derived from the 'twist' in this section of shaft and will not be equal to the torque applied. The total torsional vibration response of the shaft system is the sum of the roll and twist components of the forced vibration. The roll component is due to the rolling oscillations of the system which behaves as though it were a rigid body. This effect is the same at all points in the system and produces no twist and therefore no stress in the shaft.

As an example of this effect, the response of a rotating system was measured simultaneously with two LTVs and an in-line torque transducer, using the torque applied by the eddy current excitation system. The experimental shaft system is shown in Figure 4.9 and is discussed in detail in Section 4.3. The LTVs were arranged to measure the torsional vibration response of the two inertias either side of the transducer at location X-X. Measurements from the three instruments were taken with the excitation frequency fixed at a series of discrete values across the range of interest, with a constant magnitude applied voltage for the duration of the test. The results for one rotation speed are presented in Figure 4.10 and the first natural frequency of the system is clearly apparent at approximately 24Hz. The torque measured in the shaft by the torque transducer can be converted to the twist over the shaft section between the two rotors, which included the transducer, from the known stiffness of this section. This compares very well across the frequency range with the relative twist value determined from the difference between the measurements taken by the two LTVs. The total torsional vibration response of the shaft system is measured by the LTVs and is the sum of the roll and twist components of forced vibration. The roll component is seen to dominate the LTV measurements at low frequencies but is not measured by the torque transducer.

This was further confirmed by examining the forced vibration response of a simple lumped parameter model of this system to show that for a free-free system the torque measured by an in-line transducer, which measures the system response, is not equal to the applied torque. The simple shaft system of the experimental rig was modelled assuming lumped parameters for the shaft stiffness and inertias, in the manner detailed in Appendix B. Figure 4.11 shows the estimated shaft torque in each of the two shafts per unit applied torque across the frequency range. Below the first natural mode the torque which would be measured in the shafts is less than the applied torque due to the 'roll' effect of the free-free system. Hence, to ascertain the actual torque applied to a system from the in-line transducer value it is necessary to know the factor by which the applied and shaft torques differ, either from a suitable model or appropriate testing.

The second torque measurement method suggested infers the torque applied through measurement of the reaction on the electromagnets. This is analogous to the arrangements used for measurement of the applied force with a non-contacting electromagnetic exciter for ferromagnetic targets [4-38] and AMBs for translational excitation of rotating shafts [4-9]. Practical considerations would need to be addressed with regard to the mounting and transducer arrangements to be used. This could be achieved by mounting the electromagnets appropriately on a force transducer to measure the tangential reaction. However, for a single magnet pair applying the torque input, as used in the later experimental situation with only approximate prediction of the flux pattern incident on the disk, estimation of the moment arm introduces a considerable degree of uncertainty into the measurement. A possible redesign of the torque input system would utilise two pairs of electromagnets diametrically spaced around the rotating disk to apply a pure couple to the shaft system. Such an improvement would be complemented by the use of force transducers measuring the reaction on each electromagnet. The applied couple would be accurately estimated from the product of the force transducer outputs and the distance separating the transducers. Alternatively, a dedicated torque transducer could be utilised to measure the couple, such as the piezoelectric quartz devices currently commercially available [4-64] and such arrangements should be considered in subsequent development of this technique.

4.2.4.2 Magnetic Flux Measurement

Measurement of the magnetic flux in the air-gap could also be used to infer the torque applied to the shaft system. This could be achieved with the use of a Hall effect sensor inserted into the air-gap of the electromagnet system to give a signal representative of the flux acting on the disk. Real-time processing of the flux measurement would be necessary to obtain a signal representative of the applied torque. However, modification of the electromagnets would be required to incorporate this sensor into the magnetic circuit air-gap between the core and the disk, while increasing the air-gap length to accommodate this would reduce the torque applied.

4.2.4.3 Electromagnet Supply Current

In Section 4.2.2 the magnitude of supply current in the electromagnets was demonstrated to be approximately proportional to the flux through the rotating disk. This is a result of the relatively large air-gap in the magnetic circuit linearising the current-flux relationship and minimising the effects of hysteresis and core saturation. Furthermore, for torsional motion a constant air-gap is maintained which ensures that the relationship remains linear. The electromagnet supply current therefore provides a valid measurement for non-contact estimation of the torque applied to the shaft system.

The similarity in the magnitudes of the supply and magnetising currents in the electromagnet model allows use of the assumption that measurement of the supply current I_e will give a value approximately equivalent to the magnetising current I_m. This is assumed to be proportional to the magnetic flux density acting on the disk and, therefore, allows the simple relationship of equation {4.10} between the torque and current to be preserved. A straightforward measure of the harmonic torque input to the shaft system can be derived through processing of the measured current to give a signal proportional to its square. This is achieved in the practical system described later with a simple electronic circuit, calibrated appropriately.

However, the magnetising component of current does have a phase lag ψ with respect to the supply current, which increases with frequency as previously shown in Figure 4.8b. As torque is proportional to current-squared there will be a phase offset apparent in frequency response functions derived using this system of magnitude 2ψ. Additionally, at high frequencies there will be an over-estimate in the magnitude of torque applied. This is because the magnitude of magnetising current, and hence applied flux, is a factor of $(\cos\psi)$ smaller than the supply current, as shown in Figure 4.8a. The magnitude of the actual applied torque is therefore smaller than the value estimated from the supply current by the factor $(\cos\psi)^2$. Future refinement of the technique could 'map' the relationship between I_e and I_m with frequency and use this to improve the applied torque estimation.

These restrictions are out-weighed by the simplicity of deriving a measure of the torque input in this way. Therefore, measurement of the electromagnet supply current will subsequently be used for non-contact measurement of the torque applied to the shaft system. A low resistance shunt (0.1Ω) was used in the electromagnet supply circuit for the current measurements.

For validation of this method of obtaining a measure of the torque input it was necessary to have an independent measure of the applied torque for comparison. For the experimental arrangement considered here the use of an in-line torque transducer was seen to be the simplest arrangement. However, as discussed in Section 4.2.4.1, for consideration of the actual applied torque it was necessary to use an appropriate factor to correct the measurement. The operation of the torsional excitation system could then be studied when applying a controllable torque to a rotating system.

4.3 Experimental Test-Rig

The experimental rig, designed to be as versatile as possible for use in subsequent studies, is shown in the photograph of Figure 4.12 and consists of three inertias connected by elastic shafts and incorporates the electromagnetic exciter introduced above. A detailed sketch of the shaft system is shown in Figure 4.9 together with the main dimensions of this assembly. The shaft system will be driven at a range of rotation speeds with the drive system isolated from the main shaft to prevent transmission of unwanted torsional vibration. An LTV can be used to measure the induced torsional vibration, with easy access to the measurement points. Versatility is also required to allow attachment of torsional vibration absorbers for later studies. The rig should be free from any influence of other forms of vibration which might affect the measurements.

The excitation system makes use of an aluminium disk that is part of the shaft system under test. Two electromagnets are mounted on either side of this conducting disk, as detailed in Figure 4.4, so that the disk rotates in the air-gap between the poles of the electromagnet system. The magnetic flux is set up in the axial direction between the magnetic poles. The electromagnets are mounted on rigid aluminium support brackets, with the intention of minimising any interference or leakage within the magnetic circuit. These were set to hold the electromagnet pole faces parallel to the rotating disk. Two sheets of packing material, 0.30mm thick, were then used to set the magnet pair to be as close to the disk as possible without striking it when rotating. The brackets were aligned to set the centre of the magnet poles at the distance estimated to give maximum braking torque, as described in Section 4.2.1.1 and determined from previous studies [4-40]. The main dimensions of the electromagnet arrangement, shown previously in Figures 4.3 and 4.4, are detailed in Table 4.1.

Table 4.1: Practical dimensions of electromagnet arrangement

Parameter	Quantity	Measured value
Excitation disk diameter	D	340mm
Radial position of magnets	l	120mm
Electromagnet diameter	d_m	80mm
Disk thickness	h	4.80mm
Air-gap between magnets (incl. disk)	g	5.40mm

The shaft dimensions and inertias of the system were determined simultaneously in order to design the optimum arrangement for the required tests. The shaft had to be of sufficient diameter for the LTV to be used without performance limitations, whilst not too torsionally stiff. Approximate estimation of the torque generated by the magnet system considered the resulting deflection of the shaft to ensure this would be within the measurement range of the LTV. Physical limitations of the maximum length of the shaft and diameter of the inertias were defined to give a practical design. Additionally, the torsional natural frequencies of the rotor-shaft system were calculated so these were within the estimated excitation range of the eddy current system for later studies.

The excitation disk was aluminium as discussed in Section 4.2.1 while the central inertia and flywheel were steel. Mechanical details of the inertia disks required a simple hub for mounting onto the shaft, with pins fixing the two together. This would eliminate the possibility of wear at these connections affecting the torsional vibration behaviour.

The drive motor was selected to have sufficient power to drive the shaft system accounting for frictional losses and the operation of the torque input system. This was a 0.5hp d.c. motor universally wired, with a variable speed controller giving a no-load speed range of approximately zero to 1400rpm. A rubber belt and pulley arrangement is used to couple the shaft to the motor, providing the rotational drive input and isolating the shaft from any torsional vibration of the motor. Additionally, for modal analysis testing this should ensure that the imposed boundary conditions of the shaft approximate the 'free-free' case.

Self-lubricating pillow block type bearings with locking collars were selected for the application, requiring little maintenance. Six have been positioned along the shaft to minimise any whirling motion in the operating range and ensure accurate alignment of the rotating assembly. Sleeve couplings are provided on the central section of the shaft. These will facilitate the removal of this section for insertion of a torque transducer at point X-X in Figure 4.9. The bearings were mounted onto the raised platform on the frame of the apparatus, shown in Figure 4.12, which was rigid enough that any foundation vibration problems would be negligible. The drive motor was fixed to the base of the apparatus and the complete assembly was mounted on an 'anti-vibration' table to isolate any vibration transmitted through the floor.

For accurate, independent measurement of the shaft rotational speed, a tachometer system was used. This consisted of an opto-switch which monitored the passing of a white stripe on the flywheel once per revolution. The signal from this was converted to a TTL pulse for connection to the input of a spectrum analyser with a tachometer counter.

4.4 Experimental Investigation of the Torsional Excitation System

The theoretical background of the eddy current braking system has been discussed in previous sections for the creation of a controllable and measurable torque input. The next step is to demonstrate experimentally the application of a torque to a rotating shaft system with this excitation method and examine the relationship between electromagnet current and torque input for validation of the predicted behaviour. Initially, the input of a d.c. voltage to the electromagnets to give constant torque eddy current braking is explored. The application of a controlled harmonic torque to a shaft system with this system is then addressed, followed by calibration of the selected torque measurement method.

4.4.1 Constant Torque Input

For initial examination of the torque input of the system, a series of tests were carried out with a d.c. input to the electromagnets. For this constant torque input, with continuous drive applied by the motor, the measurement obtained from the in-line torque transducer mounted in the central shaft is equal to the torque applied by the braking system. The voltage drop across the shunt in series with the electromagnet circuit was used to measure the current drawn. Initial tests with the electromagnets connected with the same polarities, demonstrated that no braking effect was observed when the input voltage was applied. In this case the fields from the two magnets do not give a resultant flux which penetrates the disk. The eddy current braking effect was only seen to occur when the electromagnets have opposite polarities, confirming the approximate flux pattern of Figure 4.4b.

Figure 4.13 shows the torque applied by the braking system, after the effects of frictional torque have been accounted for, for a range of input voltages across the speed range. The limited linear region consistent with the relationship defined in equation {4.4} occurs below the lowest measurements obtained, at 200rpm. For the experimental results the torque increases with speed up to a maximum at approximately 400rpm and diminishes after this. The disk is rotating at relatively low speed, with magnetic Reynolds number $R_m = 3.45$ at a maximum speed of 1300rpm. Therefore this behaviour can be attributed to the effect described previously as armature reaction.

Considering the relationship between torque and current proposed earlier in equation {4.10}, the logarithms of each quantity at each speed were plotted from which the constant of proportionality K_N and the power index of the torque-current relationship can be determined. From this analysis the power index of the current was seen to be equal to $2.00 \pm 1.0\%$, confirming validity of this expression. Figure 4.14 shows the normalised torque, $\left(T/I^2\right)$, calculated from these results for the speed range covered and the proportionality constant K_N derived as above, which is therefore only a function of the rotation speed.

The temperature of the disk was considered to see if this would have a significant effect on the operation of the torque input system, through changing the conductivity of the material. In previous experimental studies of eddy current disk brakes, consistent results were obtained by avoiding large temperature fluctuations during tests [4-45]. Following initial measurements with 10V d.c. excitation and the steady-state temperature of the disk at 19°C, a series of tests was performed over 40 minutes as the excitation voltage was gradually increased to 25V. At this time the maximum disk temperature had risen to 42°C with a decrease in K_N of 2.34%. A number of factors can be related to this change, which is smaller than might be expected. The resistance of pure metals increases with temperature in accordance with the temperature coefficient of resistance, which for aluminium is 0.004 at 20°C, defining a 0.4% increase in resistance per °C rise in temperature [4-65]. However, the 8.4% decrease in conductivity estimated from this was not reflected in the K_N values. It is proposed that the conductivity decrease causes a corresponding decrease in eddy current magnitudes which reduces the effect of their magnetic field on the electromagnets, partially compensating for the reduced conductivity in producing the braking torque.

Other related concerns include heating of the electromagnet coils which will increase their resistance and result in a decrease of supply current. However, temperature measurements on the magnet casing showed only a 4°C rise over the duration of the previous test. From these results it can be concluded that small temperature variations of the disk will not be a significant factor in the torque-current relationship for the system, although every effort will be made during subsequent measurements to attain steady-state temperature conditions.

The constant (d.c.) operation of the torque input system has therefore been demonstrated to behave as discussed theoretically. The torque applied to the excitation disk of the shaft assembly was confirmed to be proportional to the square of the current input to the electromagnets as proposed in equation {4.10} and the speed-dependent constants of proportionality were found.

4.4.2 Application of a Harmonic Input

The behaviour of the torque excitation system with a harmonic voltage applied to the electromagnets was then investigated experimentally. A schematic of the equipment used for input and measurement of this signal to the electromagnets during the subsequent experimental work is detailed in Figure 4.15.

Initial results to demonstrate the operation of the system consider the application of a sinusoidal voltage to the electromagnets, exploring the resulting current and torque applied to the rotating disk. Figure 4.16 shows the time trace of the voltage applied to the electromagnets and the current flowing in the circuit, with the shaft rotating at 1000rpm and a 5Hz sinusoidal voltage 60V (pk-pk) input. The supply current has a phase lag with respect to the applied voltage as a result of the impedance (resistance and reactance) present. As discussed in the preceding sections, this impedance increases with frequency so the current in the electromagnets, and hence the applied torque, decrease as the frequency of excitation is increased. The current waveform is very close to that of a sine wave, confirmed by examining these signals in the frequency domain. This reinforces the assumption of minimal effect due to the magnetisation curve of the electromagnet system, so a predominantly sinusoidal flux should pass through the disk.

Figure 4.17 shows the spectra of the current input to the electromagnets and the resulting torque measured in the shaft. The fundamental excitation frequency is clearly apparent in the current spectrum, with components other than the fundamental more than two orders of magnitude smaller. The fundamental shaft torque frequency is twice the applied signal frequency as discussed in Section 4.2.3. The first part of this experimental study will consider the relationship between these two parameters in greater depth. The much smaller harmonics of this torque input confirm the validity of the assumption of a sinusoidal flux created by the electromagnets, with minimum distortion by their magnetic characteristics. Other torque components measured in the shaft not due to this controlled input are approximately 20dB lower and result from the rotation of the shaft system.

4.4.3 Experimental Study of Torque-Current Relationship

This section investigates the experimental operation of the torque input system, to demonstrate the application of a controllable torque to a rotating shaft system and to prove the linear relationship between applied torque and current-squared for a harmonic input.

To examine the dynamic operation of the technique, measurements were taken for two excitation frequencies, 1.5Hz and 3Hz, both of which were well below the first non-zero natural frequency of the shaft system. The shaft torque can be measured from this flat region of the response curve, where the excitation and response are in-phase below the dynamic magnification effect of the first resonance. The applied sinusoidal voltage covered the amplitude range 0 to 60V peak-peak, with rotation speeds from 200rpm to 1200rpm. For each situation the electromagnet current, at the fundamental applied frequency f, and the magnitude of torque components, both d.c. and a.c. (at frequency $2f$), were recorded. For a system with free-free boundary conditions, the shaft torque measured with an in-line torque transducer is not equal to the torque applied to the system. A factor determined from the lumped parameter model discussed in Section 4.2.4.1 was used to correctly derive the a.c. component of input torque, relating the measurement in this section of shaft to the actual torque applied by the electromagnet system.

From these experimental results the relationship between the torque and current was considered, in accordance with equation {4.17} to account for the d.c. and a.c.

components of the applied torque correctly. Figure 4.18 shows a plot of log(T) against log(I) for one example speed, for both these applied torque components. As seen for the constant torque results the relationship is linear, from which the constant of proportionality K_N and power index of the torque-current relationship can be obtained. This was carried out for all of the speeds considered and the power index in each instance, for both d.c. and a.c. components was equal to 2.00 within limits of +/-2.5%. This experimentally verifies equation {4.10}, which states that torque is proportional to current-squared, for the application of a harmonic torque excitation. This also confirms consistent operation of the braking system in accordance with the relationship stated in equation {4.17}. This considers the a.c. and d.c. components resulting from a harmonic voltage input as the applied torque is proportional to the square of the magnetic flux in the air-gap and hence current in the electromagnets. The estimates of the constant of proportionality K_N obtained are presented in Figure 4.19 for the speed range considered, for both excitation frequencies and for a.c. and d.c. components of the measured torque. The profiles of these curves are very similar to that of the constant torque results in Figure 4.14, reaching a maximum at approximately 400rpm, confirming that the basic mechanisms controlling the braking effect are the same.

It appears that the earlier assumptions were quite valid regarding the dominant effect of the air-gap in determining the linear magnetic characteristics of the electromagnet system and resulting in a sinusoidal magnetic flux on application of a sinusoidal voltage. Additionally, although a wide range of frequencies was not tested, for the results considered here the transformer e.m.f.s have not affected the operation of the braking system appreciably. It has been confirmed that the mechanisms of the braking system are similar to that for the constant (d.c.) torque braking of Section 4.4.1. However, the values of K_N from the constant torque results are different to those obtained from the dynamic torque input. This is a due to the different eddy current amplitudes resulting from the time-varying applied magnetic flux, even if the induction mechanism is predominantly the same.

The relationship between torque generated by the exciter and its input current can now be utilised fully, as it has been previously demonstrated that the magnetic flux in the air-gap is proportional to and approximately in phase with this current. A real-time measure of the applied torque can therefore be derived from the electromagnet supply current in accordance with equation {4.10}. For this an electronic circuit was used which produced a voltage proportional to the square of the current measured from the shunt in series with the electromagnets. Figure 4.20 presents the frequency spectra of the signal from the current-squared circuit and the torque measured in the shaft, showing equivalent harmonic components in the two signals at twice the applied voltage excitation frequency. The signal from this circuit can then be calibrated to derive a representative measure of the applied input torque. The values of $K_N = \left(T/I^2\right)$ determined in experimental consideration of the harmonic torque input above can be used for calibration of the torque input. This gives the 'calibration chart' of Figure 4.19, defining the value of K_N for each operating speed. The calibration of the torque input signal to the shaft system derived from the current-squared circuit is discussed in further detail in the following section.

Control of the electromagnet input will allow a range of excitations to be applied, including single frequency sinusoid, as above for swept-sine testing, or a broad-band excitation. Results for a range of excitation levels and also broad-band excitation gave very similar transfer function results for the frequency range of interest. However, with the same magnitude of signal (pk-pk) as the single frequency sine tests the torque amplitude is reduced with broad-band excitation, thereby reducing the angular displacement along the shaft, with implications for the measurement noise floor in subsequent studies.

4.4.4 Calibration of Torque Input

In order to achieve full modal analysis and derive mobility measurements in appropriate units, it is necessary to have the input to the shaft system calibrated so the relative magnitude of the response can be determined. The previous section demonstrated derivation of K_N with independent measurement of the torque and current and manual processing of the values. This section discusses further ways in which this relationship can be determined to give values of the proportionality constant of equation {4.10} for calibration purposes.

There are a number of factors influencing the value of K_N, making it very difficult to derive theoretically. From equation {4.9} the main factors defining the torque-current relationship are rotation speed, disk volume between the poles, effective moment arm, disk conductivity, effective pole area and particularly the relationship between the magnetic flux in the air-gap and the current in the electromagnets. Additional effects specific to eddy current braking include the resistance of the external current path, the eddy current magnetic field, skin depth, effective length of the magnetic circuit air-gap and factors such as flux fringing and leakage, magnetisation characteristics of the electromagnet cores and the physical attributes of the coils. In view of this and the difficulties with obtaining estimates of many of these parameters, for calibration purposes it is necessary to derive the torque-current relationship empirically for each experimental set-up.

The relationship of equation {4.10} has been experimentally demonstrated and can be used to give a measure of the torque applied to the shaft system as introduced in Section 4.2.4.3. This is achieved with a circuit set to give a known linear relationship between its voltage output and the square of its input, the voltage drop across the shunt in the electromagnet circuit, which is proportional to the exciting current in the coils I_e as the shunt has an accurately measured constant resistance. A measure of the torque input to the rotating system can therefore be obtained and Figure 4.21 shows how the ratio of transducer shaft torque to electromagnet current-squared (implied input torque) varies with frequency for one rotation speed. This was obtained by sweeping the electromagnet input through the frequency range with a signal generator. This transfer function, essentially equivalent to $\left(T_{shaft}/T_{applied}\right)$, is calibrated in torque per current-squared $\left[\mathrm{Nm}/\left(\mathrm{A}^2\right)\right]$. The flat region of the response curve, up to approximately 10Hz, indicates where the ratio between torque input and shaft torque is constant. The dynamic magnification effect of the first non-zero natural frequency of the system then starts to increase the torque and twist in this section of the shaft, as previously shown theoretically in Figure 4.11. The applied torque and shaft torque are in phase at low frequencies, before the effect of the first natural frequency of the system becomes apparent. As expected, the phase at the resonant peak is approximately 90°. The phase lag ψ due to the inaccuracy of assuming the supply current is equivalent to the magnetising component of the current in the electromagnets is also evident. This offset increases with frequency and decreases the phase of the transfer function by a maximum of 58° at 100Hz, comparing well with estimates from the electromagnet impedance model of Section 4.2.2.2. For the speed range considered experimentally this effect was seen to give a phase decrease at 100Hz of 115° for 200rpm, decreasing with increasing rotation speed to 52° at 1200rpm.

The 'free-free' boundary conditions of the shaft system result in the response measured by the torque transducer indicating the 'twist' in this section of shaft. From this transfer function, discrete values of the ratio $\left(T_{shaft}/I^2\right)$ at a single frequency from the flat region can be determined and then corrected by the appropriate factor from the modelled response to give the ratio of $\left(T_{applied}/I^2\right)$. Modelling of this simple shaft system is sufficiently accurate in this case to allow use of these theoretically derived correction factors in validation and calibration of the torque excitation system. Transfer function values were taken for a series of rotation speeds over a range of frequencies and processed in this manner and Figure 4.22 shows the calibration values obtained which are constant up to approximately 15Hz. Above that frequency the first natural frequency of the system dominates the response and the predicted and measured responses compare less closely in the absence of appropriate damping in the theoretical model. Average values of the calibration factor were calculated for the range 2-15Hz where the curves are predominantly flat and these are presented in Figure 4.23.

These values are close to those of the discrete point values of Section 4.4.3, with independent torque and current measurement, giving the same trend with rotation speed. However the electromagnet arrangement had been re-aligned between these two sets of data and direct comparison of the magnitudes cannot be made. The torque-current relationship is quite sensitive to the identified parameters, particularly the air-gap length. It is also important to avoid problems with impedance matching which might adversely affect the measurements when monitoring currents with series shunts. Small differences in the values obtained will depend on the connections across the shunt measuring the voltage drop and discrepancies in these current measurements are augmented as this signal is squared. Additionally, it is essential to ensure linear response of the squaring circuit over the frequency range.

Following calibration of the torque input system by the method detailed above, the actual applied torque to the system was derived and is shown in Figure 4.24 for constant amplitude voltage input across the frequency range. Comparison of these results with Figure 4.6 shows how the input torque is dramatically reduced at high frequencies due to the increased impedance. The interaction between electromagnet impedance effects as functions of rotation speed and frequency gives these measured torque profiles. As a result, the torque in the lower frequency range increases with rotation speed due to the decreased circuit impedance. Furthermore, the phase offset identified due to the difference between the supply and magnetising currents in the electromagnet circuit results in over-estimation of the applied torque at high frequencies. From the modelled electromagnet system impedance of Section 4.2.2.2 the over-estimation factor at 100Hz is predicted to be 1.41 at 200rpm, decreasing to 1.13 at 1200rpm. This was not included in the experimental estimation of the calibration factors used for the current signal as it changes with frequency and at the lower frequencies of interest, up to approximately 50Hz, the much smaller phase offset results in closer estimation of the applied torque.

An alternative method of calibrating the current signal to give a measure of the applied torque would use an LTV, rather than a torque transducer, to measure the system response at any convenient point on the shaft. The calibration factor is then derived from comparison of the response measurement with the predicted behaviour, similar to above. This would not require modification of the shaft system as necessitated by use of an in-line torque transducer. This would give a more versatile calibration method for application to torsional vibration studies of different shaft systems and is the subject of further work, addressed in Chapter 6.

The electromagnetic system described has therefore been demonstrated as a versatile means of creating a controllable torque input for a rotating shaft system. A measure of the applied torque magnitude can be derived from the current in the electromagnet circuit, thus eliminating the need to modify the shaft system under test to incorporate strain gauges or a torque transducer. This excitation device is seen to have distinct advantages over previous systems, providing a complimentary technique to the LTV.

4.5 Experimental Results - Torsional Modal Analysis

This section describes the application of this controllable and measurable torsional excitation for the torsional modal analysis of simple rotating shaft systems. In combination with an LTV to measure response, the real-time measurement of torque input to a system allows torsional vibration frequency response functions (FRFs) to be obtained. The aim of this work is to utilise the theory and signal processing technology used almost exclusively for conventional translational modal analysis. Hence, with standard hardware and software for data processing, this versatile technique achieves full modal analysis for rotating shaft systems. The torsional modal parameters can be extracted, with derivation of natural frequencies, mode shapes and damping factors, permitting consideration of the torsional vibration characteristics of a rotating system in unprecedented depth.

4.5.1 Simple Three Inertia System

For demonstration of this technique the test-rig introduced in Section 4.3 was used. The experimental shaft system is shown in Figure 4.25 with three disk-inertias positioned along the shaft and the series of measurement points clearly labelled. The torque input is applied to the rotating disk at measurement location 8.

A range of excitations could be applied through control of the electromagnet system input including single frequency sinusoid for swept-sine testing, as predominantly demonstrated here, or a broad-band excitation. Initial tests were carried out using a sinusoidal voltage applied to the electromagnets and this input function gave the best results due to the increased magnitude of torque applied. Limited results were obtained using broad-band input functions, which can speed up the measurement process considerably. However, application of a torque input to give a measurable response is difficult to achieve without a large power amplifier for the electromagnet signal.

For the test procedure the motor was run up to the required constant speed and the electromagnet input from the signal generator was swept through the frequency range. This encompassed the first three torsional modes of the system, including the zero frequency rigid body mode. The sweep rate was slow enough to ensure that steady-state conditions had been attained, minimising distortion of the response plot. This was confirmed by comparison of FRFs obtained from tests with frequency sweep both up and then down.

A voltage proportional to the square of the current in the electromagnet circuit gave the measure of torque input to the shaft system, calibrated as discussed in Section 4.4.4. Measurements of the torsional vibration response were taken sequentially from the numbered positions along the rotating shaft using an LTV. The use of this instrument to measure the torsional vibration response allowed the results to be obtained rapidly as it could be quickly positioned to access each measurement point. Data collection and processing using a dual channel FFT (fast Fourier transform) analyser allowed the rotating system FRF to be obtained from measurement of the torque input and torsional vibration.

The relationship expressed in equation {4.17} and the effect of increasing impedance of the electromagnet circuit with frequency indicate that, for a fixed input voltage, in addition to the a.c. component of torque being increased at lower frequencies, the d.c. component will be increased. Hence, without changing the voltage input amplitude to the electromagnets or controlling the driving motor, the speed of the shaft system will decrease with decreasing excitation frequency. Most significantly, there are obvious implications for the accuracy of torque input measured as the speed is assumed constant in the value of K_N used. For the tests described here the speed could be assumed to be essentially constant. Typically, for the drive motor used, initially set at 800rpm with 60V (pk-pk) excitation at 20Hz (40Hz torque input), the shaft speed varied from 825rpm (+3.1%) with 100Hz excitation (200Hz torque input) to 737rpm (-7.9%) for 5Hz excitation (10Hz torque input). This may be of concern in cases where the vibration characteristics are order related, such as during operation of the vibration absorber studied in Chapter 5. The speed could then be set at the required value for the critical frequency range in a measurement, remaining essentially constant over the region of interest.

4.5.1.1 Frequency Response Functions

The advantages of this excitation device over previously reported torsional vibration excitation and measurement systems are the ability to derive FRFs directly from a rotating system and the lack of substantial modifications being required for the mechanical system.

The FRF data could then be processed using standard modal analysis techniques. These results are discussed here and are seen to be typical of those derived from a torsional system of this nature.

Figures 4.26a & b show the driving point FRF from a sine-sweep test, in Bode and Nyquist formats, with the shaft rotating at a nominal speed of 1000rpm. The units of magnitude for the FRF are '(°/s)/Nm'. The first two non-zero modes, subsequently referred to as Modes I and II, are clearly identified and their natural frequencies can be easily estimated from this spectrum, with the FRF exhibiting the expected magnitude and phase characteristics. The general shape of this curve compares well with previous theoretical considerations of rotating shaft system frequency response [4-66, 4-67] and a number of important points can be identified. Results between the lowest 'anti-resonance' and zero frequency represent the cyclic speed variation of the system and thus indicate the boundary conditions of the structure. This is a result of the free-free system tending to roll as a rigid body in the direction of the applied torque at low frequencies. By increasing the frequency of excitation, the inertia torque builds up gradually and the reaction results in twist of the shaft.

The experimental results are seen to be dominated by noise above a frequency of approximately 60Hz due to the decreasing torque input with frequency. This is not a fundamental limit but exists as a result of the LTV 'noise floor', the electrical input used and the frequency response of the electromagnets, so it is possible to obtain measurements wherever a large enough response can be excited to be measured by the LTV. The increasing phase offset of the FRF due to the different phase of the supply current and the magnetising current component, as described in Section 4.4.4, is clearly apparent in the Bode form of the response. However, for modal analysis this is not a significant problem as all points on the shaft at a specific frequency will have the same phase relationship with the input, at a set rotation speed. It has also served to 'skew' the two modal circles of the Nyquist plot relative to each other and similar inaccuracies were apparent in the real and imaginary component form of the FRF. However, over local regions of the response curve the FRF phase is essentially constant in the Bode form used for the curve-fitting and will have negligible effect on subsequent modal analysis.

Figure 4.27a shows the FRF from the central inertia position of the shaft, a transfer mobility which has characteristics typical of such a measurement [4-68]. For the point mobility of Figure 4.26a discussed above, anti-resonances are expected to occur between adjacent resonances, while for a transfer mobility there should be minima occurring instead in some of these regions. The roll component of the low frequency range is apparent as before and the magnitude of Mode I response has been reduced, while that of Mode II is a maximum. The phase of Mode II has changed by approximately 180° as a result of a node for that mode located between this and the previous measurement position.

The FRF measured at the flywheel position is shown in Figure 4.27b, demonstrating much smaller response than the other points, as expected. The phase of the response at both modal peaks has changed by approximately 180° from Figure 4.27a due to the nodes occurring between these two disks for each mode. Additionally, the anti-resonances occurring between the resonances of Figure 4.26 have been replaced by minima.

A number of differences should be noted between these results and the transfer function of Figure 4.21 obtained using the torque transducer in the shaft system. It is apparent that the torsional system has changed slightly due to the stiffer section of shafting which has replaced the torque transducer and hence increased the natural frequencies. More significantly, by using the LTV the measurement obtained is the complete torsional vibration response of the system at the measurement point. This includes the 'solid-body' rolling component of this free-free system not detected by the torque transducer. Additionally, by measuring the rotational velocity of a point on the shaft with the LTV the phase of the FRF derived differs by 90° from that obtained with the torque transducer. This latter system measures relative angular displacement for which the phase lag of response relative to excitation at resonance is equal to 90°.

For comparison with the sine-sweep results, Figure 4.28 shows an FRF for which 'pseudo-random' excitation was applied to the electromagnets with a magnitude of 60V (pk-pk). The reduced energy put into the structure across the frequency range increases the noise in the FRF, despite the use of ensemble averaging. However, the two natural frequencies can be readily identified and the phase of the measurement was seen to demonstrate the same features as previous results presented, although with some loss of clarity due to noise. The low coherence of the FRF confirms the high level of noise across the measurement. Due to the increased response around the region of Mode I the coherence is close to 1.00, although a dip is apparent at the resonance, most likely due to bias error resulting from the frequency resolution of the spectrum analyser being too coarse to describe the rapidly changing function in this region for the lightly damped structure [4-69].

Low coherence can also result from excitation other than the instrumented input or non-linear response of the shaft system. The occurrence of undesired torsional excitation would affect the modal analysis accuracy as the measured response would no longer be directly related to the measured input. Possible sources might be related to the bearings, which were of the rolling-element type, or the drive input from the electric motor which would be apparent at low frequencies. For further development of random excitation with this system it would be necessary to use a suitable FRF estimator, in light of any noise present in the input and response signals [4-69, 4-70]. Broad-band (white) noise was also used as an input to the electromagnets but the wide distribution of excitation energy with frequency (40kHz range for the signal generator used) prevented any useful measurements from being achieved. It should be noted that for all the other FRFs presented in this thesis, which were from swept-sine tests and peak-averaged, the coherence was exactly 1.00 across the FRF.

Additionally, the noise characteristic of the LTV can corrupt the FRF measurement, particularly in regions where the speckle noise peaks, at harmonics of the fundamental rotation frequency, become significant. This can occur where the response is of low magnitude compared to the noise floor of the LTV, for instance where insufficient torque is applied to drive a reasonable response or close to a nodal point along the shaft for a mode. If these peaks are in close proximity to the modal peaks this has implications for the curve fit accuracy during modal analysis.

4.5.1.2 Modal Analysis

FRFs were obtained for the nine measurement locations along the shaft as indicated in Figure 4.25. By processing this data using STAR modal analysis software [4-71] the modal parameters could be extracted for the two identified modes. The modal frequencies obtained agree closely with estimates from a simple, 'free-free', lumped parameter model of the system, as demonstrated in Table 4.2. Modal damping values of 2.30% (of critical value) for Mode I and 1.13% for Mode II were obtained from this analysis and these values compare well in magnitude with published data [4-67, 4-72].

Table 4.2: Shaft system modal frequency results from experiment and lumped parameter model

	Mode I	*Mode II*
Experimental Results:		
Modal Frequency	28.29Hz	52.51Hz
Free-Free Lumped Parameter Model:		
Modal Frequency	28.69Hz	51.24 Hz
(Difference with experimental values)	*(+1.41%)*	*(-2.42%)*

The measurements taken gave sufficient points to describe the mode shapes of the system, which are shown in Figure 4.29. The torsional modal displacements are shown normal to the zero-datum for clarity and nodal points are clearly identifiable. The mode shapes have been normalised at the torque input point with unit magnitude to show the relative torsional displacement of the shaft in each mode. This normalisation has also taken into account the exact phase relationship determined in the modal analysis due to the 'complex' mode shapes obtained, so in effect this is displaying a 'snapshot' in time of the system motion. However, the relative phase of the measurement points was 0° (in-phase) or 180° (out-of-phase) to within ±15°, confirming the existence of predominantly 'normal' modes. Hence, the phase offset in the FRFs due to the impedance of the electromagnets has not prevented accurate results from being obtained as the phase relationship for points along the shaft in each mode remains constant. Comparison of the displacements with those from the simple lumped parameter model shows good agreement.

The free-free assumption for the boundary conditions of the shaft system essentially holds true, although it is of interest to note the reduced modal displacement at the ends of the shaft relative to the adjacent inertia. Therefore, these sections of shaft are not behaving as the zero-inertia, purely elastic components they are approximated to be in the lumped parameter model. As a result of their distributed inertia and effects of the end bearings of the shaft the experimental mode shapes take the form shown, highlighting inadequacies of the simple model used. This reinforces the importance of experimental torsional modal analysis for study of the real rotating shaft system vibration behaviour.

4.5.1.3 Effects of Rotation Speed

Following these initial results, a study was conducted to investigate the effect of rotation speed on the torsional vibration behaviour of the three inertia shaft system. This is with the aim of investigating the modal parameters obtained for the first two modes of the system and to develop the understanding of the behaviour and limitations of the excitation system.

To this end, FRFs were obtained for the driving point of the system for a series of rotation speeds, covering the range 200rpm to 1200rpm, with the excitation fixed at 60V (pk-pk). For each test the rotation speed was fixed at the nominal value for a mid-range frequency and the applied voltage was maintained at the constant peak-to-peak magnitude as the excitation swept down through the frequency range. Steady-state operating conditions were attained for the apparatus and the results were not taken in sequential order, preventing any influence of time related variation in the parameters. These response spectra were then processed in modal analysis software to determine modal parameters and the results were seen to be consistent and repeatable.

Figures 4.30a & b show the FRFs obtained from the system rotating at 200rpm and 1200rpm in order to identify differences which occurred progressively between these two extremes of operation. It is apparent that the lower speed has sharper resonant peaks and, therefore, less damping for the two modes, which are at marginally higher frequencies than for the rotation speed of 1200rpm. The higher speed has less noise corrupting the signal at frequencies above Mode II due to increased torque input from the excitation system. Consideration of the phase for the two FRFs shows that the same inherent features are apparent in each. However, as discussed previously, there is a phase offset which increases with frequency due to the use of the electromagnet supply current as a measure of the torque input. In agreement with previous results, this effect has decreased the phase at

100Hz from the ideal of 90° to approximately 0° for the 200rpm measurement. This effect decreases with increasing rotation speed and for the 1200rpm FRF the phase has been decreased to approximately 40° at 100Hz. This results in over-estimation of the applied torque at high frequencies by a factor determined from these results of approximately 2.00 for 200rpm at 100Hz, decreasing to 1.22 for 1200rpm. The smaller phase offset at lower frequencies gives much closer estimation of the actual applied torque.

The modal parameters obtained from the analysis of the results are presented in Figures 4.31a & b with the natural frequencies of Mode I and II decreasing with increasing rotation speed. Additionally, the modal damping increases with rotation speed for both modes, although the value for Mode I reaches a plateau at 800rpm. Although these differences are fairly small, there appears to be some physical changes occurring in the shaft system with rotation speed, which will be discussed in the following sections.

4.5.1.4 Effects of Excitation Level

As a further investigation of the influence of excitation on the response of the rotating system, results were obtained for a range of applied voltage excitation levels. The experimental procedure was as described above and the rotation speed was fixed at 1000rpm with FRFs obtained from the driving point for a range of applied excitation voltages from 10V to 60V (pk-pk).

Example FRFs are shown in Figure 4.32 with applied excitation voltages of 40V and 20V (pk-pk), for comparison with the FRF of Figure 4.26a for which the applied voltage was 60V (pk-pk). As the input voltage is decreased the response of the system is brought closer to the noise floor of the LTV, particularly because the applied torque is proportional to the square of this voltage. This is clear from the FRFs, where the harmonic speckle noise peaks become more significant with the reduced voltages and the measured response of Mode II degrades quite seriously. However, it is still possible to derive valid data in the regions around the modes where the phase information remains of suitable quality. Additionally, the reduction in excitation level results in sharper resonances, implying decreased damping for each mode.

The torsional vibration modal parameters of the system are shown in Figures 4.33a & b, as functions of the voltage applied to the electromagnets. It is apparent that the natural frequency of both modes decreases with increasing excitation magnitude. Modal damping, however, increases dramatically with excitation level.

4.5.1.5 Factors Controlling Modal Parameters

Whilst the percentage changes in modal parameters discussed in the two previous sections appear relatively insignificant, it is certainly apparent from the excitation level results that there is some influence of the torque input on the vibration behaviour of the test system. These differences will be attributed to changes in the shaft system resulting from the torque input, not due to the direct influence of the excitation system itself on the vibratory behaviour. Obviously, for the purposes of accurate modal analysis non-linear behaviour is undesirable. However, the identified changes in vibration characteristics with rotation speed require investigation and this highlights the importance of performing modal analysis of a rotating system under rotating conditions. Additionally, although the modal damping values obtained from the previous analysis compare well in magnitude with published data, the damping is seen to decrease with increasing mode number. This is not in accordance with conventional understanding of proportionally damped structures [4-68, 4-73] which is the usual assumption for torsional damping in shaft systems [4-72].

Parallels should be made between the results observed here and the effects of the excitation device on the test structure in translational modal analysis [4-69]. Conventionally, the attachment of the excitation mechanism to the test component requires some precautions to avoid inadvertent modification of the structure. Inappropriate use of excitation methods can result in mass loading or stiffening of the system under test, thereby unacceptably changing its vibratory behaviour. However, the non-contact electromagnetic system developed here should not be subject to these effects. For accurate modal analysis it is necessary to ensure that the measured input is the only excitation applied to the structure and that secondary excitation does not occur due to the coupling mechanism used to attach the exciter to the structure. While this effect can be quite common in translational modal analysis, excitation in a torsional sense should be readily applied with little or no coupling with other motions, particularly with a symmetrical shaft cross-section. Additionally, as discussed in earlier chapters, the LTV used to measure the response of the shaft system in the configuration used for these tests was only sensitive to torsional vibration.

However, the experimental excitation system, which uses a single electromagnet pole pair, applies a moment and an unbalanced force to the shaft, not just a pure couple. This effect therefore influences the dynamic behaviour of the shaft system, resulting in the observed changes to the estimated modal parameters. The unbalanced force pushes the shaft into the bearings and increases the damping of the torsional motion of the shaft. The d.c. component of the unbalanced force should have the biggest influence on this behaviour. Theoretical consideration of this damping effect would need to look at the shaft-ground damping resulting from the viscous frictional losses in the bearings [4-72].

To consider the effect of the input torque on the system response, Figure 4.34 shows the variation in modal damping, for both the sets of data discussed above, as a function of the excitation system input torque. Damping is seen to be an almost linear function of input torque, with all four curves closely related. This is consistent with the proposal that the effect is due to lateral loading of the shaft bearings with the electromagnet arrangement used. The increased applied torque and hence force on the bearings applied at the frequency of the lowest mode therefore increases its damping compared to the higher mode. It is also apparent that Mode II has slightly less damping than Mode I for equivalent results with the same input torque. This can be attributed to the particular bearings determining the damping in a mode. Considering the mode shapes presented previously, Mode I has the largest response at the excitation disk, presumably with the bearings in this region most affected by the unbalanced shaft force. For Mode II the excitation disk is close to a nodal point, so the influence of the bearings affected by the lateral loading is reduced.

In previous work considering the coupling of torsional and lateral vibration through geared systems, the lateral motion of the shaft in the bearing journals was proposed to contribute additional damping to torsional modes [4-74]. Additionally, the bearing lateral damping and stiffness coefficients were dependent on the rotational speed and the static load on the journal, thus changing the eigenvalues of the coupled system. Although the coupling between torsional and lateral motion of the system under test here is minimal, the motion of the shaft-bearing connection induced by the unbalanced force applied to the disk is proposed to have resulted in similar effects. Refinement of the excitation system to apply a pure couple to the excitation disk, through the use of two diametrically opposed magnet systems, should reduce this influence of the excitation level on modal damping. However, this clearly demonstrates the use of torsional modal analysis for examination of the effects of unbalanced lateral forces on shaft system behaviour while rotating.

Further to this, the changes in the natural frequencies of the system were considered to see if these are directly dependent on the damping behaviour. The modal analysis solution provides estimation of the modal parameters for free oscillation of a system from the measured FRFs [4-68]. If the damping applied to the shaft is assumed to be viscous, the modal damping value can be derived as a ratio compared to the critical damping for the mode. The frequency of damped oscillation ω_d for a single degree-of-freedom system can be determined from the critical damping ratio ζ and the system's undamped natural frequency ω_n [4-75];

$$\omega_d = \omega_n \sqrt{1-\zeta^2} \qquad \{4.19\}$$

Hence, for each result discussed above, the undamped natural frequency ω_n of the system can be estimated using the assumption of a single degree-of freedom for this lightly coupled structure. Theoretically the values of ω_n obtained for each mode should be the same for each of the FRF measurements considered in Sections 4.5.1.3 and 4.5.1.4. This would demonstrate that only damping is a function of the parameters discussed above and the frequency changes observed are a direct consequence of this.

However, calculation of the undamped natural frequencies from these results does not give common values for Mode I or II. The very light damping estimated for the system gives a maximum increase of 0.03% when calculating ω_n from ω_d. For example, at 200rpm the estimates of undamped natural frequencies are 28.473Hz and 52.622Hz for Modes I and II respectively. In comparison, at 1200rpm the corresponding values of ω_n are 28.078Hz and 52.104Hz. There must therefore be some effect additional to damping which changes the natural frequency of the system with rotation speed and excitation level. From consideration of fundamental principles an effective decrease in system torsional stiffness or increase in system inertia has occurred to give this trend or, alternatively, the assumptions of damping behaviour in the system do not hold true. The most likely parameter to have changed is the stiffness.

For the results showing the reduction in modal frequencies with increasing rotation speed a reduced system stiffness is implied and the modal frequencies were seen to be inversely proportional to the applied torque, However, with increased excitation level this latter effect only occurs for Mode I, as for Mode II varying the applied voltage appears to give very little variation in modal frequency. The maximum applied torque is at least 2.5 times smaller for this mode than for Mode I and is applied close to a nodal point.

These results suggest there is some weak non-linear behaviour controlling the response due to the changes in natural frequency with rotation speed and excitation level [4-68]. This did not have a major effect on the system response during experimentation, with no apparent distortion of the FRFs dependent on sweep direction, and as such does not invalidate the general linearity assumptions of modal analysis. It should be possible to attribute this behaviour to the properties of the shaft system, possibly due to bending of the shaft resulting from the unbalanced force applied or some effect related to the disk mountings or shaft couplings. These results emphasise that to consider accurately the vibration characteristics of a shaft system there is a need for use of the new torsional modal analysis tools developed to study the system under rotating conditions.

4.5.2 Four Inertia Shaft System

To consider further the use of the torsional modal analysis system, a fourth inertia was added to the shaft system on the free end, at location 9 of Figure 4.25. This would give a distinct third mode of vibration for the system and the occurrence of measurable response above the frequency range demonstrated previously allows further exploration of the excitation method and torque input measurement. These results should confirm those obtained for the three inertia system results, with illustration of further points relating to the use of the torsional modal analysis system.

4.5.2.1 Connection of the Drive Input to the Shaft System

It has been assumed that the soft rubber belt used to connect the drive motor to the shaft system serves a number of purposes, providing rotation of the system without transmission of any torsional excitation components. The low modulus of elasticity of the belt material results in the two translational springs formed by the belt and connecting the pulleys having a low extensional stiffness. For a shaft system incorporating a belt and pulley drive a value of equivalent torsional stiffness is commonly derived for the complete arrangement, to simplify modelling and discussion of the system's dynamic behaviour [4-76, 4-77]. Therefore, in this case the resilient belt drive system is presumed to have a low equivalent torsional stiffness, isolating the motor from the main shaft and ensuring it is not a part of the oscillating system. This requires that the torsional natural frequency of the motor-belt system is very low in frequency, allowing the assumption to be made that the end of the shaft attached to the motor drive is a 'free' boundary condition. This is analogous to ensuring that solid body modes are much lower than the vibration modes of interest when a free-free structure is suspended by elastic cords in conventional (non-rotating) modal analysis [4-69].

To consider the participation of the drive motor in the torsional response of the shaft system under test, Figures 4.35a & b show the torsional FRFs measured for the drive input end of the four inertia system and the motor pulley. A number of differences can be seen which confirm that the assumption of the motor being uncoupled from the main shaft is reasonable. There are a number of components of torsional vibration present at the motor pulley resulting from the operation of the motor. Most significantly this includes a large peak at 100Hz, twice the supply voltage, as is typical for this type of motor. Clearly these torsional vibration components are not transmitted to the shaft system under test and remain isolated at the motor shaft by the rubber belt. The two modes apparent on the main shaft have a reduced response on the motor pulley much lower in magnitude than the drive system harmonics.

At low frequencies, up to approximately 10Hz, the motor response closely matches that of the shaft, seeming to participate in the rolling of the free-free system. Experimental measurement of the complete rotating system moment of inertia, including the motor, in deceleration tests agreed with a calculated value for only the four inertia shaft system to within 1.00%. Consequently, the moment of inertia of the motor appears to contribute little to the torsional behaviour and is estimated to be at least an order of magnitude smaller than the shaft system. The apparent mode of vibration occurring for the motor shaft at approximately 17Hz is of limited concern as no trace of this can be seen in the main shaft response. The low resonant frequency is due to the low equivalent torsional stiffness of the rubber belt, with the main shaft acting as a fixed point in this mode. This effect was seen to be of similar magnitude and frequency for all rotation speeds with a relatively small response compared to the shaft modes. As a result, above the response of this mode, the motor shaft can be considered to be uncoupled from the shaft torsional vibration.

In analysis of the vibration characteristics of the shaft system alone the extra degree of freedom of the motor shaft has been ignored and a sufficiently complete modal model of the rotor-shaft system has been derived. Obviously, for full consideration of the torsional vibration characteristics of a system, the drive motor parameters are of significance. However, with the drive system suitably isolated from the shaft it is reasonable to assume there is no torsional constraint at this location. Criteria must be derived in subsequent work to ensure that the drive system plays no role in the measurements made.

4.5.2.2 Modal Analysis Results

A comprehensive modal analysis study was carried out for the four inertia shaft system and full sets of FRFs were obtained for a series of rotation speeds from 400rpm to 1200rpm. The aim was to investigate further the behaviour of the excitation technique and the differences in the modal parameters of the shaft system related to the rotation speed, particularly mode shapes. The experimental procedure was as described in Section 4.5.1 with the voltage input to the electromagnets fixed at a constant peak-to-peak magnitude and the excitation swept through the frequency range.

All sets of FRFs across the speed range were fairly similar in appearance, with small differences due to reduced high frequency noise at higher rotation speed and the pattern of harmonic speckle peaks, due to the LTV operation, which are more closely spaced at lower speeds. Example FRFs with the shaft rotating at 1200rpm are presented in Figures 4.36a to d and are in agreement with conventional mobility measurements in terms of relative phase and the arrangement of resonances and anti-resonances. The response at the fourth inertia position in Figure 4.36a shows the third (non-zero) mode giving a large response. Noise, including speckle peaks, is seen to dominate the measurement above 120Hz. At the excitation disk the phase of the motion for Mode III has changed by 180°, as shown in Figure 4.36b, indicating that a node for that mode exists between these two locations. The anti-resonance between Modes II and III is clear but the low response level allows noise to become significant in this region. The response of the system due to Modes I and II changes very little between these positions. At the central inertia the response is of the form of Figure 4.36c, where the largest relative motion of Mode II occurs and the phase indicates that a node is located between this and the previous measurement point. The flywheel position FRF in Figure 4.36d shows that a node exists for Mode I in the end section of shaft. Response magnitudes for all modes are significantly reduced, particularly for Mode III which is entirely masked by the LTV noise base.

For comparison, Figures 4.37a & b show the FRFs from the end location and flywheel position respectively at a rotation speed of 400rpm. The phase offset due to the impedance effects of the electromagnets is more pronounced at lower rotation speeds, as discussed in Section 4.5.1.3, which affects the accuracy of the applied torque estimation. Differences in the response of the rotating system due to rotation speed can only be considered in detail through examination of the modal parameters and this is possible with the use of torsional modal analysis.

Modal parameters for the three (non-rigid body) vibration modes were determined in modal analysis of the data obtained for each of the five rotation speeds. Curve-fit bands were carefully set by hand to ensure that no spurious noise peaks in the vicinity of a mode's response would corrupt the measurement. Frequency and damping values were taken from the maximum response point of each mode, agreeing closely with measurements from other (non-nodal) positions. To ensure consistency of results for comparison purposes it is important to have reached steady-state conditions in the temperature of the component materials. The oil film in the bearings should have a stabilised fluid viscosity as this will affect the system damping and modal frequencies. Effects such as this will contribute to a degree of scatter in the estimates of modal parameters from a system. However, the results presented here were found to be quite consistent and repeatable once steady-state conditions had been quickly attained.

The modal frequencies estimated at each rotation speed are close to one another and to estimates from a simple 'free-free' lumped parameter model of the system, as shown in Table 4.3. The model estimates of the natural frequencies are a reasonable approximation of the experimental values, although some discrepancy is apparent for Mode III. The variation of modal frequencies with rotation speed for the three modes is shown in Figures 4.38a to c. There is a general decrease in the frequency of each mode with rotation speed, as previously seen for the three inertia system.

Table 4.3 Four inertia shaft system modal frequency results from experiment at 800rpm and lumped parameter model

	Mode I	*Mode II*	*Mode III*
Experimental Results at 800rpm:			
Modal Frequency	25.67Hz	51.38Hz	101.67Hz
Free-Free Lumped Parameter Model:			
Modal Frequency	26.14Hz	49.78Hz	114.73Hz
(Difference with experimental values)	*(+1.83%)*	*(-3.11%)*	*(+12.85%)*

The estimates of modal damping for the system are shown in Figures 4.39a to c, demonstrating the variation with rotation speed for each of the three modes and decreasing with mode number, as before. The trends are similar to those discussed for the three mass system, with damping for Mode I reaching a maximum at 800rpm and decreasing slightly above this. The damping of Mode II increases with rotation speed over the speed range considered. Mode III damping is approximately constant over the range of rotation speed range, although fluctuations are apparent that can be attributed to noise in the transfer function at this frequency with reduced input torque.

The first two modes are very distinct in the FRFs and the mode shapes are presented in Figure 4.40a & b. For comparison of the results the eigenvectors have been mass normalised, that is scaled with 'unity modal mass' (UMM) as discussed in Appendix B. As before, 'snapshots' of the complex mode shapes are shown using the exact phase relationships determined in the analysis and the maximum relative phase difference of any (non-nodal) point along the shaft from the ideal of 0° or 180° was less than 15° and predominantly smaller than 5°. The results agree closely for all speeds, confirming a reasonable degree of consistency in the calibration values between speeds. All the mode shapes for the range of rotation speeds agree closely for Mode I along the whole length of the shaft. The mode shapes of Mode II are also grouped closely, although slight scatter of the modal displacements has occurred. The experimental results agree closely with the lumped parameter model predictions, although it is apparent that the ends of the shaft are not participating as expected, as seen for the three inertia results.

The mode shapes for Mode III are presented in Figure 4.40c, with accurate results only obtained from the two end points, 8 and 9, on the shaft. This is because the response of the rest of the shaft is too small in magnitude to be measured by the LTV with the low torque input at this frequency. All experimental results show the same basic mode shape although there is a general increase in modal displacement with rotation speed at the two end inertias. In addition, the experimental mass normalised displacements are noticeably smaller than the theoretical values. These effects confirm the approximate magnitude of the over-estimation factors for the applied torque predicted previously, due to the phase difference ψ between the supply current I_e and the magnetising component current I_m at this high frequency. The magnitude of the torque actually applied to the shaft system is therefore smaller than the estimated value obtained from the supply current by the factor $(\cos\psi)^2$, which increases with decreasing rotation speed. The magnitude of the FRF and hence modal displacements estimated will be too small by this factor.

It is apparent that the trends in variation of natural frequencies and damping of the shaft system with rotation speed are very similar to those for the three inertia system. The mode shapes of Modes I and II all agree quite closely, not appearing to change significantly with rotation speed. The changes in natural frequency are fairly small so no major differences would be expected. Analytical tools are limited for comparison of these results to consider the changes in the rotating system due to damping and possibly stiffness effects related to rotation speed. Additionally, the torsional vibration response of rotating shaft systems has not been studied in such detail before and therefore very little published information is available for comparison with these experimental results.

The modal damping of all three natural modes of the four inertia shaft was seen to be approximately proportional to the torque input by the electromagnetic system. It was postulated previously that this is due to the unbalanced force applied laterally to the bearings with the arrangement of electromagnets used. Additionally, by calculating the undamped natural frequency ω_n for all three modes at each of the rotation speeds, it is possible to consider whether it is principally the estimated changes in damping that result in the observed modal frequency variations. As before, for these small damping factor magnitudes the estimated undamped natural frequencies of the shaft system are not comparable over the speed range considered. Therefore, in addition to the changes in damping in the system, there must be a change in the shaft stiffness in order to give this magnitude of changes in the modal frequencies with rotation speed. The modal frequencies appear to be inversely related to the torque input, indicating the occurrence of some form of shaft stiffness reduction with rotation speed and excitation level.

Torsional modal analysis of rotating shaft systems allows a depth of study to be achieved which has not been realised with previous technology. The novel excitation system described in this chapter provided a controllable torque excitation and a measure of the torque input by non-contact means. The use of conventional modal analysis software confirmed the integrity of this new experimental method, allowing determination of modal parameters in terms of natural frequencies, torsional mode shapes and damping factors. Changes in modal parameters have been highlighted which relate to rotation speed, identifying non-linear behaviour of the shaft system and damping was dependent on the behaviour of the shaft bearings. Modal analysis of torsional vibration response is an area in which considerable insight could be realised in the design and development of rotating machinery. This would allow further consideration of the factors governing modal parameters discussed here and aspects related to development of this approach and its application to real shaft systems are discussed in Chapter 6. The use of this technology to study devices such as the centrifugal pendulum vibration absorber, considered in the next chapter, highlights its potential to provide detailed understanding of rotating system behaviour.

5. APPLICATION OF TORSIONAL MODAL ANALYSIS TO DEVELOPMENT OF A VIBRATION ABSORBER

The torsional vibration of rotating shafts can be controlled by 'tuning' of the inherent mass, stiffness, excitation, and damping characteristics of the system. However, some modifications may be found impracticable, too costly or detrimental to other performance criteria such as mass balance or efficiency. To reduce torsional vibration levels it may then be necessary to introduce tuning or damping devices. This chapter will demonstrate how one novel device, the centrifugal pendulum vibration absorber (CPVA), can control the torsional vibration behaviour of a rotating shaft system with the possibility of improved performance compared to other devices. A considerable amount of literature has described the theoretical development of the CPVA which has been used in a range of applications. However, the lack of experimental techniques for investigation of the behaviour of this device, which has to be rotating to function, has prevented full exploitation of its potential.

The aim of this work is to demonstrate the use of the new torsional modal analysis technique described in the previous chapter for investigation of the practical operation of a CPVA. The non-contact measurement method allows the shaft response to be considered experimentally without system modification, to develop a better understanding of the absorber's behaviour. Initially the potential of the CPVA for controlling torsional vibration is highlighted and previous developments of this device are considered. Based on this information an absorber has been designed for subsequent experimental studies. The operation of this device is demonstrated with results showing attenuation of torsional vibration as predicted. Detailed examination of the absorber's performance is made possible through the use of the new experimental analysis technique, permitting the tuning of the device to be explored. Finally, novel use of the LTV allows the motion of the individual pendulums to be studied, complementing the results of other sections.

5.1 Devices for Controlling Torsional Vibration

Numerous devices have been developed for the control of torsional vibration of rotating shafts. These have seen application in a wide range of rotating machines, with the requirements of each situation determining the most suitable system to use. For many of the devices designed for these applications the tuning and damping functions are closely related and for accurate description the following definitions are used [5-1]. A damper is a device which reduces vibration levels in a mechanical system through the dissipation of energy. An auxiliary vibratory system which modifies the vibration characteristics of the main system to which it is attached is known as a dynamic vibration absorber and may be damped or undamped. The following discussion considers the merits of the various arrangements used to introduce a supplementary inertia into a shaft system for torsional vibration control, which are grouped with regard to the nature of the connection between the inertia and the original system.

5.1.1 Torsional Vibration Dampers

In this arrangement the supplementary inertia is connected to the original system by frictional resistances only. The inertia oscillates relative to the hub member when torsional vibration occurs, thereby dissipating energy. These are usually called untuned vibration dampers and can be broadly split into two main types, comprising those using a form of slipping torque and those using viscous shear forces.

Slipping torque dampers dissipate energy when the acceleration of the damper assembly results in relative motion between the shaft and damper flywheel [5-2, 5-3]. The various practical forms include the classical Lanchester damper using dry-friction and hydrostatic devices such as the Sandner pumping chamber or gear-wheel type dampers. Viscous shear or 'Houdaille' dampers consist of an annular seismic mass enclosed in a casing, with the peripheral and lateral gaps between these two components filled with viscous fluid, usually silicon based [5-3, 5-4]. The liquid is sheared whenever relative motion occurs between the casing, which is attached to the rotating shaft, and the seismic mass, which is free to rotate. Commercially available devices are manufactured in this country by Holset [5-5] who produce a range of viscous shear dampers (and also elastomeric tuned absorbers) tailored to customer requirements.

The untuned dry friction damper was quickly superseded by the viscous friction damper using silicone fluid, due to the fact that the stick-slip friction characteristic of the former could only attain peak performance at one order of vibration of a given mode. The wide application of viscous friction dampers is due to their simple construction and consistent long service performance. The 'tuning' function of these dampers is to place any significant resonant zone outside the normal operating speed range and to provide sufficient damping to deal with these zones during transient operation such as starting, manoeuvring and stopping. However, it is undesirable to operate continuously in a resonant zone as there will be significant loss of power from the main system with excessive wear and overheating of the damper. In large compression ignition engines, such as those used in trucks and heavy vehicles, viscous dampers are usually employed as the limited capacity of rubber vibration absorbers to dissipate energy without overheating results in a short service life.

5.1.2 Dynamic Vibration Absorbers

The supplementary inertia in these devices is connected to the original system by a rubber or mechanical spring assembly and the wide range of practical forms have been used in a large number of applications [5-6, 5-7]. This is due to their elementary, self-contained mechanical construction which gives consistent, efficient performance with minimum maintenance. A substantial reduction in vibration amplitude can be achieved and the devices are capable of dealing with all orders in a given mode. A significant amount of inherent damping is introduced, either through the hysteresis of a rubber spring, or rubbing friction in a mechanical spring assembly. With elastomeric absorbers the connecting element provides both elasticity and damping and is shaped to achieve the required values of each. The range of example applications includes the control of gear impacts for large induction motor drives used for road tunnel ventilation [5-8] and reduction of the torsional vibration of servo-motors caused by an unbalanced supply voltage [5-9].

Rubber vibration absorbers have a better performance than viscous dampers, being smaller and lighter for a given duty. For this reason and because manufacturing tolerances are not as critical, the cost of a rubber vibration absorber is less, particularly for smaller sizes. Small viscous dampers are also vulnerable to mechanical damage which, with close internal clearances, may result in the inertia mass becoming locked in the casing. For these reasons the rubber vibration absorber has been used by the automotive industry for a range of noise and vibration control measures in passenger car powertrains [5-10, 5-11]. However, heat dissipation problems prohibit the use of rubber absorbers on larger engines in medium and slow speed applications. Tuned and damped absorbers with mechanical springs could then be utilised which have the potential to be smaller and lighter than the viscous damper alternatives. However, dampers and absorbers of these types are not suited to some applications because of weight and space limitations.

5.1.3 Centrifugal Pendulum Vibration Absorbers (CPVAs)

For this absorber the motion of the supplementary inertia is controlled by centrifugal forces, so the restoring torque is proportional to the square of the rotation speed of the attached shaft and the displacement of its centre of gravity from the centre of oscillation. As a result the natural frequency of the assembly is directly proportional to rotational speed. The CPVA is therefore capable of eliminating completely the torsional vibration for a given order of excitation at all rotational speeds when correctly matched to the characteristics of the main shaft system. Additionally, the previous devices perform both tuning and damping functions, whereas CPVAs ideally perform only a tuning function as any damping in the assembly is detrimental to performance.

Viscous friction dampers and dynamic absorbers are generally larger than CPVAs, but are less expensive and available commercially as sealed and tested units requiring little or no attention in service. In addition, a separate CPVA is required for each troublesome vibration order with implied cost penalties, whereas a viscous damper deals with all the critical peaks of a given mode. However, when correctly designed CPVAs can withstand long service periods without attention or deterioration. They have significant potential for controlling the vibration due to a specific order, with inherent advantages over other devices which have a broad-band effect or are tuned to a specific frequency of excitation.

5.1.3.1 Review of Early Developments

A comprehensive review of the historical development of the CPVA, originally conceived over sixty years ago, is presented by Ker Wilson [5-12] and will be summarised here. The earliest form of pendulum-type absorber used fluid contained in U-shaped channels in a rotating flywheel. Irregularity of the flywheel rotation displaced the fluid thus producing a counteracting torque due to the action of centrifugal forces.

Subsequently, many forms of pendulum assembly were proposed and patented between 1930 and 1940, primarily with solid pendulums. The 'roll-form' absorber was the first of these, with a solid metal cylinder operating in a larger diameter circular hole in the rotating carrier member as shown in Figure 5.1a. This arrangement could be readily accommodated in an existing component such as a gear or flywheel to minimise its space requirements. For small amplitudes of pendulum motion, up to about +/-15°, there is continuous rolling motion and absorbers based on this assumption have proved successful in service. However, accurate tuning of such a design often cannot be achieved, due to uncertain prediction of whether the cylinder will slide or roll in operation and thus change the system's natural frequency. 'Ring-form' pendulum absorbers utilised a metal ring oscillating on a pin fixed to the carrier and are illustrated in Figure 5.1b. These devices experienced similar design difficulties to the roll-form devices discussed above and the tuning is more sensitive to the rotational inertia of the moving pendulum component, which is subsequently referred to as the pendulum bob.

A further form of CPVA is shown in Figure 5.1c where the pendulum bob is suspended on a single pin which rolls in cylindrical tracks in the mass and carrier. This is known as the duplex suspension or unifilar duplex suspension, with the suspension pin acting as a secondary pendulum bob. The system is a form of compound rotating pendulum and may be regarded as half of the bifilar-type suspension arrangement to be described shortly. For small pendulum vibration amplitudes and minimal rotational inertia of the suspension pin the assembly operates with rolling friction only. The pendulum bob then oscillates with substantially lateral motion and negligible rotation about its central axis relative to the carrier due to the action of the single pin suspension. It is therefore equivalent to a simple rotating pendulum with its mass concentrated at its centre of gravity. Unifilar duplex suspensions have given reliable service in numerous cases providing the amplitude of pendulum relative to the carrier remains within the limit of +/-20°. The suspension pin gives another degree of freedom to the device and the potential for dealing with two different orders of excitation. Unfortunately, the resulting pendulum amplitudes and critical tuning of this mode prevent its use in practice and it is of academic interest only.

By attaching the pendulum bob to the carrier with two links symmetrically arranged either side of its centre of gravity, it takes the form of the bifilar suspension CPVA shown in Figure 5.2a. For small angles of oscillation relative to the carrier the pendulum is constrained to rotate about an axis midway between the links without any rotation of its centre of gravity. Hence, in this arrangement all points of the pendulum move in a circular path and its rotational inertia does not affect the motion, causing the device to behave as a simple pendulum. Larger pendulum amplitudes, up to +/-25°, can be tolerated without significant deterioration of performance making the bifilar form the most effective in terms of weight and space usage. However, for the link-form of bifilar suspension shown, friction at the hinge pins is detrimental to performance, particularly at high rotation speeds and loads, resulting in energy losses and component wear. This form is also unsuitable for tuning to control vibration of second or higher orders as the link length cannot be reduced sufficiently whilst leaving enough material to accommodate hinge pins of suitable size.

For a practical form of the bifilar suspension CPVA, Figures 5.2b & c show the use of suspension pins to provide an ingenious and compact solution to the problems of the hinged link arrangement. The pins carrying the centrifugal loads roll on the cylindrical tracks in the carrier and pendulum components, so the relative motion is opposed by rolling friction only, thus minimising damping and component wear. As before, the rotational inertia of the pendulum bob does not affect its motion relative to the carrier. Therefore this arrangement is also assumed to be a simple pendulum with the mass concentrated at its centre of gravity and has an effective pendulum length equal to the difference between the diameters of the suspension holes and pins.

The first published descriptions of the bifilar form CPVA with suspension pins were described in patents in 1935 granted to Sarazin [5-13] and one month later to Chilton [5-14] with the latter dealing with a suspension system for the crankweb balance weights of radial aero-engines. The use of rolling surfaces in contact was the primary feature which made the CPVA into a practical engineering device, reducing frictional losses to a minimum and providing a mechanism which can achieve the small effective pendulum lengths necessary to deal with excitation orders commonly encountered. This form of CPVA offers predictable, consistent and trouble-free performance through better control of the pendulum motion provided by the double support. Additionally, there is less chance of degradation of performance through friction and wear at the pins due to slipping. For these reasons the experimental study reported here will explore the behaviour of a bifilar suspension CPVA.

5.1.3.2 Simple Pendulum Theory

A large number of theoretical studies have investigated the operation of the CPVA, examining both the dynamic response of the absorber and the control of torsional vibration modes in a shaft system [for example; 5-12, 5-15 to 5-18]. The system is conventionally modelled as a simple pendulum with the equations of motion linearised to give a solution for the limits of small angles of pendulum motion. This solution is briefly discussed here to provide an understanding of the absorber behaviour and the practical form of the bifilar device is addressed in the following section. This is used as the basis for the design and development of a device to demonstrate the depth of experimental study made possible with torsional modal analysis.

The most convenient and robust theoretical approach, as used for this study, is based on Lagrange's equation with the solution summarised in what follows [5-19 to 5-22]. The simple pendulum arrangement is detailed in Figure 5.3 which shows the absorber carrier of moment of inertia J_C, attached to the shaft and rotating about its axis O with a mean angular velocity Ω. A simple pendulum AB of mass m and length L_P is attached to the carrier at A where $OA = R$.

The angular position of the carrier relative to the axes shown is θ_C and the angular displacement of the pendulum about its axis of suspension relative to its equilibrium position is ϕ_P. Neglecting the effect of gravity, centrifugal force acts to restore the pendulum to its mean position when it has been displaced relative to the carrier by torsional vibration of this component. It can be seen from the geometry of Figure 5.3 that the angular displacement γ of the pendulum from its mean position, assuming small angles of oscillation, relative to the axis of carrier rotation is;

$$\gamma = \left(\frac{L_P}{L_P + R}\right)\phi_P \qquad \{5.1\}$$

Development of equations describing the velocity of the pendulum relative to the axes allows the total kinetic energy of the system to be expressed and the equations of motion are formed using Lagrange's equation. These fully describe the two degree of freedom non-linear system of the simple pendulum and a number of simplifications are used to obtain a solution for the steady-state forced oscillation of the CPVA. Primarily, the assumption of small angles of pendulum oscillation amplitude reduces the expressions into a linear form. The torque acting on the carrier $T_C(t)$ is assumed to be harmonic and a constant, but not necessarily integer, multiple of the rotation speed of order n.

The resonant frequency of the rotating pendulum arrangement is seen to be;

$$\omega_P = \Omega\sqrt{\frac{R}{L_P}} = \Omega n_r \qquad \{5.2\}$$

where n_r is defined as the resonance tuned order of the CPVA. Thus, the resonance tuned frequency of the pendulum is directly proportional to rotation speed and is defined by the relative dimensions of the pendulum. When attached to a shaft system oscillating torsionally at this order the pendulum attains the amplitude and phase necessary to produce a torque opposing that acting on the carrier position, thus preventing torsional motion at this point of the shaft.

For non-resonance tuned cases, the ratio of the pendulum amplitude Φ_P relative to the carrier amplitude Θ_C with excitation of order n is;

$$\left(\frac{\Phi_P}{\Theta_C}\right)_n = \frac{R + L_P}{L_P - \frac{R}{n^2}} \qquad \{5.3\}$$

From this expression it is apparent that when $n = n_r$ the denominator is zero. Therefore with resonance tuning of the absorber, the reciprocal of this statement demonstrates that the carrier amplitude is reduced to zero.

The amplitude of the pendulum with resonance tuning cannot be determined from {5.3} and instead is given by solution of the forced oscillation of the system;

$$\Phi_P\big|_{n=n_r} = \frac{-T_C}{m\Omega^2 R(R+L_P)} \qquad \{5.4\}$$

Through consideration of expressions describing the acceleration of the system carrier, the 'effective inertia' of the pendulum about the axis of rotation as a function of rotation order n can be defined as;

$$J_E(n) = \frac{mR(R+L_P)^2}{(R-n^2L_P)} \qquad \{5.5\}$$

For each order there is a different value of effective inertia, which for that order has the same value at all rotation speeds. This implies that there is effectively a different equivalent vibratory system for each order when a CPVA is operating in a shaft system. A resonance tuned pendulum presents an infinite inertia with respect to the order n_r.

A CPVA can therefore provide adjustment of the effective inertia with respect to a given harmonic order, at its point of attachment to the shaft system, to almost any required value between what is conventionally described as negative and positive infinity. As a result, the outstanding characteristic of CPVAs which distinguishes them from other types of torsional vibration absorber is the ease with which they can be used to bring about modification of the resonant speed zones in rotating systems. The natural frequency of the shaft system to which the absorber is attached can potentially be raised or lowered with respect to a selected rotational order to meet most requirements, with tuning effective at all rotational speeds. The process of arranging the geometrical characteristics of the pendulum in this way is called inertia tuning. Resonance tuning is a particular case of inertia tuning and has been the main approach used previously for the design of CPVAs.

However, this disregards a vast range of possibilities for successful design through the use of inertia tuning. This is of particular importance in the case of higher order harmonics where the pendulum length is small and dimension tolerances are critical. Resonance tuning then becomes increasingly difficult to achieve when allowing for wear, thermal expansion, shaft distortion and manufacturing tolerances. These tuning effects have been demonstrated comprehensively with theoretical and experimental results for a CPVA fitted at various points on a crankshaft [5-12, 5-20]. These concepts are described in the theoretical results of Section 5.2.2, demonstrating the control of a shaft system's modes of vibration by the action of the absorber.

5.1.3.3 Bifilar Form Theory

The bifilar form of the CPVA was described earlier as the most practical arrangement of the device. The theoretical description presented here is used in subsequent design of an absorber for experimental study, for which the linear analysis is a sufficiently accurate approximation of its behaviour. Figure 5.2a shows the basic arrangement of this form, detailing the dimensions of interest. It is evident from the geometry of this arrangement that, for small angles of oscillation, the pendulum bob is constrained by its suspension to oscillate about an axis parallel to the axis of shaft rotation which is at a distance from its centre of gravity equal to the length of the suspension links. Therefore the motion which is effected by the links allows the mass of the pendulum bob to be assumed to be concentrated at its centre of gravity and the arrangement is equivalent to the simple rotating pendulum of the previous section. Proof of this behaviour has been discussed in previous research [5-20].

Hence, the equations already derived for the case of the simple pendulum are valid for an absorber with bifilar suspension, with the distance between the axes of rotation and suspension given by;

$$R = R_g - L_P \qquad \{5.6\}$$

where R_g is the radial position of the centre of gravity of the pendulum bob from the carrier rotation axis. The link form of the bifilar suspension is not practical, as discussed in

Section 5.1.3.1, primarily because geometrical considerations prevent the use of links short enough to provide the required tuning for control of the second rotation orders and above. Hence, the arrangement shown in Figure 5.2b is used, with two cylindrical suspension pins rolling in circular holes in the pendulum bob and carrier, achieving higher order tuning more easily. The equivalent length of the pendulum is then as detailed in Figure 5.2c;

$$L_P = \left(d_h - d_p\right) \tag{5.7}$$

where d_h is the hole diameter and d_p the diameter of the pins. The expression defining the resonant tuning case is derived from {5.2} as;

$$n_r = \sqrt{\frac{R_g}{d_h - d_p} - 1} \tag{5.8}$$

The expressions for the pendulum amplitudes for both inertia and resonance tuning, in {5.3} and {5.4} respectively, can then be used with appropriate substitution for L_P and R.

Additionally, the effective inertia of the bifilar form CPVA about the axis of rotation is obtained from {5.5}. The pendulum bob has no angular acceleration about its centre of gravity and can therefore be considered as a concentrated particle of mass m at this point, pivoted at the effective suspension point. However, due to the finite dimensions of the bob, its rotational inertia about the carrier rotation axis should be accounted for. The expression for the effective inertia of the complete absorber at its point of attachment, with N_p identical pendulums attached to the carrier, is then given by;

$$J_{TOTAL}(n) = J_C + N_p J_P + \frac{N_p m R_g^2 \left(R_g - L_P\right)}{R_g - \left(1 + n^2\right) L_P} \tag{5.9}$$

where J_p is the moment of inertia of the pendulum bob about an axis through its centre of gravity parallel to the axis of rotation. Strictly, the moment of inertia of the suspension pins should also be included in the analysis, as discussed by Moore [5-23]. However, this term is generally neglected as it is much smaller than the moment of inertia of the absorber carrier and pendulums.

Equations {5.6} to {5.9} are used in subsequent design of an absorber, as discussed in Section 5.2, for demonstration of the experimental technique of torsional modal analysis.

5.1.3.5 Applications of the CPVA

At a meeting of the Institute of Aeronautical Sciences in 1936, Mr Arthur Nutt, Vice-president of the Wright Aeronautical Corporation expressed the opinion that the development of the CPVA was 'without question one of the most valuable contributions to aircraft engine design in many years' [5-12]. The CPVA was put into practice by Taylor in 1935, making use of the bifilar-type suspension designed by Chilton, to eliminate torsional vibrations for the Wright 'Cyclone' series radial aircraft engine [5-24]. This was a result of the constant demand for more power output driving design changes that increased vibration to unsatisfactory levels. The devices subsequently saw wide application in radial aero-engines, making use of the massive crankweb counterweights intended initially only for mass balancing purposes to give efficient use of weight and space [5-23]. Absorbers successfully reduced crankshaft torsional stresses with excellent results and were seen to give substantial reductions in stresses and wear throughout the power plant and airscrew assembly, permitting higher take-off speeds to be used in some applications.

CPVAs were also used with excellent results on various automotive, industrial and marine engines. The bifilar form was utilised in most cases for the reasons discussed earlier, although in some applications roll-form and unifilar suspension devices proved equally successful. On the crankshafts of medium and high speed in-line engines, both spark and compression ignition, the design problem is complicated by the series of troublesome orders which exist in the operating speed range. The bifilar assemblies were then either distributed along the crankshaft as a form of counterweight, with implications for weight-savings, or mounted on a common carrier at the free-end of the crankshaft for greater accessibility and ease of manufacture. Experimental research in the automotive industry in the 1940s identified the CPVA as the most efficient of all the devices considered, when correctly matched to the characteristics of the rotating system. However, they were not put into large scale production as the less expensive rubber vibration absorber had been developed into a reliable, self-contained unit requiring no lubrication and could be mounted outside the crankcase for inspection purposes. Manufacturing costs, lubrication requirements, and the serious effect of wear on efficiency made the CPVA less economically attractive than other devices.

Development of the CPVA saw its application to large diesel engines, including locomotive powerplants and stationary power generation. When correctly designed and manufactured these absorbers would eliminate resonance problems and improve the vibratory response without dissipating energy, operating for long periods with no appreciable wear or maintenance requirements. CPVAs were also used for the control of camshaft vibration and recently have been employed in this location on a large heavy duty diesel engine [5-25]. This was with the aim of absorbing the energy of the impulse loads created by the injector pulses and was estimated to reduce the loads on the front gear train by 50%. Other example applications include reduction of the main components of driving torque transmitted to an air-compressor driven by a close-coupled electric induction motor [5-19] and to reduce the effects of fluctuating aerodynamic forces in the main rotor of a helicopter [5-26].

The actual non-linear response of the system can be drastically different from that predicted with linear analysis due to the effects of damping and dynamic stability of the periodic response for large amplitude pendulum motion [5-22, 5-27 to 5-32]. The prediction and control of this behaviour would allow more effective use to be made of the mass of the device. Large amplitude motions of a CPVA have also been shown theoretically to possess chaotic dynamics for certain ranges of parameter values [5-33]. However, in practice these absorbers are prevented from achieving excessively large amplitudes during transient behaviour by the use of motion-limiting stops [5-34]. The use of non-circular pendulum paths can be effective in ensuring the period of the motion is independent of the disturbing torque magnitude and, therefore, independent of the pendulum amplitude [5-32, 5-35, 5-36]. Many of the undesirable non-linear properties of the conventional, circular path CPVA can be eliminated by this approach and controlled large angular motion can permit the use of relatively light pendulums.

Interest has recently been revived in the use of CPVAs for automotive applications, where elimination of detrimental torsional vibration would allow the design of smaller, lighter crankshafts resulting in fuel economy improvements and a smoother torque curve comparable with engines of a greater number of cylinders [5-37, 5-38]. In addition to reducing crankshaft torsional vibration, CPVAs were considered for the reduction of engine block vibration resulting from the shaking force generated parallel to the cylinder bores in the crank throw plane [5-17, 5-37, 5-39]. Comprehensive modelling of the engine and absorber system explored these effects and importantly, an estimate of the pendulum damping was determined experimentally for use in the absorber model [5-39]. Experimental and theoretical studies confirmed that CPVAs reduced torsional vibration in these applications by over 90%, although less dramatic reductions were seen for engine block shake.

Hence, the CPVA has the potential for use as an extremely efficient device for the control of torsional vibration. However, a lack of detailed experimental work has been identified as an important factor to determine the limits of recent analytical studies [5-36]. Previously, for investigation of absorber tuning, selective component assembly to give minimisation of torsional vibration response of a system was the main approach. Comparative results of system torsional response with and without the addition of the absorber previously provided a crude measure of its effectiveness. This did not permit comprehensive study of the inertia tuning effects of the absorber on the complete response of the shaft system.

The use of torsional modal analysis will allow the effect of the CPVA in a shaft system to be examined at all frequencies, not just at its resonance tuned order. This experimental technique is demonstrated in a study of various aspects of practical CPVA behaviour to show how the potential of this absorber for wider application in torsional vibration control might be unlocked.

5.2 Development of an Absorber for Experimental Study

For demonstration of this application of torsional modal analysis a CPVA was designed which could be used to control the torsional vibration modes of a simple shaft system. Tuning of the absorber can be explored both as a complete system and with regard to each of the individual pendulums, giving significant advantages over previous limited experimental studies. The mode shapes of the system with the CPVA in use are also readily derived from experimental results, demonstrating exactly how the absorber controls the shaft system response. Estimation of the damping of each mode can also be made. The torsional modal analysis system will permit full consideration to be given to inertia tuning of the CPVA. The main features of the absorber design used in the experimentation are described here, based on previously discussed research and theoretical modelling of these absorbers. Predictions of the shaft system response with the absorber in use are then presented for validation of subsequent experimental results.

5.2.1 CPVA Design Details

The theoretical equations based on linear analysis and presented in Section 5.1.3.3 were used in the design of a bifilar suspension absorber to be used in experimental testing. The primary requirements were to develop a CPVA which would permit a range of resonance tunings to be accommodated, up to a relatively high order, for example 6th. For the assumptions of linear theory to be valid the amplitude of pendulum motions should be within the small angle limits previously discussed by providing enough effective pendulum mass to absorb the torques acting on the carrier in the rotating shaft system. The intention was to allow a series of resonance tunings to be investigated with the same carrier assembly and pendulum bobs, changing only the suspension pins to achieve the desired order. The simple and robust design should be as compact as possible with the pendulums free to move throughout their full range. Consideration should be given to the important dimensions of the device in order that its tuning is as accurate as possible. In typical applications the torsional excitation is a narrow peak at integer orders or half-orders of the rotation frequency, requiring accurate absorber tuning for effective performance. The absorber should allow various aspects of CPVA behaviour to be studied experimentally and compared with predictions.

The final form of the CPVA is shown in Figure 5.4 and the main components can be clearly identified. The absorber was designed to give nominal resonance tuning at the 2.5, 4th and 6th orders which would give reasonable dimensions for the pin diameters within realistic tolerances. Additionally, the CPVA can be located at various points on the shaft system used originally in Chapter 4 and Figure 5.5 shows the absorber in place at the central location used in the experimental tests.

In the design process it is important to consider the interplay between the main dimensions of the absorber. To achieve relatively high orders of resonance tuning, compromises were necessary to optimise the size and mass of the device and ensure a compact design. Space requirements defined the starting point for the design, by specification of the overall diameter of the absorber. From this and the required resonance tuned orders, investigation of the main dimensions looked primarily at the carrier and pendulum bob suspension hole diameter and their radial position, the suspension pin diameter, the form of the pendulum bobs and the position of their centres of gravity. These aspects also serve to define the vibration amplitude of the pendulums at resonance and, hence, the mass and size of the bobs. It was important to ensure that the mass of the pendulums was sufficient to keep the amplitude of their motion in the linear range and also that their mass was much larger than the suspension pins.

A number of areas could be identified from previous research as critical to the correct operation of the device. For the bifilar CPVA the pendulum length is not directly dependent on the pendulum bob dimensions, therefore allowing the active mass of this type of device to be a greater proportion of the total absorber mass. There is a lower limit to which the pendulum length can be practically reduced, occurring when manufacturing tolerances or wear after prolonged service cause sufficient variation of the length to produce an unacceptable change in the assembly tuning characteristics. The primary problem with achieving high orders of resonance tuning is in making the absorber compact enough whilst keeping the difference between the hole and pin diameters feasibly within dimensional limitations. This is particularly apparent when the pendulum length, $L_P = \left(d_h - d_p\right)$, is of the same order of magnitude as component tolerances or predicted wear. This sensitivity to dimensional tolerances demonstrates why inertia tuning allows a more realistic design of CPVA.

Once the dimensions had been optimised, the physical design details of the carrier and pendulums were addressed, including aspects of the shaft clamping arrangement and suspension pin configuration. Close manufacturing tolerances were required, particularly for critical dimensions, most notably the suspension pin diameter and the position and diameter of the suspension holes. Suitable tolerances were specified for the machining of component parts and careful assembly was necessary to ensure smooth operation of the bobs and pins rolling in the tracks. The following paragraphs discuss the main aspects of the final design shown in Figures 5.4 and 5.5.

The basic form of the absorber is as for most practical bifilar form CPVAs, with suspension pins rolling in cylindrical tracks and tuned to the required resonant order. A number of decisions dictated the overall configuration of the device. For control of the estimated torque which would be absorbed by the device three pendulums were arranged 120° apart around the carrier to ensure a balanced assembly. No end-stops were used to limit the amplitude of the pendulum motion, so any non-linearities would be due to deviation from small angle approximations or damping, not impacts of the pendulums.

Different suspension arrangements were considered and in the final form the carrier comprised two plates with the pendulums allowed to move freely in the space between them. This permits a simpler, more accurately produced pendulum bob component which is a critical aspect due to the importance of the position of its centre of gravity in the tuning of the absorber. The solution also encloses the pendulums between the plates, reducing the potential for interference with their motion. Accurate relative alignment of the carrier plates is of paramount importance and problems experienced in this area identified improvements for subsequent CPVA designs. Additionally, the inertia of the carrier assembly is increased and a complicated clamping method is necessitated to maintain the plate alignment. The circular suspension holes were positioned as shown, aligned with the suspension holes of the three pendulum bobs. The final dimensions of the design are presented in Table 5.1, showing the important data used in subsequent theoretical estimations of the absorber performance.

For attachment of the absorber to the shaft a clamping system was required for ease of manufacture and alignment. This was achieved with the two-piece split hub clamp of Figure 5.4, with two bolts acting to fix it tightly around the shaft. One half remains fixed between the two carrier plates to keep them rigidly aligned, while the other is free to be loosened and allow assembly onto the shaft. The friction clamping system eliminates the possibility of slipping between the carrier and shaft which would be detrimental to the absorber operation and may damage the shaft. This compact symmetrical design minimises the imbalance of the carrier and is small enough not to interfere with the pendulum motion. Easy installation of the absorber is possible at a range of points along the shaft where access can be gained.

Table 5.1: Primary dimensions of the CPVA design

Dimension	Quantity	Value
Overall absorber diameter (6th order tuning)	-	200 mm
Carrier diameter	-	190 mm
Carrier thickness	-	21 mm
Suspension hole diameter	d_h	25.0 mm
Radial position of pendulum bob centre of gravity (6th order tuning)	R_g	73.7mm
Carrier assembly (incl. clamp) moment of inertia *(about the rotation axis)*	J_C	$5.328 \times 10^{-3}\ \mathrm{kg.m^2}$
Pendulum bob moment of inertia *(about its centre of gravity)*	J_P	$3.247 \times 10^{-4}\ \mathrm{kg.m^2}$
Pendulum bob mass	m	0.297 kg

The physical form of the pendulum bobs was determined by mass and inertia performance requirements, ease of accurate manufacture and robust construction. Various shapes were considered in which examination of the geometrical restrictions and the final design allowed straightforward calculation of the position of the centre of gravity in relation to the outer radial limit. The bob dimensions have a direct effect on the overall diameter of the absorber and these were selected to achieve the smallest absorber for a given carrier hole position, with the largest pendulum length. The mass of the pendulum bob, controlled by thickness, defines its effectiveness in absorbing the torque acting on the carrier location with resonance-tuning whilst remaining within the small angle limit of operation. Additionally, the minimum speed could be estimated at which the absorber could rotate without the pendulums becoming detached from the suspension hole tracks due to gravitational effects. By equating the centrifugal force with the weight of a pendulum bob this was estimated at 110rpm for the 6th order tuning.

The suspension pins consist of a central section retained in position in the carrier holes with large flanges. These flanges are made from PTFE for minimal friction and low mass, with a long bolt passing through both. The central section can be easily interchanged to alter the tuning of the absorber and is made of steel, to minimise problems with wear, and would be hardened for a more robust design. The final suspension pin diameters for the three orders selected for resonance-tuning are detailed in Table 5.2, showing the actual tuned order achieved in the design with the dimensions selected for ease of manufacture. Additionally, these components are hollow to minimise their mass, so the motion of the pins can be neglected in the theoretical modelling of the device. Although for the largest pin diameter used (23mm for 6th order) the mass of a single suspension pin was estimated to be 14% of a pendulum bob, its centroidal moment of inertia is only 0.5% of that of the bob and the pins will have minimal effect on the absorber performance, as confirmed in the experimental results.

Table 5.2: Suspension pin diameters and estimated order of resonance tuning

Nominal order of resonance tuning, n_r	Suspension pin diameter d_p (mm)	Actual resonance tuned order
2.5	13.5	2.497
4	20.5	3.991
6	23.0	5.987

The range of required resonance tunings can therefore be readily accommodated by changing the suspension pin sections and using the same pendulum bobs. Additionally, tapped holes were provided in the carrier which allowed the pendulums to be individually restrained for subsequent experimental studies. This versatile CPVA design will be used to investigate a range of aspects related to its practical operation using advanced experimental techniques.

5.2.2 Modelling of the Shaft and Absorber System

Theoretical modelling of the complete shaft and absorber system response was used to confirm that the absorber is operating as designed. Prediction of the natural frequencies and mode shapes of the shaft system with the absorber would provide validation of the torsional modal analysis results. The effect of a CPVA when used in a multi-inertia system will be demonstrated, confirming the importance of considering the whole shaft system, rather than just the absorber attachment point in isolation, and reinforcing the need for a versatile experimental study.

The experimental shaft system is shown in Figure 5.6, identifying the two positions where the absorber was attached in the experimental testing. The absorber was to be used at the end of the shaft and at a central location to give different examples of CPVA operation. This would enable investigation of the absorber behaviour with each of the three sets of suspension pins and at a range of rotation speeds, thus changing the torsional mode of the shaft system to be affected by the action of the CPVA. For brevity, theoretical predictions of the absorber behaviour are presented here for just one example of tuning, a CPVA resonance tuned to 6th order and mounted at the central location of the shaft system. This discussion is equally applicable to the other arrangements considered in the experimental study as identified for each area.

The theoretical expressions describing the absorber behaviour in Section 5.1.3.3 were used as the basis for this modelling procedure. An appropriate form of the lumped parameter model, described in Appendix B, was then used to predict the shaft system response in terms of the resulting natural frequencies and mode shapes. The mode shapes resulting from the action of the absorber are obtained theoretically by solution of the eigenvectors of the system, but are not known to have previously been considered experimentally. This can now be achieved with the new technique of torsional modal analysis.

5.2.2.1 Effective Inertia of the Absorber

A CPVA can be used to modify the torsional natural frequencies and hence critical speeds of rotating systems by providing adjustment of the effective inertia at its point of attachment to the shaft with respect to a given rotation order. Figure 5.7a shows the variation of effective inertia of the experimental absorber with order number. This is derived from equation {5.9} using the geometric values discussed in Section 5.2.1 and is a standard approach used to consider the absorber's behaviour [5-12]. It is clearly apparent that at the resonance tuned order, 6th in this case, the absorber has an infinite inertia, with the vertical asymptote separating the branches of the diagram. The sign of the effective inertia either side of the resonance tuning point defines the phase of the pendulum motion relative to the carrier. The other suspension pin diameters gave similar variation in the effective inertia of the absorber at its attachment point, with the resonance tuned order occurring at 2.5 and 4th order as intended.

The effective inertia as a function of order is independent of rotation speed. However, for ease of understanding in the experimental system considered here, it is convenient to re-consider the ordinate of Figure 5.7a in units of frequency. Hence, the resonance tuned frequency of the absorber is a function of rotation speed and Figure 5.7b shows the variation of effective inertia with frequency for an example rotation speed of 300rpm. By changing the speed of rotation of the shaft system, the frequency at which resonance tuning occurs can be changed, to affect any torsional mode of the system.

As the absorber appears as a different inertia in the system with respect to each rotation order, control of this effect, or inertia tuning, can change the natural frequencies of the shaft system as required. The basic method of inertia tuning is to adjust the physical characteristics of the pendulum to provide a chosen value of effective inertia at the location of the absorber carrier, from almost any required value between negative and positive infinity. Determination of the required inertia value is achieved through consideration of the tuning curve, as discussed in the next section, and this technique aims to remove troublesome shaft system resonances from the service speed range. The main disadvantage with resonance tuning, using the infinite inertia of the absorber to control a mode of the shaft system, is the inherent sensitivity to geometrical tolerances. In the region of the harmonic order to which an absorber is resonance tuned small changes of the pendulum length can produce considerable changes in the value of resultant effective inertia and, therefore, in the tuning of the shaft system, resulting in new critical speeds which may be encountered during start-up or run-down. These difficulties were responsible for some of the problems experienced during the early development of resonance-tuned CPVAs. Inertia tuning provides the opportunity for utilising reasonable manufacturing tolerances with adequate wear margins.

The effect on the modes away from the resonance tuned effect of the absorber can be considered by examining the effective inertia plot of Figure 5.7a and noting the important points [5-12]. At order $n = 0$ the effective inertia of the absorber represents the condition when the pendulum bobs are, in effect, rigidly connected to the carrier at a radius equal to the distance of the centre of gravity of the pendulum bob from the carrier rotation axis. The resultant effective inertia at the absorber location can be calculated as;

$$J_{TOTAL}(0) = J_C + N_p J_P + N_p m R_g^{\,2} \qquad \{5.10\}$$

At the other extreme, as $n \to \infty$, the masses become 'virtually disconnected' from the carrier and the effective inertia approaches the sum of the CPVA carrier inertia and the centroidal inertia of the pendulum bobs;

$$J_{TOTAL}(\infty) = J_C + N_p J_P \qquad \{5.11\}$$

Additionally, an order can be identified where the resultant effective inertia of the absorber at its attachment point is effectively zero, approximately 8.0 for the experimental CPVA.

5.2.2.2 Tuning Curve

The best way to examine the effect of the absorber on the response of the shaft system is to plot the 'tuning curve' for the system. This shows how the variation of the effective inertia at the position of the CPVA controls the corresponding natural frequencies of the complete shaft system assembly. Figure 5.8 shows the tuning curve for the shaft system under consideration with the absorber attached at the central location (Position B for the experimental shaft system of Figure 5.6).

The tuning curve is plotted from the lumped parameter model derived for the system, where solution of the eigenvalues gives the natural frequencies as a function of the resultant effective inertia at the absorber attachment point. Therefore, it is possible to derive directly the natural frequencies of the system corresponding to any given value of resultant effective inertia at this point. For example, the natural frequencies of the system can be easily determined when a constant inertia is located at this position. The figure shows a series of curves, which as the frequency values increase are related to modes with an increasing number of nodes. Careful identification of the modes is necessary due to the modification of nodal position which occurs with the change in effective inertia and this is illustrated in the experimental results.

Inertia tuning of the absorber can be considered by superimposing the absorber effective inertia plot of Figure 5.7b onto this graph, allowing the natural frequencies of the shaft system to be determined. The points where the absorber effective inertia coincides with the tuning curve define the resultant natural frequencies of the shaft system. Adjustment of the effective inertia of the absorber, by changing the resonance tuning frequency of the absorber, will give a new series of natural frequencies of the system. Additionally, changing the rotation speed will change the resonance tuned point of the absorber with respect to frequency with a similar effect.

Careful selection of the required effective inertia from the tuning curve can determine if sufficient margins are available to accommodate changes in component dimensions due to manufacturing tolerances or wear, without unacceptably changing the critical speeds of the shaft system. The effect of attaching the CPVA at alternative points along the shaft can be predicted from appropriate tuning curves. The torsional response of a system can be carefully controlled through selection of the absorber position and inertia tuning.

5.2.2.3 Frequency Response Functions

The effect of the varying inertia of the absorber with respect to frequency and rotation speed is clearly apparent through consideration of theoretical FRFs predicted from forced vibration analysis of the shaft system. This used the lumped parameter model discussed previously, normalising the response across the frequency range to allow comparison with experimental FRFs. For the undamped model used, the relative phase of the points on the shaft is either 0° or 180°, exactly in or out of phase.

When adding a CPVA to a shaft system there is ambiguity in defining the unmodified system, whether this is the original shaft system, just the carrier attached or the CPVA with pendulum bobs in position but restrained to prevent their movement. In previous applications it has been common to modify existing shaft inertias, such as the counterbalance weights of a reciprocating engine crankshaft, to form the pendulums of an absorber system. Therefore, to demonstrate the effect of the CPVA on the shaft system response in this study, the behaviour will be compared to that with the pendulum bobs rigidly fixed in position. This is subsequently described as a 'locked' absorber and Figure 5.9a shows the predicted FRF for this system at the CPVA location.

For comparison, Figure 5.9b shows the modelled response for the CPVA operating with its 6th order resonance tuning in the region of Mode I of the previous system. The action of the absorber has split Mode I of the locked absorber system into two peaks separated by an anti-resonance, creating two new vibration modes for the system. These are designated Modes Ia and Ib consistent with their parent mode. Mode II is close to the previous value, but Mode III is increased from that with the locked absorber and close to the value for the system with only the carrier attached. This can be deduced from the effective inertia of the absorber at these frequencies, as discussed in Section 5.2.2.1.

Increasing the rotation speed of the shaft, with everything else remaining the same, causes the frequency of the absorber resonance tuning and the resulting anti-resonance in the shaft system response, to increase. Figure 5.10a shows the system response at 400rpm, where the absorber effect is in the minimum between Mode I and II of the locked system FRF. In this low response region the action of the absorber is not as apparent as when located directly on a mode. Although the large effective inertia of the absorber severely reduces the response magnitude at its attachment point, the new modes resulting were seen to have much increased response at the excitation disk location. Thus, it is evident that the whole system must be considered with a CPVA in use to ensure that favourable response results from the action of the absorber at all positions. At a rotation speed of 500rpm the absorber resonance tuning occurs at 50Hz as apparent in the FRF of Figure 5.10b. The absorber effect is to split Mode II from the locked system into two clear peaks.

5.2.2.4 Estimation of Natural Frequencies and Mode Shapes

For the locked absorber, or where the carrier inertia alone is attached to the shaft, it is a simple matter to derive the natural frequencies and mode shapes of the modelled shaft system. This is achieved by determination of the eigenvalues and eigenvectors of the system matrix and these are presented for comparison with the following experimental results. However, with the CPVA operating the inertia at the absorber location is no longer constant but is a function of frequency, resulting in a significantly more complex characteristic equation.

Various approaches are possible to solve this equation and determine the natural frequencies of the system. The effective inertia curve for the absorber could be superimposed on the system tuning curve, as considered above, with the points at which the two curves cross defining the resultant natural frequencies of the system. Alternatively, the expression for the absorber effective inertia can be inserted into the lumped parameter model. Solution of the characteristic equation is obtained by iteration, identifying where the calculated system eigenvalues are effectively equal to the excitation frequency. More simply, by examining the forced response of the system as given in Section 5.2.2.3 the peaks from the FRFs of the system can be located, thus indicating the resonant modes. To calculate the corresponding mode shapes from the identified natural frequencies, it is necessary to substitute each of these values into the effective inertia expression in turn and calculate the appropriate eigenvector for each case.

The natural frequencies were predicted for the shaft system with the 6th order resonance tuned absorber attached at the central shaft location. Table 5.3 lists the natural frequencies for the three non-zero modes of the system with the locked absorber. The corresponding theoretical mode shapes for this case are shown in Figure 5.11, with the nodal positions clearly identified.

Table 5.3: Predicted natural frequencies of the shaft system with locked absorber on central shaft location. 6th order suspension pins.

	Mode I	*Mode II*	*Mode III*
Modal Frequency	27.31Hz	49.94Hz	101.98Hz

Following the approach discussed above the natural frequencies of the shaft system with the 6th order absorber operating can be estimated. These are given in Table 5.4 for the shaft rotating at 300rpm. From these values the mode shapes can be predicted and are shown in Figure 5.12. It can be seen that the first two modes, labelled Ia and Ib, are both one-node modes. The different positions of the node compared to the locked system result from the effective inertia of the absorber at these frequencies. The other mode shapes are relatively unchanged from the locked absorber case due to being remote from the resonance tuned order of the absorber and the actual displacement magnitudes are related to the effective inertia at the absorber location.

Table 5.4: Predicted modes for 6th order absorber on centre section of shaft. Rotation speed 300rpm

	Mode Ia	*Mode Ib*	*Mode II*	*Mode III*
Modal Frequency	25.81Hz	32.07Hz	50.81Hz	131.61Hz
Change from locked absorber (Hz)	*-1.50*	*+4.76*	*+0.87*	*+29.63*

Modelled results for the locked 2.5 and 4th order absorbers were very similar to those presented here, with only small differences resulting from the change in inertia due to the different pin diameters. For the functioning 2.5 and 4th order absorbers with the speed arranged to put the resonance tuned frequency in Mode I, the predicted natural frequencies and mode shapes of the shaft system were also very similar to the 6th order results.

This theoretical modelling has introduced the operation of the absorber and illustrated its behaviour in controlling the torsional vibration modes of a multi-inertia shaft system. In subsequent sections experimental measurements compare well with these predictions, obtaining an unprecedented depth of information concerning CPVA operation, through the use of torsional modal analysis.

5.3 Experimental Results

To demonstrate the operation of the CPVA design introduced previously, it was fixed to an experimental shaft system in two locations. It is apparent that this device needs to rotate in order to function and this has limited the depth of previous studies. With the new experimental technology for torsional modal analysis described in Chapter 4, it is possible to excite any required frequency with a calibrated input and measure the system response.

The previous simple shaft system of Chapter 4 was used in this study and Figure 5.6 shows the two locations along the shaft labelled Position A and B, at which the absorber was attached. Obviously, to have a significant effect on a mode it is necessary to ensure the absorber is located away from the nodal positions. For comparison, results were obtained in each case for the locked absorber system to emphasise the effect of the functioning CPVA. This is analogous to modification of a crankshaft's counterweights to form pendulum absorbers without an overall weight increase.

5.3.1 Absorber on End of Shaft

The absorber was initially attached to the shaft at Position A of Figure 5.6, where it would have most effect on Mode I, with a nominal resonance tuning of $n_r = 2.5$. The results presented here show the effect of the inertia of the pendulums, both when locked in position and when functioning as absorbers.

5.3.1.1 Locked Absorber

Initial results considered the vibration behaviour of the system with the locked absorber. Figure 5.13 shows the torsional vibration FRF for the carrier position at a nominal rotation speed of 600rpm, with the first three non-zero natural frequencies of the system readily identified. Subsequent modal analysis of the set of FRFs taken from the nine locations along the shaft gave clear identification of the mode shapes of the system. Modal frequency and damping values estimated from the maximum response points of each mode are shown in Table 5.5. The mode shapes are shown in Figure 5.14, with Modes I and II quite clear and the relative phase relationship of each point along the shaft very close to 0° or 180°. The smaller response points for Mode III are close to the noise floor, although the nodal points can still be identified along the shaft.

Table 5.5: Experimental modal frequency and damping for shaft system with locked absorber attached to free-end location, Position A.

	Mode I	*Mode II*	*Mode III*
Modal Frequency	23.04Hz	50.60Hz	74.36Hz
Modal Damping	2.44%	0.972%	0.490%

5.3.1.2 Absorber Functioning

With the absorber resonance tuned to $n_r = 2.5$, the shaft system rotating at 600rpm and the pendulums allowed to move freely, the effect of the absorber is clearly apparent in the FRF of Figure 5.15. Mode I, the one-node mode previously at approximately 23Hz has been split into two smaller peaks, Modes Ia and Ib, with a drop in the maximum response compared to the locked absorber system of approximately 50%. The modal frequencies and damping estimated from these results are presented in Table 5.6.

Table 5.6: Experimental modal frequency and damping for shaft system with absorber resonance tuned to 2.5 order and attached to free-end location, Position A.

	Mode Ia	*Mode Ib*	*Mode II*	*Mode III*
Modal Frequency	20.05Hz	31.72Hz	51.39Hz	92.76Hz
Change from locked absorber (Hz)	*-2.99*	*+8.68*	*+0.79*	*+18.4*
Modal Damping	2.21%	3.85%	1.42%	1.47%

Figures 5.16a & b show the four mode shapes derived from FRFs obtained for all nine locations along the shaft. It can be seen that Modes Ia and Ib are both one-node modes, consistent with their parent mode. These mode shapes show movement of their nodal points when compared to the locked absorber case. Mode Ia has a reduced frequency compared to the Mode I, due to the increased effective inertia of the CPVA at that frequency. The higher frequency of Mode Ib confirms that the absorber effective inertia is decreased at this frequency.

The mode shape of Mode II has changed slightly from the locked absorber response, with the nodal point, which was close the excitation disk, having moved towards the centre of the shaft. The nodal positions of Mode III can also be identified between the excitation disk and the absorber position while the response of this mode approaches the instrumentation noise floor away from the free end of the system. The CPVA operation has increased the natural frequencies of these modes as the effective inertia is reduced and tends towards that of the carrier only at frequencies above the resonance tuning frequency of the absorber.

5.3.2 Absorber on Central Shaft

In further investigations, the CPVA was fixed at the central shaft section at Position B of Figure 5.6. This point was selected because, at an appropriate rotation speed, the absorber could potentially have an effect on either Mode I or II of the system. The three different sets of suspension pins were used, which set the nominal resonance tuning of the absorber at 2.5, 4th and 6th order and, initially, results were obtained with the absorber locked.

5.3.2.1 Locked Absorber with 2.5, 4th and 6th Order Suspension Pins

With the carrier in the central location, each of the three sets of suspension pins were used in turn to suspend the pendulum bobs while they were locked in place. The aim was to illustrate the minor differences which occur through changing the positions of the pendulum centres of gravity with different suspension pins.

For comparison with these results, the torsional vibration response of the system with just the carrier attached was also considered. The first three modes were evident and, most notably, the response of Mode III was measured at 144Hz. This demonstrated an increased upper frequency limit for the torsional modal analysis system. Despite some corruption of the measurements due to noise at this frequency, it was possible to estimate the nodal positions in the mode shape, occurring as expected in the shaft sections between each of the principal inertias.

With the locked absorber, the three resulting distinct natural modes of vibration can be identified in Figures 5.17a to c. These show the FRFs from the carrier location with each of the three sets of suspension pins in use and the results are all quite similar. For each of these tests the rotation speed was fixed at the value which would put the resonance tuning of the functioning absorber into the response of Mode I of the locked absorber system, which were 650rpm, 400rpm and 300rpm for the 2.5, 4th and 6th order suspension pins respectively.

Sets of FRFs from all measurement locations along the shaft were obtained and the modal frequency and damping values estimated are presented in Tables 5.7a to c for each of the three suspension pin sets. The increased pin diameters used to give higher order resonance tuning cause the pendulum bob centres of gravity to be located slightly closer to the rotation axis, reducing the total moment of inertia of the locked absorber. This marginally increases the modal frequencies, with a much greater reduction in inertia between the 4th and 6th order suspension pin results, than between the 2.5 and 4th order results. In Chapter 4, the torsional natural frequencies of the shaft system were seen to increase with decreasing rotation speed but the changes were smaller in magnitude than the predominant effect in this instance.

Table 5.7: Modal frequency and damping values with locked absorber located on central shaft section, Position B.

a. Suspension pins for 2.5 order resonance tuning. Rotation speed: 650rpm.

	Mode I	*Mode II*	*Mode III*
Modal Frequency	26.69Hz	50.20Hz	97.90Hz
Modal Damping	2.72%	0.948%	0.622%

b. Suspension pins for 4th order resonance tuning. Rotation speed: 400rpm.

	Mode I	*Mode II*	*Mode III*
Modal Frequency	27.03Hz	50.63Hz	99.97Hz
Modal Damping	2.38%	0.873%	0.523%

c. Suspension pins for 6th order resonance tuning. Rotation speed: 300rpm.

	Mode I	*Mode II*	*Mode III*
Modal Frequency	27.11Hz	50.61Hz	99.85Hz
Modal Damping	2.16%	0.745%	0.627%

The accompanying mode shapes are shown in Figures 5.18a to c and are very similar for all three tuning pin sets as expected, with only small differences existing between them due to changes in the total moment of inertia of the locked absorber. Comparison of these mode shapes with those of the locked absorber system on the end of the shaft, in Figure 5.14, shows Modes I and II to be very similar. The most notable difference is the displacement of the free-end of the shaft for Mode II and the movement of the nodes due to the absorber inertia having been moved from the end of the shaft to the centre. The mode shapes derived for Mode III gives clear identification of nodal positions and the central anti-node region.

The shaft system response predicted with the model of Section 5.2.2 agreed closely with these experimental results, with the estimated modal frequencies within +/-2% of experimentally derived values. Additionally, the experimental FRFs for the three arrangements are all close to that of Figure 5.9a although the lack of damping in the modelled results is clearly apparent. Comparing the experimental mode shapes with the theoretical ones of Figure 5.11 demonstrates that the modelled shaft system closely approximates the practical behaviour. The magnitude of predicted mass normalised modal displacements are close to the experimental values for the first two modes. The experimental unity modal mass (UMM) displacements are smaller than the modelled system results for Mode III, due to the inherent over-estimation of the torque applied by the excitation system at elevated frequencies, which increases with decreasing rotation speed as discussed in Chapter 4.

In summary, the experimental results obtained with torsional modal analysis for the locked absorber demonstrate clearly the minor changes occurring in the system. These are a result of the different suspension pin diameters moving the centre of gravity of the pendulum bobs relative to the shaft rotation axis, changing the total moment of inertia of the CPVA assembly.

5.3.2.2 Absorber Resonance Tuned to 2.5 Order

Using the 2.5 order pins, with the rotation speed of the system set nominally at 650rpm, the absorber would act to attenuate the response of the central section of shaft in Mode I. The FRF from the carrier location is shown in Figure 5.19 with the previous peak of Mode

I for the locked absorber now split into two. The modal frequencies and damping are shown in Table 5.8 and the mode shapes obtained are illustrated in Figure 5.20.

Table 5.8: Modal frequency and damping values with absorber resonance tuned to 2.5 order and located on central shaft section, Position B. Rotation speed 650rpm.

	Mode Ia	*Mode Ib*	*Mode II*
Modal Frequency	24.86Hz	30.10Hz	51.77Hz
Change from locked absorber (Hz)	*-1.83*	*+3.41*	*+1.57*
Modal Damping	3.00%	3.71%	1.82%

The mode shapes of Modes Ia and Ib are similar, with the nodal point towards the flywheel location. For Mode Ib the central section of shaft appears flatter around location 5, with reduced response of the flywheel end of the shaft compared to Mode Ia but the excitation disk participates with greater relative magnitude. Mode II has undergone a slight increase in its frequency as a result of the decreased inertia of the absorber compared to the locked absorber case. Its shape appears predominantly as before, occurring at a frequency significantly higher than the resonance tuned frequency of the absorber. It was not possible to detect Mode III in any of the experimental studies with the absorber in this location as its natural frequency has been presumably increased beyond the range excitable by the torsional modal analysis system.

5.3.2.3 Absorber Resonance Tuned to 4th Order

Using the 4th order suspension pins, the rotation speed of the system was set nominally at 400rpm to keep the resonance tuned frequency of the absorber close to Mode I of the locked absorber system. Figure 5.21 shows the FRF from the carrier location with the previously observed Mode I peak split into two smaller ones. At the anti-resonance between Modes Ia and Ib a series of minima are apparent which, it is demonstrated later, are related to the tuning of the individual pendulums. The modal frequencies and damping are shown in Table 5.9 and the mode shapes are illustrated in Figure 5.22.

The results are similar to those for the 2.5 order tuning of the absorber, with similar changes in the frequencies of the modes. As before, Modes Ia and Ib are related in appearance with the nodal point occurring towards the flywheel location. The central shaft section for Mode Ib undergoes less relative torsional displacement compared to Mode Ia and reduced response of the flywheel end of the shaft. The mode shape of Mode II has changed very little and its frequency is slightly increased from the locked absorber case due to the small change in the total moment of inertia at the absorber location.

Table 5.9: Modal frequency and damping values with absorber resonance tuned to 4th order and located on central shaft section, Position B. Rotation speed 400rpm.

	Mode Ia	*Mode Ib*	*Mode II*
Modal Frequency	24.12Hz	29.90Hz	52.02Hz
Change from locked absorber (Hz)	*-2.91*	*+2.87*	*+1.39*
Modal Damping	1.32%	1.17%	1.15%

5.3.2.4 Absorber Resonance Tuned to 6th Order

The results in this section are very similar to those of the previous two sections. The aim is to illustrate the minor differences which occur through changing the diameter of the pendulum suspension pins to achieve a higher order of resonance tuning for the absorber. This should demonstrate the effect of this practical device on the torsional vibration modes of the rotating shaft system.

With the CPVA resonance tuned at 6th order the rotation speed of the system was set nominally at 300rpm to put the resonance tuned frequency of the absorber approximately equal to Mode I of the locked absorber system. The effect of the absorber functioning is apparent in the FRF of Figure 5.23 where the split peak of Mode I is again clear. The broad anti-resonant region exhibits a series of minima, which are related to the slightly different tunings of the individual pendulums. In addition, the phase of the FRF has distinct regions where the effect of each pendulum is apparent. This phenomenon was observed in the previous results but is most apparent for this order of tuning.

Table 5.10 shows the modal analysis results obtained for the shaft system, with the mode shapes displayed in Figure 5.24. These experimental results can be compared directly with the theoretical predictions of Section 5.2.2 to confirm that the absorber is operating as designed. The FRFs, modal frequencies and mode shapes can be related to the changing effective inertia of the absorber with frequency. The modelled FRF of Figure 5.10b for the 6th order resonance tuned absorber agrees closely with the experimental result of Figure 5.23 although the lack of damping in the theoretical model sharpens the peaks. The modal frequencies were predicted to within +/-3.3% and the changes in the experimentally obtained frequencies from the locked absorber case were also of very similar magnitude to those of the theoretical results.

Table 5.10: Modal frequency and damping values with absorber resonance tuned to 6th order and located on central shaft section, Position B. Rotation speed 300rpm.

	Mode Ia	Mode Ib	Mode II
Modal Frequency	25.40Hz	31.04Hz	52.49Hz
Change from locked absorber (Hz)	*-1.71*	*+3.93*	*+1.88*
Modal Damping	1.83%	1.00%	0.887%

Comparison of the experimental and theoretical mode shapes, in Figures 5.24 and 5.12 respectively, demonstrates that the modelled absorber closely approximates the behaviour of the practical device. (Similar theoretical results were predicted for the 2.5 and 4th order resonance tunings.) The mode shape of Mode Ia for the 6th order resonance tuned absorber again shows the movement of the node away from the position defined for the locked absorber results, as a result of the increased inertia of the absorber. Mode Ib also follows the same trend seen with the other resonance tunings with the nodal point moved along the shaft towards the flywheel and reduced relative displacement at the excitation disk. Additionally, the flatter region occurring in the centre of the shaft due to the effect of the absorber inertia is confirmed in the model results. The experimental mass normalised modal displacements are generally similar in magnitude to those modelled, particularly for Mode II where the absorber inertia is changing less rapidly with frequency.

In conclusion, the absorber works as intended in controlling Mode I for each of the three order tunings used as demonstrated by experimental torsional modal analysis. The next step is to use this technique to consider in more detail the important factors determining the practical operation of the device.

5.4 Detailed Study of the CPVA Operation

Building on the previous torsional modal analysis results, key areas were identified to study the CPVA operation in detail. These were seen to be the tuning of the individual pendulums and the effect of rotation speed and excitation level on its performance. FRFs were obtained to illustrate these aspects and similar results were seen for all three of the suspension pins sets used in this study. However, for brevity only the results obtained using the 6th order resonance tuning pins will be presented here. These results provide useful insight into the practical operation of these torsional vibration control devices.

5.4.1 Individual Pendulum Tuning

To examine the tuning of the pendulums the spectrum analyser was set up to give the FRFs with the 'frequency' axis in orders of rotation frequency. This was achieved with the use of a photocell tachometer which derived a once per revolution pulse from the flywheel of the shaft system. The signal from the tachometer was fed into the triggering input of the spectrum analyser.

It was necessary to lock up the other two pendulum bobs to prevent them from moving in order to study the tuning of each pendulum individually. This was the most appropriate way to achieve this, rather than removing the unwanted bobs, for a number of reasons. Most importantly, having all three pendulums in place would minimise the resultant imbalance of the rotating system. Additionally, below the resonant tuning frequency of the absorber its inertia is similar to that with all the pendulums unlocked, since in this frequency range the pendulums behave as if they are rigidly connected to the carrier. However, when the pendulums are all unlocked, at excitation frequencies above the resonant tuning point the pendulums become, in effect, virtually disconnected from the carrier as described in Section 5.2.2.1. A further concern is that with only one of the pendulums unlocked it has to exert three times the torque in response to the excitation than when they are all unlocked, based on the conventional assumption that the pendulum motions are all in phase. This has the potential for over-excitation of the pendulum, driving it into the non-linear range due to excessive amplitude, although the absorber had been designed to avoid this occurrence.

From the results of this study, Figure 5.25a shows the response of the shaft system with all three pendulums locked. Figure 5.25b shows the system FRF with all three pendulums unlocked and operating as absorbers to control the shaft response in Mode I. These two plots are in effect identical to Figures 5.17c and 5.23 respectively but with the ordinate axis now given in orders of rotation frequency. With the absorber operating the three anti-resonances due to each of the pendulums can be clearly identified and the three torsional vibration modes of the system at this rotation speed are quite distinct.

By restraining two of the pendulums, labelled 2 and 3, the order of resonance tuning of pendulum 1 can be examined and Figure 5.25c shows the single clear anti-resonance which results. The three modal peaks appear symmetrical, implying minimal non-linear effects. Figures 5.25d & e show the corresponding results obtained for the behaviour of pendulums 2 and 3 individually unlocked. From these FRFs the order for which each pendulum is actually resonance tuned can be identified, for comparison with the nominal 6th order for which they were designed and these values are listed in Table 5.11. The locations of the three anti-resonances of Figure 5.25b are also listed and are assumed to correspond to the pendulums as shown. These compare very well with values from the individual measurements to within +/-1%, close to the resolution of the spectrum analyser which is 0.025 orders for the results shown. The noise floor of the measurements will start to become significant in these regions of low response and the exact minimum response point for the shaft system may be difficult to determine. In addition, with all the pendulums functioning, the locations of the anti-resonances are a function of the combined behaviour of the whole absorber system when attached to the shaft and the minima recorded may not be entirely attributable to the individual action of one pendulum.

From these experimental measurements of the resonance tuned order of the pendulums the variations in absorber dimensions which would result in this tuning can be estimated and compared to the geometrical tolerances of the actual CPVA. The deviation of the tuning from that intended can be attributed to any of the critical dimensions determined in the CPVA theory discussed in Sections 5.1 and 5.2. These are primarily seen to be the pin diameters, carrier and pendulum bob suspension hole diameters and the positioning of these holes.

Table 5.11: Experimentally determined orders of resonance tuning for the three individual pendulums. Nominal resonance tuning of 6th order.

Pendulum No.	Individual pendulums functioning (Figures 5.25c to e)	All pendulums functioning (Figure 5.25b)
1	5.475	5.450
2	5.675	5.650
3	5.850	5.925

All the important dimensions of the absorber were measured, demonstrating the scatter of these component sizes about the intended values. However, it is difficult to determine the relative position of the constituent parts. These measurements only give an approximate estimation of the absorber geometry and, therefore, the maximum and minimum deviations of the dimensions were considered. Measurement of the pin diameters demonstrated that these are close to the intended size, in the tolerance range -0.08mm to -0.03mm for the 6th order. Additionally, the main dimensions of the pendulum bobs had been accurately machined and their suspension hole diameters were all in the tolerance range +0.00mm to +0.14mm. Therefore, the other two governing factors, carrier hole positioning and diameter, were each considered separately with all other factors assumed fixed at their nominal values.

To give the range of resonance tunings observed, theoretical predictions showed that the variation between the minimum and maximum radial carrier hole positions would be of the order of 10mm, much greater than the measured tolerance range of approximately 0.3mm. However, the similarly predicted values of suspension hole diameter covered a range of 0.37mm to result in the recorded range of resonance tuning, compared to the measured minimum to maximum variation in this dimension of 0.46mm. It is this dimension that is most important when attempting accurate tuning of a CPVA. Furthermore, by interchanging the sets of bobs and pins between carrier hole locations in experimental tests, the tuned orders for each carrier hole location remained approximately the same. Hence, the tuning anomalies are primarily due to the carrier hole diameters. The actual tolerance range for the carrier suspension hole diameters, +0.06mm to +0.52mm, confirms why the pendulum tunings are consistently lower than those predicted in the design of the absorber.

An important point to note is that for these calculations the simplifications assumed for the bifilar suspension do not allow for the dimensions of all the parts. In the case of the suspension hole diameter, the theory uses a single value where in practice there are two sets of two holes in the carrier and two holes in each bob. For theoretical purposes these are assumed to be equal, no allowance is made for their relative position and their profile is considered to be perfectly circular. Practical problems of manufacturing processes and component alignment will result in kinematic behaviour of each pendulum which may differ from the perfect case.

These results give a clear indication of the potential of the torsional modal analysis technique, which has allowed accurate examination of the tuning of the individual pendulums of a CPVA to be determined and then related to the dimensional tolerances of the component parts. For development of a practical absorber with critical tuning this approach would prove invaluable. These results can be used to suggest improvements to the design to address the important dimensions and ensure that reliable tuning of the device can be achieved with realistic manufacturing tolerances.

5.4.2 Effect of Rotation Speed

With the intention of using the CPVA to control the response of Mode II of the system when fixed at the central shaft section, Position B of Figure 5.6, the shaft rotation speed was increased in order that the resonance-tuned order of the absorber would act at a higher frequency. Figures 5.26a to e show the FRFs recorded for the series of speed increments considered, to illustrate the effects observed. These results can be compared with the previous theoretical results of Figures 9b and 10, to confirm the actual absorber response is as predicted by the model. For completeness, Figure 5.26a gives the response of the system when rotating at 250rpm, with the absorber functioning distinctly in the region below the maximum of Mode I. Figure 5.23 discussed previously showed the behaviour of the system at 300rpm, the optimum speed for control of Mode I. With the shaft rotating above that speed, at 350rpm and 400rpm, the absorber operation is shown in

Figures 5.26b & c respectively, where the frequency of operation of the absorber passes into the minimum region between Modes I and II and its effect is hardly apparent.

With further increases in shaft rotation speed the resonance tuned frequency of the absorber enters the region of Mode II. However, at 450rpm and then 500rpm the experimental FRFs of Figures 5.26d & e do not show the expected sharp anti-resonances. For these two speeds the nominal resonance tuning of 6th order should occur at frequencies of 45Hz and 50Hz respectively. Instead, a wider spread of interruptions to the response are apparent. Repetition of these results demonstrated that consistent operation of the absorber could not be achieved in the region of Mode II and for this reason modal analysis of any results to determine the mode shapes was not carried out.

For further indication of the inconsistent operation of the absorber in the control of Mode II, Figure 5.27 shows the FRF from the carrier position at a shaft rotation speed of 500rpm with the ordinate axis in orders. For the absorber anti-resonance behaviour to occur in the region of this higher mode, only the speed of the shaft has been increased from the results of Section 5.4.1. Clearly, the absorber is no longer functioning with resonance tuning close to 6th order, as the centre of the anti-resonant region is at order $n = 6.35$. Neither of the modal peaks are as sharp as before and the phase of the FRF has less distinct change in this region. Therefore, the operation of the absorber does not agree with the design calculations, which were satisfactory in the lower mode. Some unaccounted factors must be controlling its behaviour in these cases, resulting in the problems experienced, and this effect was apparent for all three tunings used for the absorber.

From the theory of the CPVA discussed in Section 5.1.3.2 it is possible to estimate the amplitude of the pendulum motion about its axis of suspension for resonance tuning. The infinite effective inertia of the resonance tuned absorber forces a 'node' at the carrier and controls the deflection shape of the shaft system. This is apparent from the FRFs taken along the shaft in Mode I where the response is minimal at this anti-resonance point.

For accurate estimation of the resultant nth order harmonic torque acting at the carrier position, it is necessary to consider the deflections of the main inertias along the shaft in response to the excitation. This was achieved with a lumped parameter model of the shaft system and its forced vibration response was used to estimate the torque in each section of shafting. Hence, for the carrier position to be steadily rotating with no torsional vibration, the resultant torque acting at the carrier must be counteracted by the action of the absorber's pendulums. This gives a relationship between the input excitation torque to the shaft system and the torque acting on the carrier, whereby the amplitude of the pendulum motion about its axis of suspension can then be obtained from equation {5.4}.

The two factors in this equation defining the response of the absorber masses which are dependent on the experimental configuration rather than the absorber dimensions are the rotation speed Ω and the torque acting on the carrier position T_C. It is immediately apparent from the expression that increasing the speed of rotation will result in a significant reduction in pendulum motion due to the inverse-square relationship between these variables. In addition, the excitation system was demonstrated previously to have a torque input which decreases with increasing frequency and is a function of rotation speed to a limited degree. Therefore, for the higher mode the torque input to the shaft system is reduced and the displacement of points along the shaft, and hence torque acting on the carrier position, will be reduced. As a result, when the absorber is acting on Mode II, this will force a smaller displacement of the pendulums. This is the primary difference between the effect of the CPVA on Modes I and II and, therefore, the practical behaviour of the absorber must be related to this factor. Further experimental results showed that the absorber did not appear to work consistently in Mode II for the 4th order resonance tuned absorber and did not function at all for the 2.5 order tuning. Hence, there must be a limit of operation which the 4th and 6th order arrangements are close to when operating in Mode II but the 2.5 order CPVA is below.

Certainly, this phenomenon is contrary to the majority of non-linearities observed in dynamic problems where assumptions of linear behaviour in restricted operating ranges, such as small angles, have an upper limit beyond which simplified theory is no longer valid. In Section 5.4.1 the operation of the pendulums did not seem to be non-linear with increasing amplitude in the experimental range considered. Almost identical values of tuned order were obtained from measurements with individual and combined operating pendulums, although with single pendulums operating each would absorb approximately three times the torque. However, there appears to be a lower limit of pendulum motion which must be exceeded for the device to operate as intended. Possible explanations for this may be due to dimensional inaccuracies, in terms of component tolerances and geometrical alignment of the absorber, which result in pendulum motion that is not purely in one plane or in a circular path as intended. However, it is proposed that the most likely cause of this behaviour is due to some form of 'stick-slip' motion of the pendulums.

Using equation {5.4} and values of the resultant torque acting on the carrier determined from the model discussed above, the amplitude of the pendulum motion was estimated for control of the response of the system in both Modes I and II. This assumes linear response of the shaft system and the actual magnitude of the torque input at the excitation disk was obtained from the measurements of Section 4.4.4, accommodating the variations due to frequency and rotation speed. With the absorber resonance tuned to 6th order, the amplitude of pendulum bob angular displacement estimated with the system rotating at 300rpm to give the optimum Mode I anti-resonance, was ±4.03° about its axis of suspension, labelled ϕ_p in Figure 5.3. For the shaft rotating at 500rpm with the 6th order anti-resonance affecting Mode II a pendulum motion amplitude of ±0.67° was estimated. Similar results for the 4th and 2.5 order resonance tunings were considered, estimating respective pendulum motion angular displacements of ±2.44° and ±1.07° for Mode I. Hence, the Mode I amplitude for 2.5 order, where the absorber functions correctly, is greater than the amplitude for Mode II with the 6th order absorber where problems were experienced, consistent with the explanation proposed for this phenomenon.

Presumably, using only one of the pendulums on the absorber increases its amplitude in response to excitation threefold and may permit it to correctly control Mode II of the shaft system, although this was not considered in the experimental study. Assuming linear response of the absorber with only a single pendulum operating, in Mode I its motion amplitude should still be below the +/-25° limit suggested by previous research. Further to this, if the absorber weight was a critical design factor in this application then it is estimated that the mass of each pendulum bob could be reduced by a factor of 1/5 and retain predictable operation, providing the suspension pin inertia does not then become significant.

5.4.3 Effect of Excitation Level

To consider further the operation of the absorber in controlling the response of the shaft system, a series of measurements were made with reduced excitation levels from those used for the majority of the tests. This was with the aim of demonstrating the inconsistent operation of the pendulums with reduced torque input to the system under test.

To illustrate this behaviour, Figure 5.25b previously showed the response of the carrier location with a 60V (pk-pk) signal applied to the electromagnets from the power amplifier. With the ordinate axis displayed in orders of rotation, Figure 5.28 demonstrates the change in system response which occurs by decreasing the excitation to 30V (pk-pk). Therefore, the excitation torque input has been reduced by a factor of four between the two measurements. The previously sharp responses of Modes Ia and Ib have deteriorated, although the peak of Mode II is still apparent. The anti-resonances are estimated to have occurred at orders of 5.3751, 5.7751 and in the region 5.9502 to 6.1251, although the speckle noise peak in the highest range prevents determination of the exact point of lowest response. The increased noise floor of the measurement serves to limit any further assumption being made as to the exact behaviour.

In the results of Section 5.4.1, with single pendulums operating and therefore each exerting three times the torque, the tuning of the individual pendulums did not change significantly from the situation with them all operating. Figure 5.28 does show the absorber is working, but it is not doing so as efficiently as when it experiences the larger amplitude pendulum motion resulting from the 60V (pk-pk) excitation of Figure 5.25b. This is consistent with the idea of a minimum pendulum motion amplitude for predictable operation. With the torque input reduced by a factor of four then the amplitude of pendulum motion, assumed to be linearly related, is similarly reduced. Previously the absorber operated consistently with approximately this amplitude of pendulum motion for the 2.5 order resonance tuned absorber operating in Mode I. However, compared to the 6th order absorber in Mode I with 30V excitation, the torque input and the magnitude of the shaft system response for the 2.5 order absorber were significantly above the measurement system noise floor, permitting more accurate FRFs to be derived.

Further decrease of the input excitation demonstrated a more indistinct anti-resonant zone, although the increase in noise floor relative to the measured response prevents accurate examination of the effects occurring. Therefore, it is apparent that the absorber performance deteriorates when operating at lower amplitudes of excitation, supporting the proposed idea of a lower pendulum amplitude limit for successful absorber operation due to insufficient torque acting on the carrier to move the bobs. Further investigation of absorber behaviour, now made possible with torsional modal analysis, can explore these areas in more depth. Redesign of the absorber would look to minimise these effects to ensure consistent performance in controlling torsional vibration response tailored to the specific application requirements.

5.5 Experimental Measurement of Absorber Pendulum Motion

To conclude the detailed examination of the absorber's behaviour, an experimental study was undertaken to examine the motion of the pendulums on the CPVA when tuned to attenuate a resonant mode of the rotating shaft system. The LTV can be used to measure the angular velocity of a rotating component and therefore has the potential for monitoring the actual pendulum motions. This novel application of the instrument should provide useful insight into the practical operation of these torsional vibration absorbers.

Two LTVs were set up for the experimentation as shown in Figure 5.29, with one monitoring the torsional vibration of the shaft on the coupling adjacent to the attachment point of the CPVA carrier, effectively measuring $\dot{\theta}_c$. The other was incident on the outer edge of the pendulum bobs and therefore gave a signal consisting of three sections of data per revolution, corresponding to the angular motion of each pendulum as it passed through the beams. A digital oscilloscope was used to monitor the signals from both instruments simultaneously. To ensure a continuous signal could be obtained from the LTV incident on the pendulums, the central hub of the CPVA was covered with retro-reflective tape to backscatter the laser beams when they 'dropped off' in the region between the bobs. The pendulums passed the LTV in the order 3-2-1 and between pendulums 1 and 3 a section of the tape was blacked out to allow identification of a reference location.

It is important to note that an LTV measures the total angular velocity of the target component. As a result the LTV measurement on the pendulum bobs will include contributions from the angular velocity of the carrier, $\dot{\theta}_C$, and the angular velocity of the pendulums about their axes of suspension, $\dot{\phi}_P$. For these tests the CPVA was set up with suspension pins resonance tuned nominally at 6th order, to give a reasonable number of vibration cycles in each section of data observed from the passing pendulums.

To identify the modes which were studied during these tests consider the FRF of the rotating system given previously in Figure 5.23. Mode I is the parent mode for the two lower peaks in the response, corresponding to a one-node mode of the shaft system with a locked absorber attached. When the absorber is functioning to attenuate this mode it is split into lower and upper subsidiary peaks described previously as Mode Ia and Ib respectively. The anti-resonance point when the absorber is functioning in this mode is the minimum between these peaks. This should correspond with the resonant mode of the locked absorber system for most effective resonance tuning of the CPVA.

The results discussed below present the time histories of the angular velocity for each situation, recorded for the pendulums and the carrier. This was achieved by exciting the shaft system at the frequency corresponding to the maximum points of each modal peak and the anti-resonance, recording the response with the LTVs as described.

5.5.1 Pendulum Motion for Mode Ib

The raw time signals from the LTVs with the torque input system exciting Mode Ib above the anti-resonance are presented in Figures 5.30a & b, primarily to assist in the location of the reference marker between pendulums 3 and 1 which is labelled '*'. The three pendulums have been identified and the predominantly single frequency component of the motion of each is clearly apparent. The signal repeats the basic data pattern corresponding to the three pendulums with approximately equal length sections of noise and signal. The response of the carrier is also seen to comprise essentially the single excitation frequency.
These signals were filtered to remove the high frequency noise and the revised results are

shown in Figures 5.31a & b. The angular velocity fluctuations measured on the pendulums are clear and approximately in phase with that of the carrier. Therefore the carrier torsional vibration dominates the measurement as the pendulum motion should be out of phase with the carrier for this mode. The amplitude of carrier motion is quite low, close to the noise floor of the LTV. Further processing of the results can remove those sections where the pendulum motion signal 'drops-out' as the LTV beams fall off the edge of the bobs. Figure 5.32 is an example of this, permitting the individual pendulum motions for Mode Ib to be studied.

A rough estimate of the angular displacement of the pendulums could be made by subtracting the carrier torsional vibration from the angular velocity measurement from the pendulum bobs. However, no attempt was made to pursue this due to the poor quality of data obtained. Further development of this technique should address this aspect as the potential for detailed analysis of the pendulum motions is clear.

5.5.2 Pendulum Motion for Mode Ia

For the other mode resulting from the action of the absorber, Mode Ia below the anti-resonance, the motion of the pendulums and the carrier are shown in Figures 5.33a & b. The raw time signals have been processed as above and the three pendulums are labelled, following identification of the marker zone. Again, the single excitation frequency component is clear for both the pendulum and carrier motions. These appear to be in phase as would be expected for this mode, although the carrier torsional vibration dominates the pendulum LTV measurement in a similar manner to that discussed for the Mode Ib results.

5.5.3 Pendulum Motion for Mode I Anti-Resonance

The action of the absorber is to add another degree of freedom to the rotating system so at the frequency of the anti-resonance the shaft system and pendulums both have significantly reduced amplitude compared to their response in the two modes, Ia and Ib. This can be seen clearly in Figures 5.34a & b where the angular velocities of the pendulums and carrier are presented for the anti-resonant case. The carrier motion has been minimised in this arrangement due to the resonance tuned absorber acting as an infinite effective inertia in the system at this frequency. The pendulum amplitudes are much reduced from those of the two previous modes and hence are even more difficult to estimate. Additionally, the motion of pendulum 2 is more distinct than that of pendulums 1 and 3, emphasising differences in their actual resonance tuned orders.

5.5.4 Pendulum Motion for Mode II

Measurement of the FRF for the system with the rotation speed increased in order to put the action of the absorber into Mode II did not give any noticeable attenuation of this mode, as discussed in Section 5.4.2. Previously the FRF of Figure 5.26e demonstrated that with the rotation speed causing the absorber resonance tuning to occur in the Mode II response, inconsistent operation of the absorber prevented predictable control of this mode. It was proposed that this was due to a lower limit of the pendulum motion which it is necessary to exceed in order for the CPVA resonance tuning to function correctly.

Figures 5.35a & b show the corresponding pendulum and carrier angular velocities for this mode, demonstrating the extremely low level of motion resulting, below the instrument noise floor of approximately 5°/s in this case. This effect was confirmed in tests with other tunings of the absorber where no, or very inconsistent absorber effect could be observed in Mode II. For this result it is more difficult to determine the actual drop-out sections of the signal accurately and these have not been removed from the figure, although the approximate location of the transition from pendulum 3 to pendulum 1 is identified as before.

Torsional modal analysis has therefore been demonstrated successfully for an application in which previous experimental study has been limited. Together with novel use of the LTV to study the pendulum motions, this has provided significant insight into the operation of the CPVA. Future development of these techniques would aid the practical development of these absorbers into a versatile, predictable and efficient method for wider application in the control of torsional vibration.

6. CONCLUSIONS AND FURTHER WORK

6.1 Summary of Discussion

Torsional vibration has been identified as being of considerable importance during operation of rotating shaft systems, contributing significantly to machinery noise and vibration levels. Despite its importance, the exacting problem of obtaining measurements from rotating components has prevented experimental analysis from being as well developed as it is for translational vibration. This thesis reports significant new developments in experimental techniques for torsional vibration analysis of rotating shaft systems and Appendix C lists the external publications which have resulted from this work.

6.1.1 Use of the Laser Torsional Vibrometer in the Presence of Lateral Vibrations

The laser torsional vibrometer (LTV) has been developed previously for accurate non-contact measurement of the torsional oscillation of rotating components. In Chapter 3 the fundamental operation of the instrument was addressed to extend the understanding of its operation to account for the effect of all shaft motions on the measurement obtained.

The first reported experimental validation of LTV operation through the measurement of the speed fluctuations generated by an inclined Hooke's joint was presented. This confirmed the operation of the device in achieving accurate measurement up to large amplitudes of torsional displacement for the 2nd order component. Measurement of the 4th order component provided a clear indication of the noise floor of the instrument.

The LTV, whilst inherently immune to lateral target motion in most cases, was seen to be sensitive to specific types of lateral shaft motion under certain circumstances. The optical geometry removes the sensitivity of the instrument to translational motion of the target shaft, either axial or radial. However, angular lateral vibration of the shaft contributes to the measurement derived and thus is indistinguishable from the intended measurement of torsional vibration. The effect was dependent on the incidence angles of the LTV relative to the shaft, becoming more severe as this was moved away from the optimum arrangement, as often required by access restrictions. This lateral motion sensitivity was seen to comprise terms both proportional to and independent of the shaft rotation speed.

The predicted sensitivity of the instrument to angular lateral motion about both axes was confirmed experimentally. Subsequently, the significance of these effects in measurement situations was illustrated, through consideration of torsional and angular lateral vibration magnitudes experienced in real engine applications. Comparison of two simultaneous torsional vibration measurements at different LTV incidence angles showed clear differences as a result of crankshaft angular lateral vibration. Estimation of the magnitude of the shaft motion was made from this data and was used to predict the magnitude of error components which could be induced in practice due to these effects.

From this data, optimum configurations of the instrument were specified to ensure effective immunity to all lateral motion in this typical application. It was recommended that use of the instrument with the incidence angle $\alpha < 70°$ is avoided, as the magnitude of measured components induced by angular lateral vibration is potentially very significant. In the range $70° < \alpha < 80°$ the error components are of measurable magnitude and care is required in the interpretation of data. For $80° < \alpha \leq 90°$ error components were of similar or smaller magnitude than the instrument noise floor and operation is effectively immune to angular lateral motion, allowing reliable and accurate measurement of torsional vibration.

To overcome this problem more reliably, a new technique was demonstrated which provides an accurate measure of pure torsional vibration in situations where a single instrument demonstrates unacceptable sensitivity to angular lateral vibrations. Two suitably aligned LTVs are used for this method, with the measurement derived from addition of their signals whereupon any signal components due to angular lateral motion cancel. Experimental proof of this principle clearly demonstrated the ambiguous measurement from a single torsional vibrometer. The measurement derived from the two instruments showed the pure torsional vibration component.

Simultaneously this technique can provide non-contact assessment of angular lateral, or bending, vibration directly from a rotating component and this was demonstrated experimentally with bending vibration sensitivity down to the order of 1m°. However, this measurement is sensitive to angular motion about both *X* and *Y* axes. Thus, except in the simple case of motion occurring about one of these axes as demonstrated, the individual motions cannot be derived separately and the measurement is restricted to qualitative assessment.

This technique was used to study the crankshaft motion of an automotive diesel engine. Comparison of the pure torsional vibration measurement with that from a single LTV identified discrepancies due to the effects of shaft bending vibration. Furthermore, the bending vibration signal gave a clear indication of the shaft motion due to the combustion impacts. Important new results were presented from study of the crankshaft bending vibration. From the frequency spectrum of this measurement clear bending vibration peaks were present at the expected vibration orders, the first four harmonics of rotation speed. Additionally, it was possible to locate the natural frequency of the crankshaft in bending, which was excited by the firing impulses, at approximately 455Hz and this was confirmed in further modal analysis tests on the engine. During operation the magnitude of the bending motion of the crankshaft pulley for this mode about the *X*-axis was estimated to be 12m°. This application of laser vibrometry for non-contact measurements of shaft vibration represents a further step forward in the use of this technology for machinery diagnostics.

6.1.2 Torsional Modal Analysis for Rotating Shaft Systems

The importance of experimental modal analysis in the design and development process is well known but it is surprising that experimental analysis of torsional vibration for rotating systems has been limited. This is primarily due to the absence of a versatile means by which to apply an instrumented torque input and obtain measurements under rotating conditions. The research reported in Chapter 4 addressed this deficiency by providing a novel, non-contact means to input a controllable and measurable torque excitation to a rotating shaft system. Together with the use of an LTV to measure response, the key components of a modal analysis system were realised without modification to the system under test. Real-time determination of the torque input allowed torsional vibration frequency response functions to be obtained for a series of points along the shaft. These signals are processed with conventional hardware and modal analysis software. This versatile technique achieved full experimental modal analysis for the first time from a rotating shaft system, including derivation of natural frequencies, mode shapes and damping factors.

The principle behind the excitation system developed is that of eddy current braking of a rotating disk. Two electromagnets were arranged to give a magnetic field between their poles which passes through a conducting disk component that is part of the shaft system under test. As the disk rotates in the field, eddy currents were induced and their interaction with the applied magnetic field provided a tangential force, retarding the rotation. The applied torque was proportional to the square of the magnetic flux density in the air-gap between the electromagnets and, due to the near-linearity of the magnetic circuit resulting from the influence of the air-gap, this magnetic flux was proportional to the current in the electromagnet coils. The constant of proportionality between the torque and square of the current was a function of the electromagnet construction and the radial position of their poles, the rotational angular velocity, the disk conductivity and its volume in the flux region.

Application of a sinusoidal voltage to the electromagnet coils causes a current to flow with a phase lag relative to the input voltage, resulting from the impedance of the electromagnet coils. It was evident from consideration of the flux, eddy-current and velocity vectors that, whatever the direction of the magnetic field, the torque acting on the disk is always retarding the disk rotation. Hence, a sinusoidal voltage input to the electromagnets produced a braking torque input with a constant component and a component at twice the input voltage frequency. Additionally, the reactive and resistive components of the electromagnet impedance act to reduce the applied torque with increasing excitation frequency.

The magnitudes of the supply current in the coils and the current in the inductive element of the electromagnet impedance, which is assumed to give rise to the magnetic flux acting on the disk, were demonstrated to be approximately equal over the frequency range considered. A satisfactory estimation of the applied torque can therefore be derived from the square of the supply current in the electromagnet circuit. However, the magnetising component of current has a phase lag relative to the supply current which increases with frequency. This results in a phase offset in the FRF measurements which increases with frequency, with a corresponding over-estimate of the applied torque magnitude. These problems are outweighed by the ease of deriving the torque input in real-time by non-contact means. The relationship between applied torque and electromagnet current was demonstrated experimentally and calibration of the torque input was achieved. Due to the factors determining the torque-speed relationship it was necessary to determine the calibration constant experimentally for each speed range.

To validate the use of this excitation method for torsional modal analysis, results were obtained from a simple three inertia shaft system using sine sweep excitation. The frequency range of excitation encompassed the first three torsional modes of the system, including the zero frequency rigid body mode for the free-free shaft system. The FRFs obtained were consistent with conventional mobility measurements in terms of phase and magnitude and the location of resonant and anti-resonant regions. The first two non-zero modes were easily located and estimates of natural frequencies and mode shapes agreed closely with predictions from a simple lumped parameter model. Modal damping for this lightly damped structure was of the order of 1%-2% of critical, consistent with previous studies.

Increasing the shaft system rotation speed resulted in a decrease of its modal frequencies, while damping was seen to increase. A decrease in phase offset of the FRFs with increasing speed was also seen, consistent with the modelled current components from electromagnet impedance measurements. Investigation of the effects of excitation level showed the modal frequencies to decrease with increasing excitation amplitude, while modal damping increased dramatically. The influence of the torque input system on the shaft system behaviour was considered based on these parameters. Modal damping was seen to be a linear function of input torque and it was proposed that this is due to lateral loading of the shaft bearings with the force applied to the shaft by the electromagnet system. Furthermore, the observed changes in natural frequency were estimated to be of too great a magnitude to be entirely due to the changes in damping. Therefore, an effective decrease in system torsional stiffness has occurred with increasing rotation speed or excitation level. This identifies the possibility of weak non-linear behaviour controlling the response of the shaft system.

A fourth inertia was added to the shaft system to consider use of the excitation and measurement systems over an increased frequency range and the assumed boundary conditions of the motor drive connection were discussed. Modal frequencies for the three modes over a range of rotation speeds agreed closely with lumped parameter model predictions. Mode shapes presented with scaling of mass normalised values compared very well for the first two modes. However, the experimentally derived third mode shape displacements were significantly reduced compared to the predicted magnitudes. This was primarily a result of the over-estimated torque input at high frequencies due to the phase difference between the supply current and the magnetising component of the current. The variations of modal parameters with rotation speed were as seen for the three inertia system.

This new experimental technique completely satisfies its intended use and achieves experimental results which surpass previous developments in this field. Modal analysis of torsional vibration response with the use of this technology will permit realisation of considerable insight in the design and development of rotating machinery.

6.1.3 Experimental Study of a Centrifugal Pendulum Vibration Absorber

An application of torsional modal analysis was demonstrated in the experimental study of the operation of a centrifugal pendulum vibration absorber (CPVA) on a shaft system. The CPVA was identified as being superior to dampers and other absorbers to control torsional vibration in specific applications, but experimental study has been limited due to a lack of appropriate techniques with which to investigate the actual behaviour of the device. This device needs to be rotating to function and, therefore, the new torsional modal analysis technique allows an unprecedented depth of information to be realised, extending the understanding of its operation. The non-contact excitation and measurement systems allow the vibration response to be considered without modification of the shaft system.

The bifilar-form absorber designed for the experimental study was based on previous theoretical models assuming linear behaviour of the pendulums. Theoretical modelling of the absorber operation was used for validation of the torsional modal analysis results. The CPVA was fixed to the shaft system at two locations and different suspension pin sets were used during the experimentation to adjust the resonance tuning. The pendulum bobs could be restrained to give a 'locked absorber' for comparison with the system response when the pendulums were free to move and the CPVA was functioning. The natural frequencies of the torsional modes were easily obtained from the experimental FRFs. The torsional mode shapes of the shaft system were readily derived and estimation of the modal damping was possible.

The CPVA was attached to the end of the shaft system and was resonance tuned to 2.5 order at a rotation speed which would put the tuning effect in the response of Mode I of the locked absorber system. The previous one-node modal peak with the locked absorber was replaced by two smaller peaks, one below and one above the original modal frequency. Modal analysis of these results showed these two modes, labelled Ia and Ib, both to have one nodal point along the shaft, with the movement of this point along the shaft consistent with the predicted effective inertia of the absorber. Additionally, the reduced effective inertia at higher frequencies increased the natural frequencies of Modes II and III.

With the absorber at the central position with each of the three sets of suspension pins in use and the pendulums locked, minor differences in the system response were identified due to the increased pin diameters for the higher resonance tunings moving the centre of gravity of the bobs closer to the shaft axis. The resulting reduction in total moment of inertia of the locked absorber gave small increases in modal frequencies as predicted. The shaft system with only the carrier in place demonstrated an increased upper frequency limit of operation for the excitation system with identification of a mode above 140Hz.

The absorber was used to attenuate the response of the central section of shaft with the suspension pins giving CPVA resonance tuning of 2.5, 4th and 6th orders. The rotation speed was set in each case to put the resonance tuning effect in the response of Mode I of the system and as a result this peak was split into two smaller peaks. The absorber performed as predicted in controlling Mode I for each of the three sets of suspension pins. The modal frequency and damping values and mode shapes were similar for all three tunings of the absorber, with only minor differences identified due to the changes in diameter of the suspension pins. The one-node mode shapes for Modes Ia and Ib were similar, with the modal frequency values and changes in nodal positions related to the effective inertia of the absorber.

A series of minima were apparent in the absorber anti-resonance of the FRF which became increasingly apparent for the 4th and 6th order tunings. The location of these minima corresponded very closely to the tuning of each individual pendulum, determined by locking up the other bobs in the carrier. Consideration of the geometrical tolerances of the absorber identified the diameter of the suspension holes in the carrier as the critical parameter causing the measured spread of pendulum tuning. This factor is therefore important when attempting accurate tuning of a CPVA, which in practice depends also on the circularity of these holes and the alignment of the two carrier plates.

Increasing the shaft rotation speed showed the resonant frequency of the absorber to move upwards, as expected from an order-tuned device. However, it was not possible to achieve the characteristic sharp anti-resonances with the absorber resonance tuning in the region of Mode II as anticipated. For the 6th order absorber operating unsuccessfully in Mode II, the pendulum motion was estimated to be a factor of six smaller than that for successful operation in Mode I. From these results it appeared there was a lower limit of pendulum motion amplitude which must be exceeded for the absorber to operate as intended. Estimated results confirmed that for the absorber in Mode I with the 2.5 and 4th order tunings, the pendulum motions were above this lower limit, while for Mode II the pendulum amplitudes were predicted to be below this limit. It was proposed that a form of stick-slip friction acts on the motion of the pendulums preventing consistent operation of the absorber. This was confirmed with decreased excitation of the shaft system as the sharp FRF anti-resonances deteriorated and additional changes were seen in the order at which the anti-resonance minima occur.

Novel use of the LTV allowed the motion of the individual pendulums to be studied experimentally and simultaneous time histories were presented for the pendulum and carrier angular velocities for the 6th order resonance tuned absorber. With the shaft system excited at frequencies corresponding to Mode Ia and Ib the three pendulums could be identified from the repeating series of three sections of signal separated by noise where the LTV laser beams 'dropped off' between bobs, with the motion comprising essentially the single excitation frequency. With the absorber excited at the Mode I anti-resonance frequency the masses were confirmed to have reduced amplitude compared to Mode Ia and Ib operation. For Mode II excitation at an appropriate rotation speed the carrier and pendulum angular velocities were below the noise floor of the LTV.

The advantages of torsional modal analysis have therefore been exploited in the study of a CPVA to consider fully the effects of its tuning. This included not just the attenuation of a selected mode's response due to resonance tuning, but also the control of all the natural frequencies and mode shapes of a system through inertia tuning. The use of this novel excitation and measurement system has been demonstrated to give significant improvements over previous experimental techniques, with significant potential for future development.

6.2 Recommendations for Further Work

These developments in technology for experimental measurement and analysis of torsional vibration allow a much greater depth of study to be realised in the design and development of rotating machinery, with potential for further exploitation. The following sections discuss the wider application of these techniques.

6.2.1 Sensitivity of the LTV to Angular Lateral Vibration

A number of important areas can be identified from this work dealing with both torsional vibration measurement and assessment of shaft bending motion. Initial developments would address experimental validation of sensitivity of the LTV to all components of angular lateral motion of a rotating shaft, as identified in the theory presented in Chapter 3.

For the accurate measurement of pure torsional vibration from flexible shafts where it is not possible to align a conventional LTV with $\alpha = 90°$, there is a need for a dedicated instrument based on the approach of Section 3.5 which utilised two conventional LTVs. The main aim of the new design should overcome the inherent problems with the critical alignment of the instrumentation with respect to the shaft. An optical configuration is required to form the two pairs of parallel beams, which are recombined onto separate photodetectors after being incident on the target. Creation of the two parallel laser beam pairs must allow for synchronised adjustment of the incidence angle α so that this is equal for each 'half' of the instrument. An optical system incorporating mirrors which can be angularly aligned simultaneously is envisaged to accommodate the variations in application access and measurement requirements. A method is also required to identify when the equalised incidence angle condition has been achieved during alignment.

Problems experienced due to minor differences in the two LTV demodulators have identified this as a critical area for future development. One possible approach is to multiplex the demodulation of the signals from the two photodetectors with a single demodulator. Further signal processing aspects include preventing the possibility of cross-talk between the two halves of the system. Improvements in the alignment technique and minimisation of errors in the processing of the results would ensure maximum accuracy of the torsional vibration measurement in situations where optical access restrictions and shaft angular lateral motion would result in ambiguous measurement.

Additionally, the optical arrangement of such an instrument could form the basis of a technique to investigate the bending vibration of rotating shafts. However, obtaining this measurement from the difference of two LTV measurements in the manner described in Section 3.5 is sensitive to angular lateral shaft motion about both X and Y axes. It would therefore be necessary to develop a technique to derive the separate orthogonal components for accurate measurement of shaft angular lateral motion. One possible approach is to take two such measurements simultaneously, with alignment of the two new instruments in orthogonal planes. This could be done in a similar manner to that described for the measurement of rotating shaft translational lateral vibration with the use of conventional laser vibrometers [6-1]. Resolution of the individual components of angular lateral vibration could be achieved by mathematical means. However, this technique is laborious and the problems of deriving an unambiguous measurement of the shaft motion at synchronous frequencies would be similar to that reported for translational vibration.

Despite the unavoidable sensitivity of the bending vibration measurement to motion in both orthogonal planes preventing direct independent measurement, this is a useful step forward in the application of laser vibrometry to measurements on rotating components. A host of potential applications, such as engine and powertrain development, machine tool design and wear monitoring, oil and gas drilling processes and high speed turbomachinery, can be identified for this technology, all of which could benefit from the new data obtainable. In automotive engines, crankshaft bending vibration is believed to be the main source of engine 'rumble', a troublesome low frequency noise that reduces passenger comfort, particularly during acceleration [6-2 to 6-4]. Ultimately, this technique will allow quantification of the motion in all three rotational degrees of freedom of any point on a rotor by non-contact means. This confirms the continually expanding potential of optical techniques for use in machinery diagnostics.

6.2.2 Development of Modal Analysis Techniques for Torsional Vibration

The excitation system described in Chapter 4 has the potential for application to many rotating shaft systems. Future development of this experimental technique will help to establish it as a standard procedure for analysis of rotating machinery dynamic behaviour.

Development of the electromagnet system is required to optimise the torque input, in terms of frequency range, magnitude of input and ease of alignment, to allow testing at any chosen constant speed and at any required excitation frequency for the shaft system of interest. One potential application of torsional modal analysis that has been identified is the study of elastomeric vibration dampers. For testing of these devices, high amplitudes of shaft vibration would be required to simulate conditions encountered during operational cycles. At high frequencies the current in the coils, and hence flux and torque, is inversely proportional to the frequency of input. Therefore for high input torques it is necessary to have either a high input voltage or relatively low electromagnet system impedance.

With the use of two or more magnet systems spaced at equal angular intervals around the excitation disk a pure couple would be applied to the disk, with no unbalanced force acting on the shaft which might affect the torsional vibration behaviour. Additionally, it would be advantageous to consider the trade-off between size and number of electromagnets with regard to system impedance, coil current and applied torque. Improvements to the physical configuration of the electromagnets will use a design specifically intended for the purpose with the aim of maximising the air-gap flux through which the rotating conductor passes. Losses in the core should be minimised and this could be achieved with a laminated structure constructed from steel intended for alternating current applications. Modelling of the electromagnetic behaviour of the system may assist with the magnet system design and would require fundamental development of the eddy current braking theory for application of a harmonic torque input, an area not fully addressed in appropriate literature.

Application of this excitation method to various shaft arrangements should make use of a conducting disk which already exists, or a component could be modified or replaced. For example, in a crankshaft system the electromagnets would be positioned either side of the crankshaft pulley. Obviously, attaching a large diameter disk to a shaft system would give unwanted modification of its dynamic behaviour. The excitation disk material has been assumed to be conducting and non-magnetic up to this point, although it would be advantageous to make use of a ferro-magnetic disk that is already part of the shaft system. However, the behaviour of the excitation system will not be ideal due to the resulting non-linear relationship between current and torque. Direct measurement of the reaction torque on electromagnets will overcome the need to use this relationship to infer the input to the shaft and will be discussed shortly.

For translational modal analysis on non-rotating structures, swept-sine, broad-band and impulse inputs are all used to excite the test system. The electromagnet system has the potential to match this range of inputs, allowing results to be obtained more quickly and limiting shaft speed changes during tests. Reduced torque magnitude at high frequencies prevented successful use of a broad-band input function during the reported work. Increasing the current in the electromagnets and the magnetic field acting on the rotating conductor of the shaft system would address this limitation. Furthermore, the signal to noise ratio of the measurement system needs to be improved for lower levels of excitation and the resulting response. Weighting the voltage applied to the magnets during a frequency sweep test would ensure that the square of the current and hence applied torque is constant across the frequency range, ensuring that similar shaft conditions prevail for comparison of test data. A feedback system could maintain the rotation speed at a constant value during tests if variations of system behaviour with this parameter are of significant importance.

The creation of a torsional impulse to a rotating shaft system, analogous to the impulse hammer used in conventional translational modal analysis, would also be the subject of future development. For applying a rapid pulse of flux, and therefore torque, the electrical 'inertia' or impedance of the electromagnet system is a primary concern. The main strategy proposed to overcome this is the use of a large d.c. voltage to give a rapid increase in initial current growth, with current limiting to prevent overloading of the electromagnet coils during the pulse. This technique has the potential for significant improvements in the duration of experimental measurements.

Direct calibrated measurement of the torque input to the rotating system is required for reliable and accurate estimation of mobility properties. Measurement of the three quantities in the 'applied torque - magnetic flux - supply current' relationship should be re-addressed to achieve a suitably accurate and representative measure of the applied torque. Alternative approaches to the calibration of the current signal to give a calibrated measure of the applied torque would be addressed in further work. A more accurate estimate of the torque input could be derived through mapping the relationship between the supply and magnetising components in the electromagnets from the modelled impedance. A simple calibration rig, which incorporates the disk and electromagnet system to be used in the excitation of the actual shaft system, would also assist in this study, removing the need for complete disassembly and modification of the shaft system under test. A parallel can be made with translational modal analysis where measured acceleration of a known test mass gives an independent measure of the force input from an electrodynamic shaker for calibration of force transducers [6-5]. The forced response of the calibration rig shaft system would be modelled and correlated with the experimentally measured response determined by LTV to derive calibration factors. Empirical derivation of the proportionality constant for each speed range is most straightforward and of suitable accuracy for what is a very complex electromagnetic system.

However, in the light of more robust methods for measuring the applied torque, development of this area would be of limited significance. It is proposed that the most appropriate solution to derive a direct measure of the torque applied to the rotating shaft would be through measurement of the reaction force or torque on the electromagnets. With the use of two electromagnet systems to apply a pure couple to the disk, and a suitable mounting arrangement making use of either force or torque transducers, the applied torque could be accurately derived.

The intricacies of torsional modal analysis can now be addressed with this excitation system to investigate effects related to the rotation of the system and in the correlation of experimental data and theoretical predictions of system response. Deficiencies in the use of existing theory for this new application can be explored, such as the visualisation of torsional vibration with modal analysis software. Additionally, the effects of inertia or stiffness modification can be exploited using features available in existing software. Torsional modal analysis will permit improvements in modelling of the actual behaviour of real shaft systems. This includes the use of distributed mass and lumped parameter models for consideration of such effects as motion of the free ends of the shaft observed in the experimental testing.

A further area for consideration is the boundary condition assumptions used for the test structure at the rotational drive input. The test shaft system should be suitably isolated from the rotational input through the use of a resilient rubber belt or other flexible connection, to maintain the rotating condition without opposing the fluctuating input torque or transmitting unwanted torsional vibration. Criteria must be derived to ensure that the drive system plays no role in affecting the measured shaft behaviour. Additionally, changes in modal parameters have been highlighted which relate to rotation speed, excitation level and lateral loading of the bearings, identifying non-linear behaviour of the shaft system and these should be explored further.

Experimental modal analysis on non-rotating systems is widely used throughout industry and in many branches of research. The ability to perform torsional modal analysis on rotating systems will be of considerable interest to a similarly wide audience. Manufacturers and end-users of devices such as vibration dampers and absorbers, couplings and geared systems are especially likely to benefit from this work. These new techniques will improve the development of their products through the provision of data that was previously unobtainable.

6.2.3 Practical Development of the CPVA

To address market requirements for smoother, quieter machinery there is a clear requirement for devices to control vibration of rotating shafts and the links between torsional vibration and the noise and vibration of rotating machines have been introduced previously. The capabilities of the new experimental technique for torsional modal analysis allow comprehensive exploration of the dynamic response of the CPVA for potential application to a range of shaft vibration problems. Further developments in torsional modal analysis will be directly applicable to the study of the CPVA. Techniques originally intended for conventional modal analysis such as prediction of the forced vibration response of the shaft can be utilised. Structural modification theory can also be exploited to consider the effects of changes to the shaft system components.

For development of an absorber with critical tuning the depth of information provided by torsional modal analysis will prove invaluable. Significantly, this should provide insight into the practical operation of the CPVA compared to other devices for controlling torsional vibration. This will permit investigation of the limitations of manufacturing tolerances on the effectiveness of the device in controlling vibration modes of a shaft system. The results can suggest design improvements to the components with critical dimensions to ensure that reliable operation of the absorber can be realistically achieved.

Further investigation of absorber behaviour can explore the areas identified with respect to the motion of the pendulums and the proposed lower limit for consistent behaviour. Redesign of the absorber would address these issues to achieve consistent performance in controlling torsional vibration response, tailored to specific application requirements.

Additionally there is a lack of experimental work considering the effects addressed in advanced theoretical studies. These include the occurrence of non-linearities due to large amplitudes of motion and the effects of damping which may permit a device with broader tuning to be realised. Use of the LTV to measure the pendulum motions can help to unravel the practical understanding of the CPVA operation, although the instrument sensitivity would need to be addressed to improve the clarity of results. This would allow the component of pendulum angular velocity to be extracted reliably from the LTV measurement on the bobs. Inclusion of the pendulum bob motions could be used in more complete modal analysis of the CPVA. This would permit greater understanding of the limiting performance factors, for practical development of these devices into a versatile, predictable and efficient method for the control of torsional vibration.

The practical operation of rotating systems can now be considered in unprecedented depth with the use of the versatile experimental analysis techniques described in this thesis. This allows exploitation of devices like the CPVA to control undesired torsional vibration in applications including electric motor drives, geared systems and automotive powertrains. The resulting reduction in torsional vibration from these developments permits smaller, lighter shaft components to be used with the potential improvements in fuel economy, product life, reliability, noise and vibration benefiting a wide range of rotating machinery throughout industry.

6.3 Conclusions

The following developments in torsional vibration measurement by laser technology were made;

- The first reported experimental validation of LTV operation by measurement of the speed fluctuations generated by an inclined Hooke's joint was presented.
- Sensitivity of the LTV to angular lateral vibration of the target shaft was confirmed theoretically and experimentally.
- Incidence angle ranges for operation immune to this effect were defined from torsional and angular lateral vibration magnitudes determined in real engine measurements.
- A new technique was demonstrated which achieves accurate torsional vibration

measurement where a single LTV has unacceptable angular lateral vibration sensitivity.

- A simultaneous assessment of bending vibration can be derived directly from the rotating component by this non-contact method.
- Crankshaft bending and torsional vibration of a diesel engine were quantified using these new techniques, allowing identification of the crankshaft bending natural frequency.

Significant progress was achieved in the modal testing of torsional vibration;

- A controllable torsional excitation technique for rotating shaft systems was developed, based on the principle of eddy current braking with electromagnets.
- Measurement of the electromagnet coil input current provided estimation of the torque input without modification to the shaft system under test.
- Combined with use of an LTV to measure response this enabled modal analysis of torsional vibration to be performed, utilising conventional techniques for data processing.
- Simple three and four inertia systems were tested to validate the system performance and good agreement was found with theoretical predictions of the natural frequencies and mode shapes and previous estimates of torsional modal damping.

These technologies were exploited for the advanced experimental study of a CPVA;

- A CPVA was designed and used to demonstrate control of the torsional vibration modes of a rotating shaft system, when resonance-tuned to a series of rotation orders.
- Experimental natural frequencies and mode shapes agreed closely with theoretical predictions of absorber performance, showing its effect on the complete shaft response.
- Accurate measurement of each individual pendulum tuning was achieved and related to critical dimensions of the absorber components, together with examination of other effects related to successful CPVA design.
- Novel use of the LTV allowed the motion of the pendulums to be studied experimentally.

APPENDIX A

Finite Rotations of Position Vectors about Two Axes

As discussed in Chapter 3, finite rotations of a rigid body about specified axes can be expressed as vectors, but generally they do not obey the commutative law of addition [A-1]. This appendix serves to derive the result stated in equation {3.5} of Section 3.2.1.1 and used in development of subsequent theory.

As shown previously in Figure 3.4, the arbitrary point of interest P is located by position vector $\bar{r}$ before rotation. In the initial case, consider the change of this fixed magnitude position vector due to a finite rotation $\bar{\theta} = \theta\hat{n}$ of magnitude θ about an axis having the unit vector $\hat{n}$. Subsequently P is moved to P', $\bar{r}$ becomes $\bar{r}'$, and the final position vector can be expressed in terms of the original position vector and finite rotation vector;

$$\bar{r}' = \bar{r} + (1-\cos\theta)[\hat{n}\times(\hat{n}\times\bar{r})] + \sin\theta(\hat{n}\times\bar{r}) \qquad \{A.1\}$$

Fundamentally, vectors can be characterised by the attributes of magnitude, direction and obeying the commutative law of addition. However, finite rotations do not obey this final requirement as demonstrated in the following derivation.

Extending the general case, two consecutive rotations can be applied to the position vector $\bar{r}$, designated $\bar{\theta}_1 = \theta_1\hat{n}_1$ and $\bar{\theta}_2 = \theta_2\hat{n}_2$ respectively. The position vector locating point P after the first rotation is obtained from application of equation {A.1};

$$\bar{r}_a' = \bar{r} + (1-\cos\theta_1)[\hat{n}_1\times(\hat{n}_1\times\bar{r})] + \sin\theta_1(\hat{n}_1\times\bar{r}) \qquad \{A.2\}$$

Similarly, the position vector locating point P after the second rotation is given as;

$$\bar{r}_a'' = \bar{r}_a' + (1-\cos\theta_2)[\hat{n}_2\times(\hat{n}_2\times\bar{r}_a')] + \sin\theta_2(\hat{n}_2\times\bar{r}_a') \qquad \{A.3\}$$

Substituting {A.2} into {A.3} gives;

$$
\begin{aligned}
\bar{r}_a'' = \bar{r} &+ (1-\cos\theta_1)[\hat{n}_1 \times (\hat{n}_1 \times \bar{r})] + \sin\theta_1(\hat{n}_1 \times \bar{r}) \\
&+ (1-\cos\theta_2)[\hat{n}_2 \times (\hat{n}_2 \times \bar{r})] \\
&+ (1-\cos\theta_2)(1-\cos\theta_1)[\hat{n}_2 \times \{\hat{n}_2 \times [\hat{n}_1 \times (\hat{n}_1 \times \bar{r})]\}] \\
&+ (1-\cos\theta_2)\sin\theta_1\{\hat{n}_2 \times [\hat{n}_2 \times (\hat{n}_1 \times \bar{r})]\} \\
&+ \sin\theta_2(\hat{n}_2 \times \bar{r}) + \sin\theta_2(1-\cos\theta_1)\{\hat{n}_2 \times [\hat{n}_1 \times (\hat{n}_1 \times \bar{r})]\} \\
&+ \sin\theta_2 \sin\theta_1[\hat{n}_2 \times (\hat{n}_1 \times \bar{r})]
\end{aligned}
\qquad \{A.4\}
$$

Reversing the sequence of rotations, applying $\bar{\theta}_2$ then $\bar{\theta}_1$, through the use of equation {A.1} as above, the final position vector after the two consecutive rotations is;

$$
\begin{aligned}
\bar{r}_b'' = \bar{r} &+ (1-\cos\theta_2)[\hat{n}_2 \times (\hat{n}_2 \times \bar{r})] + \sin\theta_2(\hat{n}_2 \times \bar{r}) \\
&+ (1-\cos\theta_1)[\hat{n}_1 \times (\hat{n}_1 \times \bar{r})] \\
&+ (1-\cos\theta_1)(1-\cos\theta_2)[\hat{n}_1 \times \{\hat{n}_1 \times [\hat{n}_2 \times (\hat{n}_2 \times \bar{r})]\}] \\
&+ (1-\cos\theta_1)\sin\theta_2\{\hat{n}_1 \times [\hat{n}_1 \times (\hat{n}_2 \times \bar{r})]\} \\
&+ \sin\theta_1(\hat{n}_1 \times \bar{r}) + \sin\theta_1(1-\cos\theta_2)\{\hat{n}_1 \times [\hat{n}_2 \times (\hat{n}_2 \times \bar{r})]\} \\
&+ \sin\theta_1 \sin\theta_2[\hat{n}_1 \times (\hat{n}_2 \times \bar{r})]
\end{aligned}
\qquad \{A.5\}
$$

Each of the finite rotations have been assigned a direction and magnitude but, in order to be added like vectors, the parallelogram law implies that the final position vector locating point *P* must be the same in each case, irrespective of the sequence in which the rotations were applied. However, comparison of {A.4} and {A.5} demonstrates that this is generally not the case.

Finite rotations do behave as vectors in the cases where the two rotations are about a common axis or are infinitesimal. For infinitesimal rotations, terms higher than first order in expansions of θ_1 and θ_2 may be neglected and the usual small angle approximations applied. Hence, the final positions for the two sequences of rotations are equivalent and are stated as;

$$\vec{r}_a'' = \vec{r}_b'' = \vec{r} + \left(\theta_1 \hat{n}_1 + \theta_2 \hat{n}_2\right) \times \vec{r} \tag{A.6}$$

Therefore infinitesimal rotations can be classified as true vectors as they obey the commutative law of addition. This result is applied in Chapter 3 to rotations of the rotating shaft axis about the orthogonal X and Y axes.

APPENDIX B

Torsional Shaft System Lumped Parameter Model

B.1 Generalised System

To allow investigation of torsional shaft system vibration, a lumped parameter model was derived based on conventional theoretical analysis [B-1 to B-3]. This was used for comparison with, and validation of, experimental results and seen to approximate closely the physical system under test. The model is outlined here to clarify points discussed in the main text.

The inertias in the system are lumped into N discrete disks, each with a moment of inertia about the shaft axis of J_n. These inertias are connected together by N-1 massless elastic shafts of stiffness K_n. The angular displacement at each inertia is θ_n and the external torques applied to the system are labelled $T_n(t)$. To represent the dissipation of vibration energy viscous damping is incorporated into the model. Energy dissipated in the shafts and couplings is represented by dampers denoted C_n. Energy dissipated in bearings or other elements with an absolute velocity dependent torque, therefore connected to ground, are denoted B_n.

The equation of motion for each degree of freedom can be derived from Newton's laws or from Lagrange's equation and the generalised form for point n is;

$$\begin{aligned} J_n\ddot{\theta}_n + B_n\dot{\theta}_n + C_n\left(\dot{\theta}_n - \dot{\theta}_{n+1}\right) + C_{n-1}\left(\dot{\theta}_n - \dot{\theta}_{n-1}\right) \\ + K_n\left(\theta_n - \theta_{n+1}\right) + K_{n-1}\left(\theta_n - \theta_{n-1}\right) = T_n(t) \end{aligned} \quad \{B.1\}$$

By deriving appropriate expressions for each co-ordinate point, the resulting equations of motion can be assembled into matrix form;

$$\underline{J}\{\ddot{\Theta}\} + \underline{B}\{\dot{\Theta}\} + \underline{C}\{\dot{\Theta}\} + \underline{K}\{\Theta\} = \{T_N\} \quad \{B.2\}$$

B.2 Solution of Eigenvalues

With no damping, $B_n = 0$, $C_n = 0$ and the undamped torsional natural frequencies can be derived through solution of the eigenvalues and eigenvectors that describe the normal modes of the system. The equations of motion expressed in matrix form are;

$$\underline{\boldsymbol{J}}\{\ddot{\Theta}\} + \underline{\boldsymbol{K}}\{\Theta\} = \{0\} \qquad \{B.3\}$$

For example, with a four inertia shaft system the inertia and stiffness matrices are;

$$\underline{\boldsymbol{J}} = \begin{bmatrix} J_1 & 0 & 0 & 0 \\ 0 & J_2 & 0 & 0 \\ 0 & 0 & J_3 & 0 \\ 0 & 0 & 0 & J_4 \end{bmatrix} \qquad \underline{\boldsymbol{K}} = \begin{bmatrix} K_1 & -K_1 & 0 & 0 \\ -K_1 & (K_1 + K_2) & -K_2 & 0 \\ 0 & -K_2 & (K_2 + K_3) & -K_3 \\ 0 & 0 & -K_3 & K_3 \end{bmatrix} \qquad \{B.4a, b\}$$

Premultiplying equation {B.3} by the inverse of the inertia matrix gives the following;

$$\underline{\boldsymbol{I}}\{\ddot{\Theta}\} + \underline{\boldsymbol{A}}\{\Theta\} = 0 \qquad \{B.5\}$$

where $\underline{\boldsymbol{I}}$ is the identity matrix and $\underline{\boldsymbol{A}} = \underline{\boldsymbol{J}}^{-1}\underline{\boldsymbol{K}}$ is referred to as the system matrix. Assuming the system to undergo harmonic motion, $\{\ddot{\Theta}\} = -\underline{\lambda}\{\Theta\}$ and the characteristic equation of the system can be derived;

$$|\underline{\boldsymbol{A}} - \underline{\lambda}\ \underline{\boldsymbol{I}}| = 0 \qquad \{B.6\}$$

The roots of the characteristic equation are the eigenvalues of the system and the natural frequencies are obtained from the elements of the eigenvalue matrix;

$$\lambda_i = \omega_i^2 \qquad \{B.7\}$$

Substituting each eigenvalue λ_i into the matrix equation {B.3} the eigenvectors are obtained, also known as the mode shapes. For a system with n degrees of freedom, there will be n eigenvalues and n corresponding eigenvectors.

By assembling the n normal modes or eigenvectors into the columns of a square matrix, the modal matrix $\underline{\boldsymbol{P}}$ is created. Due to the orthogonal properties of the eigenvectors, using the transpose $\underline{\boldsymbol{P}}^T$ of the modal matrix, the product $\underline{\boldsymbol{P}}^T \underline{\boldsymbol{J}} \, \underline{\boldsymbol{P}}$ can be formed and the result is the diagonal generalised mass matrix. Generally the eigenvectors are subject to an arbitrary scaling factor which is not unique. However, if each of the columns of the modal matrix $\underline{\boldsymbol{P}}$ is divided by the square root of the generalised mass, the new matrix $\underline{\tilde{\boldsymbol{P}}}$ is said to be mass normalised. Therefore, the diagonalisation of the mass matrix by the mass normalised modal matrix is equal to the identity matrix;

$$\underline{\tilde{\boldsymbol{P}}}^T \underline{\boldsymbol{J}} \, \underline{\tilde{\boldsymbol{P}}} = \underline{\boldsymbol{I}} \qquad \{B.8\}$$

This treatment of the theoretical predictions of a system's eigenvectors allows direct comparison with the mode shapes derived from experimental modal analysis. The results obtained from the STAR modal analysis software were presented in an equivalent form for experimentally obtained mode shapes, with 'unity modal mass' (UMM) scaling.

For the study of the behaviour of the centrifugal pendulum vibration absorber it was necessary to insert the expression for the effective inertia of the device into the inertia matrix at the appropriate location along the shaft and assume a rotation speed for each case. The effective inertia of the absorber is a function of frequency and results in a significantly more complex characteristic equation to be solved. As discussed in Chapter 5, this was achieved using a process of iteration to determine the eigenvalues and eigenvectors in the theoretical modelling of the shaft system.

B.3 Forced Vibration Response

In addition to deriving the eigenvalues and eigenvectors for the undamped natural modes of a shaft system, it was necessary in some instances to consider the forced response. This was with the aim of predicting the frequency response functions for investigation of system behaviour, particularly with regard to the absorber performance.

For the modelling used in this study it was not necessary to include damping terms in the system equations of motion. The structures under test were very lightly damped, typically with damping estimated to be 1%-2% of critical. Thus, an undamped model would give reasonable prediction of the response, except in the immediate vicinity of the resonant peaks. Additionally, in an undamped system the degrees of freedom are entirely in phase or out of phase with each other, passing through step changes at the resonant frequencies.

The equations of motion for forced vibration of the undamped shaft system are stated in matrix form from development of {B.2} as;

$$\underline{J}\{\ddot{\Theta}\}+\underline{K}\{\Theta\}=\{T_N\} \tag{B.9}$$

Assuming the multi-degree of freedom system to be excited by harmonically varying forces, the general response is assumed to be of the form;

$$\{\Theta\}=\{\Psi\}e^{j\omega t} \tag{B.10}$$

Substitution into the equations of motion gives;

$$\left[-\omega^2\underline{J}+\underline{K}\right]\{\Psi\}=\{T_N\} \tag{B.11}$$

Premultiplying by the inverse of the impedance matrix $\underline{Z(\omega)}=\left[-\omega^2\underline{J}+\underline{K}\right]$ allows the forced vibration solution to be stated as;

$$\{\Psi\}=\underline{Z(\omega)}^{-1}\{T_N\} \tag{B.12}$$

For free-free shaft systems, the response at each inertia location contains the total roll and twist components of torsional vibration. Consideration of the relative twist of points on the shaft permits the torque in each connecting shaft section to be derived.

APPENDIX C

Publications

The following conference papers and publications have been generated from the research presented in this thesis:

- MILES T.J., LUCAS M. and ROTHBERG S.J. 'The Laser Torsional Vibrometer: Successful Operation During Lateral Vibrations', Proceedings of the 15th ASME Biennial Conference on Vibration and Noise (Boston, USA), September 1995. DE-Vol. 84-3, Part C. pp1451-1460.

- MILES T.J., LUCAS M. and ROTHBERG S.J. 'The Laser Torsional Vibrometer: Optimum Use in the Presence of Lateral Vibrations', Automotive Refinement (Mechanical Engineering Publications, London) 1996. IMechE Seminar Proceedings: Autotech 95 (Birmingham, UK) Paper C498/26/041. pp65-73.

- HALLIWELL N.A., ROTHBERG S.J., MILES T.J., EASTWOOD P.G., PICKERING C.J.P. and GATZWILLER K. 'On the Working Principle of Torsional Vibration Meter Type 2523', Brüel and Kjær Application Note, 1995.

- MILES T.J., LUCAS M. and ROTHBERG S.J. 'Bending Vibration Measurement on Rotors By Laser Vibrometry', Optics Letters, Vol. 21, No. 4, February 1996. pp296-298.

Features on this work have been included in two IOP publications:

'*Scattered light can assess vibration in rotating machines*', Opto & Laser Europe, Issue 30, May 1996. pp38-39.

'*Optics measures vibration in rotating machines*', Noise & Vibration Worldwide, Vol. 27, No. 7, July 1996. pp7-9.

Additionally, an entry submitted to the *1996 Metrology for World Class Manufacturing Awards* based on this work and entitled 'A New Instrument for Bending Vibration Measurement on Rotors' received a 'Commendation' as runner-up in its class.

* MILES T.J., LUCAS M. and ROTHBERG S.J. 'Torsional Modal Analysis of Rotating Shaft Systems', Proceedings of Sixth International Conference on Vibrations in Rotating Machinery (Oxford, UK), September 1996. IMechE Conference Transactions 1996-6, Paper C500/101/96. pp631-640.

Results from this research were also presented in the following paper:

* HALLIWELL N.A. 'The Laser Torsional Vibrometer: A Step Forward in Rotating Machinery Diagnostics', Journal of Sound and Vibration, Vol. 190, No. 3, 1996. pp399-418.

The following publications are currently in preparation for submission to the Journal of Sound and Vibration;

* MILES T.J., LUCAS M., HALLIWELL N.A. and ROTHBERG S.J. 'Torsional and Bending Vibration Measurement on Rotors Using Laser Technology',
* MILES T.J., LUCAS M. and ROTHBERG S.J. 'Torsional Modal Analysis on Rotating Systems with Application to the Development of a Vibration Absorber',

REFERENCES

Chapter 1

1-1 GRANERE V.R. 'Understand Torsional Vibration', Hydrocarbon Processing, Vol. 70, July 1991. pp53-60.

1-2 SMITH R.L. 'Torsional Vibration', Sound and Vibration, Vol. 26, September 1992. pp22-24.

1-3 BROWN R.N. 'A Torsional Vibration Problem as Associated with Synchronous Motor Driven Machines', Transactions of the ASME: Journal of Engineering for Power, Vol. 82, July 1960. pp215-220.

1-4 SIMMONS H.R. and SMALLEY A.J. 'Effective Tools for Diagnosing Elusive Turbomachinery Problems in the Field', Transactions of the ASME: Journal of Engineering for Gas Turbines and Power, Vol. 112, October 1990. pp470-477.

1-5 WRIGHT J. 'Putting the Damper on Torsional Vibration', Power Transmission Design, Vol. 30, Part 5, May 1988. pp41-44, 69.

1-6 HALLIWELL N.A. and EASTWOOD P.G. 'Marine Vehicles and Offshore Installations: Laser Diagnostics of Machinery Health', Optics and Lasers in Engineering, Vol. 16, 1992. pp337-350.

1-7 HALLIWELL N.A. and EASTWOOD P.G. 'Torsional Vibration Damper Performance: Diagnosis Using Laser Technology', Proceedings of the IMechE Conference on Automotive Diagnostics (London, UK), 1990. Paper C422/005. pp115-122.

1-8 HERSHKOWITZ H. 'Torsional Vibration Measurements in Preventative Maintenance of Rotating Machinery', Proceedings of the National Conference on Power Transmission (Chicago, IL), November 1978. Vol. 5. pp161-169.

1-9 HALLIWELL N.A. 'The Laser Torsional Vibrometer: A Step Forward in Rotating Machinery Diagnostics', Journal of Sound and Vibration, Vol. 190, No. 3, 1996. pp399-418.

1-10 KER WILSON W. 'Practical Solution of Torsional Vibration Problems', 5 volumes (Chapman & Hall, London) 3rd ed. 1969.

1-11 TUPLIN W.A. 'Torsional Vibration', (Pitman, London) 1966.

1-12 SCHWIBINGER P., HENDRICK D., WU W. and IMANISHI Y. 'Noise and Vibration Control Measures in the Powertrain of Passenger Cars', Proceedings of the 1991 Noise and Vibration Conference (Transverse City, MI). Society of Automotive Engineers P-244. SAE Paper 911053. pp123-131.

1-13 BAKER J.M., BAZELEY G., HARDING R., HUTTON D.N. and NEEDHAM P. 'Refinement Benefits of Engine Ancillary Dampers', Proceedings of the Institution of Mechanical Engineers, Vehicle NVH and Refinement (Birmingham, UK), May 1994. Paper C487/041/94. pp149-158.

1-14 KEENEY C.S. and SHIH S. 'Prediction and Control of Heavy Duty Powertrain Torsional Vibration', Proceedings of the 1993 Noise and Vibration Conference (Transverse City, MI). Society of Automotive Engineers P-264. SAE Paper 922481. pp713-722.

1-15 CHIKATANI Y. and SUEHIRO A. 'Reduction of Idling Rattle Noise in Trucks', Proceedings of the 1991 Noise and Vibration Conference (Transverse City, MI). Society of Automotive Engineers P-244, SAE Paper 911044. pp49-56.

1-16 RUST A. and BRANDL F.K. 'Definition, Identification and Elimination of Obtrusive Gear Rattle Noise', Proceedings of the SAE: XXIII FISITA Congress (Torino, Italy), May 1990. Vol. I, SAE Paper 905067. pp499-506.

1-17 YAMAMOTO K., UMEYAMA M., ISHIKAWA H., OTAKE T. and KOAYASHI K. 'Consideration of a new Type Two-Mass Flywheel', Proceedings of the 1991 Noise and Vibration Conference (Transverse City, MI). Society of Automotive Engineers P-244. SAE Paper 911059. pp161-165.

1-18 SEBULKE A. 'The Two-Mass Flywheel - A Torsional Vibration Damper for the Power Train of Passenger Cars - State of the Art and Further Technical Development', SAE Transactions, Vol. 96, Section 2, 1987. SAE Paper 870394. pp2.89-2.98.

1-19 DREXL H.J. 'Torsional Dampers and Alternative Systems to Reduce Driveline Vibrations', SAE Transactions, Vol. 96, Section 2, 1987. SAE Paper 870393. pp2.78-2.88.

1-20 OCHIAI K. and NAKANO M. 'Relation between Crankshaft Torsional Vibration and Engine Noise', SAE Transactions, Vol. 88, Section 2, 1979. SAE Paper 790365. pp1291-1298.

1-21 BEBERMEIR J. and EBERHARD G. 'Torsional Vibration Absorbers for Passenger Car Drive Lines', Proceedings of the SAE: XXIII FISITA Congress (Torino, Italy), May 1990. Vol. I, SAE Paper 905066. pp491-497.

1-22 HESTERMAN D.C. and STONE B.J. 'Secondary Inertia Effects in the Torsional Vibration of Reciprocating Engines - A Literature Review', Proceedings of the IMechE, Part C: Journal of Mechanical Engineering Science, Vol. 208, 1994. pp11-15.

1-23 HESTERMAN D.C., DREW S.J. and STONE B.J. 'Vibration of Engines Resulting from Torsional Vibration of Crankshafts', Proceedings of the 6th International Conference on Vibrations in Rotating Machinery (Oxford, UK), September 1996. Paper C500/033/96. pp713-723.

1-24 SIMMONS H.R. and SMALLEY A.J. 'Lateral Gear Shaft Dynamics Control Torsional Stresses in Turbine-Driven Compressor Train', Transactions of the ASME: Journal of Engineering for Gas Turbines and Power, Vol. 106, October 1984. pp946-951.

1-25 SCHWIBINGER P. and NORDMANN R. 'The Influence of Torsional-Lateral Coupling on the Stability Behaviour of Geared Rotor Systems', Transactions of the ASME: Journal of Engineering for Gas Turbines and Power, Vol. 110, October 1988. pp563-571.

1-26 LI X. and STONE B.J. 'Coupling Mechanisms Between Torsional and Transverse Vibration in Reciprocating Engines and Compressors', Proceedings of the 13th International Modal Analysis Conference (Nashville, TN), February 1995. Vol. II. pp1373-1377.

1-27 WAHL A.M. and FISCHER E.G. 'Investigation of Self-Excited Torsional Oscillations and Vibration Damper for Induction-Motor Drives', Transactions of the ASME: Journal of Applied Mechanics, Vol. 64, December 1942. ppA175-183.

1-28 KNIGHT W.A. 'Factors Affecting the Torsional Frequency Response of Machine Tool Drive Systems', International Journal of Machine Tool Design and Research, Vol. 12, 1972. pp65-83.

1-29 WALKER D.N., ADAMS S.L. and PLACEK R.J. 'Torsional Vibration and Fatigue of Turbine-Generator Shafts', IEEE Transactions on Power Apparatus and Systems, Vol. PAS-100, No. 11, November 1981. pp4373-4380.

1-30 RAN L., YACAMINI R. and SMITH K.S. 'Torsional Vibrations in Electrical Induction Motor Drives During Start-Up', Transactions of the ASME: Journal of Vibration and Acoustics, Vol. 118, April 1996. pp242-251.

1-31 HYDE R.L. and BRINNER T.R. 'Starting Characteristics of Electric Submergible Oil Well Pumps', IEEE Transactions on Industry Applications, Vol. IA-22, No. 1, January/February 1986. pp133-144.

1-32 BELMANS R., VANDENPUT A. and GEYSEN W. 'Influence of Torsional Vibrations on Lateral Oscillations of Induction Motor Rotors', IEEE Transactions on Power Apparatus and Systems, Vol. PAS-104, No. 7, July 1985. pp1832-1837.

1-33 VANCE J.M. 'Rotordynamics of Turbomachinery', (John Wiley & Sons, New York) 1988.

1-34 ALBRIGHT M.F. and STAFFELD D.F. 'Noise and Vibration Refinement of the Ford 3.8 Liter Powertrain', Proceedings of the 1991 Noise and Vibration Conference (Transverse City, MI). Society of Automotive Engineers P-244. SAE Paper 911073. pp291-305.

1-35 KINOSHITA M., SAKAMOTO T. and OKAMURA H. 'An Experimental Study of a Torsional/Bending Damper Pulley for an Engine Crankshaft', SAE Transactions, Vol. 98, Section 3, 1989. SAE Paper 891127. pp1605-1615.

1-36 PARK Y-S., PARK J-Y. and LEE C-W. 'Dynamic Torsional and Bending Stress Measurement from Operating Crankshaft', SAE Transactions 1986, Vol. 95, Section 1. SAE Paper 860232. pp1.1157-1165.

1-37 KURODA O. and FUJII Y. 'An Approach to Improve Engine Sound Quality', SAE Transactions, Vol. 97, Section 4, 1988. Paper 880083. pp4.73-4.82.

1-38 IDE S., UCHIDA T., OZAWA K. and IZAWA K. 'Improvement of Engine Sound Quality Through a New Flywheel System Flexibly Mounted to the Crankshaft', SAE Transactions, Vol. 99, No. 6, SAE Paper 900391, 1990. pp596-603.

1-39 ZHENDONG F. XIANGHONG W. and FANGNING S. 'Experimental Modal Analysis for Bending Vibration of Automotive Powertrains', Proceedings of the 6th International Pacific Conference on Automotive Engineering (Seoul, South Korea), October 1991. SAE Paper 912573. pp1031-1034.

1-40 GOODWIN M.J. 'Dynamics of Rotor-Bearing Systems', (Unwin Hyman, London) 1989. Ch. 9.

1-41 EHRICH F.F. 'Handbook of Rotordynamics', (McGraw-Hill, New York) 1992. Ch. 4.

1-42 ROTHBERG S.J. and HALLIWELL N.A. 'On the Use of Laser Vibrometry for Rotating Machinery Measurements', Proceedings of the Institution of Mechanical Engineers, Vibrations in Rotating Machinery (Bath, UK), September 1992. Paper C432/078. pp409-415.

1-43 ROTHBERG S.J. and HALLIWELL N.A. 'Vibration Measurements on Rotating Machinery Using Laser Doppler Velocimetry', Transactions of the ASME: Journal of Vibration and Acoustics, Vol. 116, July 1994. pp326-331.

1-44 STANBRIDGE A.B., and EWINS D.J. 'Measurement of Translational and Angular Vibration Using a Scanning Laser Doppler Vibrometer', Proceedings of the First International Conference on Vibration Measurements by Laser Techniques: Advances and Applications (Ancona, Italy), October 1994. SPIE Vol. 2358. pp37-47.

1-45 TRETHEWEY M.W., SOMMER H.J. and CAFEO J.A. 'A Dual Beam Laser Vibrometer for Measurement of Dynamic Structural Rotations and Displacements', Journal of Sound and Vibration, Vol. 164, No. 1, 1993. pp67-84.

1-46 BOKELBERG E.H., SOMMER H.J. and TRETHEWEY M.W. 'A Six-Degree-of-Freedom Laser Vibrometer, Part I: Theoretical Development', Journal of Sound and Vibration, Vol. 178, No. 5, 1994. pp643-654.

1-47 BOKELBERG E.H., SOMMER H.J. and TRETHEWEY M.W. 'A Six-Degree-of-Freedom Laser Vibrometer, Part II: Experimental Validation', Journal of Sound and Vibration, Vol. 178, No. 5, 1994. pp655-667.

1-48 FUJII K. 'A Simulation of Crankshaft Bending Vibration', Proceedings of the 6th International Pacific Conference on Automotive Engineering (Seoul, South Korea), October 1991. SAE Paper 912495. pp357-363.

1-49 KAMIYA T., ATSUMI T. and TASAKA K. 'Toyota's New Type of Crankshaft Pulley to Improve the Compartment Tone Quality', SAE Transactions, Vol. 97, Section 4, 1988. SAE Paper 880078. pp4.59-4.65.

1-50 LEE S-K., CHOI B-U. and YEO S-D. 'Identification of the Relation Between Crankshaft Bending and Interior Noise of A/T Vehicle in Idle State', New Engine Design and Engine Component Technology. Society of Automotive Engineers SP-

972, 1993. SAE Paper 930618. pp11-21.

Chapter 2

2-1 NESTORIDES E. 'A Handbook on Torsional Vibration', (Cambridge University Press, London) 1958. pp483-496.

2-2 As reference 1-4

2-3 NESTORIDES E. 'A Handbook on Torsional Vibration', (Cambridge University Press, London) 1958. pp630-636.

2-4 KER WILSON W. 'Practical Solution of Torsional Vibration Problems. Volume 5: Vibration Measurement and Analysis', (Chapman & Hall, London) 3rd ed. 1969. Ch. 36.

2-5 As reference 1-36

2-6 HOTTINGER BALDWIN MESSTECHNIK (HBM) 'Product Summary - Torque', (Germany). Trade brochure.

2-7 SUNG C-C., VARADAN V.V, BAO X-Q. and VARADAN V.K. 'Active Torsional Vibration control Experiments Using Shear-Type Piezoceramic Sensors and Actuators', Journal of Intelligent Material Systems and Structures, Vol. 5, Part 3, May 1994. pp436-442.

2-8 YEH M-K. and CHIN C-Y. ' Dynamic Response of Circular Shaft with Piezoelectric Sensor', Journal of Intelligent Material Systems and Structures, Vol. 5, Part 6, November 1994. pp833-840.

2-9 GINDY S.F. 'Force and Torque Measurement, A Technology Overview. Part II - Torque', Experimental Techniques, Vol. 9, No. 7, July 1985. pp9-15

2-10 FLEMING W.J. 'Automotive Torque Measurement: A Summary of Seven Different Methods', IEEE Transactions on Vehicular Technology, Vol. VT-31, No. 3, August 1982. pp117-124.

2-11 WILMSHURST T.H., ROTHBERG S.J. and HALLIWELL N.A. 'Laser Torquemeter: A New Instrument', Electronics Letters, Vol. 27, No. 2, 1991. pp186-187.

2-12 VIBRO-METER 'Torquemaster TM - Torque Transducers', (Switzerland). Trade brochure.

2-13 NESTORIDES E. 'A Handbook on Torsional Vibration', (Cambridge University

Press, London) 1958. pp593-601.

2-14 KER WILSON W. 'Practical Solution of Torsional Vibration Problems. Volume 5: Vibration Measurement and Analysis', (Chapman & Hall, London) 3rd ed. 1969. Ch. 31 & 32.

2-15 TUPLIN W.A. 'Torsional Vibration', (Pitman & Sons, London) 1966. Ch. 12.

2-16 KER WILSON W. 'Practical Solution of Torsional Vibration Problems. Volume 5: Vibration Measurement and Analysis', (Chapman & Hall, London) 3rd ed. 1969. Ch. 33.

2-17 KER WILSON W. 'Practical Solution of Torsional Vibration Problems. Volume 5: Vibration Measurement and Analysis', (Chapman & Hall, London) 3rd ed. 1969. Ch. 34.

2-18 STANSFIELD R. 'The Measurement of Torsional Vibrations', Proceedings of the Institution of Mechanical Engineers, Vol. 148, No. 5, 1942. pp175-193.

2-19 NESTORIDES E. 'A Handbook on Torsional Vibration', (Cambridge University Press, London) 1958. pp601-618.

2-20 VERHOEF W.H. 'Measuring Torsional Vibration', Instrumentation Technology, November 1977. pp61-66.

2-21 VANCE J.M. 'Rotordynamics of Turbomachinery', (John Wiley & Sons, New York) 1988. Ch. 8.

2-22 As reference 1-1

2-23 GRANERE V.R. 'Torsional Vibration: Are your Measurements Accurate?', Hydrocarbon Processing, Vol. 71, April 1992. pp71-3.

2-24 As reference 1-8

2-25 SCHWIBINGER P. and NORDMANN R. 'Torsional Vibrations in Turbogenerators due to Network Disturbances', Transactions of the ASME: Journal of Vibration and Acoustics, Vol. 112, No. 3, July 1990. pp312-320.

2-26 SMITH J.D. and ECHEVERRIA-VILLAGOMEZ J.S. 'Using an Encoder as a Torsional Vibration Transducer', Proceedings of the IMechE, Part C: Journal of Mechanical Engineering Science, Vol. 203, 1989. pp219-220.

2-27 VANCE J.M. and FRENCH R.S. 'Measurement of Torsional Vibration in Rotating Machinery', Transactions of the ASME: Journal of Mechanisms, Transmissions, and Automation in Design, Vol. 108, December 1986. pp565-577.

2-28 FU H. and YAN P. 'Digital Measurement Method on Rotating Shaft Torsional Vibration', Proceedings of the 14th Biennial ASME Design Technical Conference on Mechanical Vibration and Noise (Albuquerque, NM), September 1993. DE-Vol. 60. pp271-275.

2-29 WILLIAMS J. 'Improved Methods for Digital Measurement of Torsional Vibration', Proceedings of the 1996 International Truck and Bus Meeting and Exposition, (Detroit, MI), October 1996. Vol. 1203. SAE Paper 962204. pp9-15

2-30 WANG P., DAVIES P., STARKEY J.M. and ROUTSON R.L. 'Torsional Mode Shape Measurement on a Rotating Shaft', Proceedings of the 10th International Modal Analysis Conference (San Diego, CA), February 1992. Vol. I. pp676-681.

2-31 WANG P., DAVIES P., STARKEY J.M. and ROUTSON R.L. 'A Torsional Vibration Measurement System', IEEE Transactions on Instrumentation and Measurement, Vol. 41, December 1992. pp803-807.

2-32 ROUTSON R.L., STARKEY J.M., WANG P. and DAVIES P. 'Torsional and Translational Vibrations of a Drive Shaft System with a Cardan Joint', Proceedings of the 22nd Biennial ASME Mechanism Conference: Flexible Mechanisms, Dynamics and Analysis (Scottsdale, AZ), September 1992. DE-Vol. 47. pp533-542.

2-33 BIGRET R., COETZEE C.J., LEVY D.C. and HARLEY R.G. 'Measuring the Torsional Modal Frequencies of a 900MW Turbogenerator', IEEE Transactions on Energy Conversion, Vol. EC-1, No. 4, December 1986. pp99-107.

2-34 SMITH J.D. and ECHEVERRIA-VILLAGOMEZ J.S. 'Comparing Encoder and Accelerometer Measurement of Transmission Error or Torsional Vibration', Proceedings of the IMechE First International Conference on Gearbox Noise and Vibration (Cambridge, UK), April 1990. Paper C404/027. pp43-49.

2-35 HENRY M.S. 'Torsional Vibration Measurement and Analysis: A New Technique', SAE Transactions, Vol. 92, No. 3, 1983. SAE Paper 831320. pp3.977-984.

2-36 SEIDLITZ S. 'Engine Torsional Transducer Comparison', SAE Transactions, Vol. 101, Section 3, 1992. SAE Paper 920066. pp133-137.

2-37 HAYASHI A. and KITAGAWA Y. 'High-Resolution Rotation-Angle Measurement of a Cylinder Using Speckle Displacement Detection', Applied Optics, Vol. 22, No. 22, November 1983. pp3520-3525.

2-38 HANSON S.G. and HANSEN B.H. 'Laser-Based Measurement System for

Rotational Measurement of Specularly Reflective Shafts', Fibre Optic and Laser Sensors XII (San Diego, CA), July 1994. SPIE Vol. 2292. pp143-153.

2-39 HANSON S.G. 'System for Non-Contact Measurement of Torsional Vibrations of Shafts', Proceedings of Optical Velocimetry (Warsaw, Poland), May 1995. SPIE Vol. 2729, 1996. pp155-163.

2-40 HANSON S.G. and LADING L. 'Generics of Systems for Measuring Linear and Angular Velocities of Solid Objects', Proceedings of Optical Velocimetry (Warsaw, Poland), May 1995. SPIE Vol. 2729, 1996. pp81-90.

2-41 GREGORY R.W., HARRIS S.L. and MUNRO R.G. 'A Method of Measuring Transmission Error in Spur Gears of 1:1 Ratio', Journal of Scientific Instruments, Vol. 40, January 1963. pp5-9.

2-42 MUNRO R.G. and YILDIRIM N. 'Some Measurements of Static and Dynamic Transmission Errors of Spur Gears', Proceedings of the 1994 International Gearing Conference (Newcastle, UK), September 1994. pp371-376.

2-43 ROSINSKI J., HOFMANN D.A. and PENNELL J.A. 'Dynamic Transmission Error Measurements in the Time Domain in High Speed Gears', Proceedings of the 1994 International Gearing Conference (Newcastle, UK), September 1994. pp363-370.

2-44 THOMPSON S.J., HAIGH J., HOFMANN D.A., ROSINSKI J. and PENNELL J.A. 'A Four Megawatt Test Rig for Gear Noise and Vibration Research', Proceedings of the 1994 International Gearing Conference (Newcastle, UK), September 1994. pp445-451.

2-45 DRAIN L.E. 'The Laser Doppler Technique', (John Wiley & Sons, Chichester) 1980. Ch. 9.

2-46 DURST F., MELLING A. and WHITELAW J.H. 'Principles and Practice of Laser-Doppler Anemometry', (Academic Press, London) 2nd ed. 1981.

2-47 WATRASIEWICZ B.M. and RUDD M.J. 'Laser Doppler Measurements', (Butterworths, London) 1976.

2-48 HALLIWELL N.A., PULLEN H.L. and BAKER J. 'Diesel Engine Health: Laser Diagnostics', SAE Transactions, Vol. 92, Section 3, 1983. SAE Paper 831324. pp3.986-3.994.

2-49 HANSON S.G. 'Laser-Based Method for Analysing Rotational Speed and Vorticity', International Symposium on Laser Anemometry (Miami, FL), November 1985.

FED-Vol. 33. pp91-95.

2-50 WATANABE T., IWATA K. and NAGATA R. 'Optical-Heterodyne Method for Measuring Rotational Velocity', Optics Communications, Vol. 43, No. 3, October 1982. pp164-167.

2-51 HALLIWELL N.A, PICKERING C.J.D. and EASTWOOD P.G. 'The Laser Torsional Vibrometer: A New Instrument', Journal of Sound And Vibration, Vol. 93, No. 4, 1984. pp588-592.

2-52 HALLIWELL N.A. and EASTWOOD P.G. 'The Laser Torsional Vibrometer', Journal of Sound And Vibration, Vol. 101, No. 3, 1985. pp446-449.

2-53 EASTWOOD P.G., HALLIWELL N.A. and GILBERT P. 'Laser Tools for Diesel Engine Diagnostics', Proceedings of the Institution of Mechanical Engineers, Vol. 199, No. D4, 1985. pp295-300.

2-54 As reference 1-9

2-55 BRÜEL & KJÆR (Halliwell N.A., Rothberg S.J., Miles T.J., Eastwood P.G., Pickering C.J.D. and Gatzwiller K.) 'On the Working Principle of Torsional Vibration Meter Type 2523', Application Note (Denmark) 1994. Trade Brochure.

2-56 DANTEC 'Measure with a Light Hand - Vibrometer Systems. Torsional Vibrometer' (Denmark). Trade brochure.

2-57 ROTHBERG S.J. and HALLIWELL N.A. 'Laser Vibrometry: Pseudo-Vibrations', Journal of Sound and Vibration, Vol. 135, No.3; 1989. pp516-522.

2-58 ROTHBERG S.J., HALLIWELL N.A., EASTWOOD P.G. and WILMSHURST T.H. 'The Laser Torsional Vibrometer: Noise-Floor Considerations', Proceedings of SPIE, Stress and Vibration: Recent Developments in Industrial Measurement and Analysis (London, UK), March 1989. SPIE Vol. 1084. pp171-182.

2-59 LIU T.Y., BERWICK M. and JACKSON D.A. 'Novel Fiber-Optic Torsional Vibrometers', Review of Scientific Instruments, Vol. 63, No. 4, April 1992. pp2164-2169.

2-60 LEWIN A.C., ROTH V. and SIEGMUND G. 'New Concept for Interferometric Measurement of Rotational Vibrations', Proceedings of the First International Conference on Vibration Measurements by Laser Techniques: Advances and Applications (Ancona, Italy), October 1994. SPIE Vol. 2358. pp24-36.

2-61 POLYTEC 'Laser Doppler Vibrometer - Rotational Vibrometer', (Germany). Trade

Brochure.

2-62 PICKERING C.J.D., HALLIWELL N.A. and WILMSHURST T.H. 'The Laser Vibrometer: A Portable Instrument', Journal of Sound and Vibration, Vol. 107, No. 3, 1986. pp471-485.

2-63 MEYNART R. 'A Simple Interferometric Vibrometer Based on a Laser Doppler Velocimeter', Journal of Physics, E: Scientific Instruments, Vol. 17, November 1984. pp984-987.

2-64 As reference 1-6

2-65 As reference 1-7

2-66 EWINS D.J. 'Modal Testing: Theory and Practice', (Research Studies Press, John Wiley & Sons, New York) 1988.

2-67 KER WILSON W. 'Practical Solution of Torsional Vibration Problems. Volume 4: Devices for Controlling Vibration', (Chapman & Hall, London) 3rd ed. 1968. Ch. 29.

2-68 NESTORIDES E. 'A Handbook on Torsional Vibration', (Cambridge University Press, London) 1958. pp618-629.

2-69 KER WILSON W. 'Practical Solution of Torsional Vibration Problems. Volume 2: Amplitude Calculations', (Chapman & Hall, London) 3rd ed. 1963. Ch. 17.

2-70 GATZWILLER K. 'Measuring Torsional Operational Deflection Shapes', Application Note: Torsional Vibration Meter Type 2523. (Brüel & Kjær, Denmark).

2-71 LI H., ENTWISTLE R.D. and STONE B.J. 'Impact Excitation of Torsional Vibration', Modal Analysis: The International Journal of Analytical and Experimental Modal Analysis, Vol. 9, No. 3, July 1994. pp163-174.

2-72 DREW S.J. and STONE B.J. 'Impact Excitation of Torsional Vibration Systems', Proceedings of the 13th International Modal Analysis Conference (Nashville, TN), 1995. Vol. II. pp1432-1436.

2-73 KNIGHT W.A. 'Torsional Vibrations and Machine Tool Stability', PhD Thesis, Department of Mechanical Engineering, University of Birmingham, October 1967.

2-74 OPITZ H., KALKERT W. and REHLING E. 'Design and Application of Electro-Hydraulic Exciters for the Investigation of Large Machine Tools', Proceedings of the 5th Machine Tool Design Research International Conference (Birmingham, UK), 1964. pp5-21.

2-75 SERVOTEST '900 Series Rotary Vibrator', (Derriton Group, UK). Trade brochure.

2-76 TEAM CORPORATION 'Hydrashakers - Rotating Vibration System', (Gearing & Watson, UK). Trade brochure.

2-77 As reference 1-15

2-78 KNIGHT W.A. 'Factors Affecting the Torsional Frequency Response of Machine Tool Drive Systems', International Journal of Machine Tool Design and Research, Vol. 12, 1972. pp65-83.

2-79 HENTSCHEL G. and SCHWEIZERHOF S. 'The "Vibrotor" Vibration Exciter', The Engineers' Digest, Vol. 15, No. 4, April 1954. pp137-138. (Abstract from *La Recherche Aéronautique*, No. 37, January-February 1954. pp51-55.)

2-80 As reference 1-32

2-81 DREW S.J. and STONE B.J. 'Excitation of Torsional Vibration for Rotating Machinery Using a 1.7kW AC Servo-Drive', IMechE Conference Transactions of Second International Conference on Gearbox Noise, Vibration and Diagnostics (London, UK), November 1995. Paper C492/028. pp171-181.

2-82 DREW S.J. and STONE B.J. 'Torsional (Rotational) Vibration: Excitation of Small Rotating Machines', Journal of Sound and Vibration, Vol. 201, No. 4, 1997. pp437-463.

2-83 ILICH J., DREW S.J. and STONE B.J. 'The Torsional Vibration Characteristics of Couplings', Proceedings of the 6th International Conference on Vibrations in Rotating Machinery (Oxford, UK), September 1996. Paper C500/032/96. pp619-629.

2-84 As reference 1-23

Chapter 3

3-1 As reference 1-9

3-2 As reference 2-51

3-3 DRAIN L.E. 'The Laser Doppler Technique', (John Wiley & Sons, Chichester) 1980. Ch. 3.

3-4 BRÜEL & KJÆR 'The Laser Velocity Transducer - Its Principles and Applications', (Denmark).Trade brochure.

3-5 POLYTEC 'Laser Doppler Vibrometer', (Germany).Trade brochure.

3-6 DANTEC 'Measure with a Light Hand - Vibrometer Systems', (Denmark). Trade brochure.

3-7 COLLACOTT R.A. 'Vibration Monitoring and Diagnosis', (George Goodwin, London) 1979. Ch. 2.

3-8 WILLIAMS J.H. 'Fundamentals of Applied Dynamics', (John Wiley & Sons, New York) 1996. Appendix A.

3-9 BRÜEL & KJÆR 'Torsional Vibration Meter Type 2523 - Instruction Manual', (Denmark) 1992.

3-10 As reference 2-68

3-11 As reference 2-69

3-12 As reference 1-34

3-13 As reference 2-52

3-14 As reference 1-35

3-15 As reference 1-37

3-16 As reference 1-50

3-17 DIMENTBERG F.M. 'Flexural Vibrations of Rotating Shafts', (Butterworths, London) 1961. Ch. 1.

3-18 LOEWY R.G. and PIARULLI V.J. 'Dynamics of Rotating Shafts', (The Shock and Vibration Information Center, Washington) 1969. Ch. 5.

3-19 As reference 1-36

3-20 As reference 1-49

Chapter 4

4-1 As reference 2-66

4-2 NORDMANN R. 'Identification of Modal Parameters of an Elastic Rotor with Oil Film Bearings' Transactions of the ASME: Journal of Vibration, Acoustics, Stress, and Reliability in Design, Vol. 106, January 1984. pp107-112.

4-3 LEE C.W. and JEI Y-G. 'Modal Analysis of Continuous Rotor-Bearing Systems', Journal of Sound And Vibration, Vol. 126, No. 2, 1988. pp345-361.

4-4 LEE C.W., KATZ R., ULSOY G. and SCOTT R.A. 'Modal Analysis of a Distributed Parameter Rotating Shaft', Journal of Sound And Vibration, Vol. 122, No. 1, 1988. pp119-130.

4-5 ROGERS P.J. and EWINS D.J. 'Modal Testing of an Operating Rotor System Using a Structural Dynamics Approach', Proceedings of the 7th International Modal Analysis Conference (Las Vegas, NV), January 1989. Vol. I. pp466-473.

4-6 JEI Y-G. and LEE C.W. 'Modal Analysis of a Continuous Asymmetrical Rotor-Bearing Systems', Journal of Sound And Vibration, Vol. 152, No. 2, 1992. pp245-262.

4-7 BUCHER I., EWINS D.J. and ROBB D.A. 'Modal Testing of Rotating Structures: Difficulties, Assumptions and Practical Approach', Proceedings of the 6th International Conference on Vibrations in Rotating Machinery (Oxford, UK), September 1996. Paper C500/007/96. pp539-562.

4-8 JOH Y.D. and LEE C.W. 'Excitation Methods and Modal Parameter Identification in Complex Modal Testing of Rotating Machinery', Modal Analysis: The International Journal of Analytical and Experimental Modal Analysis, Vol. 8, No. 3, July 1993. pp179-203.

4-9 LEE C-W. and KIM J-S. 'Modal Testing and Suboptimal Vibration Control of Flexible Rotor Bearing System by Using a Magnetic Bearing', Transactions of the ASME: Journal of Dynamic Systems, Measurement, and Control, Vol. 114, June 1992. pp244-252.

4-10 FÖRCH P., GÄHLER C. and NORDMANN R. 'Modal Testing in Rotating Machinery Using Active Magnetic Bearings', Proceedings of the 6th International Conference on Vibrations in Rotating Machinery (Oxford, UK), September 1996. (Supplement paper).

4-11 GÄHLER C. and FÖRCH P. 'A Precise Magnetic Bearing Exciter for Rotordynamic Experiments', Proceedings of the 4th International Symposium of Magnetic Bearings (Zurich, Switzerland), August 1994. pp193-200.

4-12 NORDMANN R., MATROS M. and NEUMER T. 'Parameter Identification in Rotating Machinery by means of Magnetic Bearings', Proceedings of IFTOMM 4th International Conference on Rotor Dynamics (Chicago, IL), 1994. pp7-15.

4-13 KUANG J-H. and LIN J-F. 'Accelerometer Pair Measurements for Shaft Dynamic Parameters Analysis', Proceedings of the 12th International Modal Analysis Conference (Honolulu, HA), January 1994. Vol. II. pp1649-1655.

4-14 As reference 2-33

4-15 As reference 2-8

4-16 As reference 2-7

4-17 As reference 1-24

4-18 As reference 2-70

4-19 GADE S., GATZWILLER K. and HERLUFSEN H. 'Torsional Operational Deflection Shapes (TODS) Measurements', Proceedings of the 12th International Modal Analysis Conference (Honolulu, HA), January 1994. Vol. II. pp1356-1359.

4-20 As reference 1-28

4-21 As reference 2-73

4-22 As reference 2-82

4-23 As reference 2-71

4-24 As reference 2-72

4-25 THOMAS D.T. 'Engineering Electromagnetics', (Pergamon Press, New York) 1972. Ch. 9.

4-26 PLONUS M.A. 'Applied Electromagnetics', (McGraw-Hill, New York) 1978. Ch. 10.

4-27 STOLL R.L. 'The Analysis of Eddy Currents', (Clarendon Press, Oxford) 1974. Ch. 1.

4-28 AVALLONE E.A. and BAUMEISTER T. (Ed.) 'Marks' Standard Handbook for Mechanical Engineers', (McGraw-Hill, New York) 10th ed. 1996. Ch. 8.

4-29 GREENWOOD D.C. 'Manual of Electromechanical Devices', (McGraw-Hill, New York) 1965. Ch. 6.

4-30 MAJMUDAR H. 'Electromechanical Energy Converters', (Allyn & Bacon, Boston) 1965. Ch. 5.

4-31 SAY M.G. and TAYLOR E.O. 'Direct Current Machines', (Pitman, London) 2nd ed. 1986. Ch. 12.

4-32 SHADOWITZ A. 'The Electromagnetic Field', (Dover Publications, New York) 1988. Ch. 11.

4-33 WOODSON H.H. and MELCHER J.R. 'Electromechanical Dynamics. Part I: Discrete Systems', (John Wiley & Sons, New York) 1968. Ch. 6.

4-34 ZAHA M. 'Electromagnetic Field Theory: A Problem Solving Approach', (John Wiley & Sons, New York) 1979. Ch. 6.

4-35 HARRIS F.K. 'Electrical Measurements', (Chapman & Hall, London) 1957. Ch. 4.

4-36 HUGHES E. 'Electrical Technology', (Longman Scientific & Technical, Harlow UK) 6th ed. 1990. Ch. 26.

4-37 SALDNER H. 'Calibrated Non-Contact Exciters for Optical Modal Analysis', Proceedings of the First International Conference on Vibration Measurements by Laser Techniques: Advances and Applications (Ancona, Italy), October 1994. SPIE Vol. 2358. pp227-237.

4-38 PATTON M.E. and TRETHEWEY M.W. 'A Non-Contacting Technique for Modal Analysis', Proceedings of the 7th International Modal Analysis Conference (Las Vegas, NV), January 1989. Vol. II. pp894-900.

4-39 PLONUS M.A. 'Applied Electromagnetics', (McGraw-Hill, New York) 1978. Ch. 6.

4-40 SCHIEBER D. 'Braking Torque on a Rotating Sheet in Stationary Magnetic Field', Proceedings of the Institution of Electrical Engineers, Vol. 121, No. 2, February 1974. pp117-122.

4-41 SCHIEBER D. 'Unipolar Induction Braking of Thin Metal Sheets', Proceedings of the Institution of Electrical Engineers, Vol. 119, No. 10, October 1972. pp1499-1503.

4-42 SMYTHE W.R. 'On Eddy Currents in a Rotating Disk', Transactions of the American Institute of Electrical Engineers, Vol. 61, September 1942. pp681-684.

4-43 VENKATARATNAN K. and RAMACHANDRA RAJU D. 'Analysis of Eddy-Current Brakes with Non-Magnetic Rotors', Proceedings of the Institution of Electrical Engineers, Vol. 124, No.1, January 1977. pp67-71.

4-44 SIMEU E. and GEORGES D. 'Modelling and Control of an Eddy Current Brake', Control Engineering Practice, Vol. 4, No. 1, 1996. pp19-26.

4-45 WOUTERSE J.H. 'Critical Torque and Speed of Eddy Current Brake with Widely Separated Soft Iron Poles', IEE Proceedings - B, Vol. 138, No. 4, July 1991. pp153-158.

4-46 PLONUS M.A. 'Applied Electromagnetics', (McGraw-Hill, New York) 1978. Ch. 13.

4-47 JACKSON J.D. 'Classical Electrodynamics', (John Wiley & Sons, New York) 2nd ed. 1975. Ch. 7.

4-48 RIPPER M.D. and ENDEAN V.G. 'Eddy-Current Braking-Torque Measurements on a Thick Copper Disc', Proceedings of the IEE, No. 3, March 1975. pp301-302.

4-49 PERRY M.P. and JONES T.B. 'Eddy Current Induction in a Solid Conducting Cylinder with a Transverse Magnetic Field', IEEE Transactions on Magnetics, Vol. MAG-14, No. 4, July 1978. pp227-232.

4-50 SINGH A. 'Theory of Eddy-Current Brakes with Thick Rotating Disc', Proceedings of the Institution of Electrical Engineers, Vol. 124, No. 4, April 1977. pp373-376.

4-51 BOXMAG RAPID Electromagnets Type 7 Size 18-100 Data Sheet. Trade brochure.

4-52 BLEANEY B.I. and BLEANEY B. 'Electricity and Magnetism', (Oxford University Press, London) 3rd ed. 1976. Ch. 6.

4-53 HUGHES E. 'Electrical Technology', (Longman Scientific & Technical, Harlow UK) 6th ed. 1990. Ch. 3.

4-54 PLONUS M.A. 'Applied Electromagnetics', (McGraw-Hill, New York) 1978. Ch. 9.

4-55 HUGHES E. 'Electrical Technology', (Longman Scientific & Technical, Harlow UK) 6th ed. 1990. Ch. 7.

4-56 SLEMON G.R. and STRAUGHEN A. 'Electric Machines', (Addison-Wesley, Reading, Mass.), 1982. Ch. 1.

4-57 PLONUS M.A. 'Applied Electromagnetics', (McGraw-Hill, New York) 1978. Ch. 12.

4-58 DUFFIN W.J. 'Advanced Electricity and Magnetism', (McGraw-Hill, London) 1968. Ch. 3.

4-59 PAUL C.R. and NASAR S.A. 'Introduction to Electromagnetic Fields', (McGraw-Hill, New York) 2nd ed. 1987. Appendix B.

4-60 JEFIMENKO O.D. 'Electricity and Magnetism', (Electret Scientific, Star City) 2nd ed. 1989. Ch. 12.

4-61 KRAWCZYK A. and TEGOPOULOS J.A. 'Numerical Modelling of Eddy Currents', (Clarendon Press, Oxford) 1993.

4-62 BEWLEY L.V. 'Flux Linkages and Electromagnetic Induction', (Dover Publications, New York) 1964. Ch. 6.

4-63 PERRY M.P. 'Low Frequency Electromagnetic Design', (Marcel Dekker, New York) 1985. Ch. 4.

4-64 KISTLER 'Measure With Crystals: Piezoelectric Measuring Instruments' (Switzerland). Trade brochure.

4-65 AVALLONE E.A. and BAUMEISTER T. (Ed.) 'Marks' Standard Handbook for

Engineers', (McGraw-Hill, New York) 10th ed. 1996. Ch. 15.

4-66 NESTORIDES E. 'A Handbook on Torsional Vibration', (Cambridge University Press, London) 1958. pp428-458.

4-67 KER WILSON W. 'Practical Solutions to Torsional Vibration Problems. Volume 2: Amplitude Calculations', (Chapman & Hall, London) 3rd ed. 1963. Ch. 15.

4-68 EWINS D.J. 'Modal Testing: Theory and Practice', (Research Studies Press, John Wiley & Sons, New York) 1988. Ch. 2.

4-69 EWINS D.J. 'Modal Testing: Theory and Practice', (Research Studies Press, John Wiley & Sons, New York) 1988. Ch. 3.

4-70 Døssing O. 'Structural Testing. Part 1: Mechanical Mobility Measurements', (Brüel & Kjær, Denmark) 1987.

4-71 The STAR System: User Guide and Reference Manual. 1994.

4-72 VANCE J.M. 'Rotordynamics of Turbomachinery', (John Wiley & Sons, New York) 1988. Ch. 3.

4-73 THOMSON W.T. 'Theory of Vibration with Applications', (Prentice-Hall International, London) 3rd ed. 1988. Ch. 6.

4-74 As reference 1-25

4-75 THOMSON W.T. 'Theory of Vibration with Applications', (Prentice-Hall International, London) 3rd ed. 1988. Ch. 2.

4-76 NESTORIDES E. 'A Handbook on Torsional Vibration', (Cambridge University Press, London) 1958. pp91-94.

4-77 KER WILSON W. 'Practical Solution of Torsional Vibration Problems. Volume 1: Frequency Calculations', (Chapman & Hall, London) 3rd ed. 1956. Ch. 11.

Chapter 5

5-1 British Standard BS3015:1991 'Glossary of Terms Relating to Mechanical Vibration and Shock'.

5-2 NESTORIDES E. 'A Handbook on Torsional Vibration', (Cambridge University Press, London) 1958. pp559-569.

5-3 As reference 2-67

5-4 NESTORIDES E. 'A Handbook on Torsional Vibration', (Cambridge University Press, London) 1958. pp520-558.

5-5 HOLSET ENGINEERING Co. 'Torsional Vibration Dampers', (Halifax, UK). Trade brochure.

5-6 KER WILSON W. 'Practical Solution of Torsional Vibration Problems. Volume 4: Devices for Controlling Vibration', (Chapman & Hall, London) 1968. 3rd ed. Ch. 28.

5-7 NESTORIDES E. 'A Handbook on Torsional Vibration', (Cambridge University Press, London) 1958. pp504-519.

5-8 As reference 1-27

5-9 TOZUNE A. 'Vibration Characteristics of Motors with Dynamic Vibration Absorbers', IEE Proceedings, Part B: Electric Power Applications, Vol. 138, No. 1, January 1991. pp21-27.

5-10 As reference 1-12

5-11 BREMER R.C. 'A Practical Treatise on Engine Crankshaft Torsional Vibration Control', Society of Automotive Engineers SP-445. SAE Paper 790763. 1979.

5-12 KER WILSON W. 'Practical Solution of Torsional Vibration Problems. Volume 4: Devices for Controlling Vibration', (Chapman & Hall, London) 1968. 3rd ed. Ch. 30.

5-13 SARAZIN R.R.R., British Patent 444 222, 1935.

5-14 REED PROPELLOR Co. Inc. (CHILTON R.), British Patent 460 088,1935.

5-15 GENTA G. 'Vibration of Structures and Machines', (Springer-Verlag, New York) 1993. Ch. 5.

5-16 DICK J. 'The Pendulum Torsional Vibration Absorber', The Engineer, Vol. 162, 1936. p595.

5-17 DEN HARTOG J.P. 'Mechanical Vibrations', (McGraw-Hill, New York) 4th ed. 1956. Ch. 5.

5-18 THOMSON W.T. 'Theory of Vibration with Applications', (Prentice-Hall International, London) 3rd ed. 1988. Ch. 5.

5-19 MITCHINER R.G. and LEONARD R.G. 'Centrifugal Pendulum Vibration Absorbers - Theory and Practice', Transactions of the ASME: Journal of Vibration and Acoustics, Vol. 113, October 1991. pp503-507.

5-20 ZDANOWICH R.W. and WILSON T.S. 'The Elements of Pendulum Dampers', Proceedings of the Institution of Mechanical Engineers, Vol. 143, 1940. pp182-210. 'Communications on the Elements of Pendulum Dampers', Proceedings of the Institution of Mechanical Engineers, Vol. 144, 1940. pp217-230.

'Communication on Pendulum Vibration-Tuners for Crankshafts', Proceedings of the Institution of Mechanical Engineers, Vol. 152, 1945. pp63-68.

5-21 BAILEY S.B. and BULLEID C.H. 'The Dynamic Absorber and Its Application to Multi-Throw Crankshafts', Proceedings of the Institution of Mechanical Engineers, Vol. 145, 1941. pp73-82.

'Communications on the Dynamic Absorber and its Application to Multi-Throw Crankshafts', Proceedings of the Institution of Mechanical Engineers, Vol. 146, 1941. pp81-95.

5-22 NEWLAND D.E. 'Nonlinear Aspects of the Performance of Centrifugal Pendulum Vibration Absorbers', Transactions of the ASME: Journal of Engineering for Industry; Vol. 86, August 1964. pp257-263.

5-23 MOORE V. 'The Control of Torsional Vibration in Radial Aircraft Engines by Means of Tuned Pendulums', Journal of the Aeronautical Sciences, Vol. 9, No. 7, May 1942. pp229-244.

5-24 TAYLOR E.S. 'Eliminating Crankshaft Vibration in Radial Aircraft Engines', SAE Journal (Transactions), Vol. 38, No. 3, March 1936, pp81-89.

5-25 BALEK S.J. and HEITZMAN R.C. 'The Caterpillar 3406E Heavy Duty Diesel Engine', Proceedings of the 16th ASME Internal Combustion Engineering Division, Heavy Duty Engines; A Look at the Future, 1994. ICE - Vol. 22. pp177-186.

5-26 WACHS M.A. 'The Main Rotor Bifilar Absorber and its Effect on Helicopter Reliability/Maintainability', SAE Transactions, Vol. 82, Section 4, 1973. SAE Paper 730984. pp2972-2981.

5-27 DEN HARTOG J.P. 'Tuned Pendulums as Torsional Vibration Eliminators', Stephen Timoshenko 60th Anniversary Volume, (Macmillan, New York) 1938. pp17-26.

5-28 CROSSLEY F.R.E. 'The Free Oscillation of the Centrifugal Pendulum with Wide Angles', Transactions of the ASME: Journal of Applied Mechanics, Vol. 19, September 1952. pp315-319.

5-29 CROSSLEY F.R.E. 'The Forced Oscillation of the Centrifugal Pendulum with Wide Angles', Transactions of the ASME: Journal of Applied Mechanics, Vol. 20, March 1953. pp41-47.

5-30 SHARIF-BAKHTIAR M. and SHAW S.W. 'Effects of Nonlinearities and Damping on the Dynamic Response of a Centrifugal Pendulum Vibration Absorber', Transactions of the ASME: Journal of Vibration and Acoustics, Vol. 114, July 1992. pp305-311.

5-31 CHAO C-P., SHAW S.W. and LEE C-T. 'Stability of the Unison Response for a Rotating System with Multiple Tautochronic Pendulum Vibration Absorbers', Transactions of the ASME: Journal of Applied Mechanics, Vol. 64, March 1997. pp149-156.

5-32 SHAW S.W. and LEE C.T. 'On the Nonlinear Dynamics of Centrifugal Pendulum Vibration Absorbers', in: GURAN A. and INMAN D.J. (Ed.) 'Smart Structures, Nonlinear Dynamics, and Control', (Prentice-Hall, New Jersey) 1995. Ch. 7.

5-33 SHAW S.W. and WIGGINS S. 'Chaotic Motions of a Torsional Vibration Absorber', Transactions of the ASME: Journal of Applied Mechanics, Vol. 55, December 1988. pp952-958.

5-34 SHARIF-BAKHTIAR M. and SHAW S.W. 'The Dynamic Response of a Centrifugal Pendulum Vibration Absorber with Motion-Limiting Stops', Journal of Sound and Vibration, Vol. 126, No.2; 1988. pp221-235.

5-35 DENMAN H.H. 'Tautochronic Bifilar Pendulum Torsion Absorbers for Reciprocating Engines', Journal of Sound and Vibration, Vol. 159, No. 2, 1992. pp251-277.

5-36 LEE C-T. and SHAW S.W. 'On the Counteraction of Periodic Torques for Rotating Systems Using Centrifugally Driven Vibration Absorbers', Journal of Sound and Vibration, Vol. 191, No. 5, 1996. pp695-719.

5-37 BOROWSKI V.J., CRONIN D.L., HANISKO J.P., MIKULEC D.A., CRUM W.B., DENMAN H.H., SHAW S.W., BROOKS L.T. and ANDERSON M.P. 'Reducing Vibration of Reciprocating Engines with Crankshaft Pendulum Vibration Absorbers', SAE Transactions, Vol. 100, Section 2, Paper 911876, 1991. pp376-382.

5-38 LEE C-T. and SHAW S.W. 'Torsional Vibration Reduction in Internal Combustion Engines Using Centrifugal Pendulums', Proceedings of the 15th Biennial ASME Design Technical Conference on Mechanical Vibration and Noise (Boston, MA), September 1993. DE-Vol. 84-1, No. 3(A). pp487-492.

5-39 CRONIN D.L. 'Shake Reduction in an Automobile Engine by Means of Crankshaft-Mounted Pendulums', Mechanism and Machine Theory, Vol. 27, No. 5, 1992. pp517-533.

Chapter 6

6-1 As reference 1-43

6-2 As reference 1-12

6-3 As reference 1-37

6-4 As reference 1-49

6-5 As reference 4-69

Appendix A

A-1 As reference 3-8

Appendix B

B-1 THOMSON W.T. 'Theory of Vibration with Applications', (Prentice-Hall International, London) 3rd ed. 1988.

B-2 As reference 2-66

B-3 As reference 4-72

FIGURES

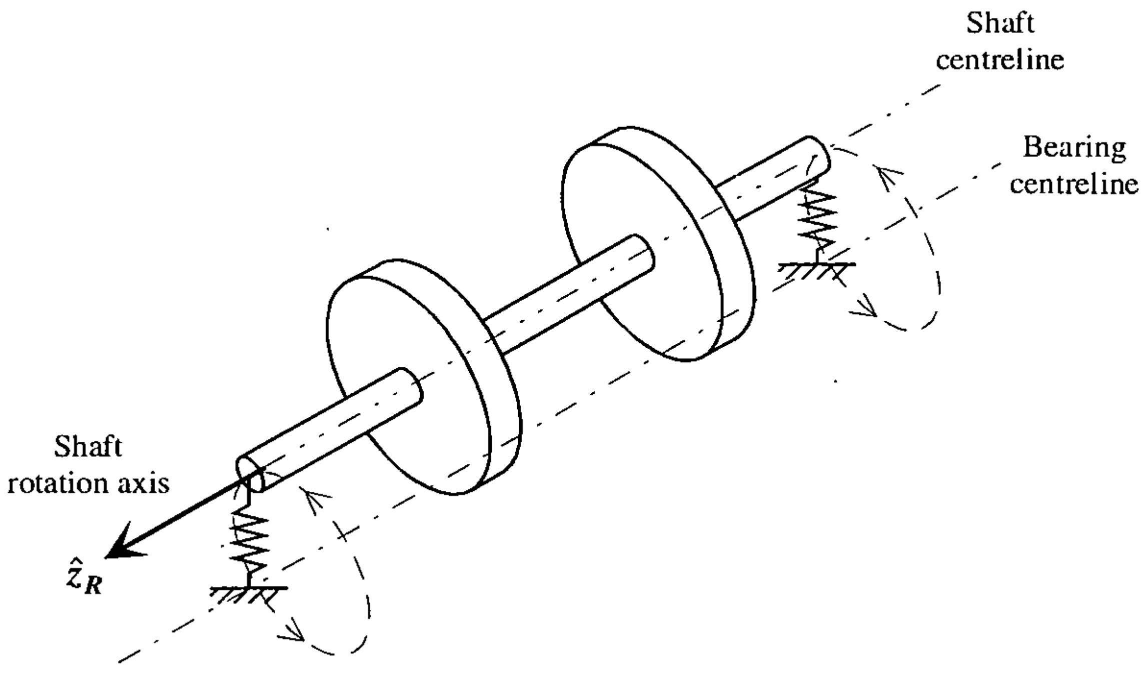

a. Cylindrical whirl orbit

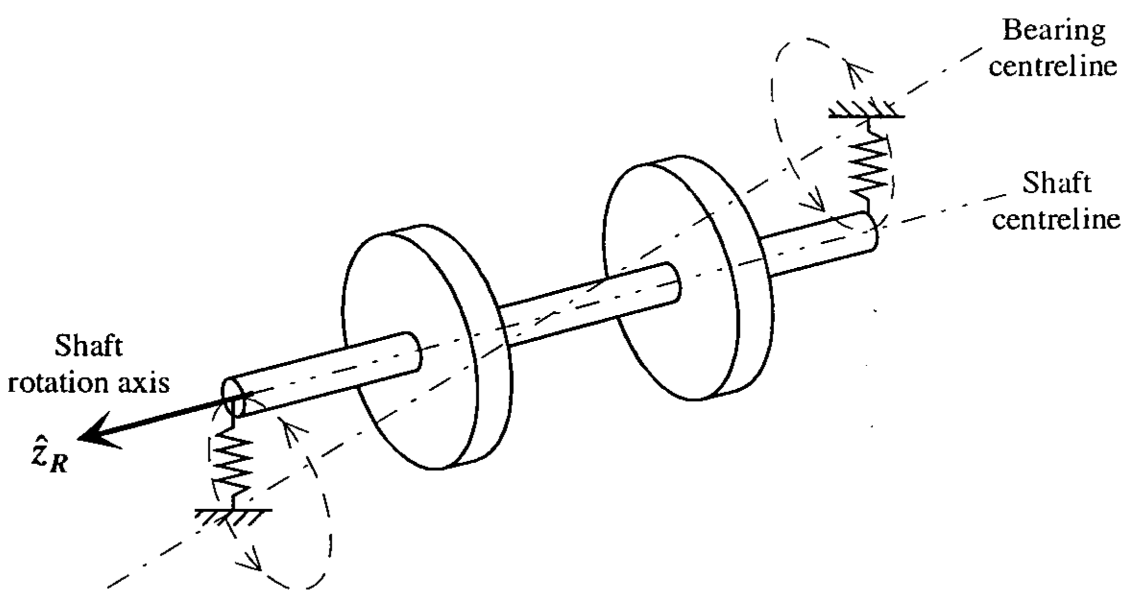

b. Conical whirl orbit

Figure 1.1: Rigid-rotor lateral vibration modes for a symmetrical rotor

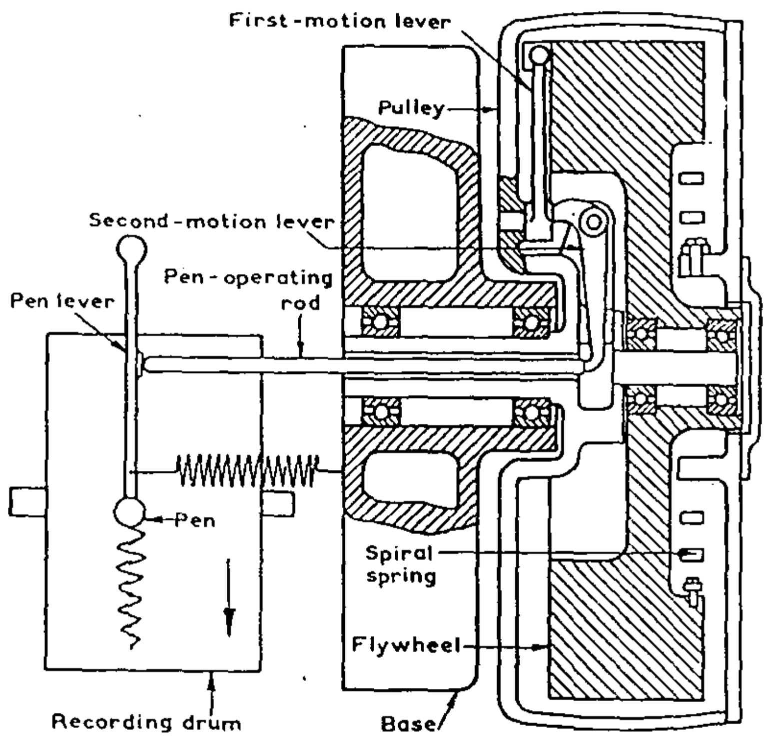

Figure 2.1: Schematic detail of a Geiger torsiograph [2-15]

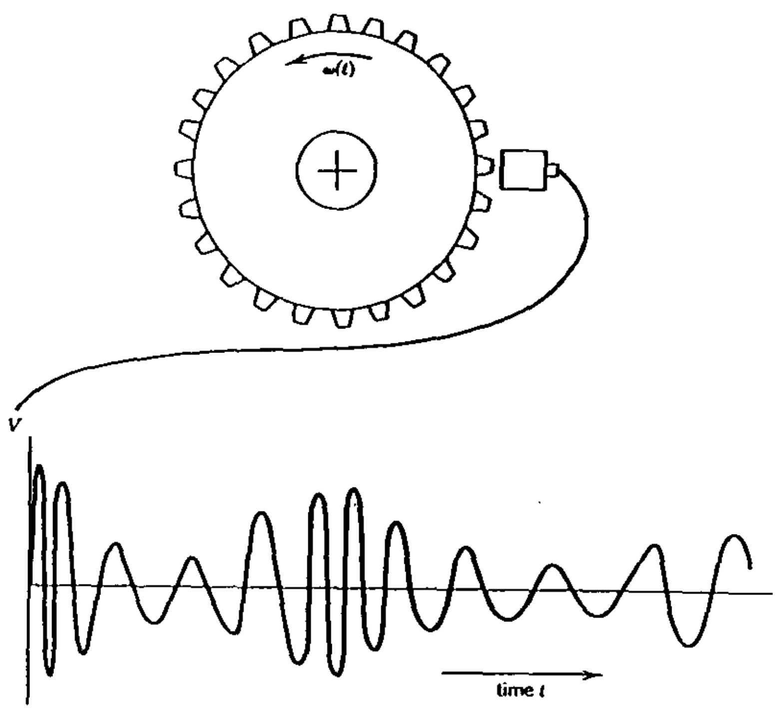

Figure 2.2: Example of carrier signal derived from a toothed wheel and magnetic pick-up for torsional vibration measurement [2-21]

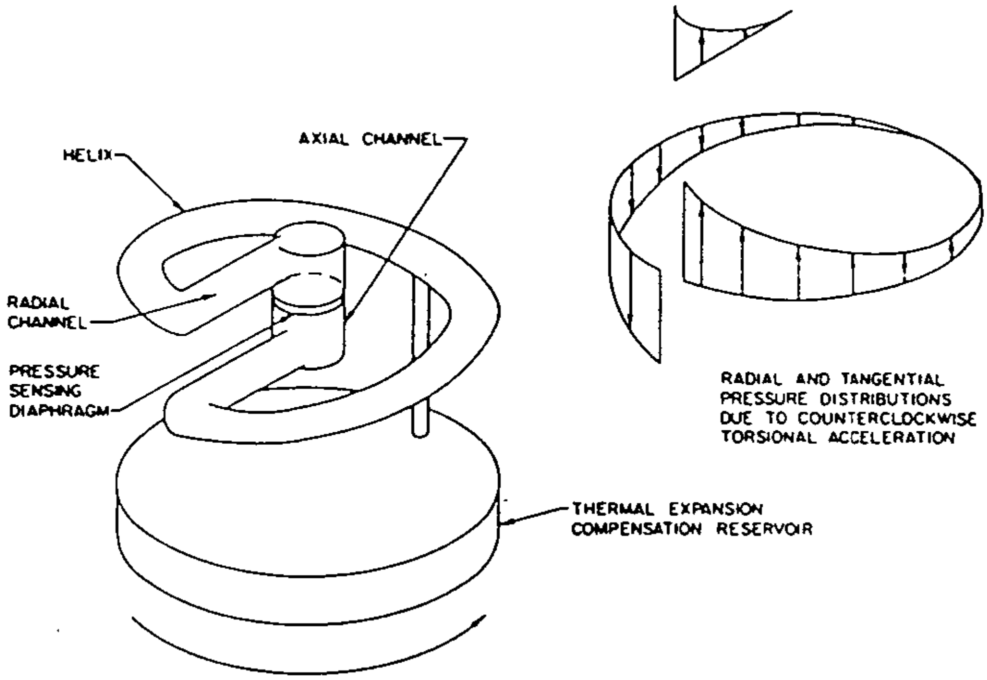

Figure 2.3: Torsional accelerometer consisting of a fluid-filled helix and pressure transducer [2-35]

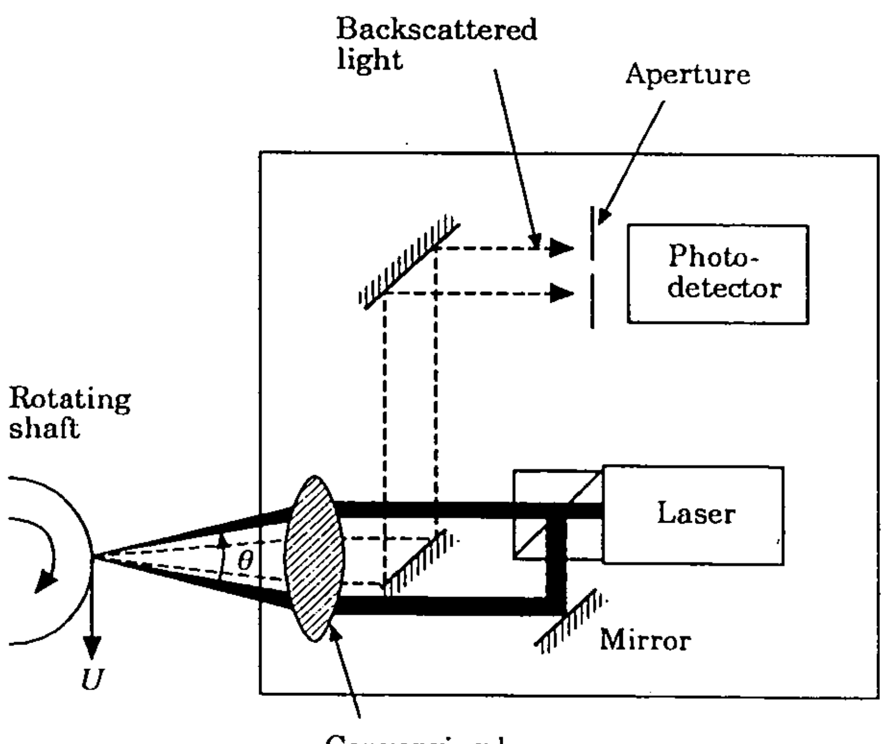

Figure 2.4: The cross-beam velocimeter [from 2-54]

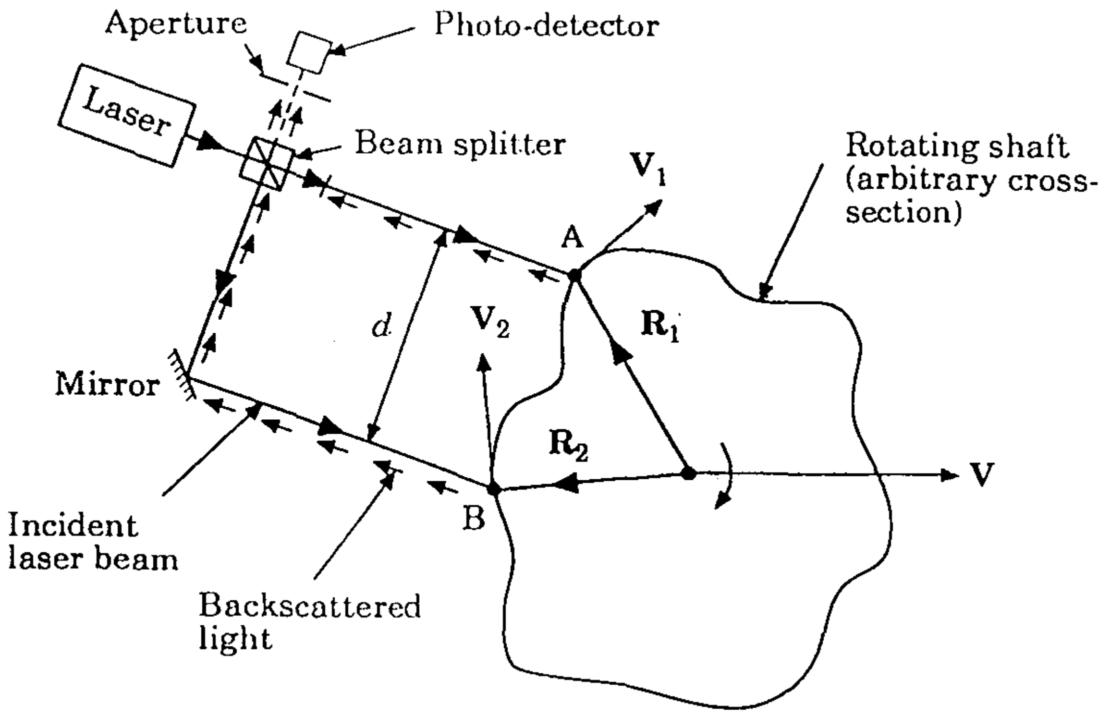

Figure 2.5: Optical arrangement of the laser torsional vibrometer [2-54]

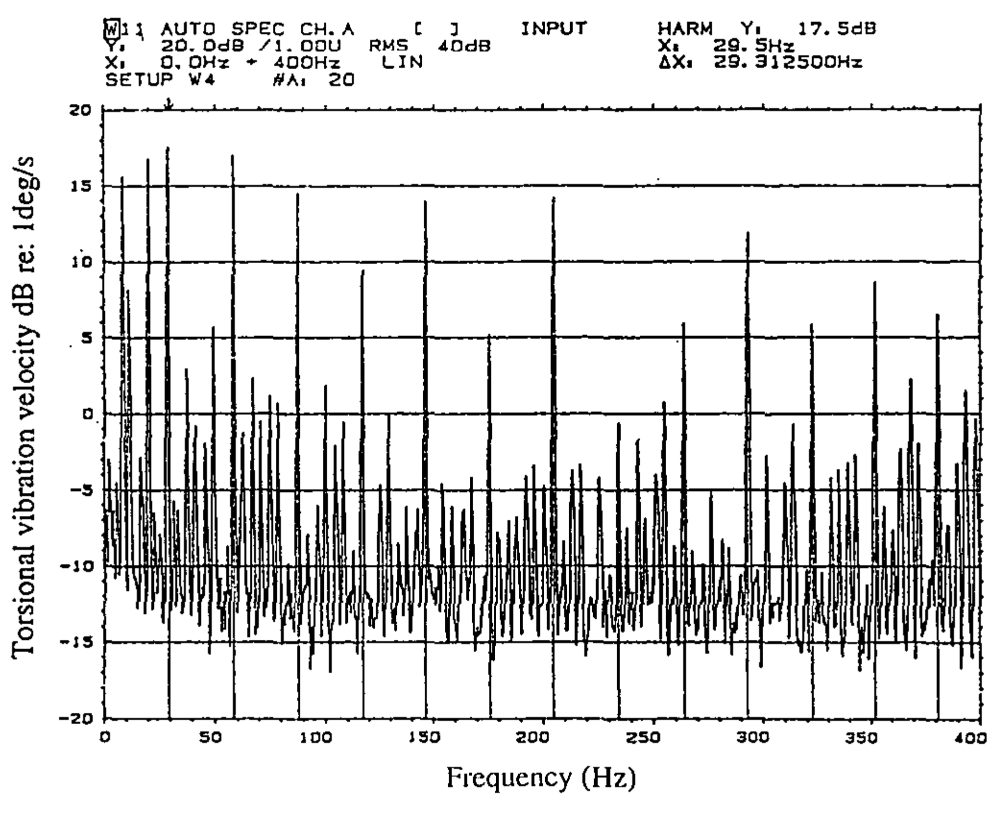

Figure 2.6: Spectrum of LTV output showing speckle noise peaks.
(Target shaft rotating at 29.5Hz)

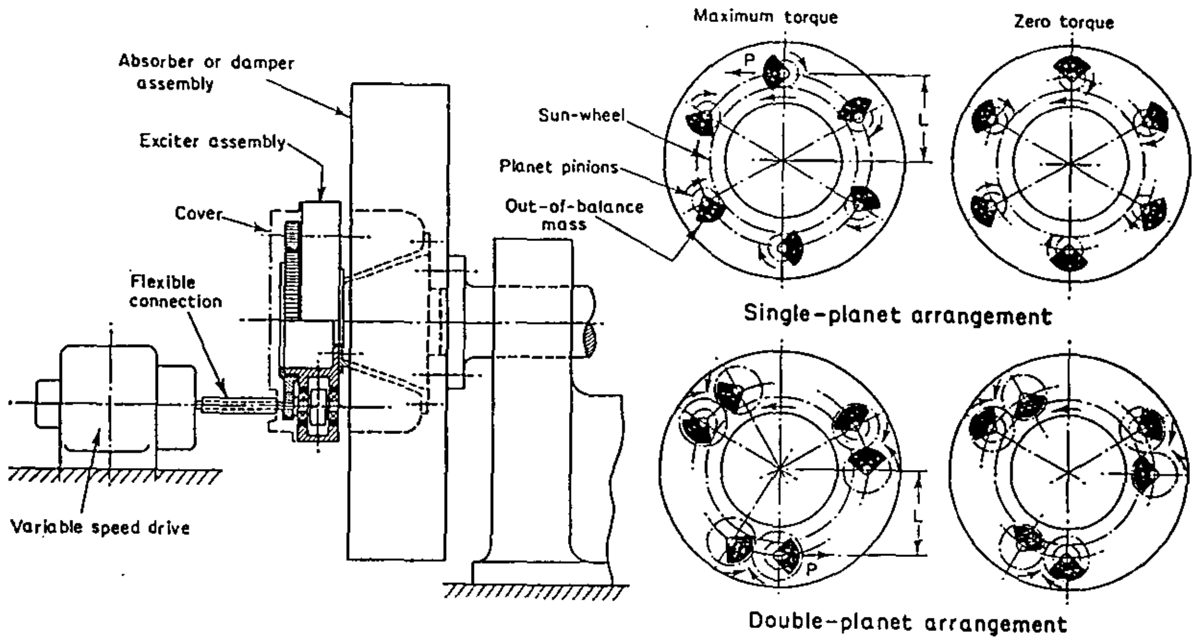

Figure 2.7: Out-of-balance exciter for non-rotating assemblies [2-67]

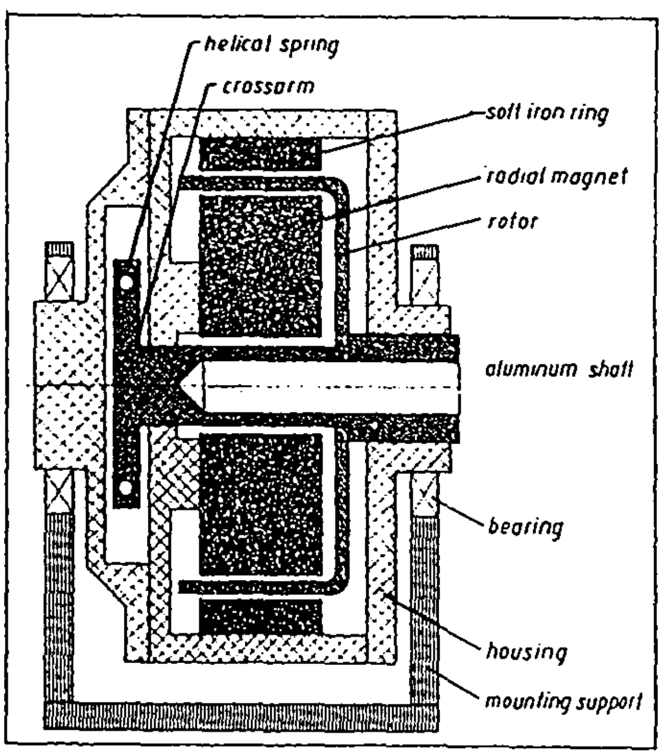

Figure 2.8: Electro-mechanical torsional exciter for rotating shafts [from 2-74]

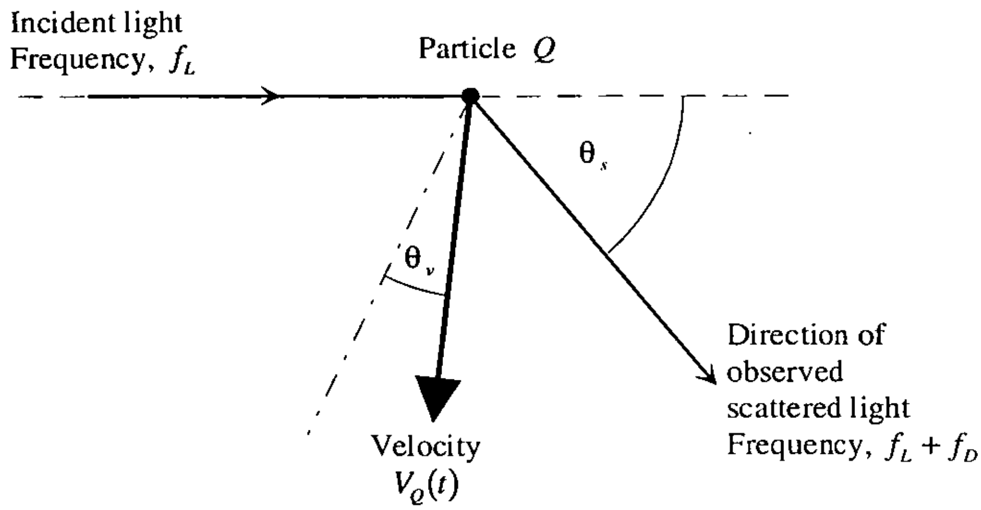

Figure 3.1: Doppler shift of scattered laser light

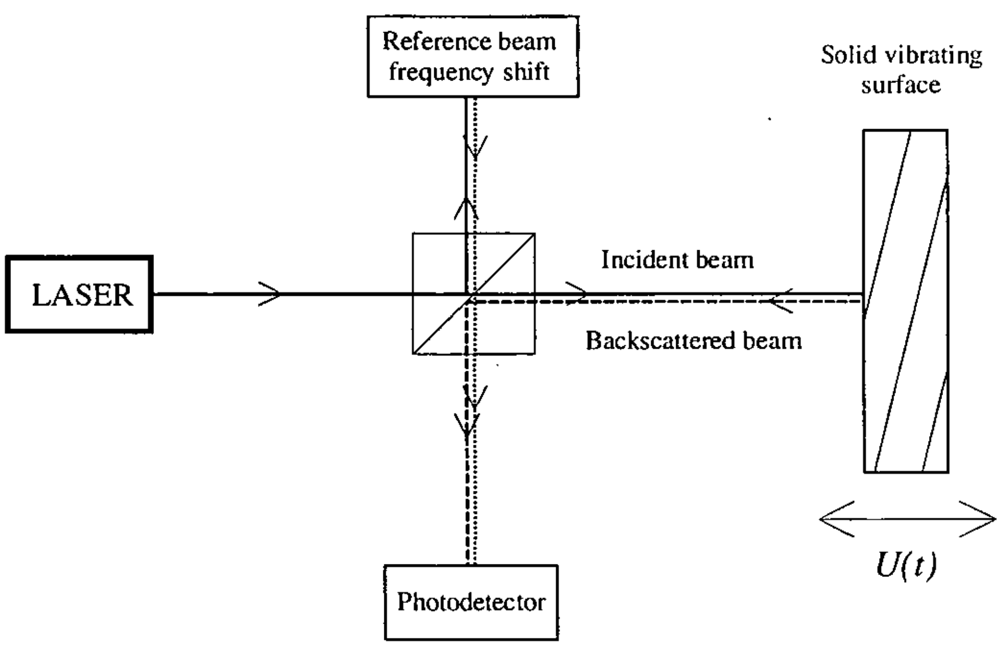

Figure 3.2: General arrangement of a laser vibrometer

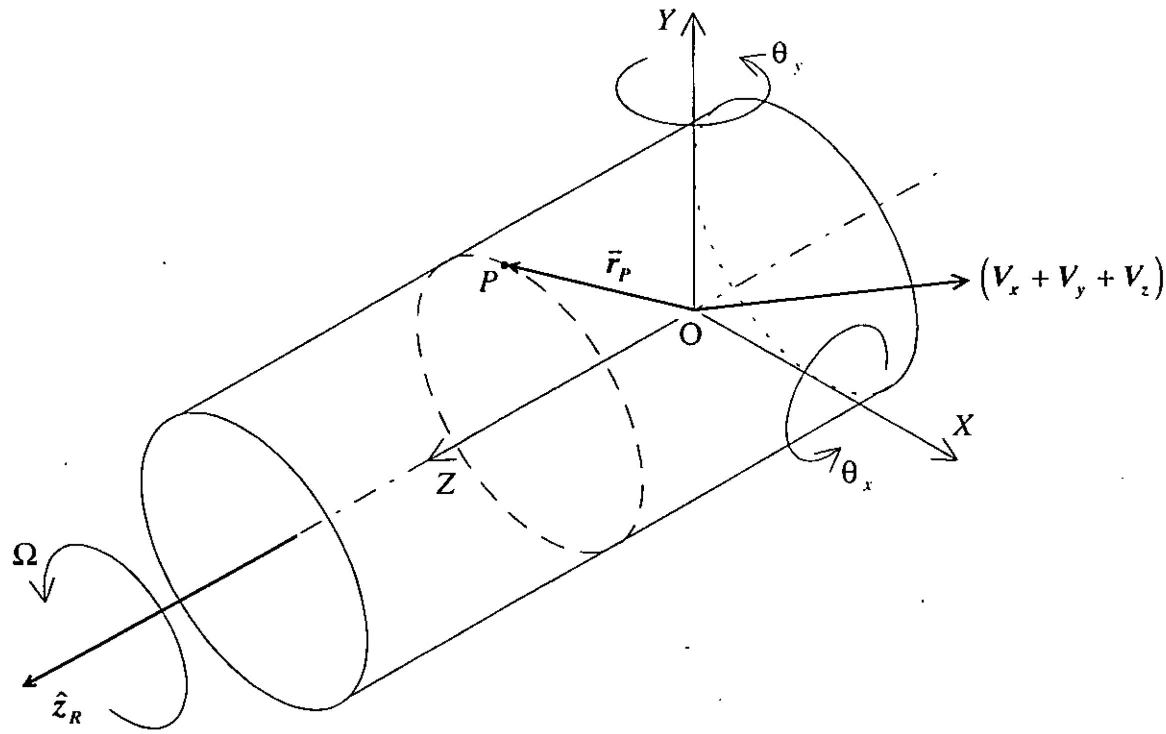

Figure 3.3: General motion of a point on a rotating shaft

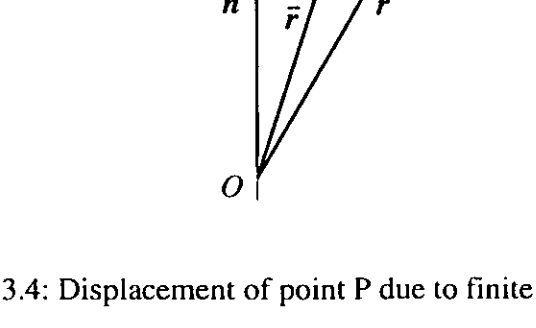

Figure 3.4: Displacement of point P due to finite rotation

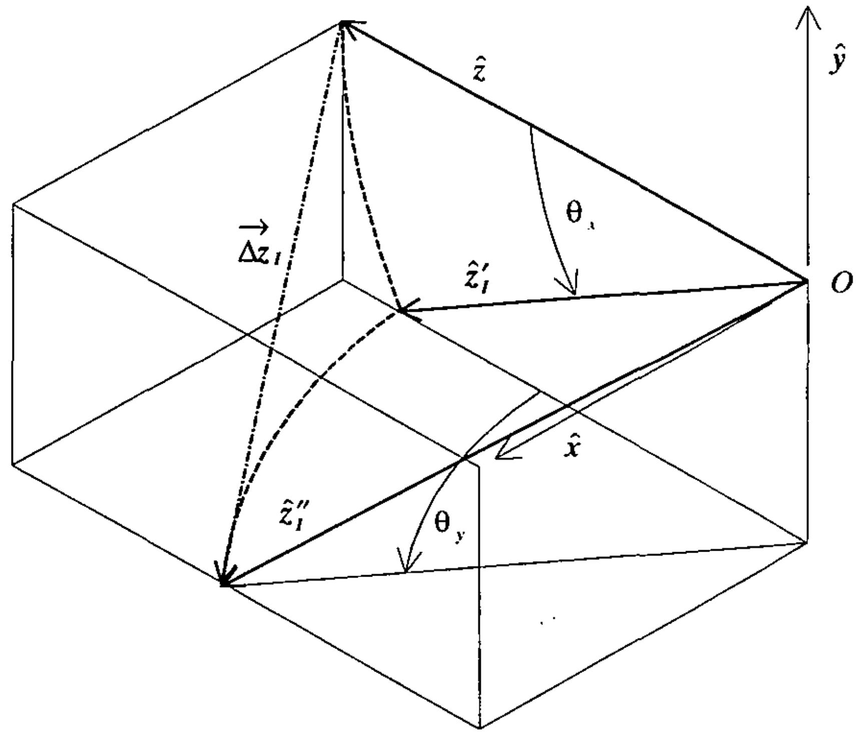

a. $\vec{\theta}_x$ followed by $\vec{\theta}_y$

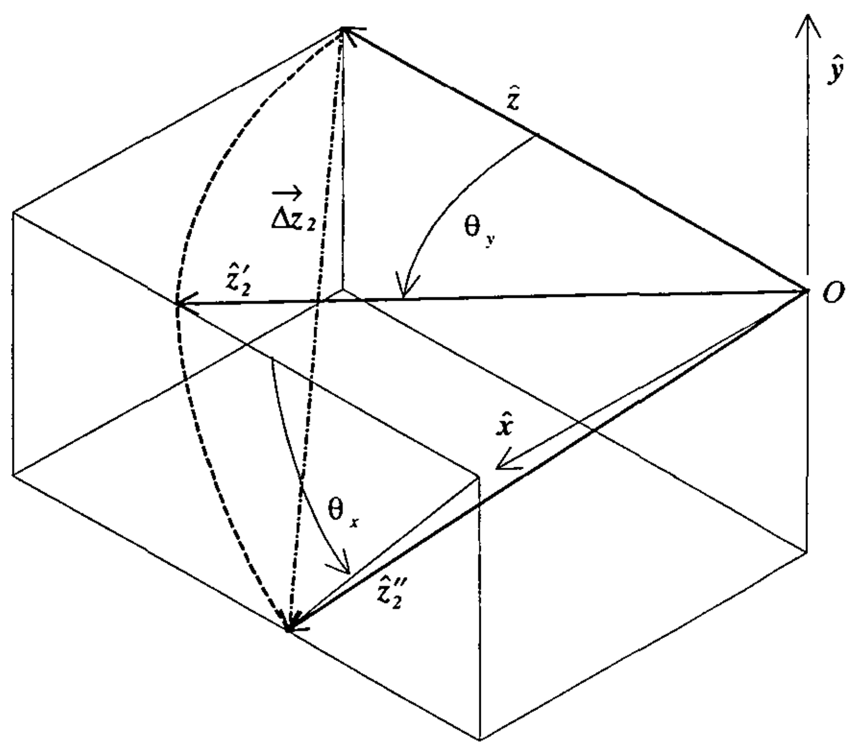

b. $\vec{\theta}_y$ followed by $\vec{\theta}_x$

Figure 3.5: Finite rotations of the shaft axis $\hat{z}$ about the co-ordinate axes

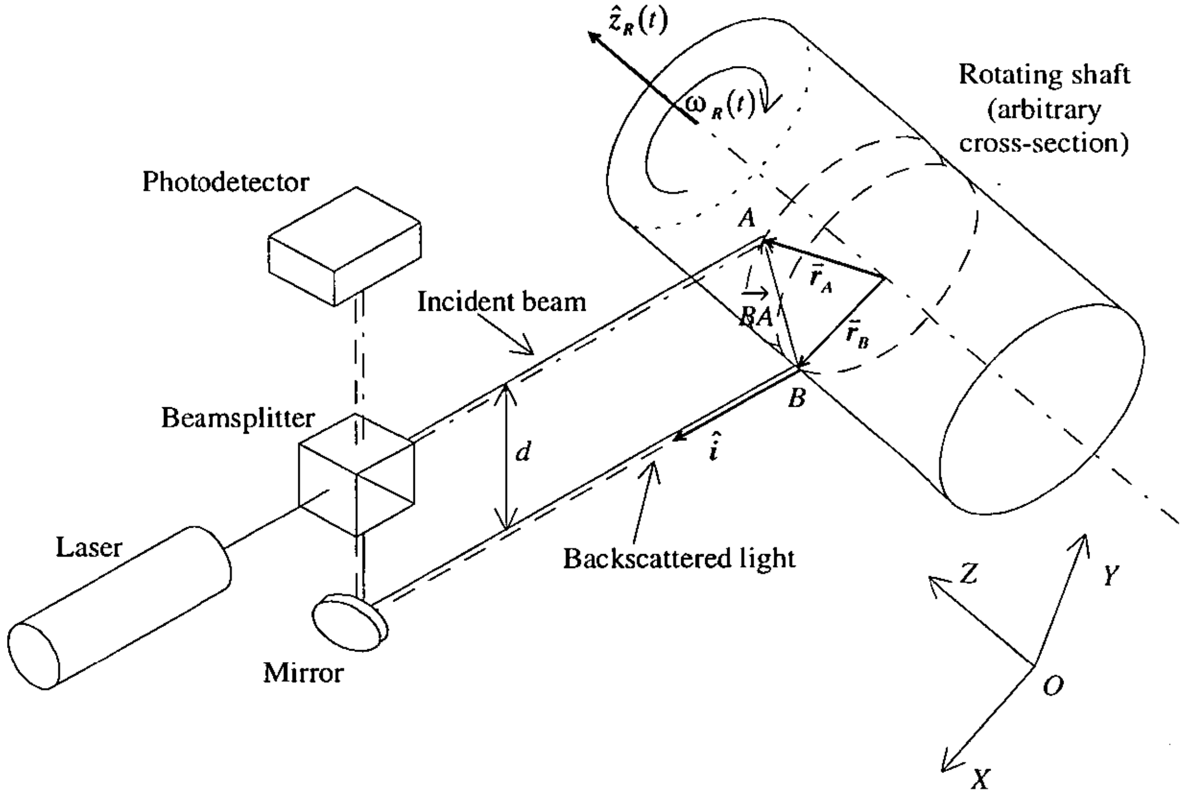

Figure 3.6: Optical geometry of the laser torsional vibrometer

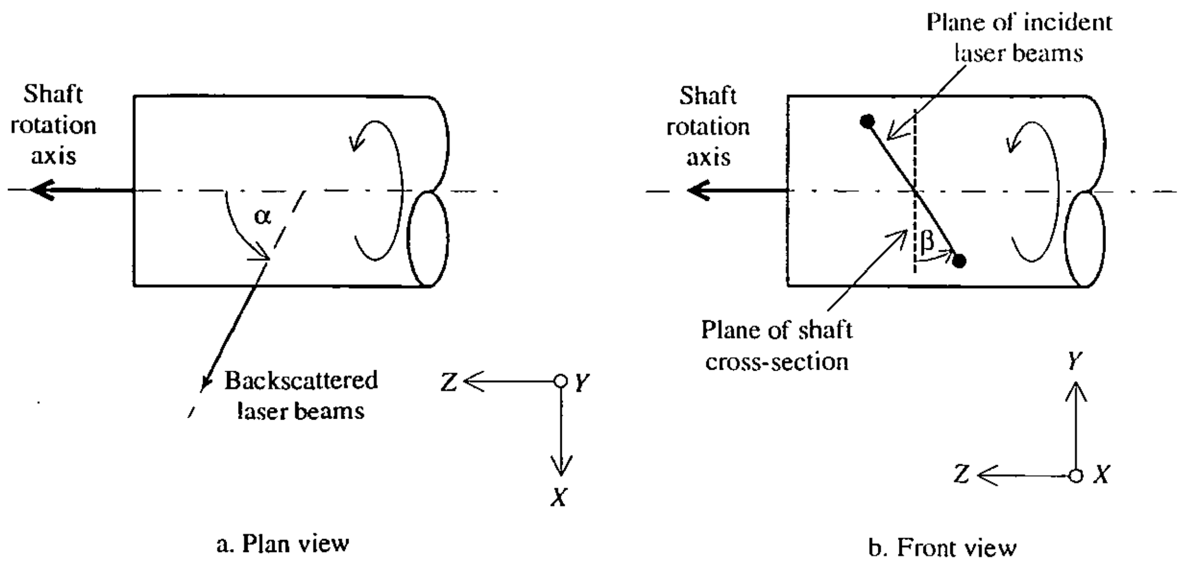

Figure 3.7: Definition of the LTV target shaft incidence angles

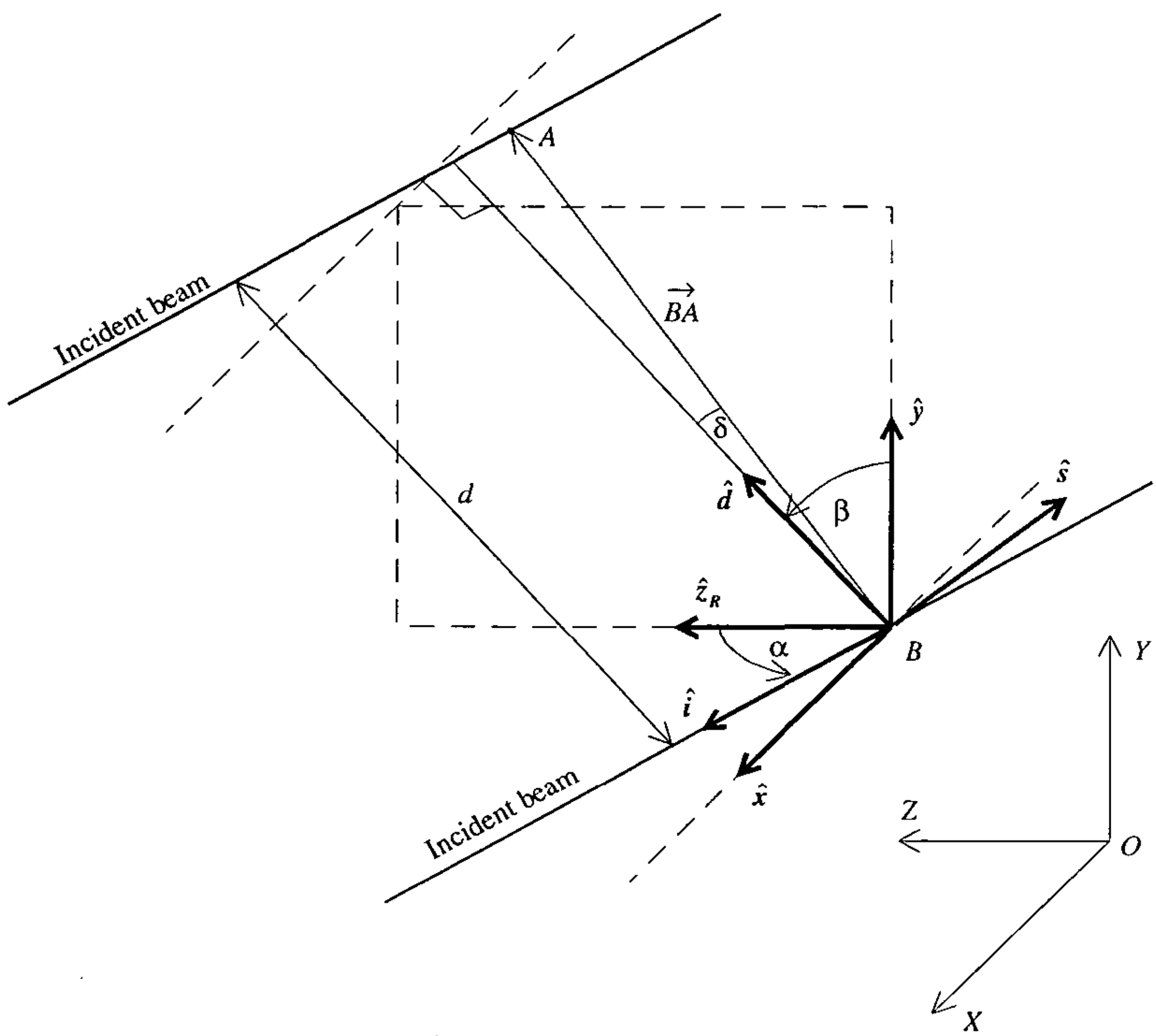

Figure 3.8: Arrangement of vectors describing instrument laser beams and target geometry

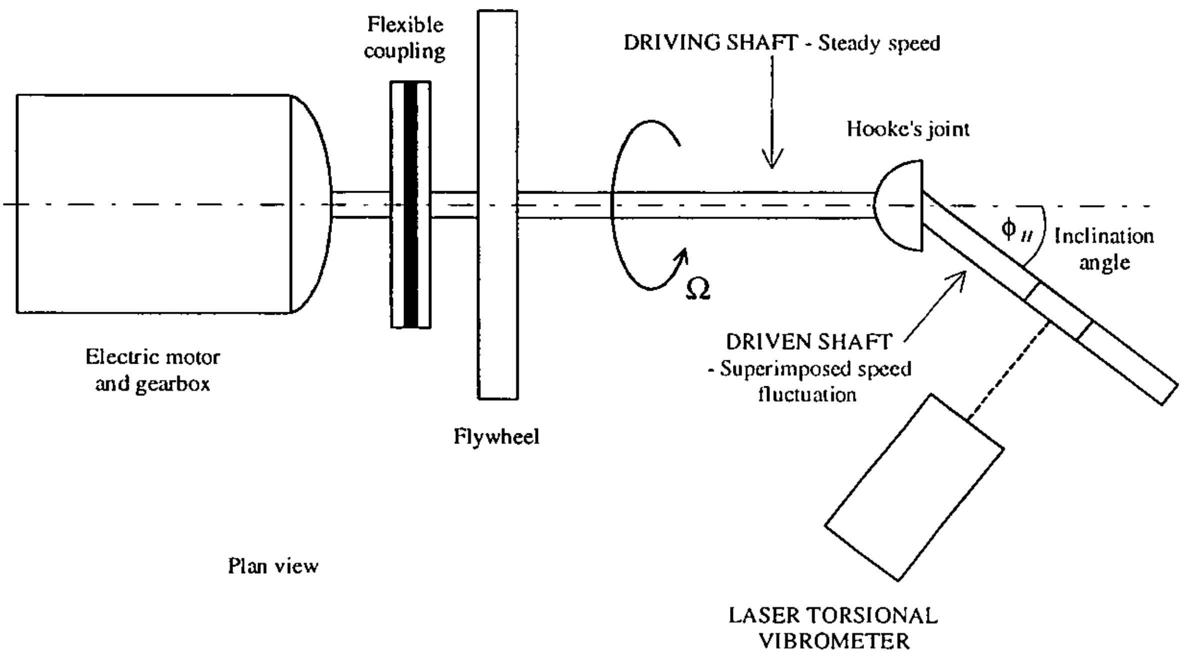

Figure 3.9: Hooke's joint apparatus for validation of torsional vibration measurement

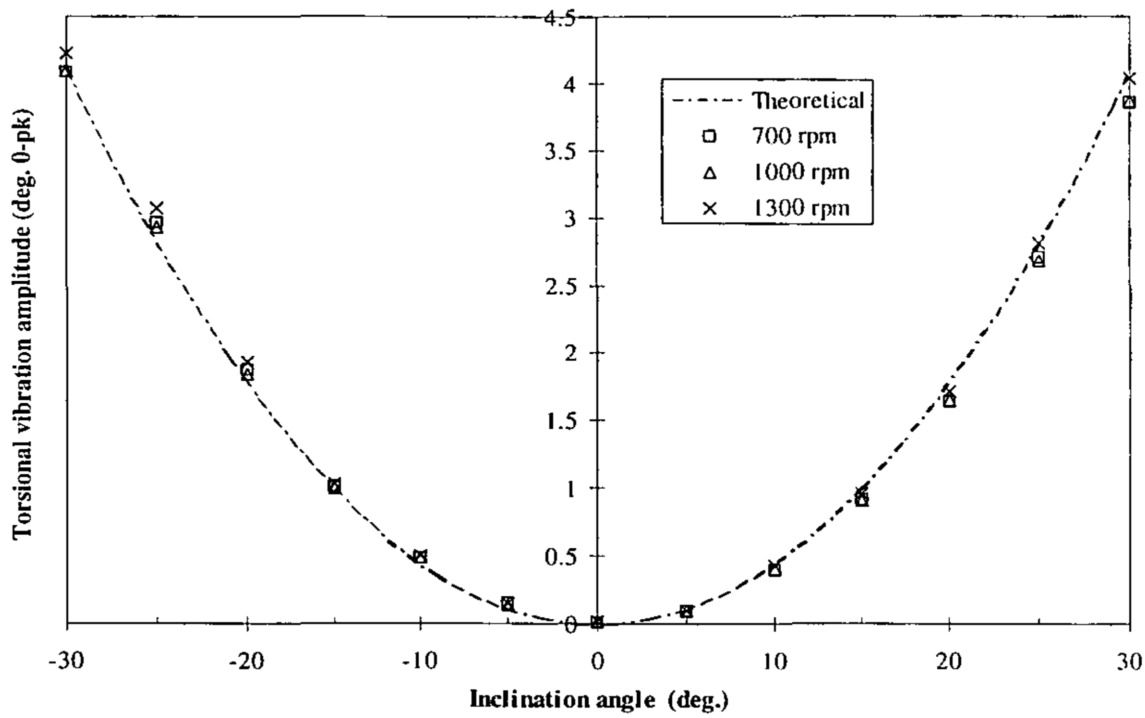

Figure 3.10: Second order torsional vibration of a Hooke's joint

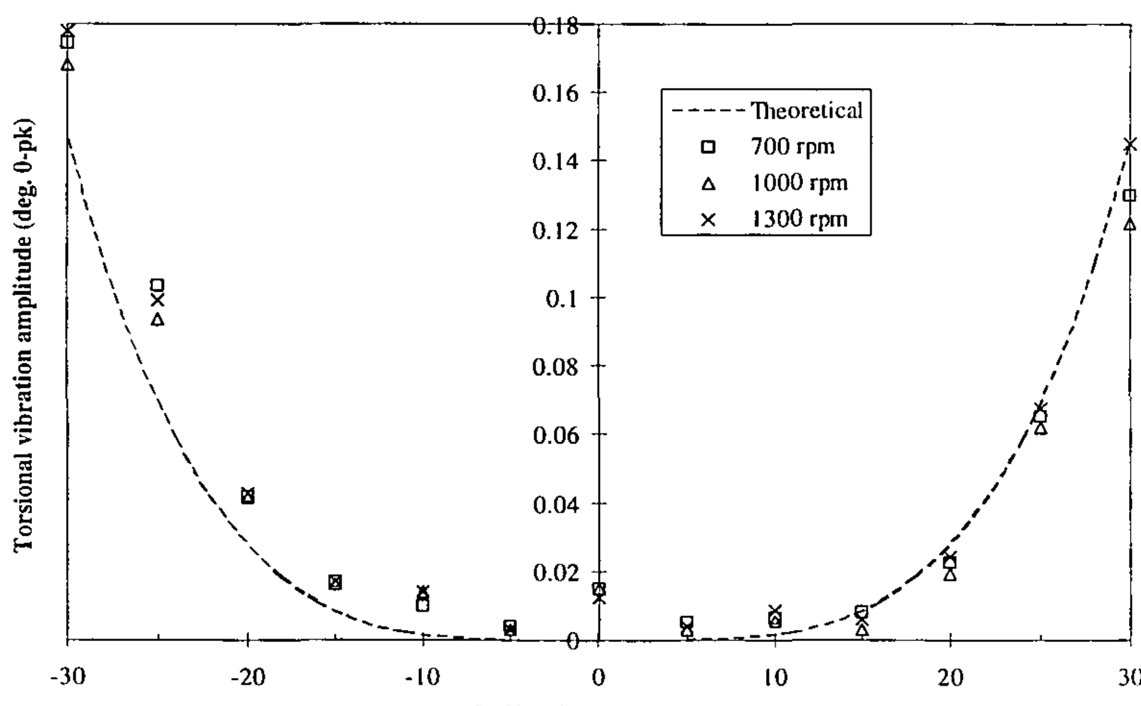

Figure 3.11: Fourth order torsional vibration of a Hooke's joint

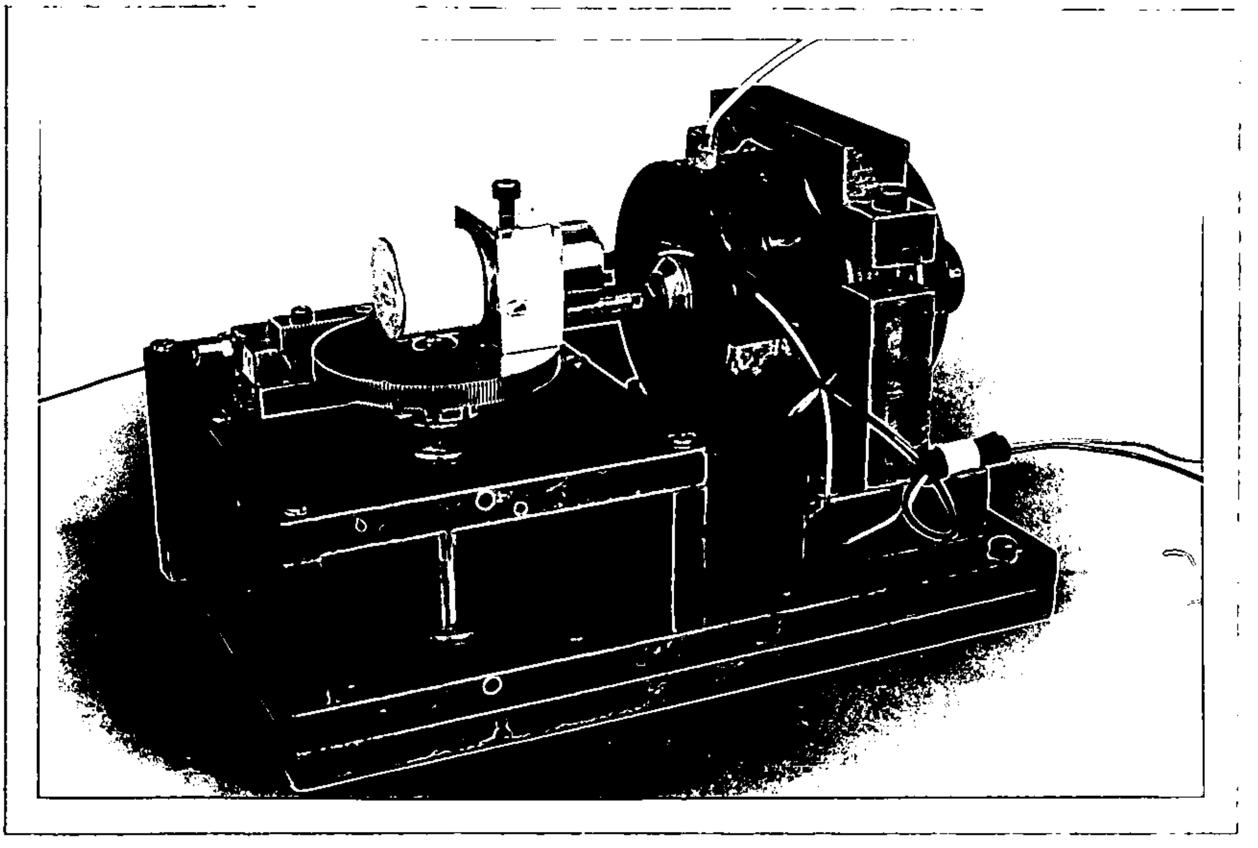

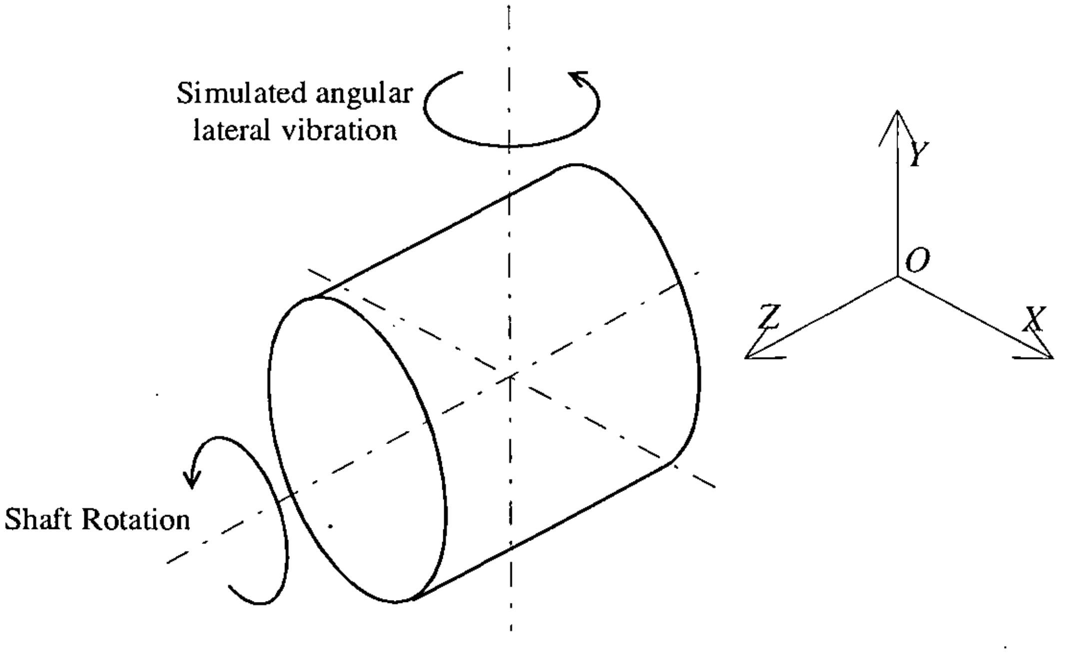

Figure 3.12: Experimental apparatus used to simulate shaft angular lateral vibration

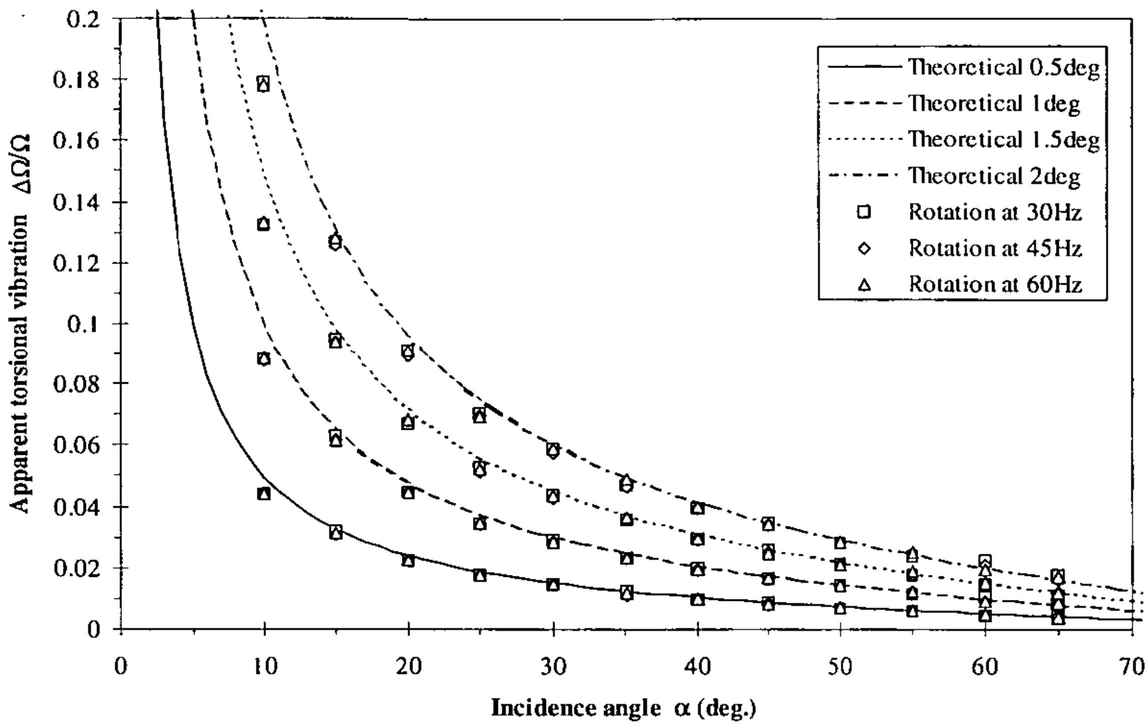

Figure 3.13: Angular lateral vibration component due to yaw motion θ_y - viewing end-face of shaft

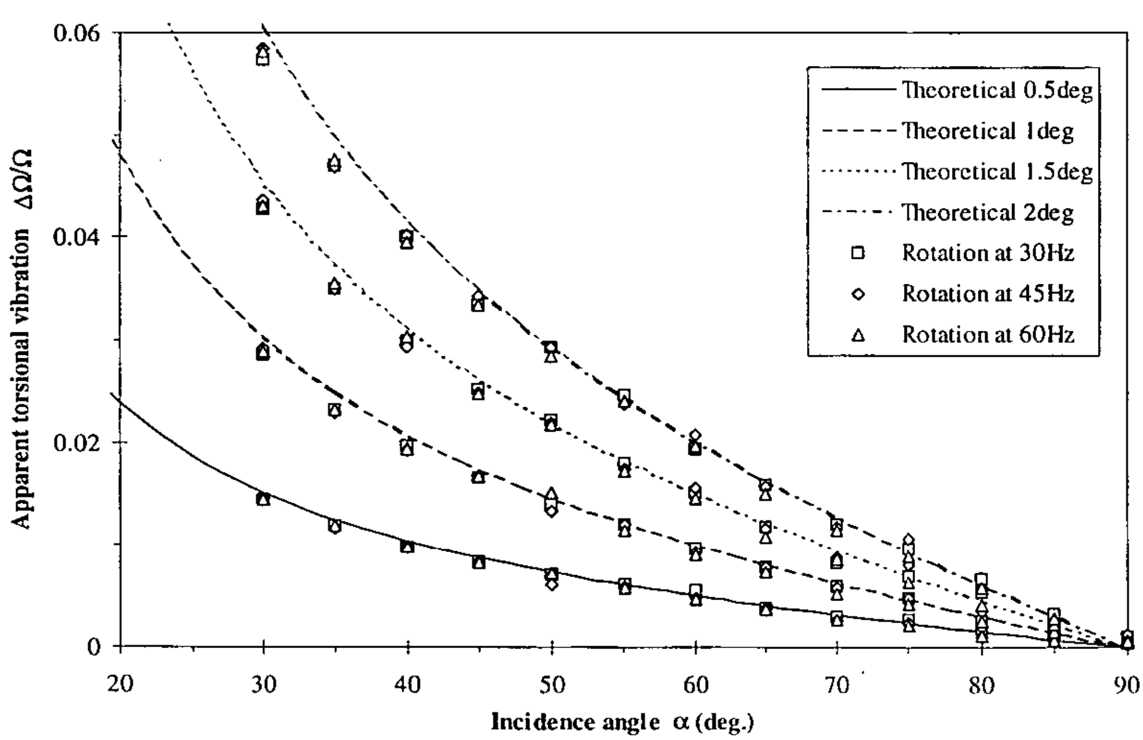

Figure 3.14: Angular lateral vibration component due to yaw motion θ_y - viewing side of shaft

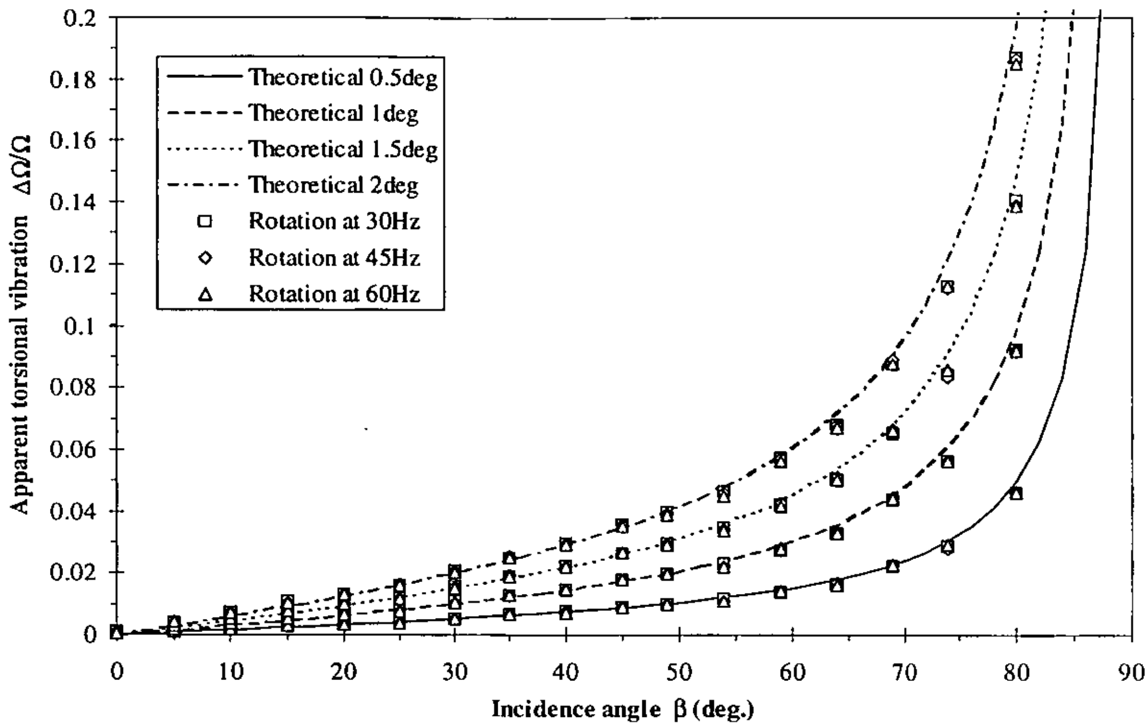

Figure 3.15: Angular lateral vibration component due to pitch motion θ_x

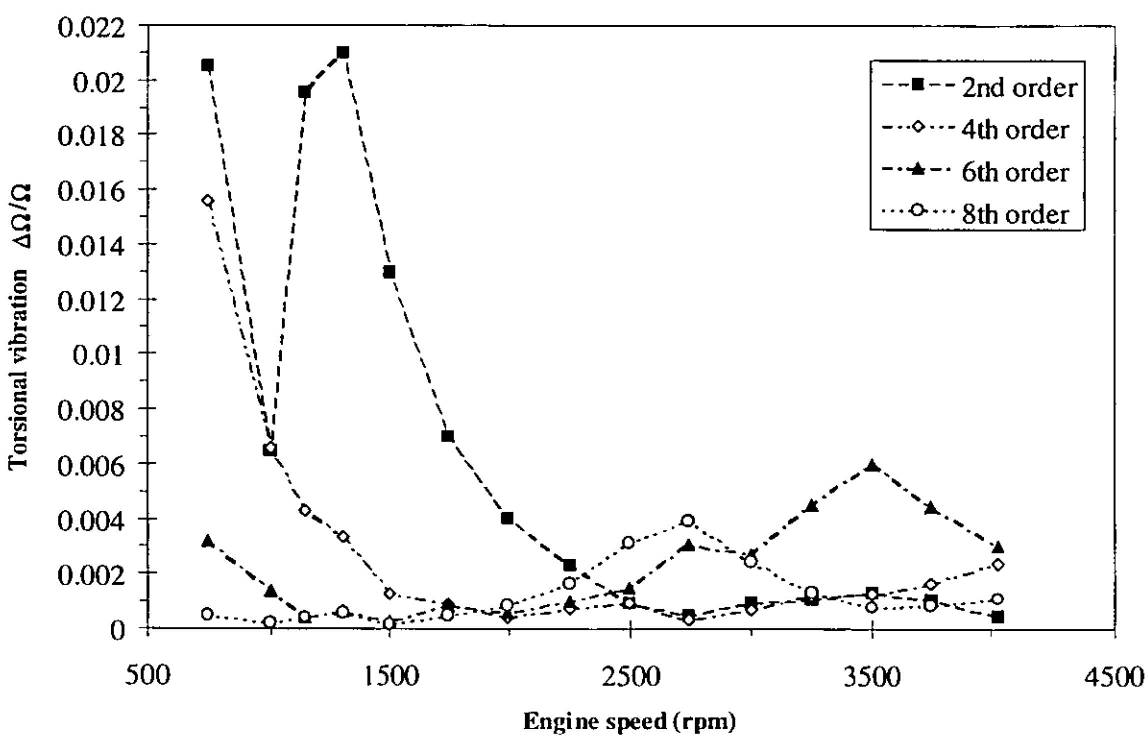

Figure 3.16: Torsional vibration magnitudes for four-cylinder four-stroke 2.0 litre diesel engine

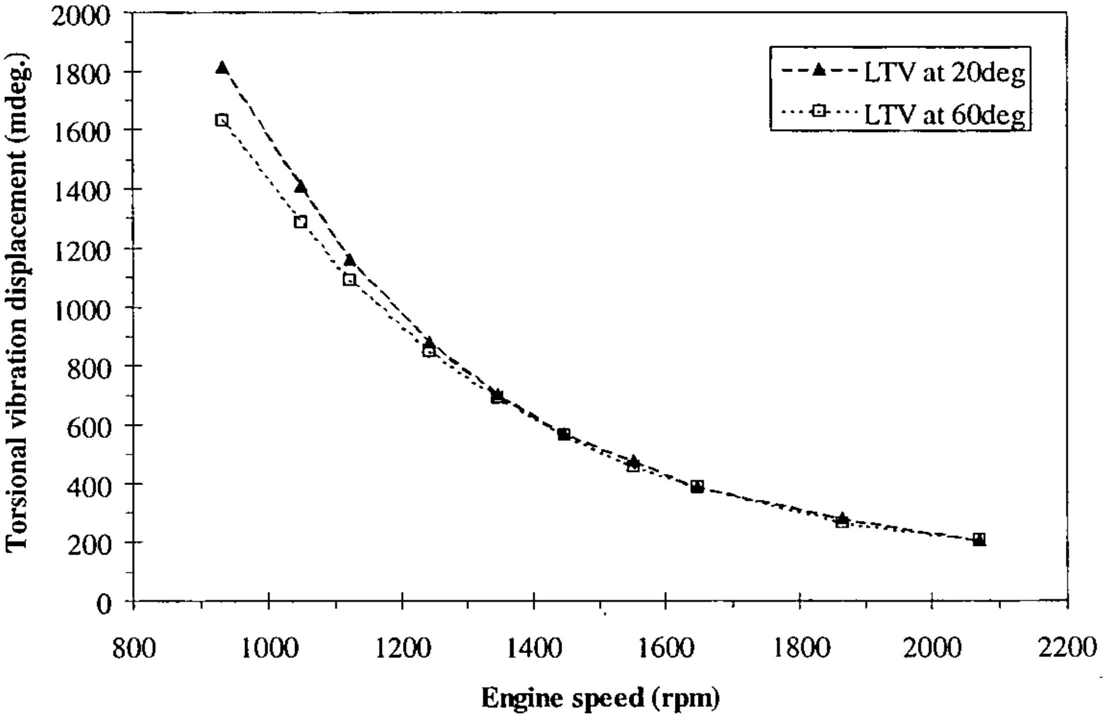

Figure 3.17: Comparison of simultaneous LTV measurements at different incidence angles

- Second order torsional vibration at crankshaft pulley of petrol engine

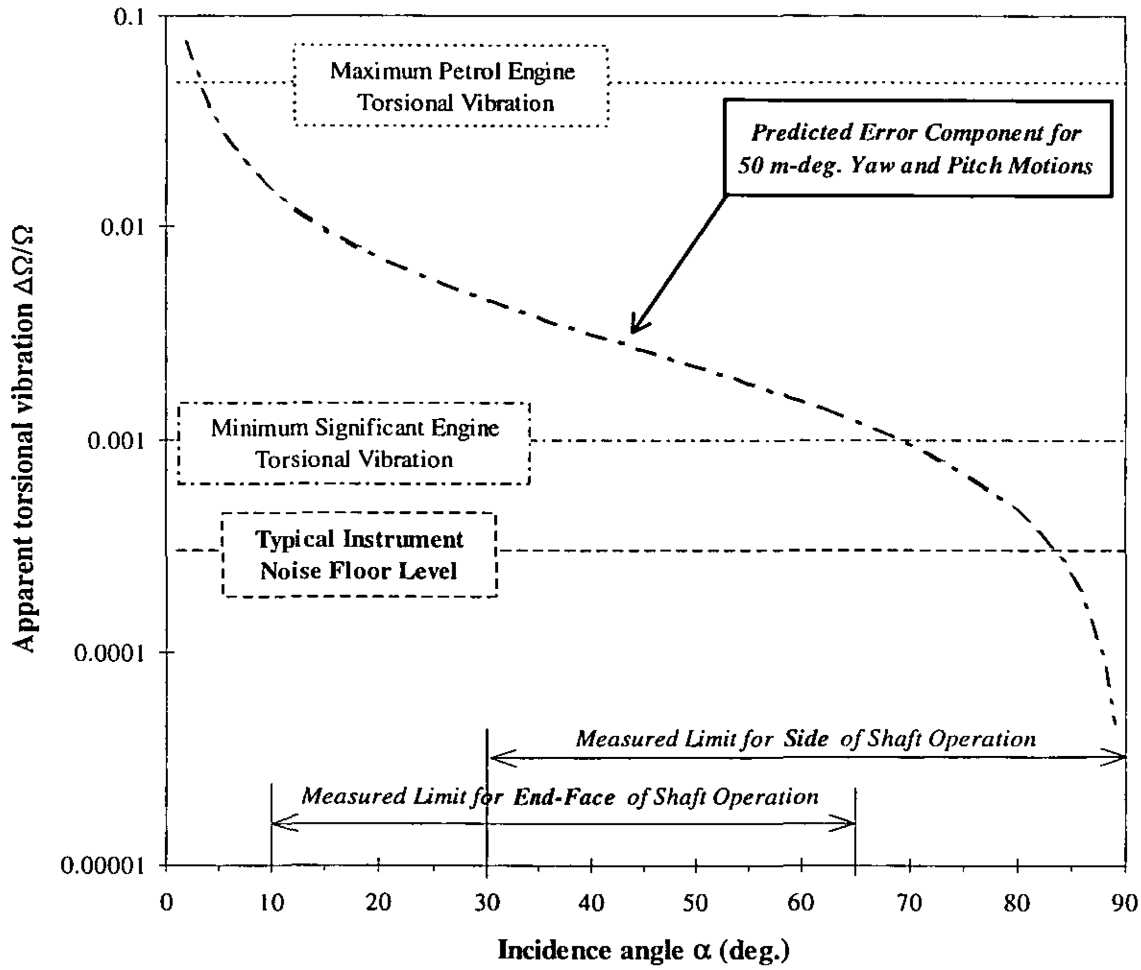

Figure 3.18: Guidelines for successful operation of the LTV with minimisation of lateral vibration errors

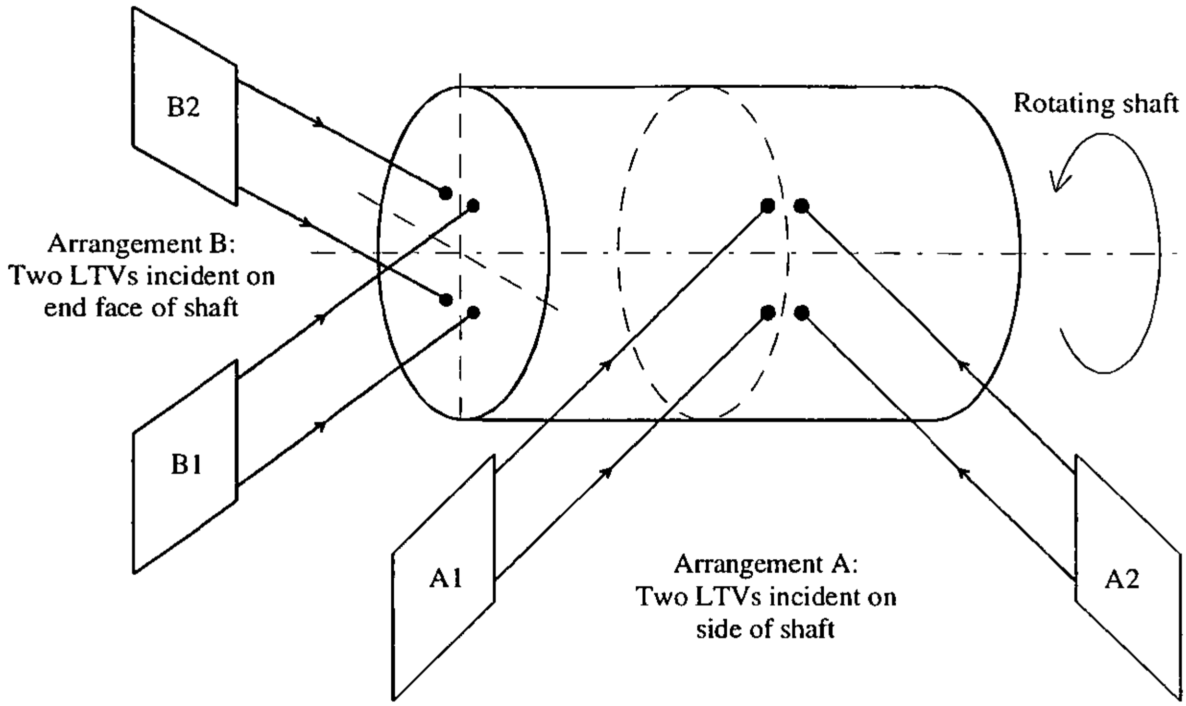

Figure 3.19: Arrangements of the two LTVs for measurement of torsional vibration immune to angular lateral vibration

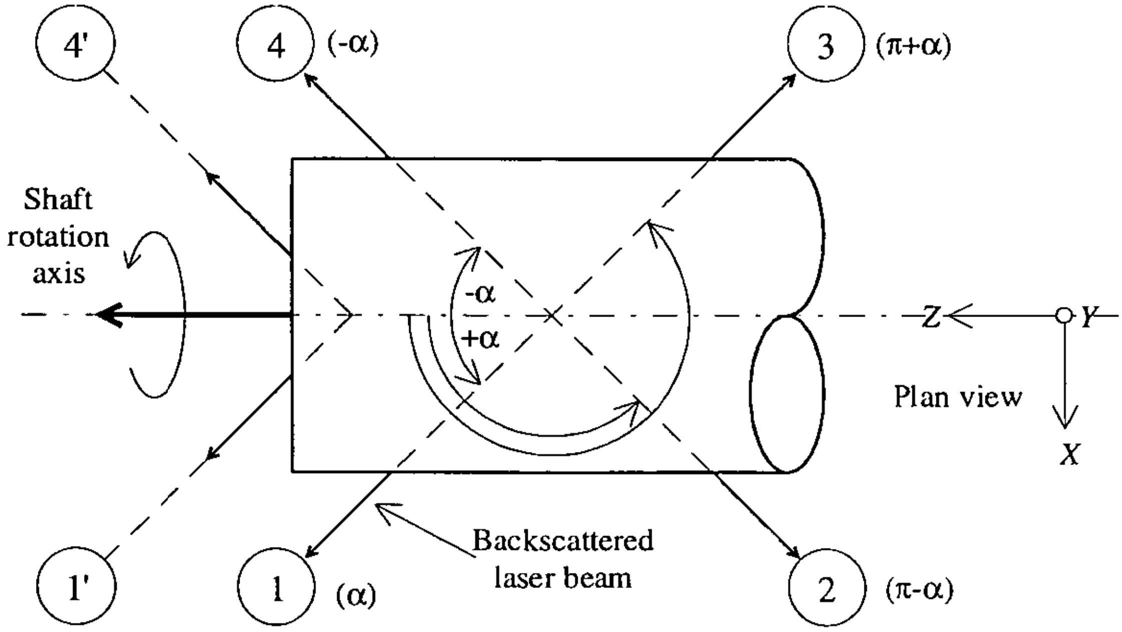

Figure 3.20: Angular positions of the LTV around the shaft in the X-Z plane

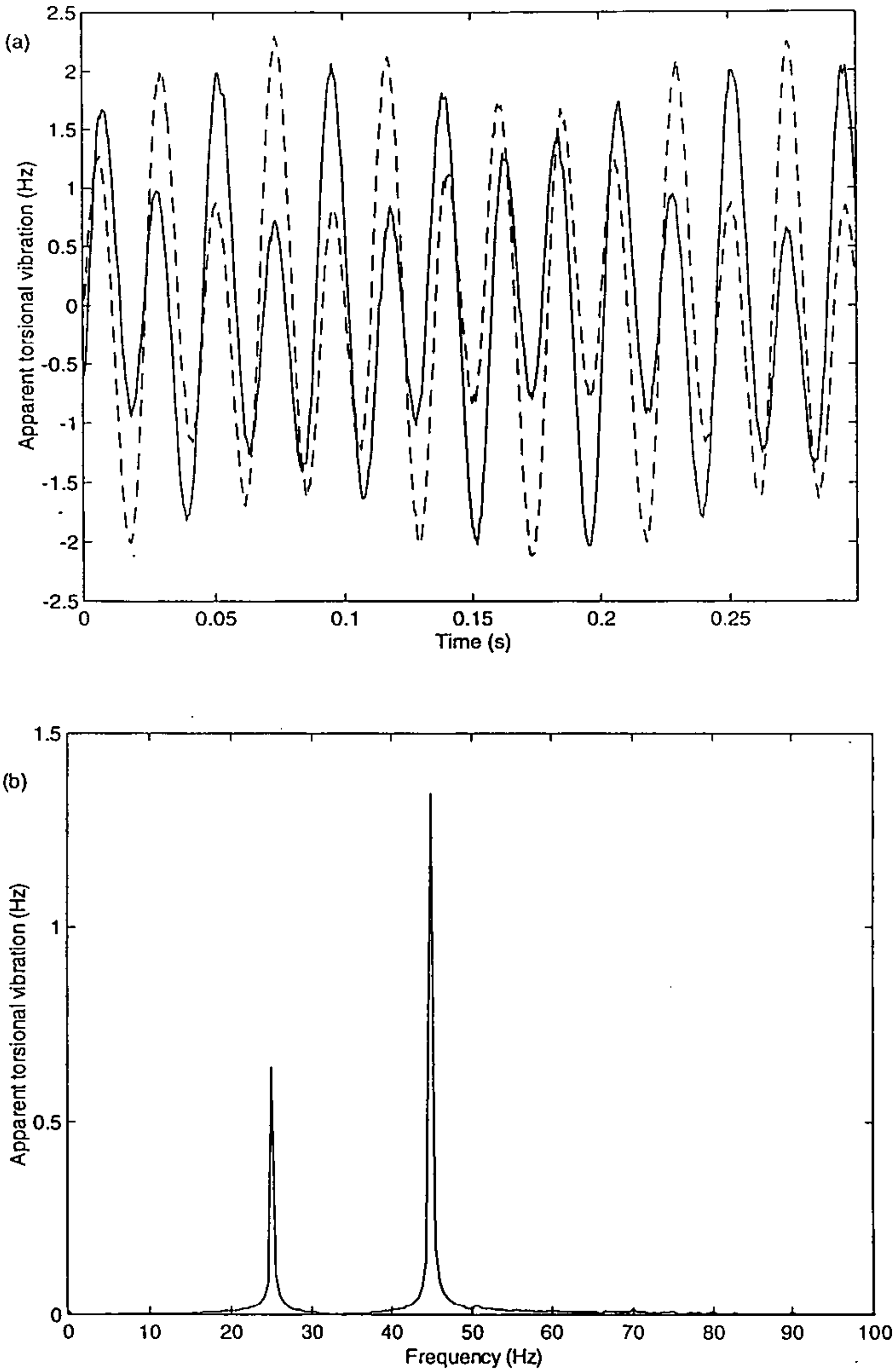

Figure 3.21: LTV outputs showing sensitivity to torsional and bending vibration
a. Time trace of instrument output: LTV1 (solid line) and LTV2 (dashed line)
b. Spectrum of LTV1 output

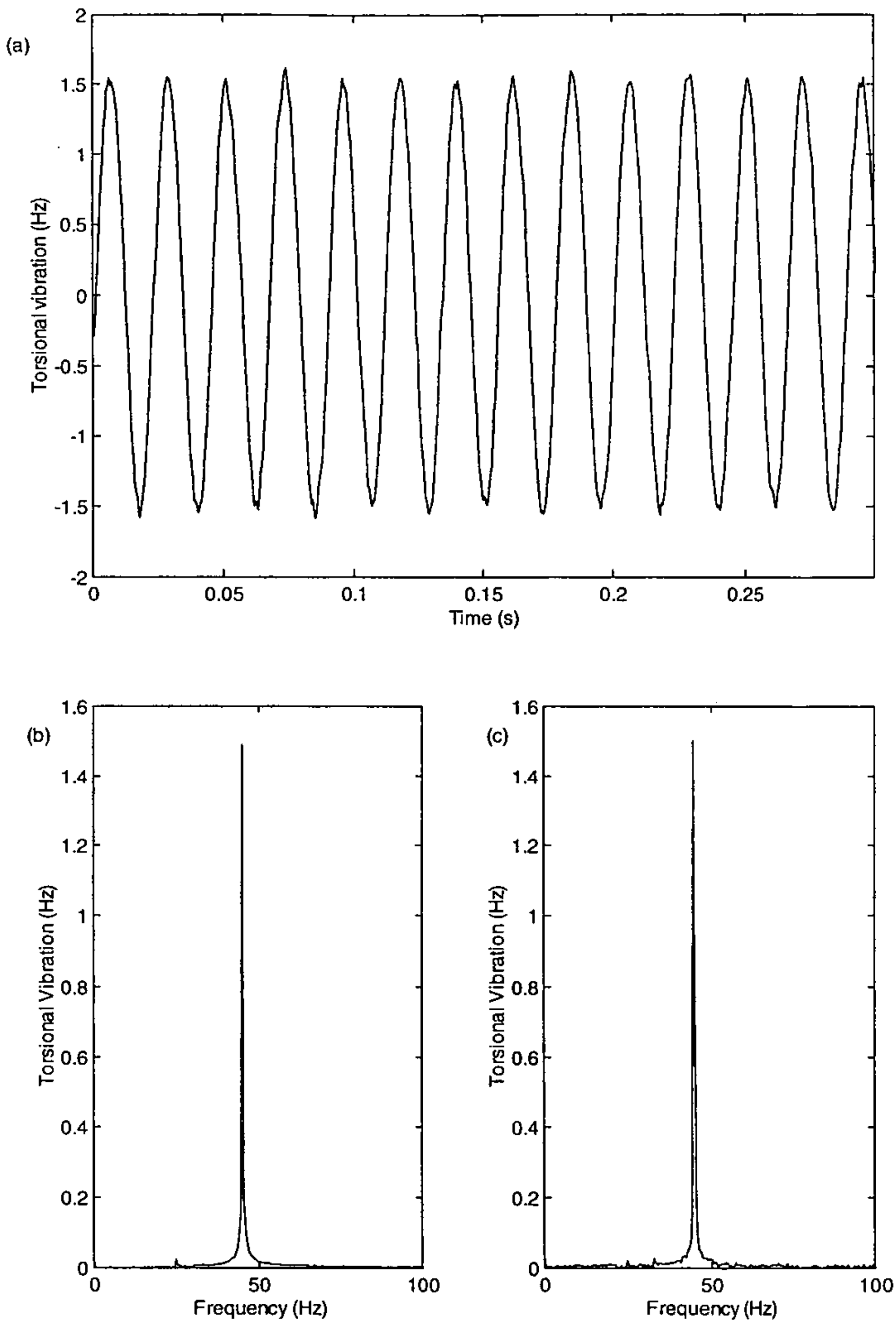

Figure 3.22: Torsional vibration measurements

a. Time trace of resolved signal

b. Resolved data from two LTVs

c. Independently measured data

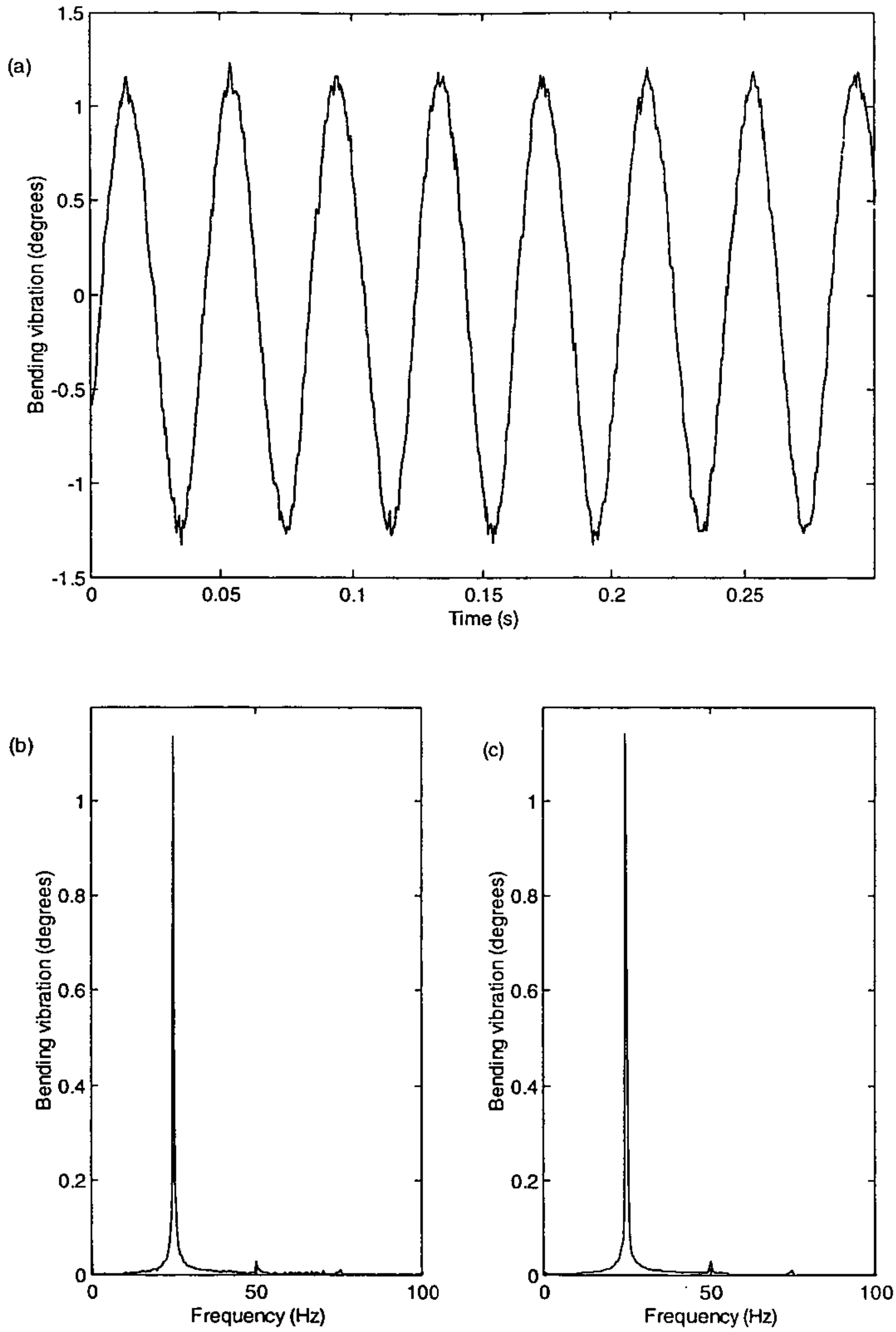

Figure 3.23: Bending vibration measurements

a. Time trace of resolved signal

b. Resolved data from two LTVs

c. Independently measured data

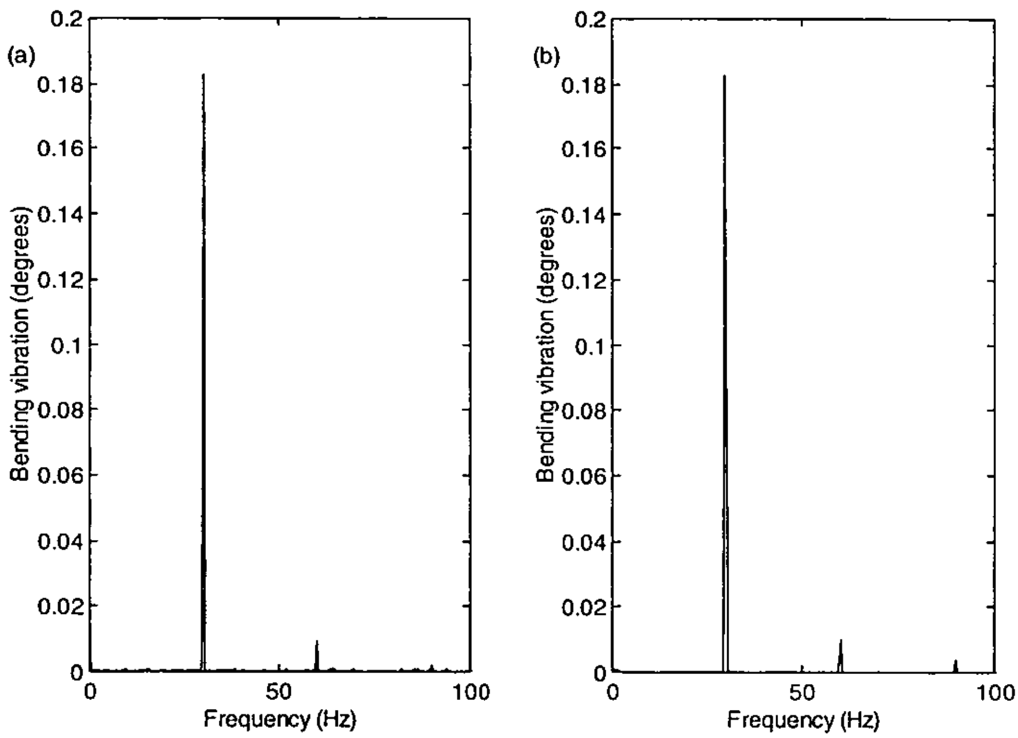

Figure 3.24: Bending vibration measurement with increased sensitivity (α=15°)

a. Resolved data from two LTVs

b. Independently measured data

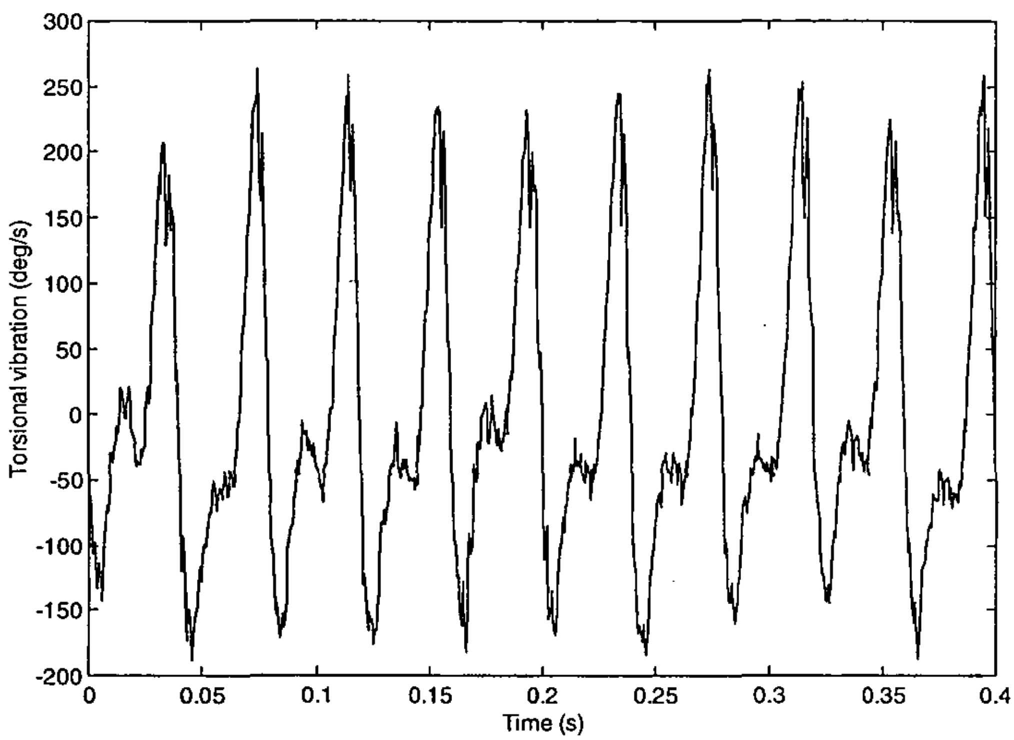

Figure 3.25: Torsional vibration time trace measurement from a diesel engine crankshaft running under load at 750rpm. Single LTV (α=35°)

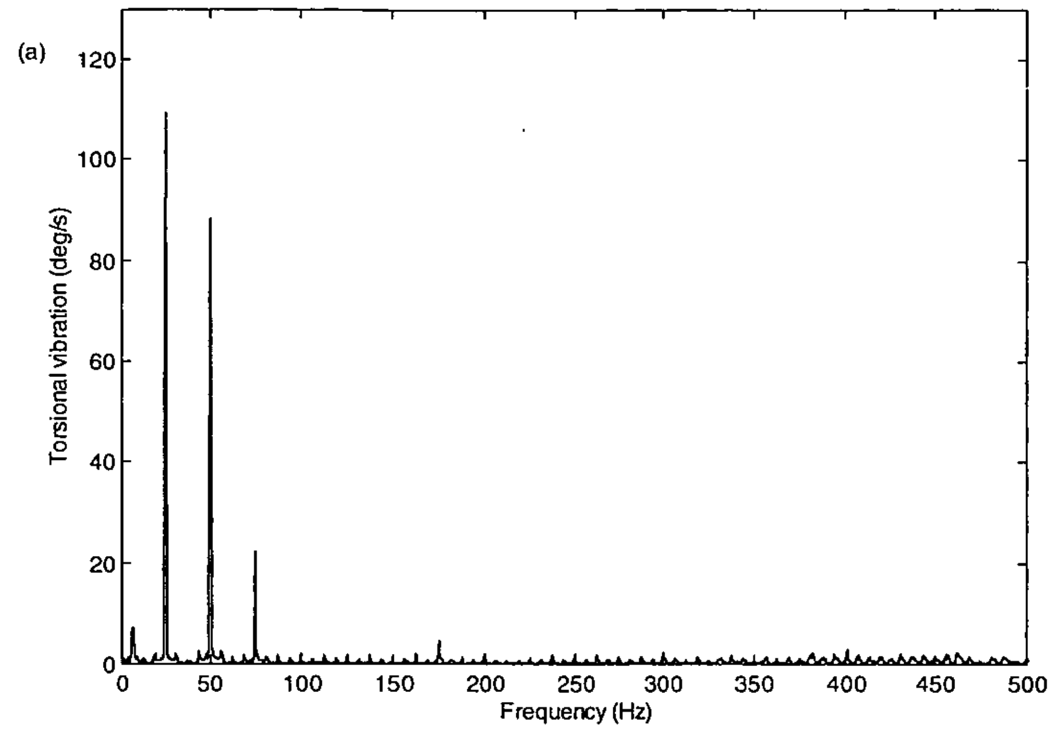

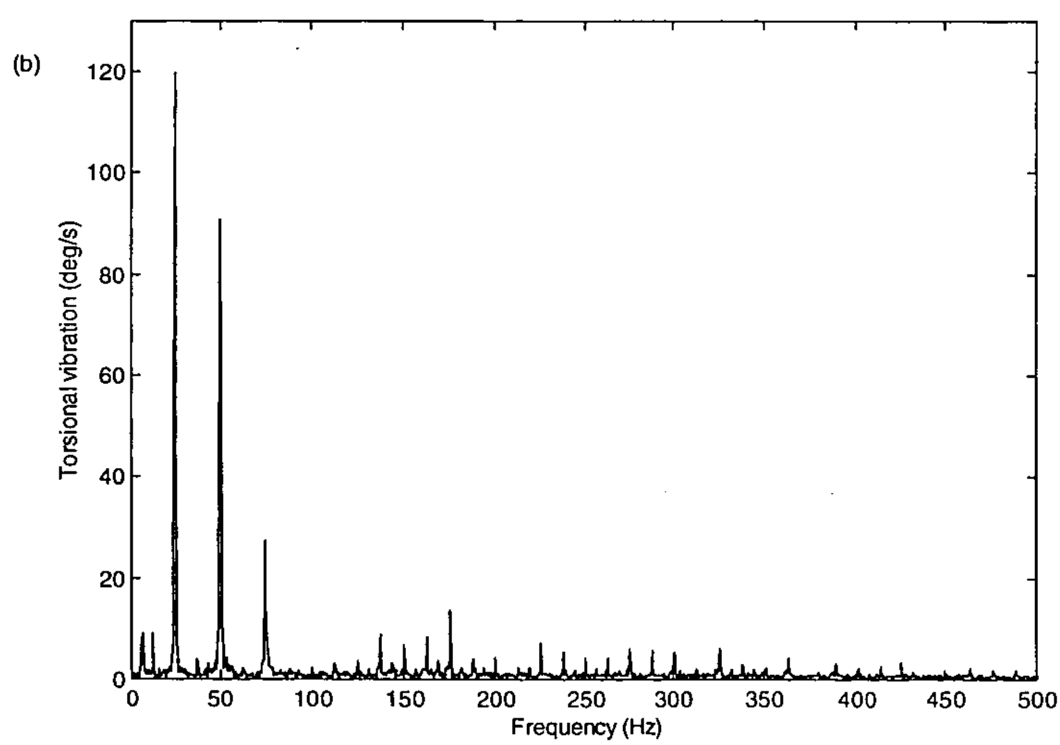

Figure 3.26: Torsional vibration spectra from diesel engine crankshaft at 750rpm

a. Single LTV (α=35°)

b. Independent LTV(α=75°)

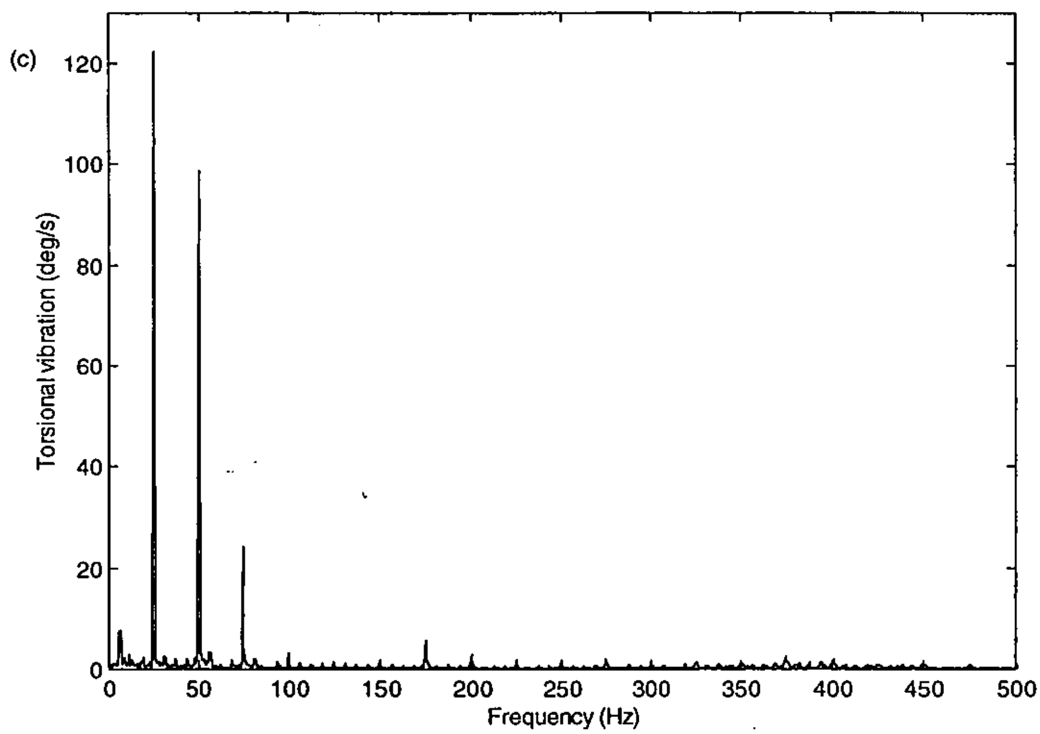

Figure 3.26: Torsional vibration spectra from diesel engine crankshaft at 750rpm
c. Resolved measurement

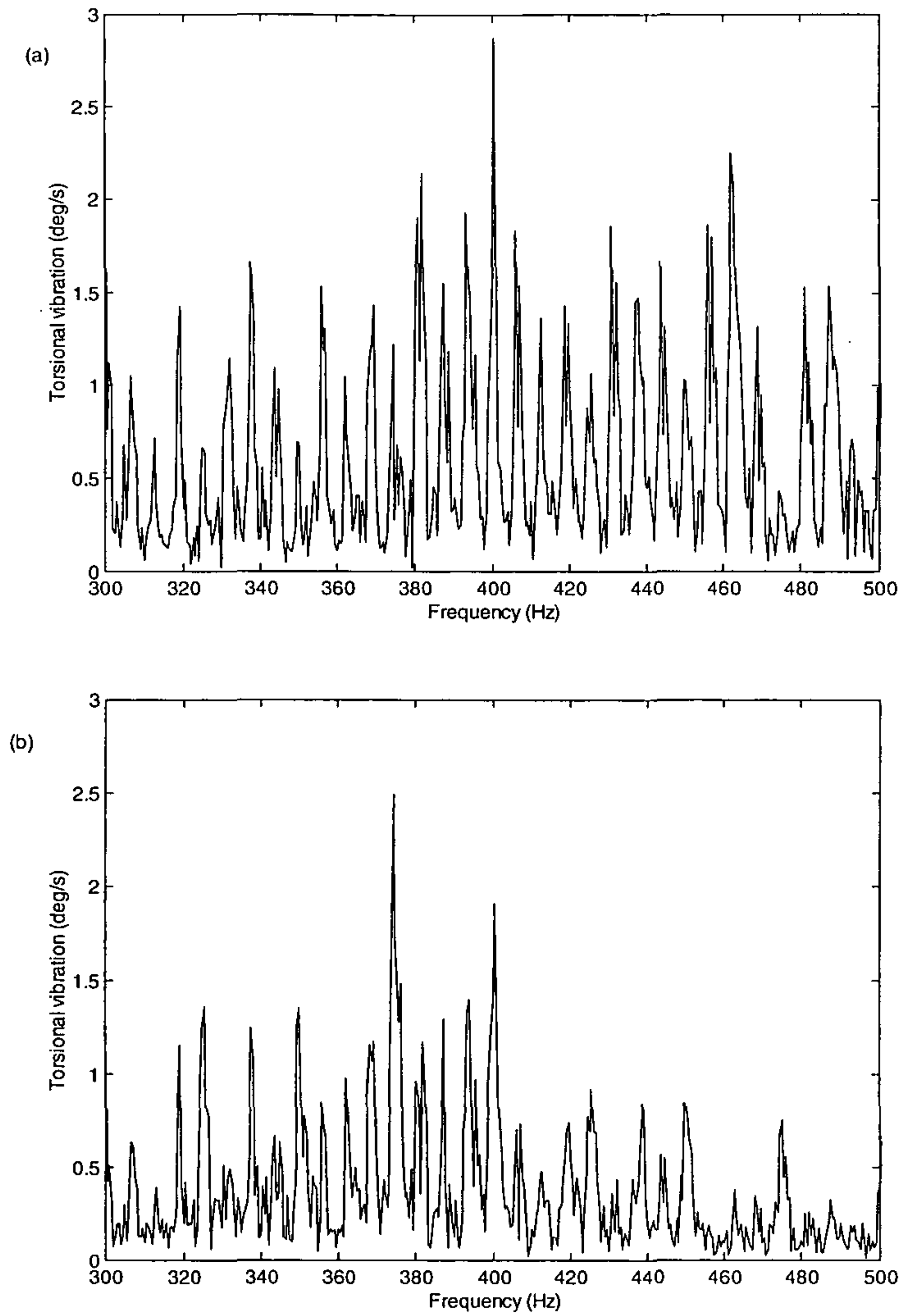

Figure 3.27: Expanded view of spectra in Figure 3.26
(Diesel engine crankshaft at 750rpm)
a. Single LTV (α=35°)
b. Resolved measurement of pure torsional vibration

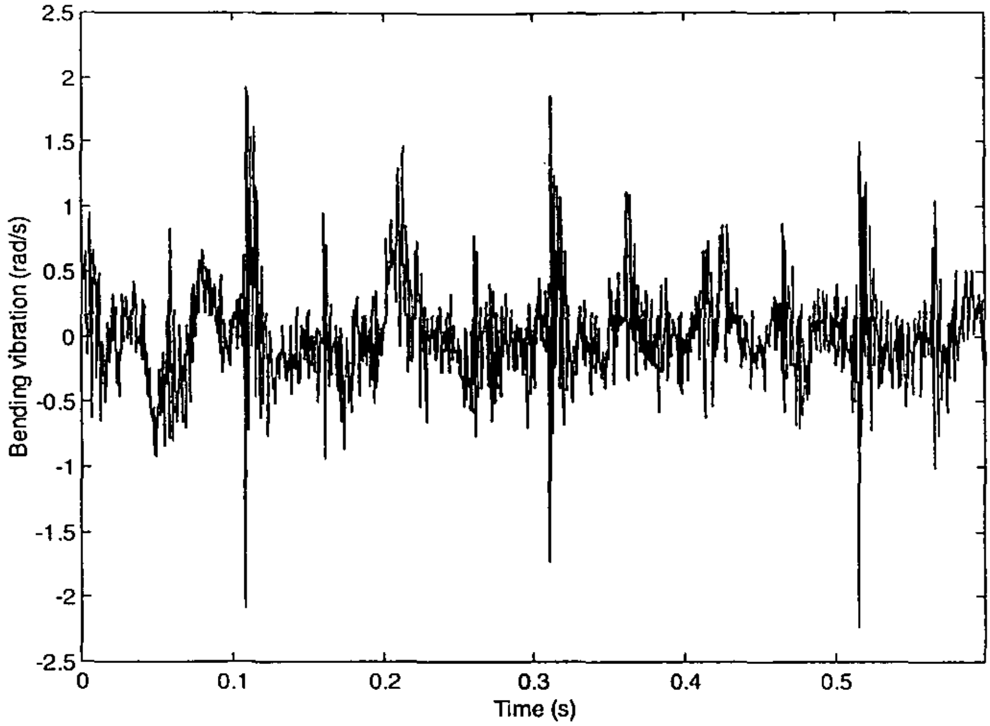

Figure 3.28: Diesel engine crankshaft bending vibration under load at 600rpm

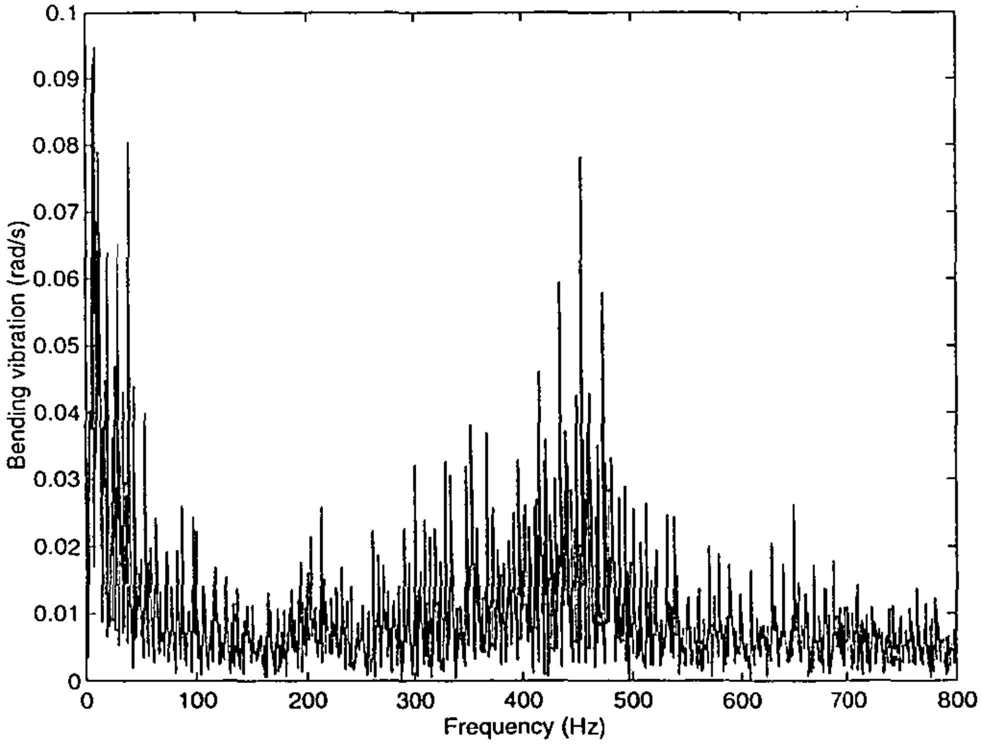

Figure 3.29: Spectrum of diesel engine crankshaft bending vibration

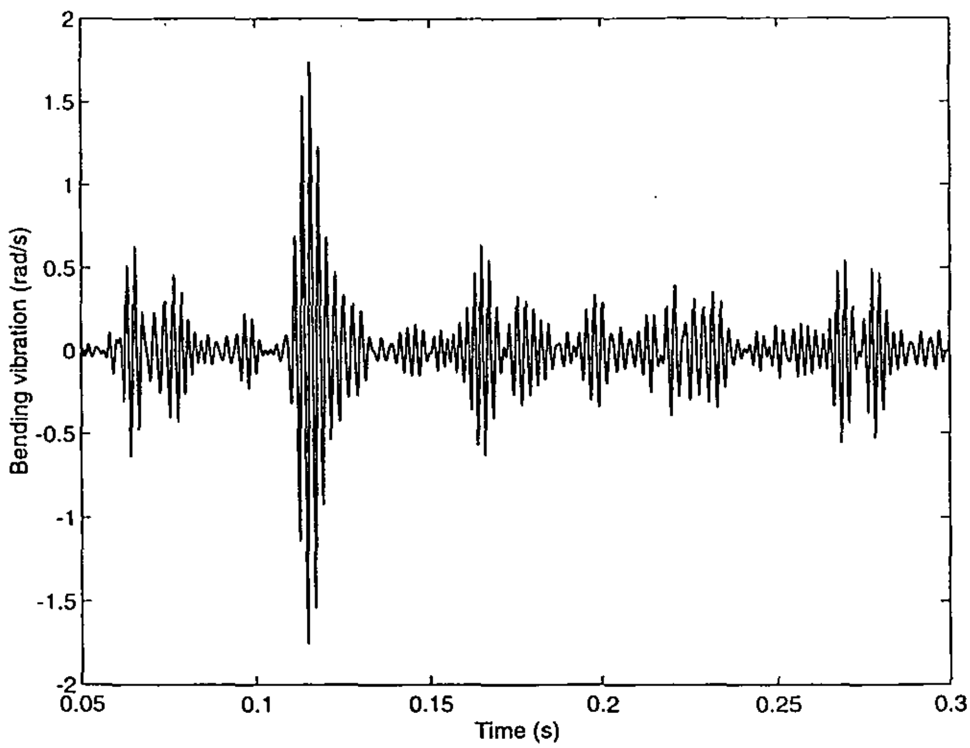

Figure 3.30: Filtered time trace of crankshaft bending vibration

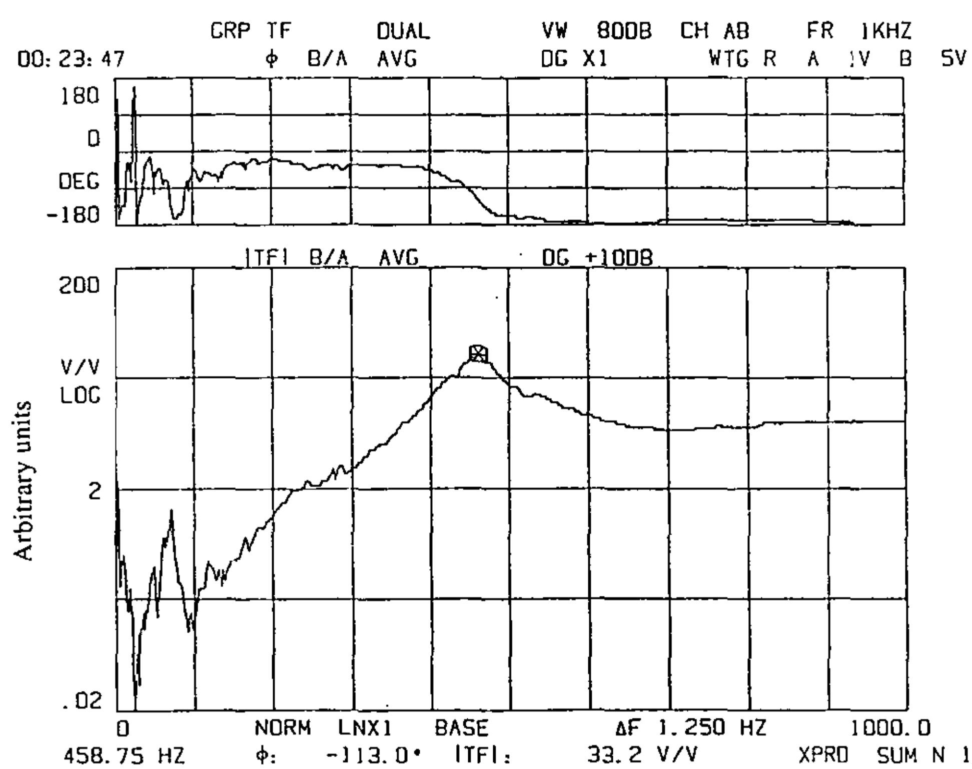

Figure 3.31: Modal analysis FRF of crankshaft from pulley position

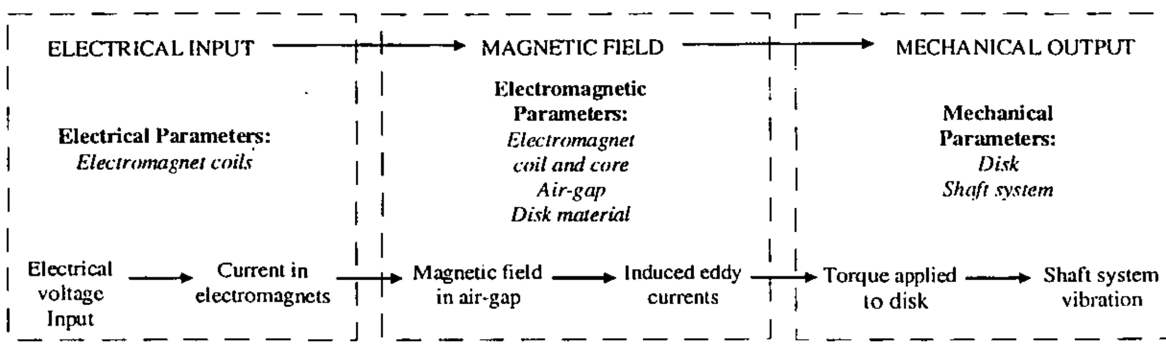

Figure 4.1: Schematic of electromagnetic torque input system.

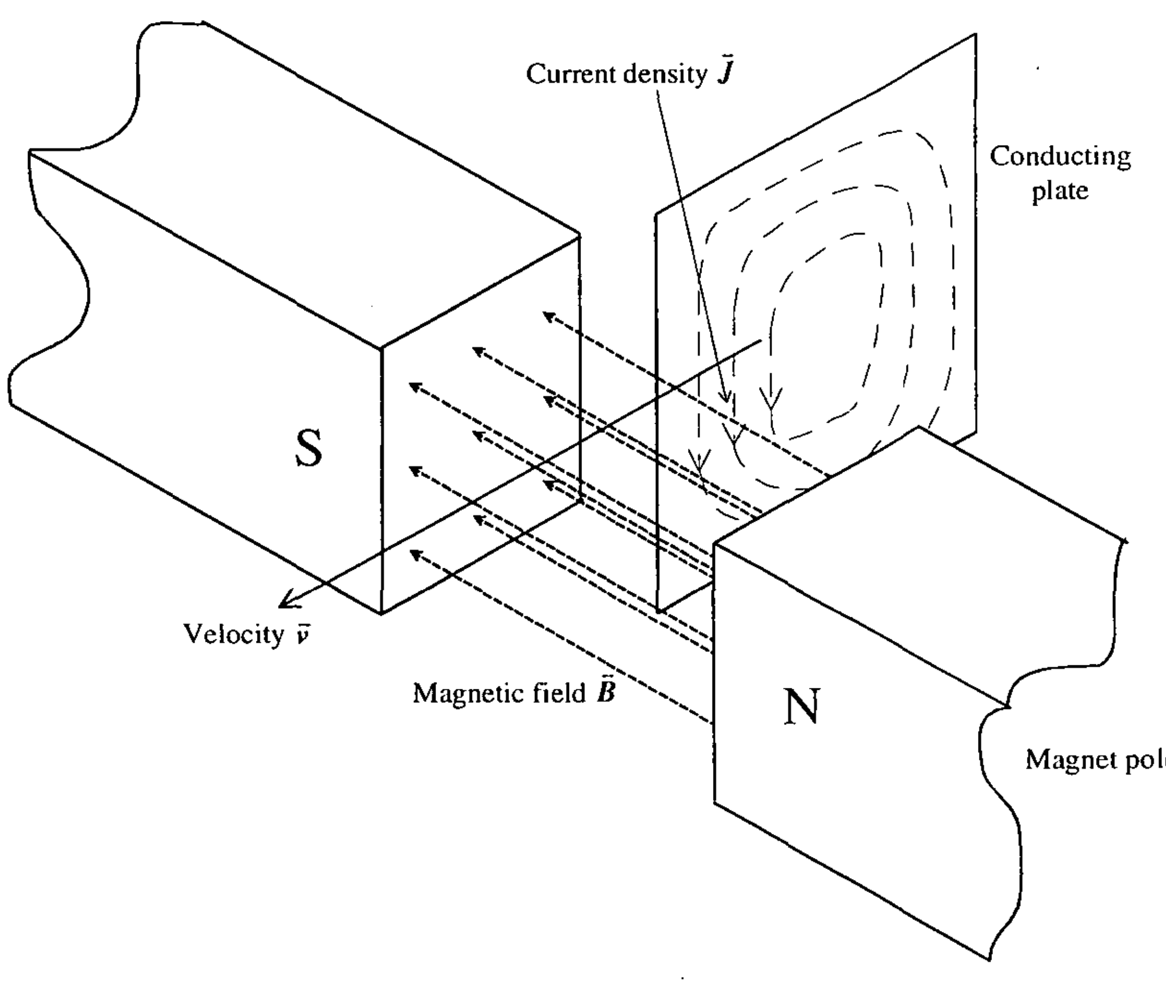

Figure 4.2: General case of a conducting plate moving through a magnetic field.

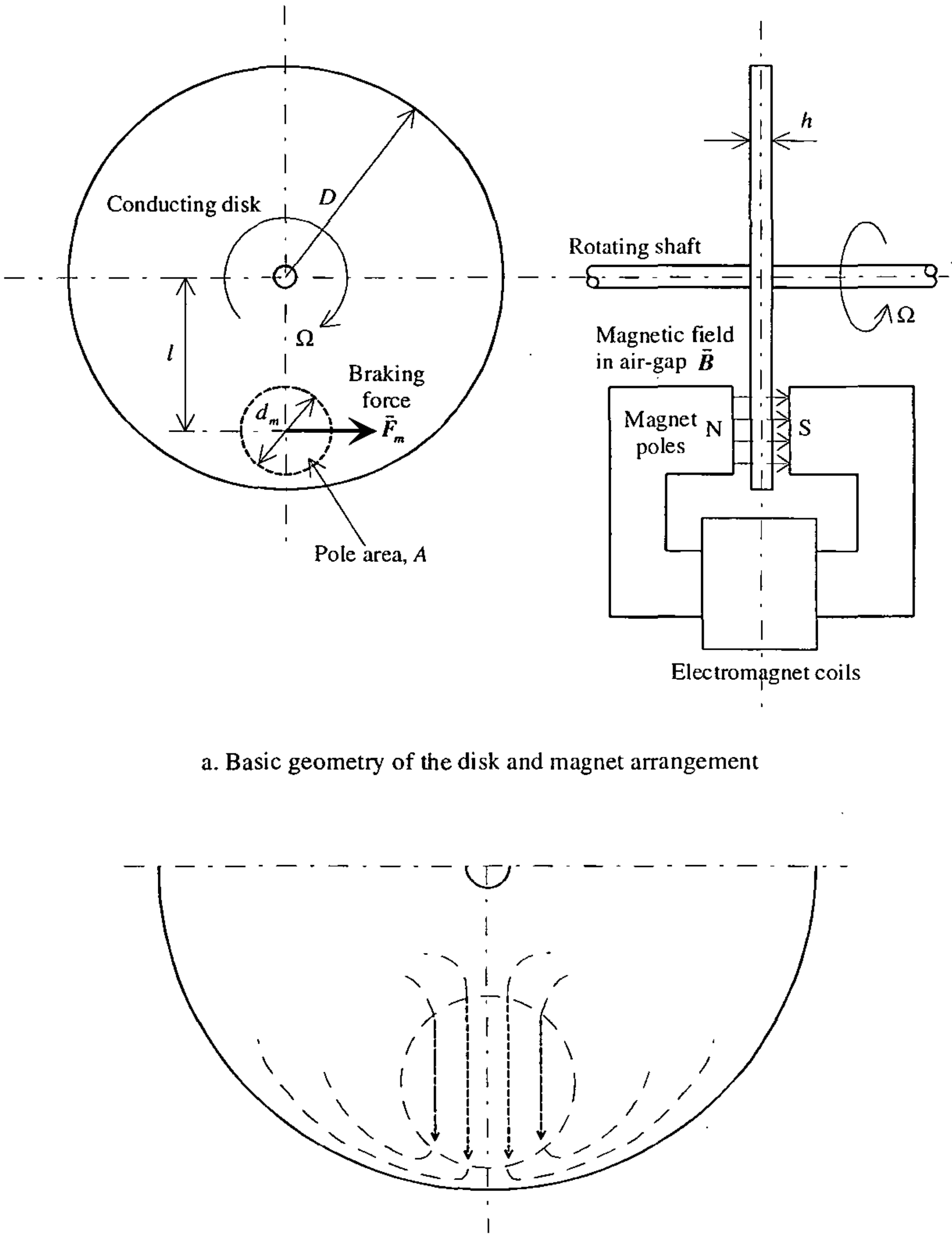

a. Basic geometry of the disk and magnet arrangement

b. Approximate eddy current pattern in vicinity of electromagnet poles

Figure 4.3: Basic arrangement of the eddy current disk braking system.

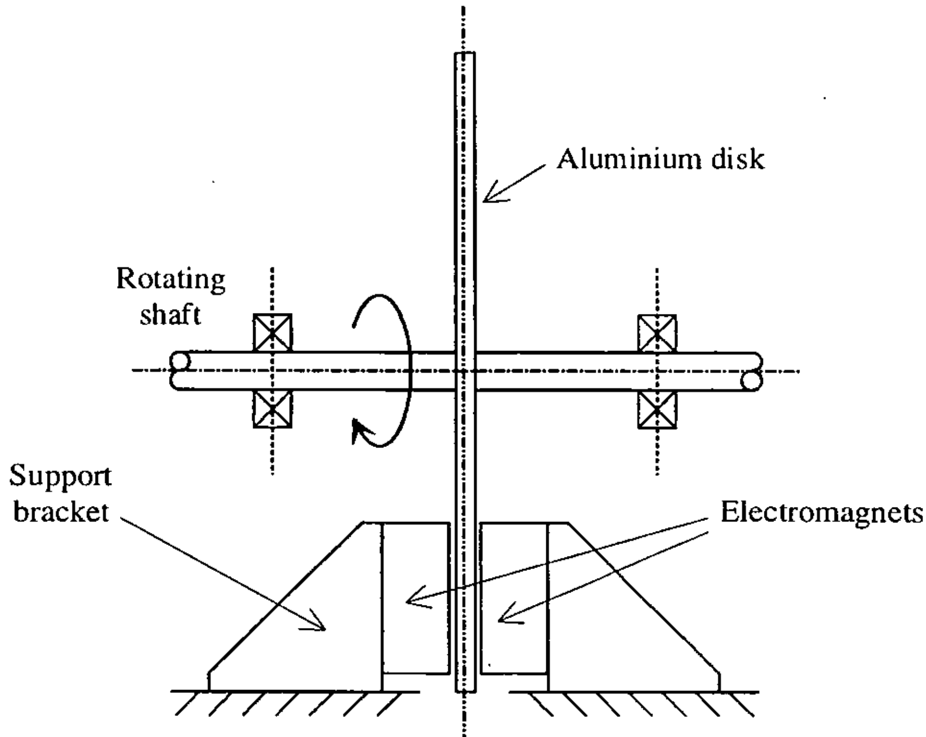

a. Actual physical arrangement of the electromagnet excitation system

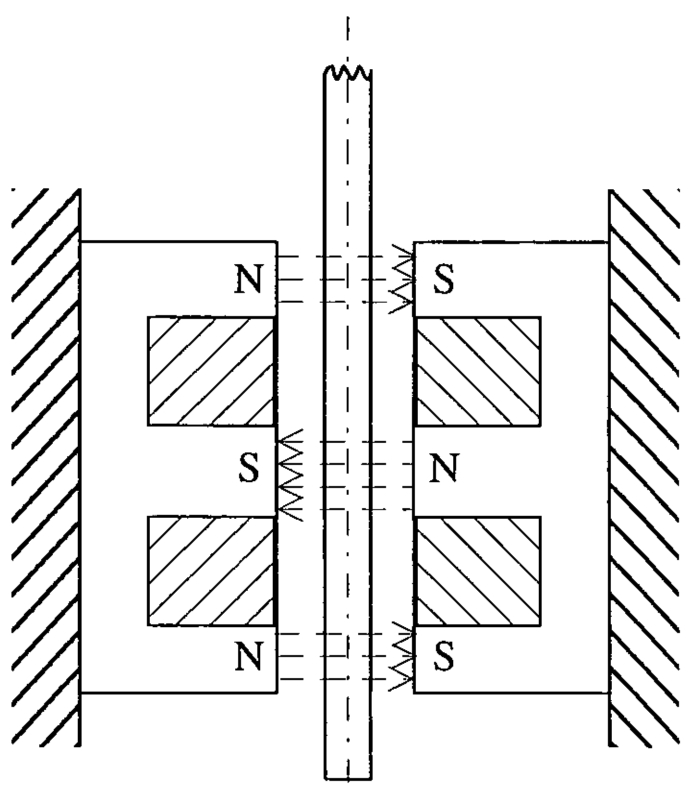

b. Detail of electromagnet cores and predicted flux pattern

Figure 4.4: Experimental electromagnet system

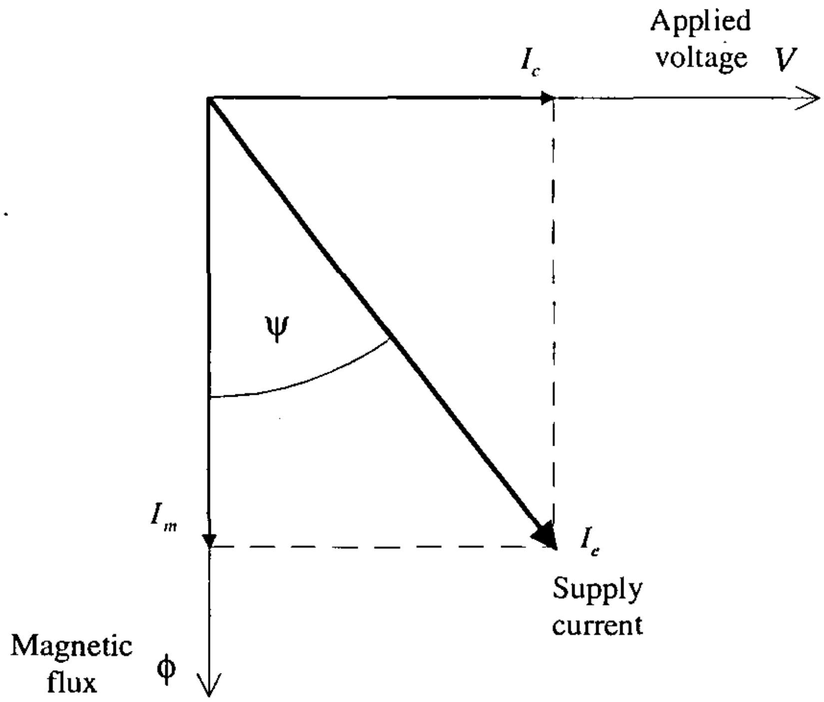

Figure 4.5: Phasor diagram for electromagnet supply excitation current components.

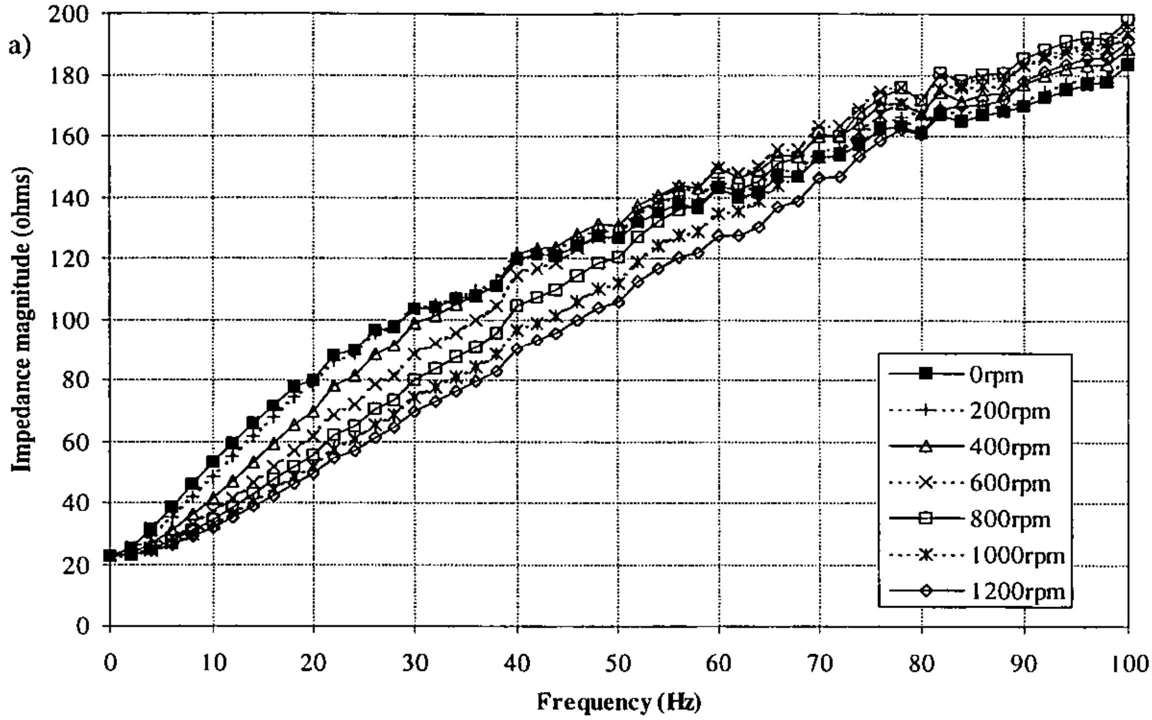

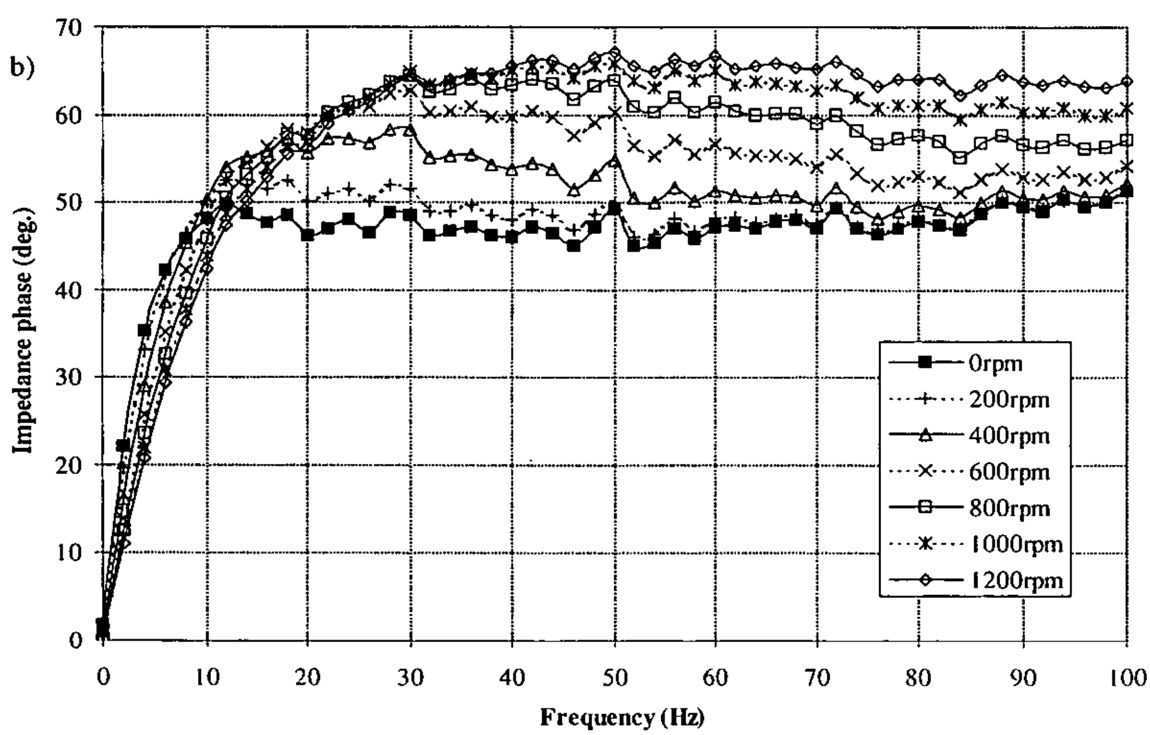

Figure 4.6: Experimentally measured impedance of electromagnet system for full range of rotation speeds. a. Magnitude, b. Phase.

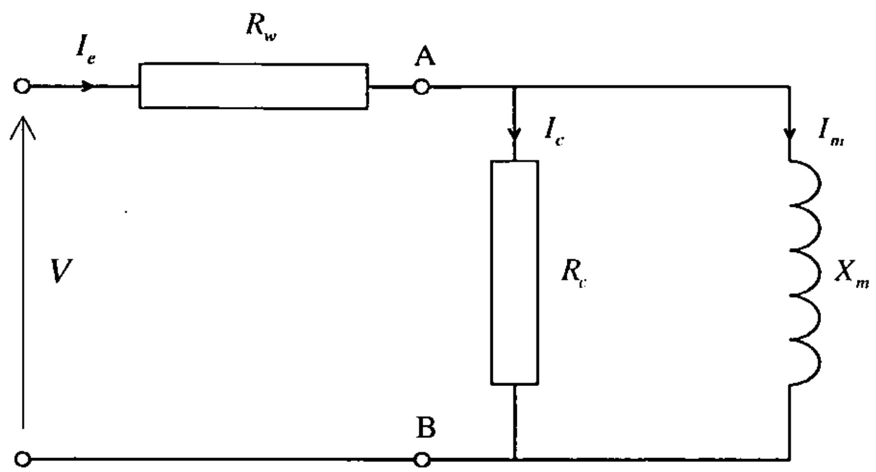

R_w = Coil winding resistance

R_c = Core loss resistance

X_m = Electromagnet inductance

a. Parallel form of electromagnet impedance model

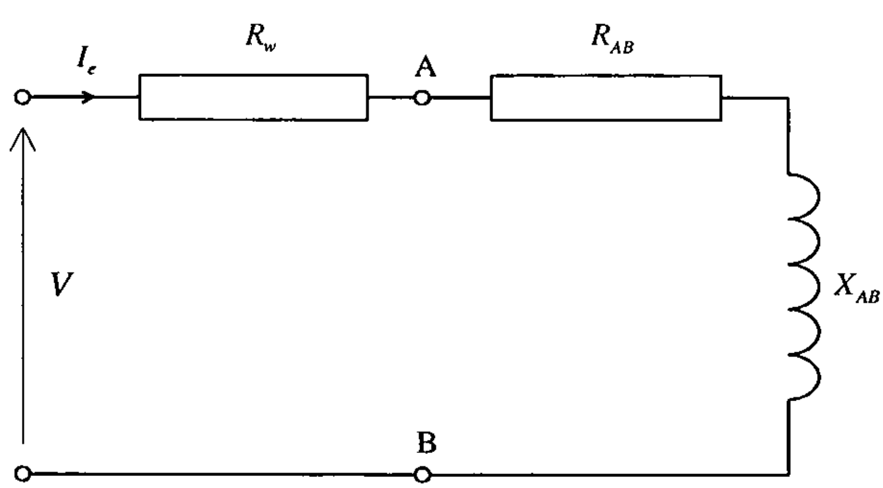

b. Series form of electromagnet impedance model

Figure 4.7: Equivalent circuit for modelling impedance of electromagnet system.

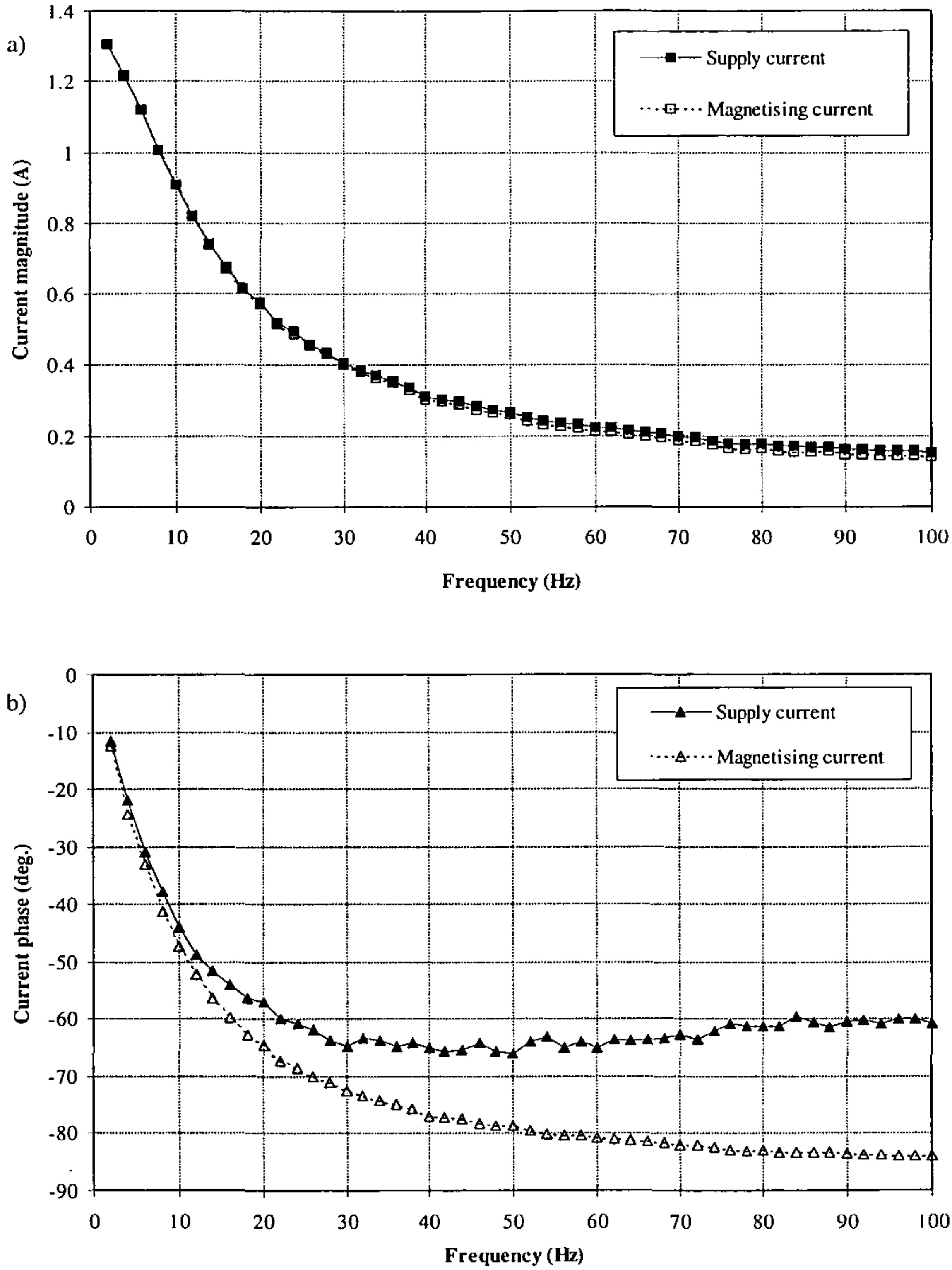

Figure 4.8: Modelled electromagnet supply I_e and magnetising component I_m currents for shaft rotation speed of 1000rpm. a. Magnitude, b. Phase.

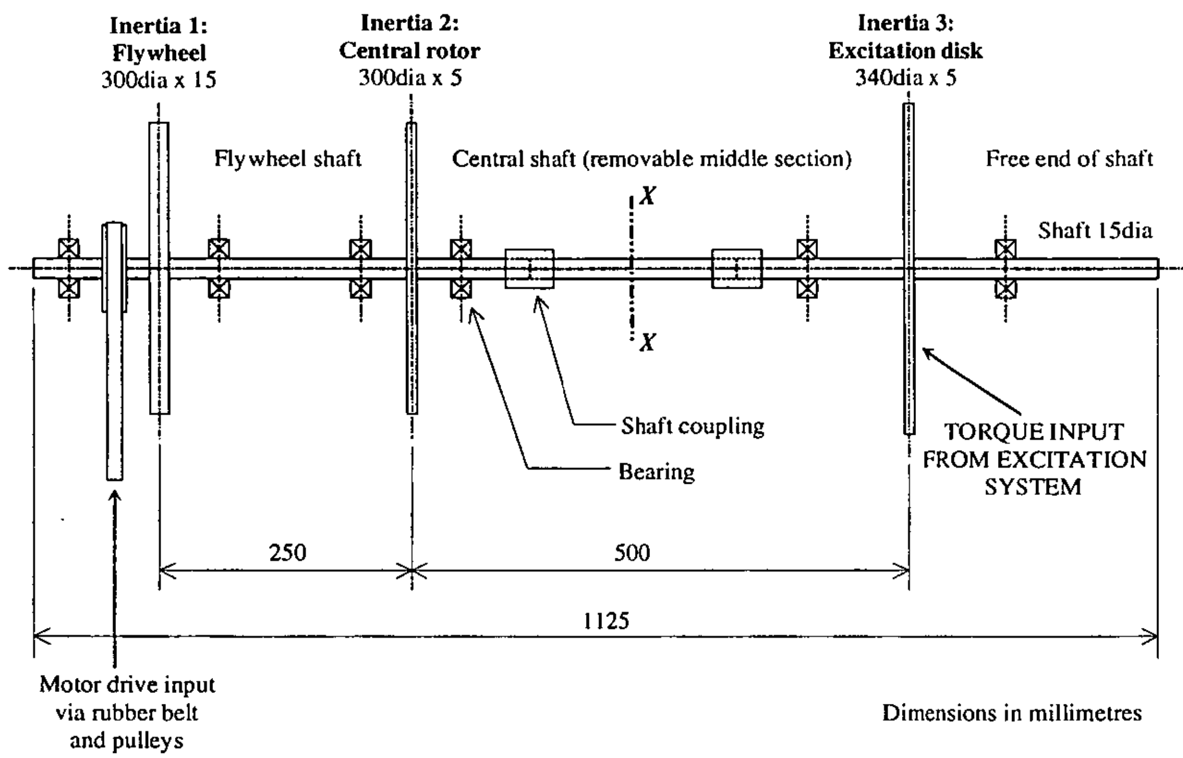

Figure 4.9: Details of experimental shaft system.

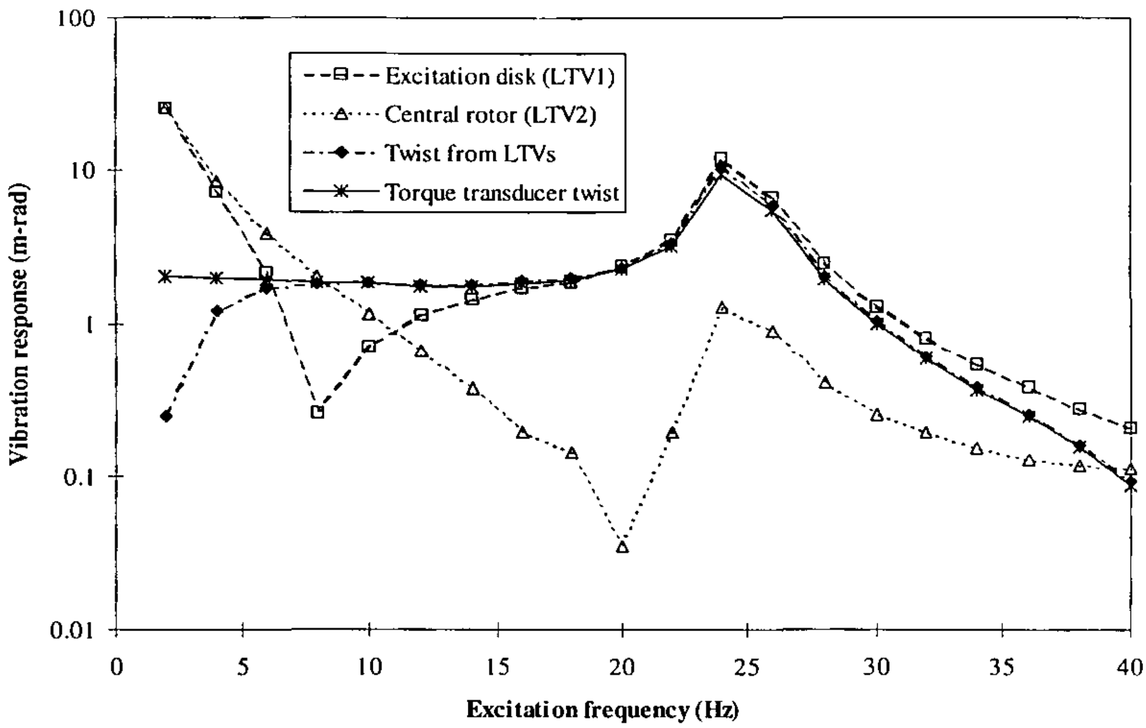

Figure 4.10: Shaft response to harmonic input, measured by in-line torque transducer and LTVs. Rotation speed 800rpm.

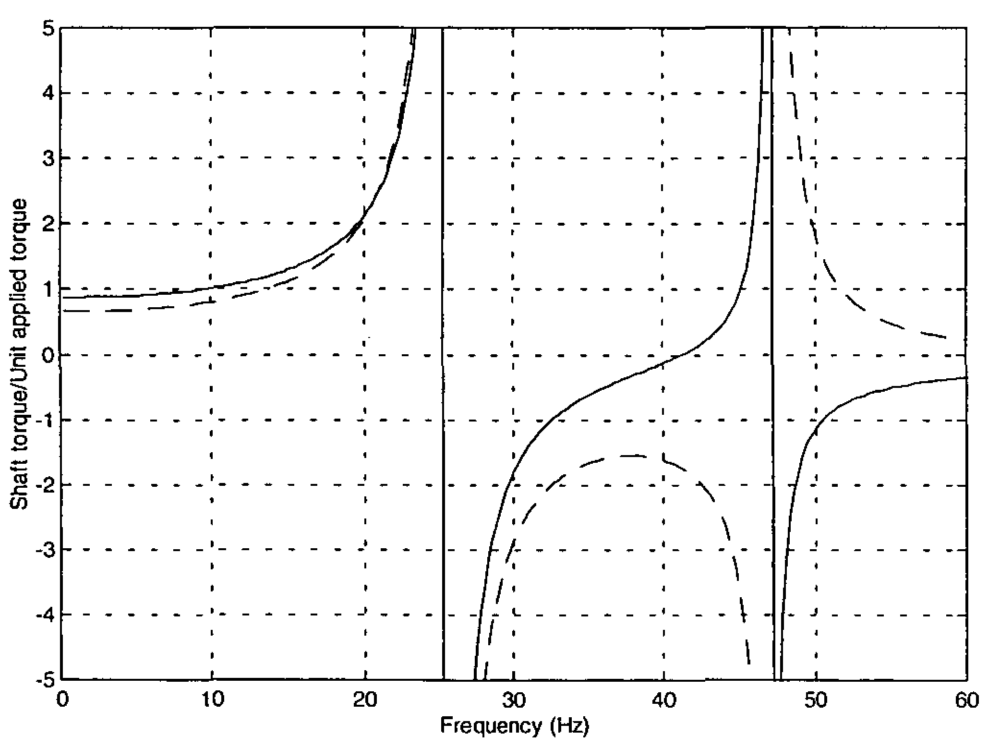

Figure 4.11: Modelled torque in shaft sections for forced response of experimental three inertia system. Central shaft with torque transducer (solid) and flywheel shaft (dashed).

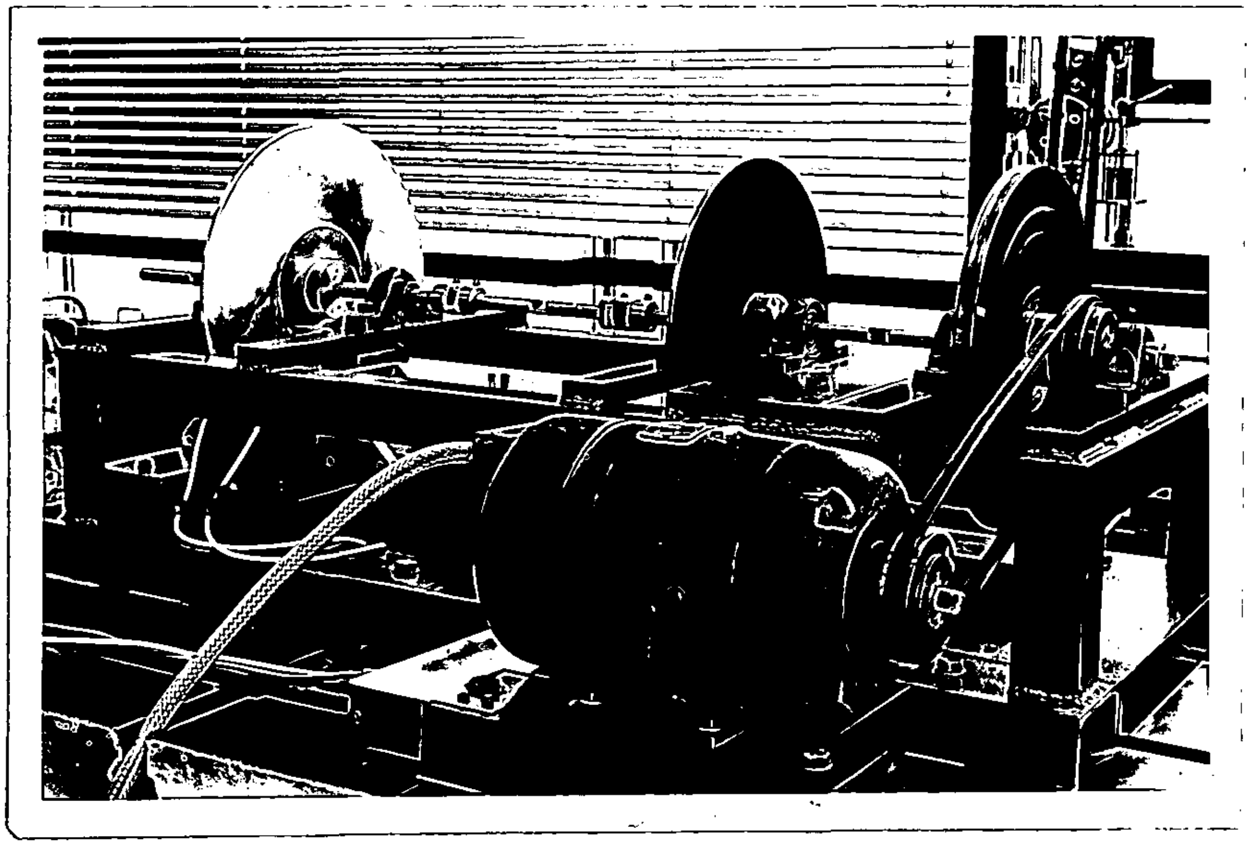

Figure 4.12: Photograph of the test-rig showing the main components.

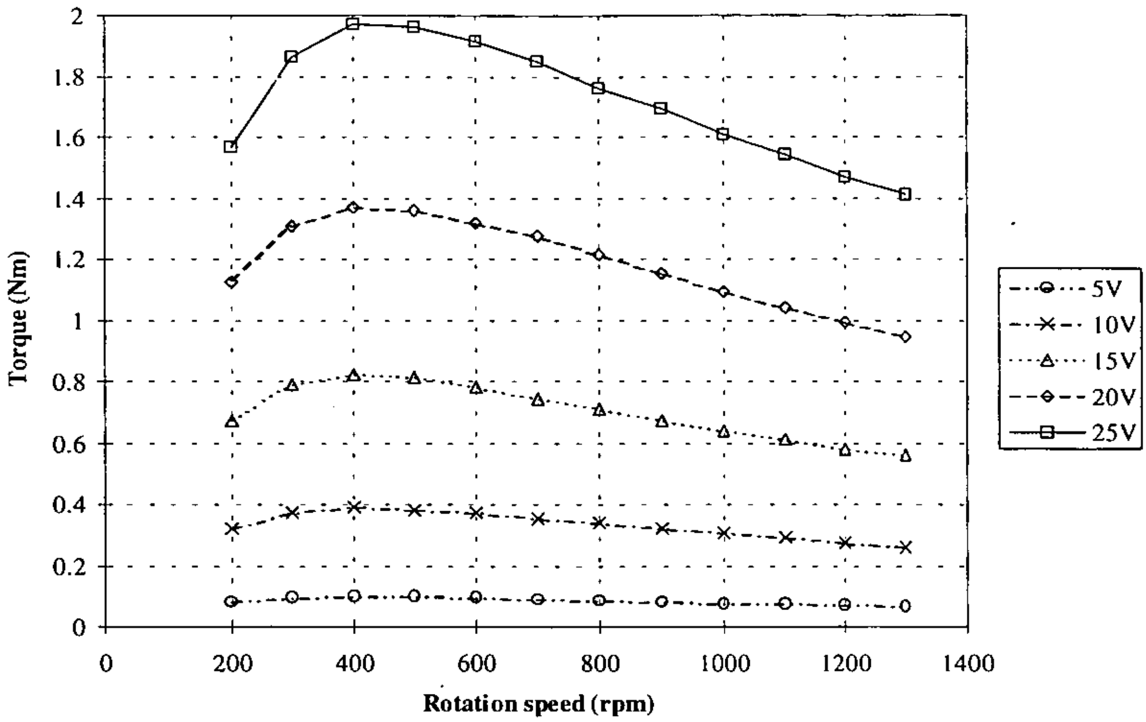

Figure 4.13: Constant (d.c.) braking torque applied by the electromagnetic system.

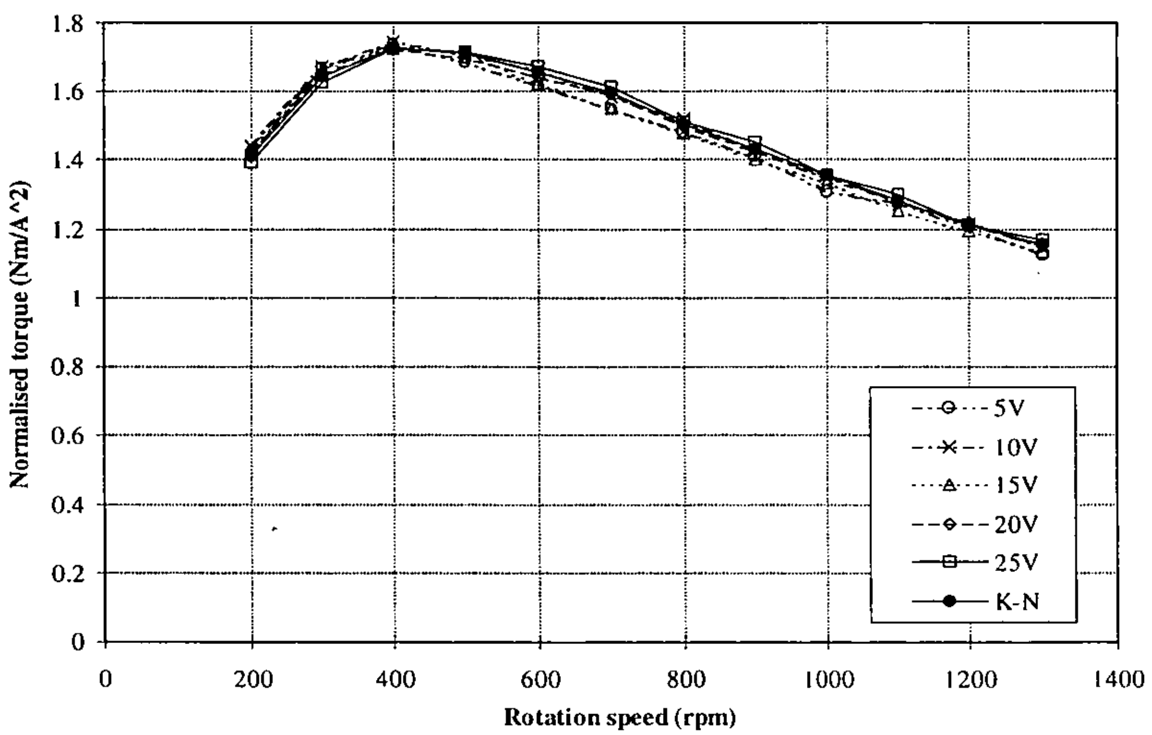

Figure 4.14: Normalised applied torque $\left(T/I^2\right)$ and proportionality constant K_N.

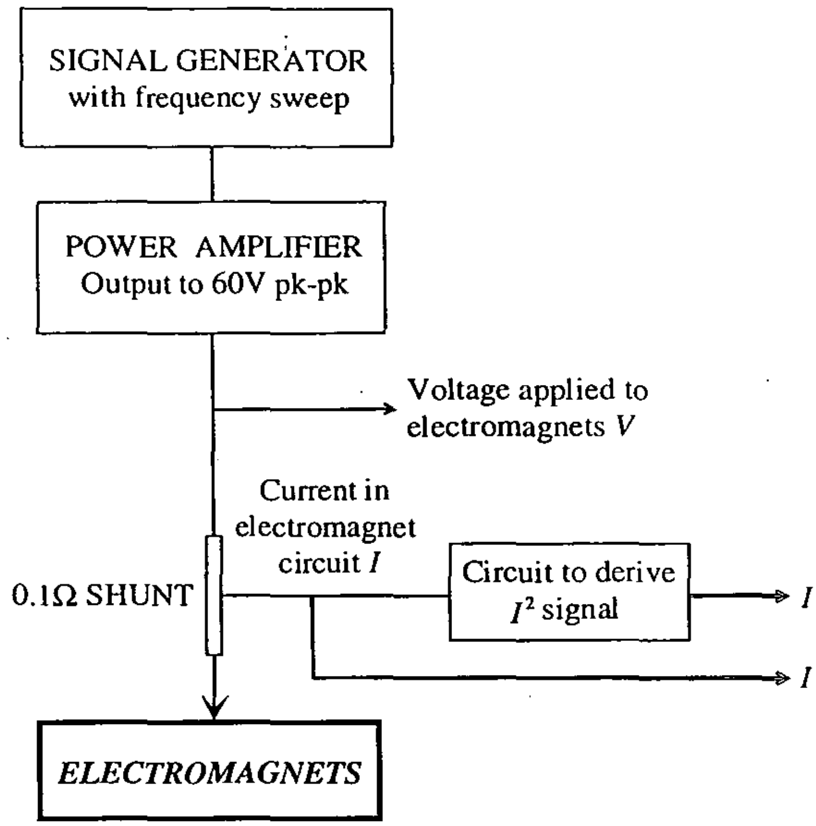

Figure 4.15: Schematic of instrumentation for harmonic voltage input to electromagnets.

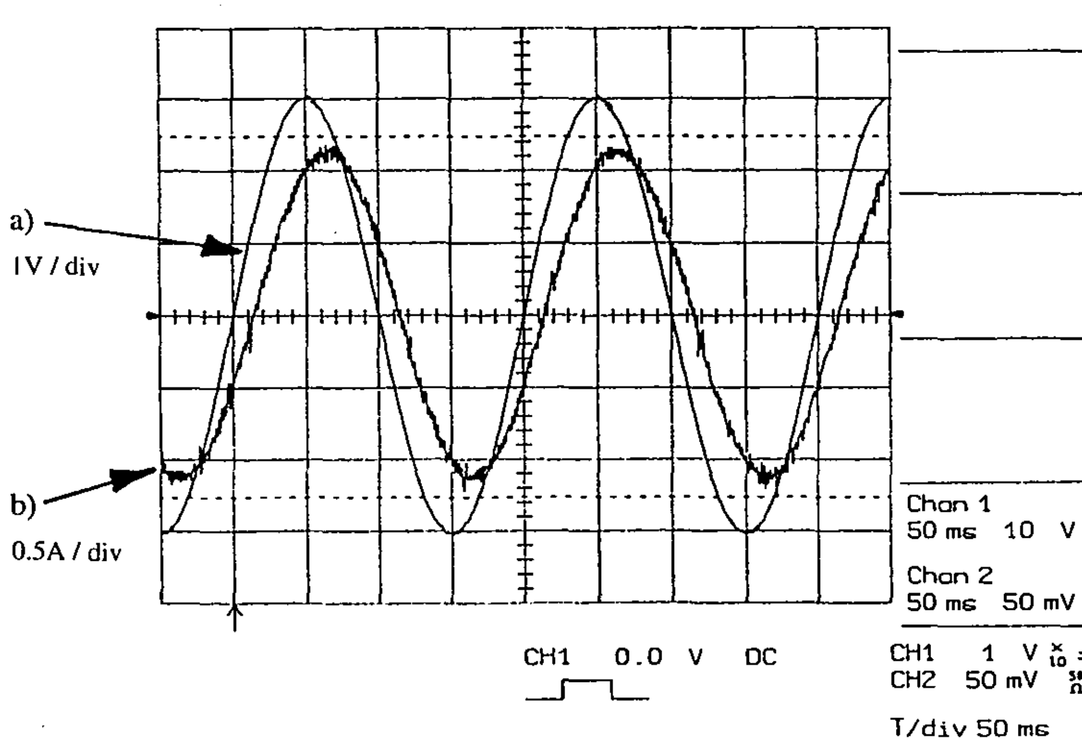

Figure 4.16: Time traces of; a) Voltage applied to electromagnets, and b) Resulting supply current. 5Hz applied voltage at 60V (pk-pk). Rotation speed 1000rpm.

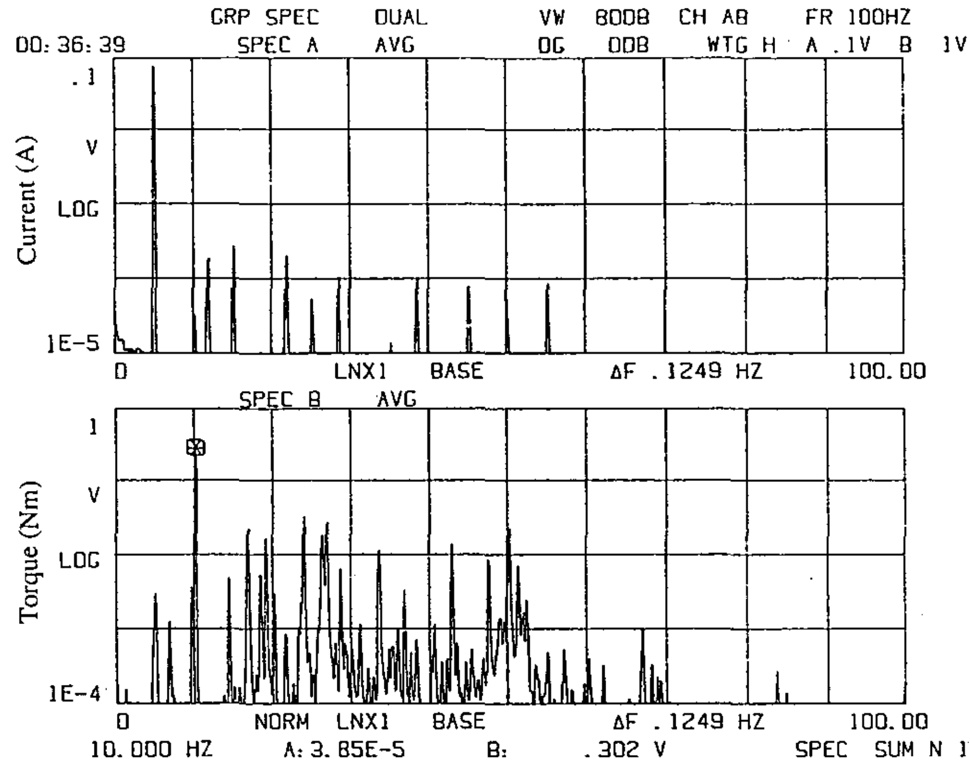

Figure 4.17: Frequency spectra of; a) Current in electromagnets, and b) Torque in shaft. Conditions as for Figure 4.16.

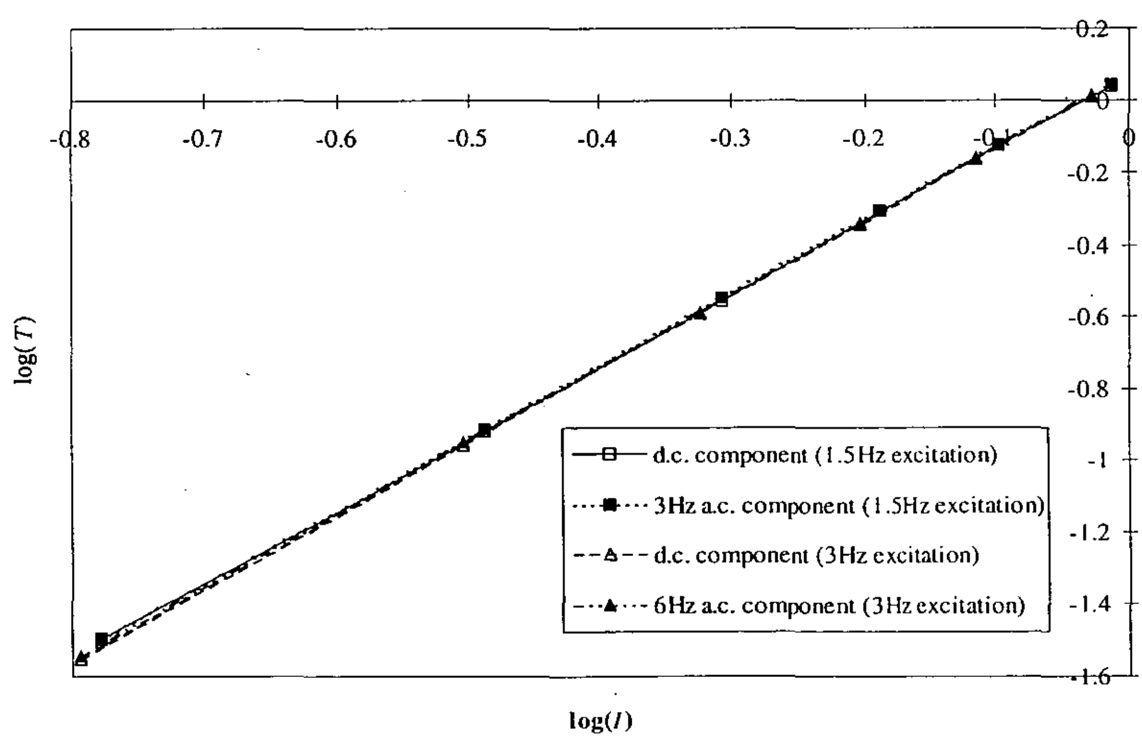

Figure 4.18: Torque-current relationship for harmonic (a.c.) input. Rotation speed 1000rpm.

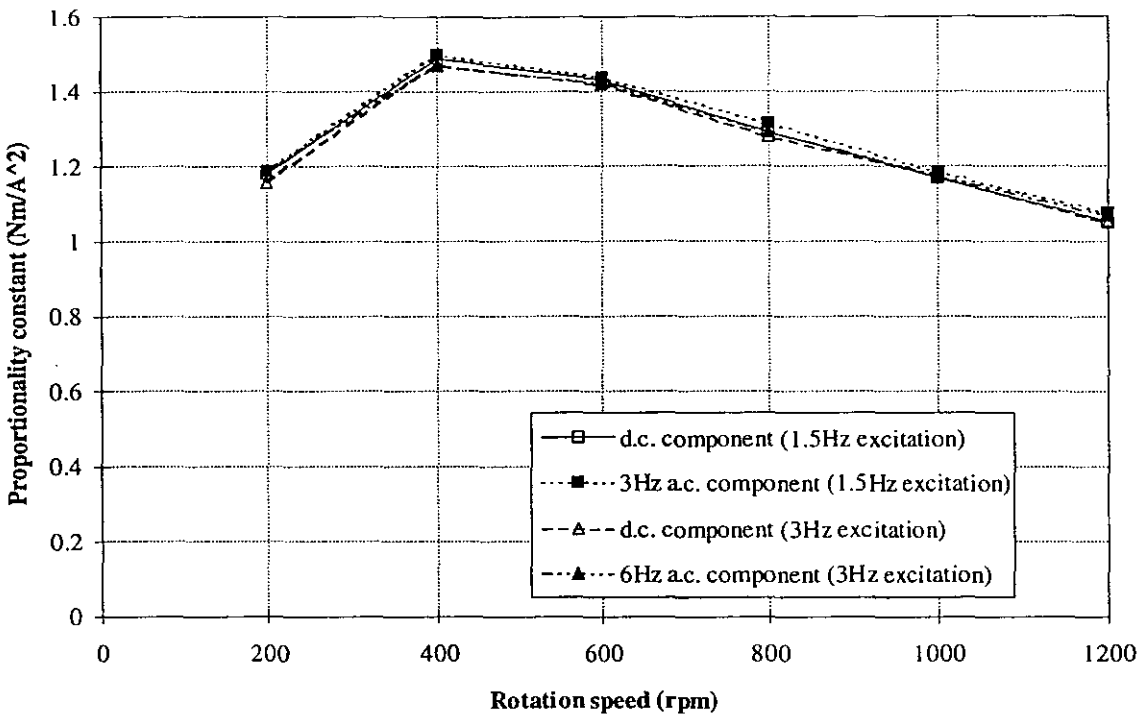

Figure 4.19: Proportionality constant K_N (calibration factor) determined from discrete harmonic (a.c.) torque input across speed range.

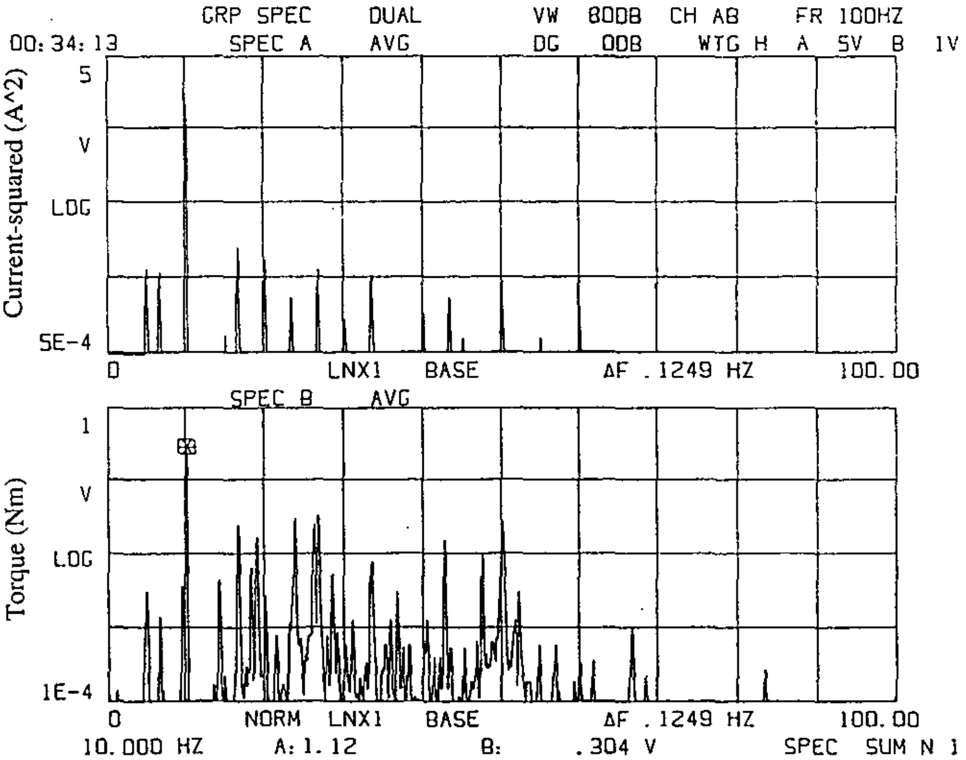

Figure 4.20: Frequency spectra of; a) Electromagnet system current-squared I^2 from circuit, and b) Torque T in shaft. Conditions as for Figure 4.16.

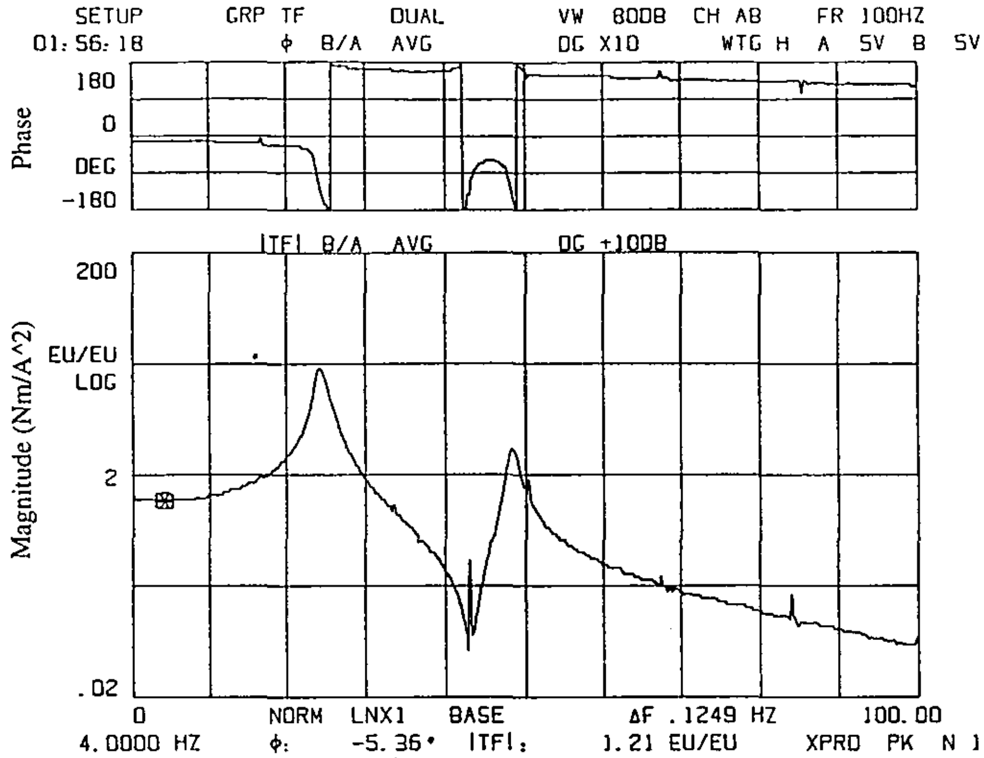

Figure 4.21: Torque/current-squared $\left(T/I^2\right)$ transfer function for calibration of electromagnetic system input. Rotation speed 1000rpm.

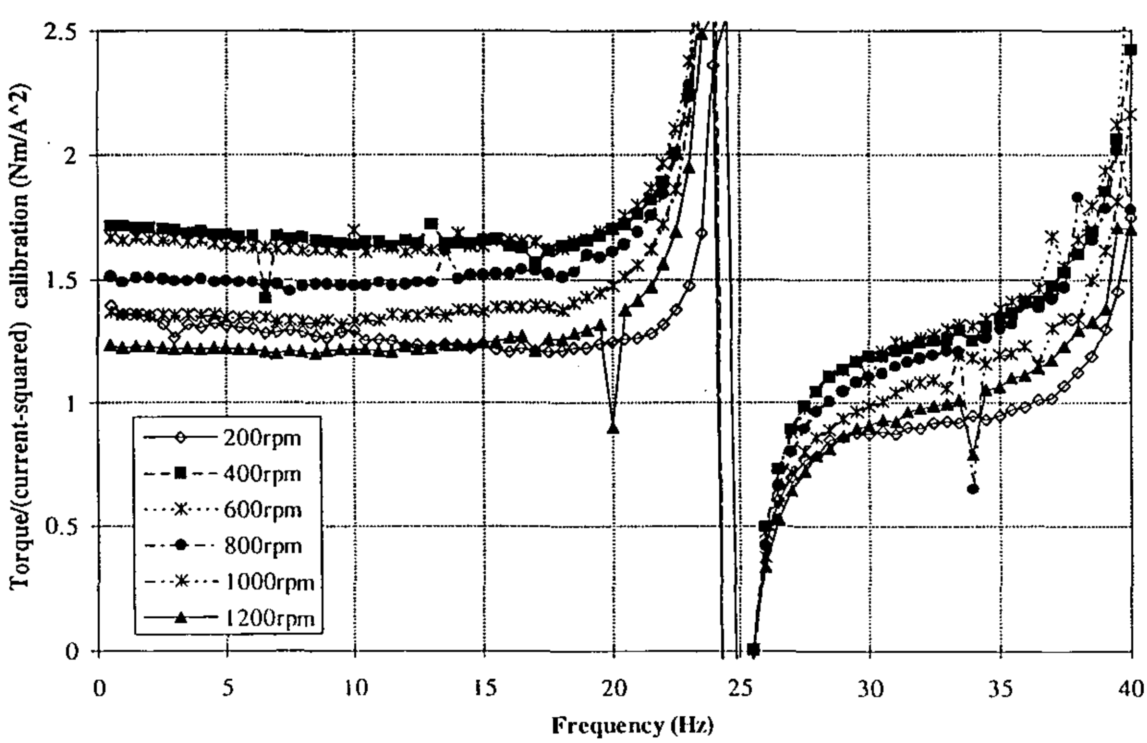

Figure 4.22: Derivation of calibration factor $K_N = \left(T/I^2\right)$ from transfer functions and lumped parameter model.

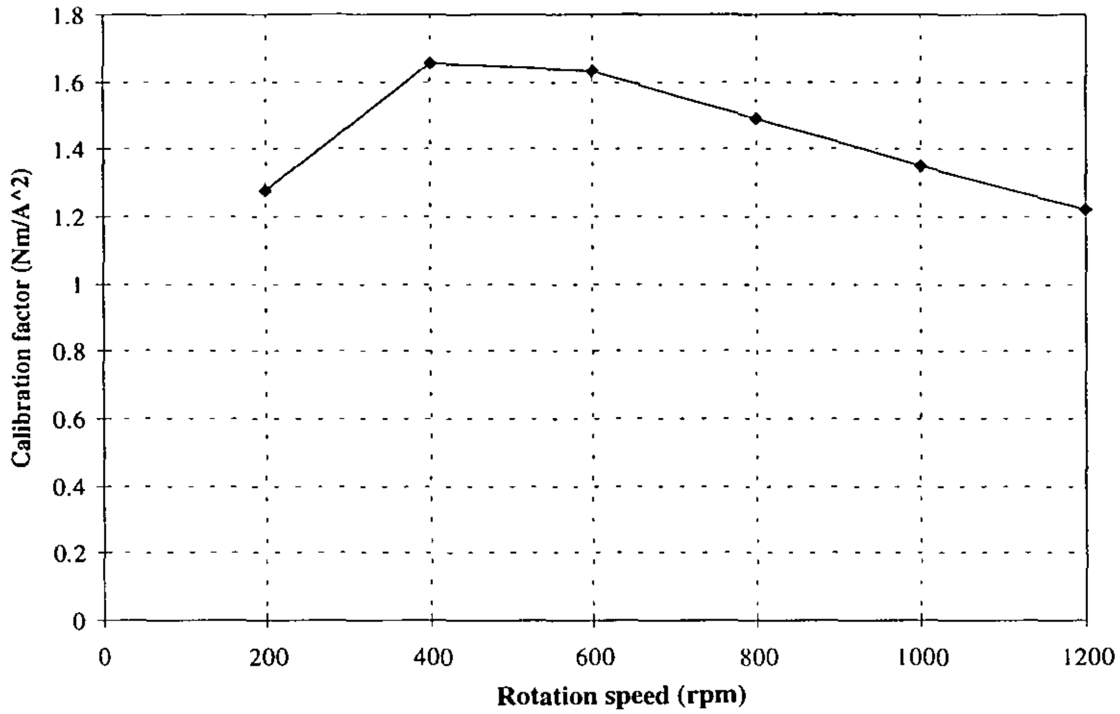

Figure 4.23: Calibration values K_N from transfer functions of input and torque response.

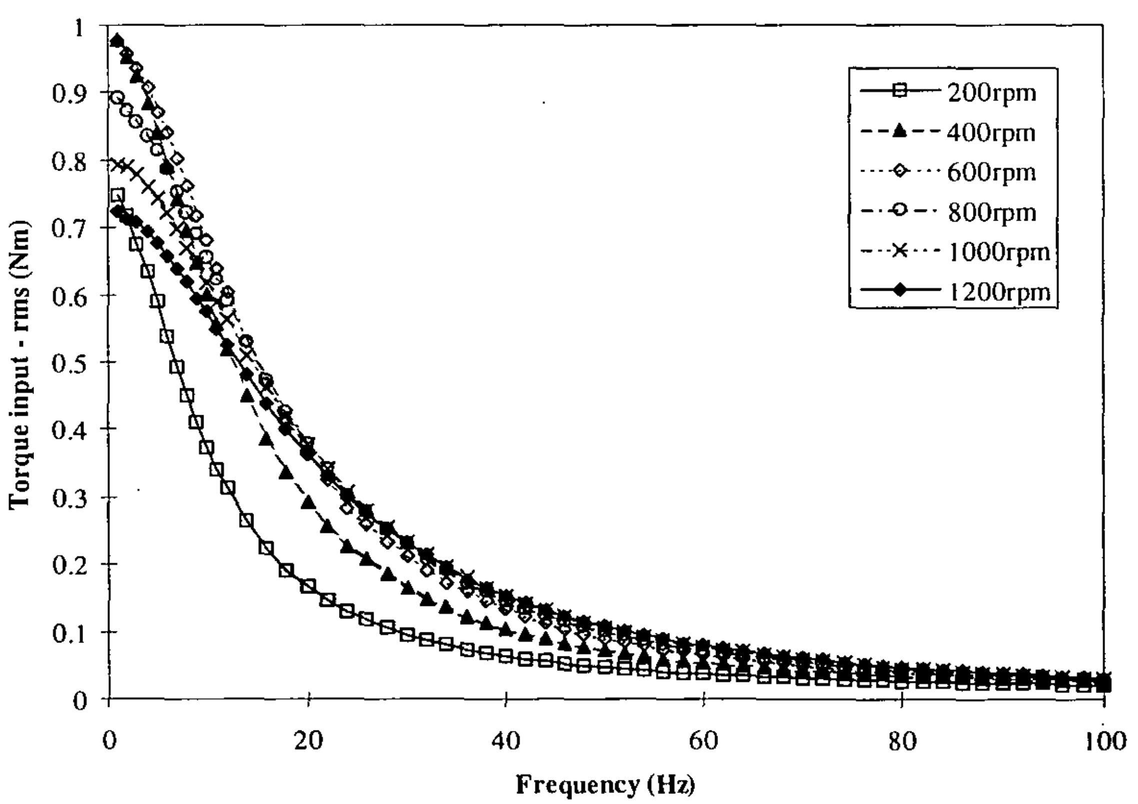

Figure 4.24: Torque magnitude applied to shaft system across frequency range for 60V (pk-pk) input to electromagnets.

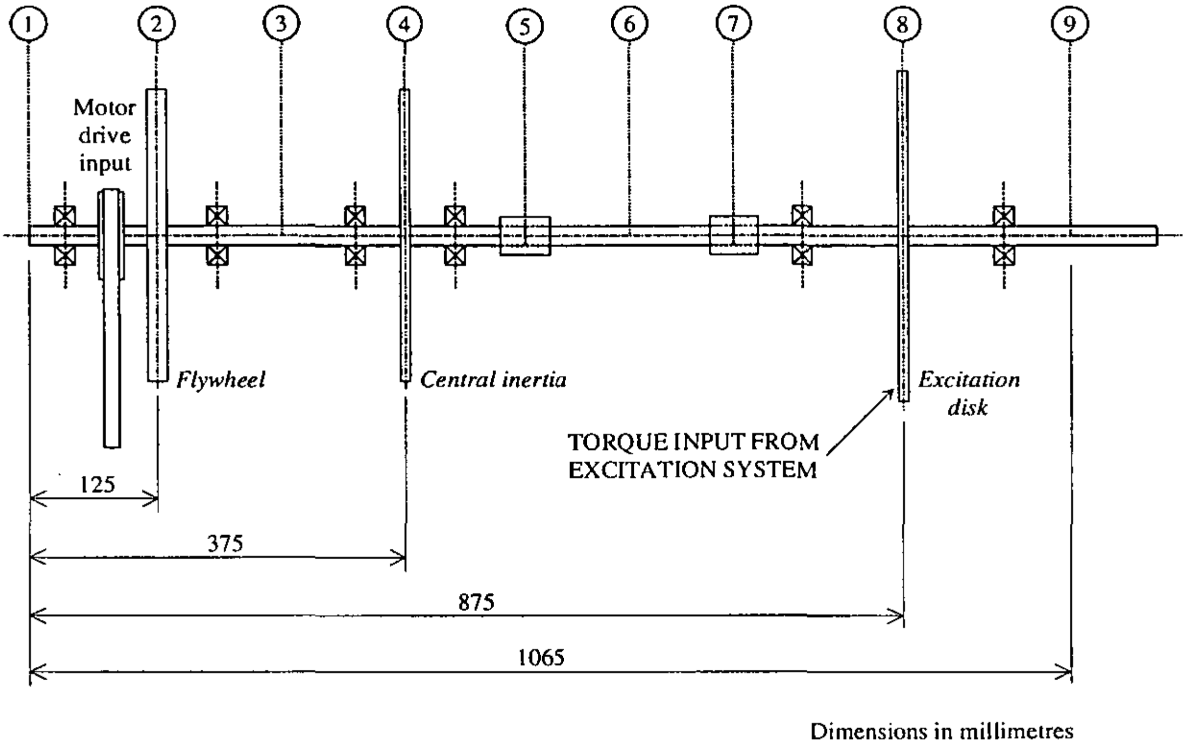

Figure 4.25: Experimental shaft system showing measurement locations.

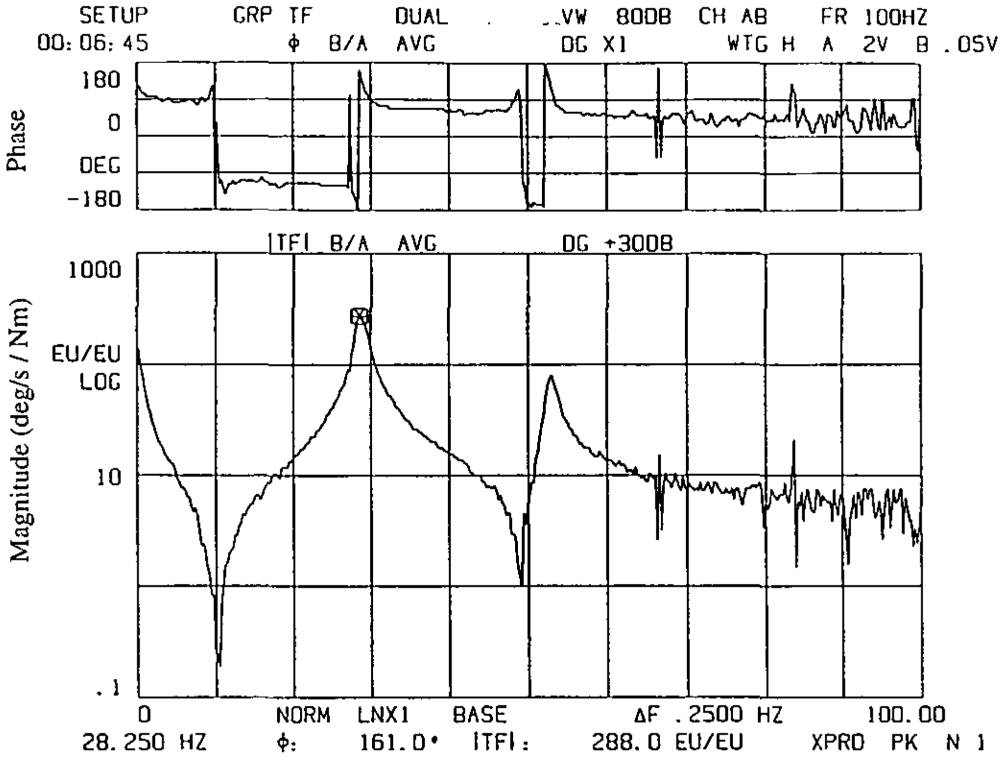

a. Bode plot (Magnitude and phase)

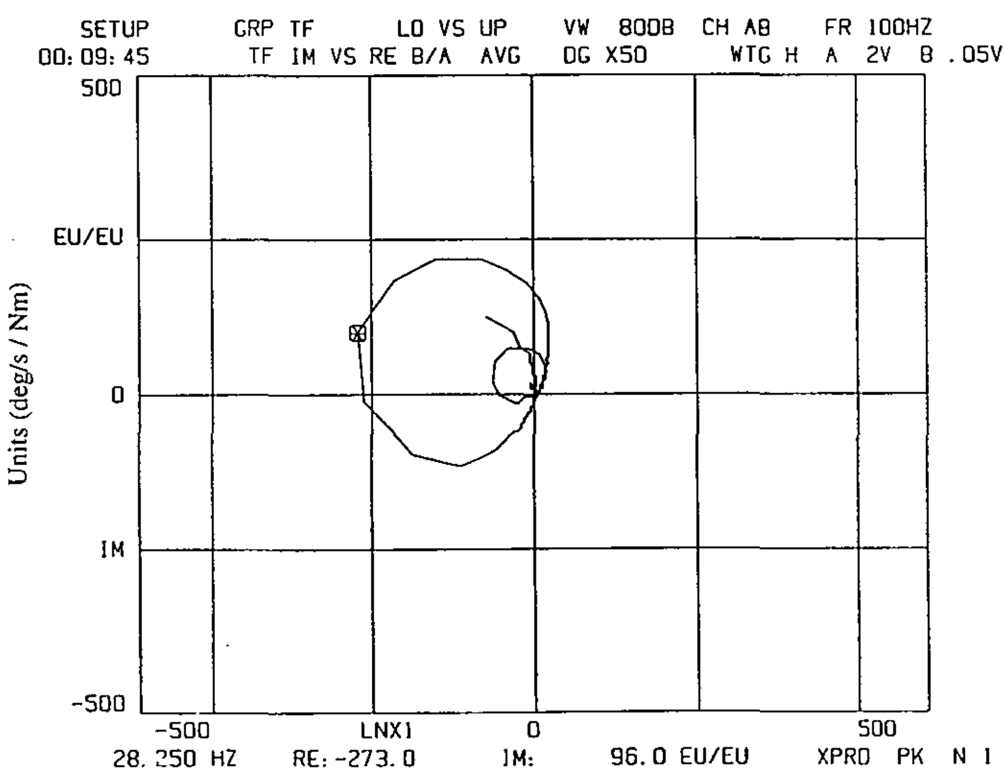

b. Nyquist plot

Figure 4.26: Torsional vibration frequency response function from driving point (location 8). Rotation speed 1000rpm.

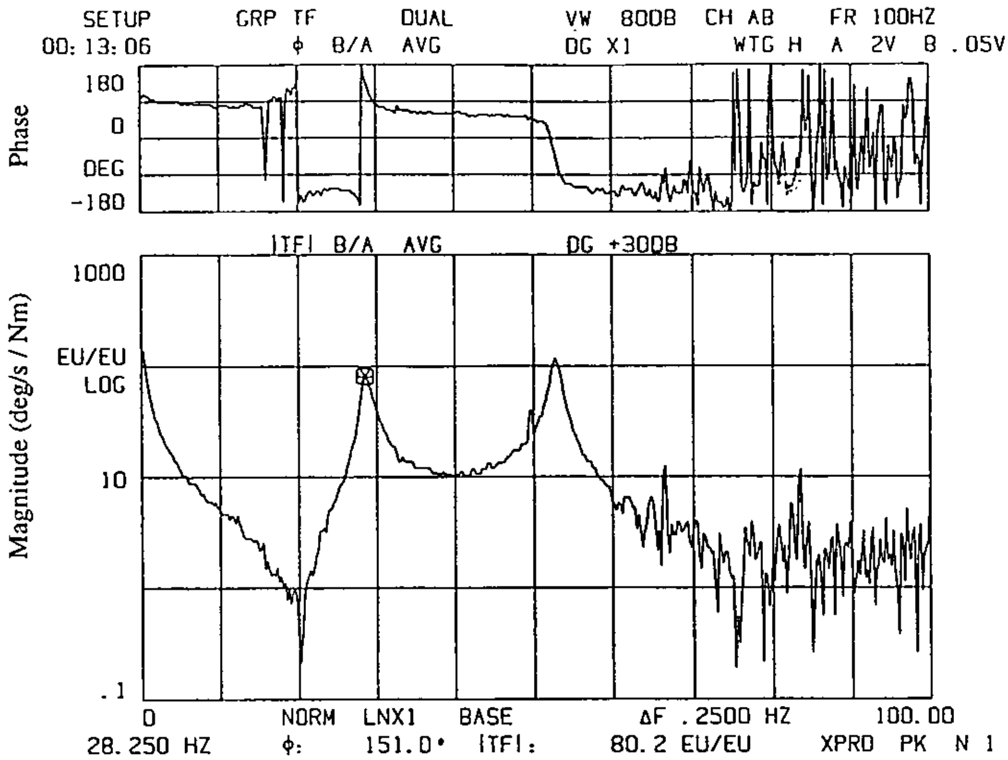

a. Central inertia (location 4)

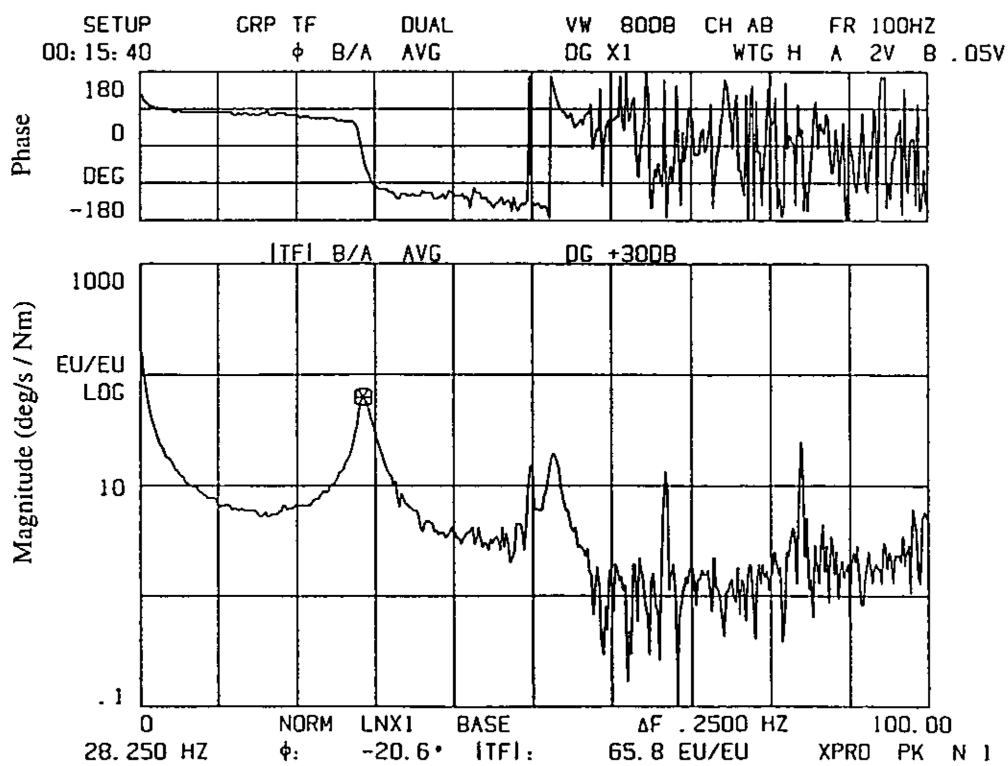

b. Flywheel (location 2)

Figure 4.27: Transfer mobility FRFs from positions along the shaft. Rotation speed 1000rpm.

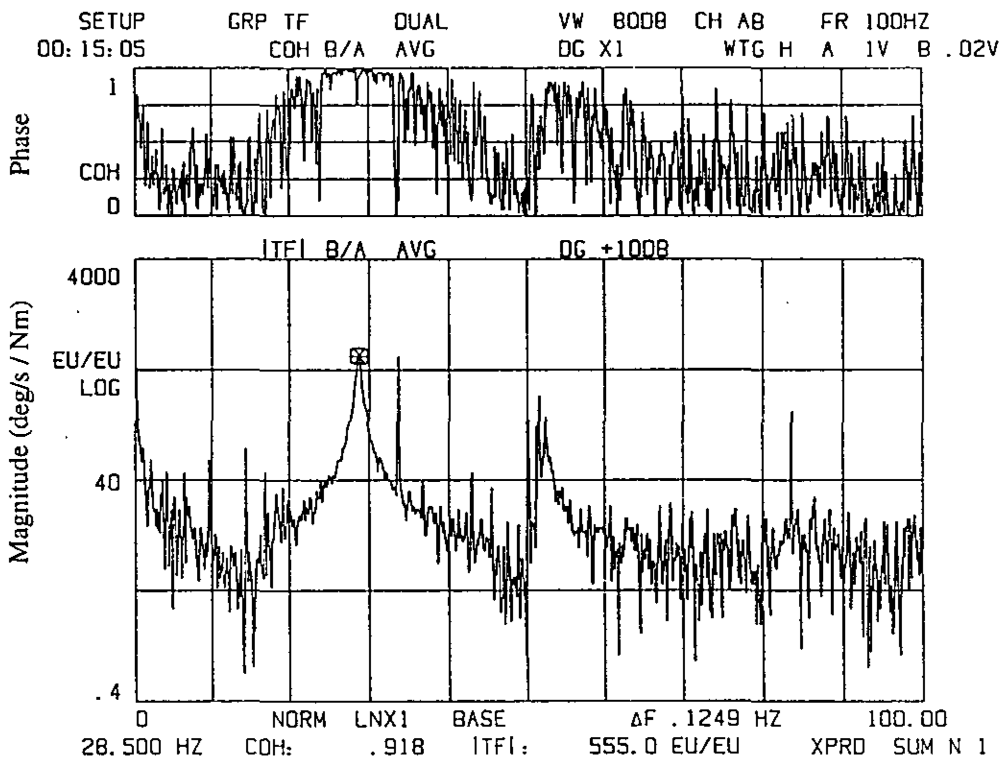

Figure 4.28: FRF from driving point with 'pseudo-random' excitation.
Rotation speed 1000rpm.

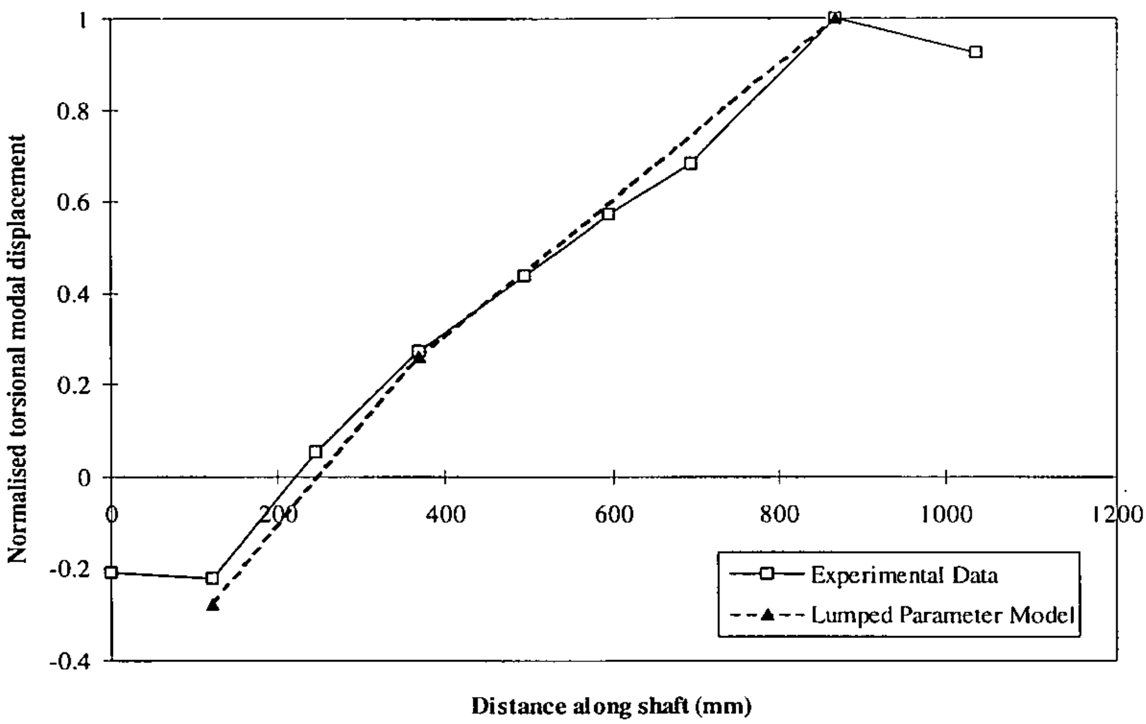

a. Mode I at 28.29Hz

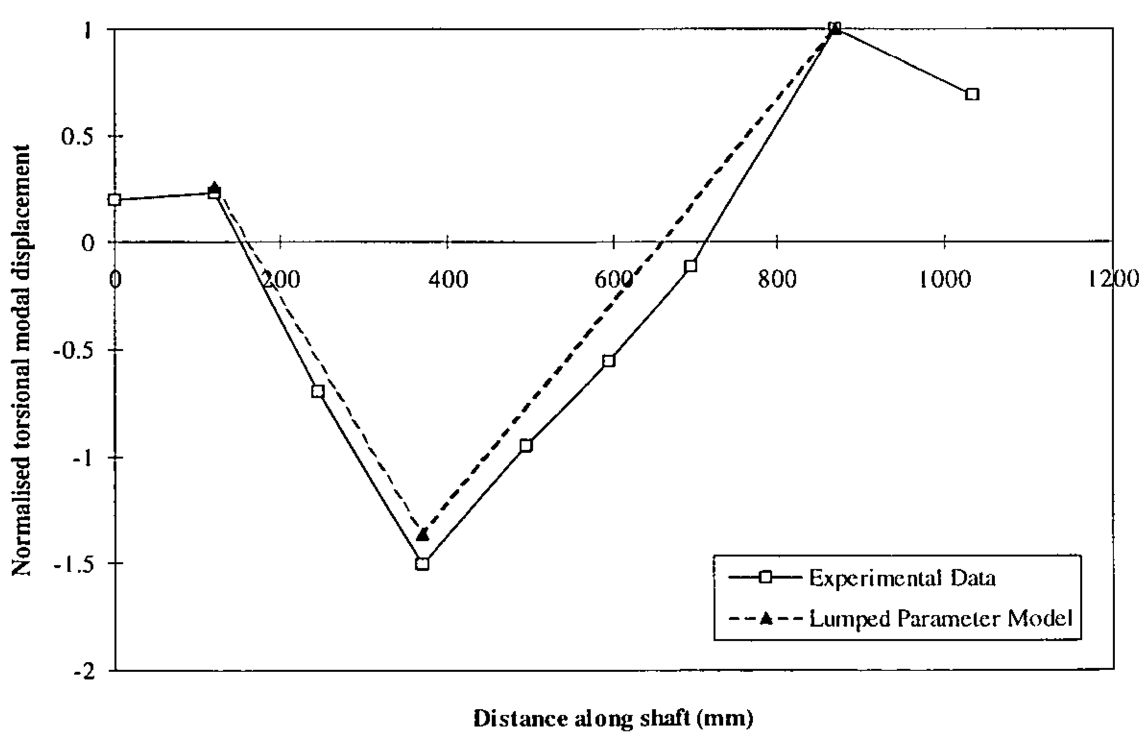

b. Mode II at 52.51Hz

Figure 4.29: Torsional mode shapes obtained for the first two natural frequencies of the shaft system.

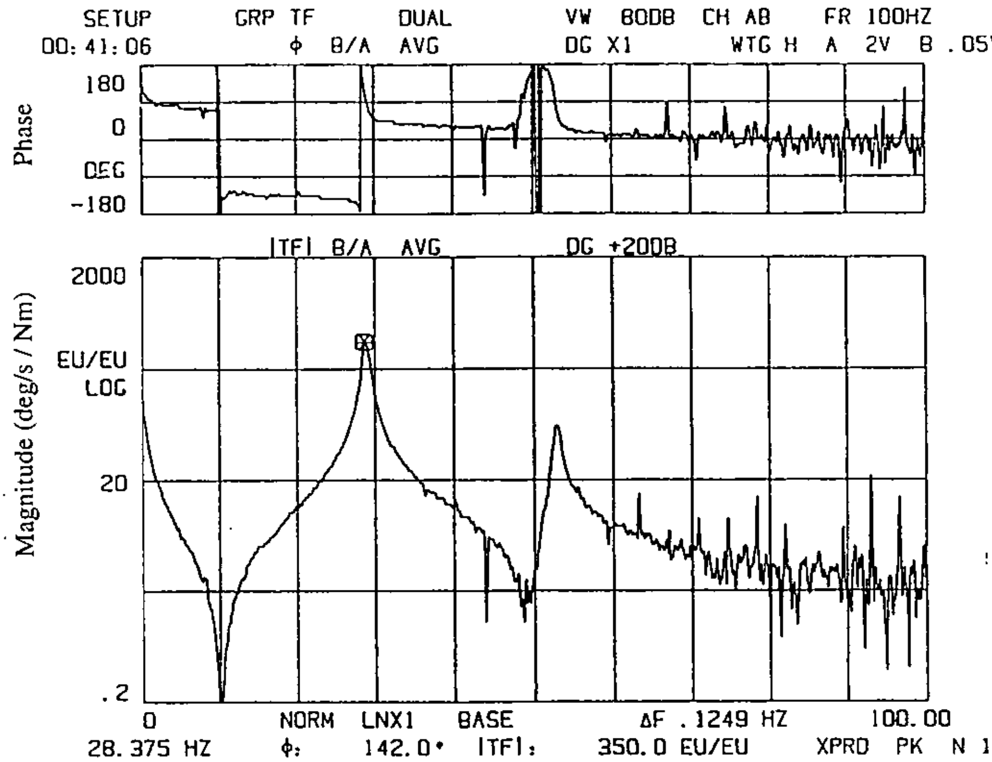

a. 200rpm.

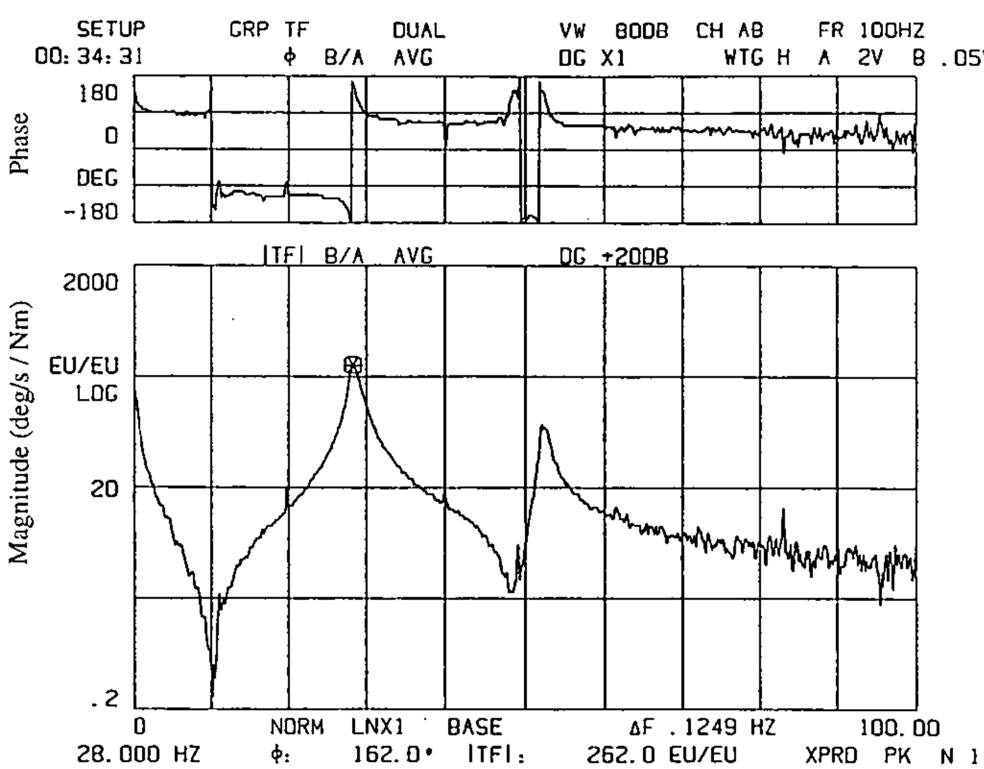

b. 1200rpm.

Figure 4.30: FRFs from the driving point at different rotation speeds.

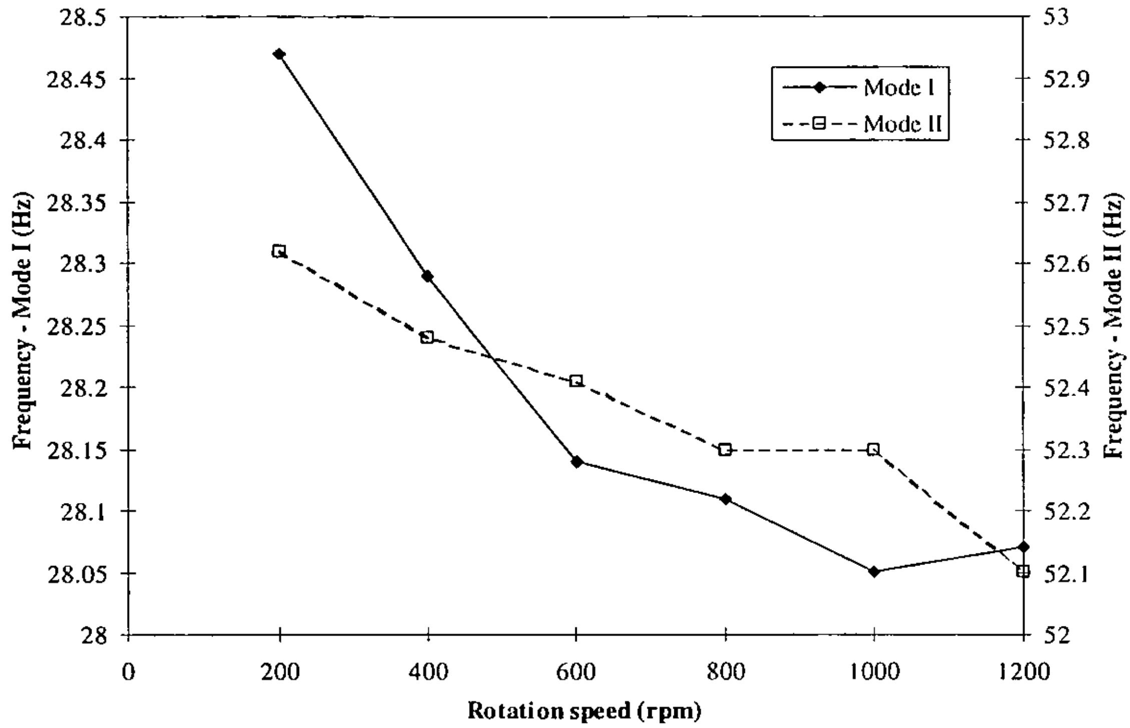

a. Modal frequency.

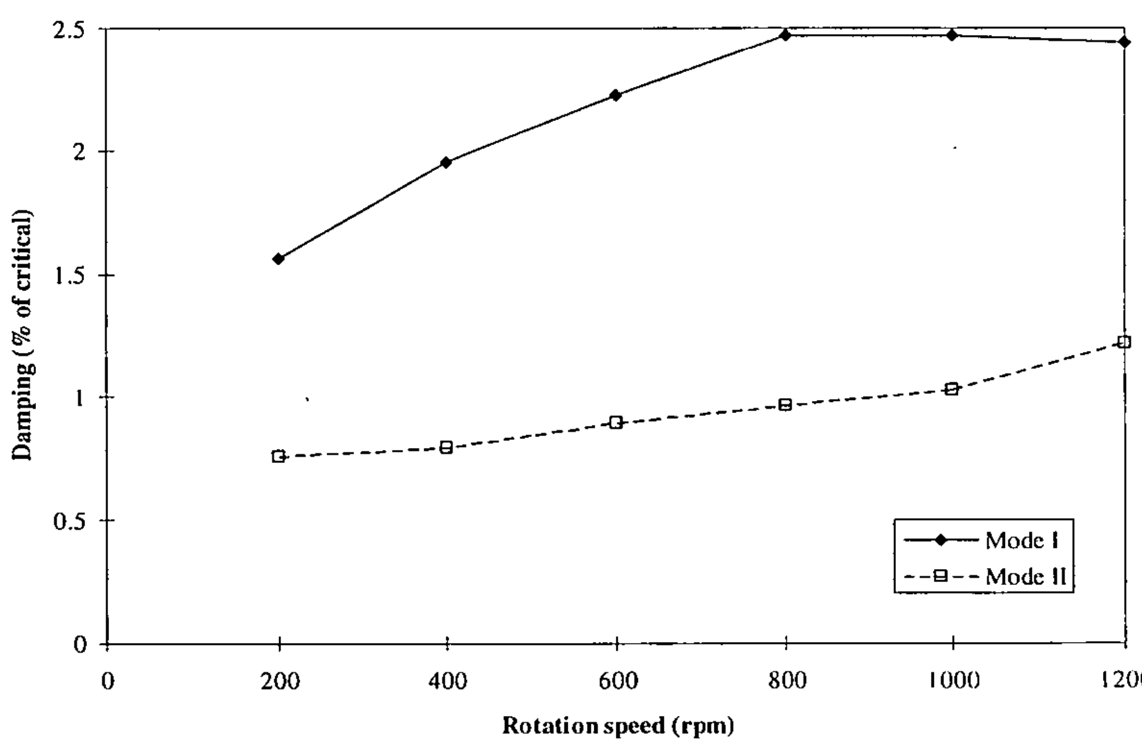

b. Modal damping.

Figure 4.31: Variation of modal parameters with rotation speed.

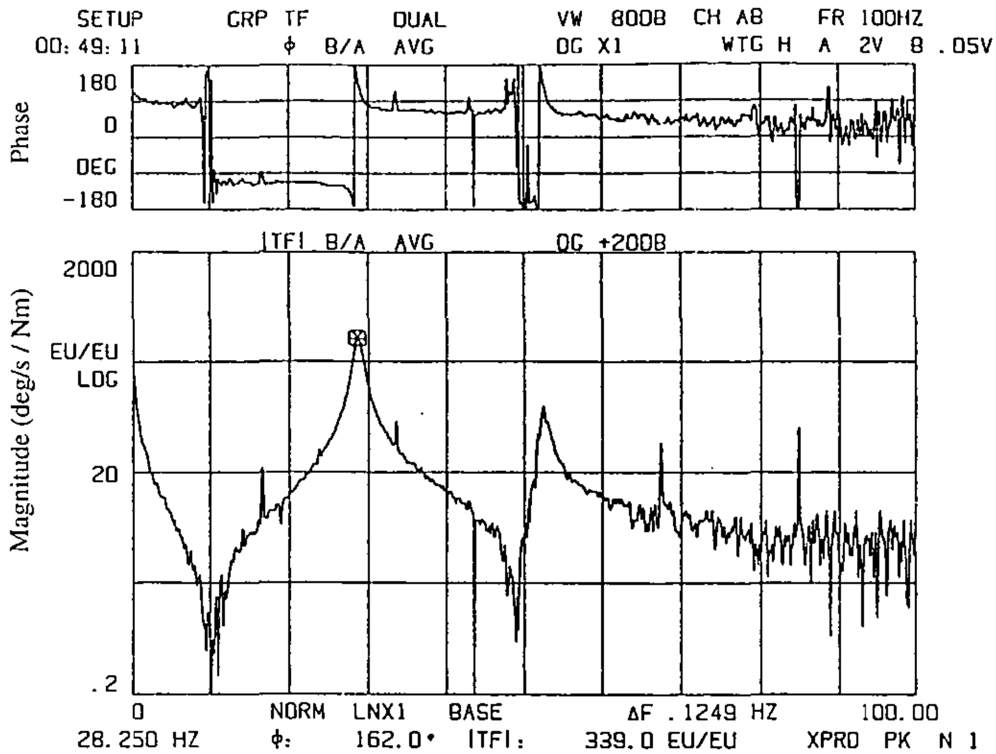

a. 40V (pk-pk)

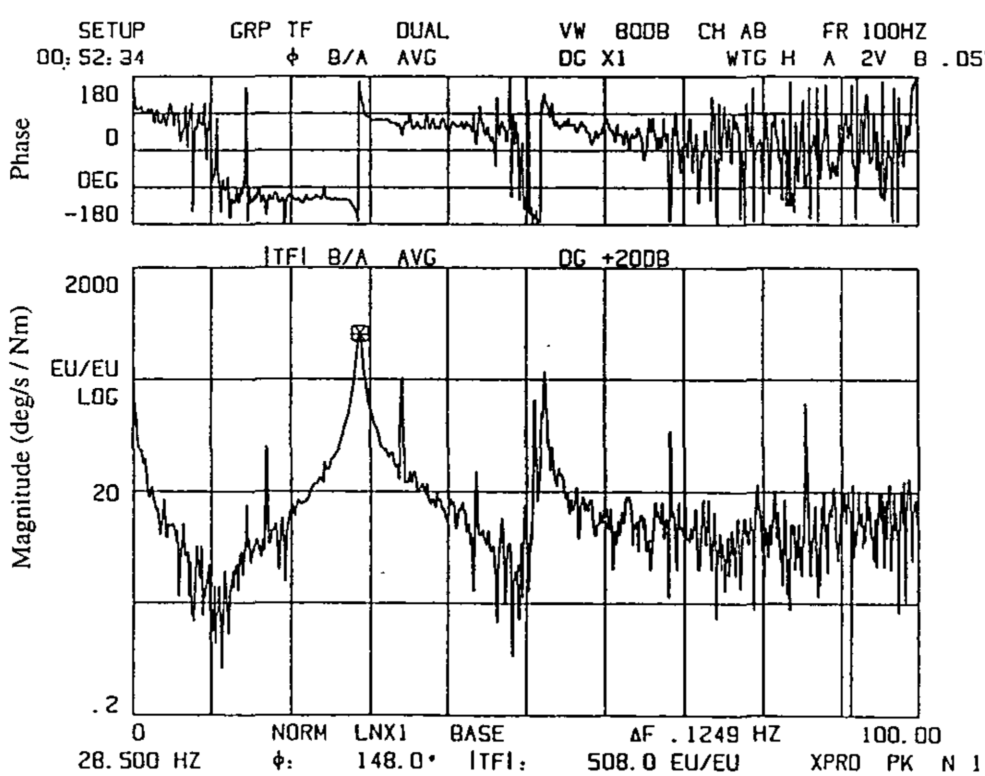

b. 20V (pk-pk)

Figure 4.32: FRFs from the driving point at rotation speed of 1000rpm with different applied excitation voltage.

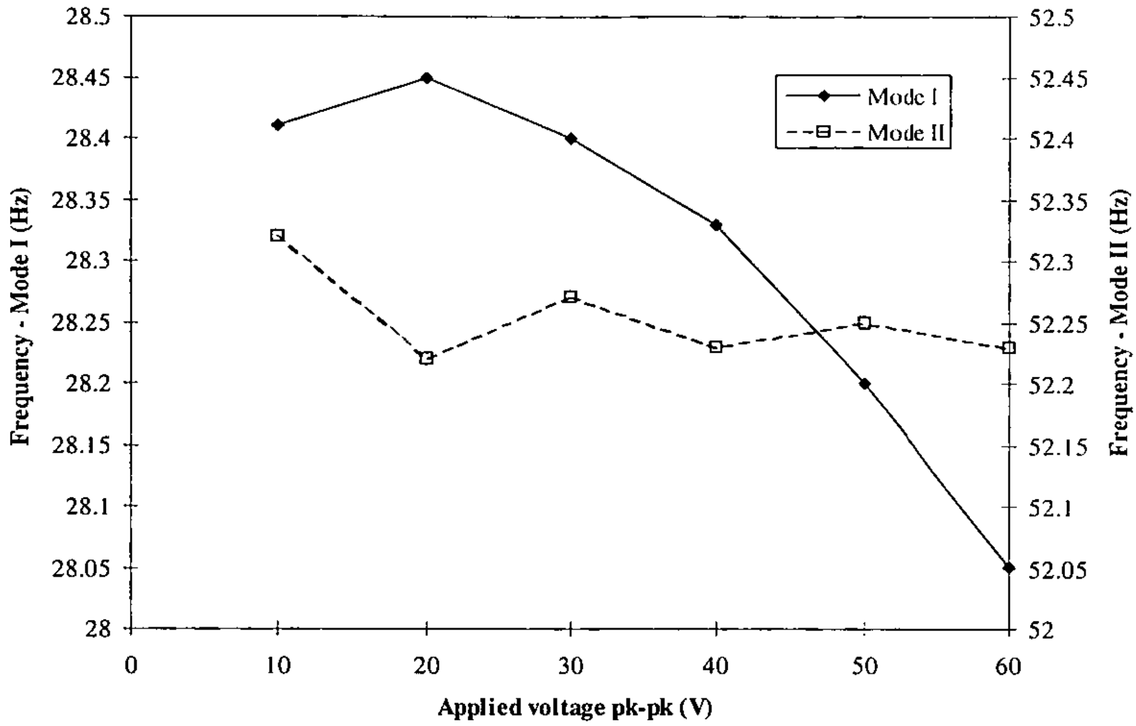

a. Modal frequency.

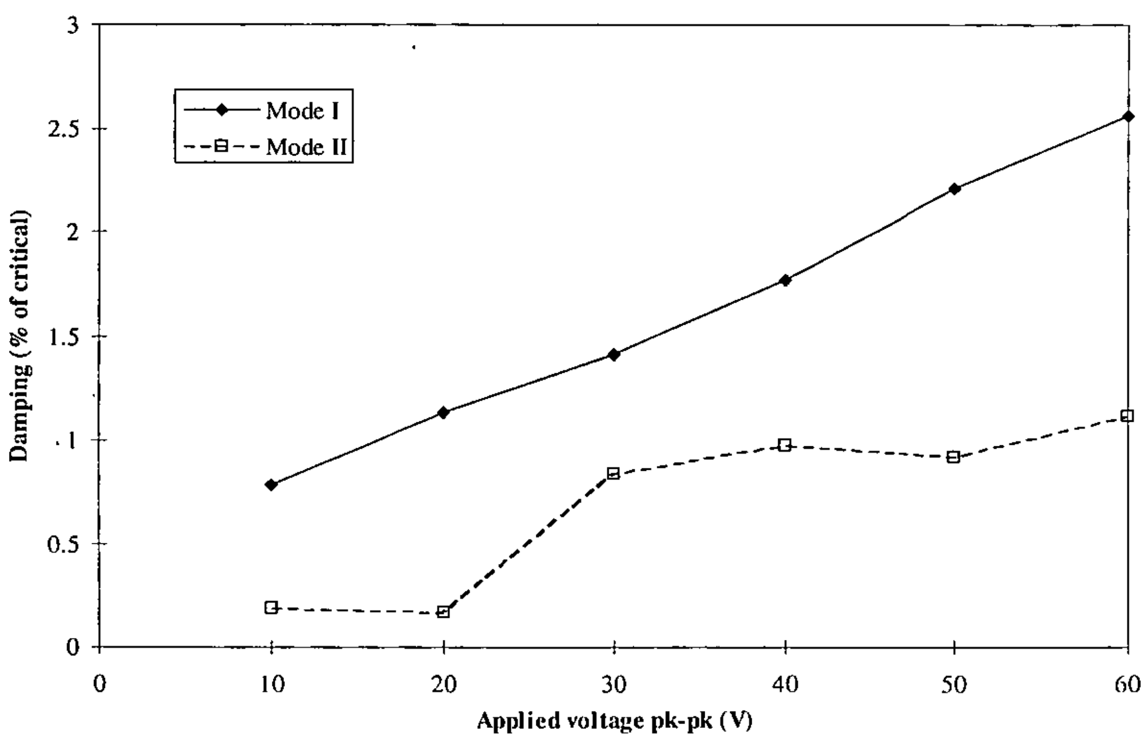

b. Modal damping.

Figure 4.33: Variation of modal parameters with applied excitation voltage.

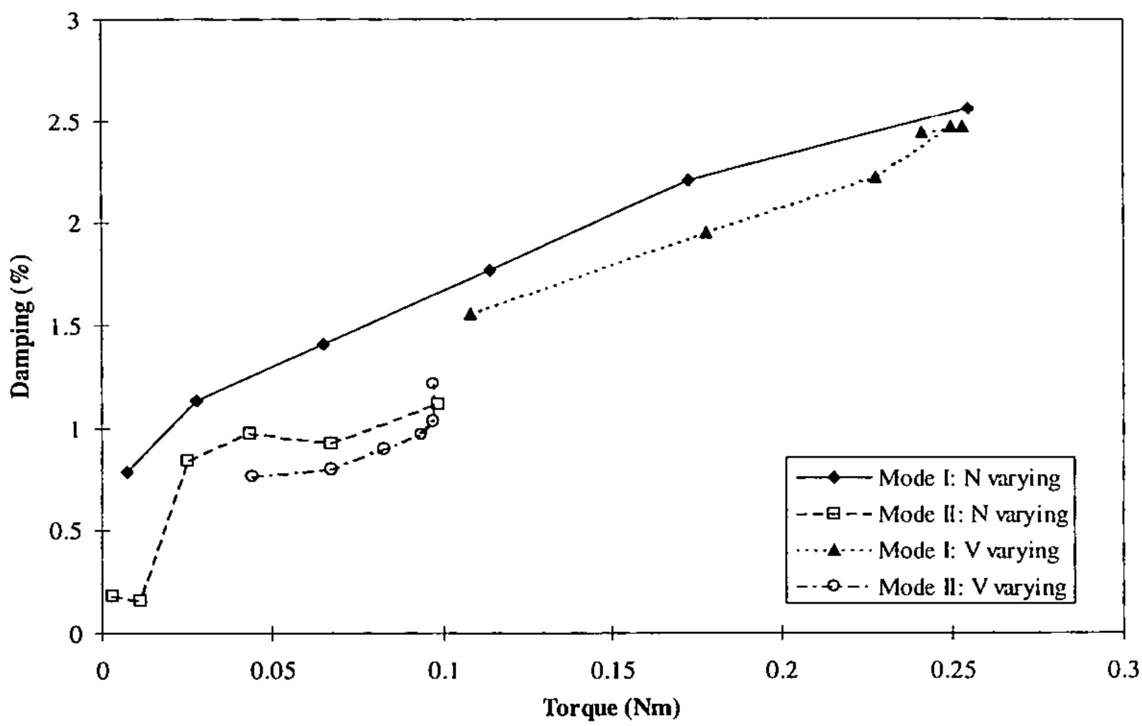

Figure 4.34: Variation of modal damping with excitation torque.

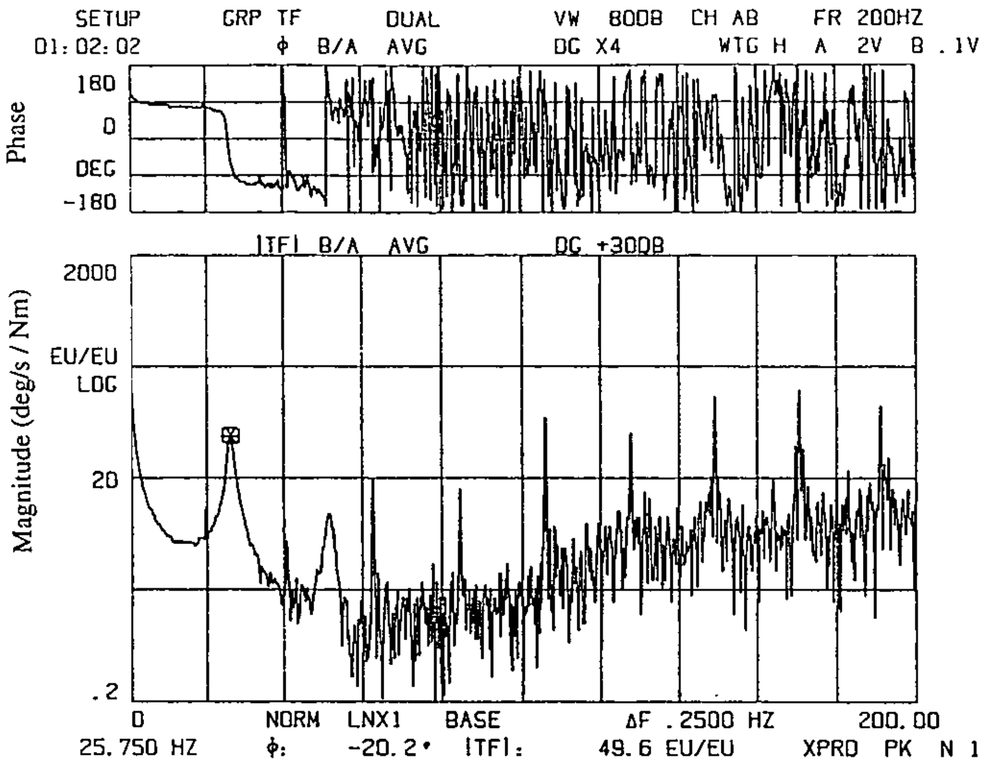

a. Drive input end of the main shaft (location 1).

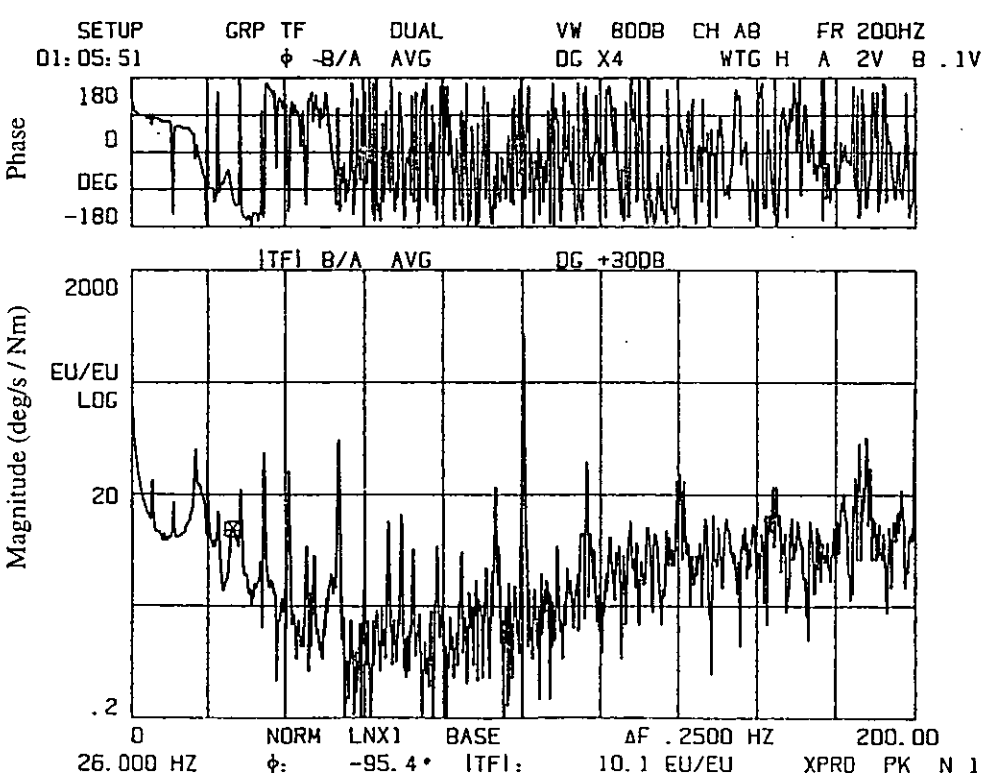

b. Motor pulley.

Figure 4.35: FRFs demonstrating the participation of the motor in the four inertia shaft system vibration. Rotation speed 1200rpm.

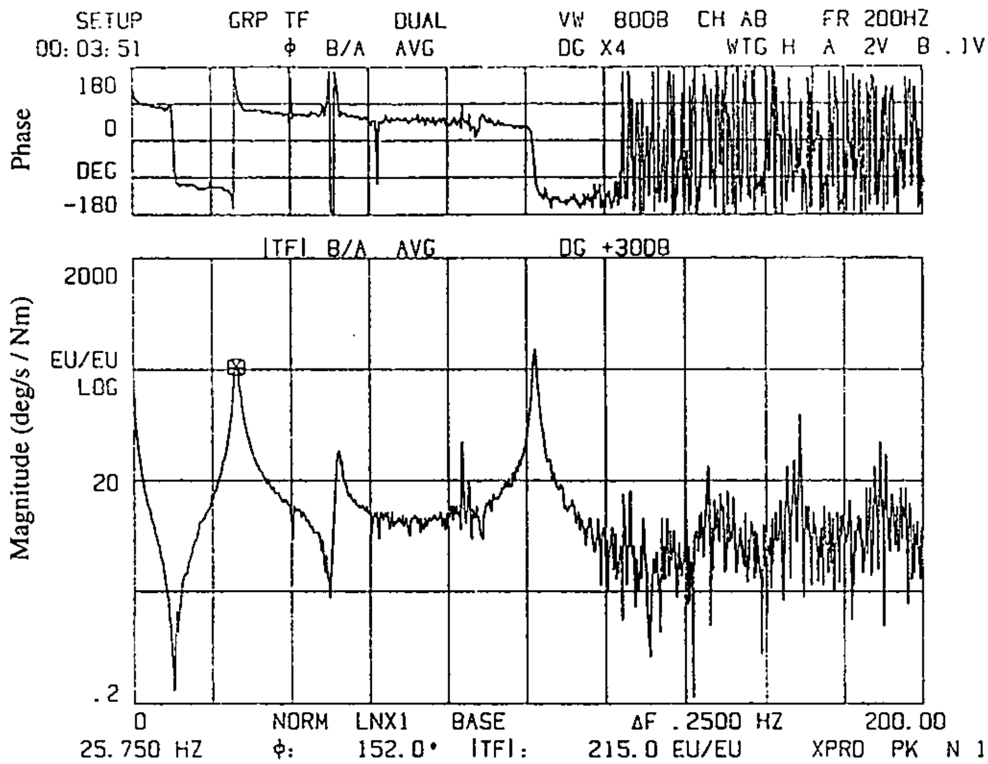

a. Fourth inertia on shaft end (location 9)

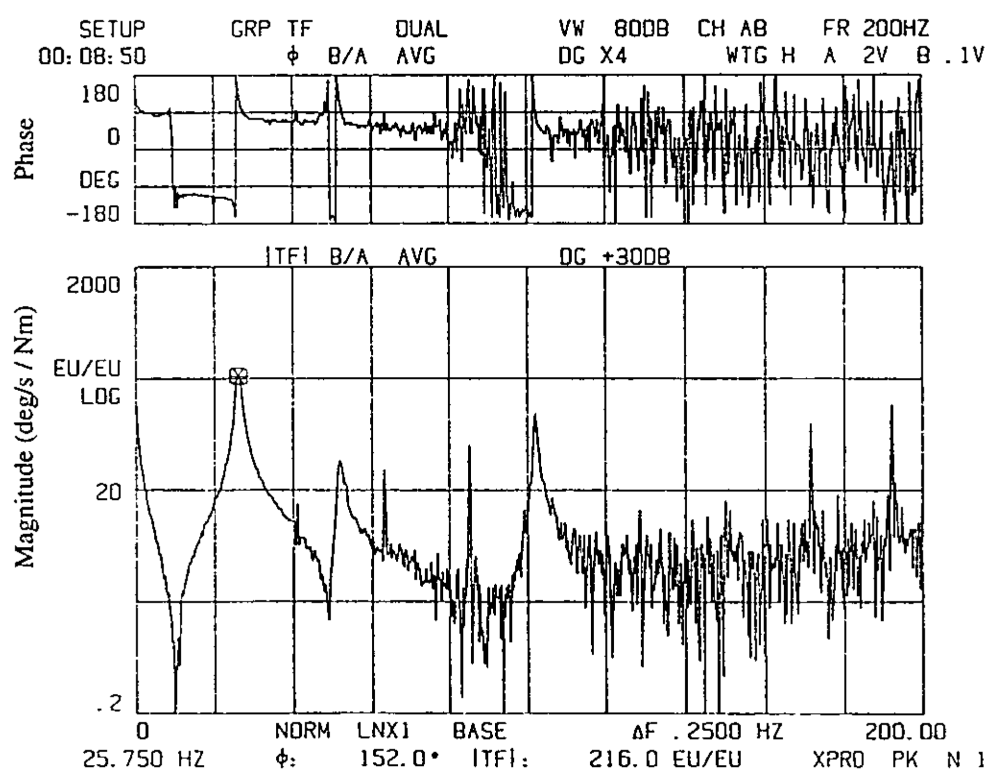

b. Excitation disk (location 8)

Figure 4.36: FRFs from four-inertia system at various locations. Rotation speed 1200rpm.

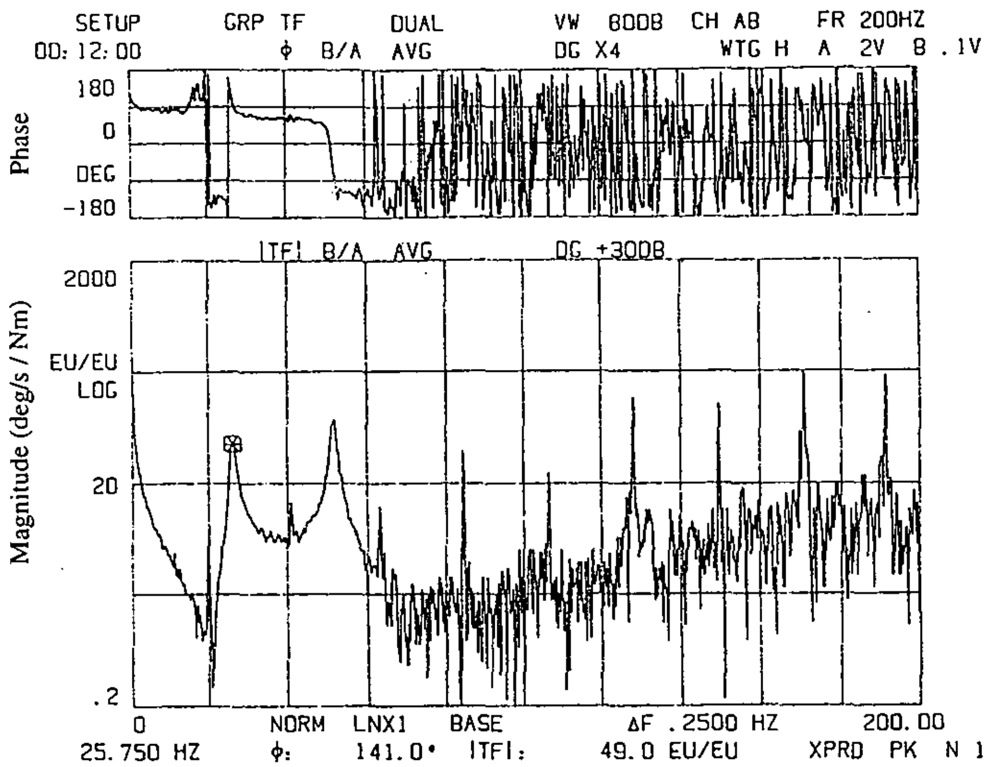

c. Central inertia (location 4)

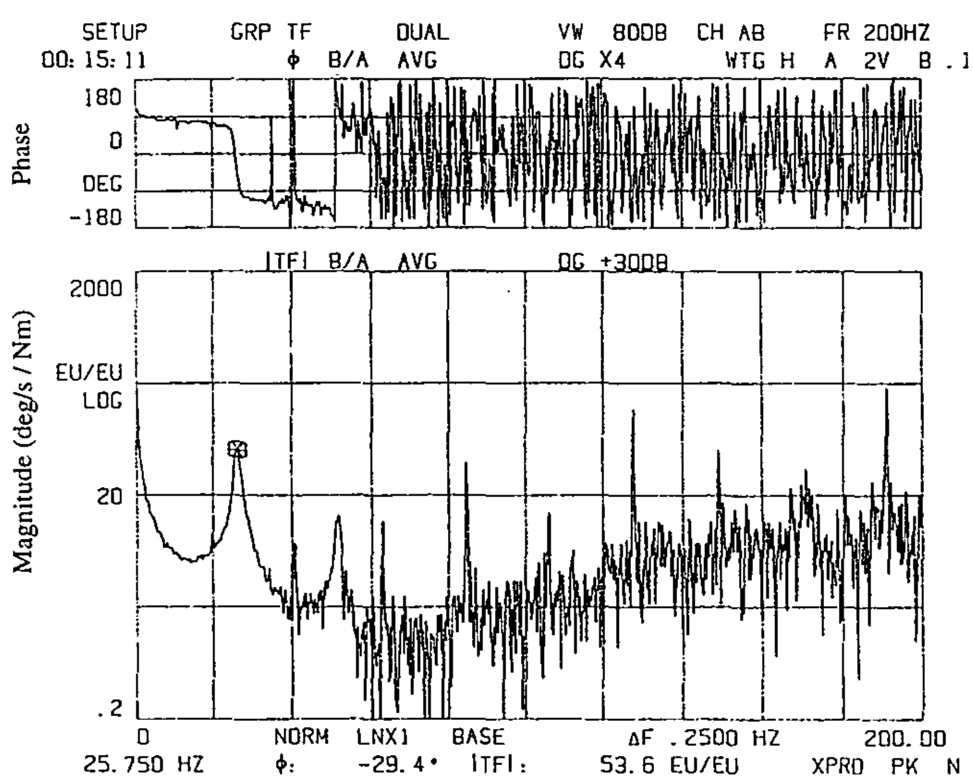

d. Flywheel (location 2)

Figure 4.36(cont.): FRFs from four-inertia system at various locations. Rotation speed 1200rpm.

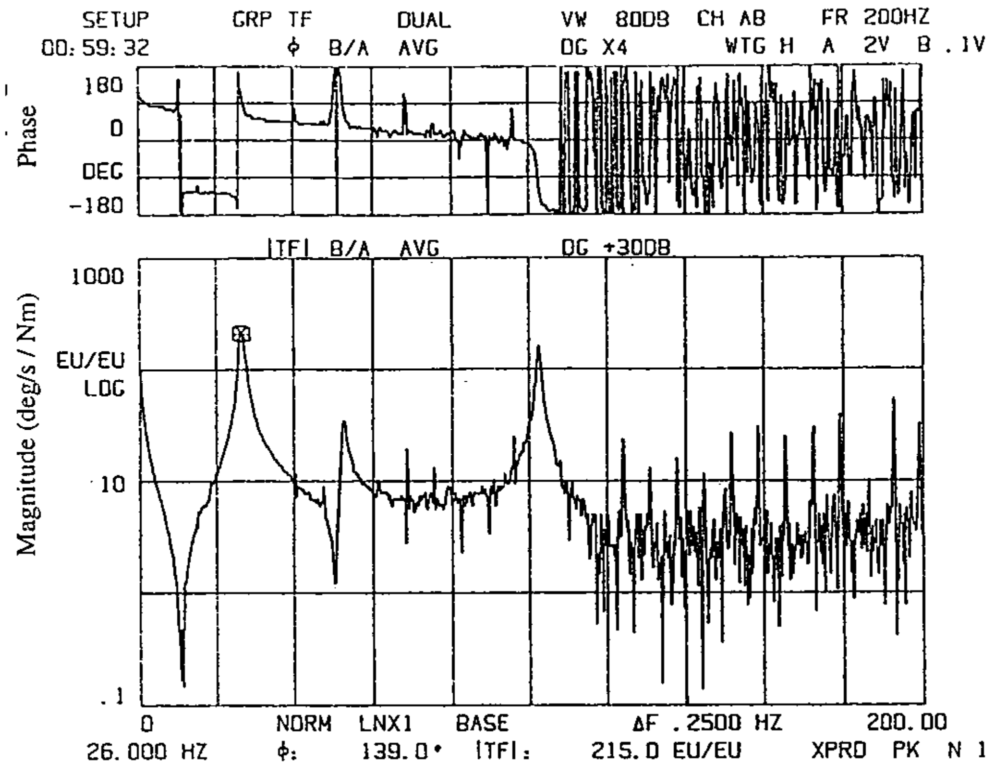

a. Fourth inertia on shaft end (location 9)

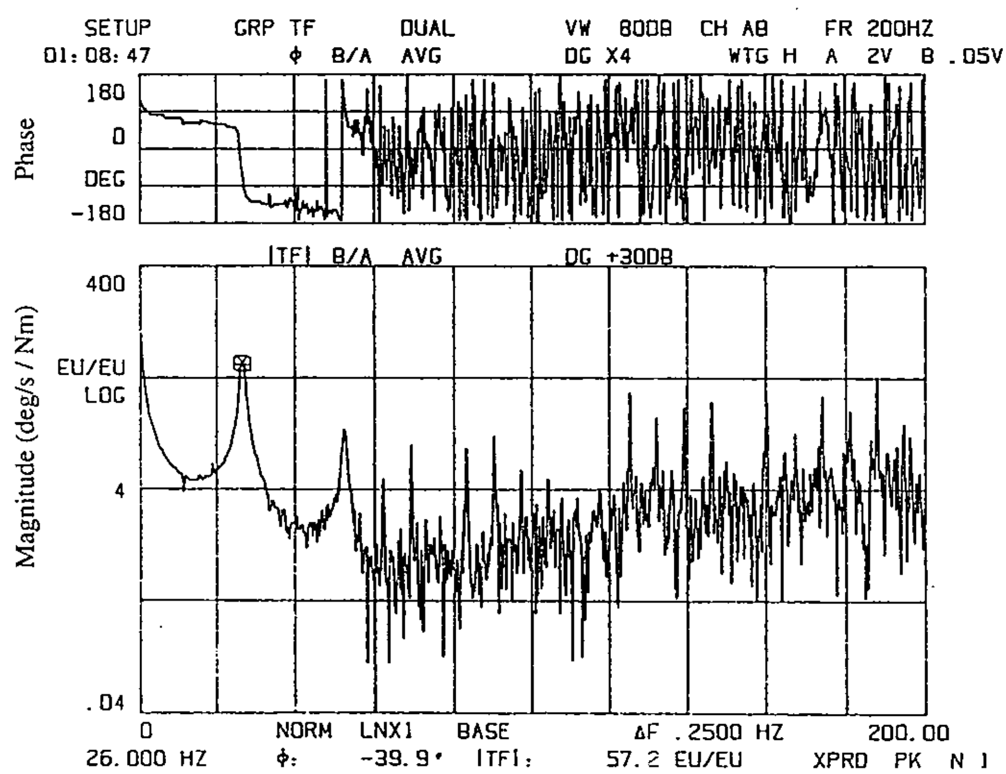

b. Flywheel (location 2)

Figure 4.37: FRFs from four-inertia system at various locations. Rotation speed 400rpm.

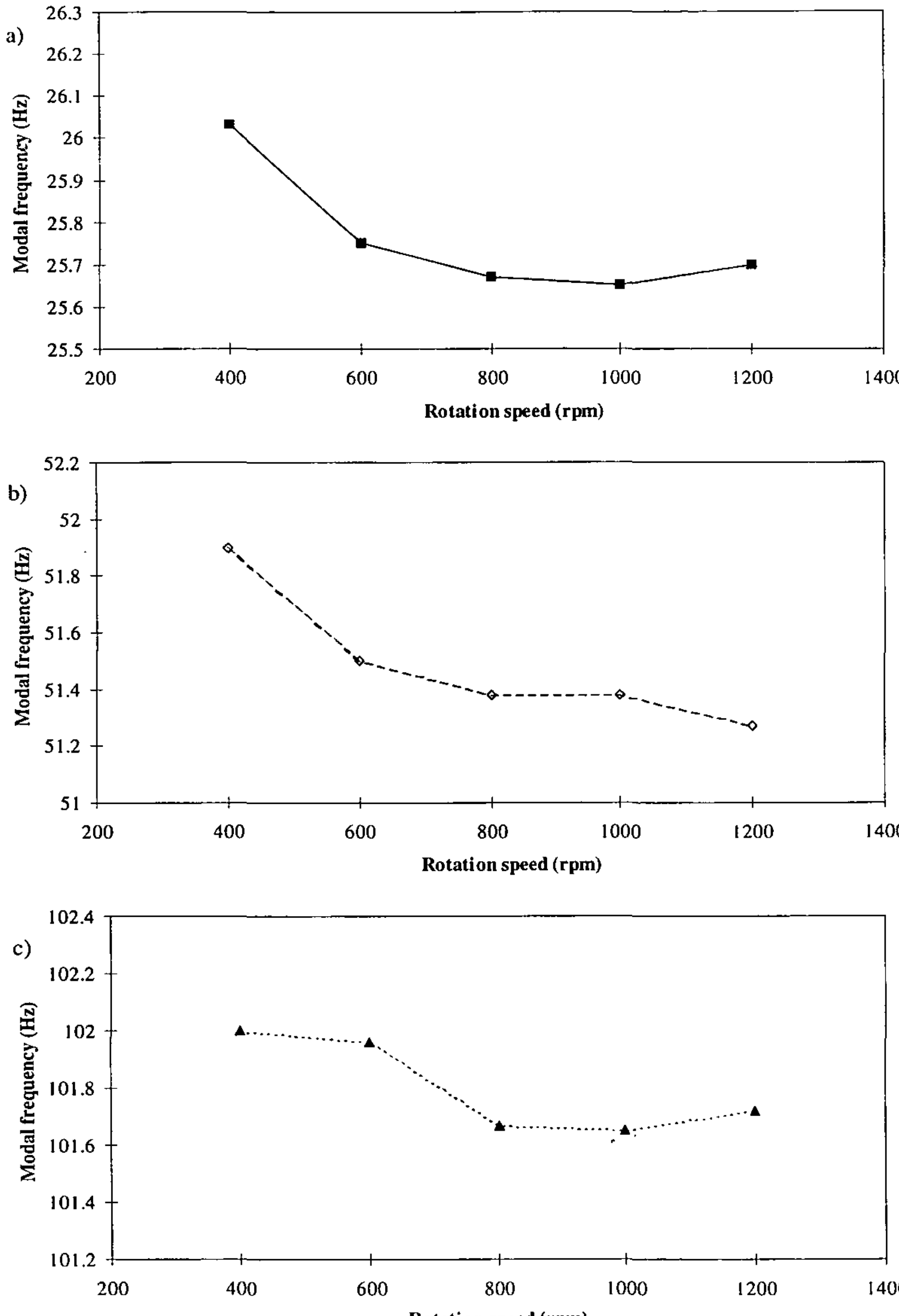

Figure 4.38: Variation of modal frequency with rotation speed for four-inertia system.
a. Mode I, b. Mode II, c. Mode III.

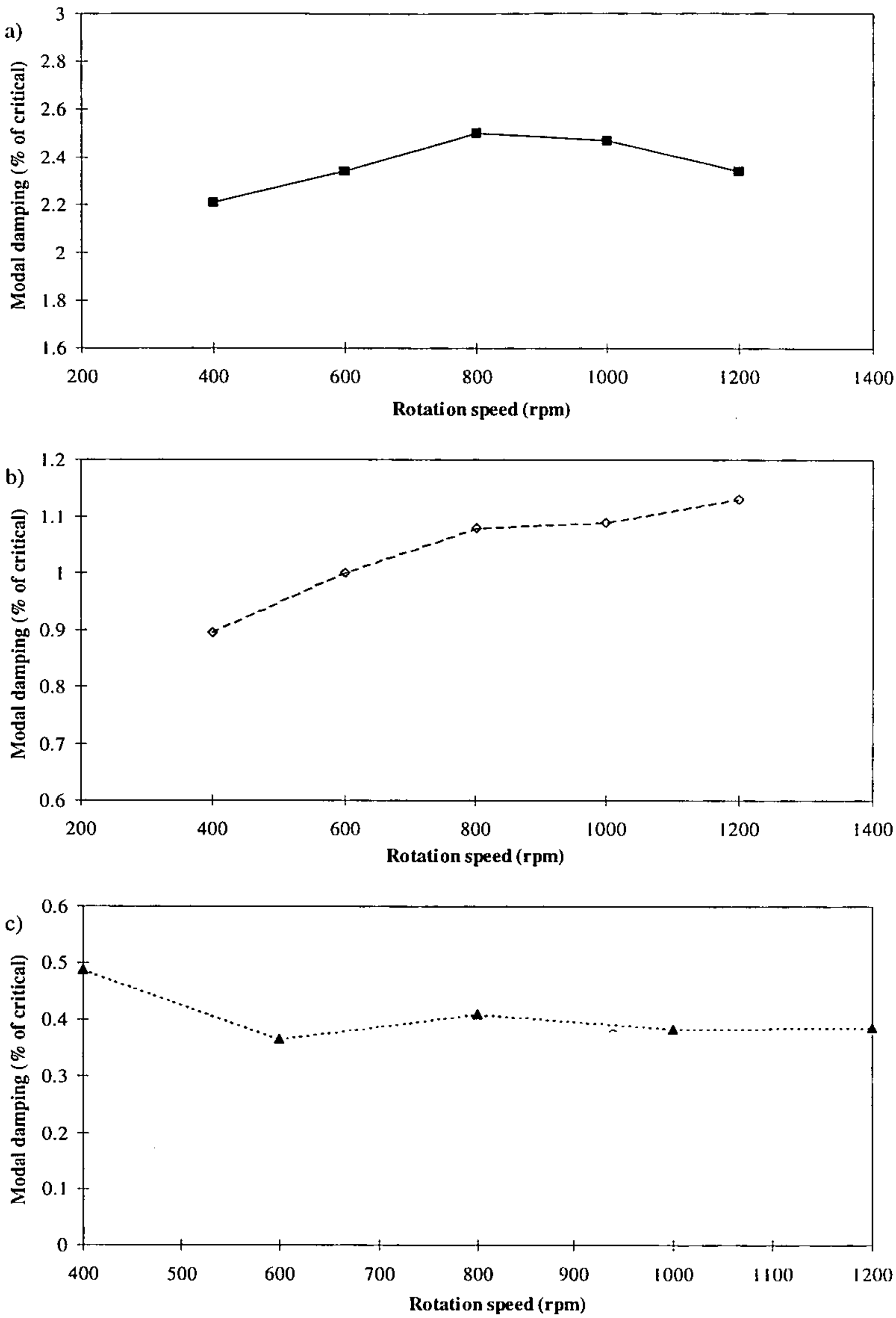

Figure 4.39: Variation of modal damping with rotation speed for four inertia shaft system. a. Mode I, b. Mode II, c. Mode III.

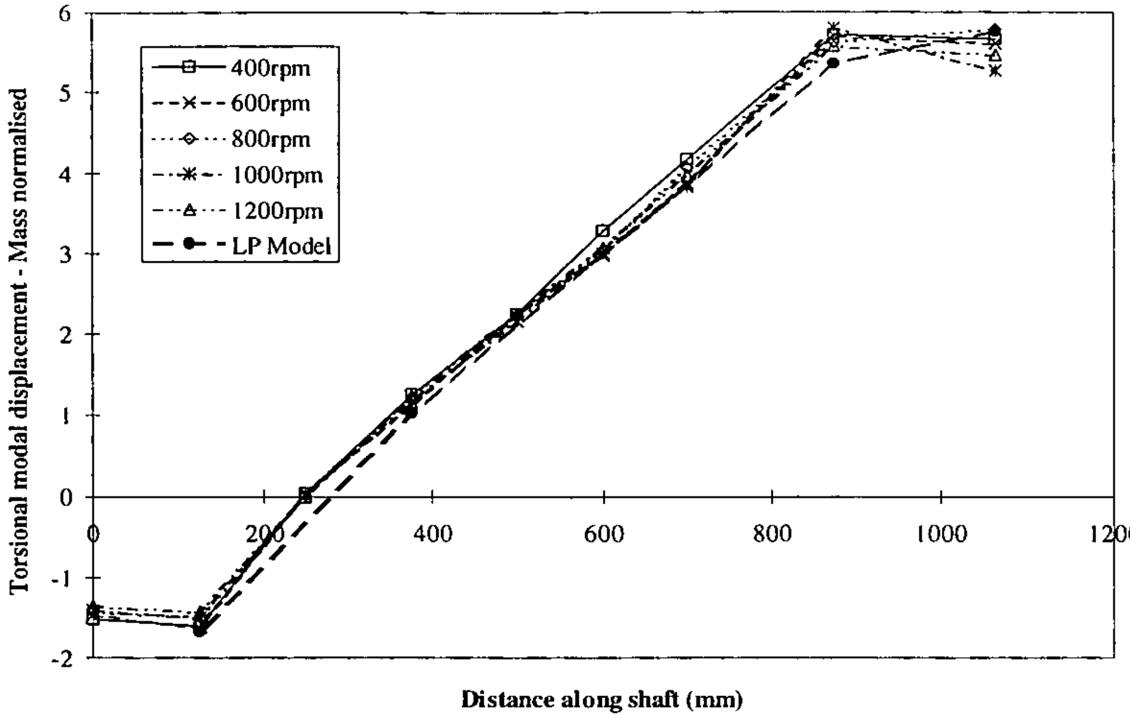

a. Mode I

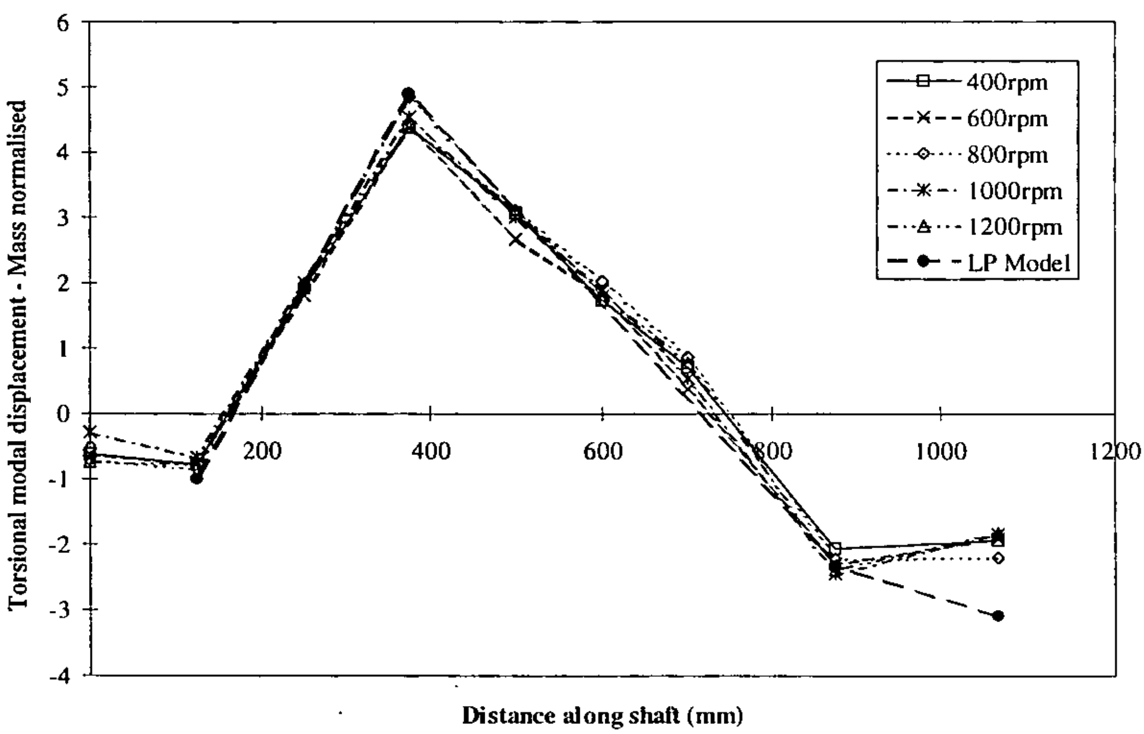

b. Mode II

Figure 4.40: Torsional mode shapes obtained for the natural frequencies of the four inertia shaft system.

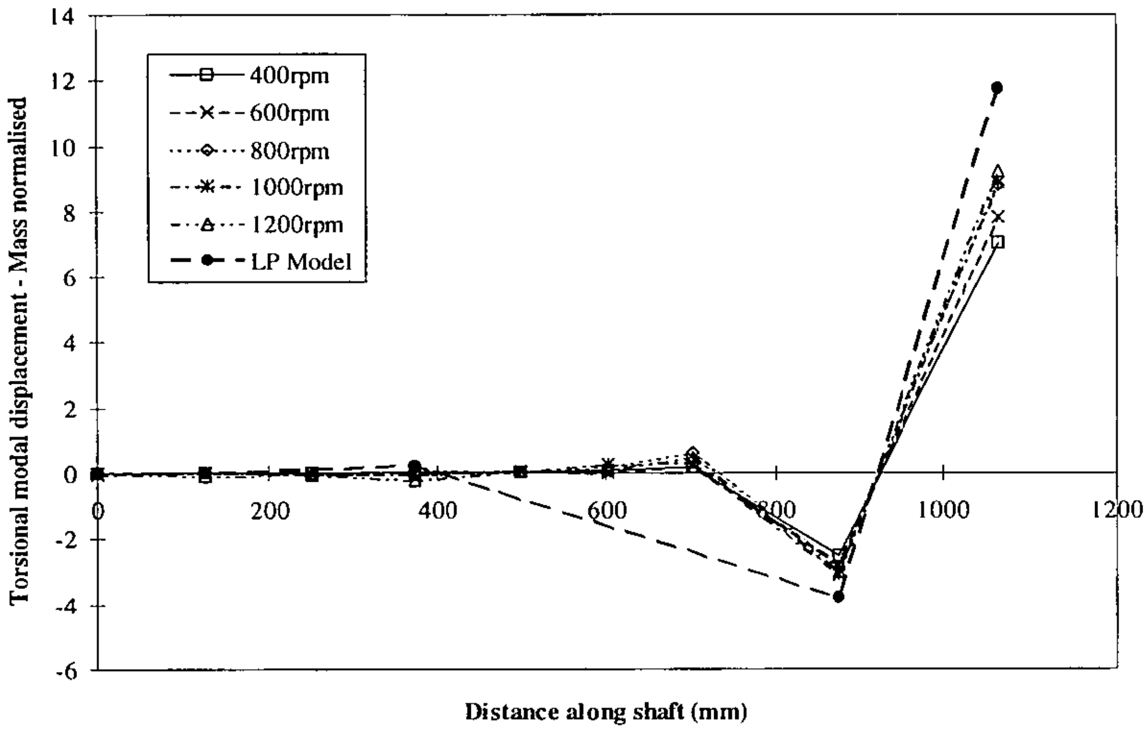

c. Mode III

Figure 4.40(cont.): Torsional mode shapes obtained for the natural frequencies of the four-inertia shaft system.

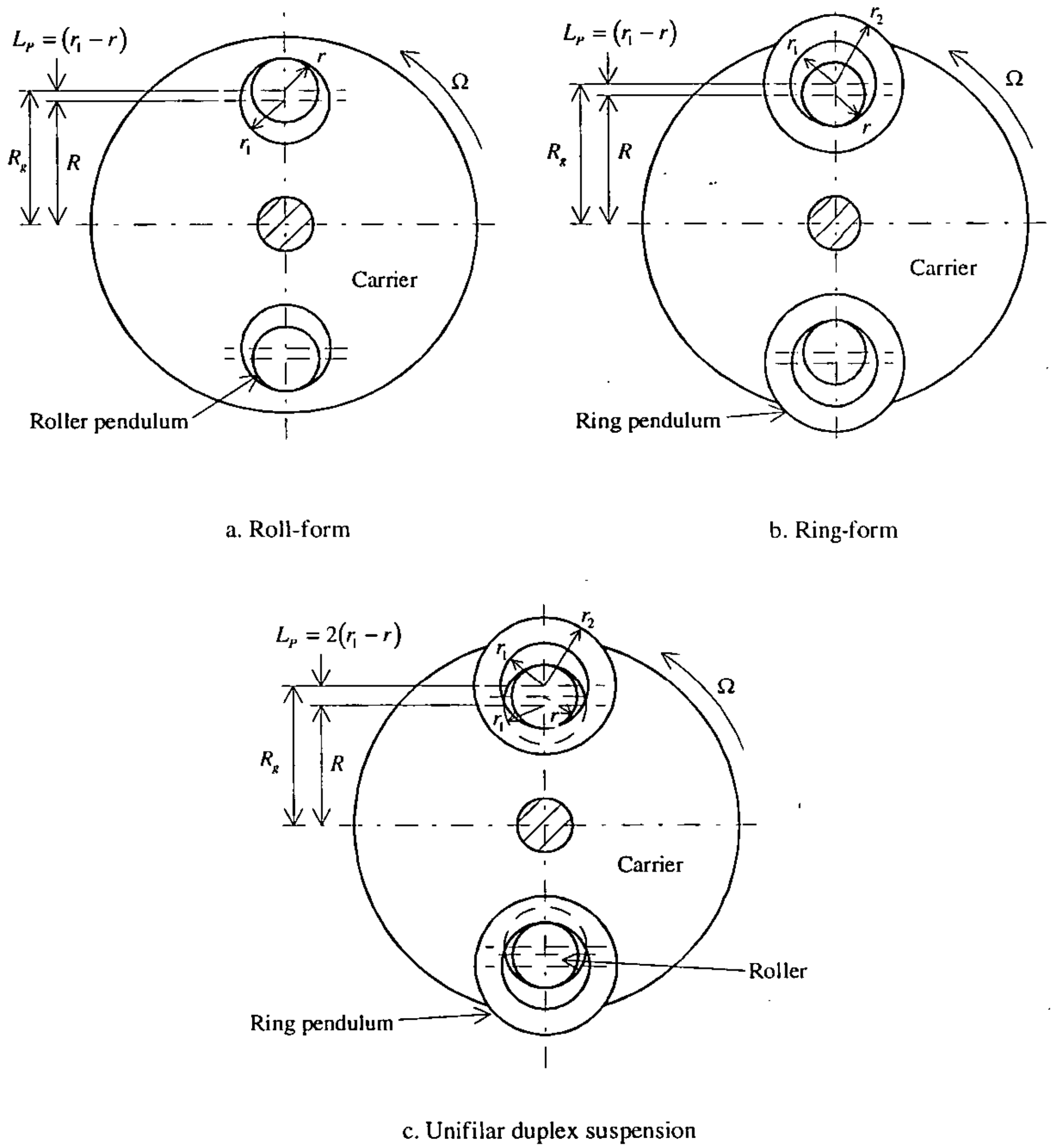

Figure 5.1: Elementary forms of the centrifugal pendulum vibration absorber.

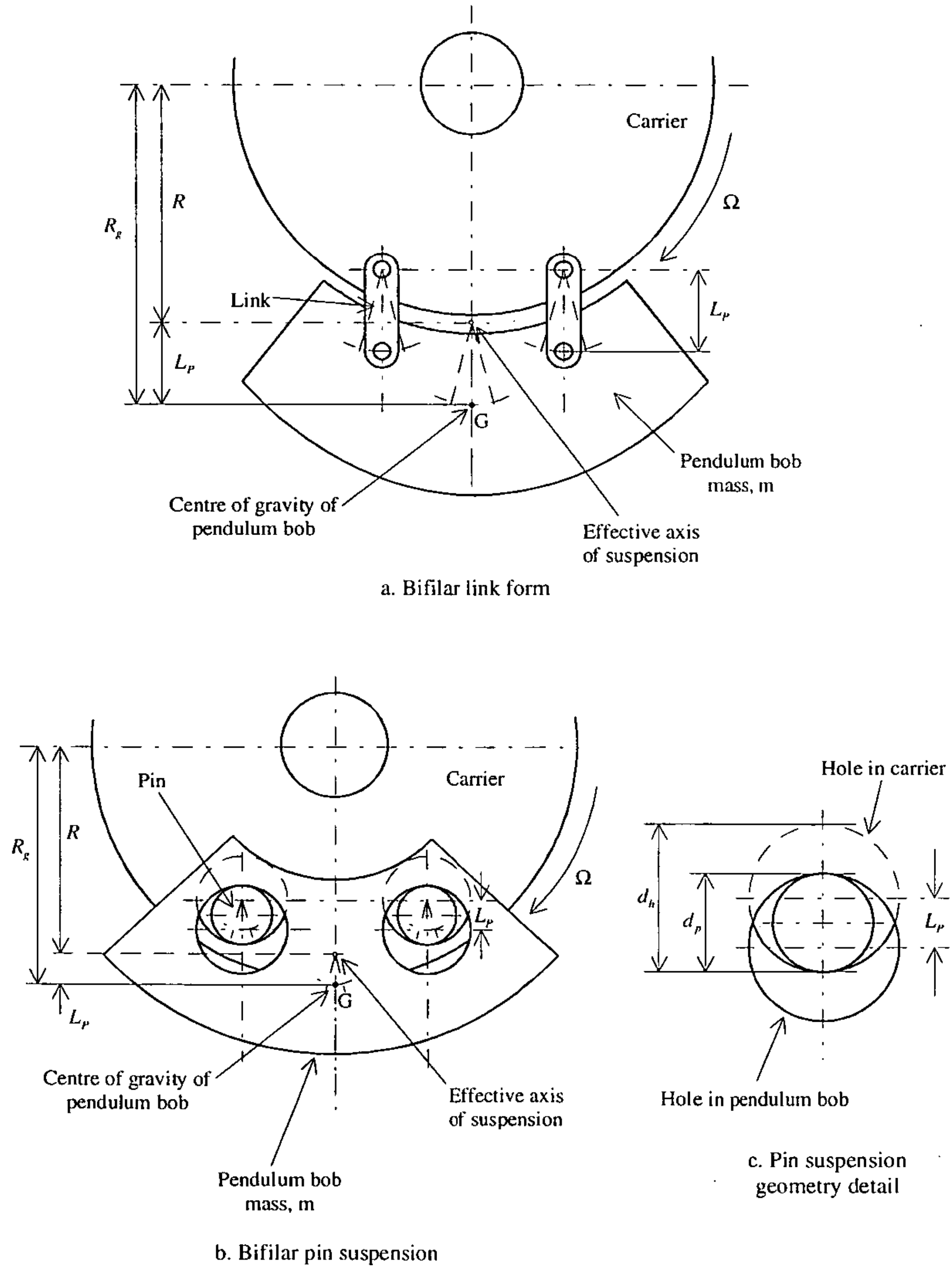

Figure 5.2: Bifilar arrangements of the CPVA.

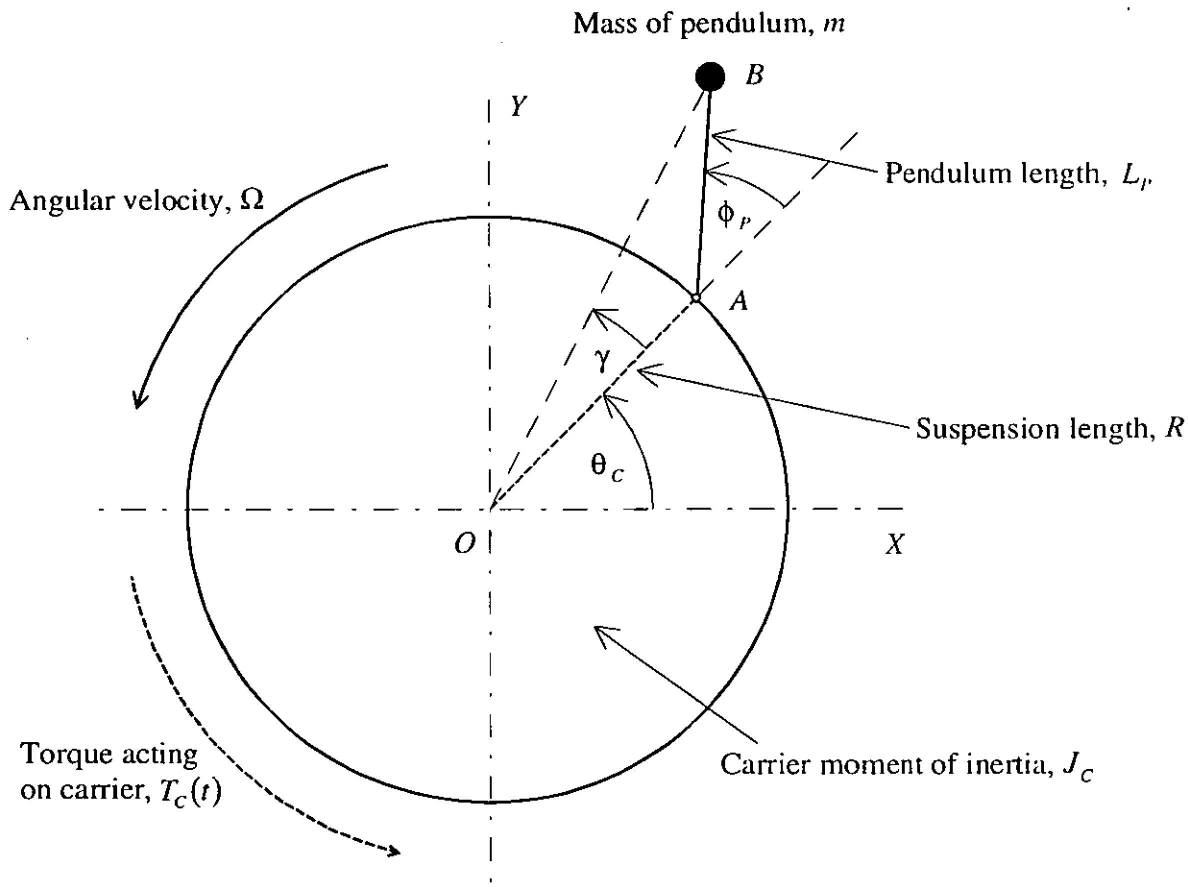

Figure 5.3: Geometry of a simple rotating pendulum

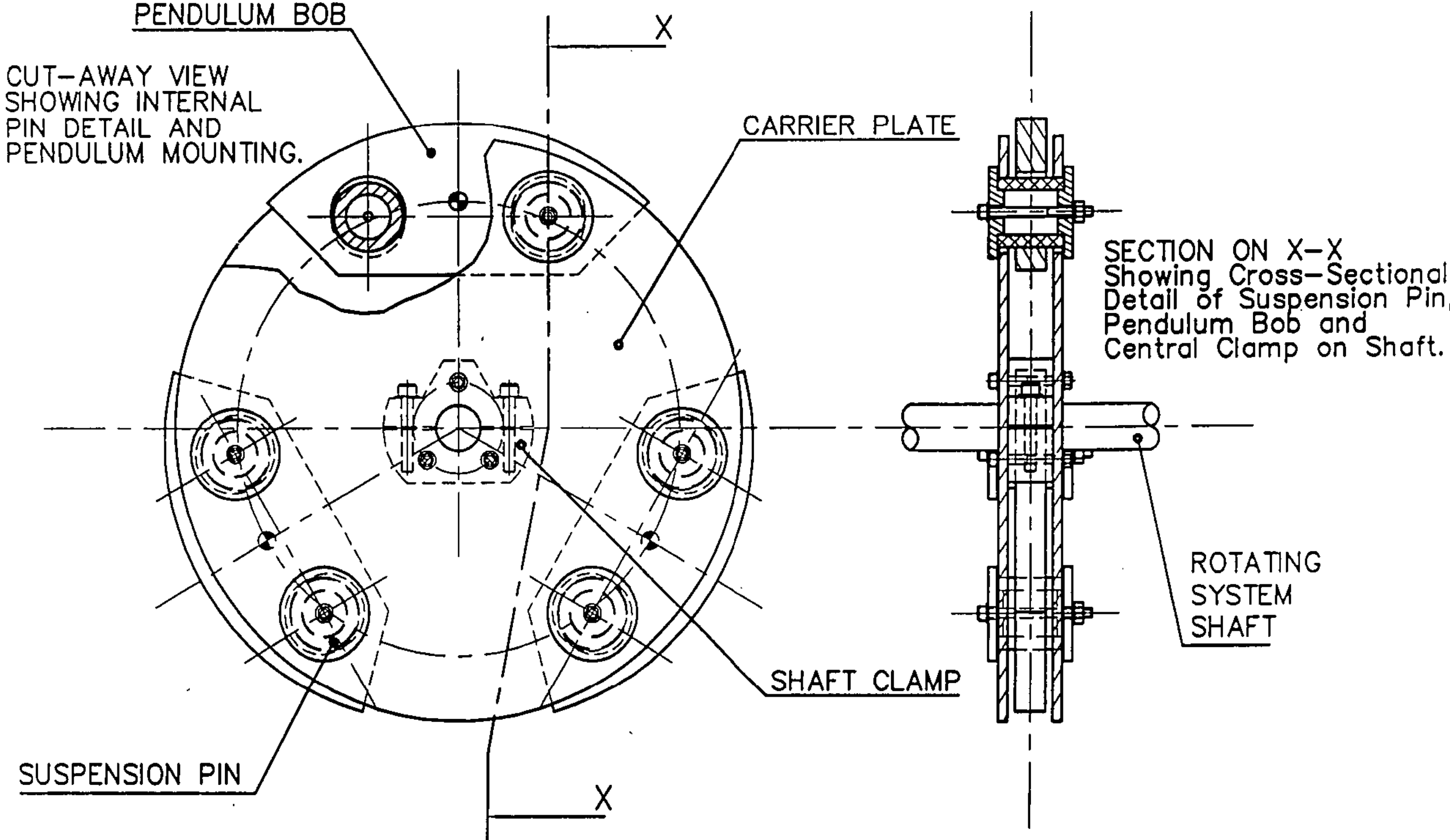

Figure 5.4: Final CPVA design used in the experimental study

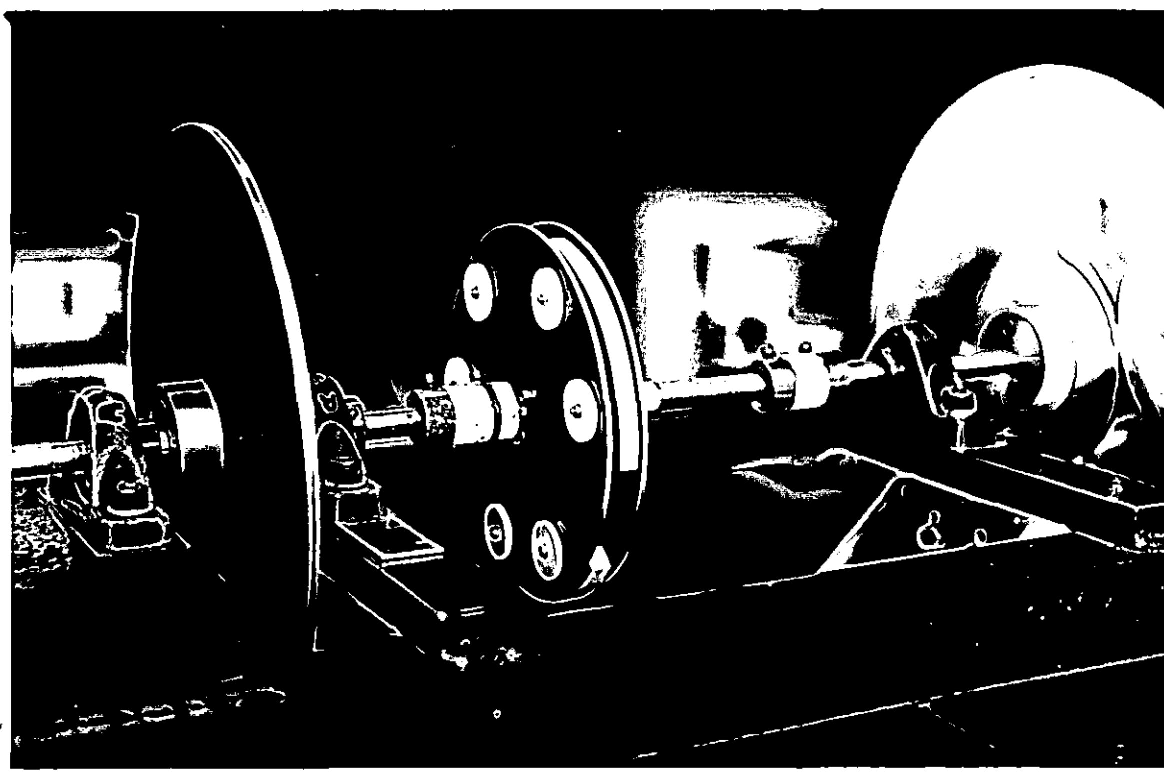

Figure 5.5: Experimental CPVA in position on centre of shaft

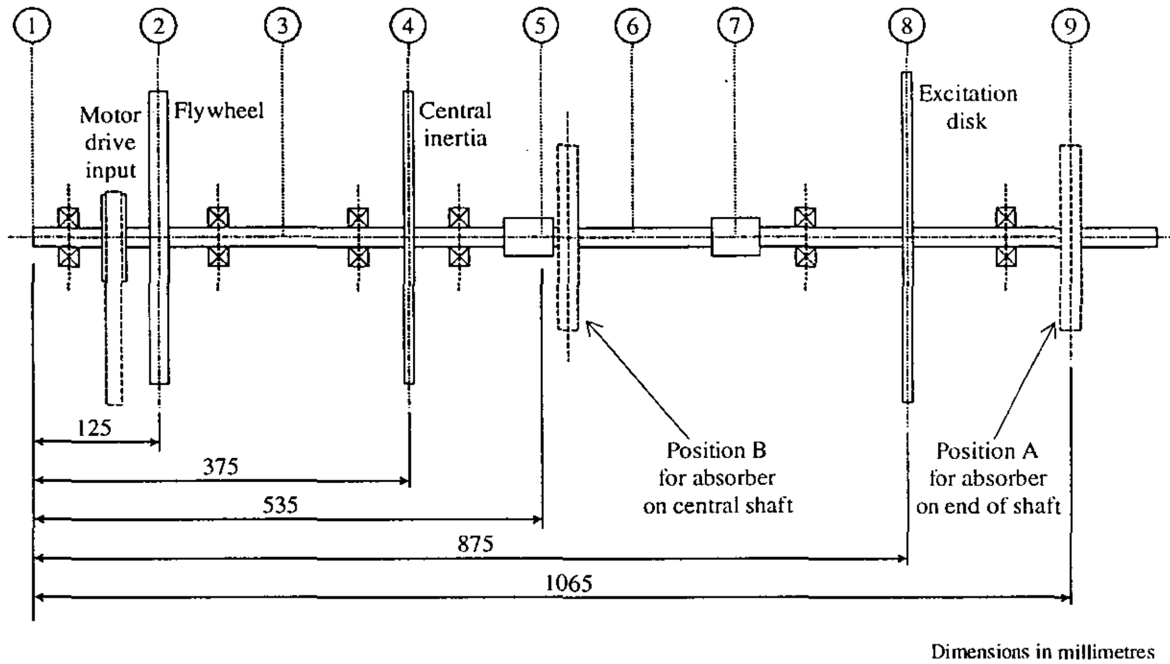

Figure 5.6: Shaft system showing absorber and measurement locations

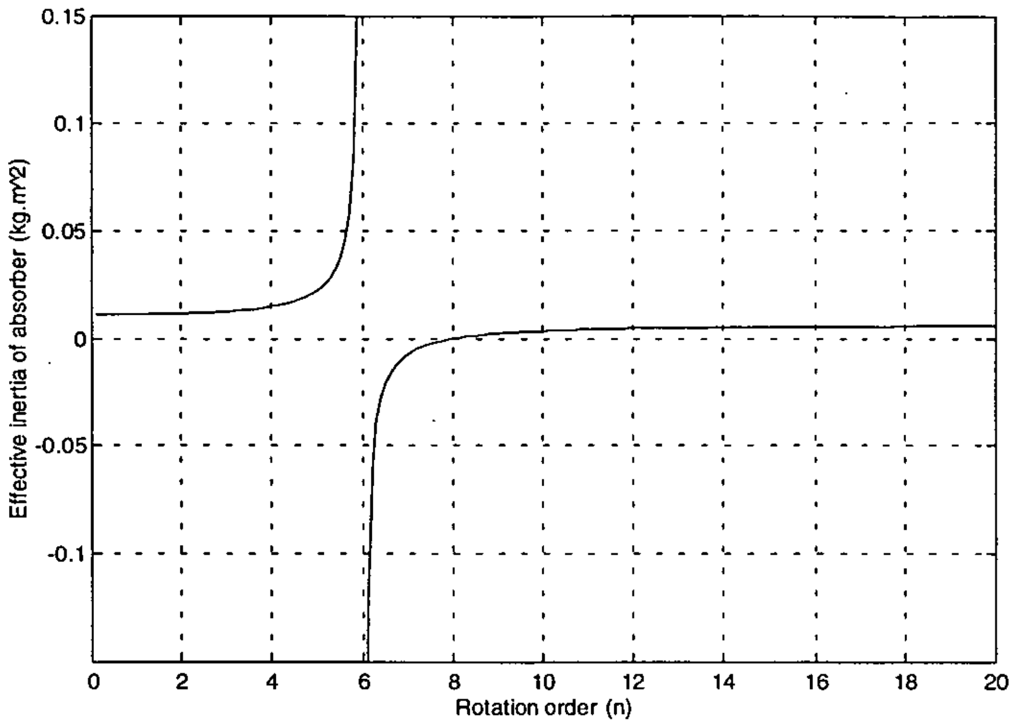

a. versus orders

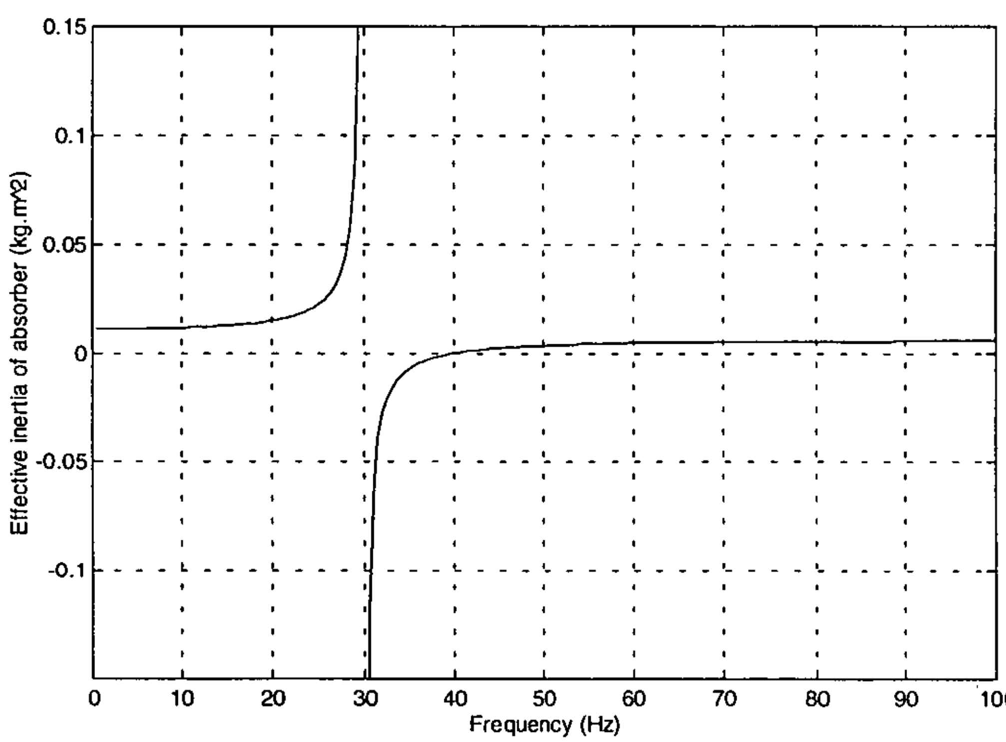

b. versus frequency at 300rpm

Figure 5.7: Variation of effective inertia for 6th order resonance tuned absorber

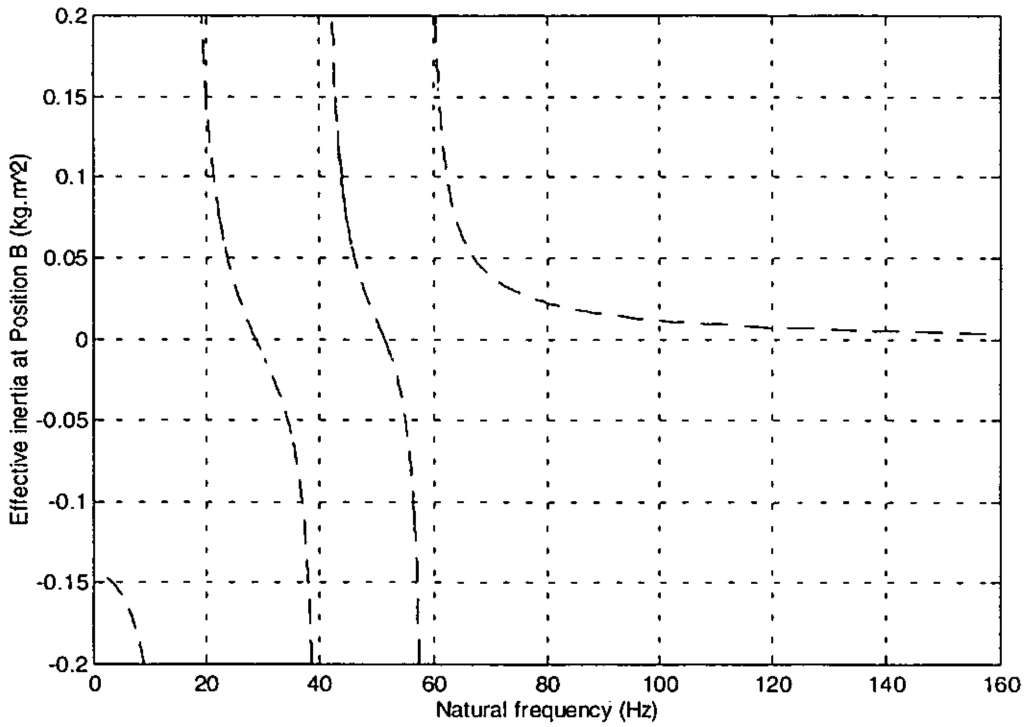

Figure 5.8: Tuning curve for central shaft absorber location:
Variation of shaft system natural frequencies with inertia at Position B

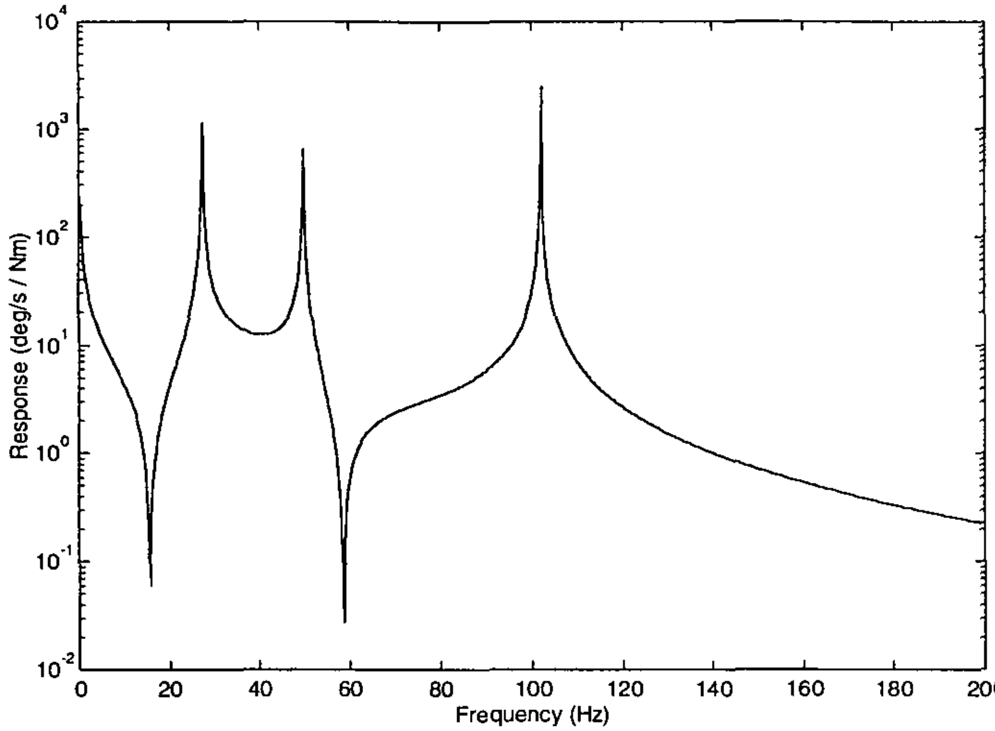

a. Locked absorber

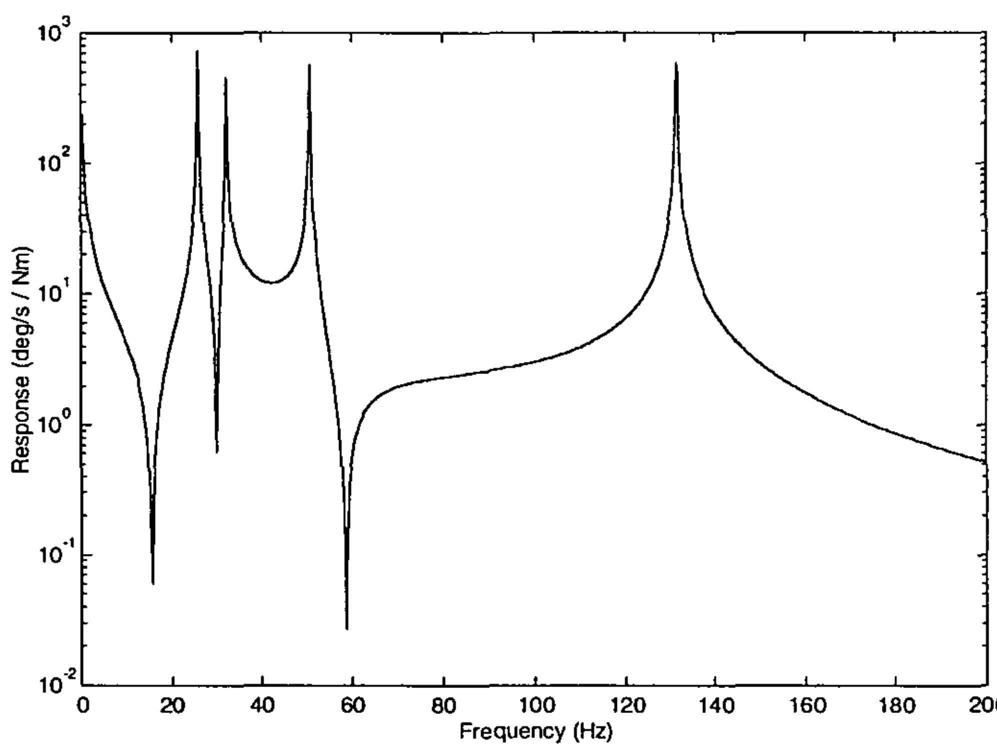

b. Functioning absorber at 300rpm

Figure 5.9: Modelled frequency response functions for absorber location with 6th order resonance tuning at central shaft position

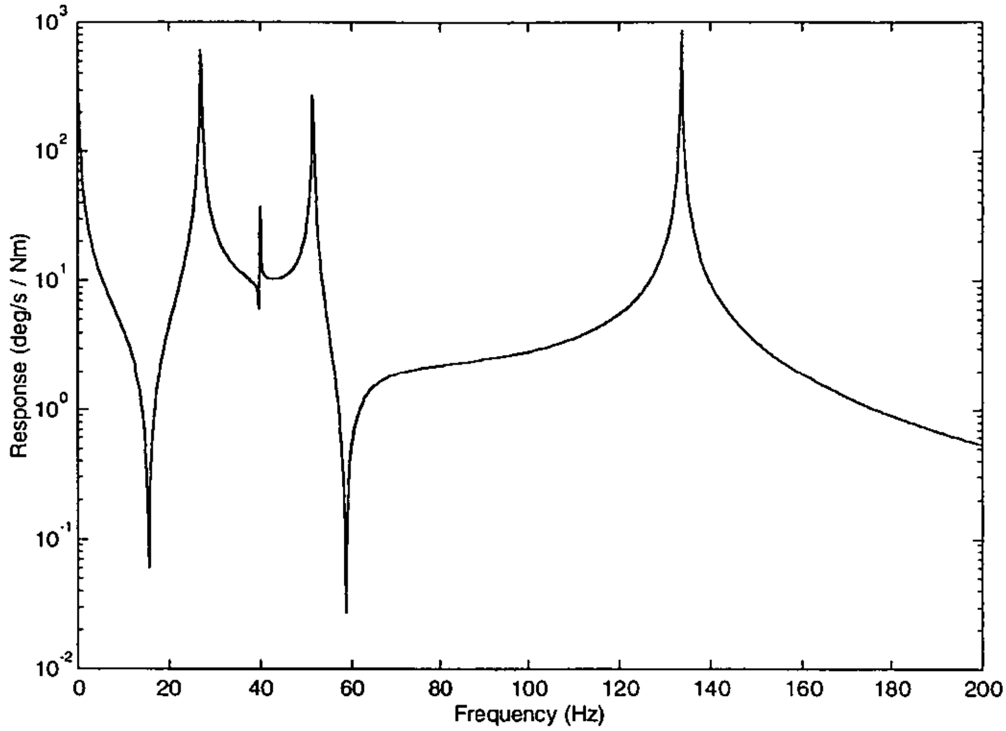

b. Functioning absorber at 400rpm

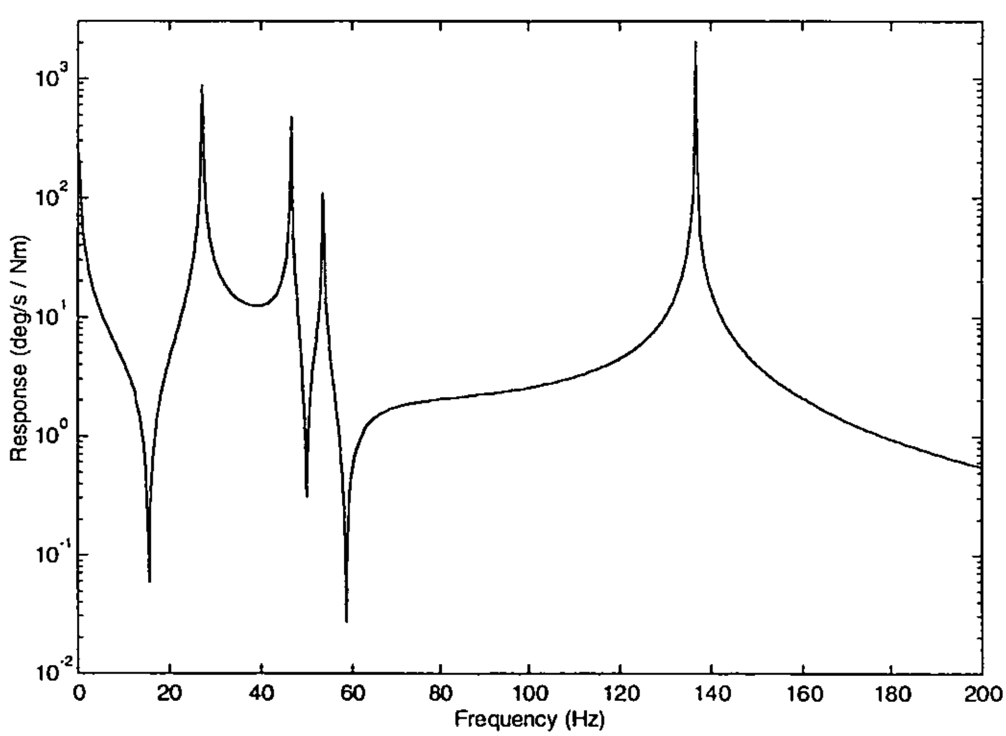

b. Functioning absorber at 500rpm

Figure 5.10: Modelled frequency response functions for absorber location with 6th order resonance tuning at central shaft position for varying rotation speeds

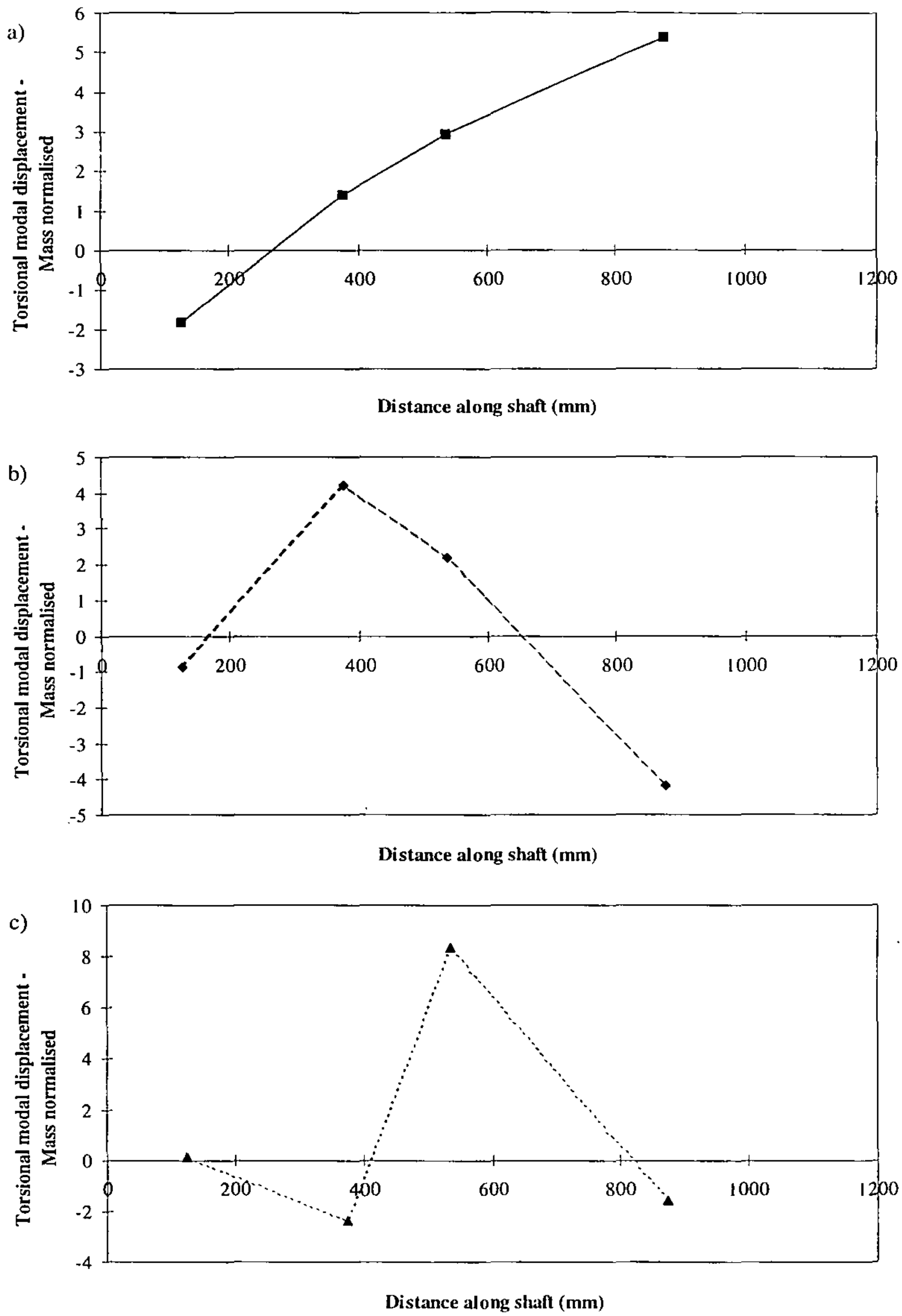

Figure 5.11: Modelled mode shapes for locked 6th order absorber at central shaft position.
a. Mode I, b. Mode II, c. Mode III

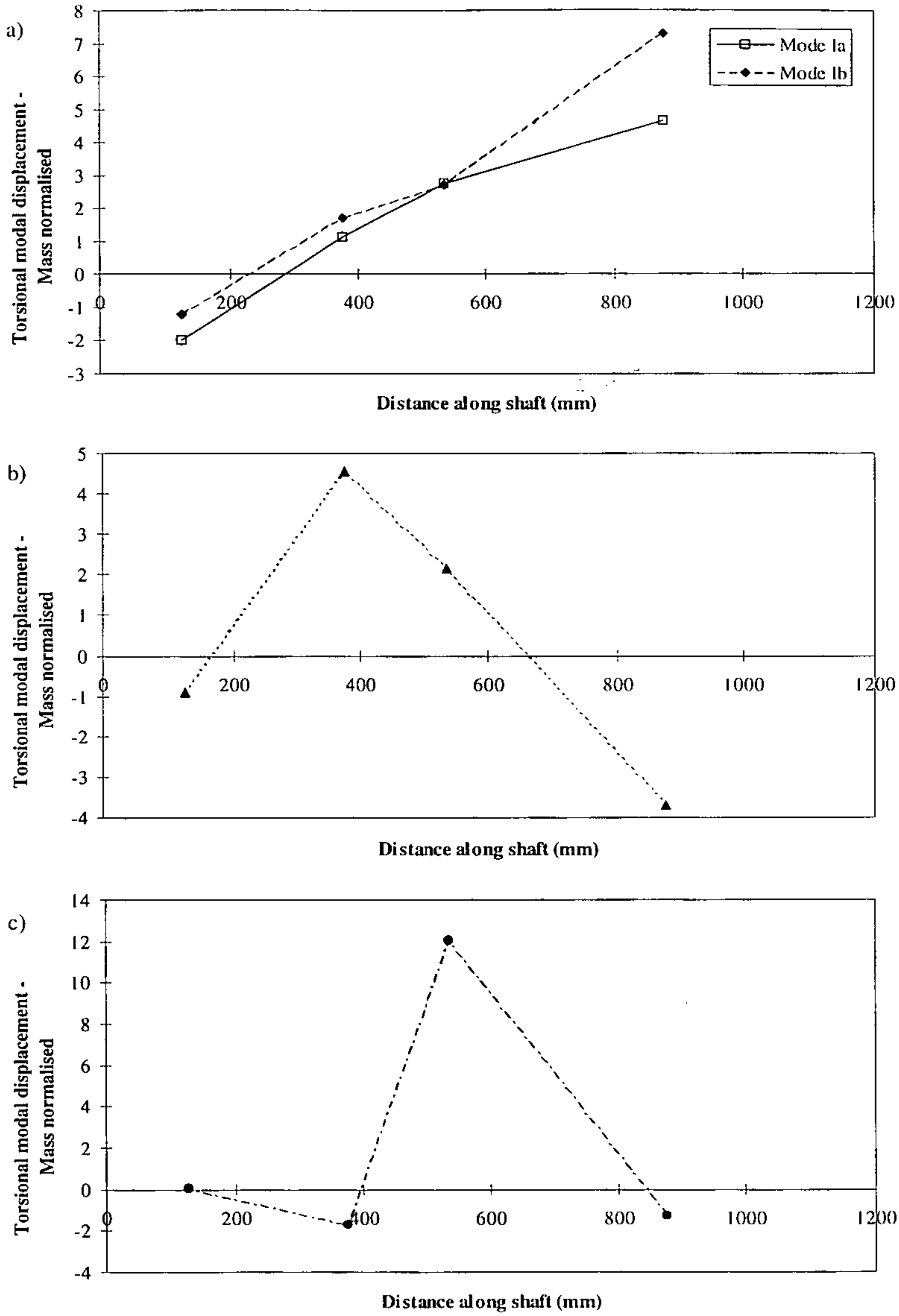

Figure 5.12: Modelled mode shapes for functioning 6th order absorber at central shaft position. Rotation speed 300rpm. a. Modes Ia and b, b. Mode II, c. Mode III

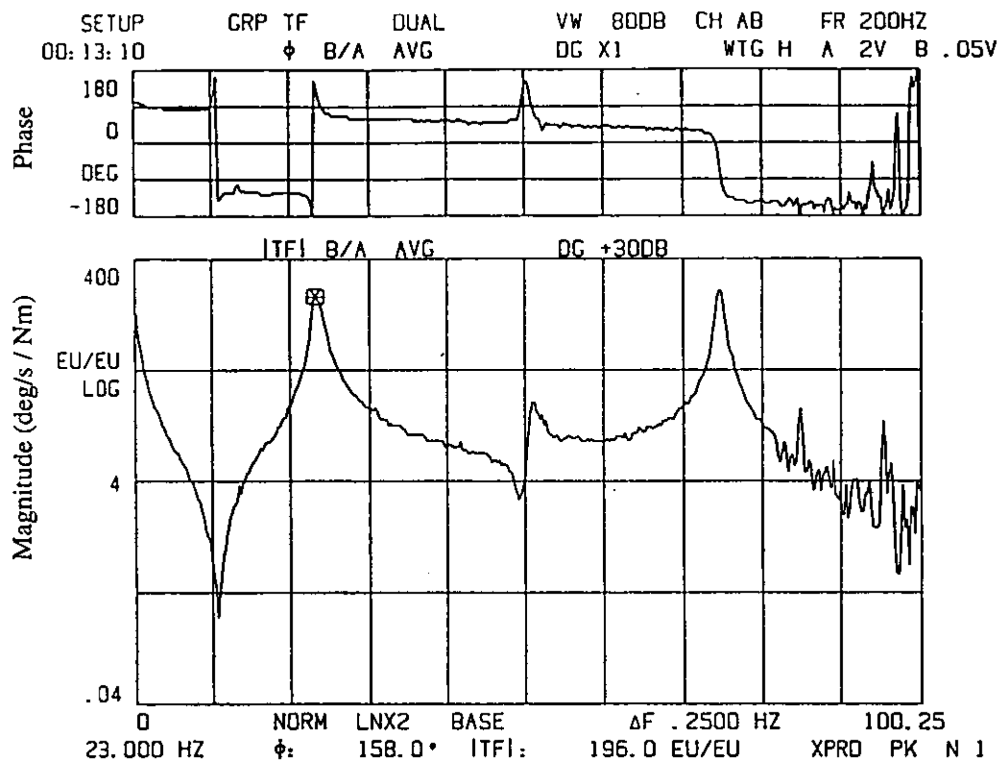

Figure 5.13: Torsional vibration FRF from location of 2.5 order locked absorber on free-end of shaft (Position A). Rotation speed 600rpm.

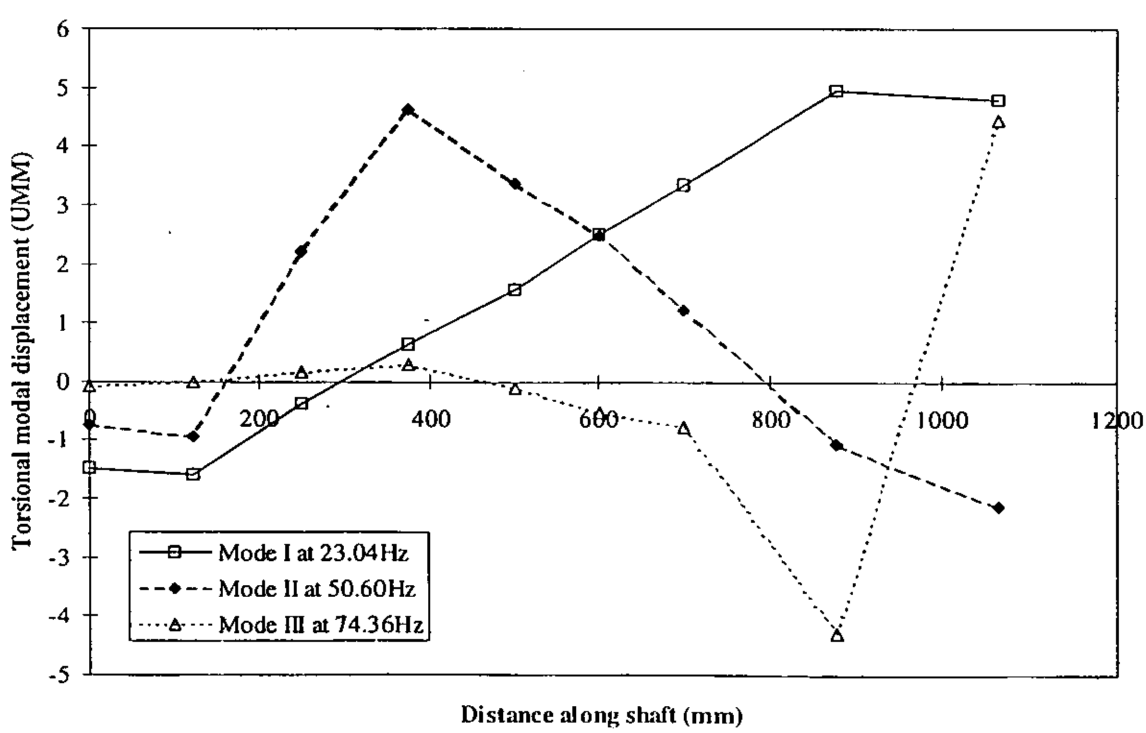

Figure 5.14: Torsional vibration mode shapes for 2.5 order locked absorber on free-end of shaft (Position A). Rotation speed 600rpm.

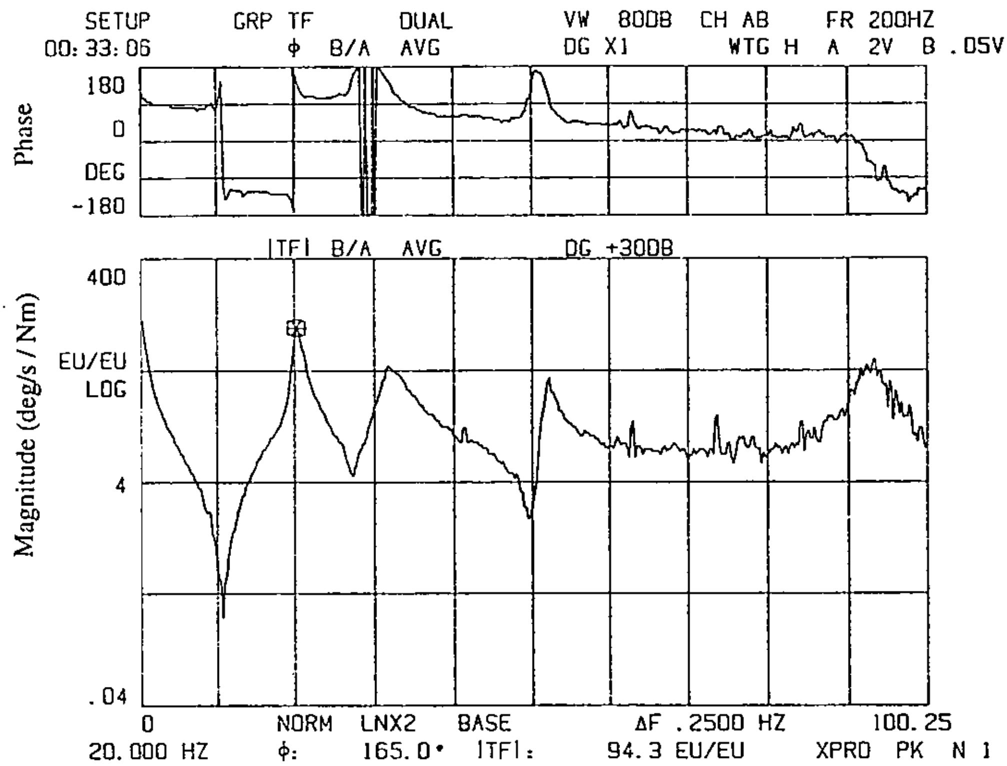

Figure 5.15: Torsional vibration FRF from absorber location with 2.5 order resonance tuning on free-end of shaft (Position A). Rotation speed 600rpm.

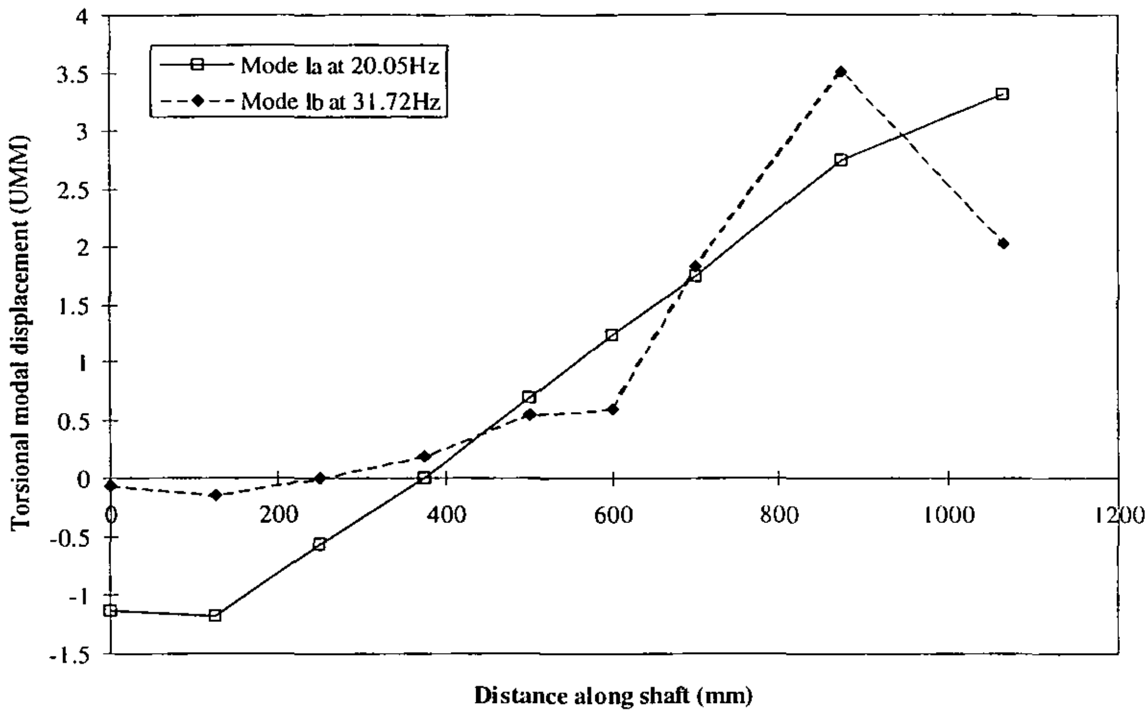

a. Modes Ia and Ib

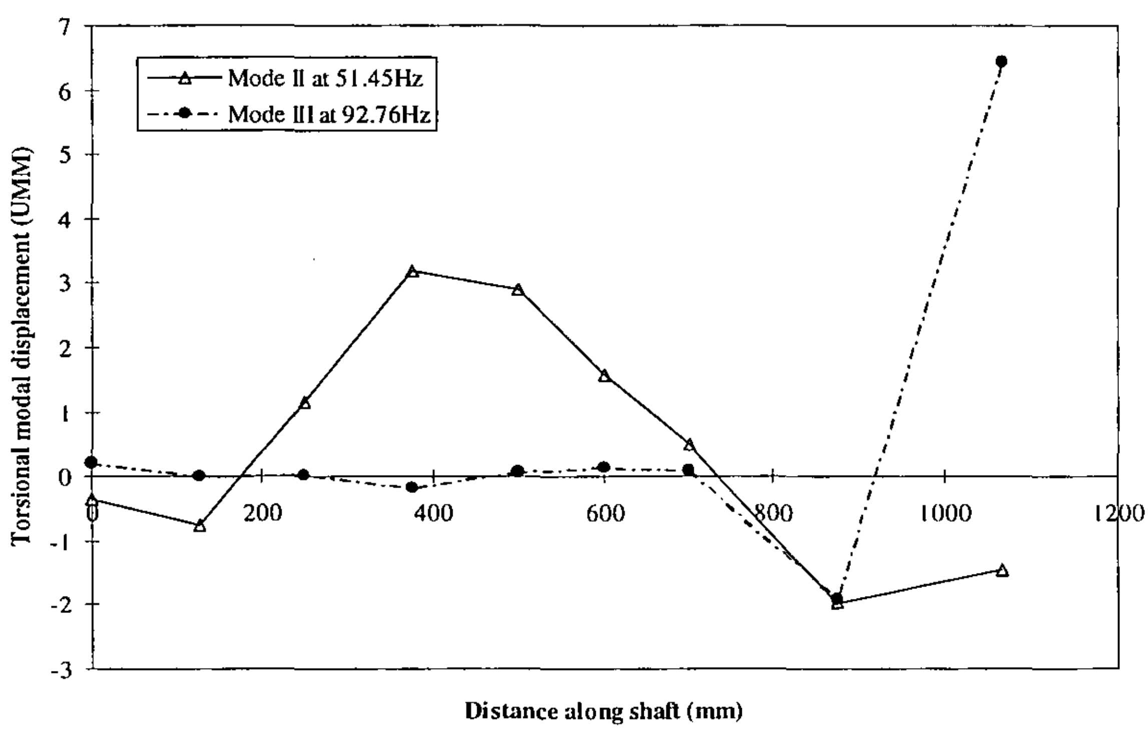

b. Modes II and III

Figure 5.16: Torsional vibration mode shapes for 2.5 order absorber on free-end of shaft (Position A). Rotation speed 600rpm.

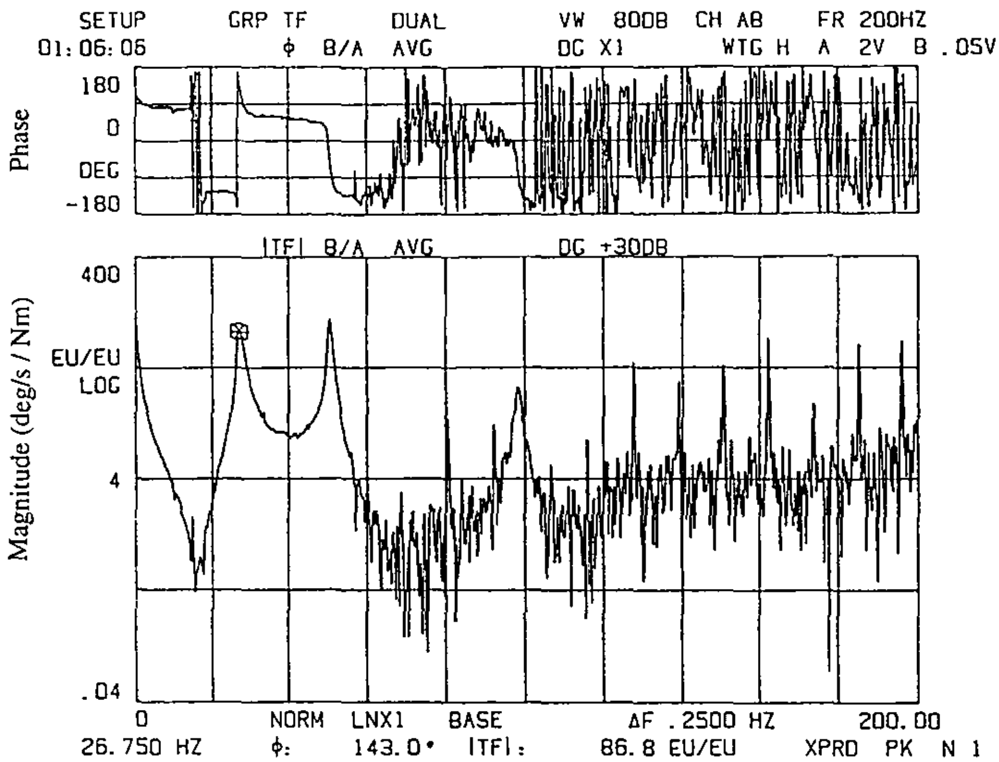

a. 2.5 order suspension pins

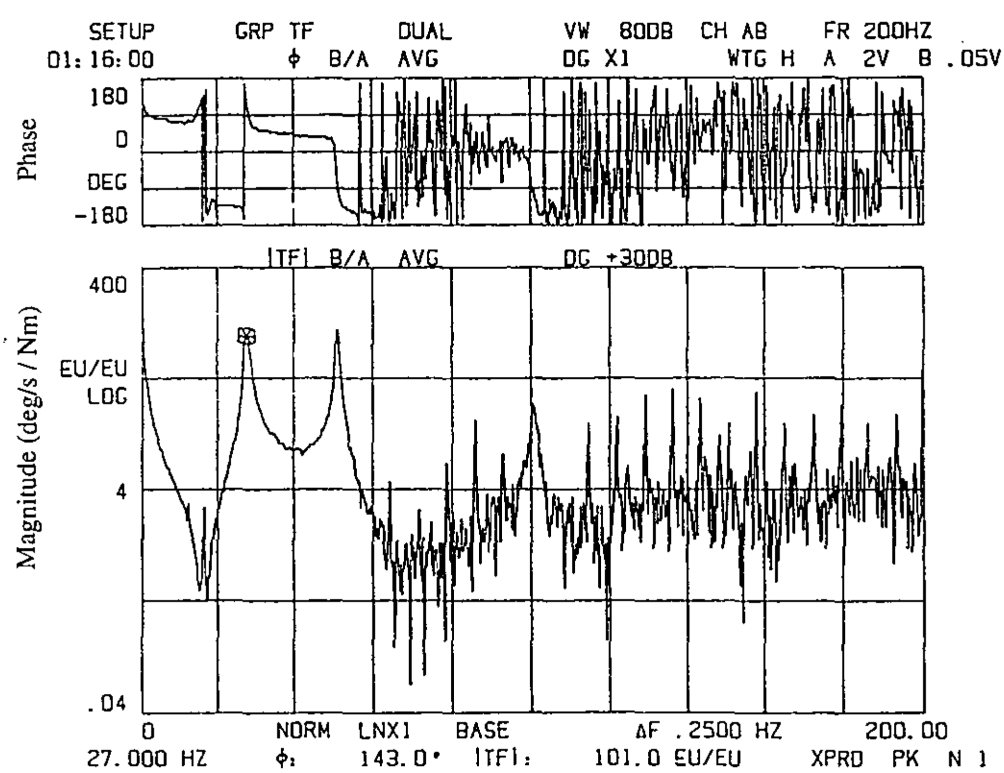

b. 4th order suspension pins

Figure 5.17: Torsional vibration FRFs from location of locked absorber on centre section of shaft (Position B).

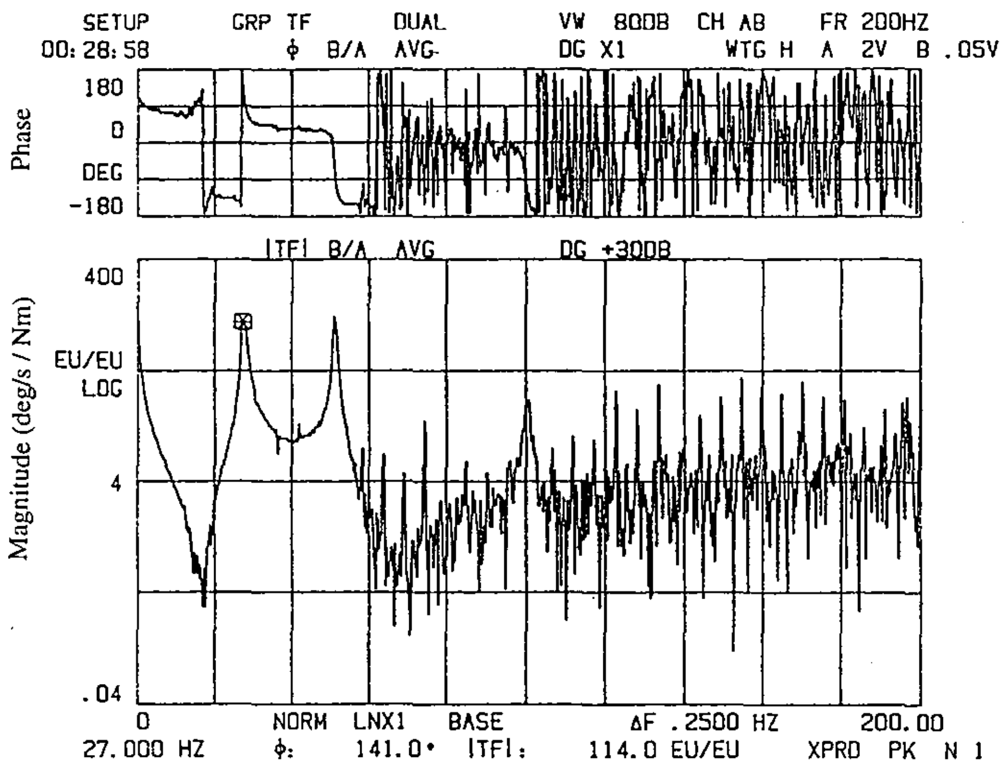

c. 6th order suspension pins

Figure 5.17(cont.): Torsional vibration FRFs from location of locked absorber on centre section of shaft (Position B).

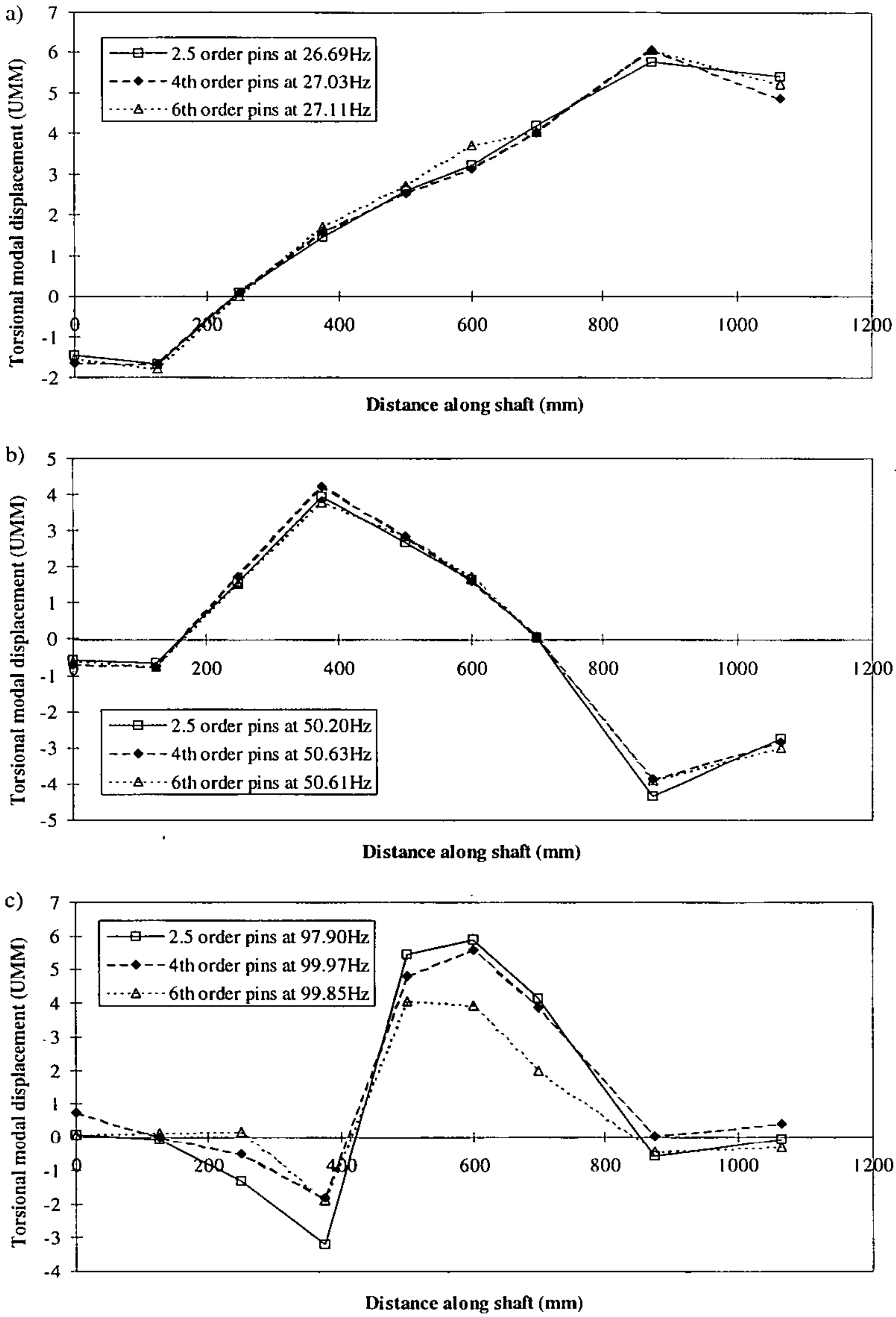

Figure 5.18: Torsional vibration mode shapes for locked absorber on centre section of shaft (Position B) with each set of suspension pins. a.Mode I, b. Mode II, c. Mode III.

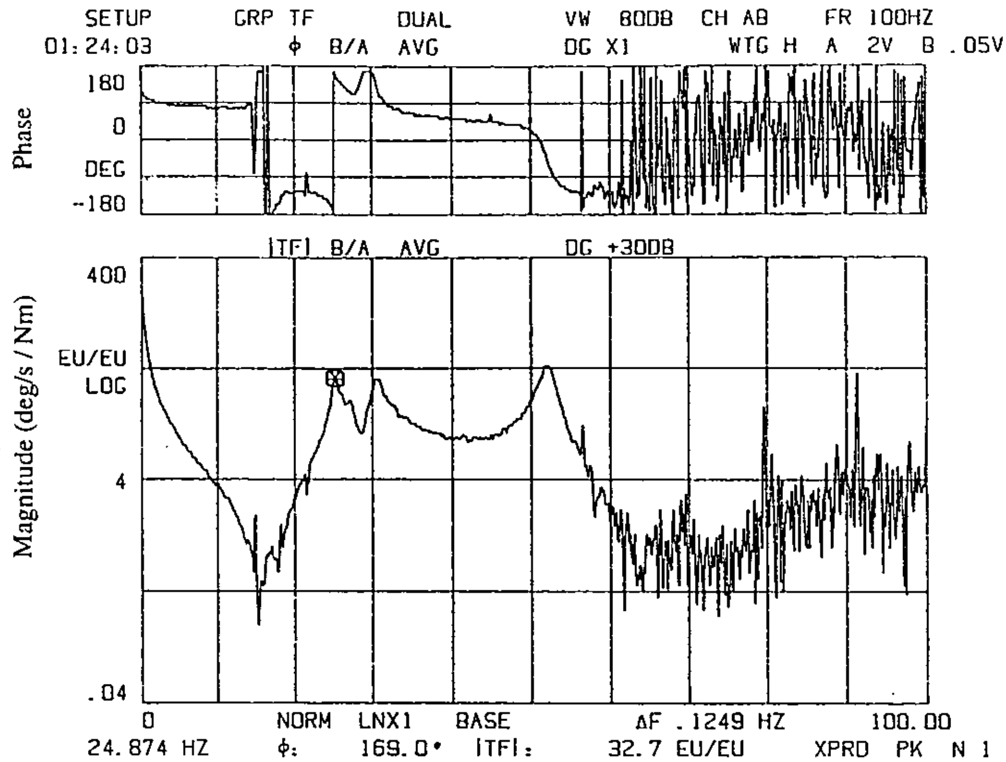

Figure 5.19: Torsional vibration FRF from absorber location on centre section of shaft (Position B) with 2.5 order resonance tuning. Rotation speed 650rpm.

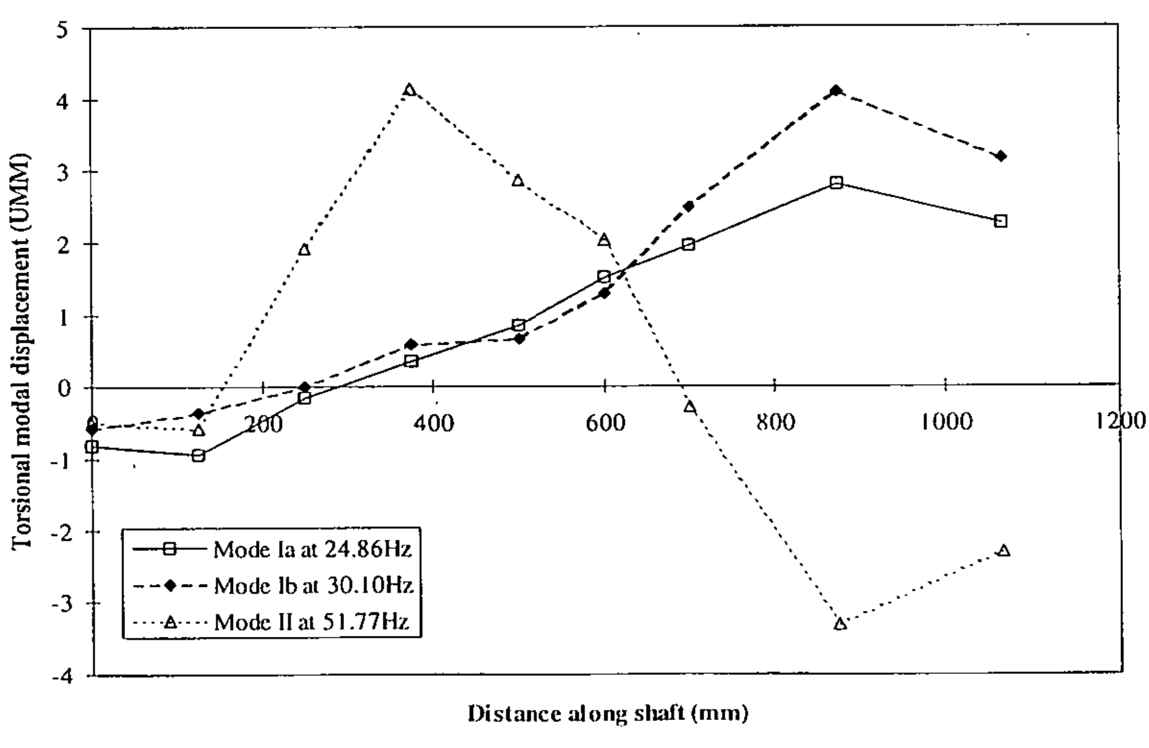

Figure 5.20: Torsional vibration mode shapes for 2.5 order absorber on centre section of shaft (Position B). Rotation speed 650rpm.

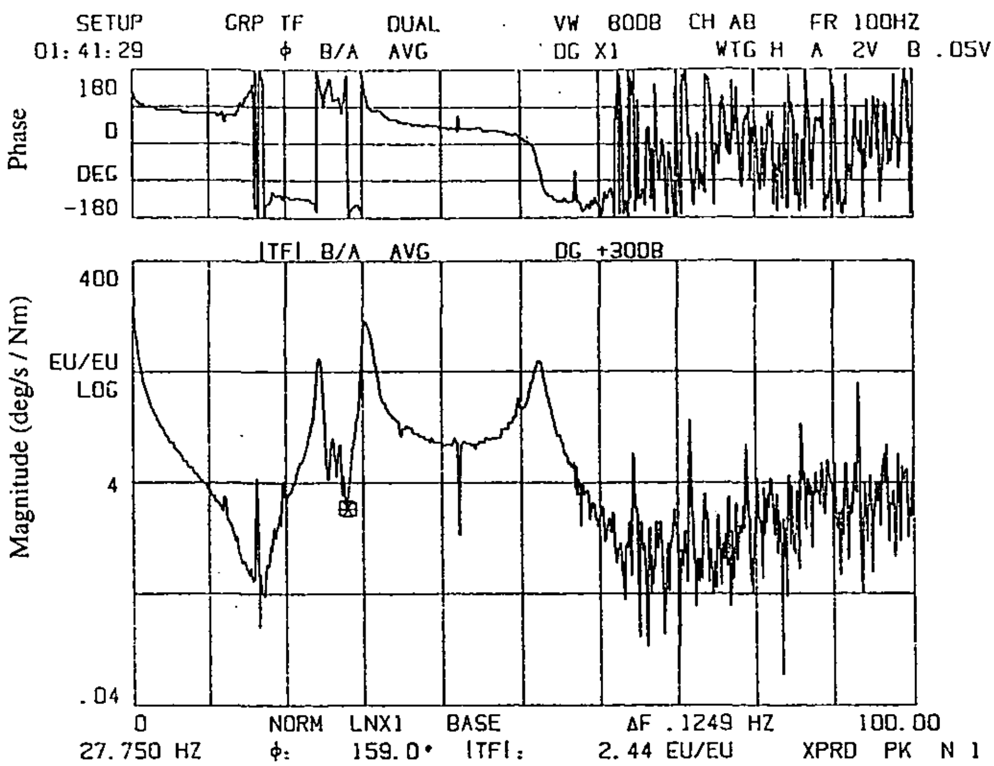

Figure 5.21: Torsional vibration FRF from absorber location on centre section of shaft (Position B) with 4th order resonance tuning. Rotation speed 400rpm.

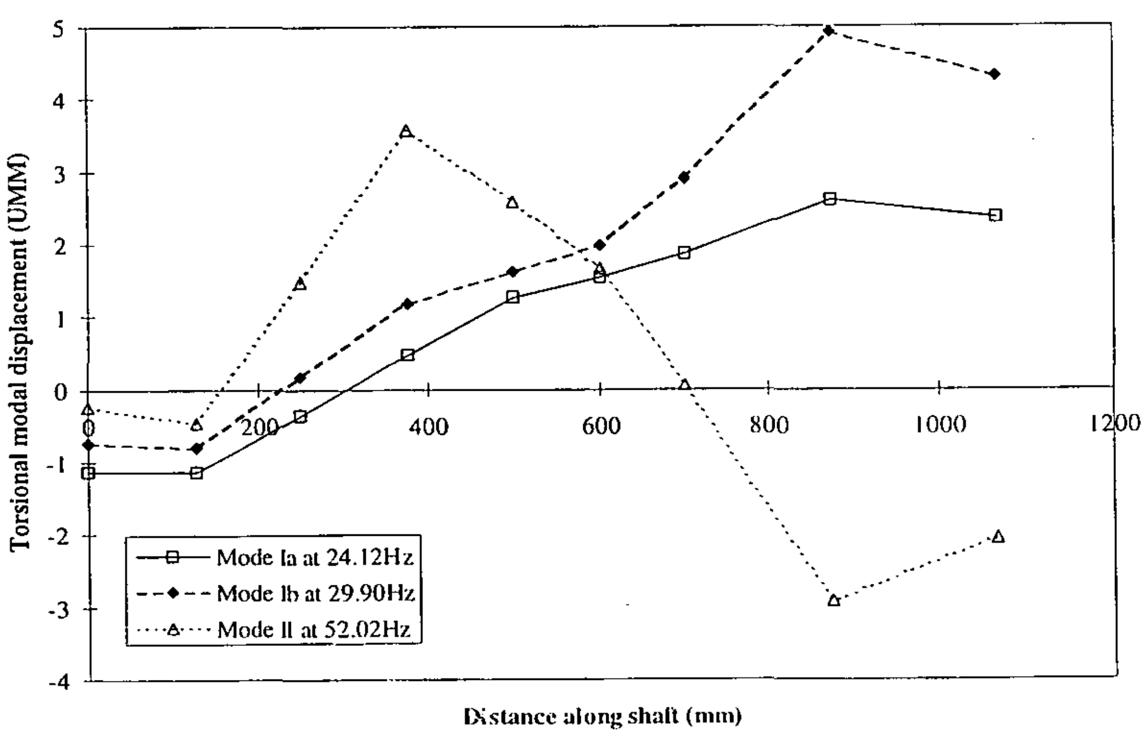

Figure 5.22: Torsional vibration mode shapes for 4th order absorber on centre section of shaft (Position B). Rotation speed 400rpm.

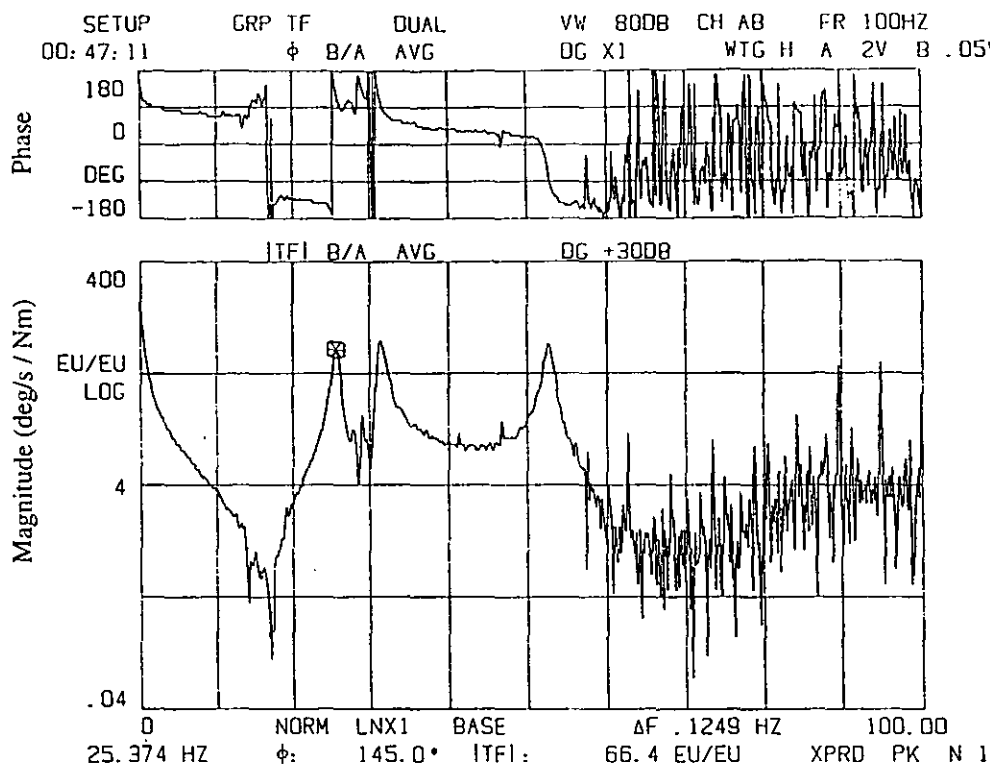

Figure 5.23: Torsional vibration FRF from absorber location on centre section of shaft (Position B) with 6th order resonance tuning. Rotation speed 300rpm.

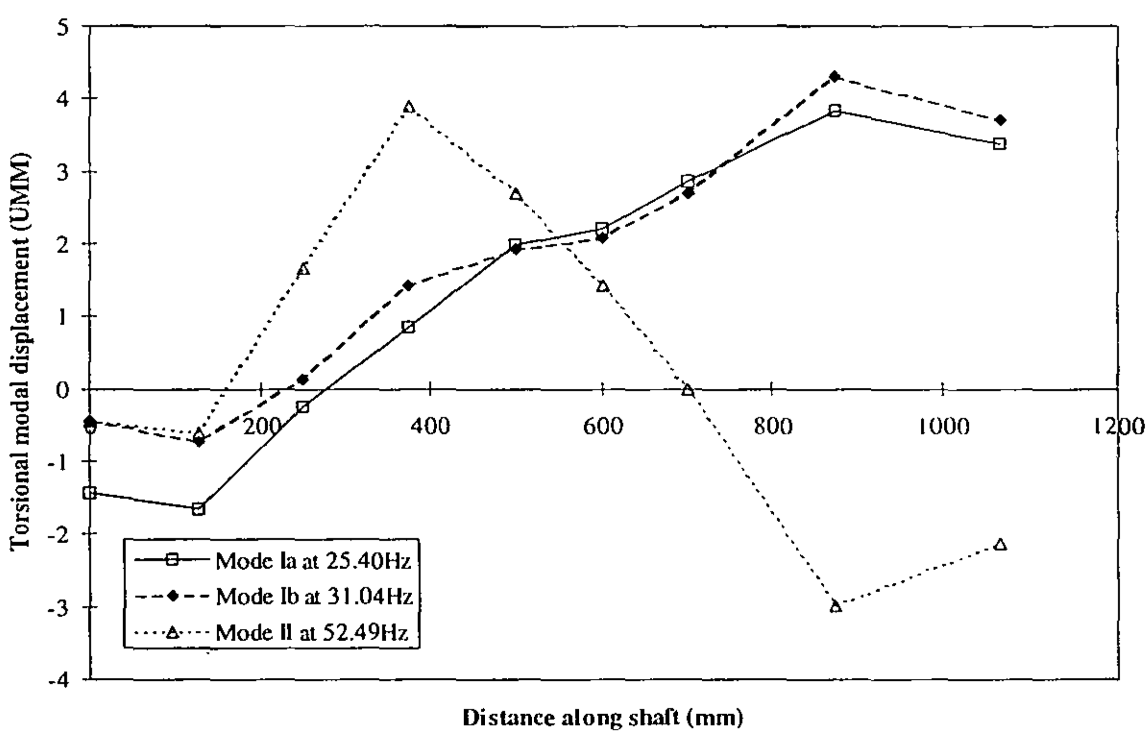

Figure 5.24: Torsional vibration mode shapes for 6th order absorber on centre section of shaft (Position B). Rotation speed 300rpm.

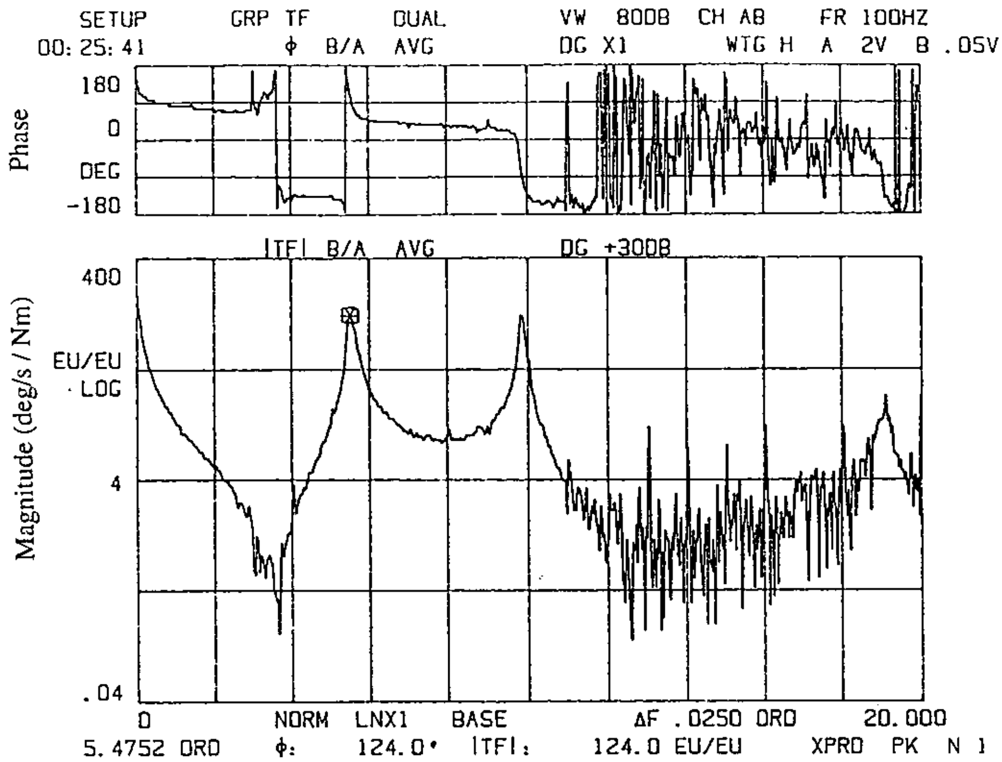

a. Locked absorber at 300rpm.

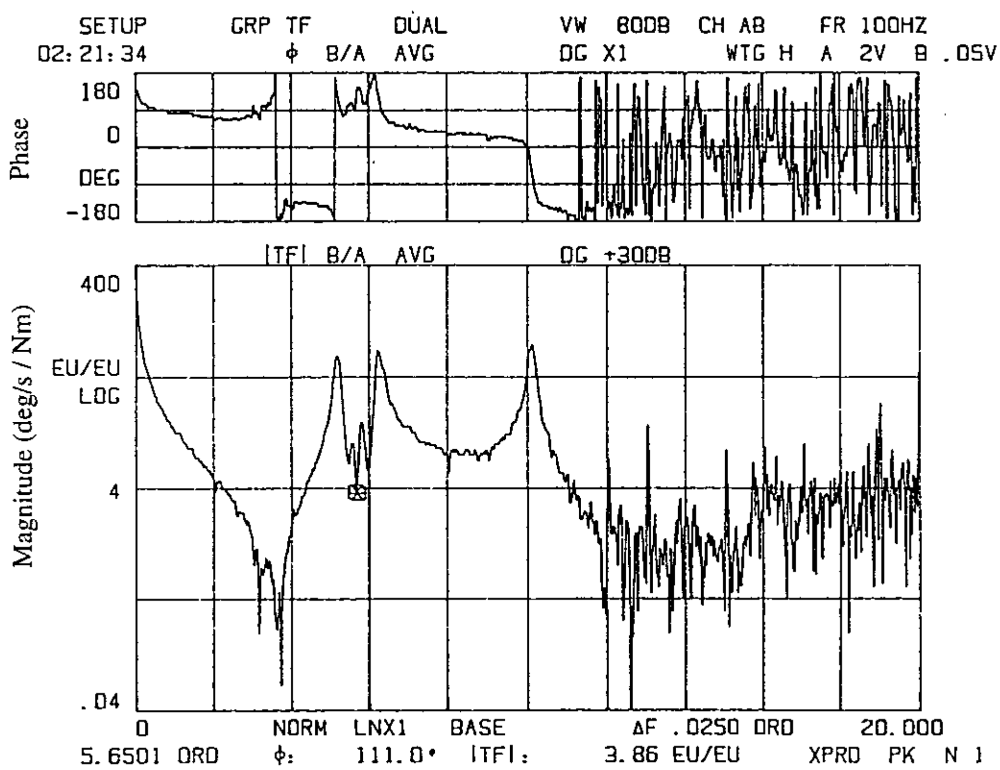

b. Functioning 6th order absorber at 300rpm.

Figure 5.25: FRFs for 6th order absorber on centre of shaft versus rotation orders.

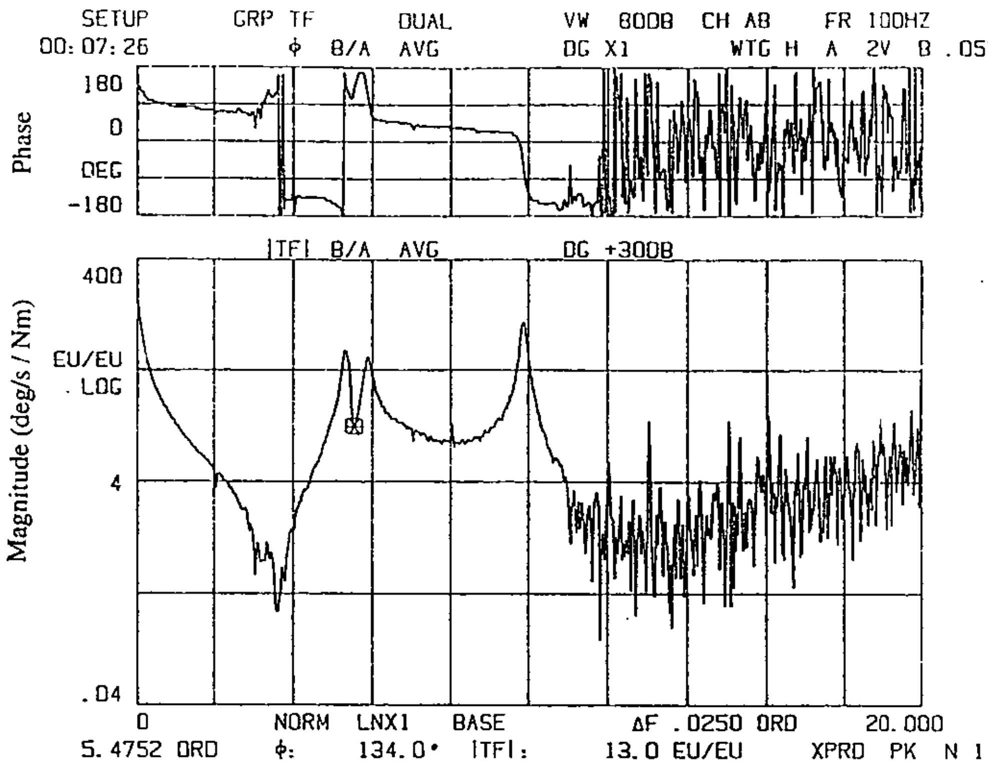

c. Absorber with only pendulum 1 unlocked.

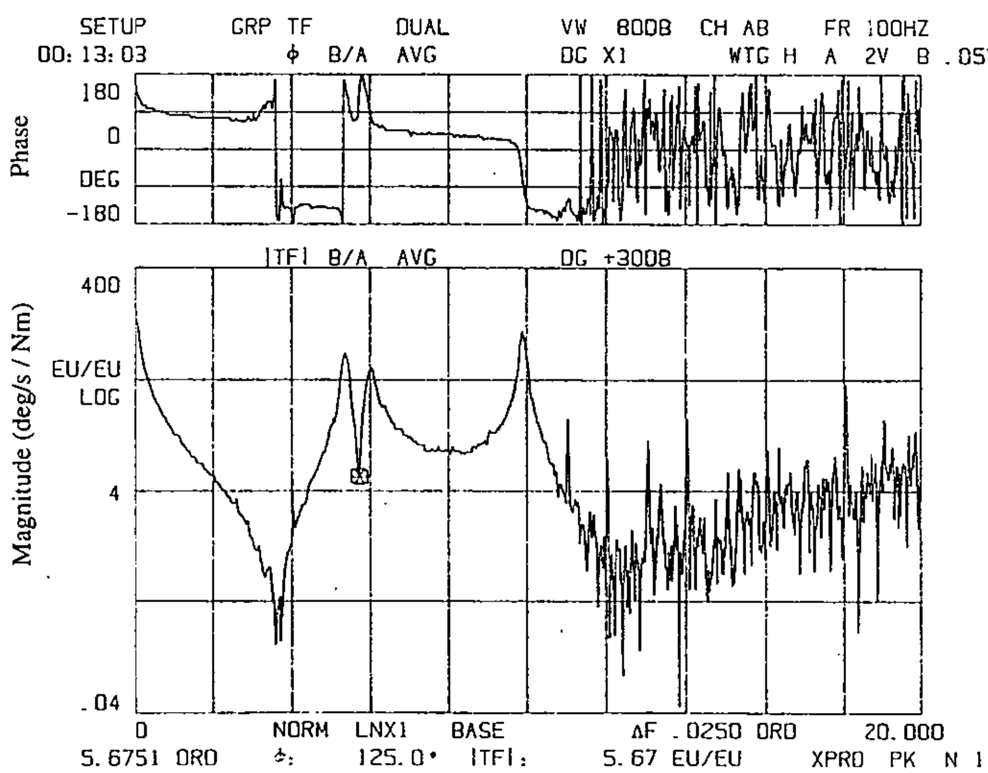

d. Absorber with only pendulum 2 unlocked.

Figure 5.25(cont.): FRFs for 6th order absorber on centre of shaft versus rotation orders.

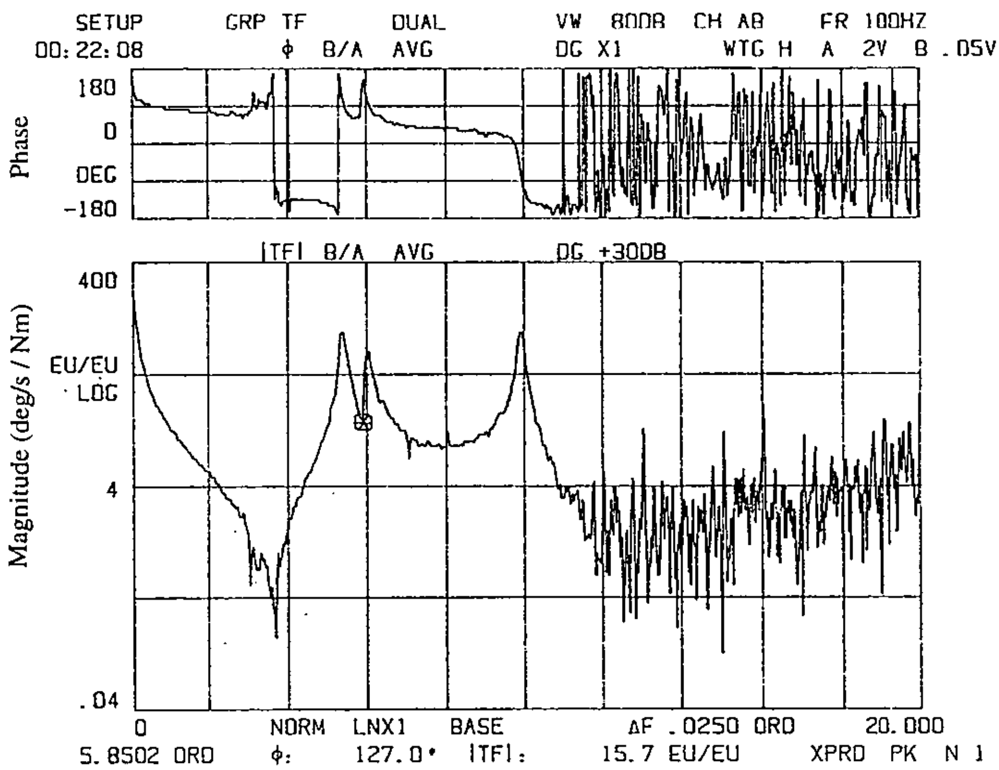

e. Absorber with only pendulum 3 unlocked.

Figure 5.25(cont.): FRFs for 6th order absorber on centre of shaft versus rotation orders.

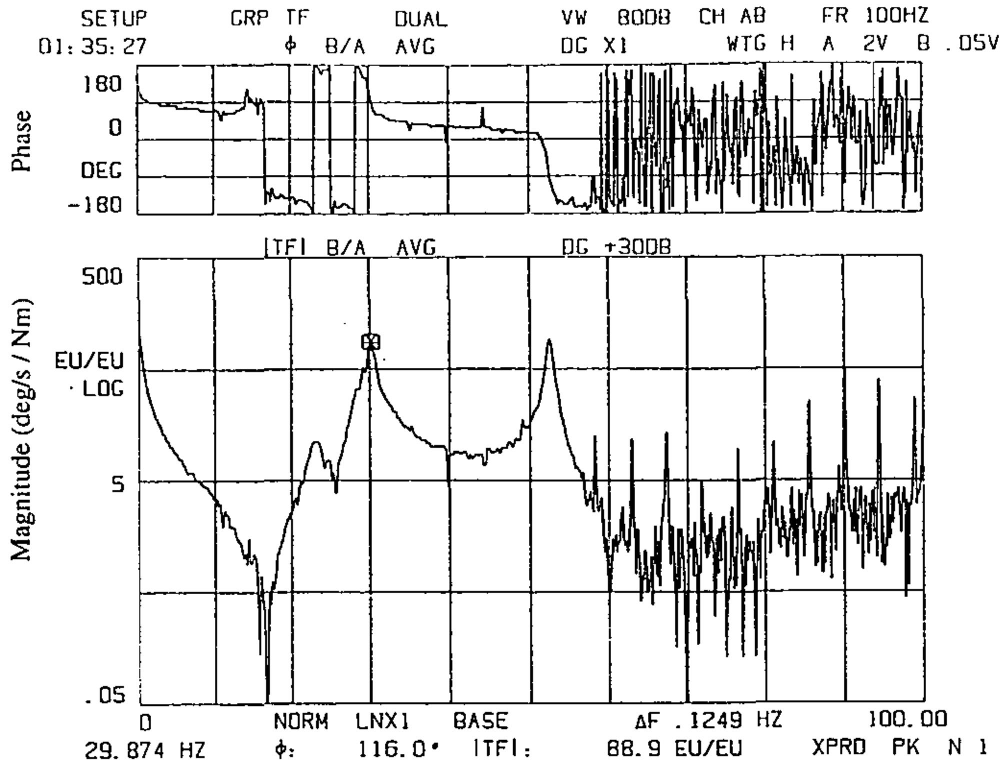

a. 250rpm

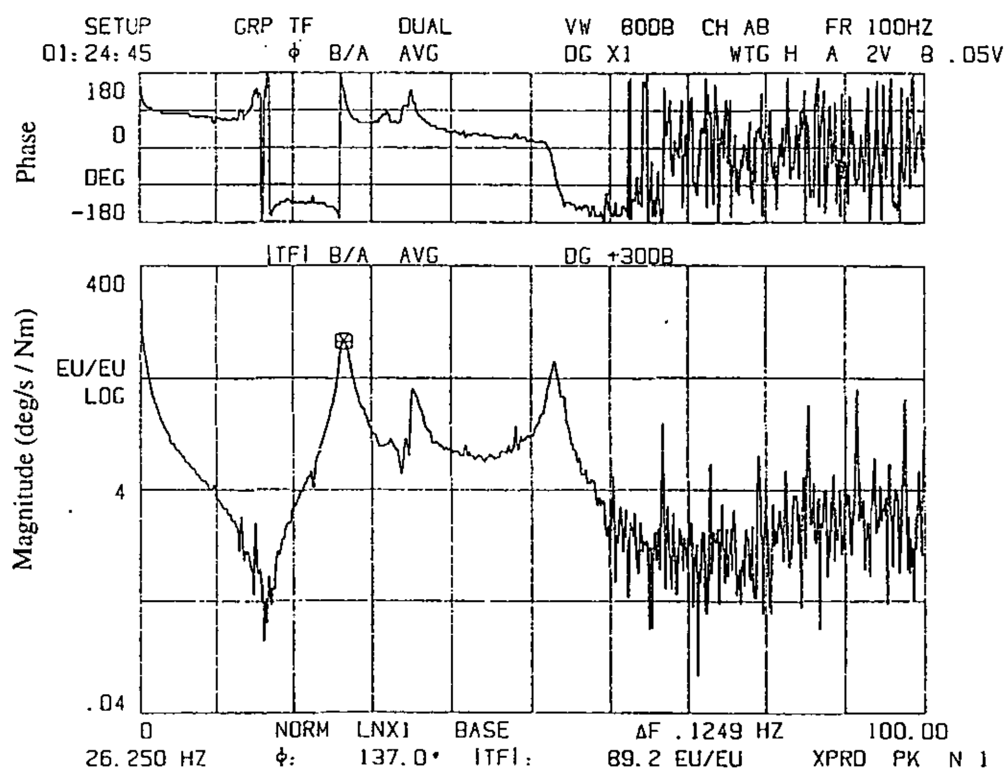

b. 350rpm

Figure 5.26: FRFs for 6th order absorber on centre of shaft at a series of rotation speeds.

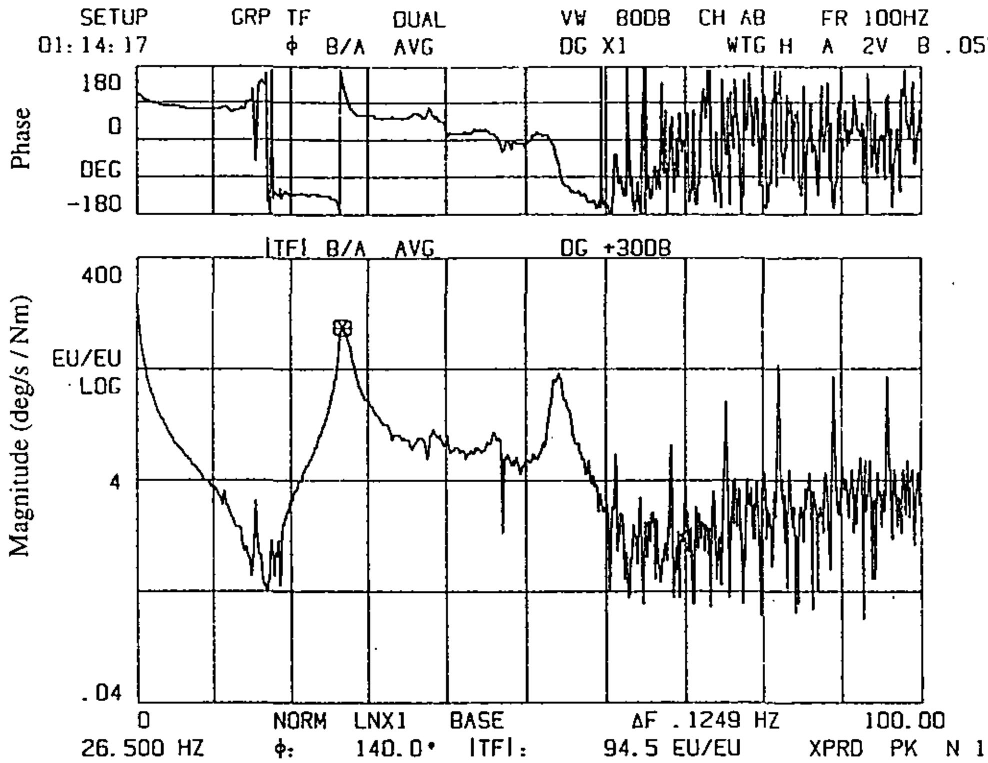

c. 400rpm

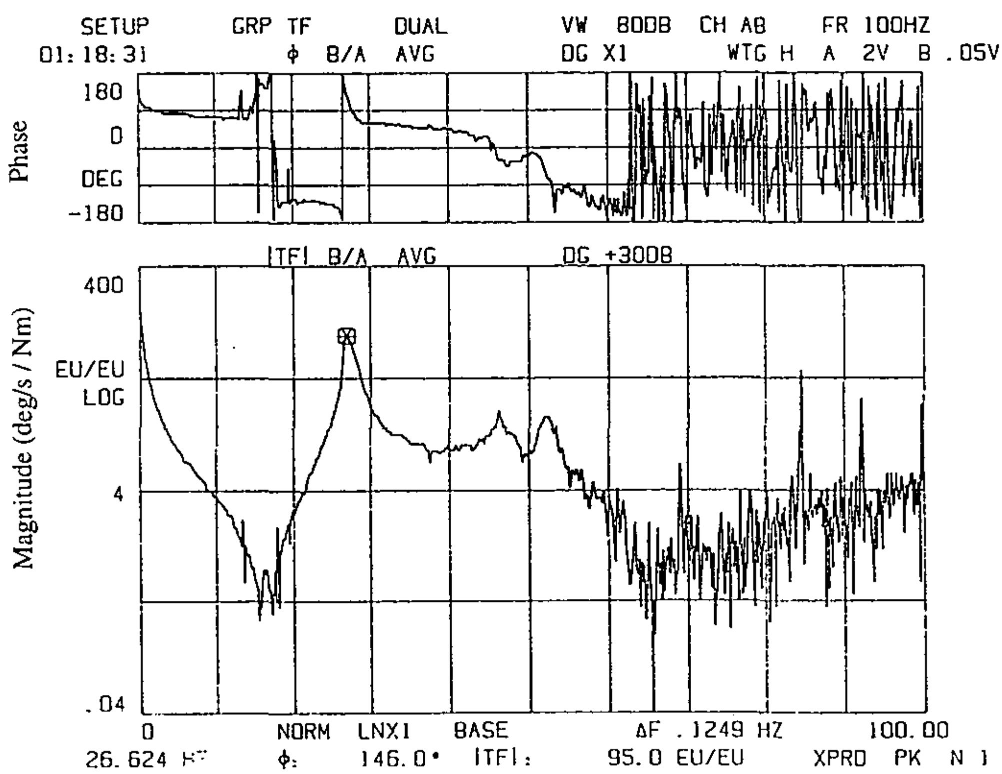

d. 450rpm

Figure 5.26(cont.): FRFs for 6th order absorber on centre of shaft at a series of rotation speeds.

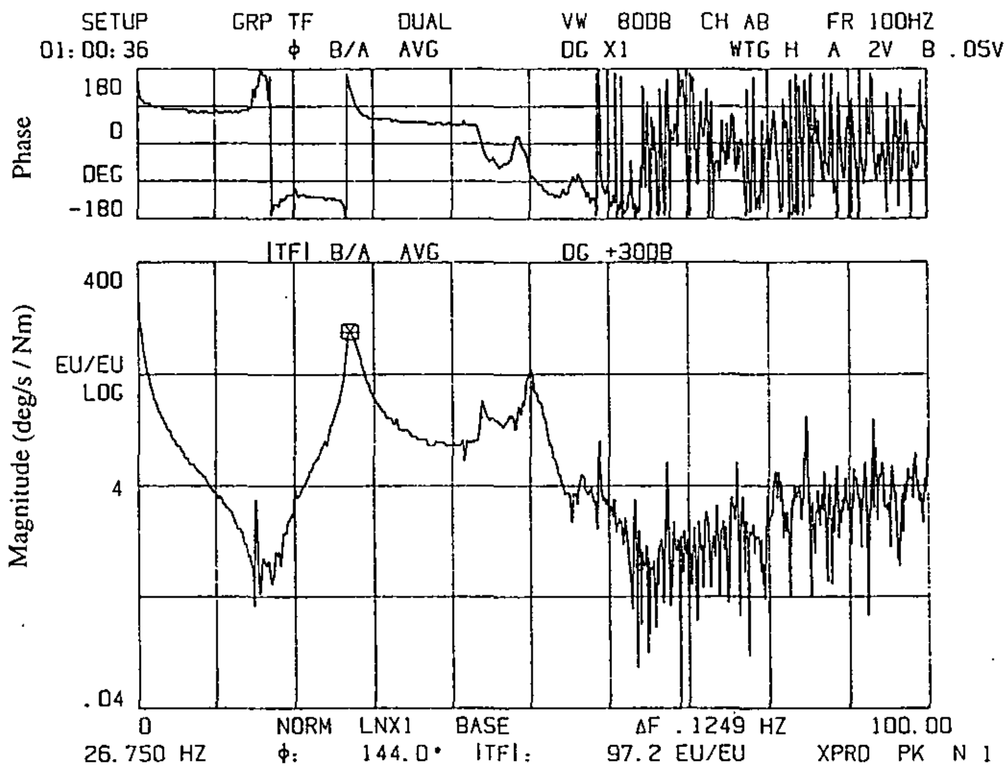

e. 500rpm

Figure 5.26(cont.): FRF for 6th order absorber on centre of shaft at a series of rotation speeds.

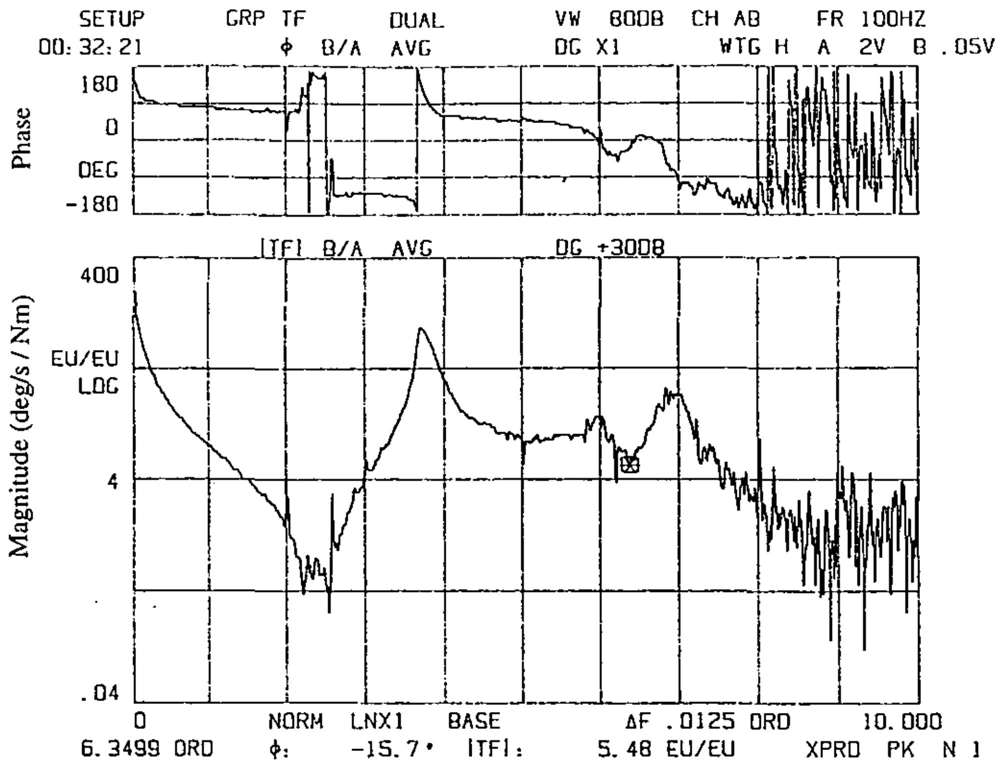

Figure 5.27: FRF for 6th order absorber versus rotation orders at 500rpm.

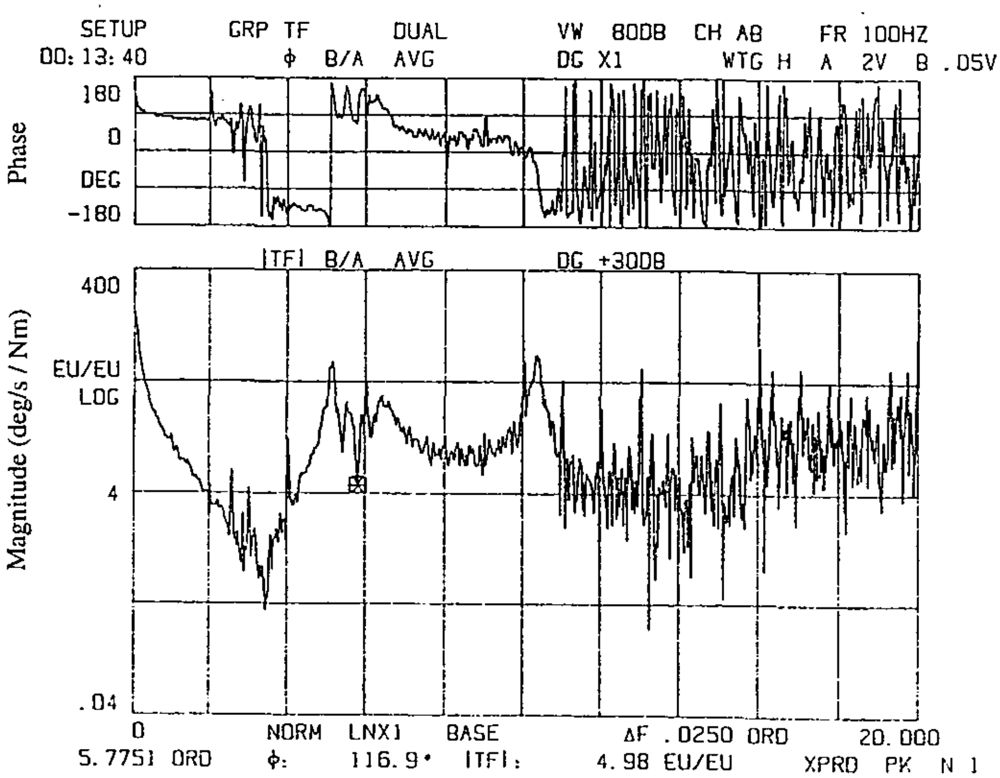

Figure 5.28: FRF for functioning 6th order absorber versus rotation orders at 300rpm and 30V (pk-pk) excitation.

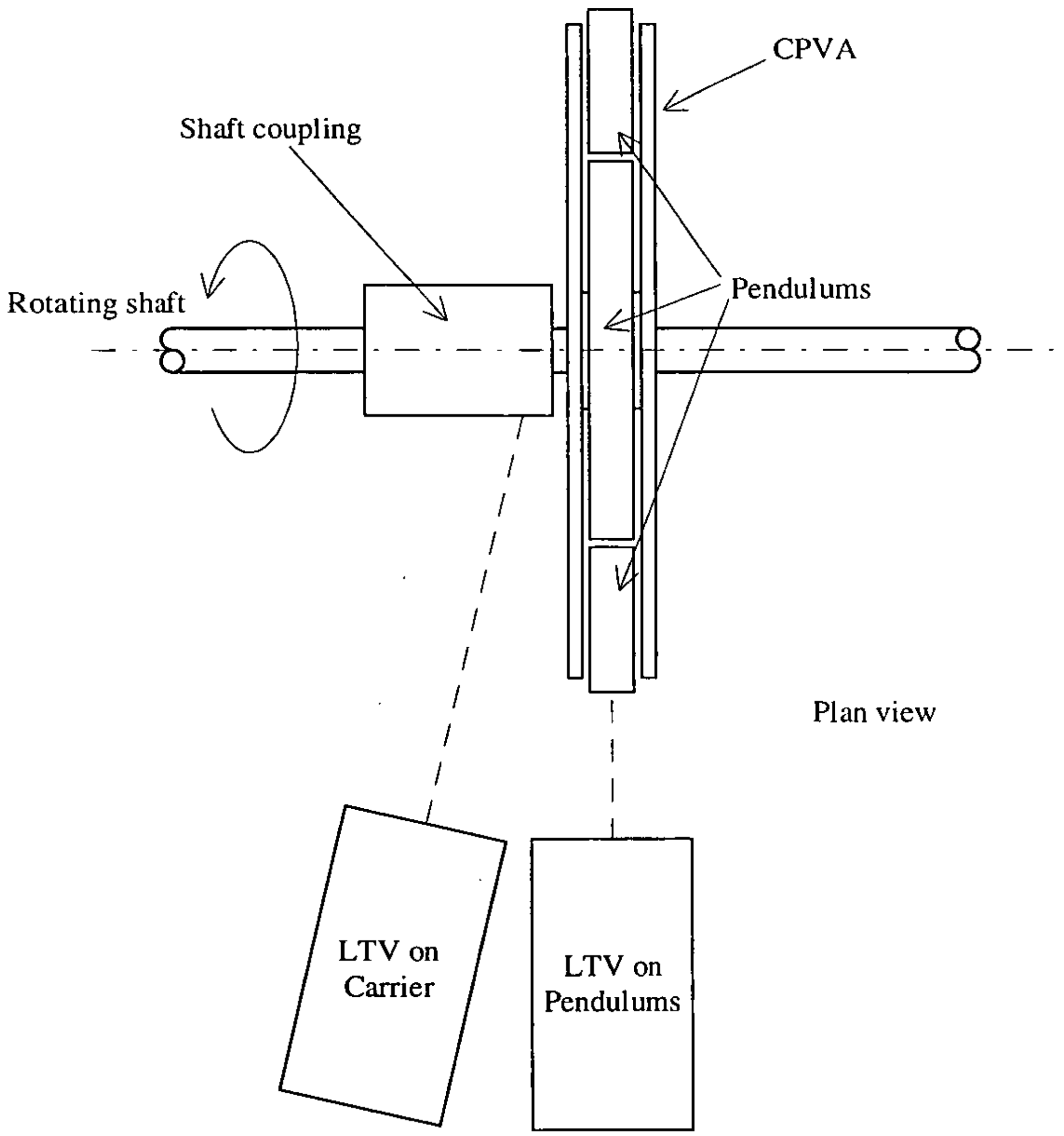

Figure 5.29: Schematic arrangement for experimental study of pendulum motion with LTVs.

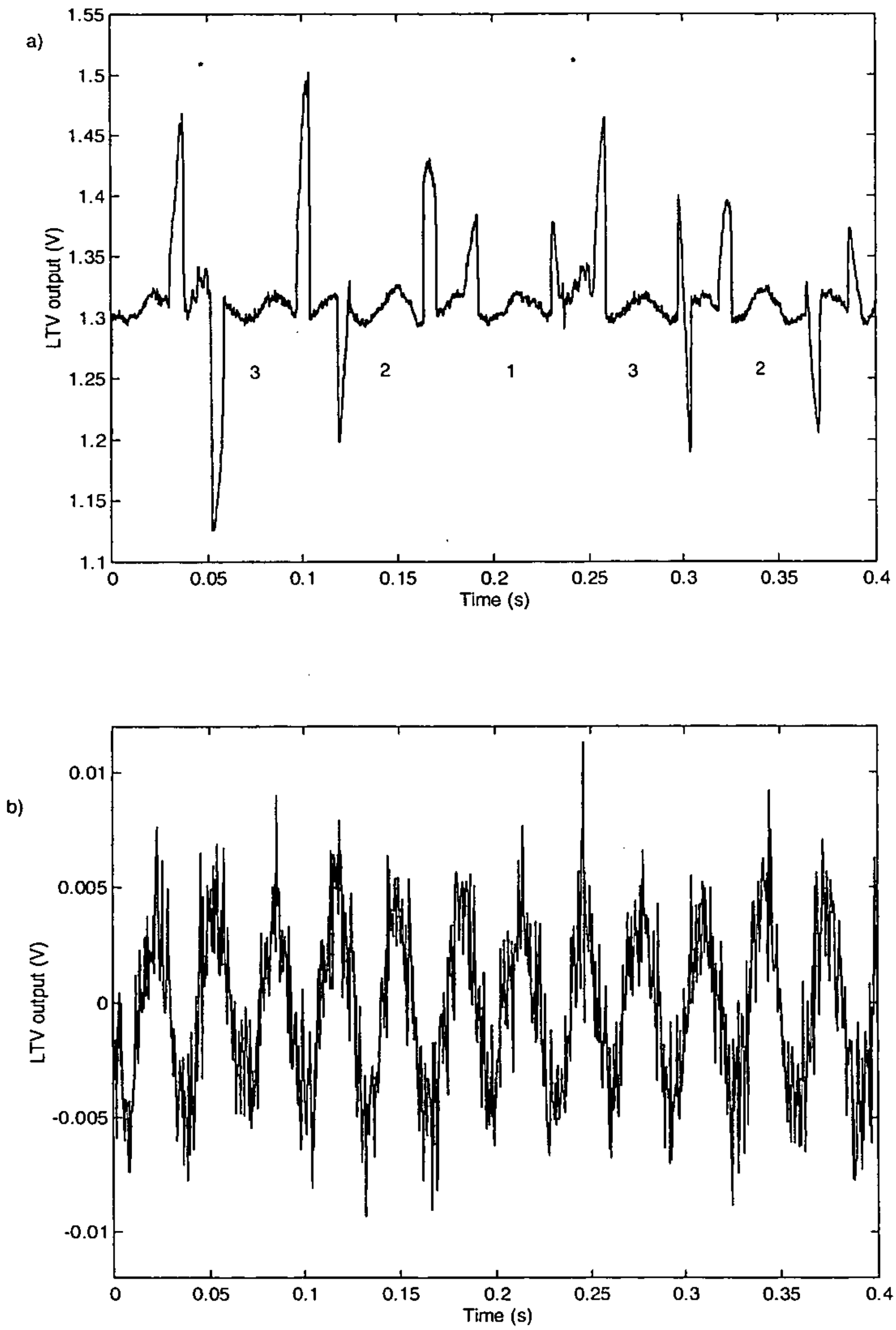

Figure 5.30: Raw LTV time signals for Mode Ib. a. Pendulum motion showing location of reference marker, b. Carrier motion.

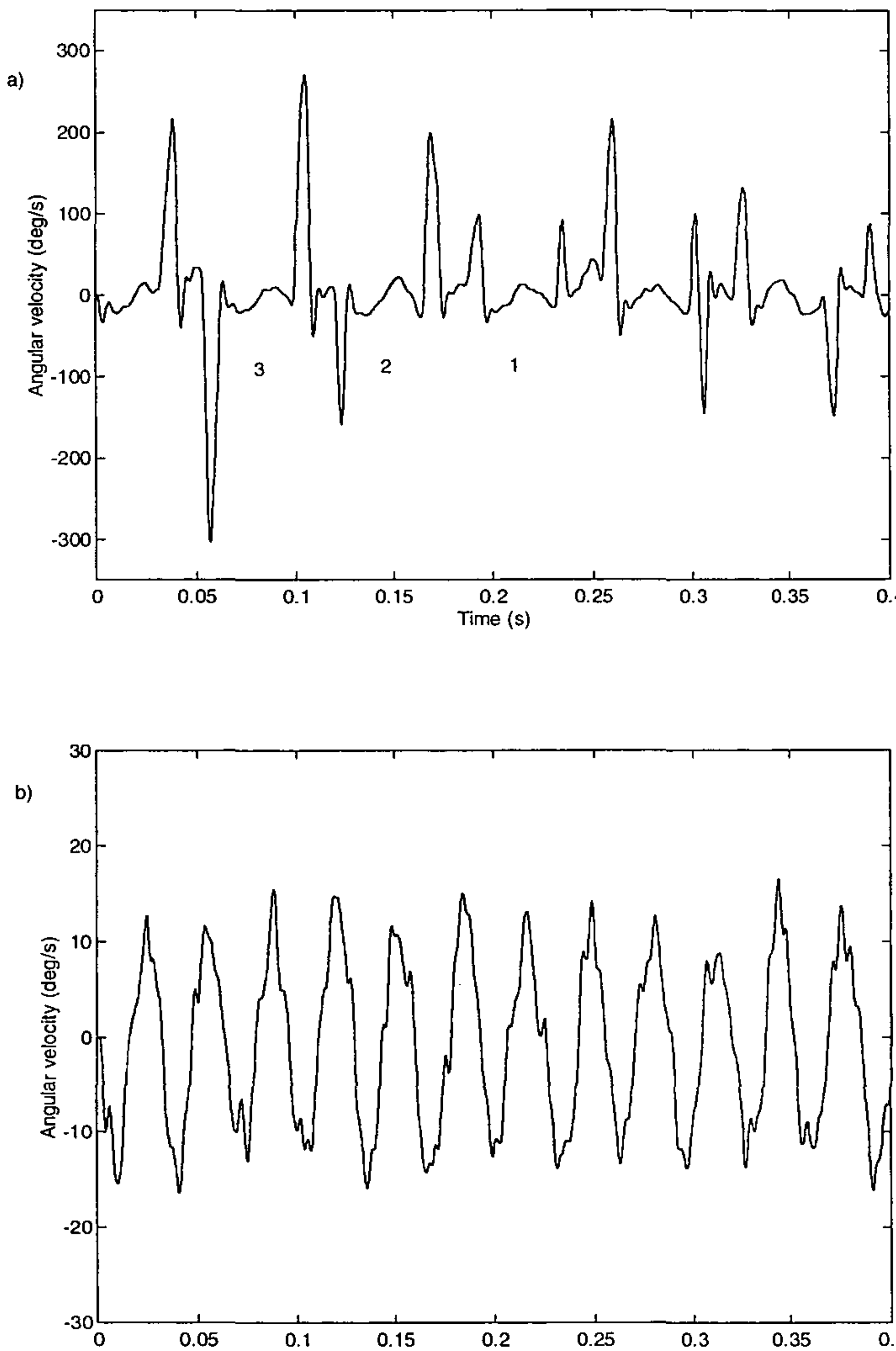

Figure 5.31: Filtered and calibrated LTV signals for Mode Ib.
a. Pendulum motion, b. Carrier motion.

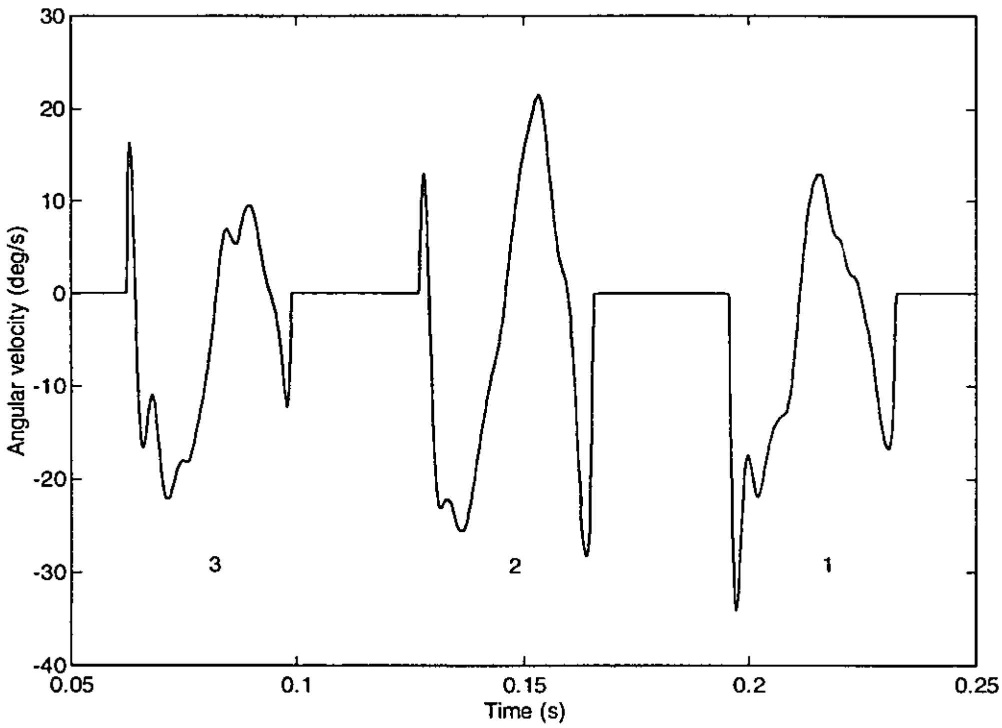

Figure 5.32: Filtered pendulum angular velocity for Mode Ib with signal drop-outs removed.

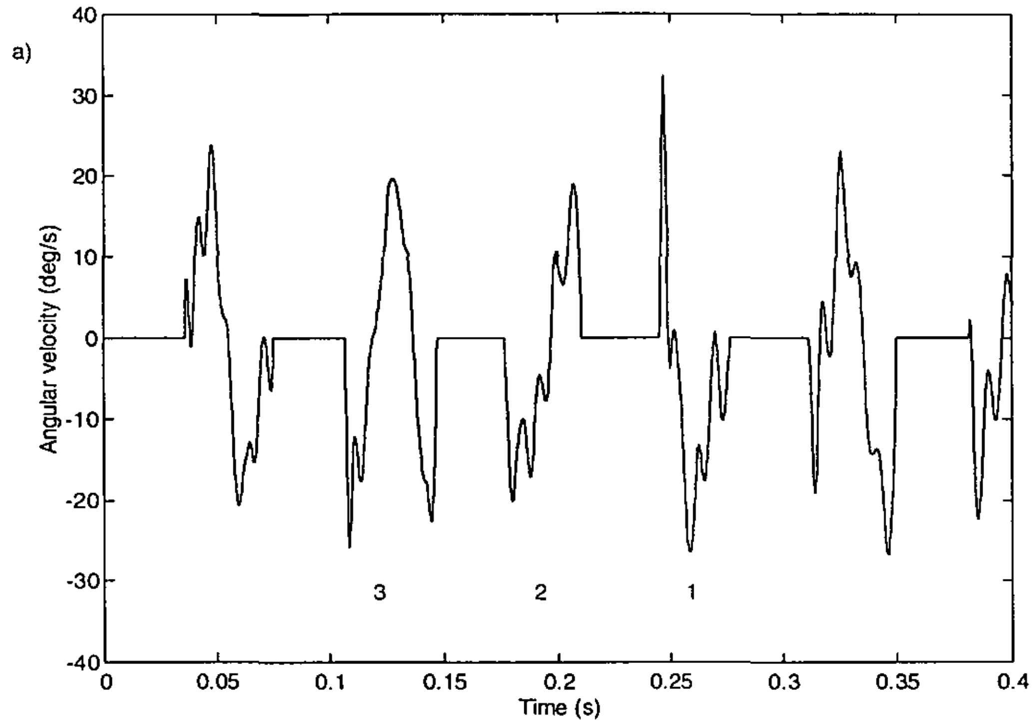

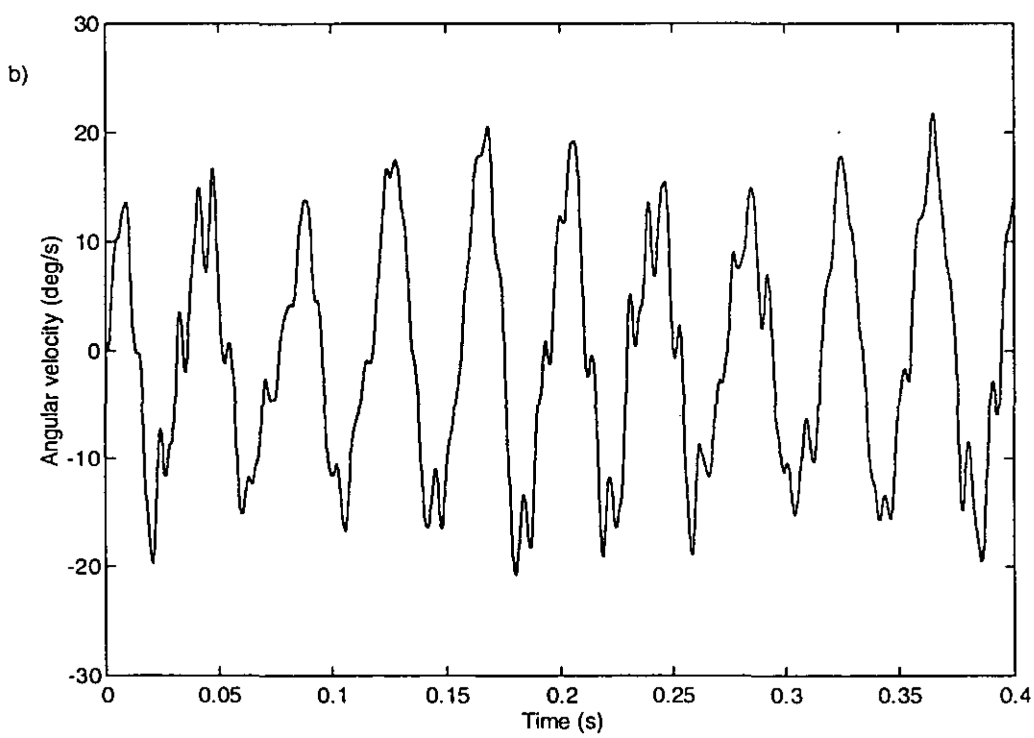

Figure 5.33: Filtered and calibrated LTV signals for Mode Ia.
a. Pendulum motion with drop-outs removed, b. Carrier motion.

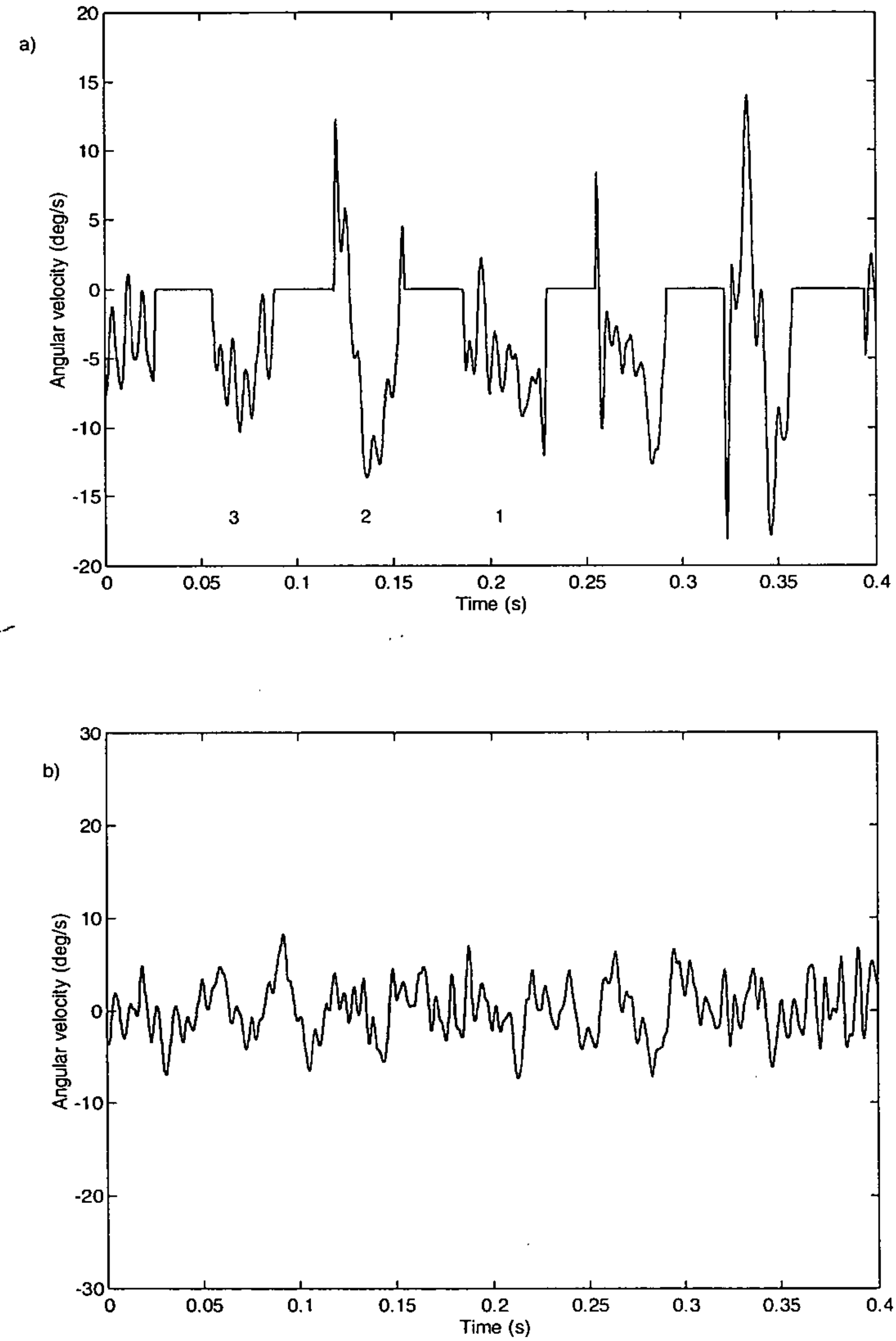

Figure 5.34: Filtered and calibrated LTV signals for Mode I anti-resonance.
a. Pendulum motion with drop-outs removed, b. Carrier motion.

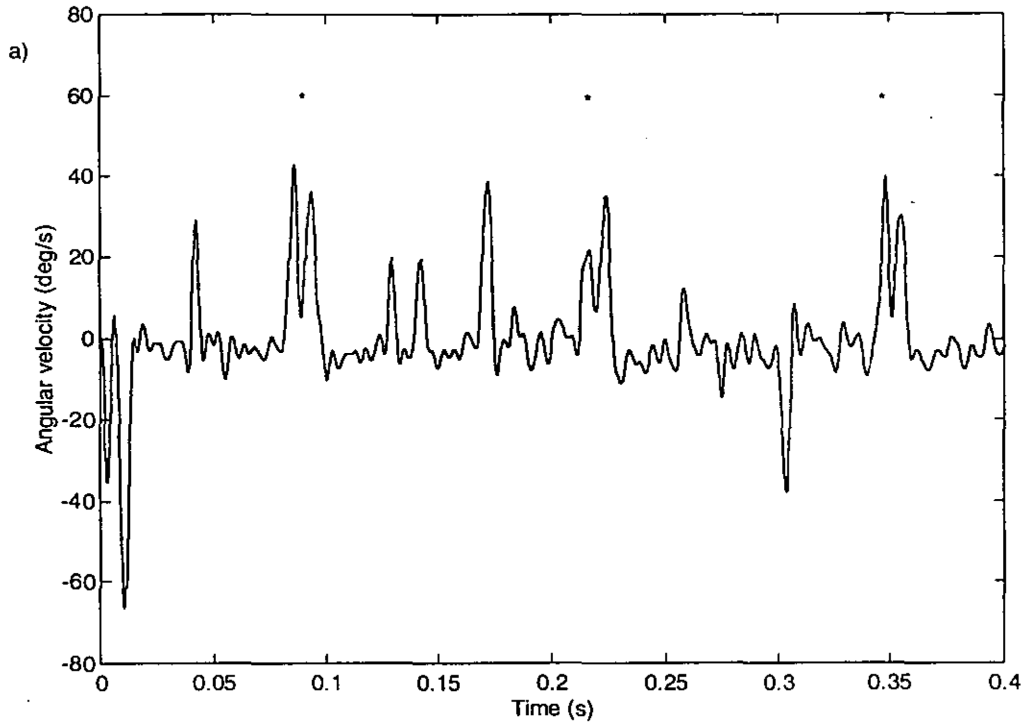

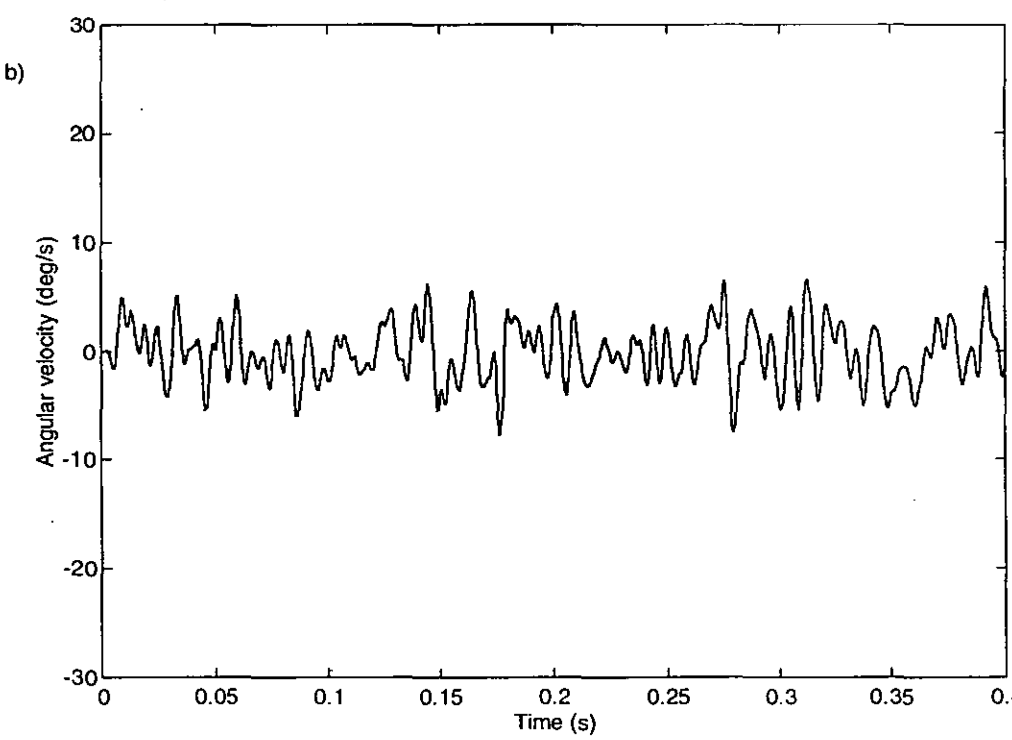

Figure 5.35: Filtered and calibrated LTV signals for Mode II.
a. Pendulum motion, b. Carrier motion.